Investigation of Required Tensile Strength Predicted by Current Reinforced Soil Design Methodologies

Erin K. Phillips

Thesis submitted to the faculty of the Virginia Polytechnic Institute and State University in partial fulfillment of the requirements for the degree of

Master of Science

In

Civil Engineering

George M. Filz, Chair

Ryan R. Berg

Russell A. Green

Joseph E. Dove

May 2, 2014

Blacksburg, Virginia

Keywords: Geosynthetic, Reinforced Soil, GRS, GRS-IBS, Reinforced Soil Design Guidance, Reinforced Soil Design Methods, Parametric Analysis

Investigation of Required Tensile Strength Predicted by Current Reinforced Soil Design Methodologies

Erin K. Phillips

ABSTRACT

Geosynthetic Reinforced Soil (GRS) is a promising technology that can be implemented in walls, culverts, rock fall barriers, and bridge abutments. Its use in walls and abutments is similar to Mechanically Stabilized Earth Walls (MSEW) reinforced with geosynthetics. Both GRS and MSEW are reinforced soil technologies that use reinforcement to provide tensile capacity within soil masses. However, the soil theories behind each method and the design methodologies associated with GRS and MSEW technologies are quite different.

Therefore, a study was undertaken to compare the required tensile strength predicted by these various reinforced soil design methodologies. For the purposes of this study, the required ultimate tensile strength was defined as the ultimate tensile strength needed in the reinforcement after all applicable factors of safety, load factors, and reduction factors were applied. The investigation explored both MSEW and GRS. GRS has been made an FHWA "Every Day Counts" initiative. Due to the push to implement GRS technology, it is critical to understand how GRS design methods differs from classic MSEW design methods, specifically in the prediction of ultimate tensile strength required.

A parametric study was performed comparing five different reinforced soil analysis methods. Two are current MSEW design methods and one was a proposed revision to an existing MSEW design method. The final two were GRS design methods. These design methods are among the most current and/or widely used design references in the United States regarding reinforced soil technology. There are significant differences between the methods in the governing soil theory particularly between GRS and MSEW design methods. The goal of the study was to understand which design parameters had the most influence on calculated values of the required ultimate tensile strength and nominal "unfactored" tensile strength. A base case was established and a reasonable set of parameter variations was determined. Two loading conditions were imposed, a roadway loading scenario and a bridge loading scenario.

Based on parametric study findings, conclusions were drawn about which design parameters had the most influence for different design methods. Additionally, the difference in overall predicted required tensile strength was assessed between the various methods. Finally, the underlying soil theory and assumptions employed by the different methods and their influence on predicted required tensile strength values was interpreted.

DEDICATION

I would like to dedicate this thesis to my parents, Thomas and Rosanne Murphy, for their continuous support of all my endeavors and their encouragement every step of the way.

ACKNOWLEDGEMENTS

First, I would like to thank the Via Department of Civil and Environmental Engineering, the Strategic Highway Research Program (SHRP2), and the Virginia Center for Transportation Innovation and Research (VCTIR) for providing me with such outstanding educational opportunities. I would like to express sincere gratitude for the support and guidance provided by my thesis advisor George Filz. His insight, encouragement, and enthusiasm for geotechnical engineering have made my time at Virginia Tech a truly rewarding experience. Additionally, I would like to thank my thesis committee members Ryan Berg, Russell Green and Joe Dove for their support of my work. Also, I appreciate the advice and direction Vern Schaefer has given throughout the course of my study. Final thanks must be given to Karla Santacruz Reyes and Andy Kost for their beneficial input on the topic of Geosynthetic Reinforced Soil. It has been a privilege to work with such exemplary individuals.

Last but certainly not least, I would like to thank my husband, Adam Phillips, for his constant love and encouragement.

TABLE OF CONTENTS

LIST OF FIGURES

LIST OF TABLES

CHAPTER 1 - INTRODUCTION

1.1 PROBLEM STATEMENT

Geosynthetic Reinforced Soil (GRS) is a promising new technology that can be implemented in walls, culverts, rock fall barriers, and bridge abutments. Its use in walls and abutments is similar to Mechanically Stabilized Earth Walls (MSEW) reinforced with geosynthetics. Both GRS and MSEW are reinforced soil technologies that use reinforcement to provide tensile capacity within soil masses. However, the current GRS design guidance indicates that the behavior of GRS systems is fundamentally different from the guidance for MSEW. GRS abutment wall design assumes that load is not transferred to the face. Therefore, the facing material is not a structural element. The wall is supported by a "composite material" in GRS systems. The opposite is true for MSEW. MSEW design methods assume the soil and reinforcement exhibit a classic soil mechanics behavior, called the "tie-back wedge approach."

Due to the fact that MSEW and GRS guidance do not make similar assumptions regarding behavior, it is critical for design engineers to know when to select one technology over the other. Additionally, it is critical for design engineers to know which design method can be utilized for a particular project. Therefore, understanding which design parameters influence performance for each type of system is necessary.

1.2 RESEARCH OBJECTIVE

The objective of this study was to understand which design parameters influenced the required tensile strength predicted by various reinforced soil design methodologies. Additionally, the results of such an evaluation can provide valuable information regarding which design method should be utilized over another.

1.3 RESEARCH TASKS

In order to achieve the research objective previously outlined, the following research tasks were performed.

Task 1: Conduct a literature review on Geosynthetic Reinforced Soil (GRS). The literature review included technology overviews, case histories, design method, numerical analyses, parametric analyses, and various GRS testing reports. The goal of this research task was to gain a broad understanding of GRS technology development, application, and use within the United States. Additionally, major differences between GRS and Mechanically Stabilized Earth Walls (MSEW) were explored throughout the literary review process.

Task 2 – Conduct a parametric analysis. The parametric study compared various reinforced soil design methodologies. A base case, reasonable parameter variation, and loading conditions were established. The goal of this research task was to compare the

nominal and required tensile strengths versus depth calculated by various reinforced soil analysis methods.

Task 3– Discussion of results and recommendations: Based on the findings of tasks 1, and 2, an assessment of the presence/absence of conservative components in each method was conducted. Observations were made regarding the difference in predicted required tensile strength expected for the various methods, and the reasons for these differences based on the underlying assumptions and the soil theories for each method were explored.

CHAPTER 2 - LITERATURE REVIEW

2.1 GRS HISTORY

Reinforced earth is an ancient methodology. Early societies used materials such as straw and plant matter to improve the strength of earth masses. The reinforcing material, though primitive, helped to improve the soil's weakness in tension. The resulting composite mass was less likely to dilate or deform. The benefit of increased confinement is still observed in modern technologies (Adams et al. 2011b).

Today, earth can be reinforced using a variety of materials including, steel strips, welded wire meshes, and geosynthetics. Geosynthetic reinforcement is derived from plastic polymers. Common polymer types include Polyester (PET), Polypropylene (PP) and High Density Polyethylene (HDPE). Geosynthetic reinforcement comes in primarily two forms, geogrids and geotextiles (Berg et al. 2009). The first recorded use of Geosynthetic Reinforced Soil (GRS) in the U.S. is by the U.S. Forest Service in the 1970s. This project used coarse grained fill and geosynthetic reinforcement, placed in closely spaced lifts, for roadway projects in mountainous terrain (Adams et al. 2011a). Prior to these efforts, the company Reinforced Earth in the 1960s began using steel strips to reinforce soil. These projects are considered the first Mechanically Stabilized Earth Walls (MSEW). MSEW designs using geosynthetics began in the 1980s (FHWA 2011).

Both MSEW and GRS systems laterally restrain a soil mass using reinforcement. Yet the behavior of these systems is inherently different according to Adams et al (1999). MSEW uses a "tie-back wedge" approach which assumes that the facing is a structural element that is restrained by the reinforcement. The "wedge" is the active stress zone behind the wall face. Therefore, the extent of the active zone must be found in MSEW design to ensure adequate length of reinforcement. GRS systems on the other hand assume a "composite behavior" approach. Assumption of composite behavior for GRS is based on the much closer reinforcement spacing for GRS than MSEW, with GRS reinforcement spacing typically less than 12 inches. Additionally, GRS reinforced fill material is typically high quality coarse grained fill that is well compacted, whereas MSEW fill can be similar to GRS fill but often lower quality fill material is used. The unique characteristics of GRS produces a composite system that strains together (Adams et al. 1999). Therefore, no active wedge develops behind the wall face and the facing is not considered a structural element (Kost et al. 2013).

GRS is used for applications such as culverts, rockfall barriers, walls, bridge piers, and bridge abutments. Additionally, GRS has been used in negative batter walls and arches (Barrett and Ruckman 2007). Over the last few years, the use of GRS technology for bridge abutments has received considerable attention. Geosynthetic Reinforced Soil Integrated Bridge System (GRS-IBS) is the coined name for a GRS wall and bridge system that was developed as part of the "Bridge of the Future" initiative by the Federal

Highway Administration (FHWA) (Adams et al. 2011a). GRS-IBS is a cost effective and efficient solution for low volume, single span bridges. Furthermore, GRS-IBS can be used under a variety of foundation soil conditions. Another noted advantage of GRS-IBS is the elimination of the "bump" at the end of the bridge. This is due to the improved performance of these systems in regards to differential settlement. However, GRS-IBS has a few shortcomings in regards to applicability. These systems are not ideal for stream scour environments or conditions of soft, deep foundation soil if large settlement is a concern (Keller and Devin 2003).

Overall, GRS-IBS is a promising technology which has been implemented in a series of successful case histories in the U.S. and abroad (Lee and Wu 2004). In 2010, GRS-IBS was made an Every Day Counts (EDC) initiative. The poor state of bridges in the U.S. prompted the EDC initiative. Many of the 600,000 bridges in the U.S. have structural deficiencies. Of these bridges, the vast majority are single span bridges no more than 90 feet in length. Currently the demand for repair and future construction of bridges does not align with government budgets. Therefore, a new efficient system is required so that more bridges can be rehabilitated and constructed at low cost. GRS-IBS is a possible solution for this dilemma (FHWA 2011).

2.2 REINFORCED SOIL DESIGN GUIDANCE

Since the introduction of reinforced soil technology in the United States, numerous methodologies for design and construction have been developed. The history of reinforced soil guidance is a complicated one, involving many great advances and setbacks. Difficulties have arisen in the past between private and public sectors. Thus, debates over best practices and over-conservatism have ensued (Christopher et al. 2013). In general, design guidance developed by the American Association of State Highway and Transportation Officials (AASHTO) and the Federal Highway Administration (FHWA) is considered to be more conservative than that developed by the National Concrete Masonry Association (NMCA) and other non-transportation related entities. Figure 1 compares conservatism between multiple methods developed before the year 1998. Conservatism was assessed by examining the service loads (L) relative to resistance of the reinforcement (R). The ratio of L/R is plotted on the horizontal axis of Figure 1. R will vary depending on the reinforcement used and therefore the resistance provided (Berg et al. 1998).

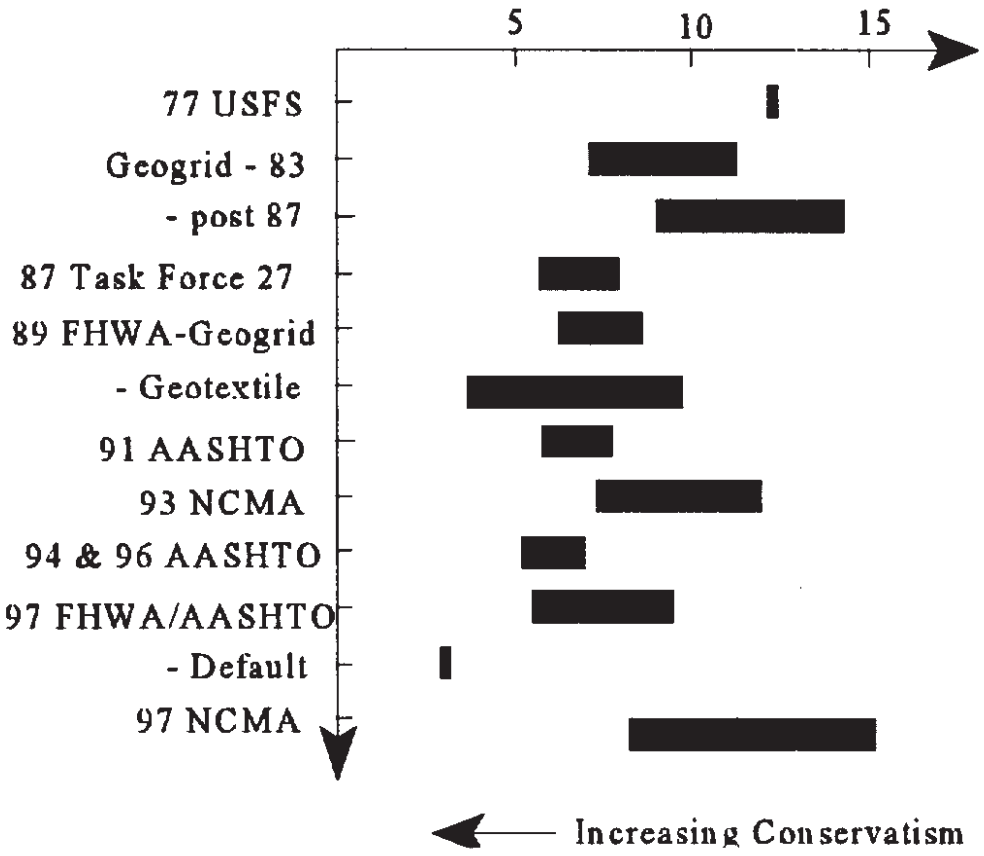

Figure 1: Conservatism of Reinforced Soil Design Guidance Berg, R. R., Allen, T. M., and Bell, J. R. (1998) "Design Procedures for Reinforced Soil Walls-AHistoric Perspective." Sixth International Conference on Geosynthetics. Used under fair use, 2014.

The paper, "Design Procedures for Reinforced Soil Walls – A Historic Perspective," by R. R. Berg, T. M. Allen and J. R. Bell should be referenced for information about the differences in calculation between these early methods, specifically in the long-term allowable design strength (LTADS) (Berg et al. 1998). Additionally, the paper describes the natural evolution of assumptions and methodologies incorporated into the internal stability calculations of these early methods. From the year 1977 to 1998, conservatism in FHWA and AASHTO design guidance has increased with time. This is likely due to increases in reduction factors and slight decreases in calculated loading of these structures (Berg et al. 1998). Figure 2 highlights the critical milestones made in reinforced soil guidance and development since 1985. Therefore, Figure 1 and Figure 2 overlap between 1985 and 1998. The paper, "Reinforced Soil Walls and Slopes: In Retrospect (i.e., The Good, the Bad, and the Ugly)," should be referenced for more information regarding the detailed history of reinforced soil guidance in the U.S. since the year 1985 (Christopher et al. 2013).

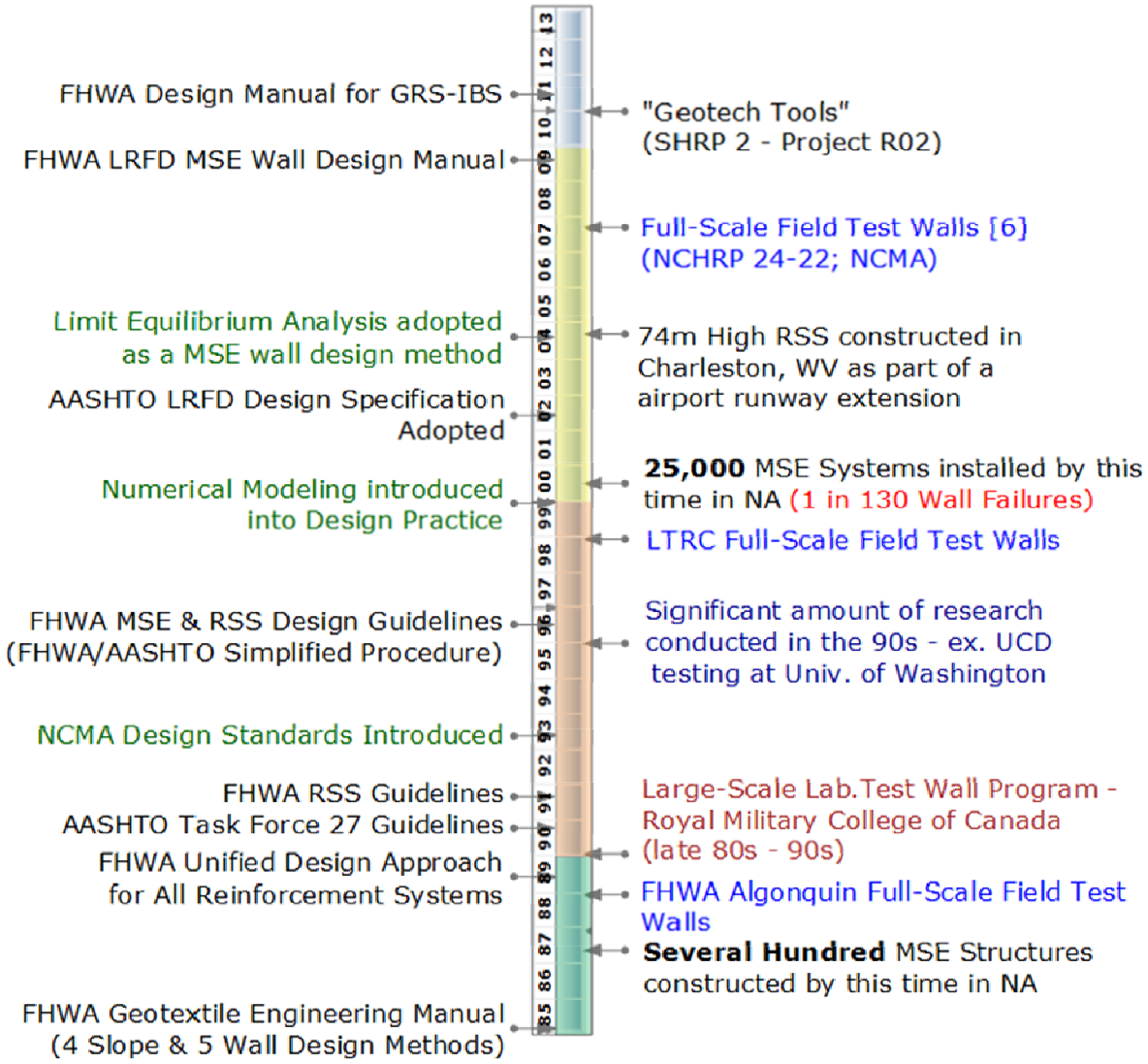

Figure 2: Timeline of Development and Advancement of Reinforced Soil Design Guidance Christopher, B. R., Holtz, R. D., Berg, R. R., and Stulgis, R. P. (2013). "Reinforced Soil Walls and Slopes: In Retrospect (i.e. The Good, the Bad, and the Ugly)." Used under fair use, 2014.

Over the last 25 years, design guidance has incorporated new insights and key features of multiple methodologies. Additionally, new resources, such as the www.geotechtools.org website, have become available to help educate diverse groups of people with varying amounts of working knowledge on the topic of reinforced earth. Education is a challenge, but advancements over the last few decades have improved design guidance and engineering resources immensely (Christopher et al. 2013).

The most current and widely applied design guidance for reinforced soil slopes (RSS) and MSEW in the U.S. is the "FHWA LRFD MSE Wall Design Manual" published in 2009 as indicated in Figure 2. This method is often called the "FHWA Simplified

Procedure" or the "AASHTO LRFD Bridge Specifications" since the method was adopted as the standard design guidance by AASHTO in 2012. The full reference is:

Berg, R.R., Christopher, B.R., and Samtani, N. (2009). "Mechanically Stabilized Earth Walls and Reinforced Slopes, Design and Construction Guidelines", *Vol. I FHWA-NHI-10-024,Vol.II-FHWA-NHI-10-025*, Federal Highway Administration, Washington, D.C.

The "FHWA Simplified Procedure" is the state of practice referenced for highway projects involving MSE and RSS. The design guidance is very comprehensive. It provides necessary information to select, design, construct, and maintain MSE and RSS structures. The "FHWA Simplified Procedure" design steps follow a Load and Resistance Factor Design (LRFD) approach. The design guidance covers a wide range of reinforcement types, including geosynthetics. Additionally, design examples and equations are provided for bridge loading conditions imposed on an abutment wall. However, the code does not incorporate the defining characteristics of GRS technology, specifically the close reinforcement spacing (Berg et al. 2009).

The state of practice design guidance for GRS-IBS is the "FHWA Design Manual for GRS-IBS" published in 2011 as indicated in Figure 2. This method is sometimes referred to as the "FHWA Method" or the "FHWA GRS-IBS Method." The manual is published in two parts and the full references are:

Adams, M., Nicks, J., Stabile, T., Wu, J.T.H., Schlatter, W., and Hartmann, J. (2011a). "Geosynthetic Reinforced Soil Integrated Bridge System—Interim Implementation Guide." *FHWA-HRT-11-026*. Federal Highway Administration, McLean, VA.

Adams, M., Nicks, J., Stabile, T., Wu, J.T.H., Schlatter, W., and Hartmann, J. (2011b). "Geosynthetic Reinforced Soil Integrated Bridge System—Synthesis Report." *FHWA-HRT-11-027*. Federal Highway Administration, McLean, VA.

The "FHWA GRS-IBS Method" provides design and construction guidance for GRS-IBS projects. The method is consistent with much of the "FHWA Simlified Procedure." However, there are instances where GRS-IBS does not fall within this framework due to unique aspects of the technology. The design guidance is comprehnsive in nature and entails necessary information regarding design, construction, maintenance, and QC/QA. The "FHWA GRS-IBS Method" also provides an LRFD procedure (Adams et al. 2011a).

Not included in Figure 2 is the "NCHRP GRS Method" published in 2006, also referred to as "NCHRP Report 556". This method provides a design methodology for GRS bridge abutments with flexible facing. The publication of this method proceeded the coining of the term GRS-IBS. However the systems detailed in the "NCHRP GRS Method" is for all intents of purposes a GRS-IBS technology. The method was intended to be a revision or compliment to the state of practice for MSEW at the time. The MSEW guidance incorporated in NCHRP GRS Method was a previous version of the "FHWA Simplified Procedure" prior to the inclusion of LRFD (Wu et al. 2006a). The full reference for the "NCHRP GRS Method" is:

Wu, J.T.H., Lee, K.Z.Z., Helwany, S.M.B., and Ketchart, K. (2006a). "Design and Construction Guidelines for GRS Bridge Abutments with a Flexible Facing." *Report No. 556.* National Cooperative Highway Research Program, Washington, D.C.

The "NCHRP GRS Method" is not the preferred GRS-IBS design guidance; the "FHWA GRS-IBS Method" is the current state of practice. However, the NCHRP GRS Method does provide a comprehensive framework for designing GRS-IBS systems including design examples. The NCHRP GRS Method reference does not include a LRFD design procedure; however, "Web-only Document 187" includes LRFD seismic design for GRS abutments with flexible facing. The "NCHRP GRS Method" differs from the "FHWA GRS-IBS Method" in multiple ways, most notably its classification of GRS-IBS characteristic spacing. The "FHWA GRS-IBS Method" sets the spacing limit at 12 inches while the "NCHRP GRS Method" sets it at 16 inches. Also, the "FHWA GRS-IBS Method" accounts for maximum particle size in design while the "NCHRP GRS Method" does not. Additionally, the methods each have differing standards for reductions factors, bearing capacity limits, friction angle used in design, strain limits, and truncation of the base (Kost et al. 2013). It should be noted that many of these differences also exist between the "FHWA GRS-IBS Method" and the "FHWA Simplified Procedure."

An additional method, which is also not included in Figure 2, is a proposed revision to the current "FHWA Simplified Procedure." This method is identical to the "FHWA Simplified Procedure" with the exception of lateral earth pressure coefficient tabulation within the reinforced fill. Therefore, this additional method is referred to by the development team as the "Simplified Procedure with K_r/K_a Adjusted." The adjustment to the lateral earth pressure coefficient in the reinforced fill (K_r) is in regards to the MSEW face batter. The change occurs when wall face batter is less than 10 degrees or nearly vertical (Berg 2013). A published reference for this method is not available at this time.

The "K-Stiffness Method" which is not included in Figure 2, takes into account the relative stiffness of all wall components in comparison to the soil stiffness. This changes the way the maximum tension in the reinforcement is calculated including its magnitude and distribution (Allen and Bathurst 2003). There are plans to incorporate "K-Stiffness Method" principals into the current "FHWA Simplified Procedure." The full reference for the "K-Stiffness Method" is:

Allen, T.M., and Bathurst, R.J. (2003). "Prediction of Reinforcement Loads in Reinforced Soil Walls." *WA-RD 522.2*, Washington State Department of Transportation, Seattle, WA.

In summary, there are several current and/or under development design methods for reinforced soil. Three pertain to MSEW structures that have larger reinforcement spacing. These are the "FHWA Simplified Procedure", the "Simplified Procedure with K_r/K_a Adjusted", and the "K-Stiffness Method." Two are design guidance for GRS-IBS specifically. These are the "NCHRP GRS Method" and the "FHWA GRS-IBS Method."

Additional details about calculation of reinforcement tension using these methods are presented in Chapter 3.

2.3 GRS CASE HISTORIES

There have been many different types of structures built using GRS technology over the last few decades; however, the primary focus of this section will be on GRS technology for the application of abutment walls. The papers, "GRS - A New Era in Reinforced Soil Technology," published in 2007 by R. Barrett and A. Ruckman, "Lateral Earth Pressure Against the Facing of Segmental GRS Walls" published in 2007 by J. T. H. Wu, and "A Synthesis of Case Histories on GRS Bridge – Supporting Structures with flexible Facing," published in 2004 by K. Z. Z. Lee and J. T. H. Wu provide further information about additional applications of GRS besides those specifically described in this section here. The case histories discussed in this section are for in-service loading conditions only. Any large scale field experiment that simulates such loading is discussed in the GRS Large Scale Testing section.

Blackhawk Bridge: The Blackhawk Bridge was constructed during the summer of 1997 in Blackhawk, Colorado (Adams et al. 1999). The bridge is also referred to as the Bobtail Road Bridge (Lee and Wu 2004). The bridge location was characterized by very steep terrain, which lead to a unique design challenge where the elevations of either side of the bridge were not equal. The abutment on the east side of the bridge was taller than the west. The eventual technology selected for the abutments was a GRS mass with pre-strained anchors running through to rock as shown in Figure 3 (Adams et al. 1999).

The bridge itself is a steel arched bridge. The bridge span is 36 meters. The east abutment height is 5.4 meters at its tallest point with reinforced soil foundation extending another 2.1 meters into the ground. The west abutment height is 2.7 meters at its tallest point, with a reinforced soil foundation extending another 1.8 meters into the ground. The reinforced fill was a SM-SC as classified using ASTM D2487. This soil was the naturally occurring soil on-site. This soil was determined to have a friction angle of 31° and cohesion of 34 kPa. The reinforcement was a PP woven geotextile with a tensile strength of 70 kN/m (Lee and Wu 2004; Wu et al. 2001). The reinforcement spacing was 0.3 meter or approximately 12 inches. Figure 4 shows a details schematic of the abutments (Wu et al. 2001). The facing element used was unique. It was a dry-stacked natural rock, which some considered to have aesthetic appeal (Adams et al. 1999).

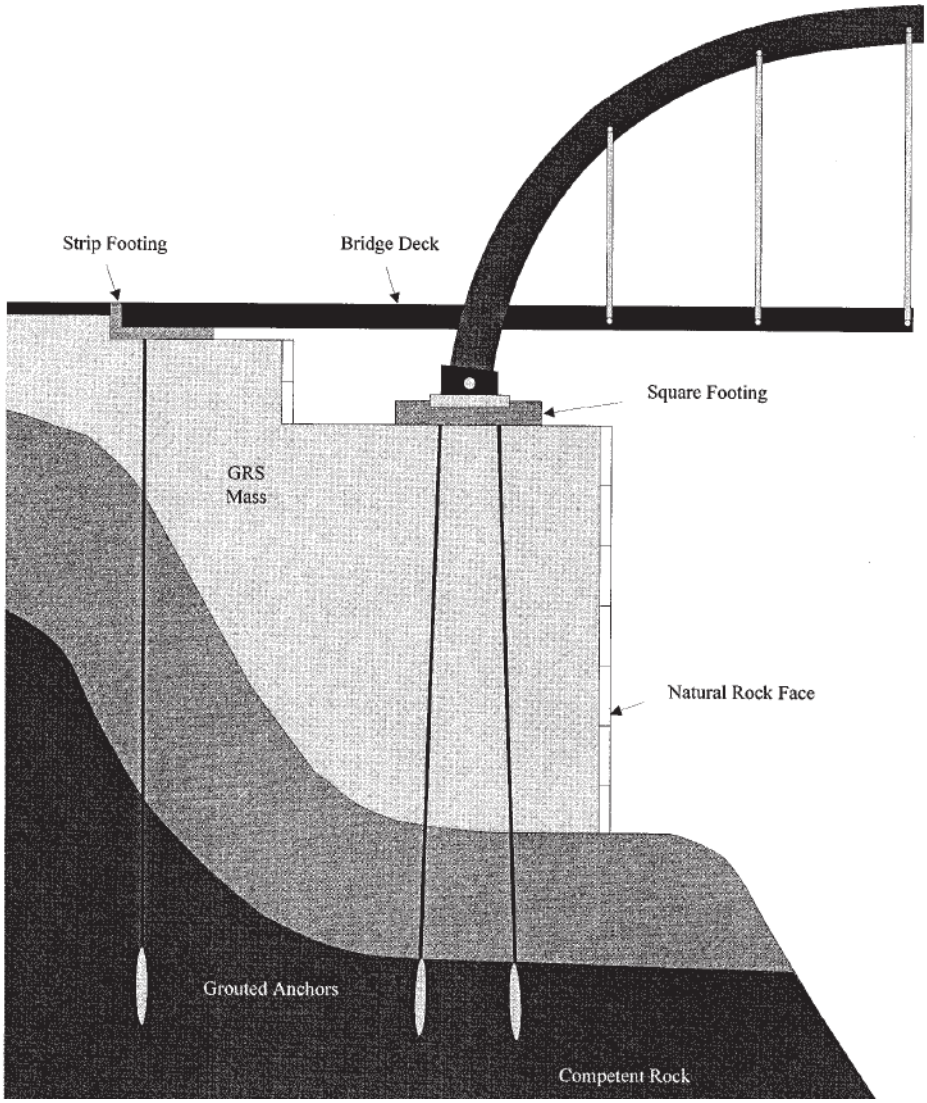

Figure 3: Schematic of the Blackhawk Bridge GRS Abutment Adams, M., Ketchart, K., Ruckman, A., DiMillio, A. F., Wu, J. T. H., and Satyanarayana, R. (1999). "Reinforced Soil for Bridge Support Applications on Low-Volume Roads." Transportation Research Board, Washington, D.C. Used under fair use, 2014.

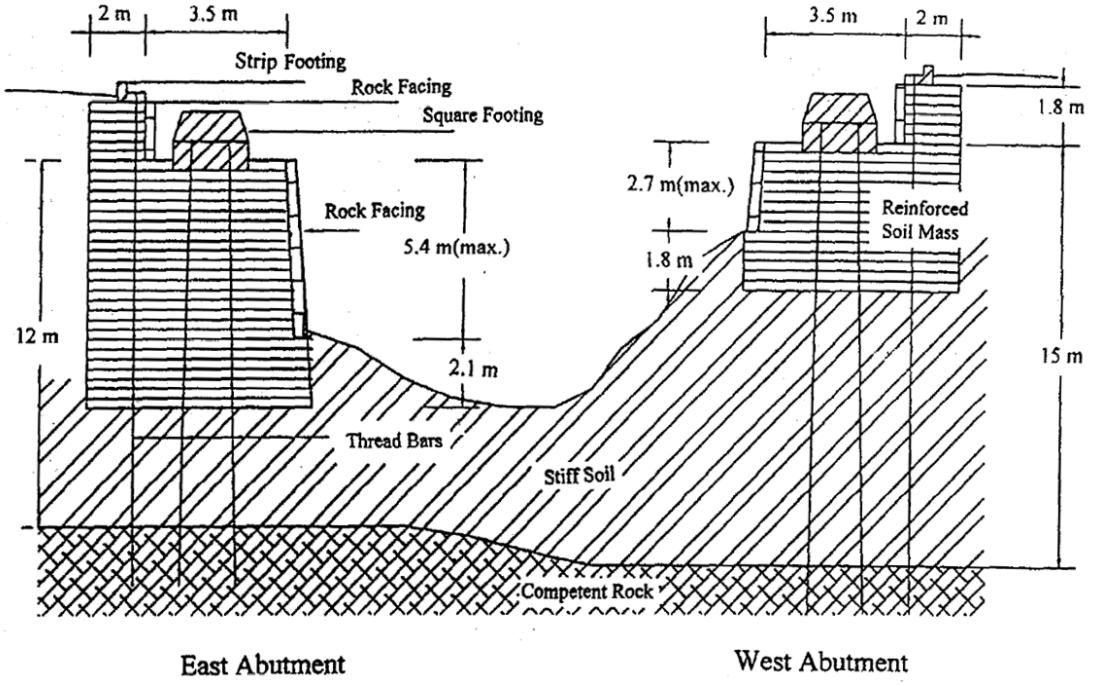

Figure 4: East and West Blackhawk Bridge Abutment Details Wu, J. T. H., Ketchart, K., and Adams, M. (2001). "GRS Bridge Piers and Abutments." *FHWA-RD-00-38*, Federal Highway Administration, McLean, VA. Used under fair use, 2014.

Three preloading cycles took place. It was concluded that preloading reduced design anticipated creep strains, settlement, and lateral movements. The max observed strain in the reinforcement was 0.2%. This was considered quite low (Lee and Wu 2004). The full instrumentation program monitored settlement, lateral movement, and reinforcement strains throughout preloading (Wu et al. 2001).

Initial construction plans detailed a bridge supported by drilled shafts. Due to cost savings, the plans were modified to incorporate a GRS mass which would directly support the bridge instead of using drilled shafts (Adams et al. 1999).

Feather Falls Trail Bridge: Constructed in 1999, the Feather Falls Trail Bridge was a small bridge for a recreational hiking trail in Plumas National Forest, California. A GRS abutment was chosen for the remote site due to the relatively simple construction process. Figure 5 shows one of the bridge abutments. All equipment and materials had to be transported via helicopter. Therefore, use of lighter materials or on site materials was a huge advantage. Construction lasted two weeks. Cost of the abutments was estimated to be $30 per square foot of wall face (Keller and Devin 2003).

Figure 5: Feather Falls Trail Abutment without Facing Keller, G. R., and Devin, S. C. (2003). "Geosynthetic-Reinforced Soil Bridge Abutments." Transportation Research Board, Washington, D.C. Used under fair use, 2014.

The reinforced fill was local rocky soil. The abutments were 5 and 8 feet high. Timber facing materials were chosen. Reinforcement spacing was approximately 6 inches. Figure 6 illustrates the layout of the GRS abutment. The chosen reinforcement was a woven PET geotextile. Two reinforcement strengths were utilized: a 52 kN/m strength and a 70 kN/m strength. Top lifts wrapped the reinforcement over the timber face, lower lifts nailed reinforcement between timbers. Drainage was accounted for through the installation of a geocomposite drain behind the abutment walls (Keller and Devin 2003).

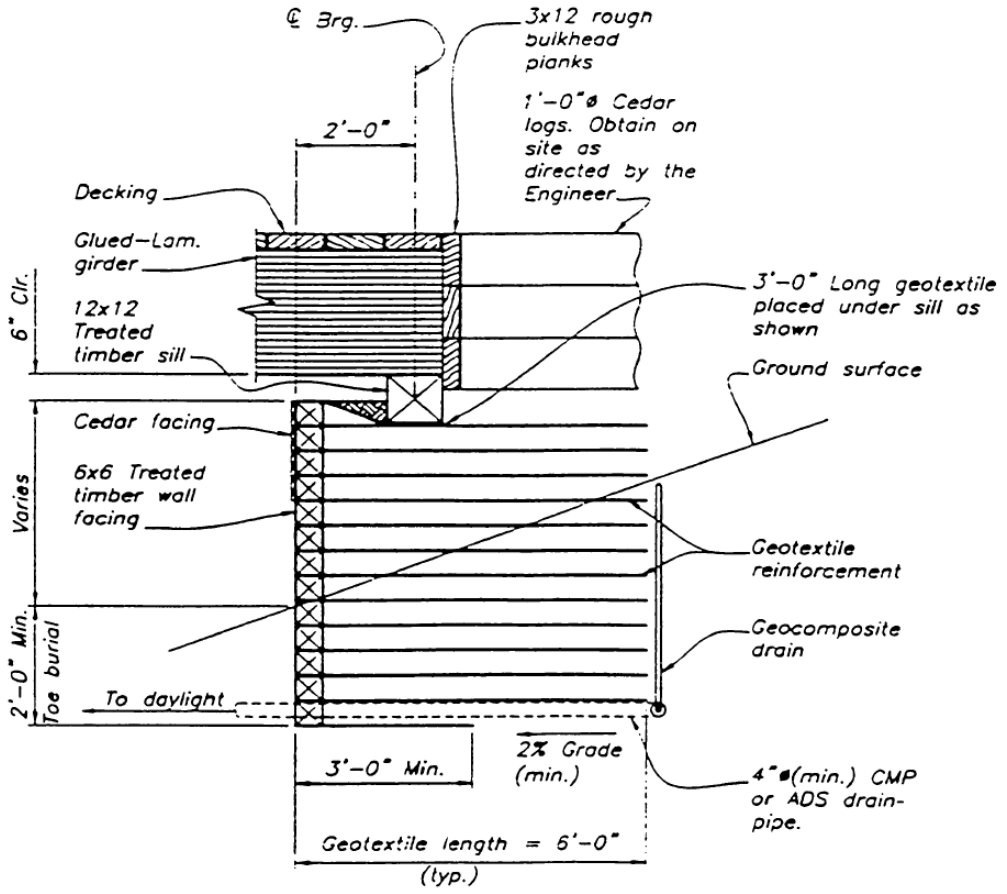

Figure 6: Feather Falls GRS Abutment Schematic Keller, G. R., and Devin, S. C. (2003). "Geosynthetic-Reinforced Soil Bridge Abutments." Transportation Research Board, Washington, D.C. Used under fair use, 2014.

Founders/Meadows Bridge: One of the first GRS style large scale projects was the Founders/Meadows Bridge Parkway Structure constructed in July of 1999 in Colorado. This system was a unique field application of GRS technology. A composite GRS mass was used to support both the bridge and the approaching roadway. The design of the bridge followed the guidance provided by Colorado Department of Transportation (CDOT) and American Association of State Highway and Transportation Officials (AASHTO) (Abu-Hejleh et al. 2000a).

The Founders/Meadows Bridge was located near Downtown Denver. The bridge was part of Colorado State Highway 86. The bridge spans 113 feet (34.5 meters) and is 113 feet (34.5 meters) wide. The bridge abutments did not utilize any deep foundation elements. The bridge, comprised of 20 precast pre-stressed concrete bridge girders, had loads entirely supported by a geosynthetic reinforced soil mass. Load was transferred through a shallow footing to that soil mass (Abu-Hejleh et al. 2000a). Figure 7 shows a photograph of the Founders/Meadows Parkway Structure.

Figure 7: Founders/Meadows Parkway Structure Wang, T. (2002). "Case History of GRS Abutment." Workshop on Geotechnical Composite Systems, Sponsored by National Science Foundation and Virginia Tech, Roanoke, VA. Used under fair use, 2014.

The reinforced wall fill was an angular, crushed stone. The fill classified as a CDOT Class 1 Backfill. The maximum aggregate size was 0.75 inches (19 millimeters) (Abu-Hejleh et al. 2000b). The fill friction angle was estimated to be 40° and the cohesion to be 70 kPa (Helwany et al. 2003). Three types of geogrid reinforcement were utilized including UX6, UX3, and UX2. The tensile strengths of the reinforcements were 157.3 kN/m, 64.2 kN/m, and 39.3 kN/m respectively. Reinforcement spacing was 16 inches (0.4 meters). Frictionally-connected, modular concrete blocks were used as facing elements. Layers of reinforcement were placed between every two rows of blocks (Abu-Hejleh et al. 2000b). Figure 8 shows a schematic of the abutment.

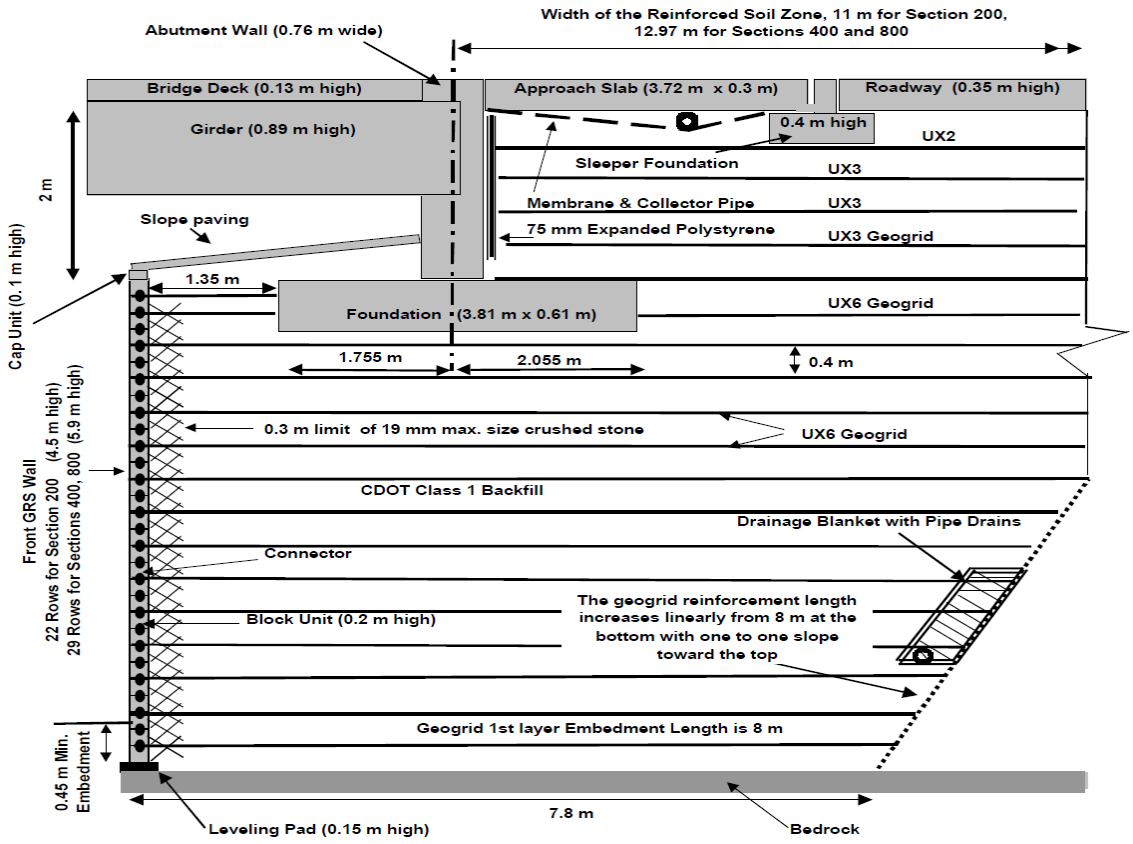

Figure 8: Founders/Meadows Composite GRS Abutment Schematic Abu-Hejleh, N., Outcalt, W., Wang, T., and Zornberg, J. G. (2000a). "Performance of Geosynthetic Reinforced Walls Supporting the Founders/Meadows Bridge and Approaching Roadway Structures - Report 1: Design, Materials, Construction, Instrumentation, and Preliminary Results." *CDOT-DTD-R-2000-5*, Colorado Department of Transportation, Denver, CO. Used under fair use, 2014.

A drainage blanket with pipe drains was installed in the bottom portion of the GRS abutment. Additionally, a geo-membrane in conjunction with a collector pipe helped prevent infiltration of water runoff into the upper wall of the soil mass (Wang 2002).

The front face of the GRS abutment and the abutment walls for 3 cross sections were monitored during construction and for 35 months while under in-service loads. The observations from instrumentation indicate that supporting bridges on GRS abutments with no deep foundation elements produces good performance. Instrumentation allowed for confirmation that AASHTO and CDOT design procedures were conservative. Additionally, results show an elimination of the “bump” at the end of the bridge, which is a typical bridge maintenance issue (Abu-Hejleh et al. 2002; Lee and Wu 2004). It was also determined that there is no risk of overturning associated with GRS bridge abutments, and that the imposed bearing pressures were well below allowable limits (Abu-Hejleh et al. 2001).

Costs associated with using deep foundation elements on the Founders/Meadows Bridge site would have been higher than the cost of the chosen design. The GRS abutment bridge support approach was a cost saving venture (Abu-Hejleh et al. 2000a).

Mammoth Lakes GRS Bridge Abutments: This project, completed in fall of 2000, involved the reconstruction of two bridges initially built in the 1930's by the USDA Forest Service. The location of the project was in the very popular Mammoth Lakes, California resort community (Keller and Devin 2003). The area was also affectionately called Lake Mamie.

The contract initially awarded was to replace the existing bridges, which had two spans, with a single span bridge supported by cast-in-place piles. In the interest of a timely construction process, GRS abutments supporting spread footings were selected to replace the pile system. The GRS abutments would be placed in a manner to avoid interference with the in-place stonemasonry abutments. This stipulation was for aesthetic concerns. Additionally, the new abutments had to meet stringent seismicity standards due to volcanic activity in close proximity to the region (Keller and Devin 2003).

The design followed "1996 AASHTO Standard Specification for Highway Bridges" but it incorporated the GRS design philosophy of high quality, well-compacted fill, placed in closely spaced lifts. Reinforcement spacing was about 6 inches for the project. The chosen reinforcement was a PP geotextile with tensile strength of 35 kN/m (Keller and Devin 2003). A schematic of one of the west abutment is shown in Figure 9.

Measured settlements of all abutments were 0.25 inches or less. The abutments were constructed and bridge decks placed in two weeks' time. The cost of the project was thousands of dollars below the traditional pile design estimate (Keller and Devin 2003).

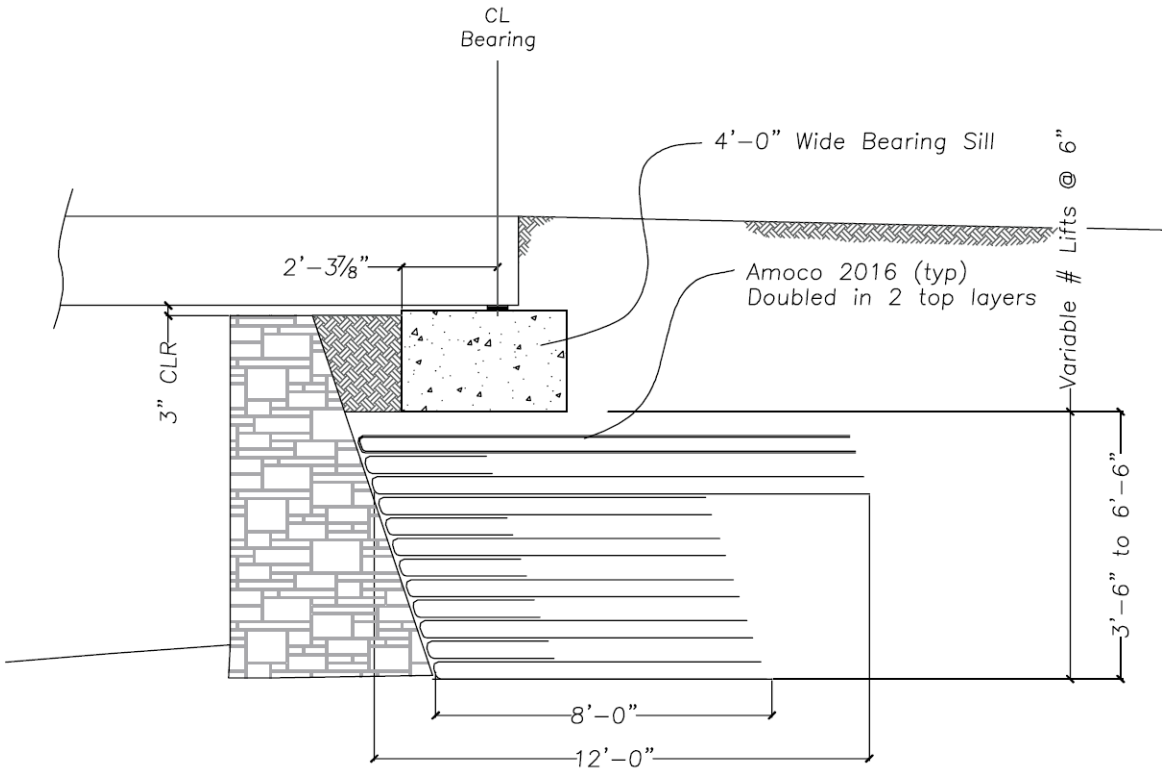

Figure 9: Mammoth Lakes West GRS Abutment Schematic Keller, G. R., and Devin, S. C. (2003). "Geosynthetic-Reinforced Soil Bridge Abutments." Transportation Research Board, Washington, D.C. Used under fair use, 2014.

Bowman Road Bridge: The Bowman Road Bridge built in fall of 2005 in Defiance County, Ohio for the crossing of Powell Creek was the first of many GRS bridge projects in the area. The 82 foot long bridge was supported directly on GRS abutments. The bridge box beams were placed on the GRS mass without the use of a concrete footing or elastomeric pad. The design of the bridge followed the guidance provided by NCHRP Report 566 and recommendations by Michael T. Adams of FHWA. The computer modeling program MSEW was also utilized in the design to evaluate global stability and reinforcement strength (Adams et al. 2007b). The Bowman Road Bridge is provided as a design example in *FHWA-HRT-11-026* (Adams et al. 2011a), which is the first two documents that describe the "FHWA GRS-IBS Method". The Bowman Road Bridge is most likely the first in-service bridge to be associated with the acronym GRS-IBS.

The required abutment height was 15.25 feet. (Adams et al. 2011a). The as-constructed east abutment was 16.9 feet tall and the west was 16.5 feet tall (Adams et al. 2011b). Reinforced fill for the abutment was a fine-gravel/coarse-sand with maximum aggregate size of 0.375 inches. The reinforced fill soil friction angle was 37°. Two variants of PP geotextiles were used for reinforcement. The tensile strengths were 4.8 kips/ft and 2.1 kips/ft (Adams et al. 2007b). The primary reinforcement spacing was 8 inches (Adams et al. 2011a). The facing elements were modular concrete blocks. The Bowman Road

Bridge was built on a reinforced soil foundation (RSF). The RSF was divided into two layers with a combined depth of 1.5 ft. The layers were comprised of well-graded compacted gravel. The layers were separated by a geotextile. Additionally, the entire RSF was wrapped in a geotextile. A Riprap slope was utilized at the toe of the abutment to help mitigate any scour (Adams et al. 2007b). A photograph of the completed bridge is shown in Figure 10.

Figure 10: Bowman Road Bridge FHWA (2011). "Geosynthetic Reinforced Soil Integrated Bridge System (GRS-IBS)." *Every Day Counts Presentation,* U.S. Department of Transportation. Used under fair use, 2014.

Using a GRS abutment resulted in time and cost savings. Construction duration lasted 6 weeks. If two crews had been hired for each abutment, construction time could have been reduced further to approximately 3 weeks (Adams et al. 2007b).

A large monitoring program was implemented for the Bowman Road Bridge Project by the Federal Highway Administration (FHWA). Both the bridge and abutment were instrumented to record critical behavior over a 2-3 year time period. No pavement cracking has been observed. Recorded settlements along the abutment wall are the result of foundation soil consolidation. Due to a grade difference, the east abutment settlement is greater than the west abutment (Adams et al. 2007b). The differential settlement was 0.19 feet and the vertical average settlement was 0.05 feet as of 2011 (Adams et al. 2011b).

Conventional cap abutments on piles could have been used at the Bowman Road Bridge. The use of this technique would have required an extension of the bridge for design from

82 ft to 110 ft. Additionally, this method would have required the construction of an approach slab. Estimated total cost at the Bowman Road Bridge location was $266,000 for the GRS abutment. Cost expenditures due to the abutment for this technique were estimated at $95,000, and the cost due to beams/waterproofing was $171,000. Estimated total cost at the Bowman Road Bridge location was $338,000 for the cap abutment on piles. Cost expenditure due to the abutment for this technique was estimated as $105,000 and cost due to beams/waterproofing was $233,000. The use of a GRS abutment provided a cost savings of about $30,000 (Adams et al. 2007b).

Steve Road Bridge over Tiffin River: In the fall of 2009, the existing bridge crossing the Tiffin River at Steve Road was replaced with a GRS-IBS structure in Defiance County, Ohio. The steel girder bridge was supported directly on GRS mass abutments (Warren et al. 2010). As of April 2013, the span of the bridge is the longest to be supported on GRS abutments. The cost of the bridge was estimated to be $616,000 (Warren et al. 2013).

The abutments were constructed in 2-4 days using a 4-6 man crew. The facing elements are CMU block and the backfill is AASHTO No. 89 crushed stone. The reinforcement is a woven geotextile. The reinforcement was spaced every 8 inches and has a tensile strength of 4800 lb/ft (70 kN/m) (Warren et al. 2013). A photograph of the original and newly constructed bridge is shown in Figure 11.

Figure 11: Steve Road Bridge over Tiffin River Warren, K. A., Whelan, M., Adams, M., and Nicks, J. (2013). "Preliminary Evaluation of Thermally Induced Strains and Pressured

The bridge performance was monitored by UNC Charlotte (Warren et al. 2010). Steel girders were instrumented with vibrating wire strain gages to assess thermal effects. Pressure cells were installed within the GRS mass. After the monitoring period, it was concluded that the bridge system and soil deform together under thermally induced loading. Additionally, the classic problem of the "bridge bump" can be avoided using GRS-IBS (Warren et al. 2013).

Mattamuskeet National Wildlife Refuge GRS Abutments: In 2011, two bridges were constructed in a wildlife refuge in Hyde County, North Carolina. The two bridges were supported on GRS abutments and replaced existing bridges supported on deficient timber structures. The first bridge over the East Canal had a 23 foot span and the second over the Central Canal had a 46 foot span. GRS abutments were chosen over traditional concrete-pile-supported abutments in order to reduce cost and for constructability purposes (Mohamed et al. 2011).

The bridges in Mattamuskeet National Wildlife Refuge were unique in that they were constructed on soft clay soil. To reduce long term settlement, the foundation soil over which the GRS abutment would be placed was preloaded. A long term monitoring program was put in place upon completion of the bridges. Using piezometers and settlement plates, it was determined that the GRS abutments were performing well (Mohamed et al. 2011).

The GRS abutments utilized a unique facing system known as a Cellular Confinement System (CCS). The facing allowed for the abutments to be vegetated, and they add to aesthetic appeal. The use of CCS requires a contractor with experience with such installations (Nguyen 2012). CCS has advantages over CMU block facing in regards to ability to tolerate settlement. Additionally, CCS performs better than CMU blocks in scour environments due to CCS's ability to withstand high water flows (Mohamed et al. 2011). A photograph of one of the completed bridges is shown in Figure 12.

Figure 12: Mattamuskeet National Wildlife Refuge GRS Bridge Nguyen, Q. (2012). "GRS Abutments for Bridge Replacement National Wildlife Refuge." A New Era of Partnerships - Investing in America's Treasures, U.S. Department of Transportation, FHWA, EFLHD. Used under fair use, 2014.

Design followed guidance provided by the ""FHWA Simplified Procedure"" outlined in the document *FHWA-NHI-10-024*. Additionally, the "NCHRP GRS Method" was referenced, specifically the document *Report No. 556*. Settlement analysis was performed using the program FoSSA (2.0) and slope stability analysis was performed using the program ReSSA (2.0). The reinforced fill had a friction angle of 34° and no cohesion. The East Canal abutments were 5 feet tall and the Central Canal Abutments were 10 feet tall. The tensile strength of geogrid reinforcement was 2,000 lb/ft. The maximum reinforcement spacing was 16 inches (Mohamed et al. 2011).

Other Completed Bridges: Listed below are some additional GRS-IBS bridges that have been completed to date (FHWA 2011). These structures do not have detailed case history reports. However, some general information can be found if needed through web-based searches.

- Ayersville Pleasant Bend Bridge
- Behnfeldt Road Bridge
- Casebeer Road Bridge
- Ayersville Road Bridge
- Huber Road Bridge
- Beerbower Road Bridge
- Scott Road Bridge
- Farmer Mark Road Bridge
- Flory Road Bridge
- Vine Street Bridge

2.4 GRS LARGE SCALE TESTING

This section contains a variety of test setups. Some are full-scale field experiments, and others are lab tests on samples that are considered "Large" in scale. All test setups in this section are roughly equal to or larger than half-scale. In other words, the test samples are no less than half the size of a structure one might see in the field.

IFF Reinforced Retaining Wall Test: The Colorado Department of Transportation constructed an Independent Full-height Facing (IFF) reinforced soil retaining wall in 1992. The wall dimensions were 9.5 feet (2.9 meters) tall and 4 feet (1.2 meters) wide. The goal of the test wall was to understand the behavior of geosynthetic reinforced soil (Wu 2007).

The reinforced fill material was Ottawa sand. The chosen reinforcement was a nonwoven geotextile. The reinforcement was not fixed or anchored to the wall face. Reinforcement spacing was 12 inches (0.3 meters). The facing panels were tied into the soil mass via steel anchors. The design of the anchors and connections aimed to allow lateral movement and to slide with the fill (Wu 2007).

The wall was monitored using instrumentation that recorded lateral deformations. The test setup was in plain strain conditions. The load reached 2.9 ksf (138 kPa) and was applied in four 0.72 ksf (34.5 kPa) intervals. From pressure cell measurements, the lateral thrust against the wall panels was estimated to be 2.25 kips (10 kN). Calculations using the Rankine active earth pressure theory predict lateral thrust values of 32.8 kips (146 kN). It was concluded that the difference was likely due to the flexibility of the facing, which provided minimal resistance and allowed the load to be carried by the reinforcement (Wu 2007).

Garden Experimental Embankment: In 1993, a full scale GRS embankment was constructed and tested in France. The experiment examined the performance of two different geosynthetic reinforcements placed on either side of the test embankment (Gotteland et al. 1997). A photograph of the embankment is shown in Figure 13, and a schematic of the experiment is shown in Figure 14.

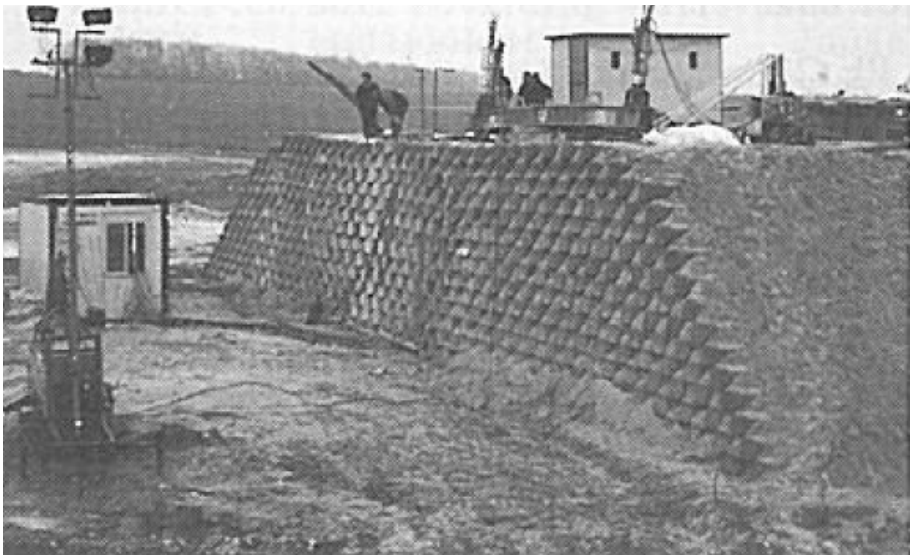

Figure 13: Garden Experimental Embankment Gotteland, P., Gourc, J. P., and Villard, P. (1997). "Geosynthetics Reinforced Structures as Bridge Abutments: Full Scale Experimentation and Comparison with Modelisations." ***Proc., International Symposium on Mechanically Stabilized Backfill,*** **J. T. H. Wu (Ed.) A.A. Balkema, Rotterdam, 25-34. Used under fair use, 2014.**

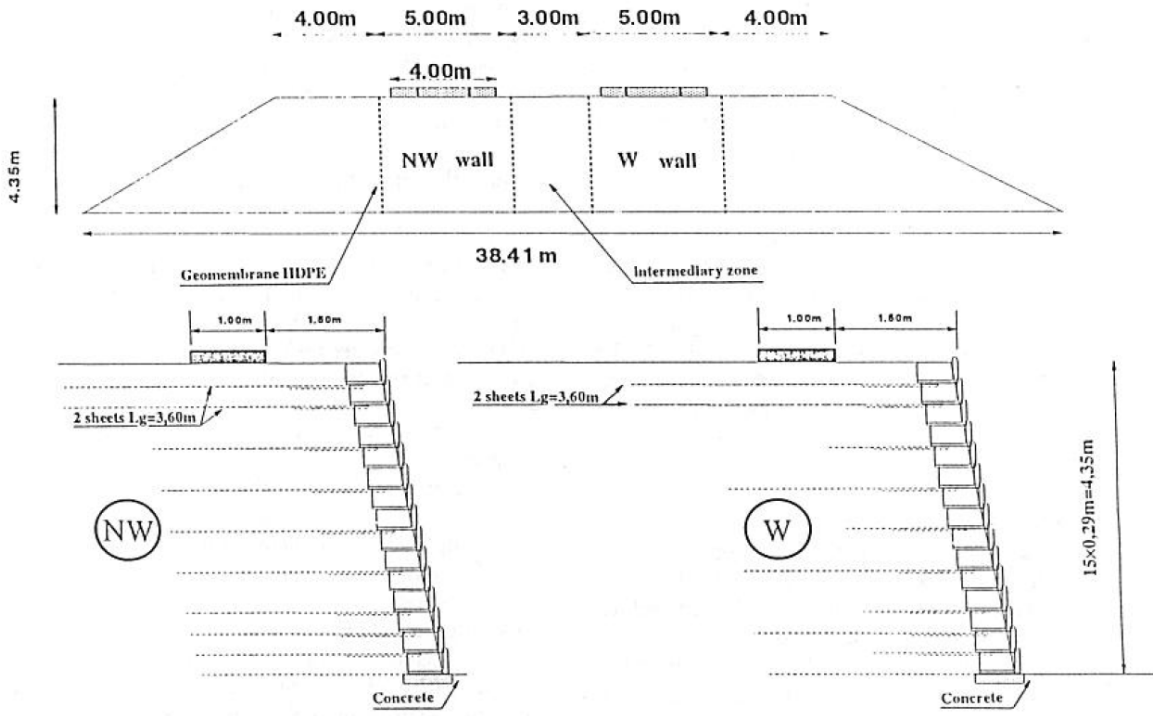

Figure 14: Garden Experimental Embankment Schematic Gotteland, P., Gourc, J. P., and Villard, P. (1997). "Geosynthetics Reinforced Structures as Bridge Abutments: Full Scale Experimentation and Comparison with Modelisations." ***Proc., International Symposium on Mechanically Stabilized Backfill,*** **J. T. H. Wu (Ed.) A.A. Balkema, Rotterdam, 25-34. Used under fair use, 2014.**

Commerce City Wall: The Colorado Department of Transportation constructed a GRS test wall in Commerce City in 1994 (Wu 2007). A photograph of the test wall is shown in Figure 15.

The fill material was gravel road base, and the facing elements were split-faced concrete blocks. The reinforcement was a geogrid and was not attached to the wall face. Reinforcement spacing was 12 inches (0.3 meters). At the connection between the soil and facing along reinforcement layers, the main reinforcing was replace by weaker geotextile called a "tail." The geotextile "tail" extended 2.95 feet (0.9 meters) into the reinforced soil mass (Wu 2007).

The wall was loaded with 40 kips (178 kN) via placement of road barriers in layers. The load remained in place for four months. Lateral deformations were monitored and then extrapolated over a 100 year period. It was concluded that lateral movement would not have exceeded 1.6 inches (40 millimeters) over that time. The test illustrated the inherent strength of a reinforced soil mass. It proved that a wall whose facing did not have strong "tie-back" support from the main geosynthetic reinforcing layers could remain stable (Wu 2007).

Figure 15: Commerce City Wall Experiment Wu, J. T. H. (2007). "Lateral Earth Pressure against the Facing of Segmental GRS Walls." ***Geosynthetics in Reinforcement and Hydraulic Applications (GSP 165),*** **Gabr, and Bowders (Eds.). ASCE, Reston, VA, 165-175. Used under fair use, 2014.**

FHWA Turner Fairbank GRS Bridge Pier: The Turner Fairbank Highway Research Center (TFHRC) constructed, instrumented, tested, and monitored a 5.4 meter tall GRS bridge pier (Adams 1997). Testing took place in the summer of 1996 (Adams et al. 1999). The pier had the characteristic close reinforcement spacing associated with GRS of about 8 inches (0.2 meters). Additionally, the pier demonstrated the efficiency of GRS construction by taking only two weeks to assemble. A schematic detailing the components of the prier is shown in Figure 16 (Adams 1997).

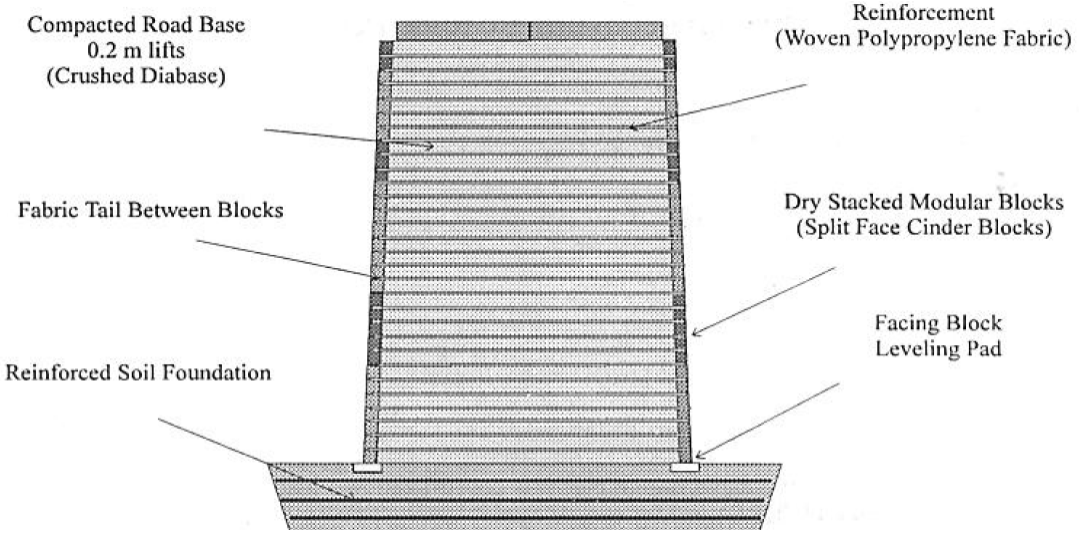

Figure 16: FHWA Bridge Pier Large Scale Experiment Schematic Adams, M. (1997). "Performance of a Prestrained Geosynthetic Reinforced Soil Bridge Pier." *Proc., International Symposium on Mechanically Stabilized Backfill*, J.T.H. Wu (Ed) A.A. Balkema, Rotterdam, 35-53. Used under fair use, 2014.

The FHWA Bridge Pier was pre-strained to help consolidate the soil mass and to ensure full mobilization of the reinforcement. Additionally, it was found that pre-straining reduced vertical settlement by an estimated 50%. It was concluded that pre-straining may be needed in situations where there are multiple bridge pier supports. Pre-straining multiple piers would help reduce differential settlements (Adams 1997).

The chosen fill material was a well-graded gravel (GW-GM) following ASTM D2487 specification, and the percent fines was 8.7%. The reinforcement was a PP geotextile with a tensile strength of 4800 lb-ft/ft (70 kN/m). The GRS pier was constructed on a Reinforced Soil Foundation (RSF) which was 4 feet (1.2 meters) deep. RSF reinforcement was Tensar BX-1100 geogrid spaced 12 inches (0.3 meters) apart. The facing elements were cinder blocks (Adams et al. 1999).

A hydraulic jack and loading pads were used to apply load uniformly across the bridge pier. Loads cells measured applied load. Additionally, pressure applied during the test was calculated from hydraulic jack pressure (Adams 1997). The pier was tested to 2,200 kips (9800 kN) (Adams et al. 1999). The pier was instrumented to record lateral and vertical displacements. Stain gages were placed in some reinforcement lifts to record

strain and creep measurements. The pier was stable even with high loads close to the faces. Quality compaction of each soil lift was thought to have a large influence on performance. Based on the performance of the piers, it was concluded that GRS technology is a viable option for simple bridge piers (Adams 1997).

Five GRS Mini Pier Experiments: In 1997, five GRS mini piers were constructed at TFHRC in Mclean, VA. The goal of the experiment was to understand the influence of reinforcement spacing on pier performance specifically in comparison to reinforcement tensile strength. The experiment also sought to illustrate the difference between how a composite mass, soil plus reinforcement, behaves in comparison to just soil (Adams et al. 2007a).

The piers were assembled on a concrete slab. The goal of the experiment was to simulate a large unconfined tri-axial compression test. The facing material was concrete masonry unit (CMU) blocks. The fill material was gravel classified as GW-GM according to ASTM D2487. The chosen reinforcement for the piers was a woven PP geotextile. Spacing varied from pier to pier. One pier had no reinforcement, another had spacing between 16 inches (0.4 meters) to 24 inches (0.6 meters), another had spacing of 16 inches (0.4 meters), and the last two piers had spacing of 8 inches (0.2 meters). The reinforcement tensile strength was the same for three of the pier at 4800 lb/ft (70 kN/m). The tensile strength of the fourth reinforced pier was 1440 lb/ft (21 kN/m). The piers were 4.6 feet (1.39 meters) wide, and 6.4 feet (1.94 meters) tall (Adams et al. 2007a). A photograph showing one of the five pier test setups is shown in Figure 17.

Figure 17: One of Five GRS Mini Pier Experiments Adams, M., Ketchart, K., and Wu, J. T. H. (2007a). "Mini Pier Experiments: Geosynthetic Reinforcement Spacing and Strength as Related to Performance." ***Geosynthetics in Reinforcement and Hydraulic Applications (GSP 165)*****, Gabr, and Bowders (Eds.), Reston, VA, 98-106. Use under fair use 2014.**

Load was applied using a hydraulic jack and measured using a load cell. Settlement and lateral deformations were monitored throughout the tests. Piers were loaded to failure. The results of the experiments indicate that the strength of the reinforcement has less of an impact on performance than reinforcement spacing. Additionally, piers with closer reinforcement spacing had greater capacity (Adams et al. 2007a).

CDOT GRS Piers and Abutment Experiment: An abutment and two bridge piers were constructed in Denver, Colorado at a location known as the Havana Site (Adams et al. 1999). The test setup is often referred to as the Havana Yard Bridge Pier and Abutments. Figure 18 is a photograph of the test setup (Wu et al. 2001).

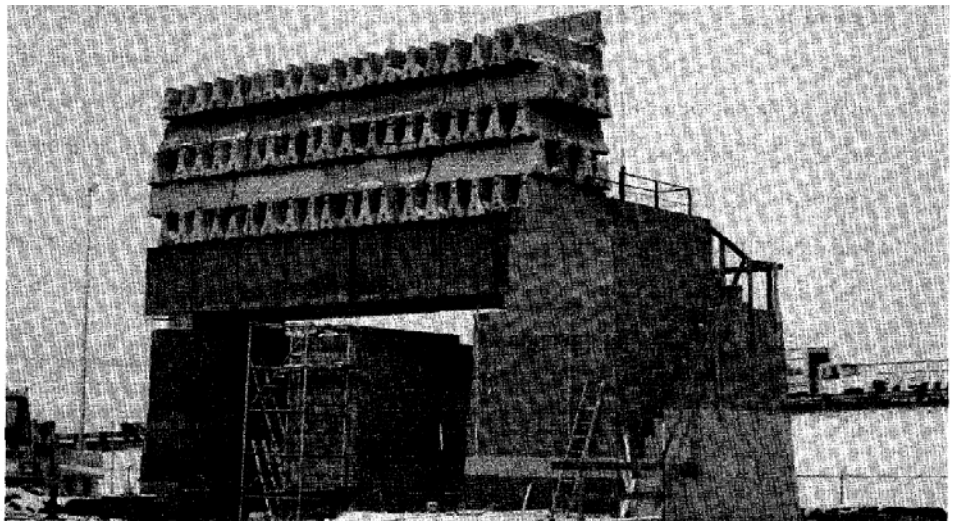

Figure 18: CDOT GRS Piers and Abutment Test Setup Wu, J. T. H., Ketchart, K., and Adams, M. (2001). "GRS Bridge Piers and Abutments." *FHWA-RD-00-38*, Federal Highway Administration, McLean, VA. Used under fair use, 2014.

The setup was constructed on top of a RSF. Then a concrete pad 6 inches (0.15 meters) thick was placed for supporting the the piers and abutment (Ketchart and Wu 1997). The center pier was 24 feet (7.3 meters) tall; while the other pier and abutment were both 25 feet (7.6 meters) tall. The reinforcement utilized was a PP geotextile ,and the fill material was coarse grained, classifying as a GW-GM following ASTM D2487. The percent fines of the fill was 13%. Reinforcement spacing was 8 inches (0.2 meters) (Adams et al. 1999). It should be noted that the outer and center piers had different base shapes. In plan view, one appears as an oval and the other a rectangle as shown in Figure 19 (Ketchart and Wu 1997). Designing with the oval pier shape was done to push the limits of GRS technology (Adams et al. 1999).

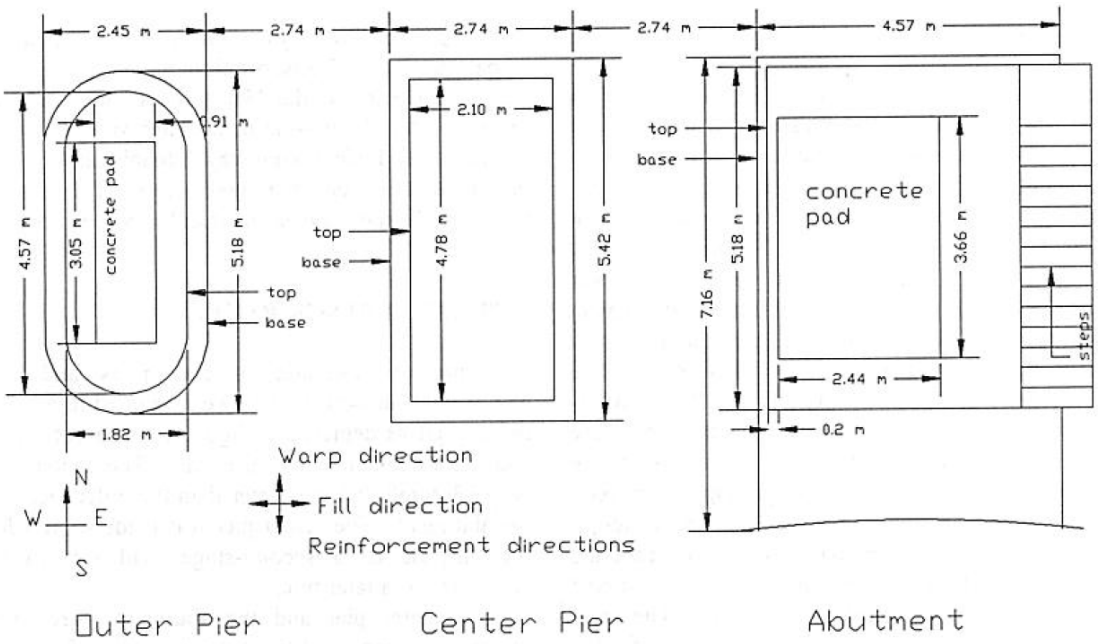

Figure 19: CDOT GRS Experiment in Plan View Ketchart, K., and Wu, J. T. H. (1997). "Performance of Geosynthetic-Reinforced Soil Bridge Pier and Abutment." *Proc., International Symposium on Mechanically Stabilized Backfill*, J. T. H. Wu (Ed.) A.A.Balkema, 101-116. Used under fair use, 2014.

Load was applied via concrete barriers stacked seven layers high (Wu et al. 2001). A total of 124 barriers were used (Adams 1997). The long term performance of the structures under dead loading was monitored (Wu et al. 2001). The dead load from the concrete barriers was maintained for around a year. The center pier was not loaded. The outer pier and abutment were instrumented to measure lateral deformations and vertical settlements. Strain gages measured reinforcement deformation (Adams et al. 1999).

The settlement of the outer pier was 1.44 inches (36.6 millimeters), and the abutment settlement was 1.07 inches (27.1 millimeters). Maximum lateral displacement was 0.5 inches (12.7 millimeters) for the outer pier and 0.17 inches (4.3 millimeters) for the abutment. Creep displacements were larger in the outer pier than in the abutment. The majority of creep deformation took place within the first 15 days, and then continued overtime. The outer pier had a lower compaction effort than the abutment. This is thought to be the reason for the difference in creep performance. Reinforcement strains were less than 1.0% (Ketchart and Wu 1997).

Vegas GRS Mini Pier Experiment: The Vegas GRS Mini Pier Experiment, often referred to as just the Vegas Mini Pier, was constructed and tested in early 2000. The pier was a demonstration conducted at the National Concrete Masonry Association Exposition. The annual event took place in Las Vegas, Nevada that year, thus the name of the experiment. The goal of the demonstration was to expose the wider segmental retaining wall community to the promising GRS technology (Adams et al. 2002). A photograph of the test pier after loading is shown in Figure 20.

Figure 20: Vegas GRS Mini Pier after Testing Adams, M., Nicks, J., Stabile, T., Wu, J. T. H., Schlatter, W., and Hartmann, J. (2011a). "Geosynthetic Reinforced Soil Integrated Bridge System—Interim Implementation Guide." *FHWA-HRT-11-026*, Federal Highway Administration, McLean, VA. Used under fair use, 2014.

The pier was constructed of alternating layers of coarse grained fill, classified as a GP-GM following ASTM D2488, and reinforcement. The chosen reinforcement was a woven geotextile with tensile strength of 2400 lb/ft (35 kN/m). The reinforcement was spaced in 6 inch lifts. However, directly underneath top bearing layers, the spacing was reduced to 3 inches (Adams et al. 2002). Modular block facing was utilized for the test on all faces of the pier. The block height was 6 inches, and to construct corners, blocks were split. The facing blocks were only frictionally connected (Adams et al. 2002).

Vertical load applied was 280 kips. A schematic of the test dimensions and load frame is shown in Figure 21. The assembly was built on a concrete test pad and elevated using cinderblocks. A vertical pressure was applied in intervals of 5.11 psi or 731 psf (35 kPa). Settlement and lateral deformation were monitored throughout the test (Adams et al. 2002).

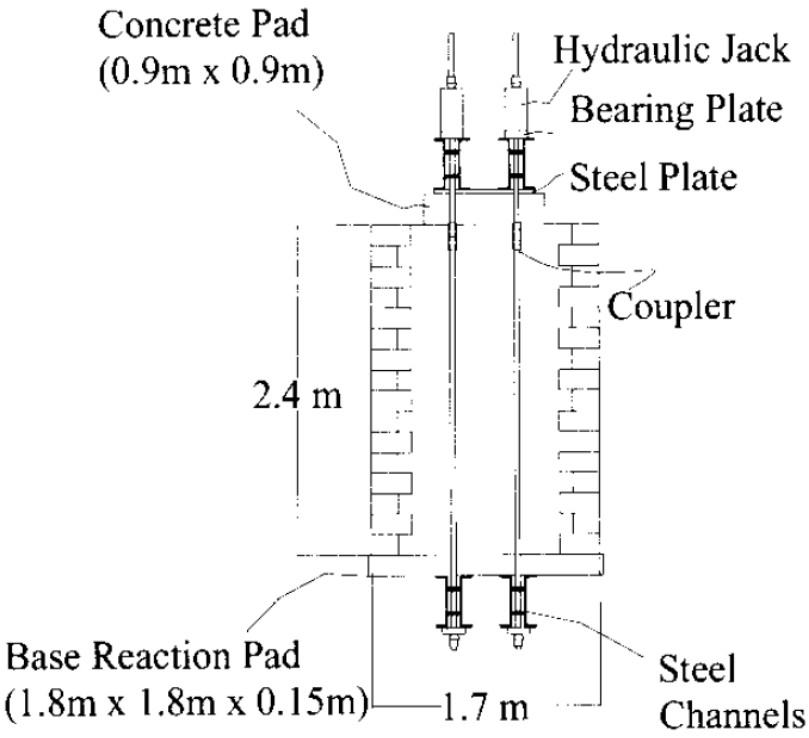

Figure 21: Vegas GRS Mini Pier Test Setup Adams, M., Lillis, C. P., Wu, J. T. H., and Ketchart, K. V. (2002). "Vegas GRS Mini Pier Experiment and the Postulate of Zero Volume Change." ***Proc., 7th International Conference on Geosynthetics,*** **P. Delmas, J. P. Gourc, and H. Girard (Eds.). Swets & Zeitlinger, Lisse, France, 389-394. Used under fair use, 2014.**

A conclusion drawn from the experiment was that the vertical applied pressure and the observed settlement had a linear relationship. Additionally, the experiment led to the "postulate of zero volume change" from the observation that the reduction in volume as the soil is compressed is approximately the same as the volume increase from lateral expansion (Adams et al. 2002).

Large Scale Unconfined Cylindrical GRS Tests: In order to assess the behavior of a soil mass reinforced with geosynthetics and to estimate the tensile force in that reinforcement, a series of large scale GRS tests were performed. Figure 22 shows a cylindrical test sample before and during loading. The samples were 2.5 feet (0.76 m) wide and 5 feet (1.52 meters) tall. The assembly rested on a steel end platen, placed on top of steel sections. The soil specimens were loaded by a 300 kip (1335 kN) hydraulic ram (Elton and Patawaran 2004).

Fill material was poorly graded sand (SP) according to the Unified Soil Classification System. The fill friction angle was 40°, and the cohesion 0.6 ksf (29 kPa). The chosen reinforcement was a nonwoven PP geotextile. Varying masses of the reinforcement over different areas were utilized in the experiment. The reinforcement spacing for the tests

was 6 inches (0.15 meters). Placement of the fill and reinforcement was conducted within a cardboard cylindrical mold (Elton and Patawaran 2004).

Figure 22: Test Setup Before and During Testing Elton, D. J., and Patawaran, M. A. B. (2004). "Mechanically Stabilized Earth Reinforcement Tensile Strength from Tests of Geotextile-Reinforced Soil." Transportation Research Board, Washington, D.C. Used under fair use, 2014.

Results of the tests indicate that reinforcement strength correlates to deformation resistance. The stronger the reinforcement, the better the reinforced soil mass performed in terms of resisting deformations. Reinforced soil peak strengths were observed to be between 4.8 ksf (230 kPa) and 9.6 ksf (460 kPa). From tear patterns of the reinforcement observed after testing, it was concluded that central reinforcement layers mobilize first. Based on results of the experiment, an equation to estimate the maximum tension carried by the reinforcement was developed. The proposed relationship predicted required reinforcement strengths, needed to produce a desired reinforced-soil strength, that were much lower than predicted by other methods. The findings imply that lower strength reinforcement could be used in designing walls and abutments, which could reduce overall project costs (Elton and Patawaran 2004).

NCHRP Full Scale Test Abutments: Two full scale abutments were tested at TFHRC in 2003. The goal of the experiments was to more fully understand the behavior of GRS technology and in doing so provide verification to an analytical model conducted in conjunction with the tests (Wu et al. 2006a).

The abutments height was 15.25 feet (4.65 meter) tall. A photograph of a test abutment is shown in Figure 23. A schematic of the test setup where the abutments are back to back is shown in Figure 24 (Wu et al. 2006a).

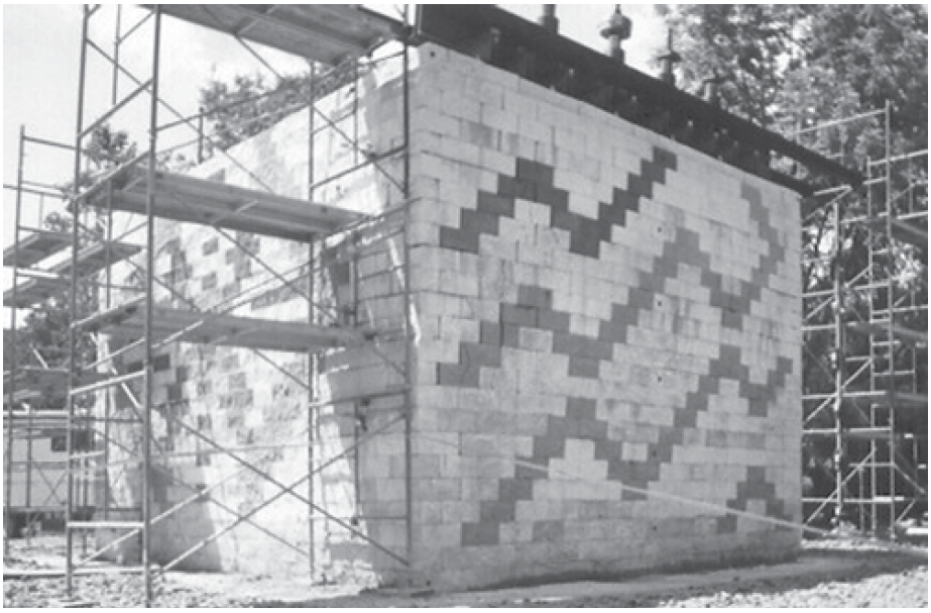

Figure 23: NCHRP Full Scale Abutment Wu, J. T. H., Lee, K. Z. Z., Helwany, S. M. B., and Ketchart, K. (2006a). "Design and Construction Guidelines for GRS Bridge Abutment with a Flexible Facing." ***Report No. 556,*** **National Cooperative Highway Research Program, Washington, D.C. Used under fair use, 2014.**

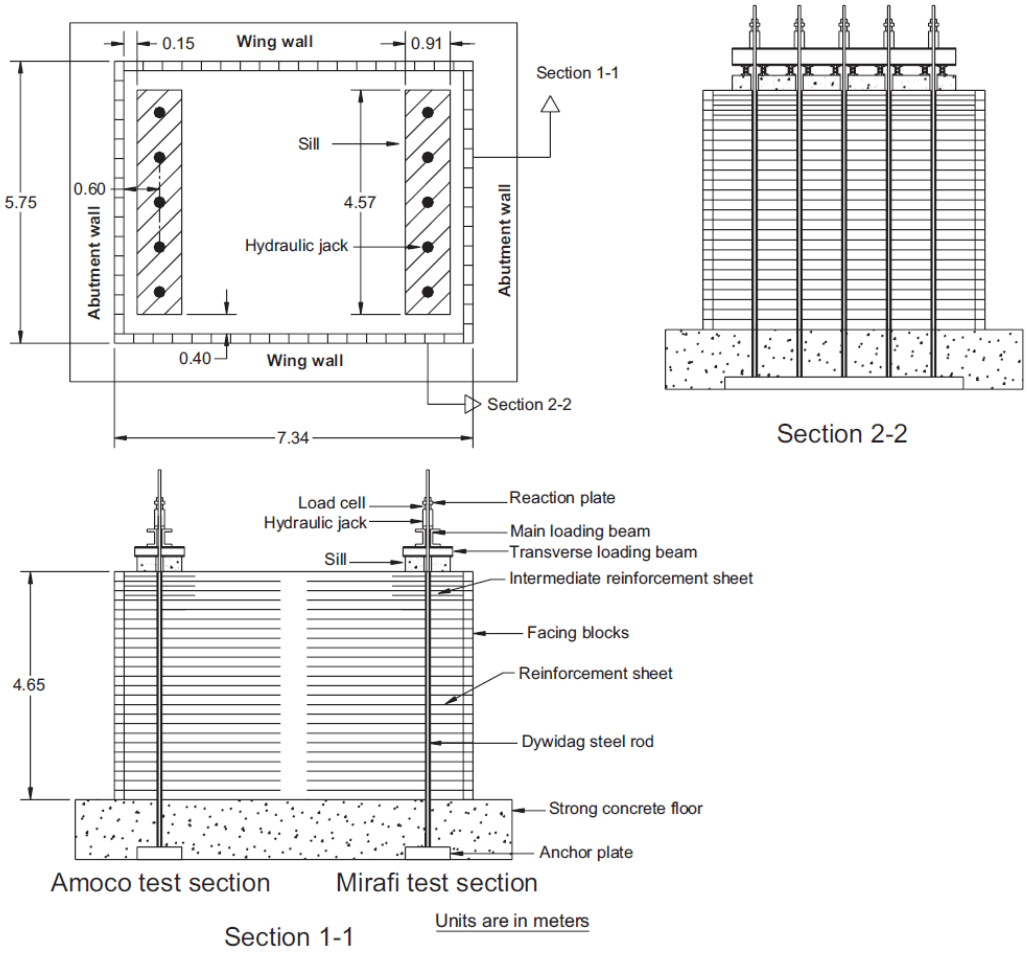

Figure 24: NCHRP Full Scale Abutments Test Setup Wu, J. T. H., Lee, K. Z. Z., Helwany, S. M. B., and Ketchart, K. (2006a). "Design and Construction Guidelines for GRS Bridge Abutment with a Flexible Facing." *Report No. 556*, National Cooperative Highway Research Program, Washington, D.C. Used under fair use, 2014.

The entire assembly was constructed on a rigid floor with dimensions of 30 ft (9.1 m) long by 24 feet (7.3 m) wide and a thickness of 3 feet (0.9 m) (Helwany et al. 2007). A concrete sill was placed on top of both abutments. Reinforced fill material was non-plastic silty sand (SP-SM) according to the Unified Soil Classification System. This soil type was chosen over a gavel fill to represent a marginal quality fill that could be encountered in the field. The fill's friction angle was 34.8° and the cohesion was 0.29 ksf (13.8 kPa). The chosen reinforcement was a PP woven geotextile. One abutment used reinforcement with tensile strength of 4,800 lb/ft (70 kN/m) and the other with tensile strength of 1,440 lb/ft (21 kN/m) (Wu et al. 2006a).

The Amoco test section with reinforcement strength of 4,800 lb/ft (70 kN/m), indicated in Figure 24 was tested first. Loading was conducted in 1.0 ksf (50 kPa) intervals with increases every 30 minutes. The vertical load at the end of the test was 17 ksf (814 kPa). Loading was terminated due to the equipment reaching maximum extension, not due to wall failure. The second abutment, Mirafi test section with reinforcement strength of

1,440 lb/ft (21 kN/m), loading terminated at 414 kPa. Loading was terminated due to observed extreme deformations. Reinforcement strain, vertical, and lateral movements were monitored throughout testing. Additionally, the contact pressure between the abutment and rigid foundation was recorded. A summary of the abutment performance is shown in Table 1 (Wu et al. 2006a). The results show that deformations are tolerable at working loads of about 4,000 psf.

Table 1: NCHRP Full Scale Abutments Test Results Summary Wu, J. T. H., Lee, K. Z. Z., Helwany, S. M. B., and Ketchart, K. (2006a). "Design and Construction Guidelines for GRS Bridge Abutment with a Flexible Facing." *Report No. 556,* National Cooperative Highway Research Program, Washington, D.C. Used under fair use, 2014.

	Amoco Test Section	Mirafi Test Section
Reinforcement	Amoco 2044, T_{ult} = 70 kN/m	Mirafi 500x, T_{ult} = 21 kN/m
Upon termination of loading:		
Average Applied Pressure	814 kPa	414 kPa
Sill Settlement (front)	175 mm (6.9 in.)	189 mm (7.4 in.)
Sill Settlement (back)	152 mm (6.0 in.)	160 mm (6.3 in.)
Max. lateral movement in abutment wall	82 mm @ 4.5 m from base	115 mm @ 4.5 m from base
Max. lateral movement in wing wall	33 mm @ 3.8 m from base	86 mm @ 3.8 m from base
At 200 kPa (limiting bearing capacity, per NHI manual)		
Applied Pressure (average)	207 kPa	214 kPa
Sill Settlement (front)	45 mm (1.8 in.)	81 mm (3.2 in.)
Sill Settlement (back)	35 mm (1.4 in.)	64 mm (2.5 in.)
Max. lateral movement in abutment wall	24 mm @ 4.5 m from base	36 mm @ 4.5 m from base
Max. lateral movement in wing wall	18 mm @ 3.8 m from base	30 mm @ 3.8 m from base
Observed Behavior: • The sills in both tests tilted toward the abutment wall face (i.e. the front of the sill settled more than the back; Left and right sides of the sill settled evenly. • The abutment wall leaned forward with the maximum movement occurring near the top of the wall. The top three courses of facing blocks were pushed outward at higher loads. • The wing wall also leaned forward with the maximum movement occurring at approximately 1/6H from the top of the wall. • In both tests, tension cracks occurred parallel to the wall face and were located at end of the reinforcement. Tension cracks initiated around 150–200 kPa average applied pressure. • Most strain gauges were damaged by moisture due to the long delay of actual loading experiments; maximum strain at 200 kPa was about 2.0% • The measured contact pressure on the rigid foundation was larger in front and decreased linearly toward the back. The computation procedure in the NHI Manual yielded about the average value of the contact pressures at a given applied load.		

GSGC Laboratory Experiments: Five Generic Soil-Geosynthetic Composite (GSGC) tests were devised and performed by Pham (2009). The goal of the experiments was to understand the fundametal behavior of GRS. The claim was made that unique GRS composite behavior was not captured in existing design guidance, specifically regarding the required tensile strength. The tests provided data that demonstrated the comopsite behavior of GRS. This data could then be verified against a numerical model (Pham 2009). A photograph of one of the test setups is shown in Figure 25: GSGC Test Setup. One of the failed samples after testing is shown in Figure 26.

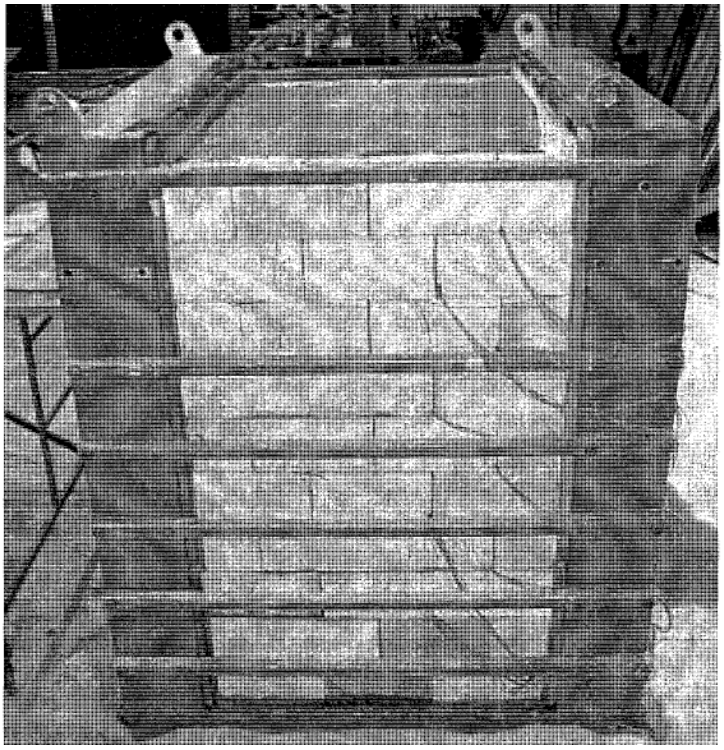

Figure 25: GSGC Test Setup Pham, T. (2009). "Investigating Composite Behavior of Geosynthetic-Reinforced Soil (GRS) Mass." University of Colorado at Denver, Denver, CO. Used under fair use, 2014.

Figure 26: GSGC Soil Mass at Failure Pham, T. (2009). "Investigating Composite Behavior of Geosynthetic-Reinforced Soil (GRS) Mass." University of Colorado at Denver, Denver, CO. Used under fair use, 2014.

A Detailed schematic of the testsetup is shown in Figure 27. Test results support the claim that GRS behavior is different from MSEW and thus a unique technology. Additionally, the tests provided additional understanding of composite behavior. Test data was used to verify proposed design equations and numerical models (Pham 2009). Finally, the results showed that spacing has a larger impact on GRS mass performance than reinforcement strength (Wu et al. 2013).

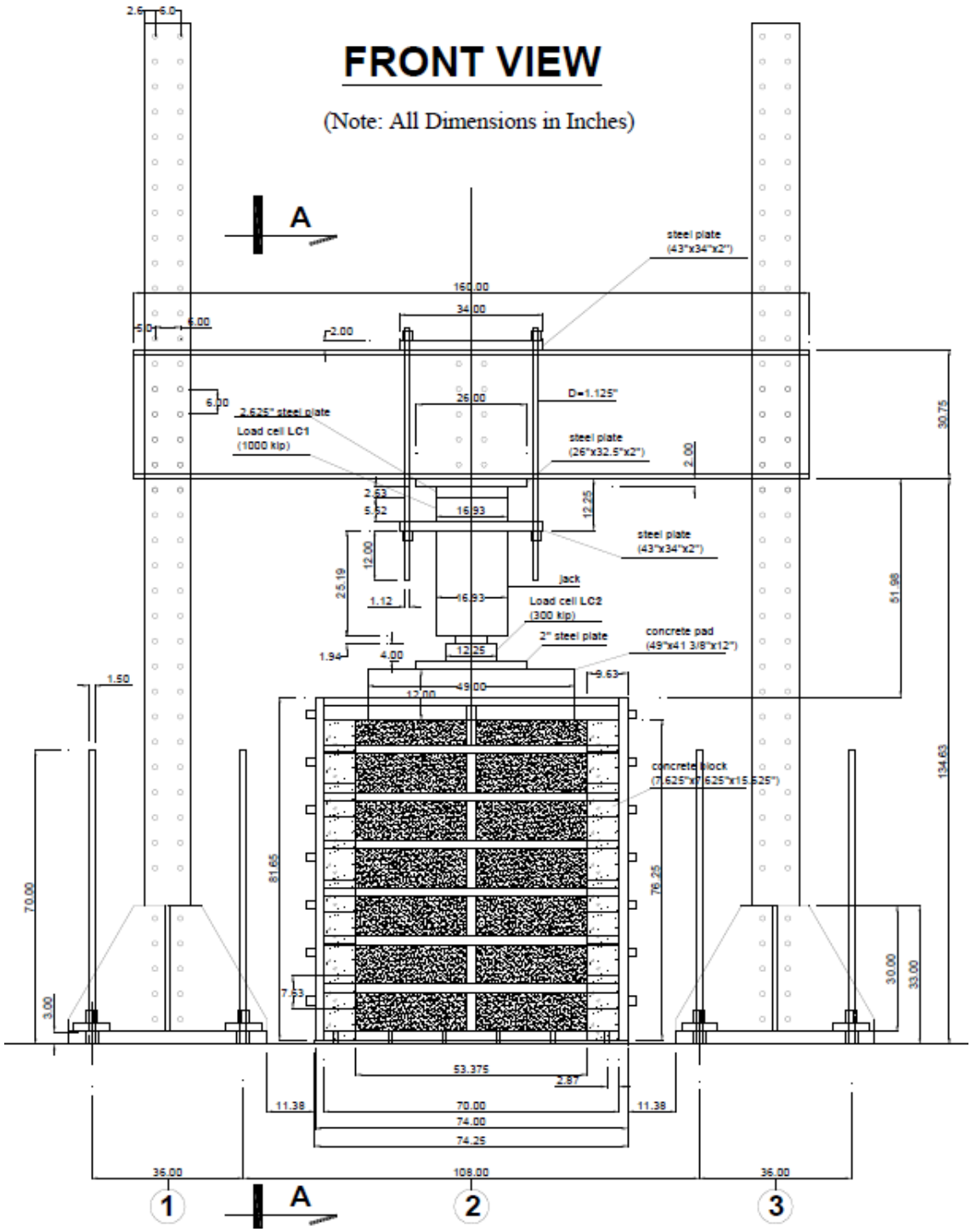

Figure 27: GSGC Test Detailed Schematic Wu, J. T. H., Pham, T. Q., and Adams, M. T. (2013). "Composite Behavior of Geosynthetic Reinforced Soil Mass." *Publication No. FHWA-HRT-10-077.*, Federal Highway Administration, McLean, VA. Used under fair use, 2014.

Virginia Tech Abutment Wall: An investigation of a GRS test abutment's performance in regards to differential foundation settlement was conducted in 2013 at Virginia Tech.

Projects that utilize GRS abutments could experience differential settlement at the foundation from the presence of very soft soils underlying an RSF or the influence of scour (Kost et al. 2014).

A field test abutment was designed and constructed in accordance with FHWA guidelines (Adams et al. 2011a). The abutment dimensions were about 10 feet tall and 24.5 feet long. A photograph of the test abutment is shown in Figure 28. The chosen geometry would be similar to that of an abutment supporting a small bridge. The abutment was constructed atop a RSF. The chosen primary reinforcement for the abutment was a TenCate Mirafi Hp570 woven PP geotextile with tensile strength of 4,800 lb/ft (70 kN/m). The reinforcement was spaced at 8 inches. The reinforced fill material was an open-graded crushed rock fill, ASTM No. 8. The facing elements were frictionally connected CMU blocks. An equivalent bridge surcharge load was applied across the top of the abutment wall by placing 20 concrete blocks, with dimensions 2 ft x 2 ft x 6 ft, in two layers of 10 blocks each (Kost et al. 2014).

Figure 28: Photograph of the Virginia Tech Abutment Wall Kost, A., Filz, G., and Cousins, T. (2014). "Differential Settlement of a GRS Abutment: Full-Scale Investigation." *Virginia Center for Transportation Innovation and Research* Charlottesville, VA. Used under fair use, 2014.

The left and right corners of the abutment and RSF were constructed atop Geofoam inclusions as shown in Figure 29. These Geofoam inclusions acted as temporary support prior to the testing of foundation settlement. The left side of the abutment, labeled side B, had 16 inches of Geofoam placed beneath it while the right side, labeled side A, had 8 inches. Once testing began, one inclusion at a time was exposed to an eco-friendly solvent. The solvent dissolved the Geofoam and thus removed the temporary foundation support. This created a differential foundation settlement condition. The process of

dissolving took place in two phases each per side, labeled area B1, B2, A1 and A2 (Kost et al. 2014).

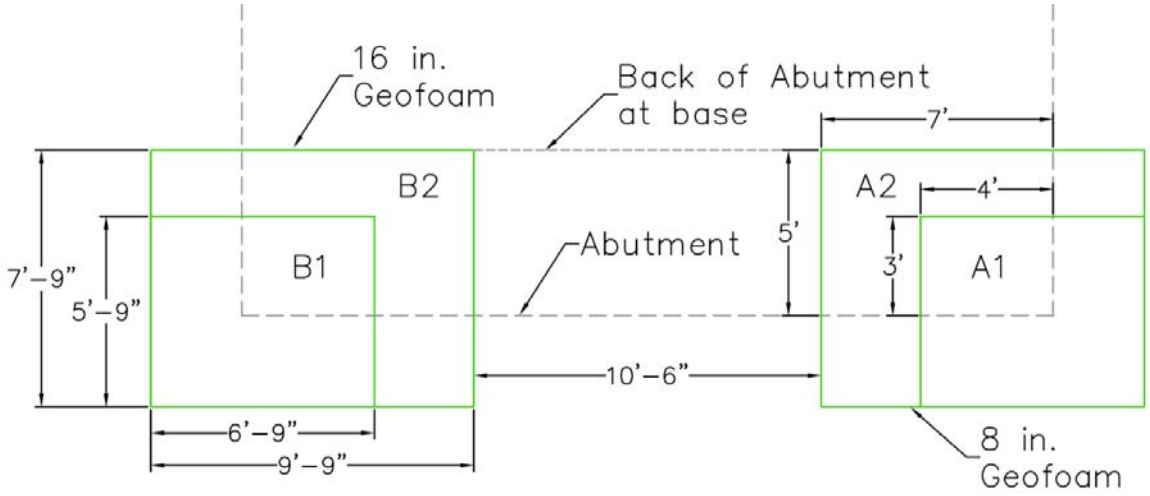

Figure 29: Geofoam Inclusion Layout beneath the Virginia Tech Abutment Kost, A., Filz, G., and Cousins, T. (2014). "Differential Settlement of a GRS Abutment: Full-Scale Investigation." ***Virginia Center for Transportation Innovation and Research*** **Charlottesville, VA. Used under fair use, 2014.**

The results of the experiment were that a GRS abutment could be constructed rapidly and handle the effects of extreme differential foundation settlement in a robust manner. The abutment after both sides were tested is shown in Figure 30. A GRS abutment subject to normal levels of field differential settlement is anticipated to perform very well. However, it is recommended that fill protection from scour conditions be employed due to the fact the after even small amounts of settlement the fill material will be subject to water action from gaps in the block facing (Kost et al. 2014).

Figure 30: Virginia Tech Abutment Wall after Testing Kost, A., Filz, G., and Cousins, T. (2014). "Differential Settlement of a GRS Abutment: Full-Scale Investigation." *Virginia Center for Transportation Innovation and Research* Charlottesville, VA. Used under fair use, 2014.

2.5 GRS SMALL SCALE TESTING

The definition of which GRS tests are "small scale" is rather qualitative. Any test setup that utilized dimensions of feet to define specimen size was classified as "large scale" while "small scale" tests were considered to be tests with sample sizes defined in units of either centimeter, millimeter, or inches. This section contains a variety of test setups, which were considered "small" in nature.

Modified SGIP Test: A modified Soil-Geosynthetic Interactive Performance (SGIP) test was developed to understand the behavior of geosynthetic reinforced soil over time. The test involved a reinforced soil sample being loaded in plain strain conditions. Deformations in the lateral and vertical dimensions were recorded. A series of SGIP tests were performed, and the behavior they exhibited was compared to measured field values. A diagram of the test setup is shown in Figure 31 (Ketchart and Wu 2002).

The tests conducted using the aparatus varied the soil type and the reinforcement type. A gravel road base material and a clayey soil where both tested. One clay and one road base soil sample were not reinforced. Two woven PP geotextiles were tested. One with tensile strnegth of 4,800 lb/ft (70 kN/m) and another with tensile strength of 1,440 lb/ft (21 kN/m). The third reinforcement type tested was a nonwoven PP geotextile with tensile strength of 411 lb/ft (6 kN/m) (Ketchart and Wu 2002).

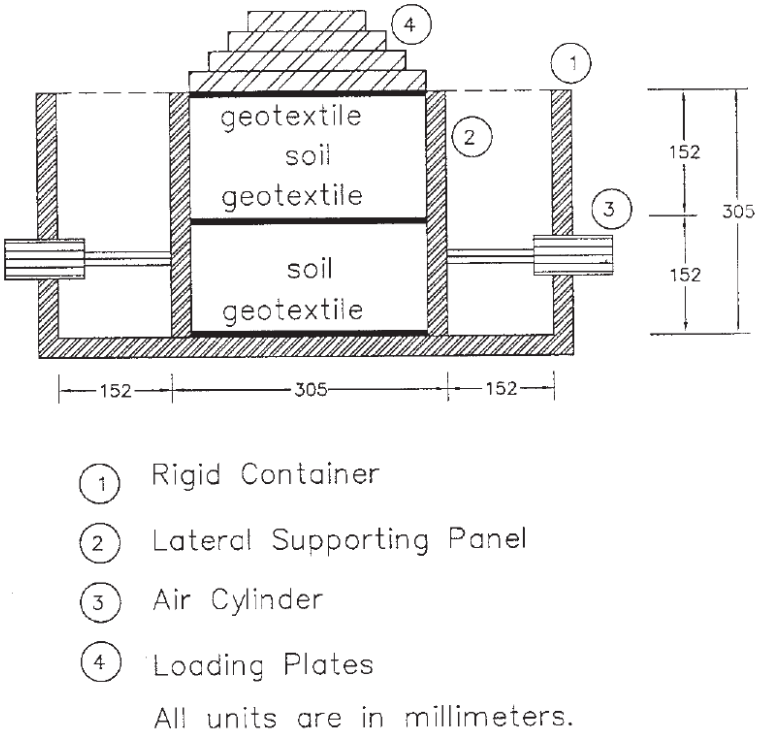

Figure 31: SGIP Test Setup Ketchart, K., and Wu, J. T. H. (2002). "A Modified Soil-Geosynthetic Interactive Performance Test for Evaluating Deformation Behavior of GRS Structures." *Geotechnical Testing Journal*, 25(4), 405-413.

Eight tests total were performed using SGIP. To understand creep behavior, two tests were conducted at elevated temperatures. The temperature advanced the creep sucestibility of the reinforcement. The testing program was assessed for repeatability and was considered to satisfy the repeatability criteria (Ketchart and Wu 2002).

The testing program confirmed that the center of the reinforced soil composite sample was sucetable to the maximum tensile loading. This conclusion was drawn from the location of rupture of the reinforcement. Additionally, it was shown that reinforcement provided both lateral and vertical restraint of the reinforced soil mass. This was found through comparing samples that were identical except one contained reinforcement and another did not. Performance was measured through examining deformation characteristics of the samples. The performance was found to correlate well with field measurements. The field measurements were from the FHWA Turner Fairbank GRS Bridge Pier experiment (Ketchart and Wu 2002). Later, the test was recommended for use in design when the reinforced fill was not ideal. In other words, if the fill is not coarse grained, an SGIP test will provide valuable insite into the long-term creep behavior of the reinforced soil mass (Wu and Adams 2007).

Long Term Creep Testing: Small scale creep tests were conducted to assess the long term performance of a geosynthetic reinforced soil mass. In particular, the test was trying to demonstrate that knowledge of the time-dependent deformation of the soil was critical.

Undestanding how the soil behaved over time was necessary to understanding how the reinforced soil mass would behave. Creep potential of the geosynthetic reinforcement only partly controlled performance (Wu and Helwany 1996).

The reinforced soil sample was placed in a rigid container. The development of tensile load in the reinforcement was soley from a vertically applied load and the self-weight of the soil. The container restained movement perpendicular to the plexiglass face, thus creating a plane strain condition. A schematic of the test setup is shown in Figure 32. Two types of confining soils were tested, a clean sand and a clay (Wu and Helwany 1996).

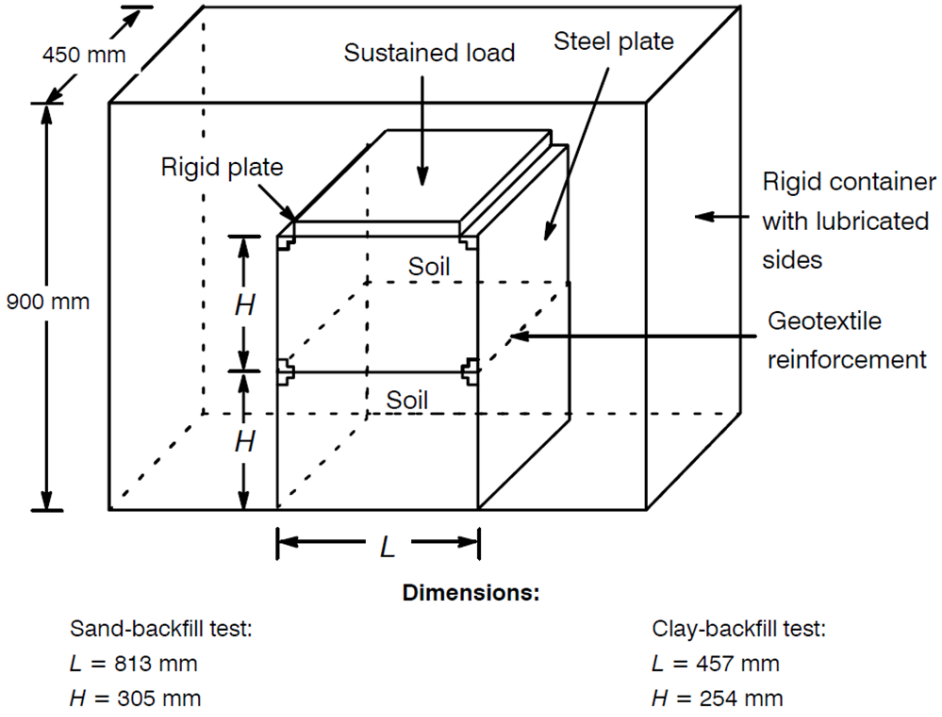

Figure 32: Creep Performance Test Setup Wu, J. T. H., and Helwany, S. M. B. (1996). "A Performance Test for Assessment of Long-Term Creep Bhavior of Soil-Geosynthetic Composites." *Geosynthetics International*, 3(1), 107-124. Used under fair use, 2014.

The tests showed that the behavior of the confining soil affected creep deformations in the reinforcement. The sand and clay confining soils exhibited different creep behvior. In the sand sample, the soil deformed more slowly than the reinforcement. Additionally, creep testing of just the reinforcement overpredicted the strains that actually developed in the sample. For the clay sample, the opposite was true. The clay soil deformed faster than the reinforcement, and the creep testing of just the reinforcement under-predicted the actual strains exhibited in the sample (Wu and Helwany 1996). The conclusion was made that creep deformation found from testing the geosynthetic alone, often called an “element test”, cannot be correlated to creep deformations exhibited by the geosynthetic in a reinforced soil mass without the use of a comprehensive numerical model (Wu et al. 1997).

2.6 GRS NUMERICAL MODELING

Numerous analytical assessments have been conducted to understand the behavior of GRS. This section will provide a brief look at some of the numerical modeling that has been conducted.

Finite Element Analysis of SGIP Tests: A finite element analysis was conducted of the SGIP test which assessed the degree of influence reinforce fill material played on long term creep performance. It was found that creep deformations for a clay backfill were much larger than a coarse grained backfill (Wu and Adams 2007).

Finite Element Analysis Comparing Backfill Influence on Long Term Creep: A finite element analysis was conducted to compare identical 10 ft (3 meter) tall GRS walls that had different reinforced fill. The first fill type was a moist clay, the second was a coarse grained material. It was found that the strain in the reinforcement for the coarse grained backfill remained nearly constant after construction for the next 15 years. For the clay material, strain increased 3.5% over the 15 year period. Additionally, the strain in the reinforcement was 6% greater for the clay backfill than the coarse grained backfill at the end of construction. Therefore, coarse grained backfill should be employed to avoid long term creep strains (Wu and Adams 2007).

Finite Element Analysis of a GRS Wall along Three Planes: The program DACSAR (Ohta and Iizuka 1986) was utilized to assess the lateral earth pressure of a GRS wall along three planes. These planes included the wall face, the back of the reinforced zone, and the plane along which the maximum tension load occurred in the reinforcement. The analysis showed that the load at the wall face was very low in comparison to the other planes and nearly constant with depth (Wu 2007). This is shown in Figure 33.

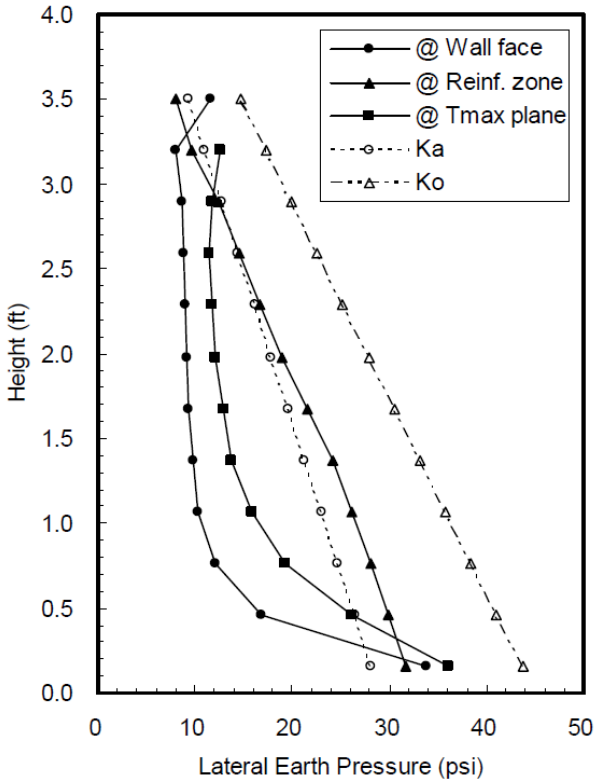

Figure 33: Results of Finite Element Analysis along Three Planes Wu, J. T. H. (2007). "Lateral Earth Pressure against the Facing of Segmental GRS Walls." *Geosynthetics in Reinforcement and Hydraulic Applications (GSP 165)*, Gabr, and Bowders (Eds.). ASCE, Reston, VA, 165-175. Used under fair use, 2014.

The results contrasted with typical Rankine or Coulomb theories which indicate an increase in lateral earth pressure with depth. The claim was made that there is actually little need for a heavy, rigid facing block system with connections to the reinforcement (Wu 2007).

Finite Element Analysis of GRS Wall: The program AFENA (Carter and Balaam 1990) was utilized in an assessment of a GRS retaining wall. The retaining wall was analyzed under plain strain 2D conditions. A schematic of the finite element mesh and wall is shown in Figure 34. The model illustrated that a GRS wall could withstand sudden differential settlements at the foundation and could mitigate "bridge bump" effects. Based on stability assessments, it is recommended in future design of GRS walls to examine the stability at the toe of the wall specifically (Skinner and Rowe 2005).

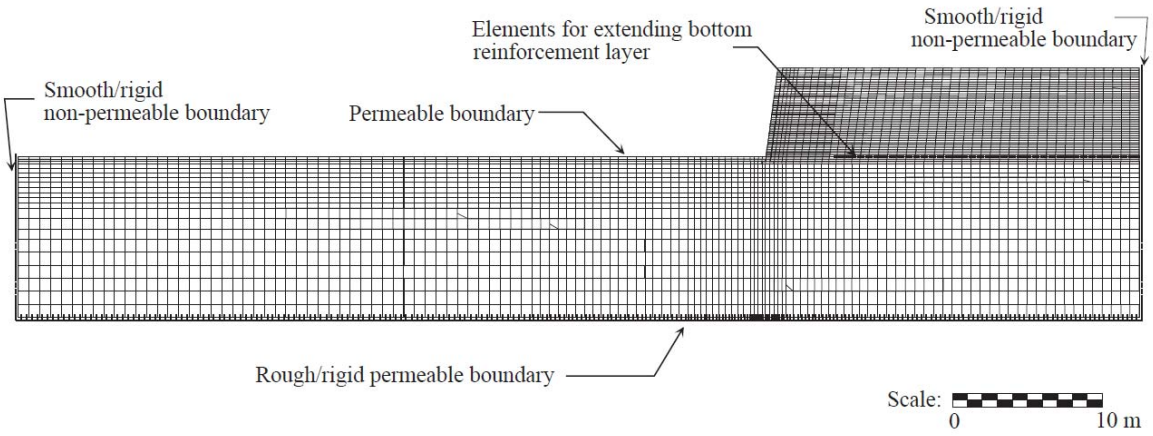

Figure 34: Finite Element GRS Wall showing Mesh Skinner, G. D., and Rowe, R. K. (2005). "Design and Behaviour of a Geosynthetic Reinforced Retaining Wall and Bridge Abutment on a Yielding Foundation." *Geotextiles and Geomembranes*, 23(3), 234-260. Used under fair use, 2014.

Finite Element Analysis of NCHRP Full Scale Test Abutments: The program Dyna3d (Hallquist and Whiley 1989) was used to assess the two full scale NCHRP test abu

tments analytically. The assessment was a plane-strain finite element analysis, and it demonstrated that the performance of a GRS abutment under various loading conditions could be modeled accurately (Helwany et al. 2007).

Numerical Model Compared against Five Full Scale Bridge Abutment Experiments: A numerical model of a GRS bridge abutment was developed using the programs DYNA3d and LS-DYNA. The model was compared against measured field data. The data came from five full-scale tests. Two were spread footing experiments, the third was the FHWA Turner Fairbank GRS Bridge Pier, the fourth was the Garden Experimental Embankment, and the last was the NCHRP Full Scale Test Abutments. There was significant agreement between the measured data and the model. The results of the analysis provided the information needed to develop a design procedure for allowable bearing pressure (Wu et al. 2006a; Wu et al. 2006b). This analysis and accompanying design procedure were included in the "NCHRP GRS Method" design guidance, Report No. 556 (Wu et al. 2006a).

Analytical Models of CIS, Composite Behavior, and Required Reinforcement Strength: Three analytical models were built to assess particular aspects of GRS technology. The first was to understand the compaction-induced stresses (CIS) observed in a GRS mass. The second was to explore fully the nature of a GRS composite mass, specifically the soil properties associated with this behavior. Finally, the last model was designed to assess the required tensile strength of reinforcement used in GRS structures. The analytical models were verified against collected data from GSGC testing. A finite element analysis was also conducted to simulate the behavior exemplified in GSGC testing. The code Plaxis 8.2 was utilized for the work. The resulting models can be used

to estimate CIS within an earth fill, and to predict the required tensile reinforcement strength value based on the allowable lateral movements desired for the wall (Pham 2009).

Analytical Support of GRS Composite Behavior: A large effort was undertaken to numerically model particular aspects of GRS composite behavior. The first model calculates lateral movement and connection forces associated with a GRS wall. The second was a model capturing the composite properties and required reinforcement strength. A presentation of these models, their verification, and all related finite element analyses are summarized in an FHWA report. As a result of these efforts, a better understanding of GRS composite behavior was achieved (Wu et al. 2013).

2.7 GRS PARAMETRIC ANALYSES

Multiple parametric analyses have been conducted on particular aspects of GRS technology. This section summarizes these assessments and their major findings.

Investigation of Foundation Soil Effects on GRS: The program DACSAR was used to vary foundation soil parameters in order to assess its effects on GRS performance. The DACSAR model was verified against field measured values from the Founders/Meadows Bridge (Helwany et al. 2003).

It was found that loose sand and medium-dense sand foundation soil result in higher abutment displacements than dense sand. However, performance of all sand foundation soils was considered tolerable. Additionally, the modeled abutment performance was satisfactory for stiff to medium clay foundation soils. The parametric analysis demonstrated the versatility of GRS abutments (Helwany et al. 2003).

Parametric Study of Bottom Reinforcement Layer in a GRS Wall: The goal of the assessment was to see if increasing the stiffness and length of the bottom reinforcement layer would in turn increase external stability. The assessment examined bearing capacity and global stability factors of safety. Two GRS wall cases were studied using finite element analysis with the program AFENA. The same model shown in Figure 34 was utilized (Skinner and Rowe 2005).

Results indicate that stiffening or lengthening the bottom reinforcement layer has little overall impact on external stability for a wall system that is already considered stable. A stiffer bottom layer did result in lower deformations at the base for one of the explored GRS wall cases. Lengthening reinforcement had a stabilizing effect in the backfill past the reinforced zone. This prevented the development of a global stability failure mechanism (Skinner and Rowe 2005).

Parametric Analysis of GRS Abutment: An investigation was conducted to assess the effects of varying live and dead bridge loads on a GRS abutment with modular block facing elements. Additionally, parameters such as backfill properties, reinforcement stiffness, and reinforcement spacing were varied (Helwany et al. 2007).

The base case geometry for the abutment was modeled after the Founder/Meadows Bridge. Load was distributed evenly over the abutment seat and increased until failure. The configuration of the parametric study base case is shown in Figure 35. Friction angle of the reinforced fill was 34° for the base case. Reinforced fill soil with friction angles of 37° and 40° were also investigated. The reinforcement spacing base case was 8 inches (20 centimeters). Spacings of 16 inches (40 centimeters) and 24 inches (60 centimeters) was also simulated. The base case reinforcement stiffness was 390 kips/ft (530 kN/m). Values of 3,900 kips/ft (5,300 kN/m) and 39 kips/ft (53 kN/m) were also explored (Helwany et al. 2007).

The results of the parametric analysis indicated that reinforced fill properties have a large impact on abutment performance, specifically the friction angle and degree of compaction. Increases in friction angle resulted in decreases in displacement. Additionally, reinforcement stiffness and spacing also influence abutment performance. As reinforcement spacing increases, the displacement at the abutment seat increases. Finally, lower reinforcement stiffness resulted in higher displacements (Helwany et al. 2007).

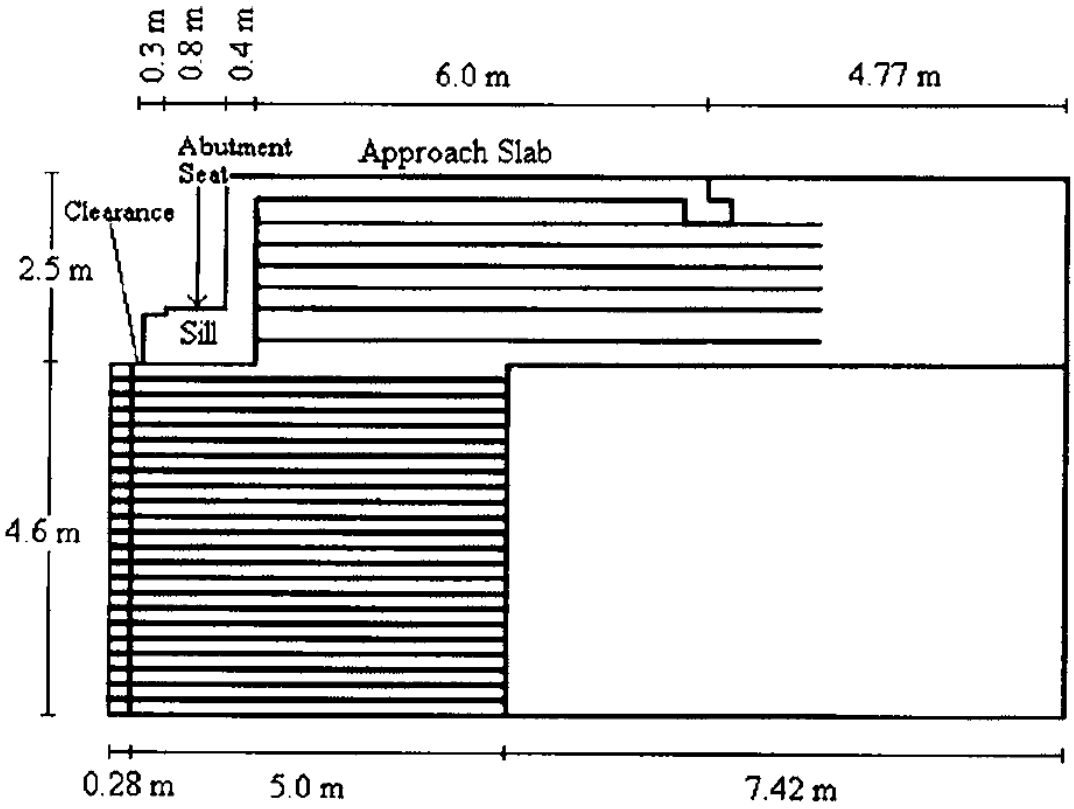

Figure 35: Base Case Geometry of Parametric Study Helwany, S. M. B., Wu, J. T. H., and Kitsabunnarat, A. (2007). "Simulating the Behavior of GRS Bridge Abutments." ***Journal of Geotechnical and Geoenvironmental Engineering,*** **133(10), 1229-1240. Used under fair use, 2014.**

The parametric analysis was included in the "NCHRP GRS Method" design guidance, Report No. 556. The study helped in understanding the factors driving performance of a GRS abutment and approach fill. The results of the analysis provided a framework for preliminary GRS abutment design guidance (Wu et al. 2006a).

CHAPTER 3 – PARAMETRIC ANALYSIS

3.1 PURPOSE OF STUDY

This chapter describes in detail a parametric analysis of reinforced soil. The purpose of the analysis was to compare reinforcement tensile load and required strength information predicted by several of the most current and/or emerging reinforced soil design methods. In recent years, concerns have arisen regarding the difference in behavior assumed by Mechanically Stabilized Earth Walls (MSEW) and Geosynthetic Reinforced Soil (GRS) analysis methods. It is often unclear when to use one technology over the other and which analysis method will be appropriate for a given project. Therefore, the goal of the parametric analysis was to investigate the significance of this issue by evaluating several MSEW and GRS design procedures using the same set of parameter values and wall geometries.

3.2 SCOPE OF PARAMETRIC ANALYSIS

A parametric study was performed to investigate the variation in required tensile strength predicted by five different reinforced soil design methods. Required tensile strength is defined as the minimum tensile strength each method requires for a given reinforcement layer once all factors of safety, reduction factors, and load factors are applied. This quantity is represented by the variable T_{req}. Additionally, the nominal maximum load in the reinforcement per layer was also compared for each of the five methods. The nominal maximum load in the reinforcement is defined as the "unfactored" tension in the reinforcement and is represented by the variable T_{max}. Load factors are often applied to T_{max} in order to obtain a factored tensile strength, which is represented by the variable $T_{max,f}$. The factored tensile strength is then used to determine the required tensile strength, T_{req}. Often resistance factors, factors of safety, and reduction factors for reinforcement material properties are applied to a $T_{max,f}$ value to obtain an ultimate required tensile strength, T_{req}, for the wall at a given layer.

The analysis was limited to internal stability. Only the tensile load, both nominal and factored, and required tensile strength were compared for the various reinforced soil design methods. No external stability values were compared such as eccentricity, factor of safety against bearing capacity, or global stability. The scope of the analysis focused on the tensile strength and tensile load predicted by the methods because the soil theories supporting these prediction methods varied the most widely. The soil theory supporting GRS and MSEW design guidance are fundamentally different. The most apparent difference is in the manner the soil and reinforcement are assumed to interact. Therefore, reinforcement tension was the primary focus of the comparison.

3.3 REINFORCED SOIL DESIGN METHODS

A parametric study compared five different reinforced soil design methods. Of these five methods, three were MSEW design methods and two were GRS design methods. These

methods are listed below and major features of each method are discussed in the reinforced soil design guidance section of the literature review chapter.

Method 1: FHWA Simplified Procedure

Method 2: Simplified Procedure with Kr/Ka Adjusted

Method 3: K-Stiffness Method

Method 4: NCHRP GRS Method

Method 5: FHWA GRS-IBS Method

These methods were chosen because they are the most current and/or widely used design methodologies available to practicing engineers. Method 1 is the most commonly used design method for MSEW. Method 2 is a refinement to Method 1. Method 3 is a design method that takes into account the relative stiffness of all wall components in comparison to the soil stiffness. There are plans for the principles of Method 3 to be incorporated into Method 1 design guidance. Method 4 was the first GRS abutment design method. Method 4 utilized a great deal of the framework outlined in an earlier publication of Method 1 before the incorporation of LRFD. Method 5 is the most current and widely used GRS design method. It has the most significant theoretical differences in assumed soil behavior in comparison to Method 1.

3.4 PARAMETRIC STUDY SETUP

This section describes the initial framework for conducting the parametric analysis. The following section details the chosen base case geometry, base case parameters, parameter variation, and loading conditions.

Loading Condition: The parametric analysis evaluated two loading conditions. The first was a roadway loading condition with a wall configuration as shown in Figure 36. The second was a bridge loading condition with abutment wall configuration as shown in Figure 37.

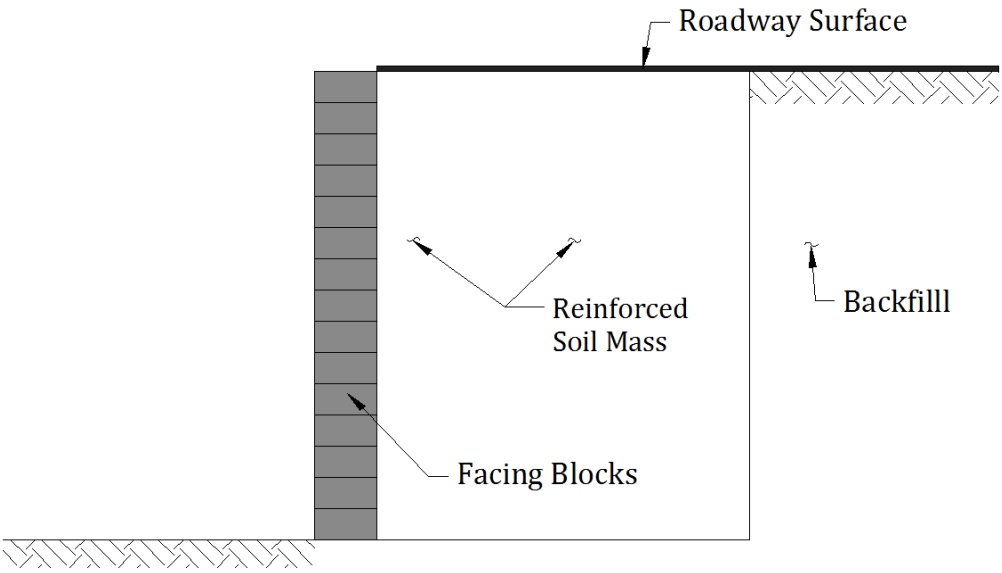

Figure 36: Wall Schematic for Roadway Loading Condition

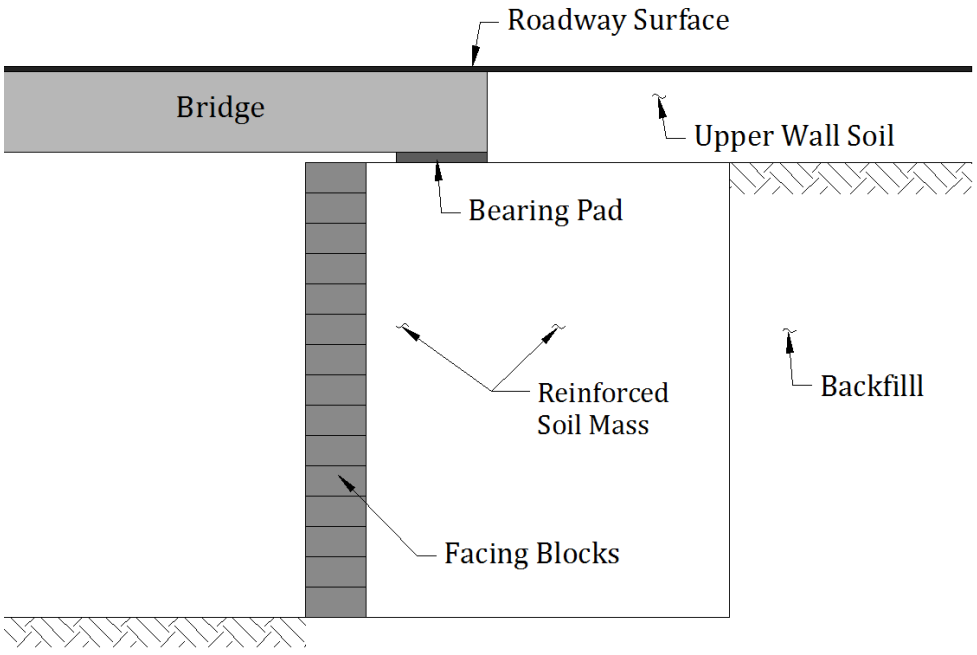

Figure 37: Abutment Wall Schematic for Bridge Loading Condition

The roadway loading condition had only one uniformly distributed pressure across the top of the wall. This was a surcharge load for traffic as shown in Figure 38. The bridge loading condition also had the uniform traffic surcharge over the road surface but it also had pressures associated with the bridge. The bridge pressure is broken into dead load and live load distributions as shown in Figure 39. It should be noted that an isolated sill was assumed for the parametric analysis instead of an integrated sill or footing. This assumption was made to allow for the most direct comparison across all methods.

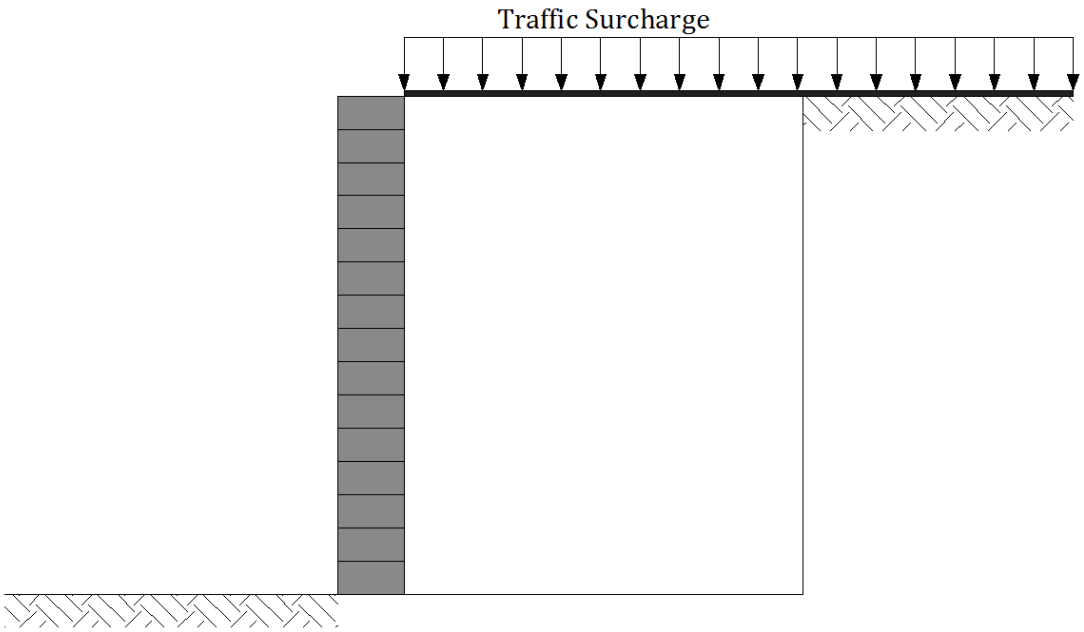

Figure 38: Roadway Loading Condition

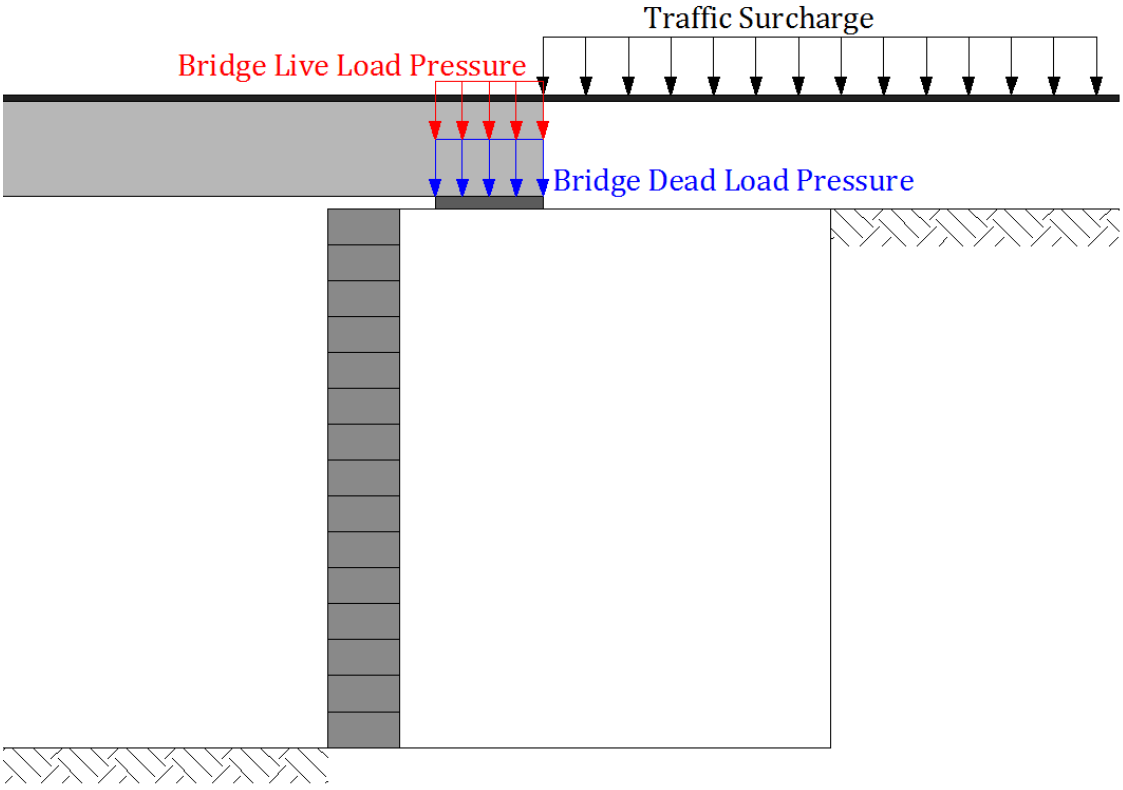

Figure 39: Bridge Loading Condition

Base Case: Base case values were chosen to be illustrative of a typical reinforced soil wall or abutment. The base case values were selected upon review of work conducted by

Karla Santacruz Reyes and Andy Kost while both were graduate research assistants at Virginia Tech. These initial values were evaluated against case history information and example designs provided in Methods 4 and 5. Additionally, the base case values were reviewed by practicing engineers with familiarity in reinforced soil wall design. Initial base case data for work conducted by Karla Reyes-Santacruz was reviewed by Jennifer Nicks from FHWA Turner Fairbank Research Center and final review of base case data was conducted by Ryan Berg of Ryan Berg and Associates.

Base case data was divided into two parts. The first was the base case information for the wall loading condition shown in Table 2; the second was for the bridge loading condition shown in Table 3. The base case values were varied as part of the parametric analysis. Figure 40 and Figure 41 illustrate how the variables are applied to the roadway loading and bridge loading conditions. It should be noted that within calculations specific to each method, often other parameters were introduced. Sometimes these parameters were not varied due to their specificity to a particular method, and they are defined in the governing calculation descriptions in this section of the report.

Table 2: Base Case Values for Wall Loading Condition

Design Property		*Variable*	*Units*	*Base Case Value*
Wall Height		H	ft	16
Traffic Load		q	psf	250
Reinforced Fill	Friction Angle	ϕ'_r	degrees	38
	Max Particle Diameter	d_{max}	in	0.5
	Unit Weight	γ_r	pcf	125
Reinforcement	Spacing	S_v	in	8
	Type	NA	NA	PET geogrid
	Reduction Factor for Installation Damage	RF_{ID}	NA	1.3
	Reduction Factor accounting for Creep	RF_{CR}	NA	1.45
	Reduction Factor for Degradation	RF_D	NA	1.15
	Reduction Factor Product RF_{ID} x RF_{CR} x RF_D	RF	NA	2.17
Facing Block Dimensions		b x h_{eff}	in x in	12 x 8

Table 3: Base Case Values for Bridge Loading Condition

Design Property		*Variable*	*Units*	*Base Case Value*
Wall Height		H	ft	16
Upper Wall Height		h	ft	3
Sill Width		b	ft	3
Setback Distance		d	ft	1
Bridge Live Load		q_{LL}	ksf	3.34
Bridge Dead Load		q_b	ksf	3.34
Traffic Load		q	psf	250
Reinforced Fill	Friction Angle	ϕ'_r	degrees	38
	Max Particle Diameter	d_{max}	in	0.5
	Unit Weight	γ_r	pcf	125
Reinforcement	Spacing	S_v	in	8
	Type	NA	NA	PET geogrid
	Reduction Factor for Installation Damage	RF_{ID}	NA	1.3
	Reduction Factor accounting for Creep	RF_{CR}	NA	1.45
	Reduction Factor for Degradation	RF_D	NA	1.15
	Reduction Factor Product RF_{ID} x RF_{CR} x RF_D	RF	NA	2.17
Facing Block Dimensions		b x h_{eff}	in x in	12 x 8

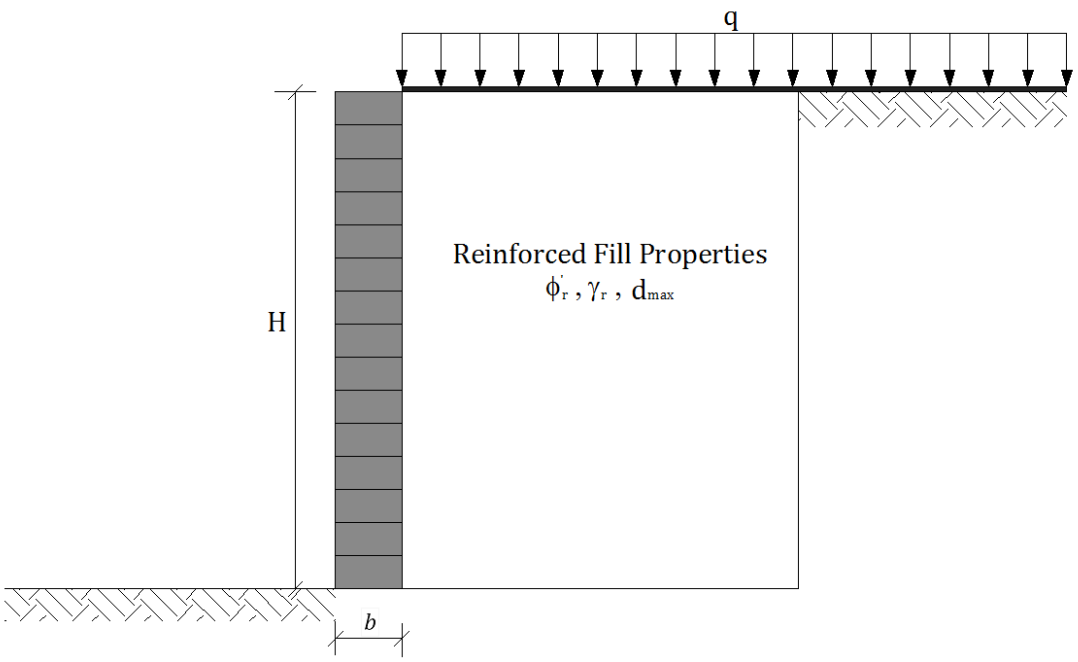

Figure 40: Base Case Wall for Roadway Loading Condition

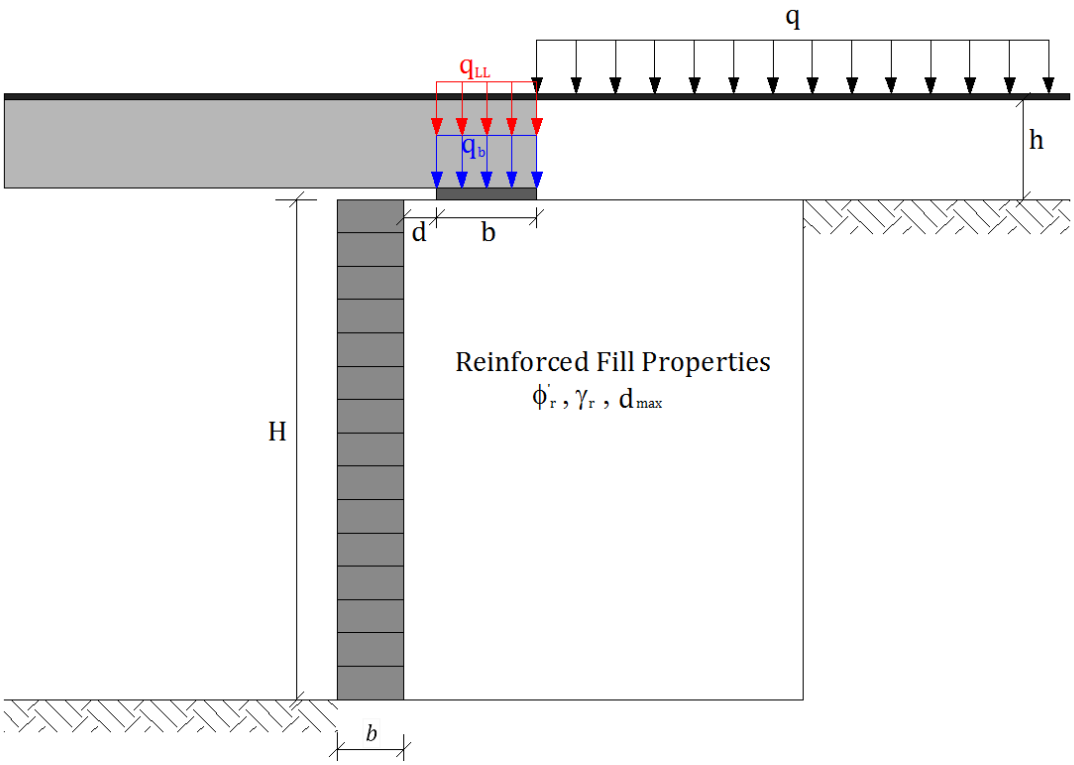

Figure 41: Base Case Abutment Wall for Bridge Loading Condition

Parameter Variation: A reasonable set of parameter variations were established for both the roadway and bridge loading conditions. The parameter variation values were selected upon review of work conducted by Karla Reyes-Santacruz and Andy Kost.

These initial values were evaluated against case history information and example designs provided in Methods 4 and 5. Additionally, the parameter variation values were reviewed by practicing engineers with familiarity in reinforced soil wall design. Initial variation data for work conducted by Karla Santacruz Reyes was reviewed by Jennifer Nicks from FHWA Turner Fairbank Research Center, and final review of parameter variation data was conducted by Ryan Berg of Ryan Berg and Associates.

The majority of parameter variations were the same between the two loading conditions. The summary of parameter variations for the roadway loading conditions is shown in Table 4. The summary of parameter variations for the bridge loading condition is shown in Table 5. The step variation between the lowest and highest parameters was different for each parameter. Step size was adjusted to ensure the variation in T_{req} and T_{max} was easily discernable. Intermediate values are not shown in Table 4 and Table 5. However, the intermediate values are presented graphically in the results section for many parameters.

Table 4: Parameter Variation for Roadway Loading Condition

Design Property		*Variable*	*Units*	*Lowest Parameter Variation*	*Base Case Value*	*Highest Parameter Variation*
Wall Height		H	ft	10	16	28
Traffic Load		q	psf	230	250	300
Reinforced Fill	Friction Angle	ϕ'_r	degrees	34	38	55
	Max Particle Diameter	d_{max}	in	0.5	0.5	2
	Unit Weight	γ_r	pcf	115	125	150
Reinforcement (1)	Spacing	S_v	in	8	8	24
	Reduction Factor Product	RF	NA	2.17	2.17	8.19
Facing Block Dimensions(2)		b x h_{eff}	in x in	8 x 8	12 x 8	48 x 24

(1) The reinforcement type was varied as part of the parametric study. The base case reinforcement was a PET geotextile. with RF_{ID} = 1.3, RF_{CR} = 1.45, RF_D = 1.15.A PP geotextile, PET geogrid, and a HDPE geogrid were also examined. The reduction factors were varied to reflect which reinforcement was being examined. For a PP geotextile RF_{ID} = 1.4, RF_{CR} = 4.5, RF_D = 1.3. For a PET geotextile RF_{ID} = 1.4, RF_{CR} = 2.0, RF_D = 1.6. For a HDPE geogrid RF_{ID} = 1.2, RF_{CR} = 2.6, RF_D = 1.1. For the parameter variation of friction angle, the base case PET geogrid RF_{ID} value will increase to 1.8 for friction angles greater than or equal to 40°.

(2) The facing block dimensions were varied based on anticipated block sizes utilized in industry. The combination of b x h_{eff} compared in the parametric analysis include an 8 in x 8 in block, 12 in x 8 in block, 24 in x 18 in, 36 in x 18 in, and 48 in x 24 in. The lowest and highest parameters listed in the table are the smallest and largest facing blocks compared in the analysis.

Table 5: Parameter Variation for Bridge Loading Condition

Design Property		*Variable*	*Units*	*Lowest Parameter Variation*	*Base Case Value*	*Highest Parameter Variation*
Wall Height		H	ft	10	16	28
Upper Wall Height		h	ft	1	3	5
Sill Width		b	ft	2	3	7
Setback Distance		d	ft	1	1	2.3
Bridge Live Load		q_{LL}	ksf	1.5	3.34	5.5
Bridge Dead Load		q_b	ksf	1.3	3.34	6.5
Traffic Load		q	psf	230	250	300
Reinforced Fill	Friction Angle	ϕ'_r	degrees	34	38	55
	Max Particle Diameter	d_{max}	in	0.5	0.5	2
	Unit Weight	γ_r	pcf	115	125	150
Reinforcement (1)	Spacing	S_v	in	8	8	24
	Reduction Factor Product	RF	NA	2.17	2.17	8.19
Facing Block Dimensions(2)		b x h_{eff}	in x in	8 x 8	12 x 8	48 x 24

(1) The reinforcement type was varied as part of the parametric study. The base case reinforcement was a PET geotextile. with RF_{ID} = 1.3, RF_{CR} = 1.45, RF_D = 1.15. A PP geotextile, PET geogrid, and a HDPE geogrid were also examined. The reduction factors were varied to reflect which reinforcement was being examined. For a PP geotextile RF_{ID} = 1.4, RF_{CR} = 4.5, RF_D = 1.3. For a PET geotextile RF_{ID} = 1.4, RF_{CR} = 2.0, RF_D = 1.6, For a HDPE geogrid RF_{ID} = 1.2, RF_{CR} = 2.6, RF_D = 1.1. For the parameter variation of friction angle, the base case PET geogrid RF_{ID} value will increase to 1.8 for friction angles greater than or equal to 40°.

(2) The facing block dimensions were varied based on anticipated block sizes utilized in industry. The combination of b x h_{eff} compared in the parametric analysis include an 8 in x 8 in block, 12 in x 8 in block, 24 in x 18 in, 36 in x 18 in, and 48 in x 24 in. The lowest and highest parameters listed in the table are the smallest and largest facing blocks compared in the analysis.

3.5 GOVERNING EQUATIONS

This section details the calculations each method employs for determining T_{max} and T_{req}. The section is broken into subsections for each of the five methods compared in the parametric analysis. All variables utilized in the governing equations presented in each calculation summary are defined. A common set of variable definitions was chosen to define design parameters across all methods. Table in APPENDIX details the original variable given within the literature of each method and the corresponding variable definition used for the parametric study in this report. All references utilized in developing each calculation are cited. A distinction is made between nominal and factored parameters throughout the calculation summaries. Often a method's references only calculate a nominal or a factored parameter. Yet if possible, both a nominal and a factored parameter calculation are presented in this report. A variable is indicated as a

factored parameter by adding the subscript f. For example T_{max} is a nominal parameter where $T_{max,f}$ is the factored form of the same parameter.

Method 1: FHWA Simplified Procedure Calculation Summary: Method 1 is the state of practice design method for Mechanically Stabilized Earth Walls. The following references were utilized in developing the calculation summary for Method 1. Method 1 references include methodologies for calculation of T_{max} and T_{req} for both a bridge loading and a roadway loading condition.

AASHTO (2011) "Laboratory Evaluation of Geosynthetic Reinforcement: Final Product Qualification Report for Miragrid XT Geogrid Product line." *NTPEP Report REGEO-2011-01-001*

Berg, R.R., Christopher, B.R., and Samtani, N.C. (2009a). "Design of Mechanically Stabilized Earth Walls and Reinforced Soil Slopes – Volume I." *FHWA-NHI-10-024*. National Highway Institute, Federal Highway Administration, Washington, D.C.

Berg, R.R., Christopher, B.R., and Samtani, N.C. (2009b). "Design of Mechanically Stabilized Earth Walls and Reinforced Soil Slopes – Volume II." *FHWA-NHI-10-025*. National Highway Institute, Federal Highway Administration, Washington, D.C.

Elias, V., Fishman, K.L., Christopher, B.R., and Berg, R.R. (2009). "Corrosion and Degradation of Soil Reinforcements for Mechanically Stabilized Earth Walls and Reinforced Soil Slopes." *FHWA-NHI-09-087*. National Highway Institute, Federal Highway Administration, Washington, D.C.

Calculation of Nominal Load in the Reinforcement, T_{max} for Roadway Loading Condition: The parametric study calculated a series of T_{max} values, one at each reinforcement layer depth.

Equation 1 (after Equation 4-32a Berg et al 2009a)

$$\mathbf{T_{max} = \sigma_h S_v}$$

Where:

T_{max} = Maximum nominal load in the reinforcement

σ_h = Nominal horizontal stress, this parameter is defined in Equation 2

S_v = Reinforcement spacing, this parameter was varied as part of the analysis

Equation 2 (developed from Equation 4-30 Berg et al 2009a)

$$\mathbf{\sigma_h = K_r \left(\gamma_r \left(z + h_{eq}\right)\right)}$$

Where:

K_r = Lateral earth pressure coefficient of the reinforced fill, this parameter is defined in Equation 3

γ_r = Unit weight of the reinforced fill, this parameter was varied as part of the analysis

z = Depth below top of reinforced zone, this parameter was varied as part of the analysis over the same range as the parameter wall height, H

h_{eq} = Equivalent uniform soil surcharge height, a constant value of 2 ft was utilized in the parametric analysis

> **Equation 3** (after Equation 4-25 and Figure 4-10, presented as Figure 42 in this report, of Berg et al 2009a)
>
> $$\mathbf{K_r = (1.0)\, K_a = \tan^2\left(45 - \frac{\phi'_r}{2}\right)}$$

Where:

K_r = Lateral earth pressure coefficient of the reinforced fill

K_a = Rankine lateral earth pressure coefficient for the active condition

ϕ'_r = Friction angle of the reinforced fill, this parameter was varied as part of the analysis

K_r was set equal to (1.0) K_a based on Figure 42 presented in Method 1 reference material. The figure indicates that the ratio of K_r/K_a for geosynthetics is equal to 1.0.

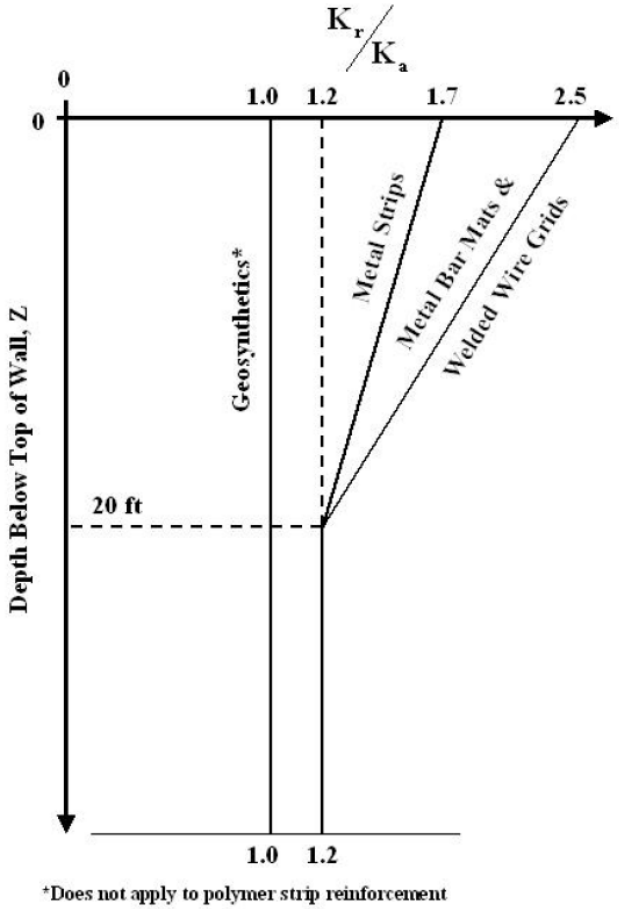

Figure 42: Variation in Ratio of K_r/K_a with Reinforcement Type Berg, R. R., Christopher, B. R., and Samtani, N. (2009). "Mechanically Stabilized Earth Walls and Reinforced Slopes, Design and Construction Guidelines." ***Vol. I - FHWA-NHI-10-024, Vol. II – FHWA-NHI-10-025*****, Federal Highway Administration, Washington, D.C. Used under fair use, 2014.**

Calculation of Maximum Factored Load in the Reinforcement, $T_{max,f}$ for Roadway Loading Condition: The parametric study calculated a series of $T_{max,f}$ values, one at each reinforcement layer depth.

Equation 4 (after Equation 4-32a Berg et al 2009a)

$$\mathbf{T_{max,f}} = \sigma_{\mathbf{h,f}}\,\mathbf{S_v}$$

Where:

$T_{max,f}$ = Maximum factored load in the reinforcement

$\sigma_{h,f}$ = Factored horizontal stress for roadway loading condition, this parameter is defined in Equation 5

S_v = Reinforcement spacing, this parameter was varied as part of the analysis

Equation 5 (after Equation 4-30 Berg et al 2009a)

$$\sigma_{\mathbf{h,f}} = \mathbf{K_r}\left(\gamma_{\mathbf{r}}\left(\mathbf{z}+\mathbf{h_{eq}}\right)\gamma_{\mathbf{EV-MAX}}\right)$$

Where:

K_r = Lateral earth pressure coefficient of the reinforced fill, this parameter is defined in Equation 3

γ_r = Unit weight of the reinforced fill, this parameter was varied as part of the analysis

z = Depth below top of reinforced zone, this parameter was varied as part of the analysis over the same range as the parameter wall height, H

h_{eq} = Equivalent uniform soil surcharge height, a constant value of 2 ft was utilized in the parametric analysis

$\gamma_{EV\text{-}MAX}$ = Load factor corresponding to a vertical pressure from a dead load earth fill, a value of 1.35 was used in the parametric analysis

Calculation of Nominal Load in the Reinforcement, T_{max} for Bridge Loading Condition: The parametric study calculated a series of T_{max} values, one at each reinforcement layer depth.

Equation 6 (after Equation 4-32a Berg et al 2009a)

$$\mathbf{T_{max}} = \sigma_{\mathbf{h}}\,\mathbf{S_v}$$

Where:

T_{max} = Maximum nominal load in the reinforcement

σ_h = Nominal horizontal stress for bridge loading condition, this parameter is defined in Equation 7

S_v = Reinforcement spacing, this parameter was varied as part of the analysis

Equation 7 (developed from Equation 4-31 Berg et al 2009a)

$$\sigma_{\mathbf{h}} = \mathbf{K_r}\left(\gamma_{\mathbf{r}}\left(\mathbf{z}+\mathbf{h_{eq}}\right)+\mathbf{h}\,\gamma_{\mathbf{u}} + \Delta\sigma_{\mathbf{v}}\right) + \Delta\sigma_{\mathbf{h}}$$

Where:

σ_h = Nominal horizontal stress for bridge loading condition

K_r = Lateral earth pressure coefficient of the reinforced fill, this parameter is defined in Equation 3

γ_r = Unit weight of the reinforced fill, this parameter was varied as part of the analysis

z = Depth below top of reinforced zone, this parameter was varied as part of the analysis over the same range as the parameter wall height, H

h_{eq} = Equivalent uniform soil surcharge height, a constant value of 2 ft was utilized in the parametric analysis

h = Height of the upper wall also known as the back wall, this parameter was varied as part of the analysis

γ_u = Unit weight of the upper wall soil, a value of 120 pcf was used in the parametric analysis

$\Delta\sigma_v$ = Nominal vertical pressure from the bearing pad, this parameter is defined in Equation 8

$\Delta\sigma_h$ = Nominal horizontal pressure from the upper wall, this parameter is defined in Equation 14

Equation 8 (after $\Delta\sigma_{v\text{-footing}}$ Equation on Page E5-19 Berg et al 2009b)

$$\Delta\sigma_{\mathbf{v}} = \frac{\mathbf{P_{wL}}}{(\mathbf{b} - \mathbf{2e}) + \left(\mathbf{d} + \frac{\mathbf{z}}{\mathbf{2}}\right)}$$

Where:

$\Delta\sigma_v$ = Nominal vertical pressure from the bearing pad

P_{wL} = Nominal load on base of the bearing pad, this parameter is defined in Equation 9

b = Sill width or width of the bearing pad, this parameter was varied as part of the analysis

e = eccentricity from center of bearing pad, this parameter is defined in

Equation 16

d = Clear or setback distance, this parameter was varied as part of the analysis

z = Depth below top of reinforced zone, this parameter was varied as part of the analysis over the same range as the parameter wall height, H

Equation 9 (after P_{wL} Equation on Page E5-16 Berg et al 2009b)

$$\mathbf{P_{wL}} = \mathbf{V_{Ab}} - \mathbf{h}\,\gamma_{\mathbf{u}}\,(\mathbf{b} + \mathbf{d}) - \gamma_{\mathbf{r}}\,\mathbf{h_{eq}}\,(\mathbf{b} + \mathbf{d})$$

Where:

P_{wL} = Nominal load on the base of the bearing pad

V_{Ab} = Sum of the nominal vertical forces from the bearing pad, this parameter is defined in Equation 10

h = Height of the upper wall also known as the back wall, this parameter was varied as part of the analysis

γ_u = Unit weight of the upper wall soil, a value of 120 pcf was used in the parametric analysis

b = Sill width or width of the bearing pad, this parameter was varied as part of the analysis

d = Clear or setback distance, this parameter was varied as part of the analysis

γ_r = Unit weight of the reinforced fill, this parameter was varied as part of the analysis

h_{eq} = Equivalent uniform soil surcharge height, a constant value of 2 ft was utilized in the parametric analysis

Equation 10 (after V_{Ab} Equation on Page E5-16 Berg et al 2009b)

$$\mathbf{V_{Ab} = V_1 + DL + LL}$$

Where:

V_{Ab} = Sum of the nominal vertical forces from the bearing pad

V_1 = Nominal vertical load from the weight of the bearing pad, this parameter is defined in Equation 11

DL = Nominal dead load from the bridge, this parameter is defined in Equation 12

LL = Nominal live load on the bridge, this parameter is defined in Equation 13

Equation 11 (after V_1 Equation in Table E5-4.1 on Page E5-8 Berg et al 2009b)

$$\mathbf{V_1 = \gamma_c\, b\, h_1}$$

Where:

V_1 = Nominal vertical load from the weight of the bearing pad

γ_c = Unit weight of concrete, a value of 150 pcf was used in the parametric analysis

b = Sill width or width of the bearing pad, this parameter was varied as part of the analysis

h_1 = Height of the bearing pad, a value of 4 inches was used in the parametric analysis

Equation 12 (developed from Figure E5-2 on Page E5-7 Berg et al 2009b)

$$\mathbf{DL = q_b\, b}$$

Where:

DL = Nominal dead load from the bridge

q_b = Nominal dead load pressure from the bridge, this parameter was varied as part of the analysis

b = Sill width or width of the bearing pad, this parameter was kept constant at the base case value of 3 ft for calculation of DL , therefore DL varied from 3.9 k/ft to 19.5 k/ft due to variation in q_b

Equation 13 (developed from Figure E5-2 on Page E5-7 Berg et al 2009b)

$$\mathbf{LL = q_{LL}\, b}$$

Where:

LL = Nominal live load on the bridge

q_{LL} = Nominal live load pressure on the bridge, this parameter was varied as part of the analysis

b = Sill width or width of the bearing pad, this parameter was kept constant at the base case value of 3 ft for calculation of LL, therefore LL varied from 4.5 k/ft to 16.5 k/ft due to variation in q_{LL}

Equation 14 (after $\Delta\sigma_H$ Equation on Page E5-25 Berg et al 2009b)

$$\Delta\sigma_{\mathbf{h}} = \frac{\mathbf{2\, F_A\, (\, L_1 - z)}}{\mathbf{L_1^2}} \quad \mathbf{when} \quad \mathbf{z \leq L_1}$$

$$\Delta\sigma_{\mathbf{h}} = \mathbf{0} \quad \mathbf{when} \quad \mathbf{z > L_1}$$

Where:

$\Delta\sigma_h$ = Nominal horizontal pressure from upper wall

F_A = Sum of horizontal nominal pressures from upper wall, this parameter is defined in Equation 24

L_1 = Depth of influence for the lateral load acting on the base of the bearing pad, this parameter is defined in Equation 15

z = Depth below top of reinforced zone, this parameter was varied as part of the analysis over the same range as the parameter wall height, H

The distribution of the nominal horizontal pressure from the upper wall, $\Delta\sigma_h$, is depicted in Figure 43. The distribution assumes that all of the horizontal pressures from the upper wall, F_A, go into the reinforced zone and are picked up by the reinforcement. No hoizontal pressure is applied to the bridge.

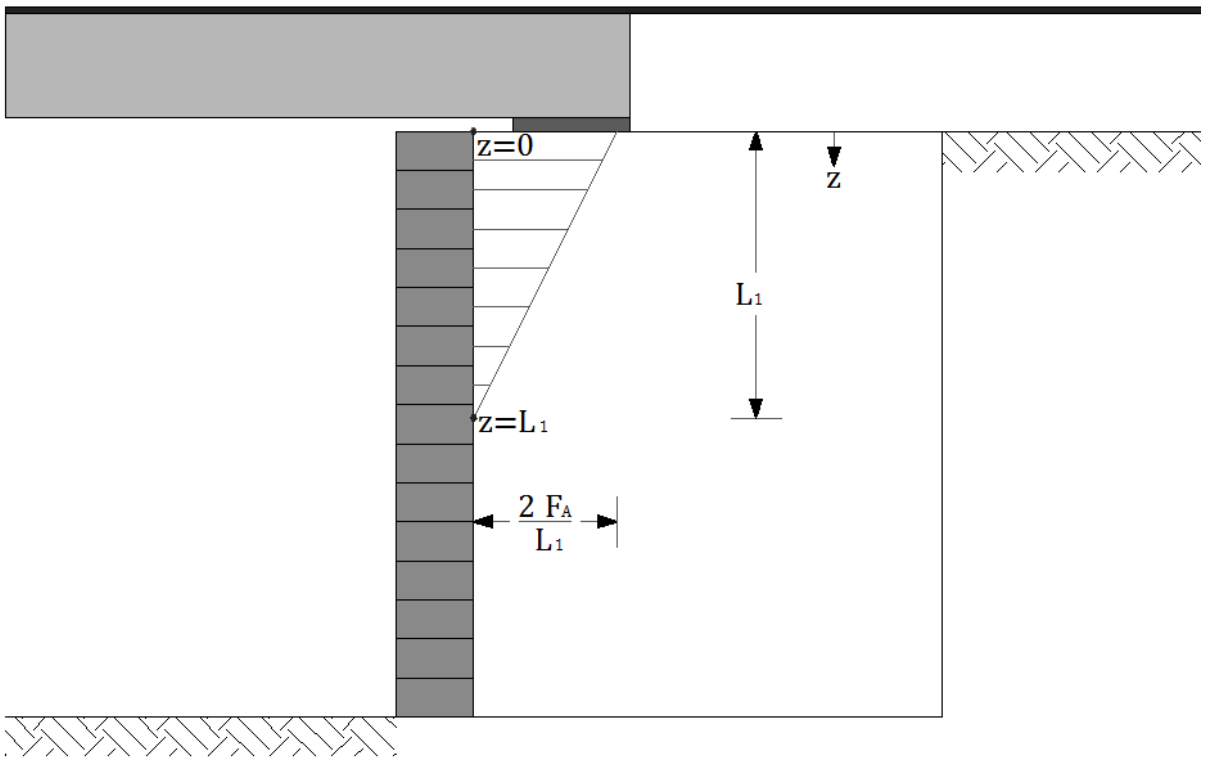

Figure 43: Distribution of Nominal Horizontal Pressure from the Upper Wall

Equation 15 (after L_1 Equation in Table E5-6.3 on Page E5-13 Berg et al 2009b)

$$\mathbf{L_1 = (\,d + (b - 2e))\,\tan\left(45 + \frac{\phi'_r}{2}\right)}$$

Where:

L_1 = Depth of influence for the lateral load acting on the base of the bearing pad

d = Clear or setback distance, this parameter was varied as part of the analysis

b = Sill width or width of the bearing pad, this parameter was varied as part of the analysis

e = eccentricity from center of bearing pad, this parameter is defined in

Equation 16

ϕ'_r = Friction angle of the reinforced fill, this parameter was varied as part of the analysis

Equation 16 (after e_f Equation in Table E5-6.3 on Page E5-13 Berg et al 2009b)

$$\mathbf{e = \frac{1}{2}\,b - a_{wl}}$$

Where:

e = eccentricity from the center of the bearing pad

b = Sill width or width of the bearing pad, this parameter was varied as part of the analysis

a_{wl} = Location of the resultant from point A, which corresponds to the location of the front edge of the footing closest to the wall face, this parameter is defined in Equation 17

Equation 17 (after a_{wl} Equation in Table E5-6.3 on Page E5-13 Berg et al 2009b)

$$\mathbf{a_{wl} = \frac{M_A}{V_{Ab}}}$$

Where:

a_{wl} = Location of the resultant from point A, which corresponds to the location of the front edge of the footing closest to the wall face

M_A = Nominal moment at point A, which corresponds to the location of the front edge of the footing closest to the wall face, this parameter is defined in Equation 18

V_{Ab} = Sum of the nominal vertical forces from the bearing pad, this parameter is defined in Equation 10

Equation 18 (developed from M_A, M_{OA}, and M_{RA} Equations in Table E5-6.3 on Page E5-13 Berg et al 2009b)

$$\mathbf{M_A = MV_1 + MDL + MLL - MF_1 - MF_{S1}}$$

Where:

M_A = Nominal moment at point A, which corresponds to the location of the front edge of the footing closest to the wall face

MV_1 = Moment due to the nominal vertical force from the weight of the footing, this parameter is defined in

Equation 19

MDL = Moment due to the nominal dead load from the bridge, this parameter is defined in Equation 20

MLL = Moment due to the nominal live load on the bridge, this parameter is defined in Equation 21

MF_1 = Moment due to the horizontal nominal earth pressure force from upper wall soil, this parameter is defined in Equation 22

MF_{S1} = Moment due to the horizontal nominal earth pressure force from traffic surcharge, this parameter is defined in Equation 23

Equation 19 (after V_1 Equation and detailed moment arm at point A in Table E5-4.1 on Page E5-8 Berg et al 2009b)

$$\mathbf{MV_1 = V_1 \left(\frac{b}{2}\right)}$$

Where:

M_A = Nominal moment at point A, which corresponds to the location of the front edge of the footing closest to the wall face

V_1 = Nominal vertical load from the weight of the bearing pad, this parameter is defined in Equation 11

b = Sill width or width of the bearing pad, this parameter was varied as part of the analysis

Equation 20 (developed from detailed moment arm at point A for DL in Table E5-4.1 on Page E5-8 and Figure E5-2 on Page E5-7 Berg et al 2009b)

$$\mathbf{MDL = DL\left(\frac{b}{2}\right)}$$

Where:

MDL = Moment due to the nominal dead load from the bridge

DL = Nominal dead load from the bridge, this parameter is defined in Equation 12

b = Sill width or width of the bearing pad, this parameter was varied as part of the analysis

Equation 21 (developed from detailed moment arm at point A for LL in Table E5-4.1 on Page E5-8 and Figure E5-2 on Page E5-7 Berg et al 2009b)

$$\mathbf{MLL = LL\left(\frac{b}{2}\right)}$$

Where:

MLL = Moment due to the nominal live load on the bridge

LL = Nominal live load on the bridge, this parameter is defined in Equation 13

b = Sill width or width of the bearing pad, this parameter was varied as part of the analysis

Equation 22 (after F_1 Equation and detailed moment arm at point A in Table E5-4.2 on Page E5-8 Berg et al 2009b)

$$\mathbf{MF_1 = F_1\left(\frac{h}{3}\right)}$$

Where:

MF_1 = Moment due to the horizontal nominal earth pressure force from upper wall soil

F_1 = Horizontal nominal earth pressure force from the upper wall soil, this parameter is defined in Equation 25

h = Height of the upper wall also known as the back wall, this parameter was varied as part of the analysis

Equation 23 (after F_{S1} Equation and detailed moment arm at point A in Table E5-4.2 on Page E5-8 Berg et al 2009b)

$$\mathbf{MF_{S1} = F_{S1}\left(\frac{h}{2}\right)}$$

Where:

MF_{S1} = Moment due to the horizontal nominal earth pressure force from traffic surcharge

F_{S1} = Horizontal nominal earth pressure force from traffic surcharge, this parameter is defined in Equation 27

h = Height of the upper wall also known as the back wall, this parameter was varied as part of the analysis

Equation 24 (after F_A Equation in Table E5-4.2 on Page E5-8 Berg et al 2009b)

$$\mathbf{F_A = F_1 + F_{S1}}$$

Where:

F_A = Sum of horizontal nominal pressures from upper wall

F_1 = Horizontal nominal earth pressure force from the upper wall soil, this parameter is defined in Equation 25

F_{S1} = Horizontal nominal earth pressure force from traffic surcharge, this parameter is defined in Equation 27

Equation 25 (after F_1 Equation in Table E5-4.2 on Page E5-8 Berg et al 2009b)

$$\mathbf{F_1 = \frac{1}{2} K_{a,u}\, \gamma_u\, h^2}$$

Where:

F_1 = Horizontal nominal earth pressure force from the upper wall soil

$K_{a,u}$ = Lateral earth pressure coefficient of the upper wall, this parameter is defined in

Equation 26

γ_u = Unit weight of the upper wall soil, a value of 120 pcf was used in the parametric analysis

h = Height of the upper wall also known as the back wall, this parameter was varied as part of the analysis

Equation 26 (after K_{a3} Equation on Page E5-6 Berg et al 2009b)

$$\mathbf{K_{a,u} = \tan^2\left(45 - \frac{\phi'_u}{2}\right)}$$

Where:

$K_{a,u}$ = Lateral earth pressure coefficient of the upper wall

ϕ'_u = Friction angle of the upper wall soil, a value of 30° was used in the parametric analysis

Equation 27 (after F_{S1} Equation in Table E5-4.2 on Page E5-8 Berg et al 2009b)

$$\mathbf{F_{S1} = K_{a,u}\, h_{eq}\, \gamma_r\, h}$$

Where:

F_{S1} = Horizontal nominal earth pressure force from traffic surcharge

$K_{a,u}$ = Lateral earth pressure coefficient of the upper wall, this parameter was defined in Equation 26

h_{eq} = Equivalent uniform soil surcharge height, a constant value of 2 ft was utilized in the parametric analysis

γ_r = Unit weight of the reinforced fill, this parameter was varied as part of the analysis

h = Height of the upper wall also known as the back wall, this parameter was varied as part of the analysis

Calculation of Factored Load in the Reinforcement, $T_{max,f}$ for Bridge Loading Condition: The parametric study calculated a series of $T_{max,f}$ values, one at each reinforcement layer depth.

Equation 28 (after Equation 4-32a Berg et al 2009a)

$$\mathbf{T_{max,f}} = \sigma_{\mathbf{h,f}}\, \mathbf{S_v}$$

Where:

$T_{max,f}$ = Maximum factored load in the reinforcement

$\sigma_{h,f}$ = Factored horizontal stress for bridge loading condition, this parameter is defined in Equation 29

S_v = Reinforcement spacing, this parameter was varied as part of the analysis

Equation 29 (after Equation 4-31 Berg et al 2009a)

$$\sigma_{\mathbf{h,f}} = \mathbf{K_r}\left(\left(\gamma_{\mathbf{r}}\left(\mathbf{z}+\mathbf{h_{eq}}\right)+\mathbf{h}\,\gamma_{\mathbf{u}}\right)\gamma_{\mathbf{EV-MAX}} + \left(\Delta\sigma_{\mathbf{v}}\right)\gamma_{\mathbf{ES-MAX}}\right) + \Delta\sigma_{\mathbf{h}}\,\gamma_{\mathbf{ES-MAX}}$$

Where:

$\sigma_{h,f}$ = Factored horizontal stress for bridge loading condition

K_r = Lateral earth pressure coefficient of the reinforced fill, this parameter is defined in Equation 3

γ_r = Unit weight of the reinforced fill, this parameter was varied as part of the analysis

z = Depth below top of reinforced zone, this parameter was varied as part of the analysis over the same range as the parameter wall height, H

h = Height of the upper wall also known as the back wall, this parameter was varied as part of the analysis

h_{eq} = Equivalent uniform soil surcharge height, a constant value of 2 ft was utilized in the parametric analysis

γ_u = Unit weight of the upper wall soil, a value of 120 pcf was used in the parametric analysis

$\gamma_{EV\text{-}MAX}$ = Load factor corresponding to a vertical pressure from a dead load earth fill, a value of 1.35 was used in the parametric analysis

$\Delta\sigma_v$ = Nominal vertical pressure at the base of the bearing pad, this parameter is defined in Equation 8

$\gamma_{ES\text{-}MAX}$ = Load factor corresponding to earth surcharge loading, a value of 1.5 was used in the parametric analysis

$\Delta\sigma_h$ = Nominal horizontal pressure from the upper wall, this parameter is defined in Equation 14

Calculation of Required Reinforcement Strength, T_{req} for Roadway Loading Condition:

The parametric study calculated a series of T_{req} values, one at each reinforcement layer depth.

Equation 30 (developed from Equation 4-33 and Equation 4-34 Berg et al 2009a and Equation 4-1 Elias et al 2009)

$$\mathbf{T_{req}} = \frac{\mathbf{T_{max,f}\ RF_{ID}\ RF_{CR}\ RF_{D}}}{\phi}$$

Where:

T_{req}= Required tensile strength

$T_{max,f}$ = Maximum factored load in the reinforcement for roadway loading condition, this parameter is defined in Equation 4

RF_{ID} = Reduction factor accounting for installation damage, this parameter was varied as part of the parametric analysis depending on reinforcement type

RF_{CR} = Reduction factor accounting for creep, this parameter was varied as part of the parametric analysis depending on reinforcement type

RF_{D} = Reduction factor accounting for degradation, this parameter was varied as part of the parametric analysis depending on reinforcement type

ϕ = Resistance factor accounting for geosynthetic reinforcement, a value of 0.9 was utilized in the parametric analysis

Calculation of Required Reinforcement Strength, T_{req} for Bridge Loading Condition:

The parametric study calculated a series of T_{req} values, one at each reinforcement layer depth.

Equation 31(developed from Equation 4-33 and Equation 4-34 Berg et al 2009a and Equation 4-1 Elias et al 2009)

$$\mathbf{T_{req}} = \frac{\mathbf{T_{max,f}\ RF_{ID}\ RF_{CR}\ RF_{D}}}{\phi}$$

Where:

T_{req}= Required tensile strength

$T_{max,f}$ = Maximum factored load in the reinforcement for bridge loading condition, this parameter is defined in Equation 28

RF_{ID} = Reduction factor accounting for installation damage, this parameter was varied as part of the parametric analysis depending on reinforcement type

RF_{CR} = Reduction factor accounting for creep, this parameter was varied as part of the parametric analysis depending on reinforcement type

RF_D = Reduction factor accounting for degradation, this parameter was varied as part of the parametric analysis depending on reinforcement type

ϕ = Resistance factor accounting for geosynthetic reinforcement, a value of 0.9 was utilized in the parametric analysis

Method 2: Simplified Procedure with K_r/K_a Adjusted: Method 2 is a proposed revision to Method 1 Mechanically Stabilized Earth Walls design guidance based on review of instrumented structures to date. Method 2 is identical to Method 1 except for the determination of the lateral earth pressure coefficient of the reinforced fill material. The following references were utilized in developing the calculation summary for Method 2. Method 2 references include methodologies for calculation of T_{max} and T_{req} for both a bridge loading and a roadway loading condition.

AASHTO (2011) "Laboratory Evaluation of Geosynthetic Reinforcement: Final Product Qualification Report for Miragrid XT Geogrid Product line." *NTPEP Report REGEO-2011-01-001*

Berg, R.R., Christopher, B.R., and Samtani, N.C. (2009a). "Design of Mechanically Stabilized Earth Walls and Reinforced Soil Slopes – Volume I." *FHWA-NHI-10-024*. National Highway Institute, Federal Highway Administration, Washington, D.C.

Berg, R.R., Christopher, B.R., and Samtani, N.C. (2009b). "Design of Mechanically Stabilized Earth Walls and Reinforced Soil Slopes – Volume II." *FHWA-NHI-10-025*. National Highway Institute, Federal Highway Administration, Washington, D.C.

DRAFT revised geosynthetic Kr/Ka relationship plot presented to AASHTO T-15 subcommittee.

Elias, V., Fishman, K.L., Christopher, B.R., and Berg, R.R. (2009). "Corrosion and Degradation of Soil Reinforcements for Mechanically Stabilized Earth Walls and Reinforced Soil Slopes." *FHWA-NHI-09-087*. National Highway Institute, Federal Highway Administration, Washington, D.C.

The parametric study calculated a series of T_{max} and $T_{max,f}$ values, one at each reinforcement layer depth, for both roadway and bridge loading conditions. Additionally T_{req} values were calculated for both loading conditions. The calculation summary for these parameters are identical to Method 1 with the exception of lateral earth pressure

coefficient, K_r. Therefore all equations from Method 1 should be utilized, except Equation 3. For Method 2, Equation 32 should be used in place of Equation 3.

Equation 32 (after Equation 4-25 of Berg et al 2009a and Figure 44)

$$\mathbf{K_r} = \left(\frac{\mathbf{K_r}}{\mathbf{K_a}}\right) \mathbf{K_a} = \left(\frac{\mathbf{K_r}}{\mathbf{K_a}}\right) \mathbf{tan^2}\left(\mathbf{45} - \frac{\phi'_{\mathbf{r}}}{\mathbf{2}}\right)$$

Where:

K_r = Lateral earth pressure coefficient of the reinforced fill

K_a = Rankine lateral earth pressure coefficient for the active condition

ϕ'_r = Friction angle of the reinforced fill, this parameter was varied as part of the analysis

K_r/K_a = ratio of lateral earth pressure coefficient, was determined based on Figure 44, the value of K_r/K_a is equal to 0.5 when $z \geq 20$ ft and $\left(\frac{0.2}{20}\right)(20 - z) + 0.5$ from $z = 0$ to 20 ft, where z is the depth below top of the reinforced zone, and z was varied as part of the analysis over the same range as the parameter wall height, H

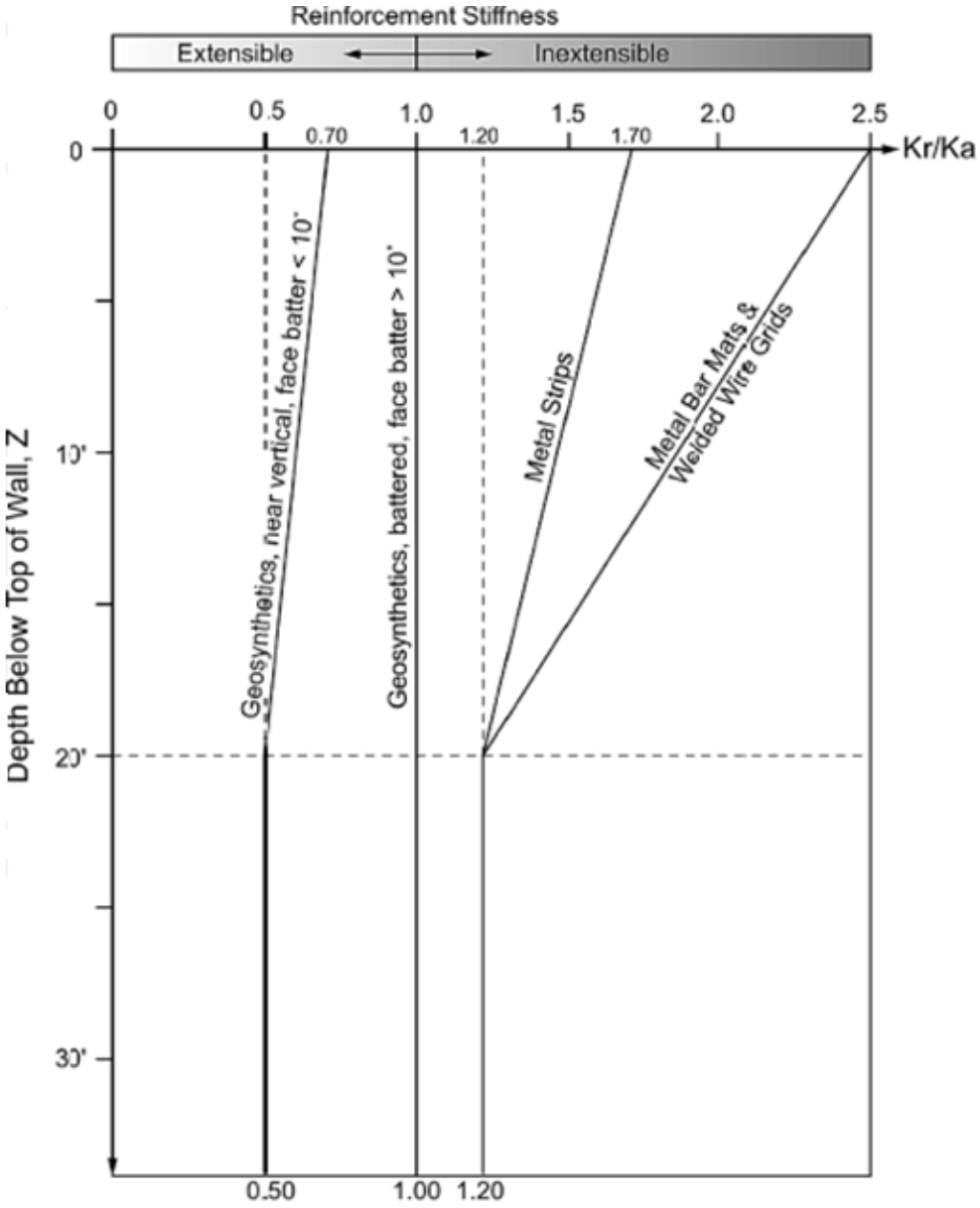

Figure 44: Revised Variation in Ratio of K_r/K_a with Reinforcement Type Berg, R. R. (2013). "Simplified Procedure with Kr/Ka Adjusted." E. K. Phillips, ed. Used under fair use, 2014.

Method 3: K-Stiffness Method: Method 3 is known as the K-stiffness method which takes into account the relative stiffness of all wall components in comparison to the soil stiffness. The design guidance for Method 3 was based on empirical case history data. The following references were utilized in developing the calculation summary for Method 3. Method 3 references include methodologies for calculation of T_{max} and T_{req} for only the roadway loading condition.

AASHTO (2011) “Laboratory Evaluation of Geosynthetic Reinforcement: Final Product Qualification Report for Miragrid XT Geogrid Product line.” *NTPEP Report REGEO-2011-01-001*

AASHTO (2011) “Laboratory Evaluation of Geosynthetic Reinforcement: Final Product Qualification Report for Tensar UX-MSE/UX-HS Geogrid Product line.” *NTPEP Report REGEO-2010-8507.4*

Allen, T. M., and Bathurst, R. J. (2003) “Prediction of Reinforcement Loads in Reinfored Soil Walls.” *WA-RD 522.2*, Washington State Department of Transportation, Seattle, WA.

Bathurst, R. J., Miyata, Y., Nernheim, A., and Allen, A. M. (2008). “Refinement of K-stiffness Method for Geosynthetic Reinforced Soil Walls.” *Geosynthetics International*, 15 (4), 269-295

Elias, V., Fishman, K.L., Christopher, B.R., and Berg, R.R. (2009). "Corrosion and Degradation of Soil Reinforcements for Mechanically Stabilized Earth Walls and Reinforced Soil Slopes." *FHWA-NHI-09-087*. National Highway Institute, Federal Highway Administration, Washington, D.C.

Washington State Department of Transportation (2012) “Geotechnical Design Manual.” *M 46-03.07*. Environmental and Engineering Programs: Geotechnical Services

Calculation of Maximum Nominal Load in the Reinforcement, T_{max} for Roadway Loading Condition: The parametric study calculated a series of T_{max} values, one at each reinforcement layer depth.

Equation 33 (after Equation 7.1 Allen and Bathurst 2003 and Equation 15-2 WSDO 2012)

$$\mathbf{T_{max} = \sigma_v K_r S_v D_{tmax} \Phi_{fb} \Phi_g \Phi_{fs} \Phi_{local} \Phi_c}$$

Where:

T_{max} = Maximum nominal load in the reinforcement

σ_v = Nominal vertical stress for roadway loading condition, this parameter is defined in Equation 34

K_r = Lateral earth pressure coefficient of the reinforced fill, this parameter is defined in Equation 35

S_v = Reinforcement spacing, this parameter was varied as part of the analysis

D_{tmax} = Empirical load distribution factor based on layer location that modifies reinforcement load, the value ranges from 0 to 1, and this parameter is defined in Equation 37

Φ_{fb} = Correction factor for wall face batter, for vertical or near vertical walls a value of 1.0 can be assumed, thus 1.0 was utilized in the parametric analysis

Φ_g = Correction factor for global stiffness, this parameter is defined in Equation 38

Φ_{fs} = Correction factor for facing stiffness, this parameter is defined in Equation 43

Φ_{local} = Correction factor for local reinforcement stiffness, this parameter is defined in Equation 46

Φ_c = Correction factor for soil backfill cohesion, the cohesion of the parametric study backfill is zero, therefore a value of 1.0 was utilized

Equation 34 (developed from Equation 7.2 Allen and Bathurst 2003, Equation 15-1 and Equation 15-2 WSDOT 2012)

$$\sigma_v = \frac{1}{2}\gamma_r\left(H + h_{eq}\right)$$

Where:

σ_h = Nominal horizontal stress for roadway loading condition

γ_r = Unit weight of the reinforced fill, this parameter was varied as part of the analysis

H = Height of the wall, this parameter was varied as part of the analysis

h_{eq} = Equivalent uniform soil surcharge height, a constant value of 2 ft was utilized in the parametric analysis

Equation 35 (after Equation 7.3 Allen and Bathurst 2003 and in text definition of K on page 15-45 WSDOT 2012)

$$K_r = K_0 = 1 - \sin\left(\phi_{ps}\right)$$

Where:

K_r = Lateral earth pressure coefficient of the reinforced fill

K_0 = Lateral earth pressure coefficient for the at-rest condition, utilized based on empirical observations not because at-rest conditions are assumed

ϕ_{ps} = Peak secant plane strain soil friction angle, this parameter is defined in Equation 36

Equation 36 (after Equation A1 Bathurst et al 2008 and Equation 15-14 WSDOT 15-14)

$$\phi_{ps} = 1.5\,\phi'_r - 17°$$

Where:

ϕ_{ps} = Peak secant plane strain soil friction angle

ϕ'_r = Friction angle of the reinforced fill, this parameter was varied as part of the analysis and is assumed to be the secant friction angle determined from a triaxial test, when $\phi'_r \leq 32°$ no adjustment is required.

Equation 37 (after in text definition of D_{tmax} on page 220 Allen and Bathurst 2003 and Figure 15-8 WSDOT 2012)

$$\mathbf{D_{tmax}} = \frac{\mathbf{1}}{\mathbf{0.4}}\left(\frac{\mathbf{z + h_{eq}}}{\mathbf{H + h_{eq}}}\right) \textbf{ when } \left(\frac{\mathbf{z + h_{eq}}}{\mathbf{H + h_{eq}}}\right) < \mathbf{0.4}$$

$$\mathbf{D_{tmax}} = \mathbf{1.0} \textbf{ when } \left(\frac{\mathbf{z + h_{eq}}}{\mathbf{H + h_{eq}}}\right) \geq \mathbf{0.4}$$

Where:

D_{tmax} = Empirical load distribution factor based on layer location that modifies reinforcement load, the value ranges from 0 to 1

z = Depth below top of reinforced zone, this parameter was varied as part of the analysis over the same range as the parameter wall height, H

h_{eq} = Equivalent uniform soil surcharge height, a constant value of 2 ft was utilized in the parametric analysis

H = Height of the wall, this parameter was varied as part of the analysis

Equation 38 (after Equation 7.6 Allen and Bathurst 2003 and Equation 15-4 WSDOT 2012)

$$\Phi_{\mathbf{g}} = \alpha\left(\frac{\mathbf{S_{global}}}{\mathbf{P_a}}\right)^{\beta}$$

Where:

Φ_g = Correction factor for global stiffness

α = Influence factor coefficient resulting from empirically fitting case history data for global stiffness, a value of 0.25 was utilized in the parametric analysis

S_{global} = Global reinforcement stiffness, this parameter is defined in Equation 39

P_a = Atmospheric pressure, a value of 2117 psf for the parametric analysis

β = Influence factor exponent resulting from empirically fitting case history data, a value of 0.25 was utilized in the parametric analysis

Equation 39 (after Equation 7.7 Allen and Bathurst 2003 after Equation 15-3 WSDOT 2012)

$$\mathbf{S_{global}} = \frac{\Sigma \mathbf{J}}{\mathbf{H}}$$

Where:

S_{global} = Global reinforcement stiffness

ΣJ = Sum of reinforcement stiffness over each reinforcement layer

H = Height of the wall, this parameter was varied as part of the analysis

Equation 40 (developed from Equation 7.7 Allen and Bathurst 2003)

$$\Sigma \mathbf{J} = \mathbf{J_{2\%,layer1}} + \mathbf{J_{2\%,layer2}} + \mathbf{J_{2\%,layer3}} + \mathbf{J_{2\%,layer4}} \cdots$$

Where:

ΣJ = Sum of reinforcement stiffness over each reinforcement layer

$J_{2\%layer,i}$ = Reinforcement stiffness at a particular reinforcement layer, a different regression relationship exists depending on which polymer type is used in the reinforcement, therefore possible parameter definitions are given by Equation 41 and Equation 42

Equation 41 (developed from creep stiffness equation on Page 6 of *NTPEP Report REGEO-2011-01-001)*

$$\mathbf{J_{2\%\ layer\ i}} = \mathbf{5.501}\ (\mathbf{T_{MARV}}) - 57.378\,\frac{\mathbf{lb}}{\mathbf{ft}}$$

Where:

$J_{2\%\ layer\ i}$ = Reinforcement stiffness at 2% for PET geogrid

T_{MARV}= The minimum average ultimate tensile strength for a grade of reinforcement, for the base case a low grade strength was assumed for a typical PET geogrid of 3,500 lb/ft

Equation 42 (developed from creep stiffness equation on Page 8 of *NTPEP Report REGEO-2010-8507.4)*

$$\mathbf{J_{2\%\ layer\ i}} = \mathbf{6.473}\ (\mathbf{T_{MARV}}) - 9172.6\,\frac{\mathbf{lb}}{\mathbf{ft}}$$

Where:

$J_{2\%\ layer\ i}$ = Reinforcement stiffness at 2% for HDPE geogrid

T_{MARV}= The minimum average ultimate tensile strength for a grade of reinforcement, for the parameter variation of reinforcement type the lowest grade strength was assumed for a typical HDPE geogrid of 4,800 lb/ft

Equation 43 (after Equation 7.15 Allen and Bathurst 2003 and Equation 15-11 WSDOT 2012)

$$\Phi_{\mathbf{fs}} = \eta(\mathbf{F_f})^{\mathbf{k}}$$

Where:

Φ_{fs} = Correction factor for facing stiffness

η = Influence factor coefficient resulting from empirically fitting case history data for facing stiffness, a value of 0.69 was utilized in the parametric analysis

F_f = Facing stiffness parameter, this parameter is defined in Equation 44

k = Influence factor exponent resulting from empirically fitting case history data for facing stiffness, a value of 0.11 was utilized in the parametric analysis

Equation 44 (after Equation 15-10 WSDOT 2012)

$$\mathbf{F_f} = \frac{\mathbf{1.5\ H^3\ P_a}}{\mathbf{E}\ \boldsymbol{b}^{\mathbf{3}} \left(\frac{\mathbf{h_{eff}}}{\mathbf{H}}\right)}$$

Where:

F_f = Facing stiffness parameter

S_v = Reinforcement spacing, this parameter was varied as part of the analysis

H = Height of the wall, this parameter was varied as part of the analysis

P_a = Atmospheric pressure, a value of 2117 psf for the parametric analysis

E = Modulus of the facing material, for dry cast concrete a value of 209,000 ksf was utilized in the parametric analysis

b = Width of the facing block, this parameter was varied as part of the analysis

h_{eff} = Facing block height, this parameter was varied as part of the analysis

Equation 45 (after Equation 7.9 Allen and Bathurst 2003 and Equation 15-5 WSDOT 2012)

$$\mathbf{S_{local}} = \frac{\mathbf{J_{2\%layer,i}}}{\mathbf{S_v}}$$

Where:

S_{local}= Local reinforcement stiffness, this parameter is calculated for each reinforcement layer and therefore varies with depth, z

$J_{2\%layer,i}$ = Reinforcement stiffness at a particular reinforcement layer, a different regression relationship exists depending on which polymer type is used in the reinforcement, therefore possible parameter definitions are given by Equation 41 and Equation 42

S_v = Reinforcement spacing, this parameter was varied as part of the analysis

Equation 46 (after Equation 15-6 WSDOT 2012)

$$\Phi_{\mathbf{local}} = \left(\frac{\mathbf{S_{local}}}{\mathbf{S_{global}}}\right)^{\mathbf{a}}$$

Where:

Φ_{local} = Correction factor for local reinforcement stiffness

a = Influence factor exponent resulting from empirically fitting case history data for local reinforcement stiffness, a value of 1.0 was utilized in the parametric analysis

S_{global} = Global reinforcement stiffness, this parameter is defined in Equation 39

S_{local}= Local reinforcement stiffness, this parameter is defined in Equation 45

Calculation of Maximum Factored Load in the Reinforcement, $T_{max,f}$ for Roadway Loading Condition: The parametric study calculated a series of $T_{max,f}$ values, one at each reinforcement layer depth.

Equation 47 (after Equation 7.1 Allen and Bathurst 2003 and Equation 15-2 WSDO 2012)

$$\mathbf{T_{max,f}} = \sigma_{\mathbf{v,f}}\,\mathbf{K_r}\,\mathbf{S_v}\,\mathbf{D_{tmax}}\,\Phi_{\mathbf{fb}}\Phi_{\mathbf{g}}\Phi_{\mathbf{fs}}\Phi_{\mathbf{local}}\,\Phi_{\mathbf{c}}$$

Where:

$T_{max,f}$ = Maximum factored load in the reinforcement

$\sigma_{v,f}$ = Factored vertical stress for roadway loading condition, this parameter is defined in Equation 48

K_r = Lateral earth pressure coefficient of the reinforced fill, this parameter is defined in Equation 35

S_v = Reinforcement spacing, this parameter was varied as part of the analysis

D_{tmax} = Empirical load distribution factor based on layer location that modifies reinforcement load, the value ranges from 0 to 1, this parameter is defined in Equation 37

Φ_{fb} = Correction factor for wall face batter, for vertical or near vertical walls a value of 1.0 can be assumed, thus 1.0 was utilized in the parametric analysis

Φ_g = Correction factor for global stiffness, this parameter is defined in Equation 38

Φ_{fs} = Correction factor for facing stiffness, this parameter is defined in Equation 43

Φ_{local} = Correction factor for local reinforcement stiffness, this parameter is defined in Equation 46

Φ_c = Correction factor for soil backfill cohesion, the cohesion of the parametric study backfill is zero, therefore a value of 1.0 was utilized

Equation 48 (developed from Equation 7.2 Allen and Bathurst 2003, Equation 15-1, Equation 15-2, and Table 15-5 WSDOT 2012)

$$\sigma_{v,f} = \frac{1}{2}\gamma_r \left(H + h_{eq}\right)\gamma_{EV-MAX}$$

Where:

$\sigma_{h,}$ = Factored horizontal stress for roadway loading condition

γ_r = Unit weight of the reinforced fill, this parameter was varied as part of the analysis

H = Height of the wall, this parameter was varied as part of the analysis

h_{eq} = Equivalent uniform soil surcharge height, a constant value of 2 ft was utilized in the parametric analysis

γ_{EV-MAX} = Load factor accounting for vertical earth pressure from a dead load fill, a value of 1.55 was utilized in the parametric analysis

Calculation of Required Reinforcement Strength, T_{req} for Roadway Loading Condition:

The parametric study calculated a series of T_{req} values, one at each reinforcement layer depth.

Equation 49 (developed from Equation 15-16 WSDOT 2012)

$$T_{req} = \frac{T_{max,f}\, RF_{ID}\, RF_{CR}\, RF_D}{\phi\, R_C}$$

Where:

T_{req}= Required tensile strength

$T_{max,f}$ = Maximum factored load in the reinforcement, this parameter is defined in Equation 47

RF_{ID} = Reduction factor accounting for installation damage, this parameter was varied as part of the parametric analysis depending on reinforcement type

RF_{CR} = Reduction factor accounting for creep, this parameter was varied as part of the parametric analysis depending on reinforcement type

RF_D = Reduction factor accounting for degradation, this parameter was varied as part of the parametric analysis depending on reinforcement type

ϕ = Resistance factor accounting for geosynthetic reinforcement, a value of 0.9 was utilized in the parametric analysis

R_C = Coverage ratio, a strip layout of geosynthetic reinforcement was not utilized for the parametric study instead full sheets of reinforcement were assumed, therefore a value of 1.0 was utilized in the parametric study

In addition to selecting a required reinforcement strength for design, a creep stiffness at 2% strain must be selected. To ensure the stiffness of the reinforcement will minimize the strain of the reinforcement in service, a strain check is imposed as shown in Equation 50.

Equation 50 (developed from Equation 15-15 WSDOT 2012)

$$\boldsymbol{\varepsilon_{targ} \geq \frac{T_{max}}{\phi_{sf}\, J_{2\%}}}$$

Where:

ε_{targ} = target reinforcement strain, a value of 2% was utilized in the parametric analysis

T_{max} = Maximum nominal load in the reinforcement, this parameter is defined in Equation 33

ϕ_{sf} = Resistance factor to account for uncertainties in the target strain, since a default value of ε_{targ} is utilized in the parametric study ϕ_{fs} was set equal to 1.0

$J_{2\%}$ = Reinforcement stiffness at 2%, shown in Equation 41 and Equation 42

For all parameter variations and base case values for Method 3, the reinforcement strain check predicted by Equation 50 was satisfied.

Calculation of Nominal Load in the Reinforcement, T_{max}, Factored Load in the Reinforcement, $T_{max,f}$,Reuired Reinforcement Strength, T_{req}, for Bridge Loading Condition: T_{max}, $T_{max,f}$, and T_{req} values were not calculated for Method 4 because no guidance was provided for this parameter. At this time, the K-Stiffness method is not recommended to be used for wall designs which directly support another structure, such as a bridge abutment.

Method 4: NCHPR GRS Method: Method 4 is a GRS abutment design method for systems with flexible facing. The guidance was the first to utilize closer reinforcement spacing characterized by GRS systems. Method 4 is a revision to an earlier publication of Method 1 prior to the inclusion of LRFD. The following references were utilized in

developing the calculation summary for Method 4. Method 4 references include methodologies for calculation of T_{max} and T_{req}.

Berg, R.R., Christopher, B.R., and Samtani, N.C. (2009a). "Design of Mechanically Stabilized Earth Walls and Reinforced Soil Slopes – Volume I." *FHWA-NHI-10-024*. National Highway Institute, Federal Highway Administration, Washington, D.C.

Berg, R.R., Christopher, B.R., and Samtani, N.C. (2009b). "Design of Mechanically Stabilized Earth Walls and Reinforced Soil Slopes – Volume II." *FHWA-NHI-10-025*. National Highway Institute, Federal Highway Administration, Washington, D.C.

Wu, J.T.H., Lee, K.Z.Z., Helwany, S.M.B., and Ketchart, K. (2006a). "Design and Construction Guidelines for GRS Bridge Abutment with a Flexible Facing." *Report No. 556*. National Cooperative Highway Research Program, Washington, D.C.

Calculation of Nominal Load in the Reinforcement, T_{max} for Roadway Loading Condition: The parametric study calculated a series of T_{max} values, one at each reinforcement layer depth. Method 4 references do not specifically address a roadway loading condition. However, Method 4 equations can be adapted for the imposed roadway loading conditions, resulting in a nominal tensile load identical to Method 1. Therefore, the calculation summary for this parameter is identical to Method 1. For the parametric study the T_{max} parameter was defined using Equation 1.

Calculation of Maximum Factored Load in the Reinforcement, $T_{max,f}$ for Roadway Loading Condition: $T_{max,f}$ values were not calculated for Method 4 because no guidance was provided for this parameter.

Calculation of Nominal Load in the Reinforcement, T_{max} for Bridge Loading Condition: The parametric study calculated a series of T_{max} values, one at each reinforcement layer depth.

Equation 51 (after T_{max} Equation on page 118 Wu et al 2006a)

$$\mathbf{T_{max}} = \sigma_{\mathbf{h}}\, \mathbf{S_v}$$

Where:

T_{max} = Maximum nominal load in the reinforcement

σ_h = Nominal horizontal stress, this parameter is defined in Equation 52

S_v = Reinforcement spacing, this parameter was varied as part of the analysis

Equation 52 (after σ_h Equation on page 118 Wu et al 2006a)

$$\sigma_{\mathbf{h}} = \mathbf{K_r}\left(\gamma_{\mathbf{r}}\left(\mathbf{z} + \mathbf{h_{eq}}\right) + \mathbf{h}\,\gamma_{\mathbf{u}} + \Delta\sigma_{\mathbf{v}}\right) + \Delta\sigma_{\mathbf{h}}$$

Where:

σ_h = Nominal horizontal stress

K_r = Lateral earth pressure coefficient of the reinforced fill, this parameter is defined in Equation 53

γ_r = Unit weight of the reinforced fill, this parameter was varied as part of the analysis

z = Depth below top of reinforced zone, this parameter was varied as part of the analysis over the same range as the parameter wall height, H

h_{eq} = Equivalent uniform soil surcharge height, a constant value of 2 ft was utilized in the parametric analysis

h = Height of the upper wall also known as the back wall, this parameter was varied as part of the analysis

γ_u = Unit weight of the upper wall soil, a value of 120 pcf was used in the parametric analysis

$\Delta\sigma_h$ = Nominal horizontal pressure from upper wall, parameter is defined in Equation 14

Equation 53 (after $K_{a(rf)}$ Equation on page 115 Wu et al 2006a)

$$\mathbf{K_r = K_a = \tan^2\left(45 - \frac{\phi'_r}{2}\right)}$$

Where:

K_r = Lateral earth pressure coefficient of the reinforced fill

K_a = Rankine lateral earth pressure coefficient for the active condition

Unlike Method 1, which uses the Simplified Method for correlating a lateral earth pressure coefficient ratio, Method 4 assumes $K_r = K_a$. Figure 42 was not referenced in Method 4 guidance.

Equation 54 (after $\Delta\sigma_v$ Equation on page 118 Wu et al 2006a)

$$\Delta\sigma_v = \frac{V_{Ab}}{D}$$

Where:

$\Delta\sigma_v$ = Nominal vertical pressure at the base of the bearing pad

V_{Ab} = Sum of the nominal vertical forces from the bearing pad, this parameter is defined in Equation 10

D = Effective width of applied bridge load at depth, parameter is defined in Equation 55

Equation 55 (after D Equation on page 118 Wu et al 2006a)

$$\mathbf{D = (b - 2e) + z \quad when \quad z \leq 2d}$$

$$\mathbf{D = d + (b - 2e) + \frac{z}{2} \quad when \quad z > 2d}$$

Where:

D = Effective width of applied bridge load at depth

b = Sill width or width of the bearing pad, this parameter was varied as part of the analysis

e = eccentricity from the center of bearing pad, this parameter is defined in

Equation 16

z = Depth below top of reinforced zone, this parameter was varied as part of the analysis over the same range as the parameter wall height, H

d = Clear or setback distance, this parameter was varied as part of the analysis

Calculation of Factored Load in the Reinforcement, $T_{max,f}$ for Bridge Loading Condition: $T_{max,f}$ values were not calculated for Method 4 because no guidance was provided for this parameter.

Calculation of Required Reinforcement Strength, T_{req} for Roadway Loading Condition: The parametric study calculated a single T_{req} value that represents the required reinforcement strength at every reinforcement layer.

Equation 56 (developed from T_{ult} Equation on page 110 Wu et al 2006a)

$$\mathbf{T_{req} = T_{@\varepsilon=1\%}\, FS}$$

Where:

T_{req}= Required tensile strength

$T_{@\varepsilon=1\%}$= Minimum reinforcement stiffness, this parameter is defined in Equation 57

FS = Factor of safety accounting for reinforcement, FS=5.5 for S_v < 16 inches, FS=3.5 for $S_v \geq 16$ inches.

Equation 57 (developed from $T_{@\varepsilon=1\ percent}$ Equation on page 110 Wu et al 2006a)

$$\mathbf{T_{@\varepsilon=1\%} = \sigma_{h,max}\, S_v}$$

Where:

$T_{@\varepsilon=1\%}$= Minimum reinforcement stiffness

$\sigma_{h,max}$ = Nominal maximum horizontal stress for roadway loading condition, this parameter is the highest σ_h value found using Equation 2 as z is varied

S_v = Reinforcement spacing, this parameter was varied as part of the analysis

Calculation of Required Reinforcement Strength, T_{req} for Bridge Loading Condition: The parametric study calculated a single T_{req} value that represents the required reinforcement strength at every reinforcement layer.

Equation 58 (developed from T_{ult} Equation on page 110 Wu et al 2006a)

$$\mathbf{T_{req} = T_{@\varepsilon=1\%}\, FS}$$

Where:

T_{req}= Required tensile strength

$T_{@\varepsilon=1\%}$= Minimum reinforcement stiffness, this parameter is defined in Equation 59

FS = Factor of safety accounting for reinforcement, FS=5.5 for S_v < 16 inches, FS=3.5 for Sv $\geq$ 16 inches.

Equation 59 (developed from T_{ult} Equation on page 110 Wu et al 2006a)

$$\mathbf{T_{@\varepsilon=1\%} = \sigma_{h,max} S_v}$$

Where:

$T_{@\varepsilon=1\%}$= Minimum reinforcement stiffness

$\sigma_{h,max}$ = Nominal maximum horizontal stress for bridge loading condition, this parameter is the highest σ_h value found using Equation 52

S_v = Reinforcement spacing, this parameter was varied as part of the analysis

Method 5: FHWA GRS-IBS Method: Method 5 is the current state of practice design method for GRS integrated bridge abutments (GRS-IBS). The guidance was the first to utilize the term GRS-IBS, and it includes provisions for LRFD. The following references were utilized in developing the calculation summary for Method 5. Method 5 references include methodologies for calculation of T_{max} and T_{req}.

Adams, M., Nicks, J., Stabile, T., Wu, J.T.H., Schlatter, W., and Hartmann, J. (2011a). "Geosynthetic Reinforced Soil Integrated Bridge System—Interim Implementation Guide." *FHWA-HRT-11-026*. Federal Highway Administration, McLean, VA.

Adams, M., Nicks, J., Stabile, T., Wu, J.T.H., Schlatter, W., and Hartmann, J. (2011b). "Geosynthetic Reinforced Soil Integrated Bridge System—Synthesis Report." *FHWA-HRT-11-027*. Federal Highway Administration, McLean, VA.

AASHTO (2011) "Laboratory Evaluation of Geosynthetic Reinforcement: Final Product Qualification Report for Miragrid XT Geogrid Product line." *NTPEP Report REGEO-2011-01-001*

AASHTO (2011) "Laboratory Evaluation of Geosynthetic Reinforcement: Final Product Qualification Report for Tensar UX-MSE/UX-HS Geogrid Product line." *NTPEP Report REGEO-2010-8507.4*

Calculation of Maximum Nominal Load in the Reinforcement, T_{max} for Roadway Loading Condition: The parametric study calculated a series of T_{max} values, one at each reinforcement layer depth.

Equation 60 (after Equation 31 Adams et al 2011a)

$$\mathbf{T_{max} = \left(\frac{\sigma_h}{0.7^{\left(\frac{S_v}{6\, d_{max}}\right)}} \right) S_v}$$

Where:

T_{max} = Maximum Nominal load in the reinforcement

σ_h = Nominal horizontal stress for roadway loading condition, this parameter is defined in Equation 2, except that Equation 53 should be used for K_r instead of Equation 3

S_v = Reinforcement spacing, this parameter was varied as part of the analysis

d_{max} = Maximum particle diameter, this parameter was varied as part of the analysis

Calculation of Maximum Factored Load in the Reinforcement, $T_{max,f}$ for Roadway Loading Condition: The parametric study calculated a series of $T_{max,f}$ values, one at each reinforcement layer depth.

Equation 61 (after Equation 84 Adams et al 2011a)

$$\mathbf{T_{max,f}} = \left(\frac{\sigma_{\mathbf{h,f}}}{\mathbf{0.7}^{\left(\frac{S_v}{6\, d_{max}}\right)}} \right) \mathbf{S_v}$$

Where:

$T_{max,f}$ = Maximum factored load in the reinforcement

$\sigma_{h,f}$ = Factored horizontal stress for roadway loading condition, this parameter is defined in Equation 62, except that Equation 53 should be used for K_r instead of Equation 3

S_v = Reinforcement spacing, this parameter was varied as part of the analysis

d_{max} = Maximum particle diameter, this parameter was varied as part of the analysis

Equation 62 (developed from Equation 86 Adams et al 2011a)

$$\sigma_{\mathbf{h,f}} = \mathbf{K_r} \left(\gamma_{\mathbf{r}}\, \mathbf{z}\, \gamma_{\mathbf{EH-MAX}} + \mathbf{h_{eq}} \gamma_{\mathbf{r}}\, \gamma_{\mathbf{LS}} \right)$$

Where:

$\sigma_{h,f}$ = Factored horizontal stress for roadway loading condition

K_r = Lateral earth pressure coefficient of the reinforced fill, this parameter is defined in Equation 53

γ_r = Unit weight of the reinforced fill, this parameter was varied as part of the analysis

z = Depth below top of reinforced zone, this parameter was varied as part of the analysis over the same range as the parameter wall height, H

$\gamma_{EH\text{-}MAX}$ = Load factor accounting for horizontal earth pressure in the active condition, a value of 1.5 was used in the parametric analysis

h_{eq} = Equivalent uniform soil surcharge height, a constant value of 2 ft was utilized in the parametric analysis

γ_{LS} = Load factor corresponding to live load surcharge, a value of 1.75 was used in the parametric analysis

Calculation of Nominal Load in the Reinforcement, T_{max} for Bridge Loading Condition:

The parametric study calculated a series of T_{max} values, one at each reinforcement layer depth.

Equation 63 (after Equation 31 Adams et al 2011a)

$$\mathbf{T_{max}} = \left(\frac{\sigma_h}{\mathbf{0.7}^{\left(\frac{S_v}{6\, d_{max}}\right)}} \right) \mathbf{S_v}$$

Where:

T_{max} = Maximum Nominal load in the reinforcement

σ_h = Nominal horizontal stress for bridge loading condition, this parameter is defined in Equation 64

S_v = Reinforcement spacing, this parameter was varied as part of the analysis

d_{max} = Maximum particle diameter, this parameter was varied as part of the analysis

Equation 64 (developed from Equation 32, 2, 34, and 35 Adams et al 2011a)

$$\sigma_h = \mathbf{K_r}\left(\gamma_r \mathbf{z} + \mathbf{h_{eq}}\gamma_r + \mathbf{h}\,\gamma_u\right) + \sigma_{h,bridge,eq}$$

Where:

σ_h = Nominal horizontal stress for bridge loading condition

K_r = Lateral earth pressure coefficient of the reinforced fill, this parameter is defined in Equation 53

γ_r = Unit weight of the reinforced fill, this parameter was varied as part of the analysis

z = Depth below top of reinforced zone, this parameter was varied as part of the analysis over the same range as the parameter wall height, H

h_{eq} = Equivalent uniform soil surcharge height, a constant value of 2 ft was utilized in the parametric analysis

h = Height of the upper wall also known as the back wall, this parameter was varied as part of the analysis

γ_u = Unit weight of the upper wall soil, a value of 120 pcf was used in the parametric analysis

$\sigma_{h,bridge,eq}$ = Nominal lateral earth pressure from equivalent bridge load, this parameter is defined in Equation 65

Equation 65 (after Equation 33, Adams et al 2011a)

$$\sigma_{h,bridge,eq} = \mathbf{K_r}\left(\frac{(\mathbf{q_b} + \mathbf{q_{LL}}) - \left(\mathbf{h}\,\gamma_u + \mathbf{h_{eq}}\gamma_r\right)}{\pi}\right)\left(\alpha_b + \mathbf{sin}(\alpha_b)\mathbf{cos}\left(\alpha_b + \mathbf{2}\beta_b\right)\right)$$

Where:

$\sigma_{h,bridge,eq}$ = Lateral earth pressure from equivalent bridge load

K_r = Lateral earth pressure coefficient of the reinforced fill, this parameter is defined in Equation 53

q_b = Nominal dead load pressure from the bridge

q_{LL} = Nominal live load pressure on the bridge

h = Height of the upper wall also known as the back wall, this parameter was varied as part of the analysis

γ_u = Unit weight of the upper wall soil, a value of 120 pcf was used in the parametric analysis

h_{eq} = Equivalent uniform soil surcharge height, a constant value of 2 ft was utilized in the parametric analysis

γ_r = Unit weight of the reinforced fill, this parameter was varied as part of the analysis

α_b = Angle for calculation of pressure distribution from bridge load, this parameter is defined in Equation 67

β_b = Angle for calculation of pressure distribution from bridge load, this parameter is defined in Equation 66

Equation 66 (after Equation 92 Adams et al 2011a)

$$\beta_b = \tan^{-1}\left(\frac{-b}{2\,z}\right)$$

Where:

β_b = Angle for calculation of pressure distribution from bridge load

b = Sill width or width of the bearing pad, this parameter was varied as part of the analysis

z = Depth below top of reinforced zone, this parameter was varied as part of the analysis over the same range as the parameter wall height, H

Equation 67 (after Equation 91 Adams et al 2011a)

$$\alpha_b = \tan^{-1}\left(\frac{b}{2\,z}\right) - \beta_b$$

Where:

α_b = Angle for calculation of pressure distribution from bridge load

b = Sill width or width of the bearing pad, this parameter was varied as part of the analysis

z = Depth below top of reinforced zone, this parameter was varied as part of the analysis over the same range as the parameter wall height, H

β_b = Angle for calculation of pressure distribution from bridge load, this parameter is defined in Equation 66

Calculation of Factored Load in the Reinforcement, $T_{max,f}$ for Bridge Loading Condition: The parametric study calculated a series of $T_{max,f}$ values, one at each reinforcement layer depth.

Equation 68 (after Equation 84 Adams et al 2011a)

$$\mathbf{T_{max,f}} = \left(\frac{\sigma_{\mathbf{h,f}}}{\mathbf{0.7}\left(\frac{S_v}{6\, d_{max}}\right)} \right) \mathbf{S_v}$$

Where:

$T_{max,f}$ = Maximum factored load in the reinforcement

$\sigma_{h,f}$ = Factored horizontal stress for bridge loading condition, this parameter is defined in Equation 69

S_v = Reinforcement spacing, this parameter was varied as part of the analysis

d_{max} = Maximum particle diameter, this parameter was varied as part of the analysis

Equation 69 (developed from Equation 86, 87, 89, and 90 Adams et al 2011a)

$$\sigma_{\mathbf{h,f}} = \mathbf{K_r}\left(\gamma_{\mathbf{r}}\, \mathbf{z}\, \gamma_{\mathbf{EH-MAX}} + \mathbf{h_{eq}}\gamma_{\mathbf{r}}\, \gamma_{\mathbf{LS}} + \mathbf{h}\, \gamma_{\mathbf{u}}\gamma_{\mathbf{ES-MAX}}\right) + \sigma_{\mathbf{h,bridge,eq,f}}$$

Where:

$\sigma_{h,f}$ = Factored horizontal stress for bridge loading condition

K_r = Lateral earth pressure coefficient of the reinforced fill, this parameter is defined in Equation 53

γ_r = Unit weight of the reinforced fill, this parameter was varied as part of the analysis

z = Depth below top of reinforced zone, this parameter was varied as part of the analysis over the same range as the parameter wall height, H

$\gamma_{EH\text{-}MAX}$ = Load factor accounting for horizontal earth pressure in the active condition, a value of 1.5 was used in the parametric analysis

h_{eq} = Equivalent uniform soil surcharge height, a constant value of 2 ft was utilized in the parametric analysis

γ_{LS} = Load factor corresponding to live load surcharge, a value of 1.75 was used in the parametric analysis

h = Height of the upper wall also known as the back wall, this parameter was varied as part of the analysis

γ_u = Unit weight of the upper wall soil, a value of 120 pcf was used in the parametric analysis

$\gamma_{ES\text{-}MAX}$ = Load factor corresponding to earth surcharge loading, a value of 1.5 was used in the parametric analysis

$\sigma_{h,bridge,eq}$ = Nominal lateral earth pressure from equivalent bridge load, this parameter is defined in Equation 70

Equation 70 (after Equation 88 Adams et al 2011a)

$$\sigma_{\mathbf{h,bridge,eq,f}} = \mathbf{K_r}\left(\frac{\left(\gamma_{\mathbf{DC-MAX}}\mathbf{q_b} + \gamma_{\mathbf{LL}}\mathbf{q_{LL}}\right) - \left(\gamma_{\mathbf{ES-MAX}}\mathbf{h}\,\gamma_{\mathbf{u}} + \gamma_{\mathbf{LS}}\mathbf{h_{eq}}\gamma_{\mathbf{r}}\right)}{\pi}\right)\left(\alpha_{\mathbf{b}} + \mathbf{sin}(\alpha_{\mathbf{b}})\mathbf{cos}\left(\alpha_{\mathbf{b}} + \mathbf{2}\beta_{\mathbf{b}}\right)\right)$$

Where:

$\sigma_{h,bridge,eq,f}$ = Factored lateral earth pressure from equivalent bridge load

K_r = Lateral earth pressure coefficient of the reinforced fill, this parameter is defined in Equation 53

$\gamma_{DC\text{-}MAX}$ = Load factor accounting for components and attachments, a value of 1.25 was used in the parametric analysis

q_b = Nominal dead load pressure from the bridge

γ_{LL} = Load factor accounting for live load, a value of 1.75 was used in the parametric analysis

q_{LL} = Nominal live load pressure on the bridge

$\gamma_{ES\text{-}MAX}$ = Load factor corresponding to earth surcharge loading, a value of 1.5 was used in the parametric analysis

h = Height of the upper wall also known as the back wall, this parameter was varied as part of the analysis

γ_u = Unit weight of the upper wall soil, a value of 120 pcf was used in the parametric analysis

γ_{LS} = Load factor corresponding to live load surcharge, a value of 1.75 was used in the parametric analysis

h_{eq} = Equivalent uniform soil surcharge height, a constant value of 2 ft was utilized in the parametric analysis

γ_r = Unit weight of the reinforced fill, this parameter was varied as part of the analysis

α_b = Adjustment parameter for location of bridge pressure acting on the sill, this parameter is defined in Equation 67

β_b = Adjustment parameter for location of bridge pressure acting on the sill, this parameter is defined in Equation 66

Calculation of Required Reinforcement Strength, T_{req} for Roadway Loading Condition:

Method 5 methodology dictates a series of three requirements that must be checked before an engineer can select the necessary required ultimate reinforcement strength. The required reinforcement strength that an engineer should select at a given reinforcement

layer is the highest value predicted by these three relationships. The relationships used to predict T_{req} are shown in Equation 71, Equation 72, Equation 73, Equation 74, and Equation 75.

The parametric study calculated a series of T_{req} values, one at each reinforcement layer depth based on what developers refer to as the "Analytical Method" presented in Method 5 references. The "Analytical Method" utilizes the factored form of the T_{max} relationship. The T_{max} relationship was developed from finite element analyses and soil-geosynthetic testing results.

Equation 71 (developed from Equation 93 Adams et al 2011a)

$$\mathbf{T_{req}} = \frac{\mathbf{T_{max,f}}}{\phi}$$

Where:

T_{req}= Required tensile strength from the analytic method

$T_{max,f}$ = Maximum factored load in the reinforcement, this parameter is defined in Equation 61

ϕ = Resistance factor accounting for geosynthetic reinforcement, a value of 0.4 was utilized in the parametric analysis

The parametric study calculated a series of T_{req} values, one at each reinforcement layer depth based on an additional check required in Method 5 references. The additional check is meant to capture the effects of differing load deformation characteristics of geosynthetic reinforcements using particular polymer types. The check requires the comparison of the maximum nominal tensile reinforcement load, T_{max}, to the tensile strength at 2% strain for a particular reinforcement. To more clearly compare results, the nominal tensile strength at 2% strain is converted to an equivalent ultimate T_{req} value through a ratio. For a variety of reinforcement types, the ratio of ultimate strength to tensile strength at 2% strain was found. This numeric value is then multiplied by T_{max} to compute an equivalent T_{req}. This T_{req} value is presented below for various reinforcements compared in the parametric analysis.

Equation 72 (developed from end of section C.2.2.3 text Adams et al 2011a and NTPEP Report REGEO-2011-01-001, AASHTO 2011)

$$\mathbf{T_{req}} = \mathbf{T_{max}}\ \mathbf{4.792}$$

Where:

T_{req}= Required tensile strength that is equivalent to the tensile strength at 2% strain for PET geogrid

T_{max} = Maximum factored load in the reinforcement, this parameter is defined in Equation 60

Equation 73 (developed from end of section C.2.2.3 text Adams et al 2011a and NTPEP Report REGEO-2010-8507.4, AASHTO 2011)

$$\mathbf{T_{req}} = \mathbf{T_{max}}\ \mathbf{3.689}$$

Where:

T_{req}= Required tensile strength that is equivalent to the tensile strength at 2% strain for HDPE geogrid

T_{max} = Maximum factored load in the reinforcement, this parameter is defined in Equation 60

Equation 74 (developed from end of section C.2.2.3 text Adams et al 2011a and Mirafi Product Testing Data)

$$\mathbf{T_{req} = T_{max}\ 5.420}$$

Where:

T_{req}= Required tensile strength that is equivalent to the tensile strength at 2% strain for PP geotextile

T_{max} = Maximum factored load in the reinforcement, this parameter is defined in Equation 60

The parametric study plotted a series of T_{req} values, one at each reinforcement layer depth based on an additional requirement of the ultimate required reinforcement tensile strength being a least equal to or above 4,800 lb/ft.

Equation 75 (developed from end of section C.2.2.3 text Adams et al 2011a and NTPEP Report REGEO-2010-8507.4, AASHTO 2011)

$$\mathbf{T_{req} = 4{,}800\ \frac{lb}{ft}}$$

Where:

T_{req}= Required tensile strength of 4,800 lb/ft, an additional requirement for ultimate tensile strength

Calculation of Required Reinforcement Strength, T_{req} for Bridge Loading Condition:

Method 5 methodology dictates a series of three requirements that must be checked before an engineer can select the necessary required ultimate reinforcement strength. The required reinforcement strength that an engineer should select at a given reinforcement layer is the highest value predicted by these three relationships. The relationships used to predict T_{req} are shown in The parametric study calculated a series of T_{req} values, one at each reinforcement layer depth based on what developers refer to as the "Analytical Method" presented in Method 5 references. The "Analytical Method" utilizes the factored form of the T_{max} relationship. The T_{max} relationship was developed from finite element analyses and soil-geosynthetic testing results.

Equation 76, Equation 77, Equation 78, and Equation 79.

The parametric study calculated a series of T_{req} values, one at each reinforcement layer depth based on what developers refer to as the "Analytical Method" presented in Method 5 references. The "Analytical Method" utilizes the factored form of the T_{max} relationship. The T_{max} relationship was developed from finite element analyses and soil-geosynthetic testing results.

Equation 76 (developed from Equation 93 Adams et al 2011a)

$$\mathbf{T_{req}} = \frac{\mathbf{T_{max,f}}}{\phi}$$

Where:

T_{req}= Required tensile strength

$T_{max,f}$ = Maximum factored load in the reinforcement, this parameter is defined in Equation 68

ϕ = Resistance factor accounting for geosynthetic reinforcement, a value of 0.4 was utilized in the parametric analysis

The parametric study calculated a series of T_{req} values, one at each reinforcement layer depth based on an additional check required in Method 5 references. The additional check is meant to capture the effects of differing load deformation characteristics of geosynthetic reinforcements using particular polymer types. The check requires the comparison of the maximum nominal tensile reinforcement load, T_{max}, to the tensile strength at 2% strain for a particular reinforcement. To more clearly compare results, the nominal tensile strength at 2% strain is converted to an equivalent ultimate T_{req} value through a ratio. For a variety of reinforcement types, the ratio of ultimate strength to tensile strength at 2% strain was found. This numeric value is then multiplied by T_{max} to compute an equivalent T_{req}. This T_{req} value is presented below for various reinforcements compared in the parametric analysis.

Equation 77 (developed from end of section C.2.2.3 text Adams et al 2011a and NTPEP Report REGEO-2011-01-001, AASHTO 2011)

$$\mathbf{T_{req}} = \mathbf{T_{max}}\ \mathbf{4.792}$$

Where:

T_{req}= Required tensile strength that is equivalent to the tensile strength at 2% strain for PET geogrid

T_{max} = Maximum factored load in the reinforcement, this parameter is defined in Equation 63

Equation 78 (developed from end of section C.2.2.3 text Adams et al 2011a and NTPEP Report REGEO-2010-8507.4, AASHTO 2011)

$$\mathbf{T_{req}} = \mathbf{T_{max}}\ \mathbf{3.689}$$

Where:

T_{req}= Required tensile strength that is equivalent to the tensile strength at 2% strain for HDPE geogrid

T_{max} = Maximum factored load in the reinforcement, this parameter is defined in Equation 63

Equation 79 (developed from end of section C.2.2.3 text Adams et al 2011a and Mirafi Product Testing Data)

$$\mathbf{T_{req} = T_{max}\ 5.420}$$

Where:

T_{req}= Required tensile strength that is equivalent to the tensile strength at 2% strain for PP geotextile

T_{max} = Maximum factored load in the reinforcement, this parameter is defined in Equation 63

In addition to the required ultimate tensile strength presented in The parametric study calculated a series of T_{req} values, one at each reinforcement layer depth based on what developers refer to as the "Analytical Method" presented in Method 5 references. The "Analytical Method" utilizes the factored form of the T_{max} relationship. The T_{max} relationship was developed from finite element analyses and soil-geosynthetic testing results.

Equation 76, Equation 77, Equation 78, and Equation 79 the additional check presented in Equation 75 is also applicable for the bridge loading condition.

3.6 PARAMETRIC STUDY RESULTS

First, the required tensile strength predicted by each method for the base case set of parameters is detailed. Then the results of varying individual parameters are presented, each in a separate section. If a method did not include a parameter in the governing equations, then that method is not included in the section. Furthermore, each section is divided into subsections based on the loading case. Therefore each parameter varied in the study will be assessed and summarized for both the roadway loading and bridge loading scenarios.

Predicted Tensile Values for Base Case Parameters: The required ultimate tensile strength, T_{req}, and the maximum nominal load in the reinforcement, T_{max}, predicted by each of the five methods for both loading conditions are presented in this section. Results are detailed graphically by plotting T_{max} and T_{req} with depth below the wall. Base case values are outlined in Table 2 and Table 3.

Roadway Loading: All methods predicted a T_{max} and T_{req} for the roadway loading condition. The variations in predicted values between methods are shown in Figure 45 and Figure 46.

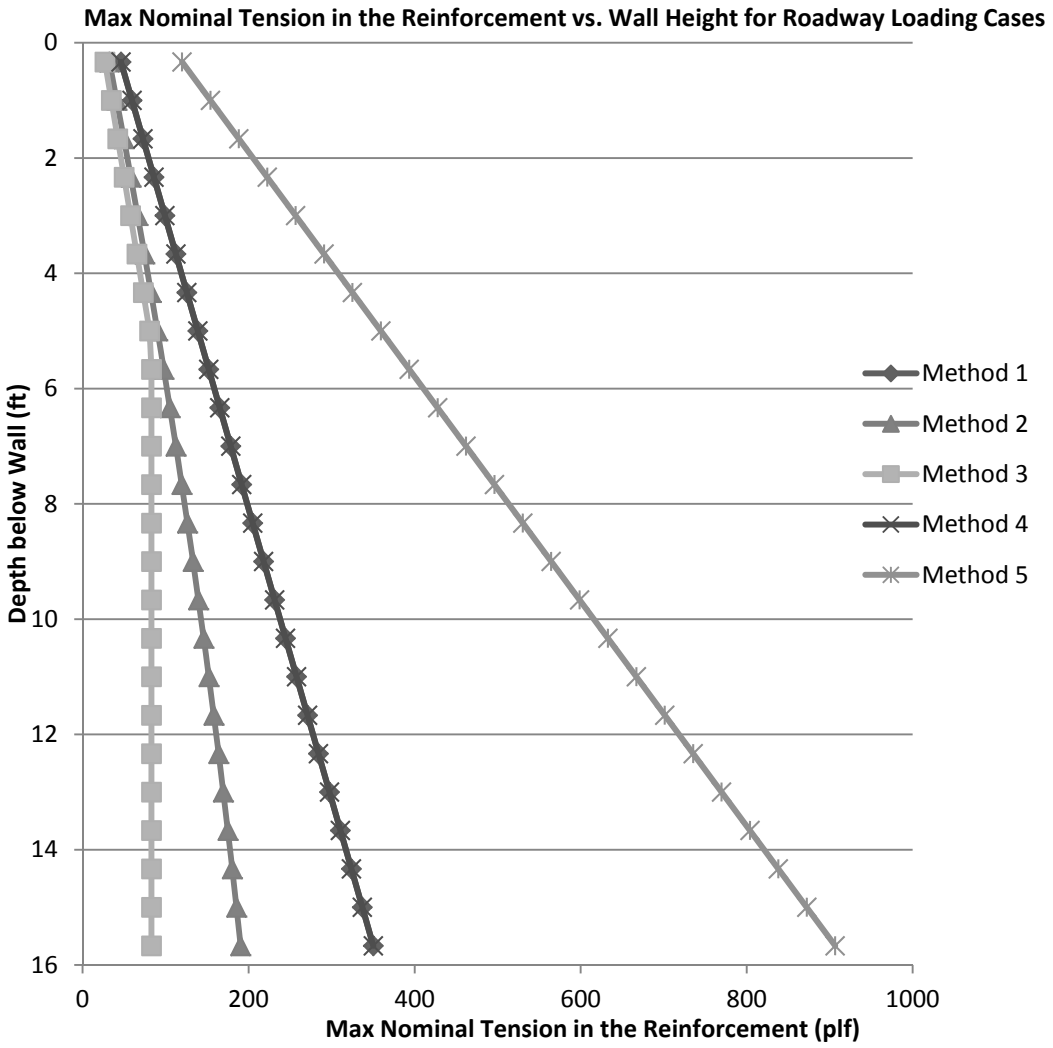

Figure 45: Base Case Roadway Loading Comparison of T_{max} for All Five Methods

Figure 45 shows that the predicted T_{max} values are identical for Methods 1 and 4. Method 3 predicts the lowest variation of T_{max} and Method 5 the highest. Due to the influence of the load distribution factor, Method 3 does not have the standard linear distribution of tensile load with depth predicted by the other methods. Method 2 has a nearly linear distribution that is the result of the variation in the ratio of K_r/K_a with depth and based on reinforcement type. Method 5 utilizes a different reinforced soil theory than the other Methods. Method 5 was developed for GRS-IBS or bridge loading conditions. It was adapted for the roadway loading condition in this study. Method 2 governing equations are identical to Method 1 with the exception of how to calculate the reinforced fill lateral earth pressure coefficient, K_r. As a consequence, Method 2 predicted T_{max} values that are lower than Method 1.

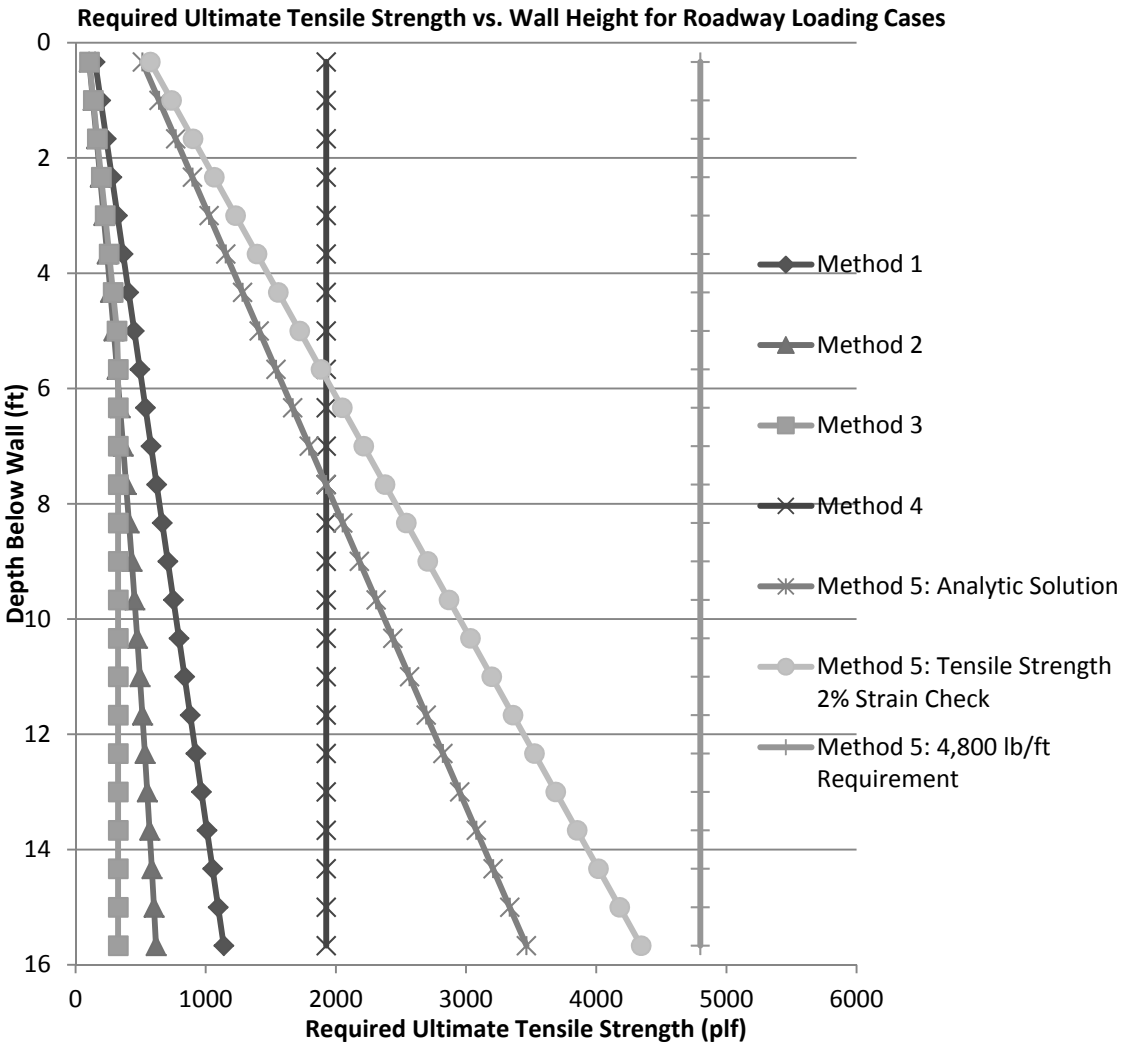

Figure 46: Base Case Roadway Loading Comparison of T_{req} for All Applicable Methods

Figure 46 shows that Method 4 selects a single ultimate T_{req} value for the entire soil profile behind the wall. Additionally, Method 5 has a requirement that if the predicted required reinforcement ultimate strength, T_{req}, is less than 4,800 lb/ft then reinforcement with at least 4,800 lb/ft of ultimate tensile strength should be used. This requirement plots as a straight line in Figure 46 and is the highest predicted value on the plot. Due to the influence of the load distribution factor, Method 3 does not have the standard linear distribution of tensile load with depth predicted by the other methods. Method 2 has a nearly linear distribution that is the result of the variation in the ratio of K_r/K_a with depth and based on reinforcement type. For the base case geosynthetic material, PET geogrid, the tensile strength at 2% strain equivalent T_{req} value predicted by Method 5 is higher at all reinforcement layers than the analytic T_{req} value predicted by Method 5, see Equation 71 and Equation 72.

In addition to the predicted tensile load for each method, the horizontal or lateral earth pressure, σ_h, was compared. σ_h is the nominal lateral earth pressure, and the factored form of this pressure, $\sigma_{h,f}$, was also evaluated. It should be noted that the nominal earth

pressure was used in determining the nominal tension required in a reinforcement layer, T_{max}. However, the factored form of lateral earth pressure, if a method calculated one, is used to predict T_{req}. Values of σ_h and $\sigma_{h,f}$ are plotted in Figure 47 and Figure 48 respectively.

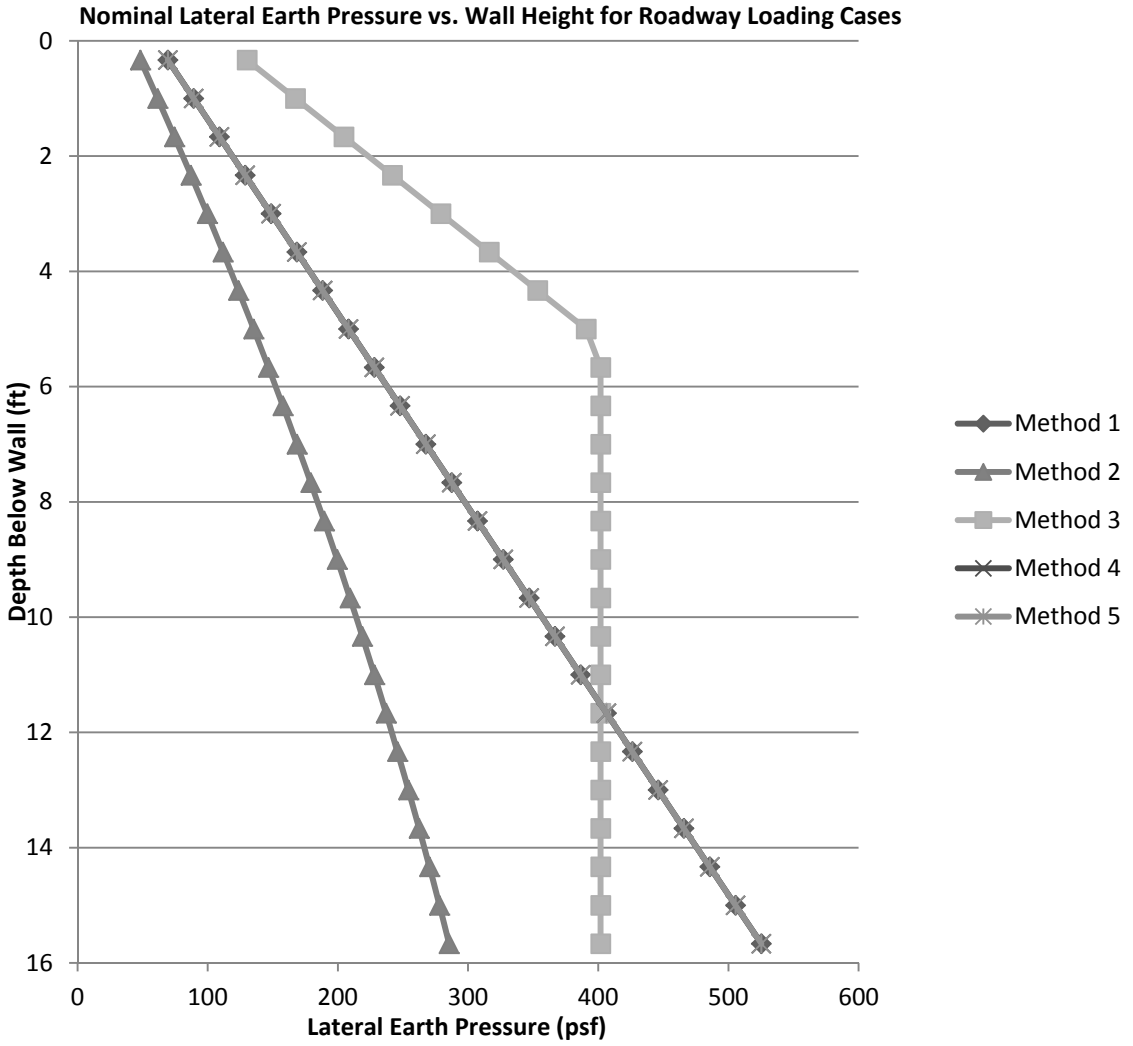

Figure 47: Base Case Roadway Loading Comparison of σ_h for All Methods

Figure 47 shows that Methods 1, 4, and 5 all predict the same distribution of horizontal earth pressures for the roadway loading case. Method 2, which has a predicted lateral earth pressure coefficient that varies with depth, predicts the lowest σ_h value. All these distributions have a linear or very near linear shape. Method 3 uses a very different approach for estimating lateral earth pressure. A lateral earth pressure roughly halfway down the wall is calculated, and then a distribution factor, which varies with depth, is applied to that single value. Method 3 is based on empirical observation of case histories, where the typical triangular distribution of earth pressure was not recorded. Instead, field measurements revealed a more trapezoidal shaped distribution (Bathurst et al. 2008). The Method 3 approach reflects these findings. However, it should be noted that the reason

lateral earth pressure numeric values are so much higher than predicted required ultimate tensile strengths, T_{req}, for Method 3 is the application of the Φ values, see Equation 38 through Equation 46 for the definition of Φ values calculated as part of the parametric study.

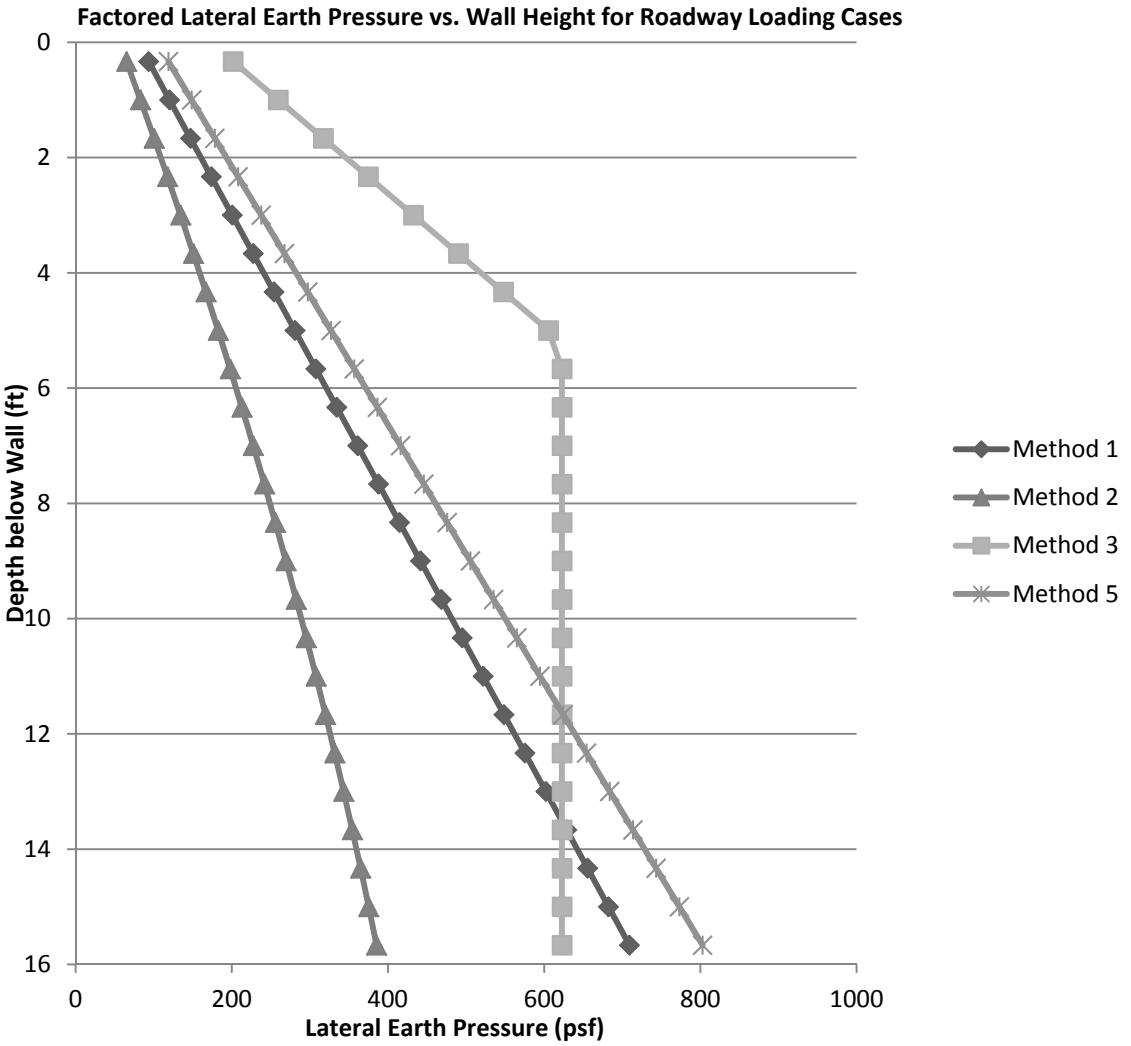

Figure 48: Base Case Roadway Loading Comparison of $\sigma_{h,f}$ for All Applicable Methods

Figure 48 shows that though Methods 1 and 5 have the same nominal lateral earth pressure distribution, different factors are applied. Thus the factored lateral earth pressure is different, with Method 5 predicting higher values at all depths. Methods 1, 2 and 5 all have linear or near linear distribution shape. Method 4 is not included on this figure because it does not evaluate a factored lateral earth pressure, $\sigma_{h,f}$. Method 3 continues to have a unique distribution controlled by a distribution factor. The shape is trapezoidal instead of triangular.

Bridge Loading: Not all methods predict T_{max} and T_{req} values for the bridge loading condition. Method 3, the K-Stiffness Method, was not adapted for the bridge loading

case for the parametric study. The variations in predicted value for the other methods are shown in Figure 49 and Figure 50.

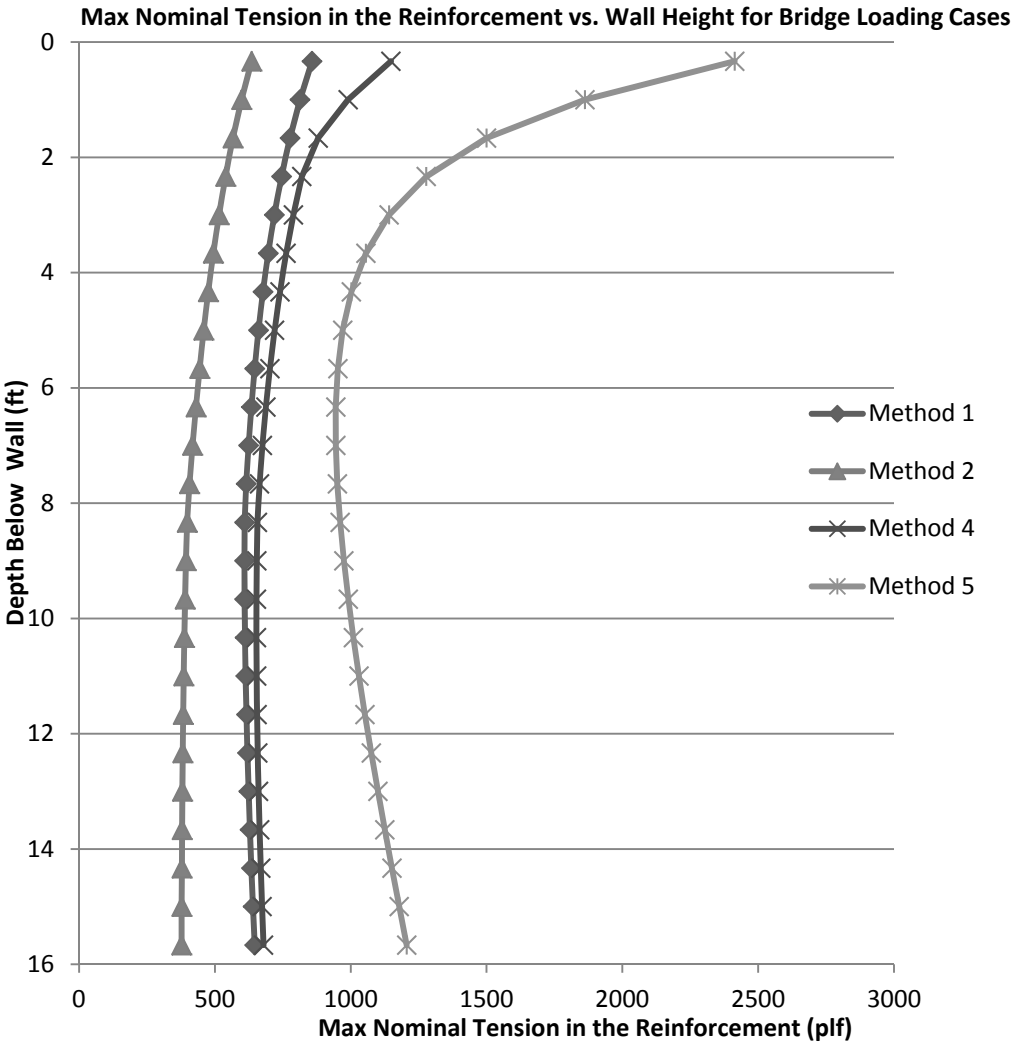

Figure 49: Base Case Bridge Loading Comparison of T_{max} for Methods 1, 2, 4, and 5

Figure 49 shows that the predicted T_{max} values for Method 5 are the largest and for Method 3 the smallest. Method 2 is identical to Method 1 with the exception of determining the value of lateral earth pressure coefficient. As a result, the distribution shapes are similar but Method 2 predicts lower values than Method 1. Method 4 results are close in value to Method 1 values for a large portion of the profile largely because Method 4 was developed from an earlier publication of Method 1. The guidance methodology is very similar and based on similar soil theory. Method 5 predicts a distribution of T_{max} values that has higher values than the other methods and a different shape. This is likely due to the differences in governing equations and soil theory between Method 5 and the other methods.

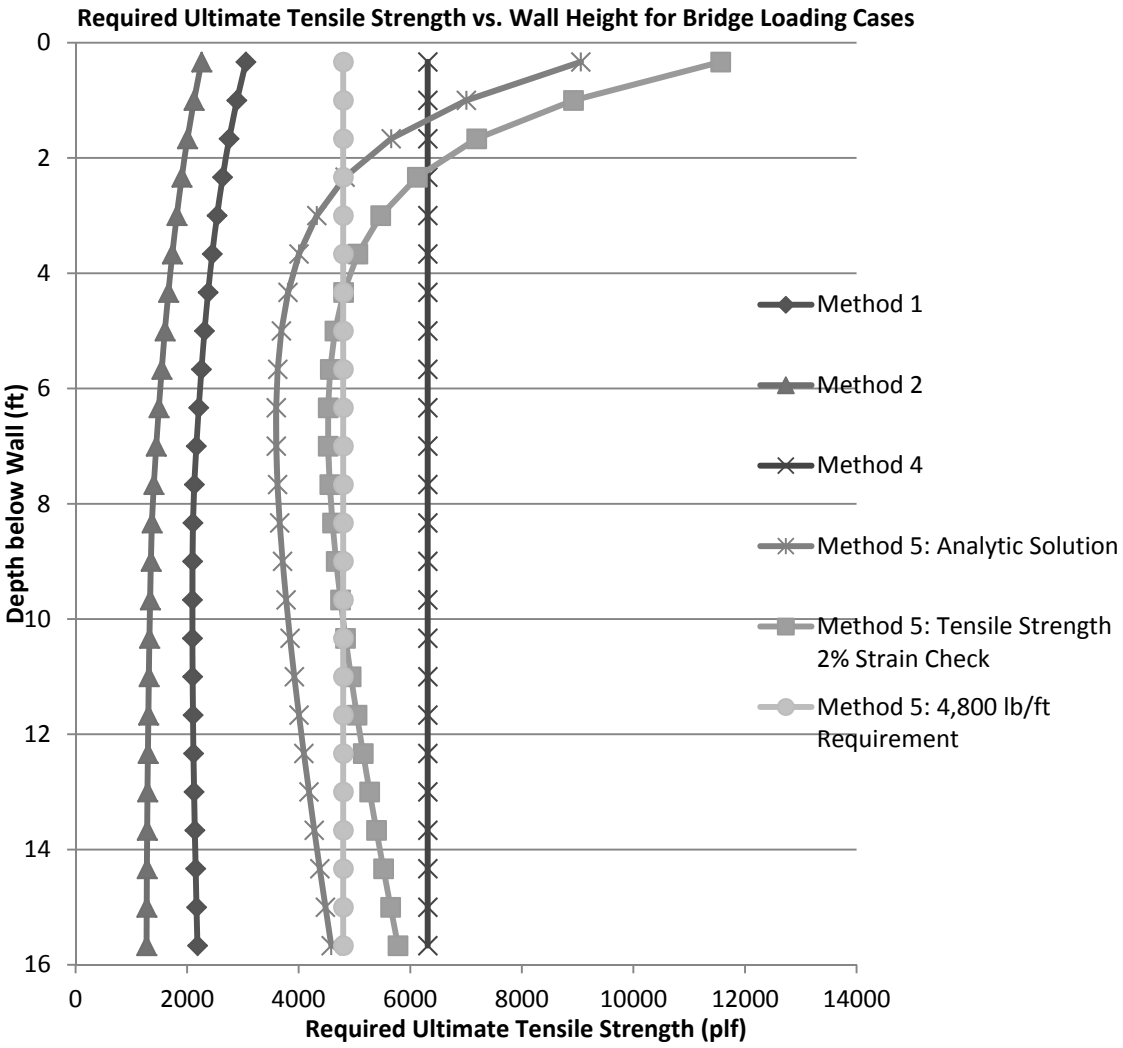

Figure 50: Base Case Bridge Loading Comparison of T_{req} for Methods 1, 2, 4, and 5

Figure 50 shows that there is not a single method that predicts the highest T_{req} value at every reinforcement layer for this loading condition. However, Method 2 predicts the lowest T_{req} value for every reinforcement depth for the base case wall bridge loading case. Method 4 selects a single ultimate T_{req} value for the entire soil profile behind the wall. Additionally, Method 5 has a requirement that if the predicted required reinforcement ultimate strength, T_{req}, is less than 4,800 lb/ft then reinforcement with at least 4,800 lb/ft of ultimate tensile strength should be used. The result is a straight line plotted at 4,800 lb/ft in Figure 50. Methods 1 and 2 continue to have very similar shaped distributions with Method 2 predicting lower values than Method 1. Additionally, the Method 5 T_{req} values for its analytical solution and the tensile strength at 2% strain check have the same distribution shape. However for the base case geosynthetic material, PET geogrid, the tensile strength at 2% strain equivalent T_{req} value is higher at all reinforcement layers than the analytic T_{req} value.

In addition to the predicted tensile load for each method, the horizontal or lateral earth pressure, σ_h, was compared. σ_h is the nominal lateral earth pressure, factored form of

this pressure, $\sigma_{h,f}$, was also evaluated. It should be noted that the nominal earth pressure was used in determining the nominal tension required in a reinforcement layer, T_{max}. However, the factored form of lateral earth pressure, if a method calculated one, is used to predict T_{req}. Values of σ_h and $\sigma_{h,f}$ are plotted in Figure 51 and Figure 48 respectively.

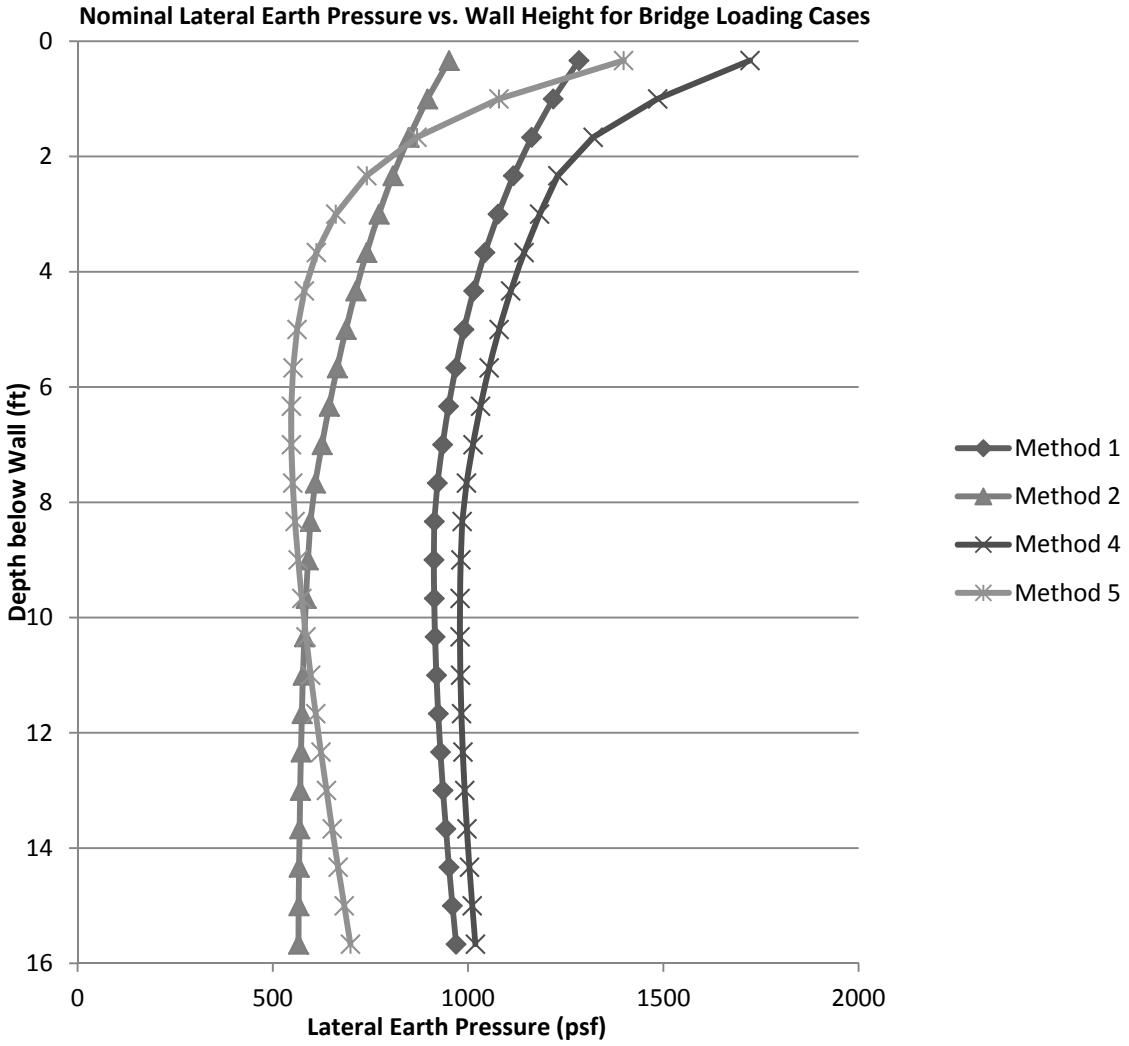

Figure 51: Base Case Bridge Loading Comparison of σ_h for All Applicable Methods

Figure 51 shows that for the nominal lateral earth pressure comparison, Method 4 predicts the highest value. Method 1 predicts higher values than Method 2. All methods display a curved distribution which would be anticipated for the bridge loading scenario. Method 5 is the only method that shows a significant increase in lateral earth pressure at the bottom portion of the wall. Additionally, Method 5 shows a more pronounced variation in σ_h in comparison to other methods. This is likely due to the fact that Method 5 is influenced by parameters not included in the other methods such as shape factors α and β, which are angles for calculation of pressure distribution from bridge loading.

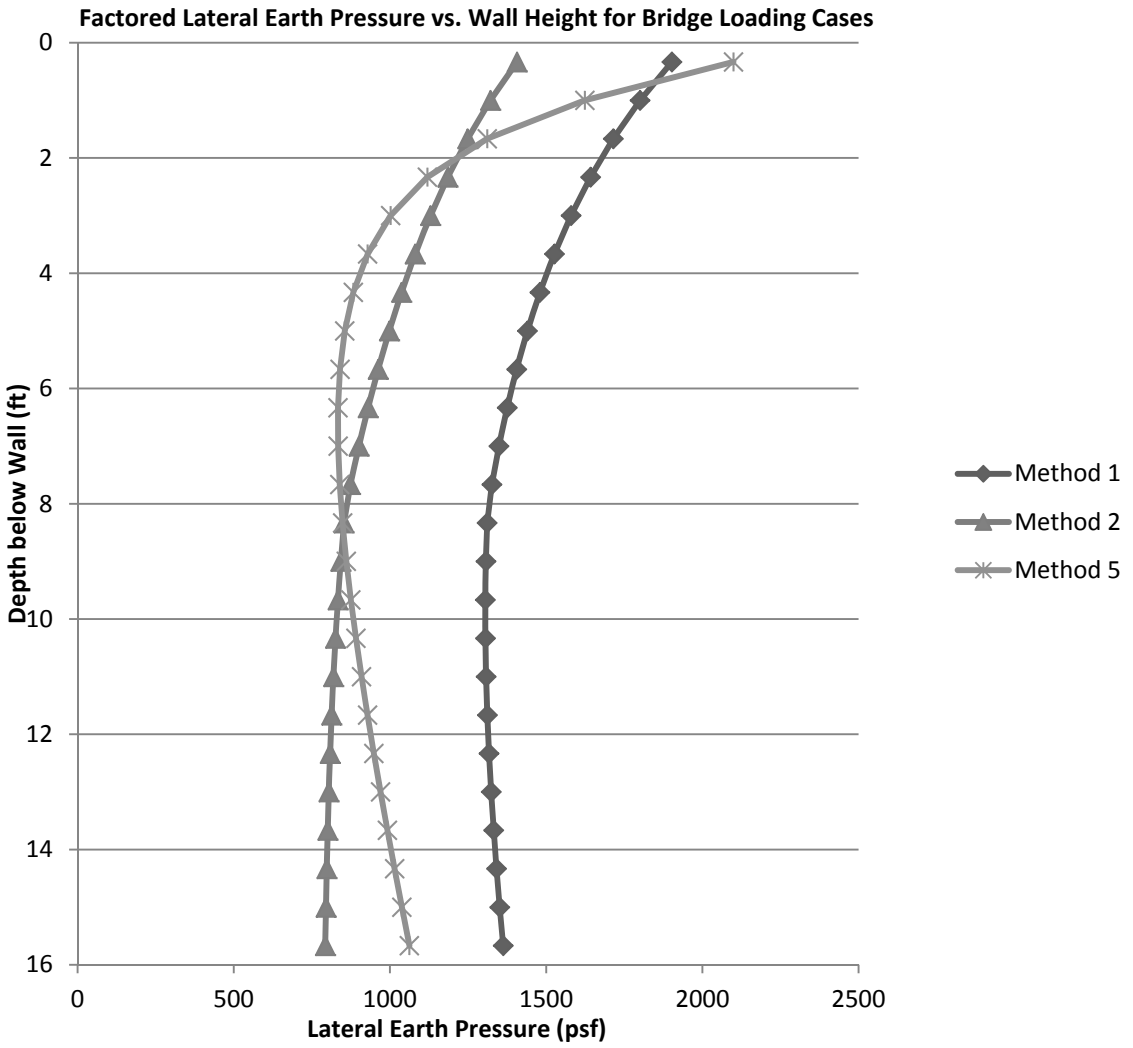

Figure 52: Base Case Bridge Loading Comparison of $\sigma_{h,f}$ for All Applicable Methods

Figure 52 shows that for the factored lateral earth pressure comparison, Method 1 predicts higher values than Method 2. Method 4 is not compared because it does not evaluate a factored lateral earth pressure. All methods continue to display a curved distribution which would be anticipated for the bridge loading scenario. Method 5 again is the only method that shows a significant increase in lateral earth pressure at the bottom portion of the wall. Additionally, Method 5 shows a more pronounced variation in $\sigma_{h,f}$ in comparison to other methods. This is likely due to the fact that Method 5 is influence by parameters not included in the other methods such as shape factors α and β, which are angles for calculation of pressure distribution from bridge loading.

Impact of Wall Height Variation: The following section explores the influence of varying the parameter, wall height, over the range detailed in Table 4 for the roadway loading condition and Table 5 for the bridge loading case.

Roadway Loading: For the roadway loading scenario, both T_{max} and T_{req} can be compared across all methods. Figure 53, Figure 54, Figure 55, Figure 56, Figure 57,

Figure 58, and Figure 59 show the variation in tension for the entire soil profile with change in wall height for each of the 5 methods. The vertical axis, depth below top of the wall, of these figures is normalized with wall height. Wall height varied from 10 feet in height up to a wall of 28 feet. Variation was in 2 foot intervals.

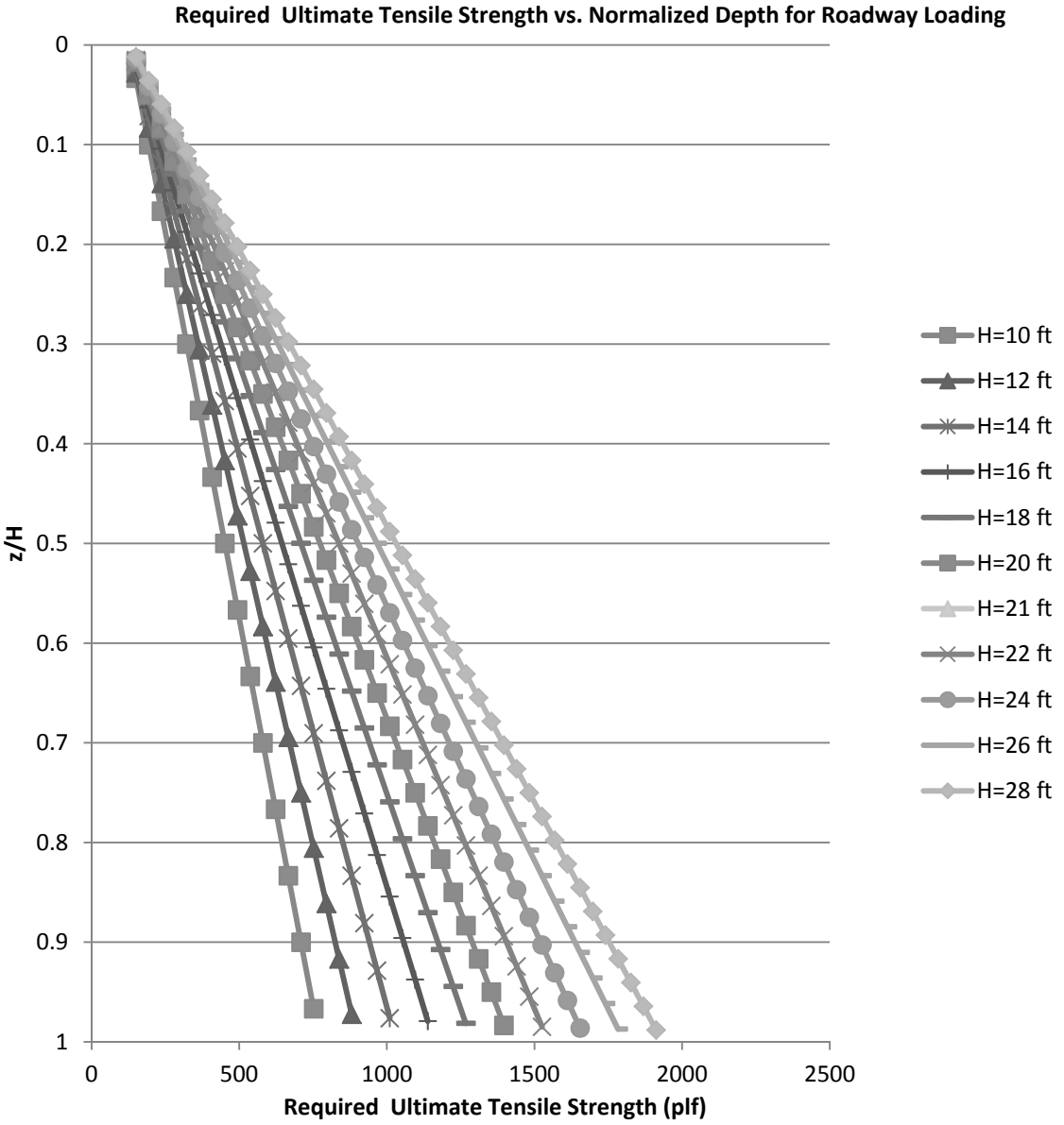

Figure 53: Influence of Wall Height on Ultimate Required Tension for Roadway Loading for Method 1: The Simplified Procedure

Figure 53 shows that for Method 1, the influence of increasing wall height results in an increase in predicted ultimate required tension, T_{req}, for the entire wall profile. The shapes of the distributions remain linear at all wall heights.

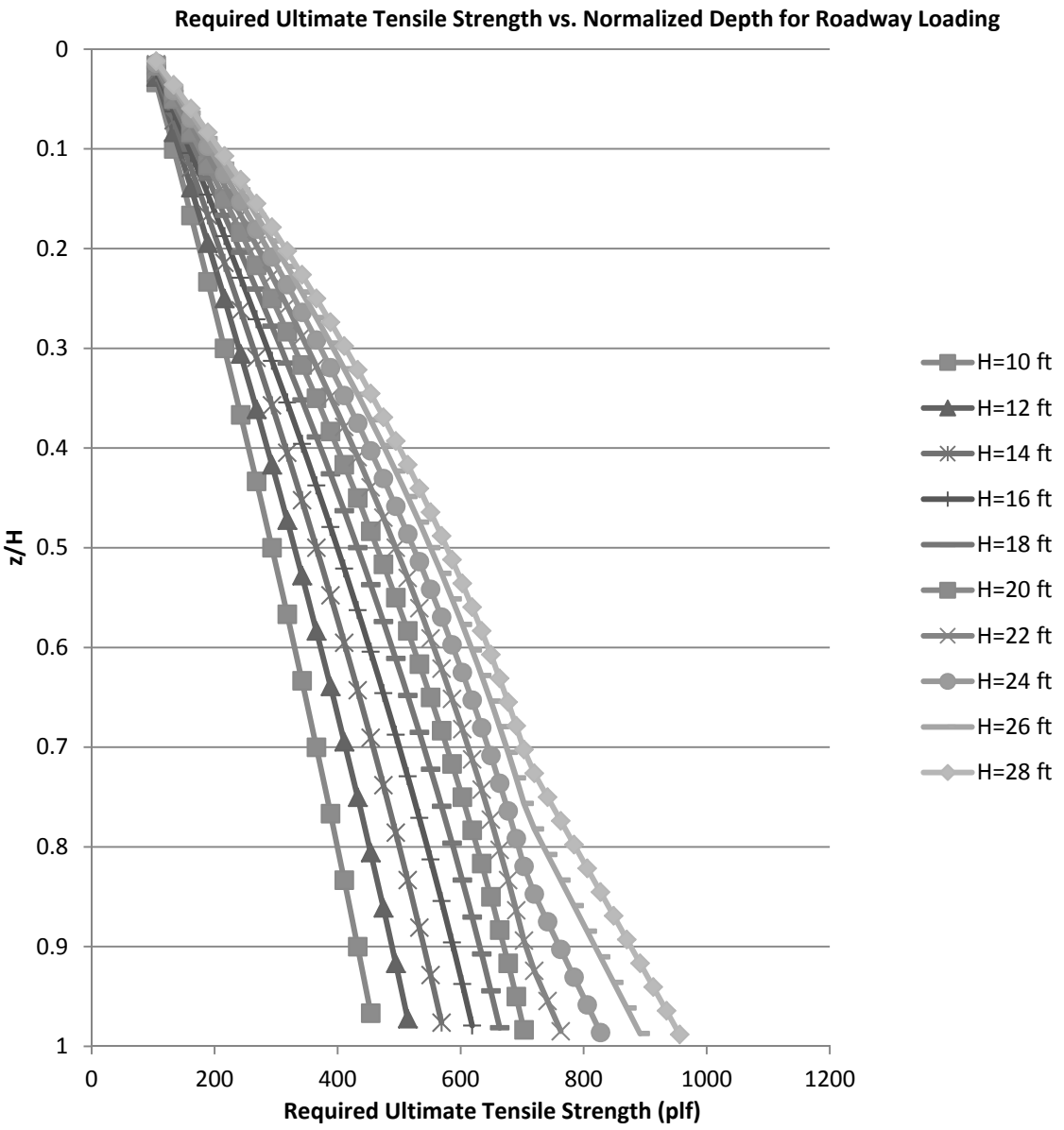

Figure 54: Influence of Wall Height on Ultimate Required Tension for Roadway Loading for Method 2: The Simplified Procedure with K_r/K_a Adjusted

Figure 54 shows that for Method 2, the influence of increasing wall height results in an increase in predicted ultimate required tension, T_{req}, for the entire wall profile. However, unlike Method 1, Method 2 does not predict a perfectly linear distribution at all depths. This is due to the proposed variation in Kr/Ka with depth for a vertical wall. Unlike Method 1, which holds this ratio constant at 1.0, Method 2 varies this value until a depth of 20 feet below the top of the wall's reinforced zone. After 20 feet, the ratio is held constant at a value of 0.5. Therefore the slight decrease in slope at the lower portion of the distributions only appears in curves with wall heights above 20 feet. As the wall

height increases, the location at which the slope decreases moves upward on the plot due to the normalization of the vertical axis with wall height.

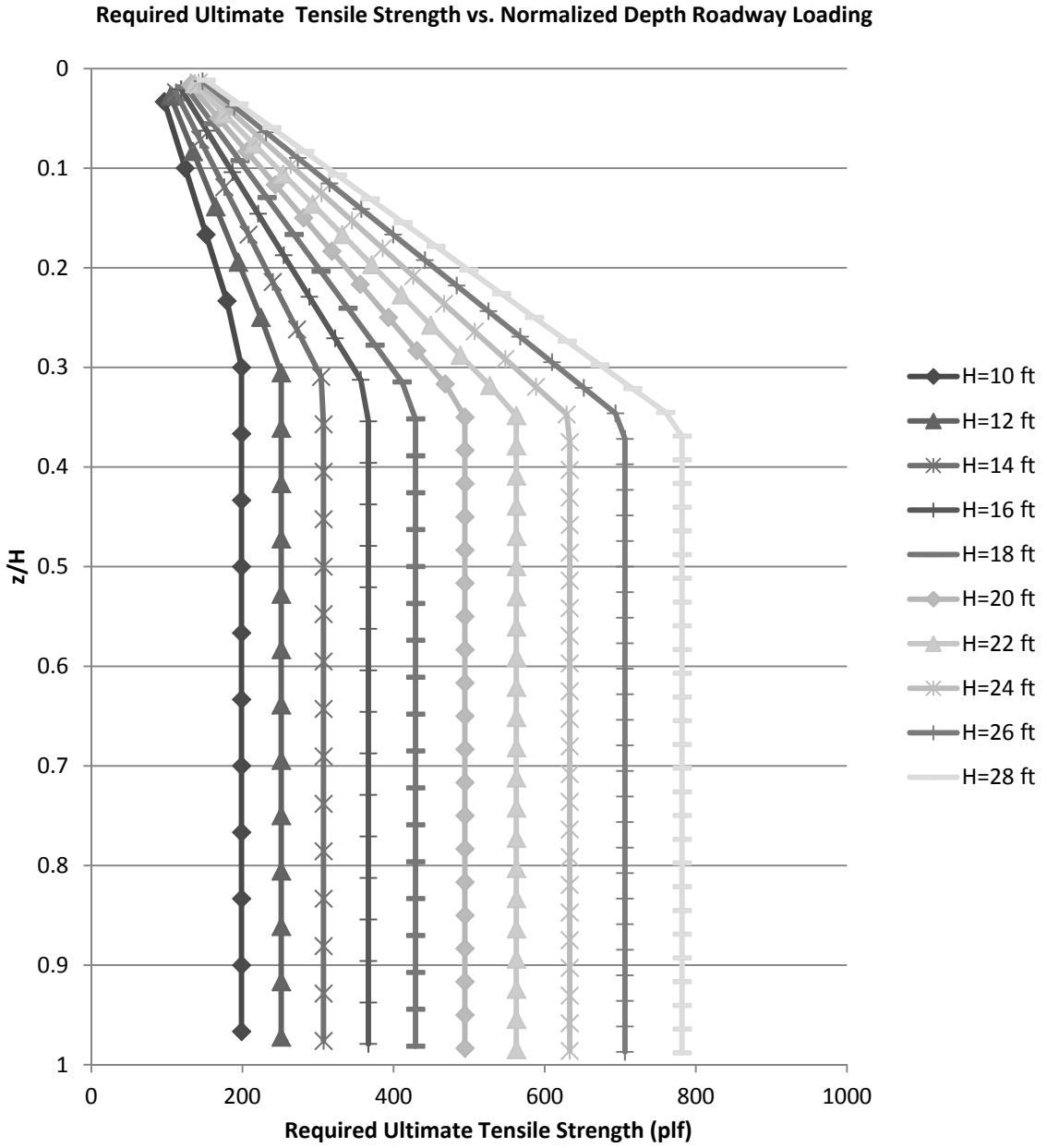

Figure 55: Influence of Wall Height on Ultimate Required Tension for Roadway Loading for Method 3: K-Stiffness Method

Figure 55 shows that for Method 3, the distribution shape is controlled by a load distribution factor. This results in the trapezoidal shape of the profiles instead of a linear increase with depth. Due to the normalization, the point at which the T_{req} value remains constant is roughly the same location of z/H. With increasing wall height the slope of the upper portion of the distribution decreases and is no longer as steep. For all locations of the soil profile, increasing wall height increases the value of T_{req}.

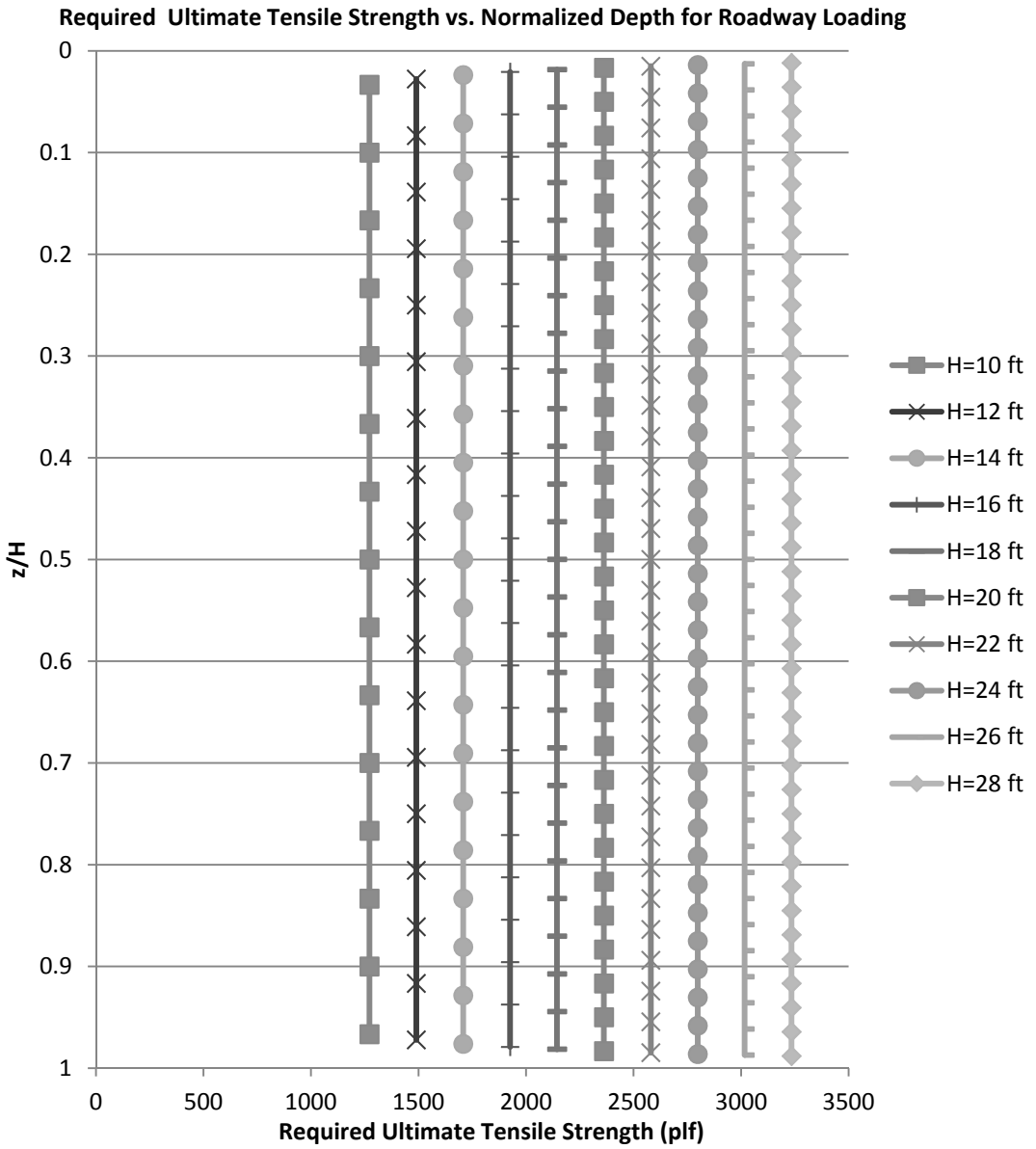

Figure 56: Influence of Wall Height on Ultimate Required Tension for Roadway Loading for Method 4: NCHRP GRS Method

Figure 56 shows that For Method 4, the entire profile is assigned a required ultimate tensile strength, T_{req}, value equal to the highest value that occurs in the wall. Therefore, the variation plots as a vertical line. With increasing wall height, the maximum value in the profile also increases. This was also highlighted in Figure 61. To look more closely at the variation of tension at each reinforcement layer, the variation in nominal maximum tensile load, T_{max}, with depth was plotted for each variation in wall height. These relationships are plotted in Figure 57.

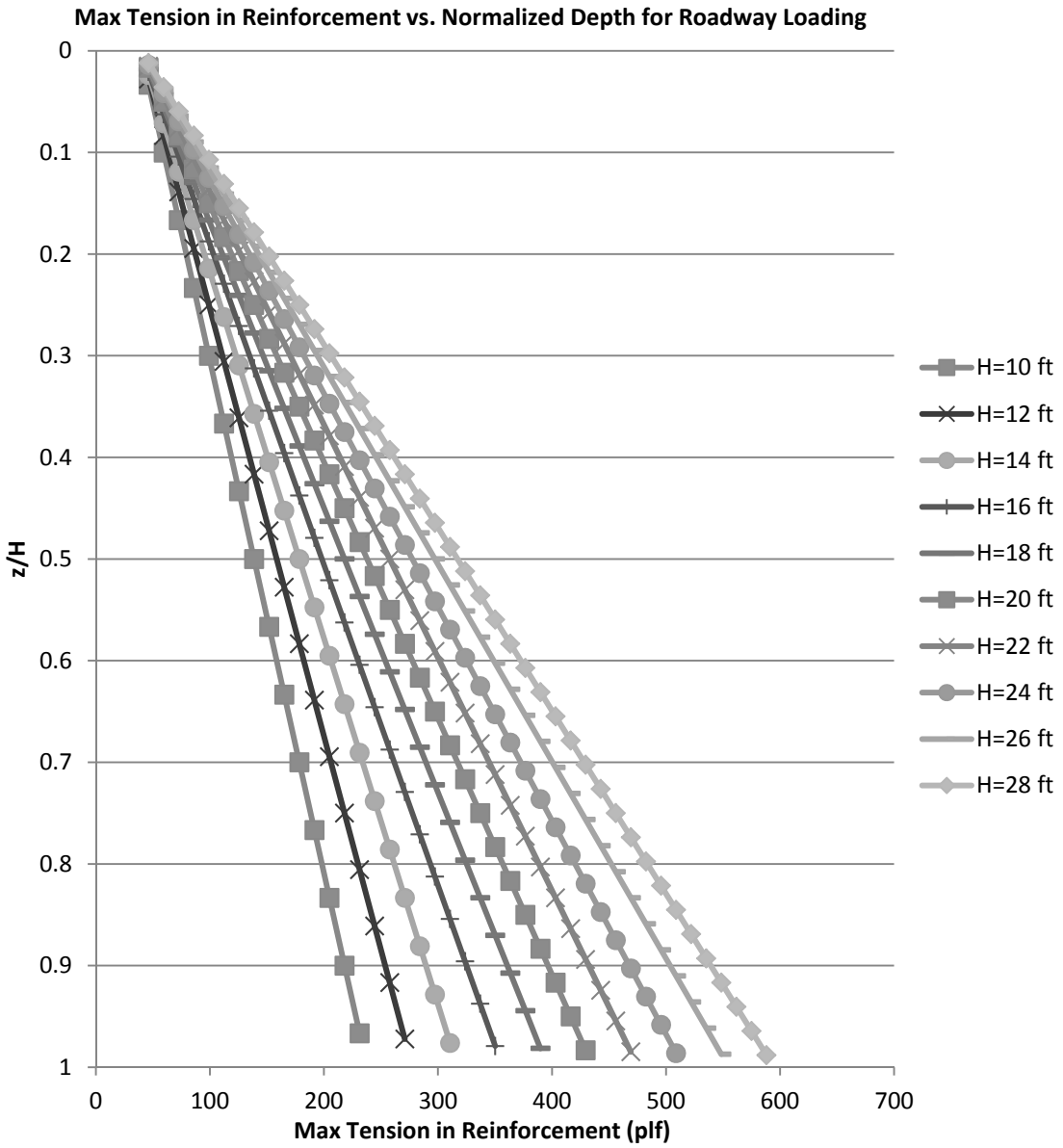

Figure 57: Influence of Wall Height on Max Tensile Load in the Reinforcement for Roadway Loading for Method 4: NCHRP GRS Method

Figure 57 shows that for Method 4, increasing wall height will increase the nominal maximum tensile load, T_{max}, at all depths below the top of the reinforced zone. The shape of each distribution remains linear through the entire soil profile.

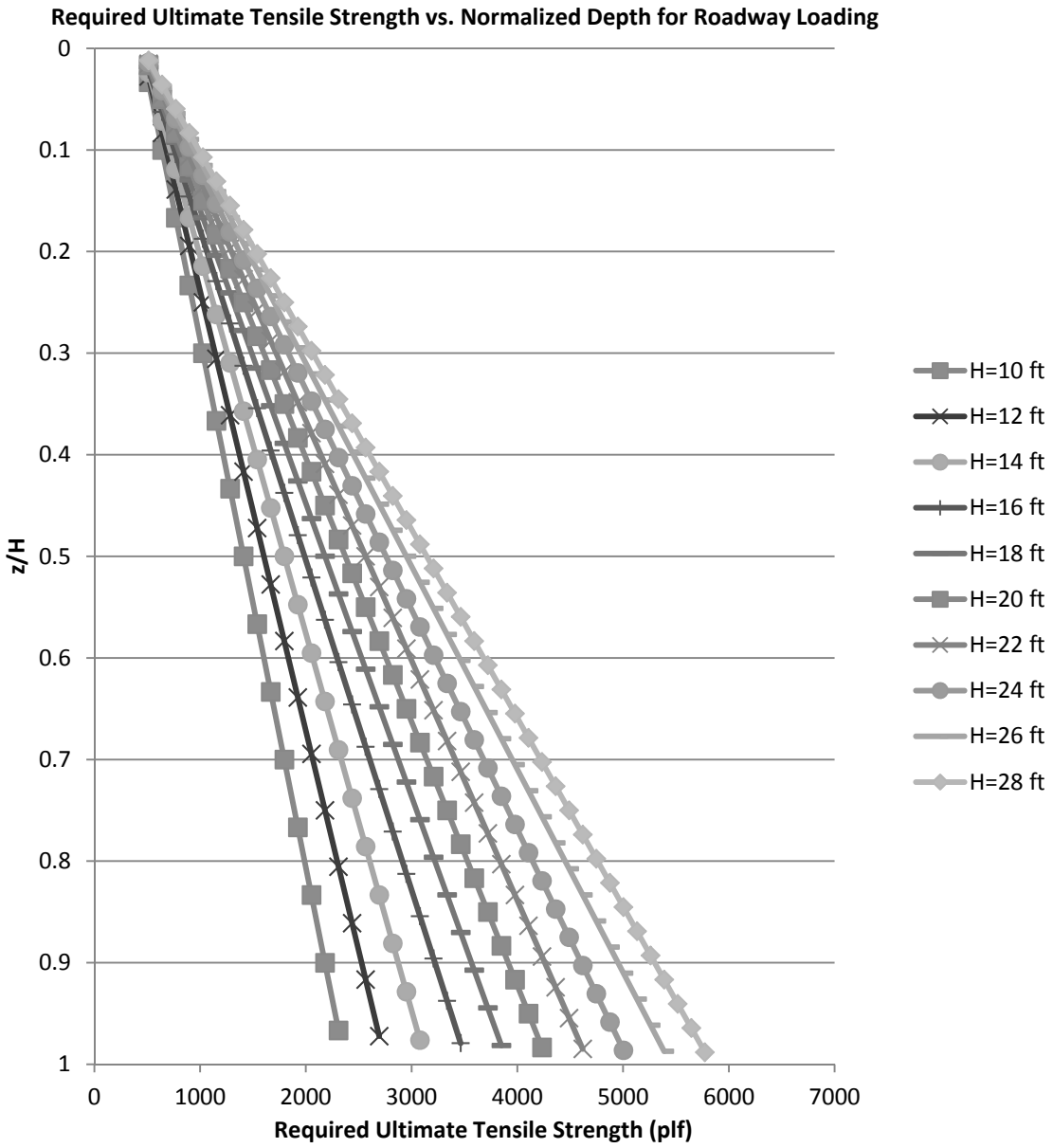

Figure 58: Influence of Wall Height on Ultimate Required Tension for Roadway Loading for Method 5: FHWA GRS-IBS Method Analytic Solution

Figure 58 shows that for Method 5, three requirements have to be checked in regards to predicted ultimate required tension T_{req}. The values of T_{req} predicted by these three checks are compared and the highest is utilized in design. Figure 58 illustrates the influence of wall height on the predicted analytic solution of Method 5, shown in Equation 71. As wall height increases the analytic solution also increases at each reinforcement layer depth. The shapes of the distributions of each wall height variations remain linear at all depths.

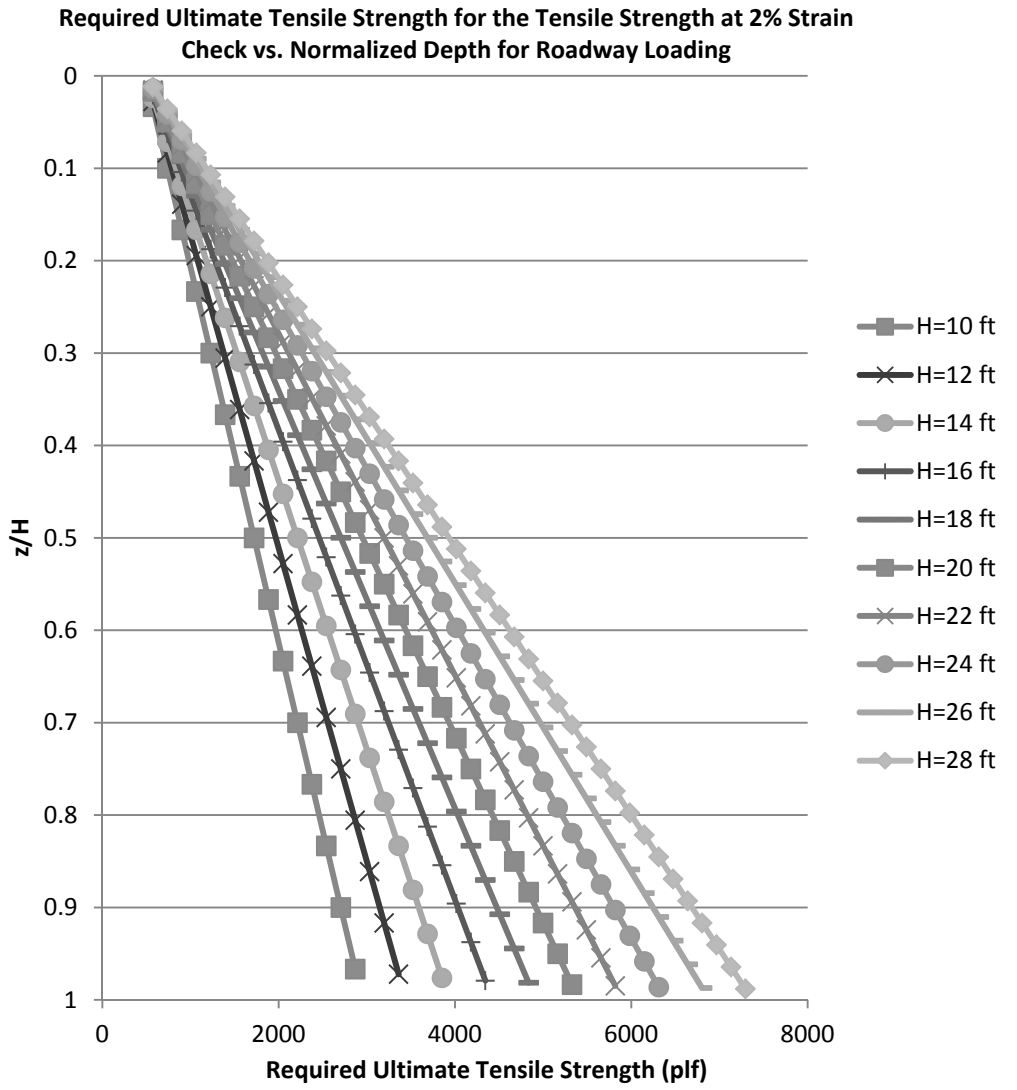

Figure 59: Influence of Wall Height on Ultimate Required Tension for Roadway Loading for Method 5: FHWA GRS-IBS Method Tensile Strength at 2% Strain Check

Of the three requirements for Method 5, the tensile strength at 2% strain check is plotted in Figure 59. The plotted value is an equivalent ultimate required tensile strength for design that is equivalent to the reinforcement that would meet the tensile strength at 2% strain check. For the base case, the reinforcement selected was a PET geogrid. For this check, the values of T_{req} predicted increase with increasing wall height. The shapes of the distributions of each wall height variations remain linear at all depths. The third check, a requirement that for design T_{req} be equal to or greater than 4,800 lb/ft is not plotted. If plotted, this relationship would be a vertical line at 4,800 lb/ft and would not be influenced by increasing wall height.

The variation in predicted maximum value of T_{max} and T_{req} was computed for a wall from 10 feet in height up to a wall of 28 feet in 2 foot intervals. The variation in T_{max} is shown

in Figure 60, and the variation of T_{req} is shown in Figure 61. The relationships presented in Figure 60 and Figure 61 only show the variation of the highest values of T_{max} and T_{req}.

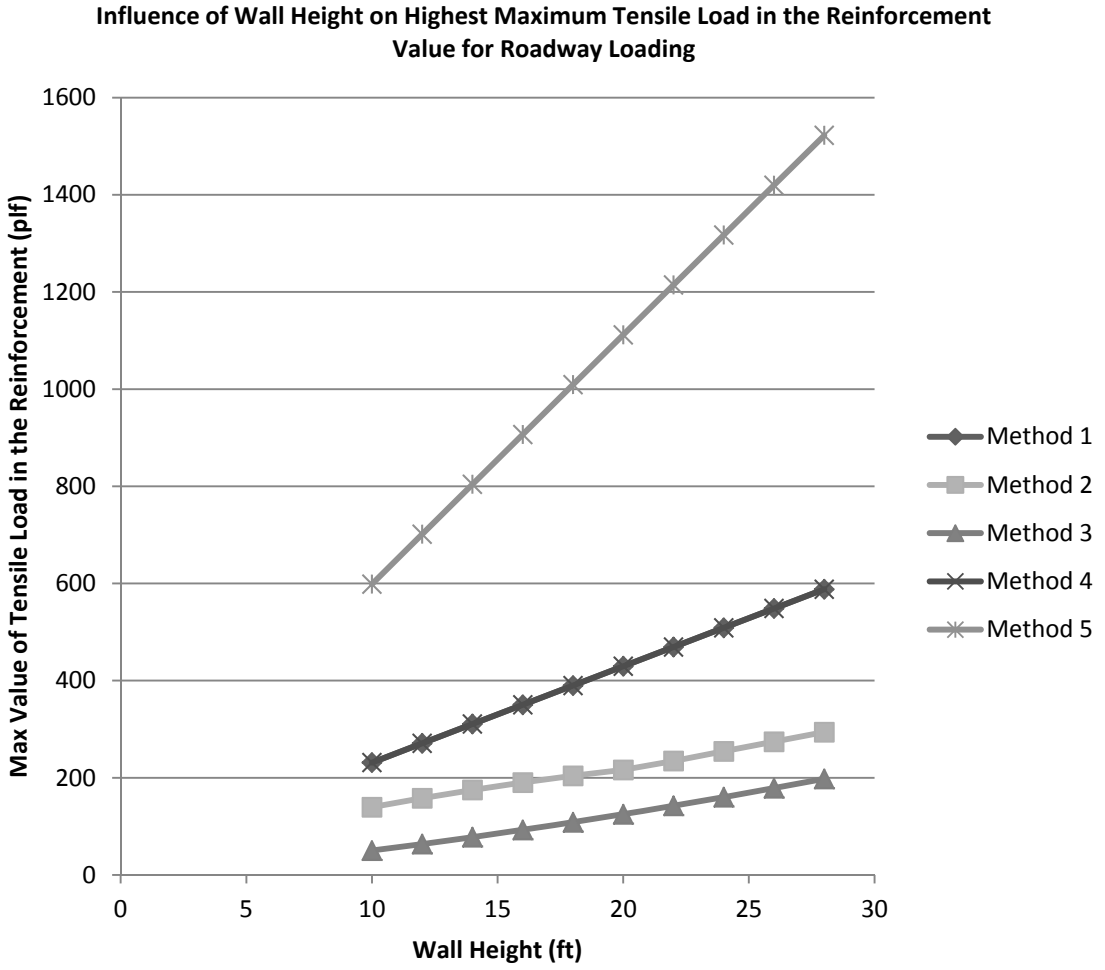

Figure 60: Influence of Wall Height on Max Load in the Reinforcement for the Roadway Loading Condition

Figure 60 shows that in general across all methods, increasing wall height will increase the maximum predicted tensile load, $T_{max,}$ in the reinforcement. Additionally, the relationship between wall height and T_{max} is roughly linear across all methods. The degree of influence can be correlated to the slope of the distributions in Figure 60. Therefore wall height has about the same level of influence between Methods 2 and 3. For Methods 1 and 4, the influence of wall height is also the same and is in both cases a little higher than Methods 2 and 3. Finally, wall height has the greatest influence on predicted tensile load for values predicted using Method 5.

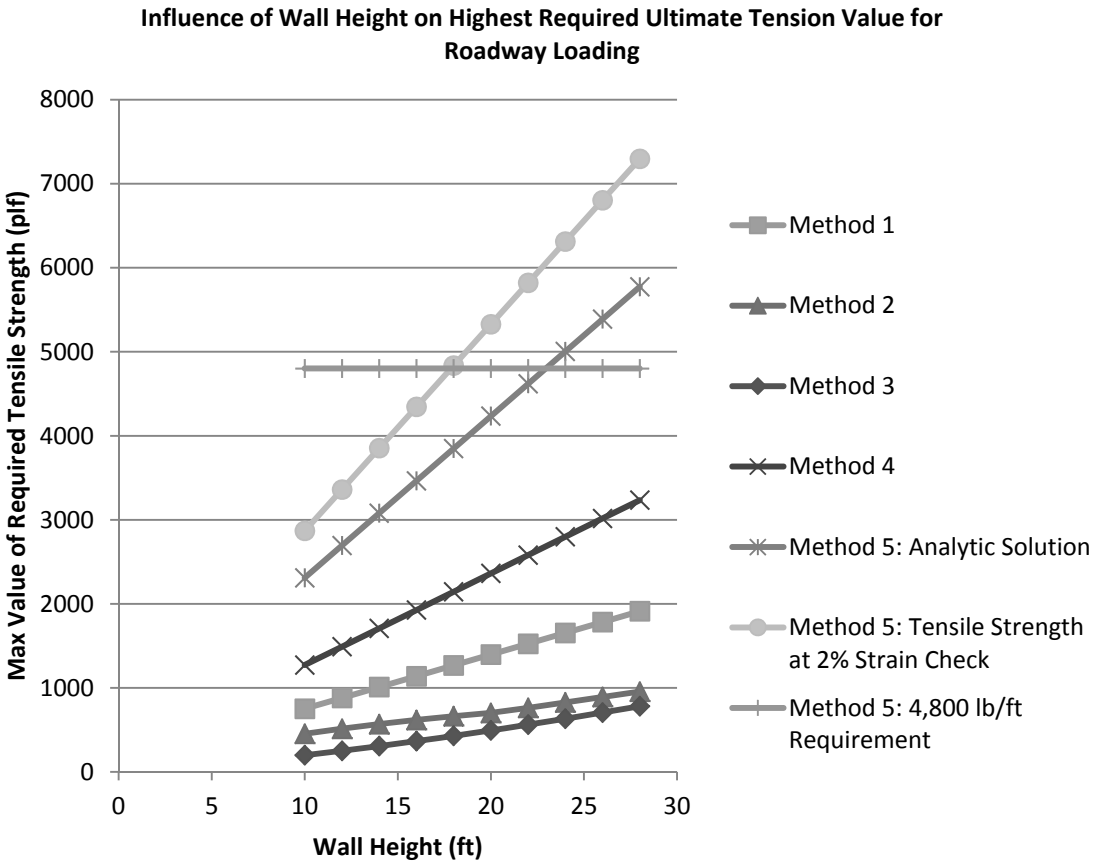

Figure 61: Influence of Wall Height on the Highest Predicted Ultimate Required Tension for the Roadway Loading Condition

Figure 61 shows that the only predicted ultimate tensile value that did not increase linearly was the 4,800 lb/ft additional requirement imposed for Method 5 guidance. This requirement was plotted as a horizontal line. All other Methods, including the tensile check at 2% strain for Method 5, increased linearly with increasing wall height. The degree of influence can be correlated to the slope of the distributions in Figure 61. Therefore wall height has a very similar level of influence for Methods 2 and 3. For Methods 1 and 4, wall height had a higher degree of influence than for Methods 2 and 3. Method 5's analytic solution and additional check of tensile strength at 2% strain equivalent T_{req} values were both more sensitive to wall height than the other methods with the tensile strength at 2% strain equivalent T_{req} being the most influenced by the parameter wall height.

Bridge Loading: For the bridge loading scenario, both T_{max} and T_{req} can be compared across all methods except Method 3, the K-Stiffness Method. The K-Stiffness Method cannot be applied to a wall that supports other structures such as bridges. Figure 62, Figure 63, Figure 64, Figure 65, and Figure 66 show the variation in tension for the entire soil profile with change in wall height for each of the 5 methods. The vertical axis,

depth below top of the wall, of these figures is normalized with wall height. Wall height varied from 10 feet in height up to a wall of 28 feet. Variation was in 2 foot intervals.

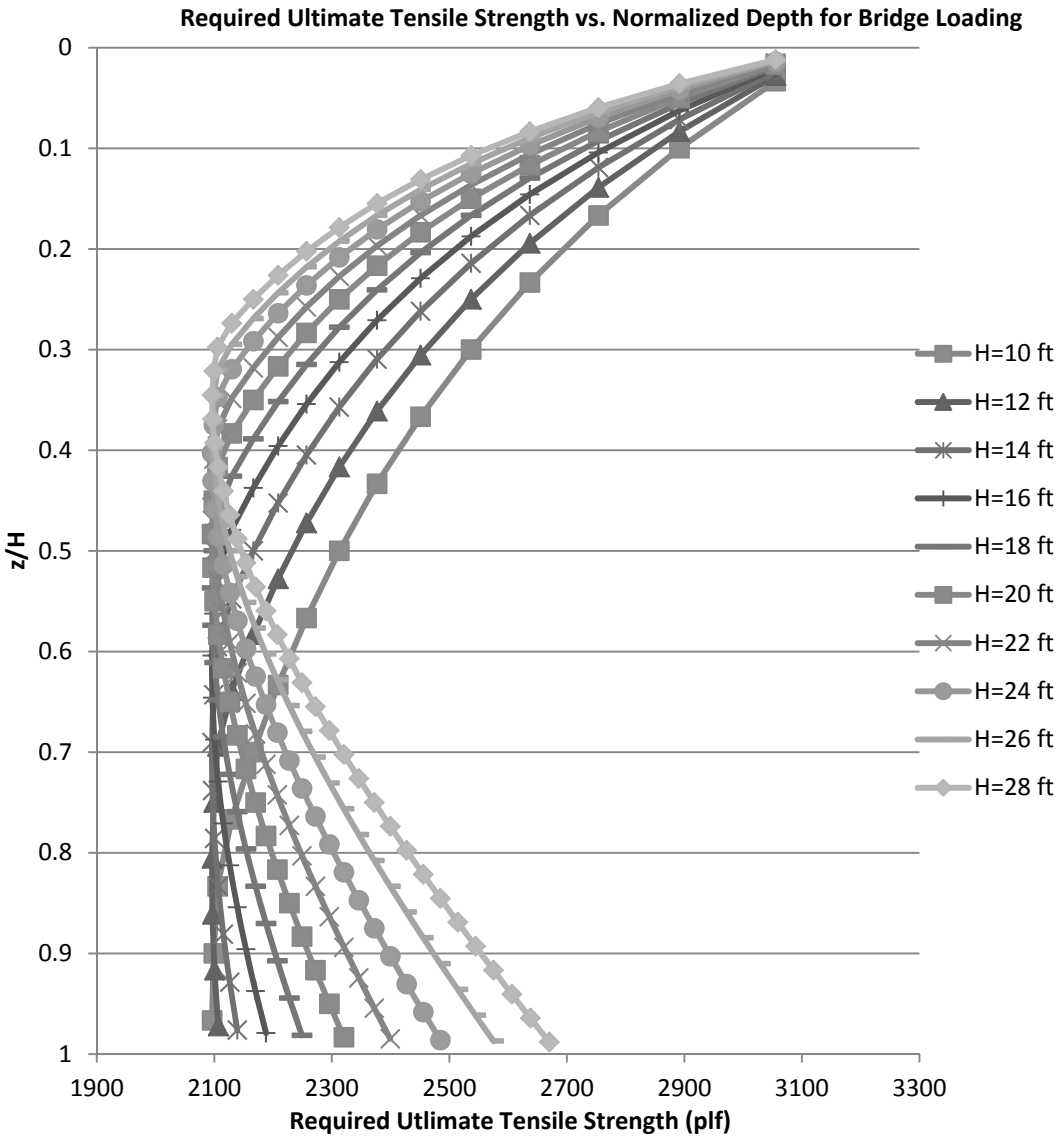

Figure 62: Influence of Wall Height on Ultimate Required Tension for Bridge Loading for Method 1: The Simplified Procedure

For Method 1 bridge loading condition, the variation in wall height has a more complicated influence on predicted ultimate required tensile strength, T_{req}, than for the roadway loading scenario. Increasing wall height will increase the degree of curvature exhibited by the distributions in Figure 62. As wall height increases the load at the lower portion of the wall increases and causes the curvature to increase. The T_{req} value at the lowest portion of the soil profile will increase with increasing wall height. The curvature of the wall distribution of T_{req} is also influenced by the depth to which bridge loads

influence the lateral earth pressure. A taller wall will not have bridge loads that influence lateral earth pressures as far into the reinforced zone, proportionally, as for a short wall.

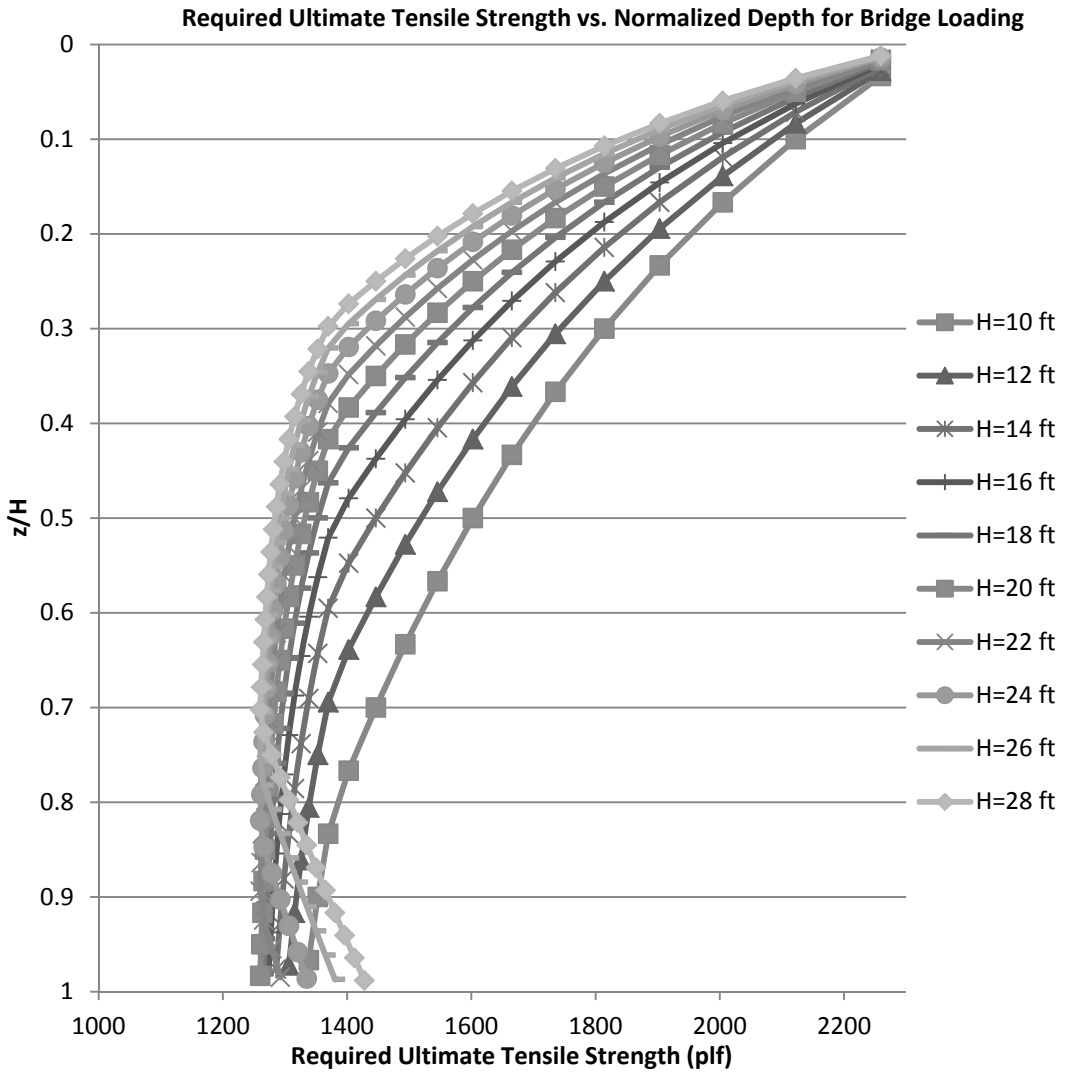

Figure 63: Influence of Wall Height on Ultimate Required Tension for Bridge Loading for Method 2: The Simplified Procedure with K_r/K_a Adjusted

Figure 63 shows that Method 2, like Method 1, has an increase in curvature of the predicted T_{req} profile with increasing wall height. However, the degree to which the bottom portion of the profile curves in comparison to Method 1 is less. This is due to the proposed variation in Kr/Ka with depth for a vertical wall. Unlike Method 1, which holds this ratio constant at 1.0, Method 2 varies this value until a depth of 20 feet below the top of the wall's reinforced zone. After 20 feet, the ratio is held constant at a value of 0.5. Therefore, the marked change in curve shape for the lower portion of the distribution does not occur until a wall height of 20 feet is reached for the parameter variation. The curvature of the wall distribution of T_{req} is also influenced by the depth to which bridge loads influence the lateral earth pressure. A taller wall will not have bridge loads that

influence lateral earth pressures as far into the reinforced zone, proportionally, as for a short wall.

For Method 4, since a single value is given for the entire T_{req} profile of the maximum value and due to the fact that the wall height has no influence on this maximum load which occurs at the top of the soil profile, no plot for Method 4 predicted T_{req} values is included. The plot would have a single straight vertical line at the same location for each wall height variation. Therefore to more clearly understand the influence of wall height in tension, the maximum nominal tensile load, T_{max}, for the entire soil profile is presented in Figure 64.

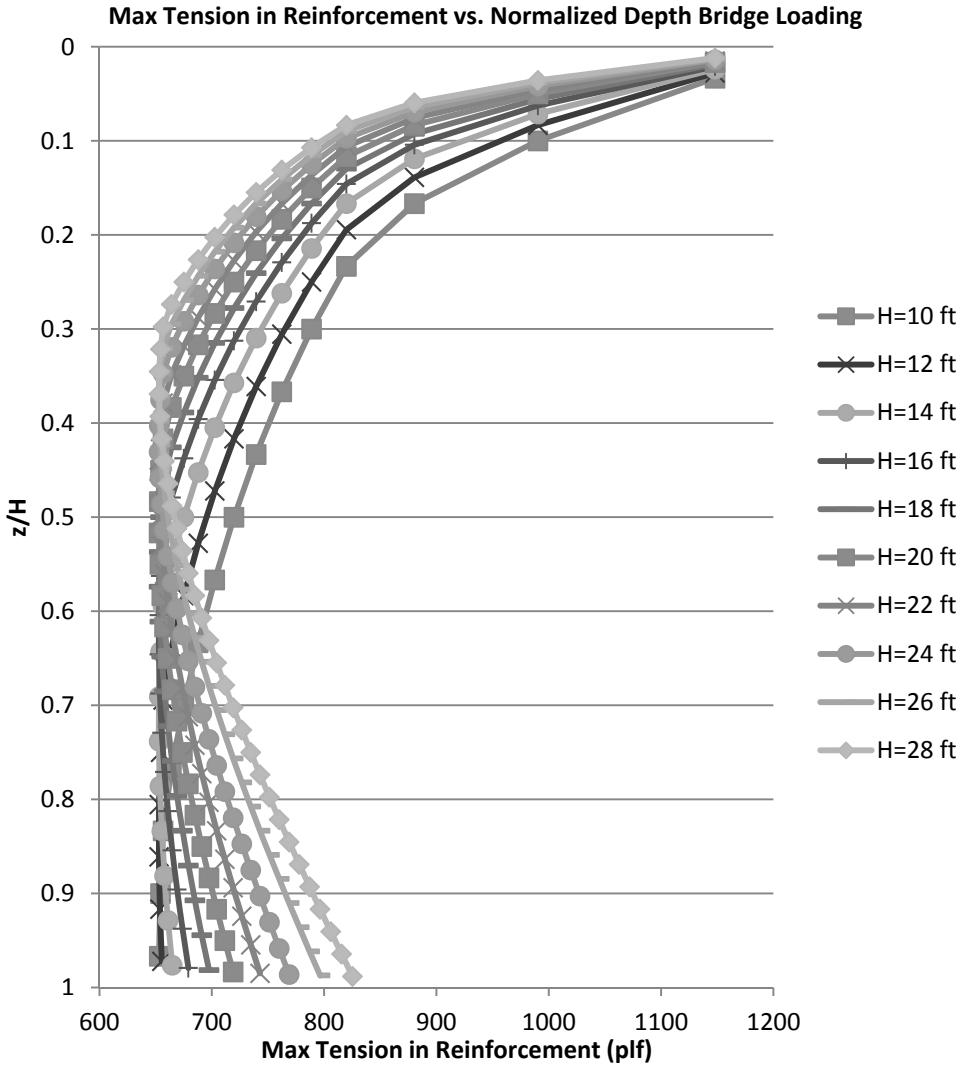

Figure 64: Influence of Wall Height on Max Tensile Load in the Reinforcement for Bridge Loading for Method 4: NCHRP GRS Method

Figure 64 shows that the distributions of T_{max} for Method 4 have a very similar shape to the T_{req} profile predicted by Method 1. The degree of curvature of the distributions increase with increasing wall height similar to Method 1. Additionally, as wall height

increases the load at the lower portion of the wall increases and causes the curvature to increase. The T_{max} value at the lowest portion of the soil profile will increase with increasing wall height. The curvature of the wall distribution of T_{max} is also influenced by the depth to which bridge loads penetrate the soil profile. A taller wall will not have bridge loads penetrating as far into the reinforced zone proportionally, as a short wall.

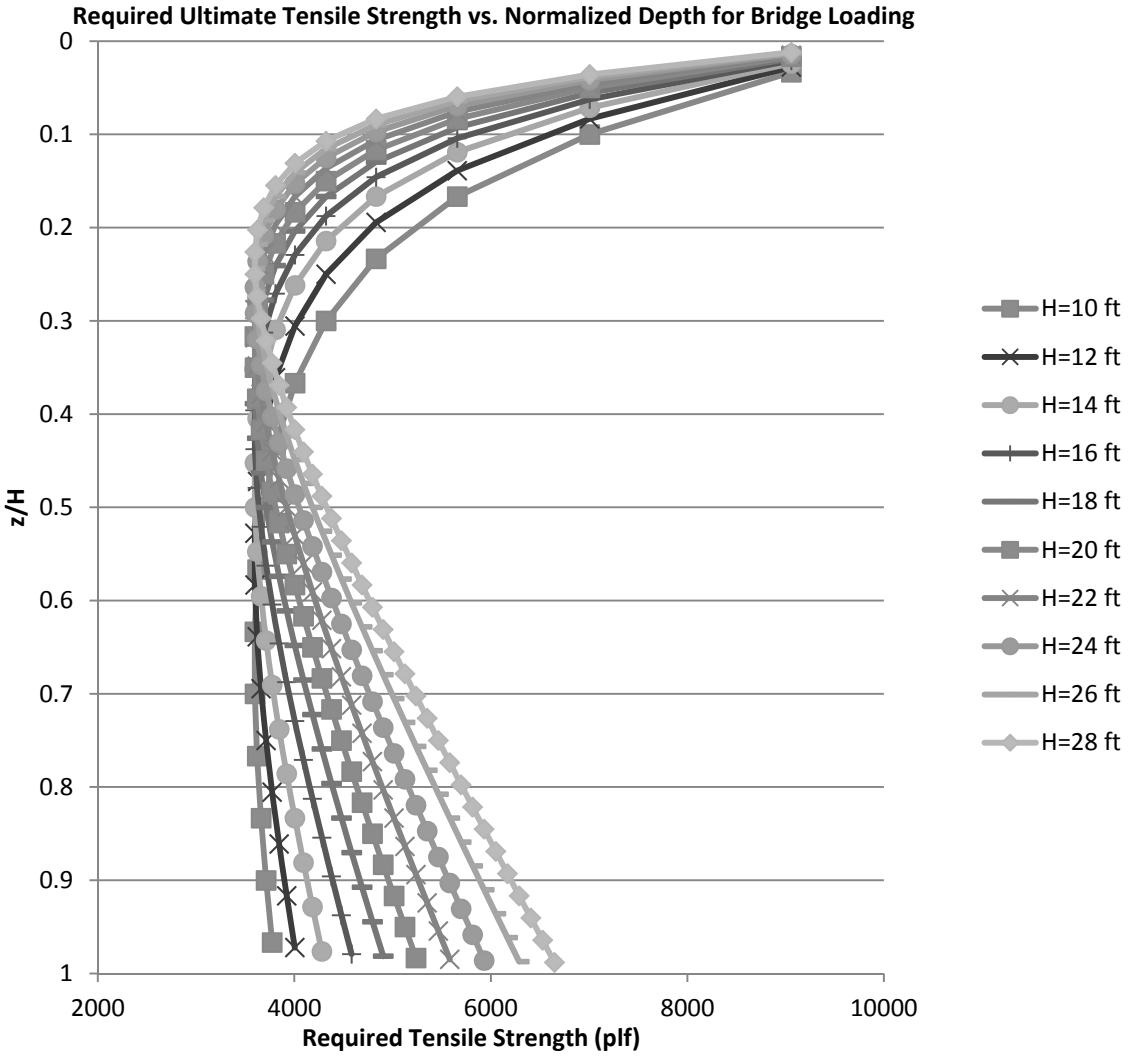

Figure 65: Influence of Wall Height on Ultimate Required Tension for Bridge Loading for Method 5: FHWA GRS-IBS Method Analytic Solution

Figure 65 shows that for Method 5's analytic solution, the degree of curvature expressed in the T_{req} profile increases with increasing wall height. The depth proportionally, where the distribution curves to the right occurs at a higher location for Method 5 than the other methods. This is likely due to the fact that the distribution is influenced by additional factors, such as α, β, and d_{max}, and that the governing equation for the analytic solution T_{req} value takes a dissimilar form in comparison to the other methods. These calculation differences are due to differences in assumed soil theory between Method 5 and other

methods. As wall height increases, the load at the lower portion of the wall increases and causes the curvature to increase. The T_{req} value at the lowest portion of the soil profile will increase with increasing wall height. The curvature of the wall distribution of T_{req} is also influenced by the depth to which bridge loads penetrate the soil profile. A taller wall will not have bridge loads penetrating as far into the reinforced zone proportionally, as a short wall. All these trends are the same for the additional Method 5 check of tensile strength at 2% strain shows in Figure 66. However, the loads are slightly higher than shown for the analytic solution.

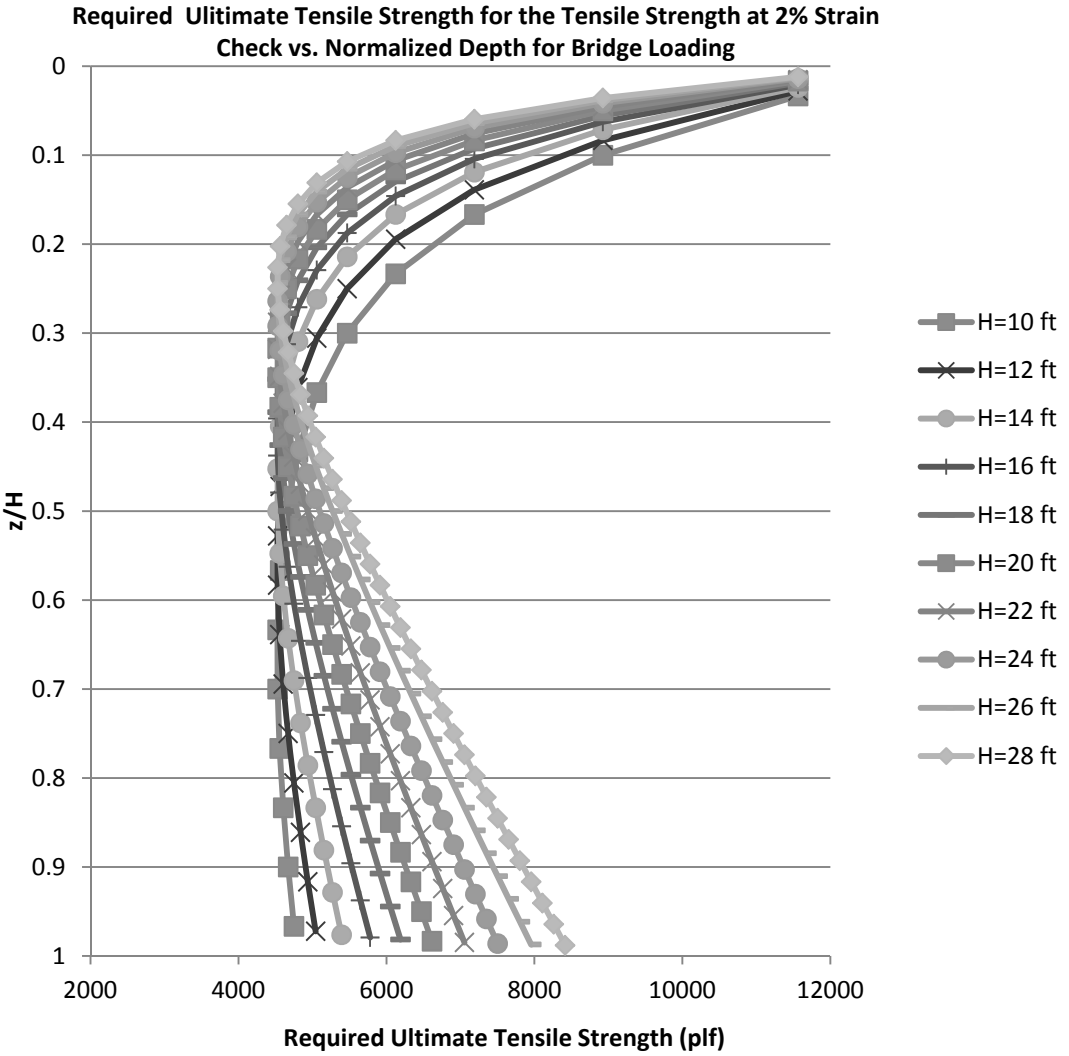

Figure 66: Influence of Wall Height on Ultimate Required Tension for Bridge Loading for Method 5: FHWA GRS-IBS Method Tensile Strength at 2% Strain Check

The third check of Method 5 in regards to 4,800 lb/ft was not plotted. It would appear as a straight line at 4,800 lb/ft and would not be influenced by change in wall height.

The variation in predicted maximum value of T_{max} and T_{req} was computed for a wall from 10 feet in height up to a wall of 28 feet in 2 foot intervals. The variation in T_{max} is shown in Figure 67 and the variation of T_{req} in Figure 68. The relationships presented in Figure 67 and Figure 68 only show the variation of the highest values of T_{max} and T_{req} across all applicable methods.

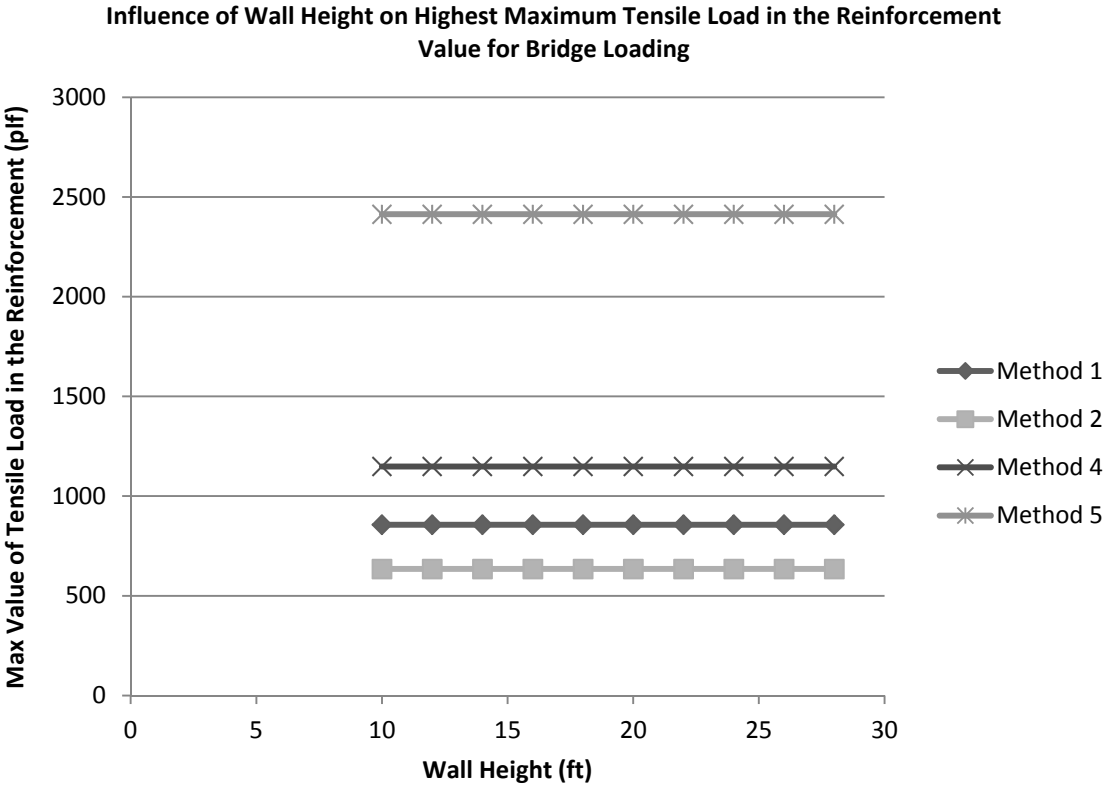

Figure 67: Influence of Wall Height on Max Load in the Reinforcement for the Bridge Loading Condition

Figure 67 shows that the highest value of maximum load in the reinforcement, T_{max}, is at the top of the wall profile for the bridge loading condition. Therefore the change in wall height does not influence this maximum value. Therefore, Methods 1, 2, 4, and 5 have maximum T_{max} values that plot as a straight horizontal line in Figure 67.

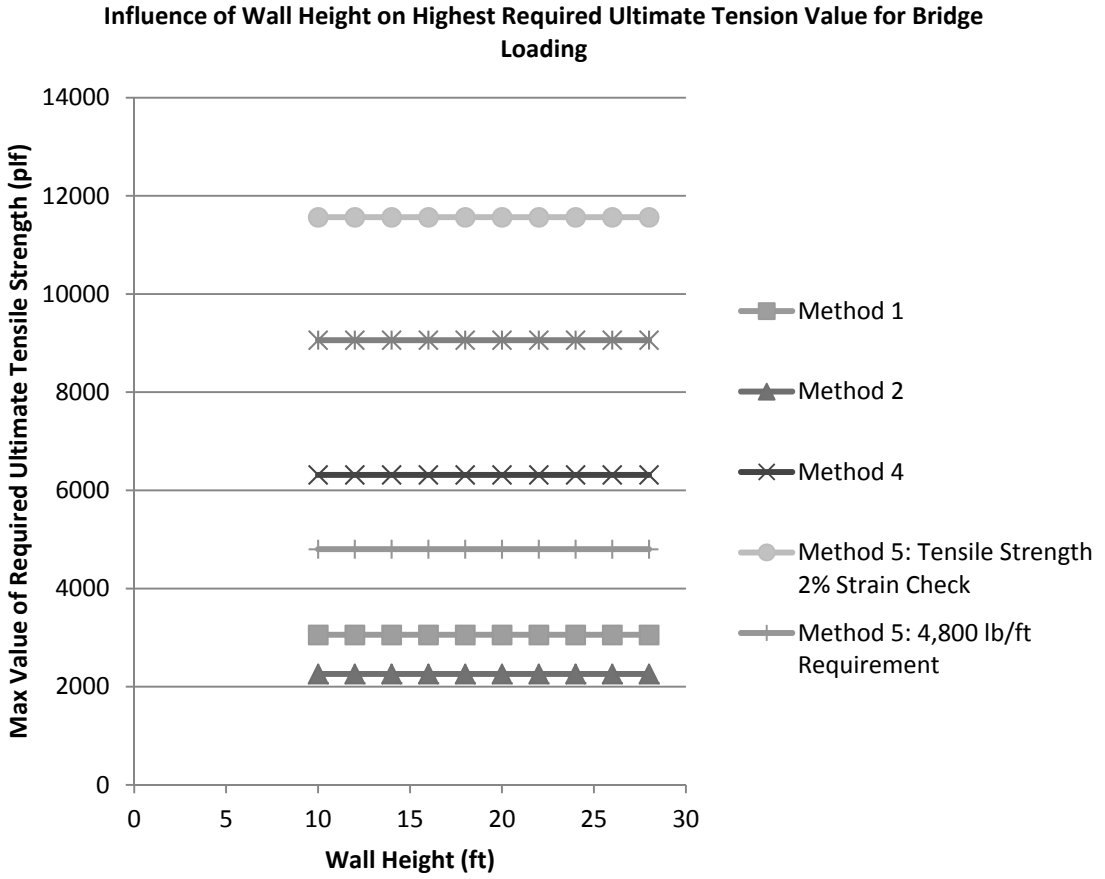

Figure 68: Influence of Wall Height on the Highest Predicted Ultimate Required Tension for the Bridge Loading Condition

Figure 68 shows that the highest predicted ultimate required tensile strength, T_{req}, is at the top of the wall profile for the bridge loading condition. Therefore the change in wall height does not influence this highest value, and Methods 1, 2, 4, and 5 have maximum T_{req} values that plot as a straight horizontal line in Figure 68.

Impact of Reinforced Fill Unit Weight Variation: The following section investigates the influence of varying the reinforced fill unit weight over the range detailed in Table 4 for the roadway loading condition and Table 5 for the bridge loading case, with other parameters left at the base-case values.

Roadway Loading: For the roadway loading scenario, both T_{max} and T_{req} can be compared across all methods. Figure 69, Figure 70, Figure 71, Figure 72, Figure 73, Figure 74, and Figure 75 show the variation in tension for the entire soil profile with change in unit weight for each of the 5 methods.

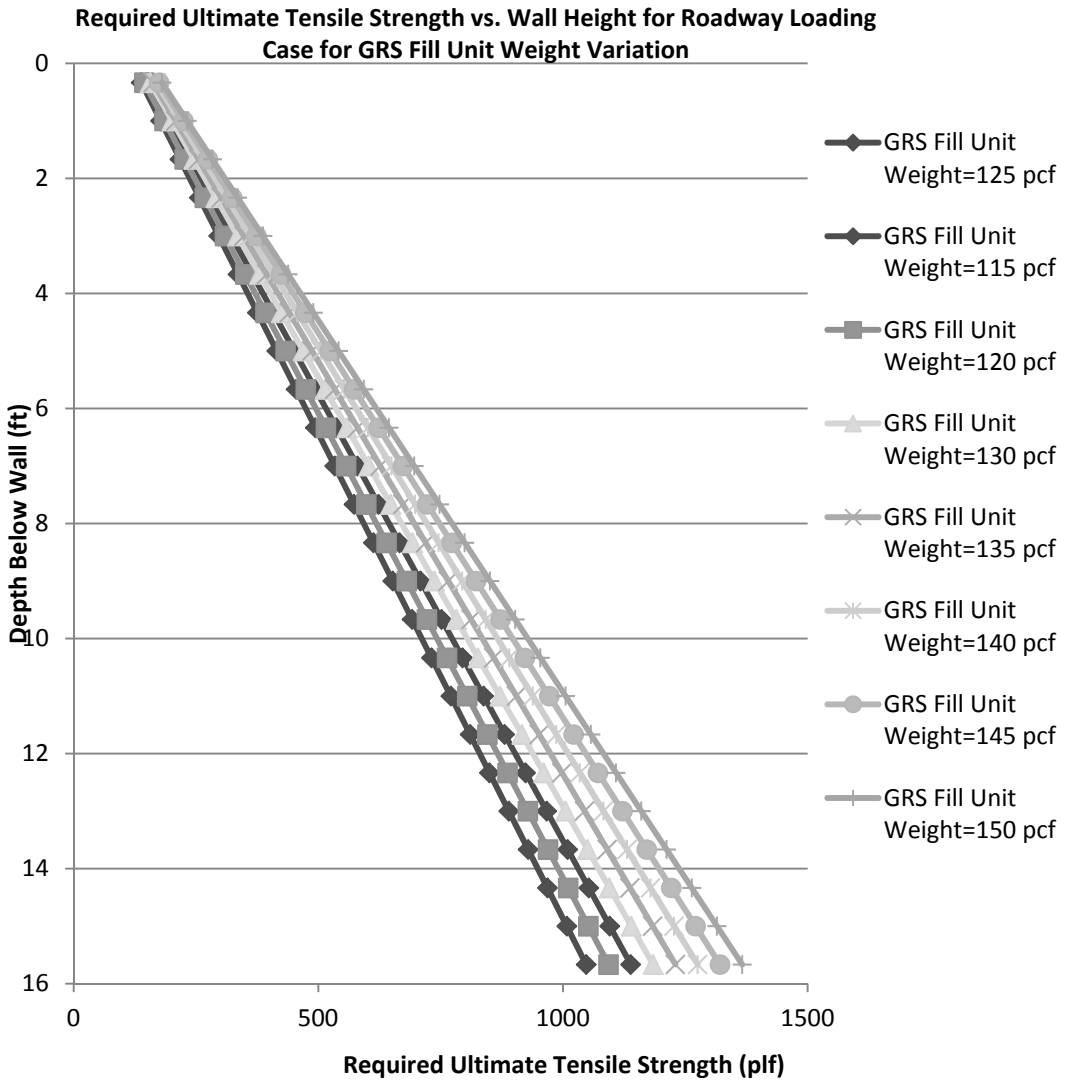

Figure 69: Influence of Unit Weight on Ultimate Required Tension for Roadway Loading for Method 1: The Simplified Procedure

For Method 1, as unit weight of the reinforced fill increases the predicted required ultimate tensile strength, T_{req}, increases as shown in Figure 69. All distributions have a linear shape for the entire soil profile. The T_{req} value both at the top and the bottom increase with unit weight of the reinforced fill with the increase at the bottom being greater than at the top of the wall.

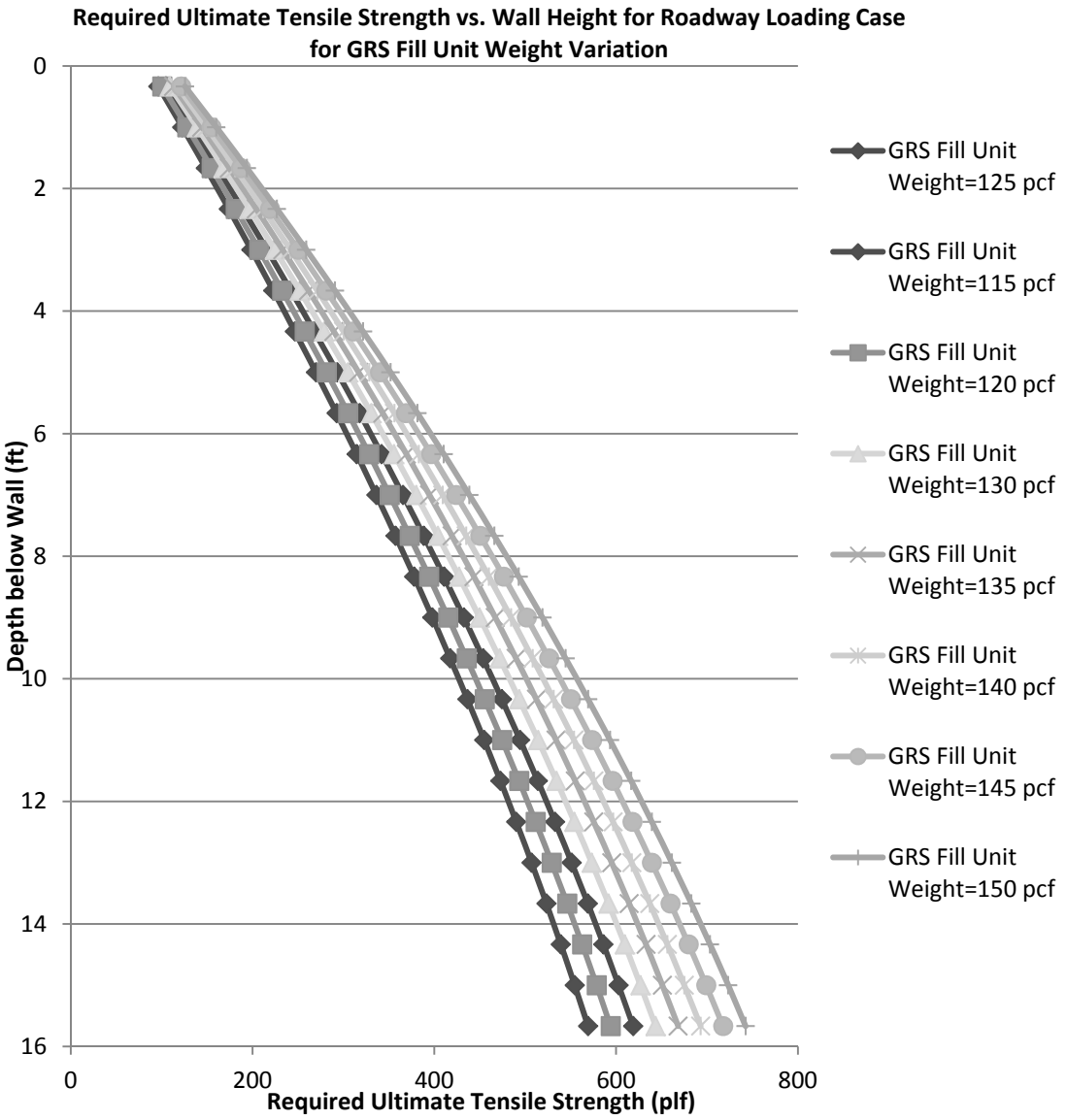

Figure 70: Influence of Unit Weight on Ultimate Required Tension for Roadway Loading for Method 2: The Simplified Procedure with K_r/K_a Adjusted

For Method 2, as unit weight of the reinforced fill increases the predicted required ultimate tensile strength, T_{req}, increases as shown in Figure 70. All distributions have a slightly curved shape with the degree of curvature decreasing with increasing reinforced fill unit weight. The T_{req} value both at the top and the bottom increase with unit weight of the reinforced fill with the increase at the bottom being greater than at the top of the wall.

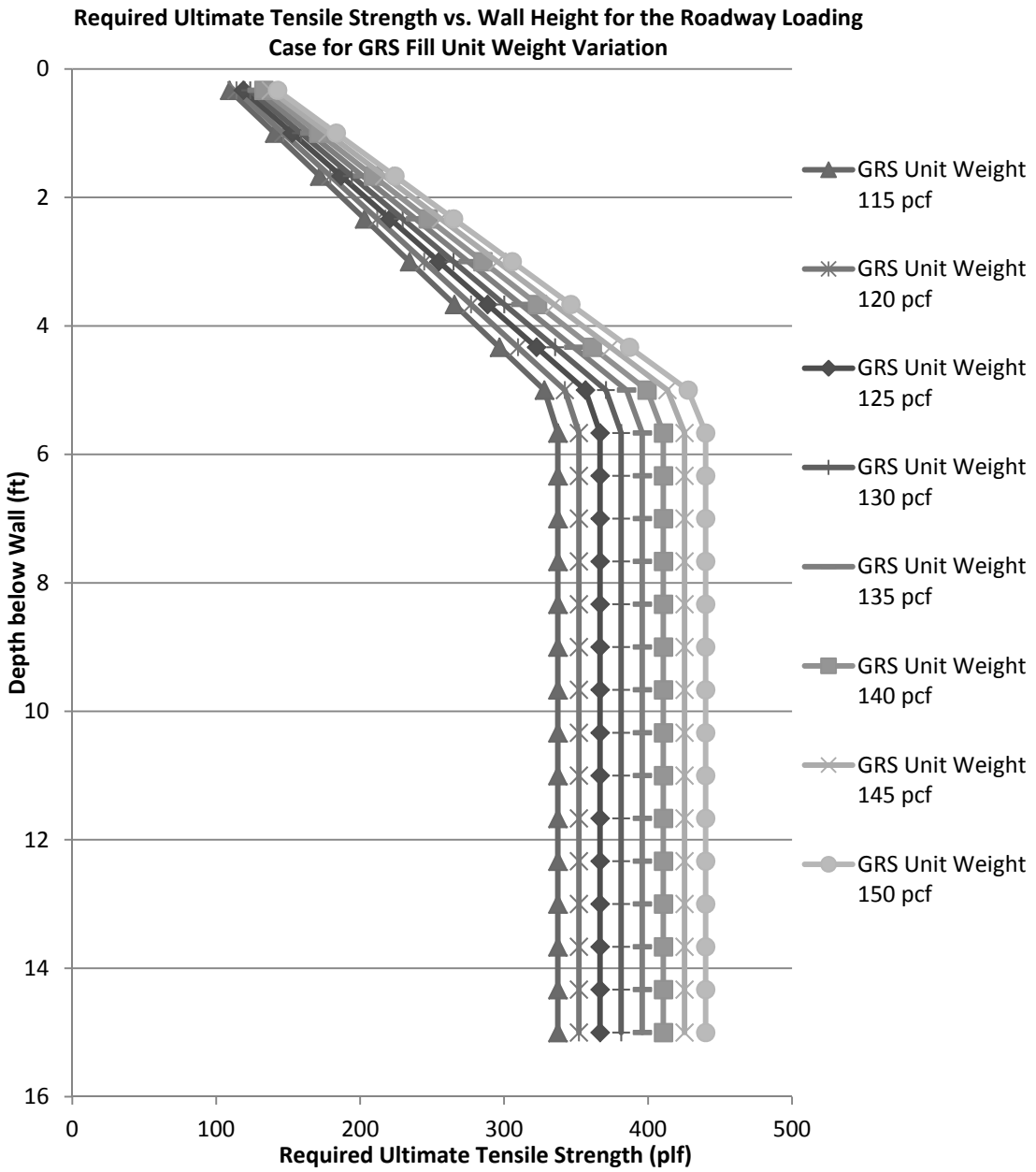

Figure 71: Influence of Unit Weight on Ultimate Required Tension for Roadway Loading for Method 3: K-Stiffness Method

For Method 3, as unit weight of the reinforced fill increases, the predicted required ultimate tensile strength, T_{req}, increases for the entire soil profile as shown in Figure 71. The shape of the distribution is controlled by the load distribution factor. Values at the bottom half of the profile display lower values in comparison to other methods.

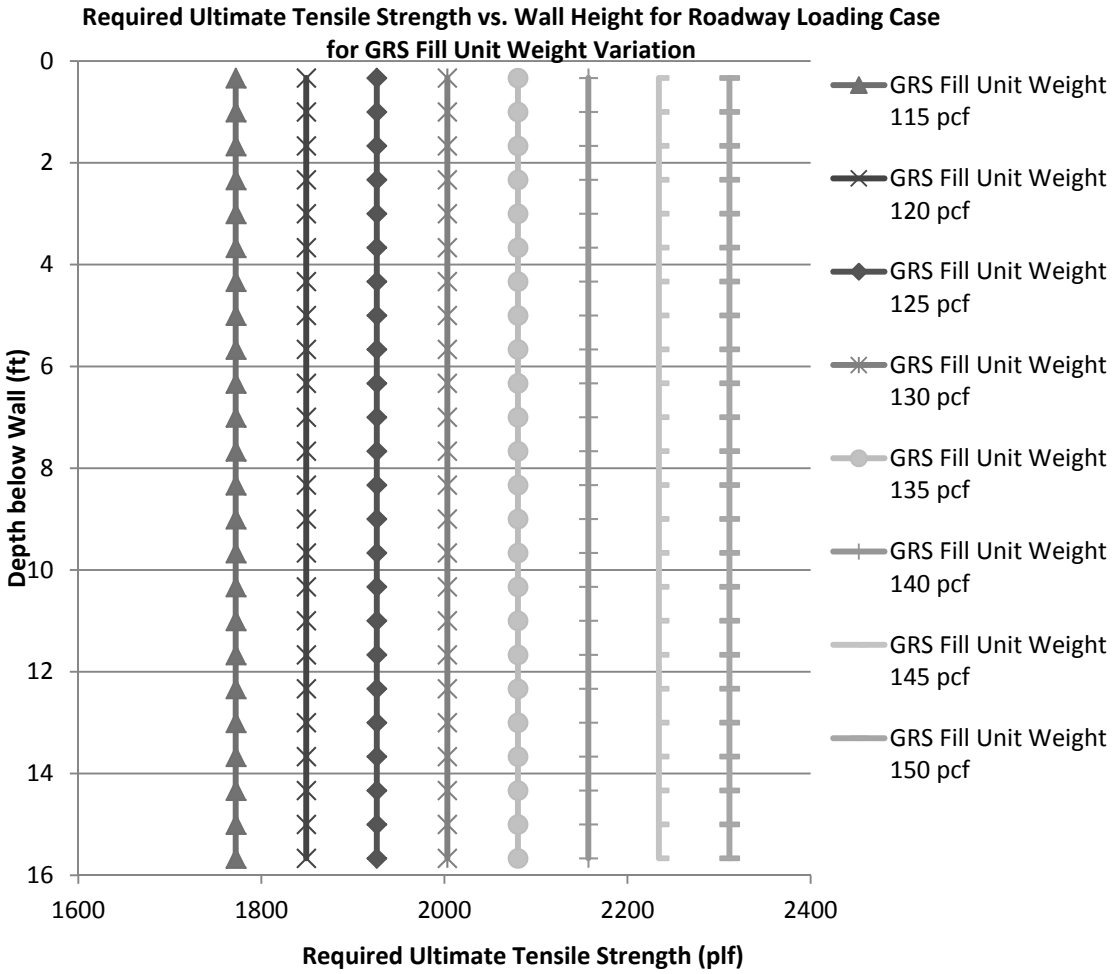

Figure 72: Influence of Unit Weight on Ultimate Required Tension for Roadway Loading for Method 4: NCHRP GRS Method

Figure 72 shows that for Method 4, the entire profile is assigned a required ultimate tensile strength, T_{req}, value equal to the highest value that occurs in the wall. Therefore, the distributions plot as vertical lines. With increasing reinforced fill unit weight, the maximum T_{req} value in the profile also increases. To look more closely at the variation of tension at each reinforcement layer, the variation in nominal maximum tensile load, T_{max}, with depth was plotted for each variation in unit weight. These relationships are plotted in Figure 73.

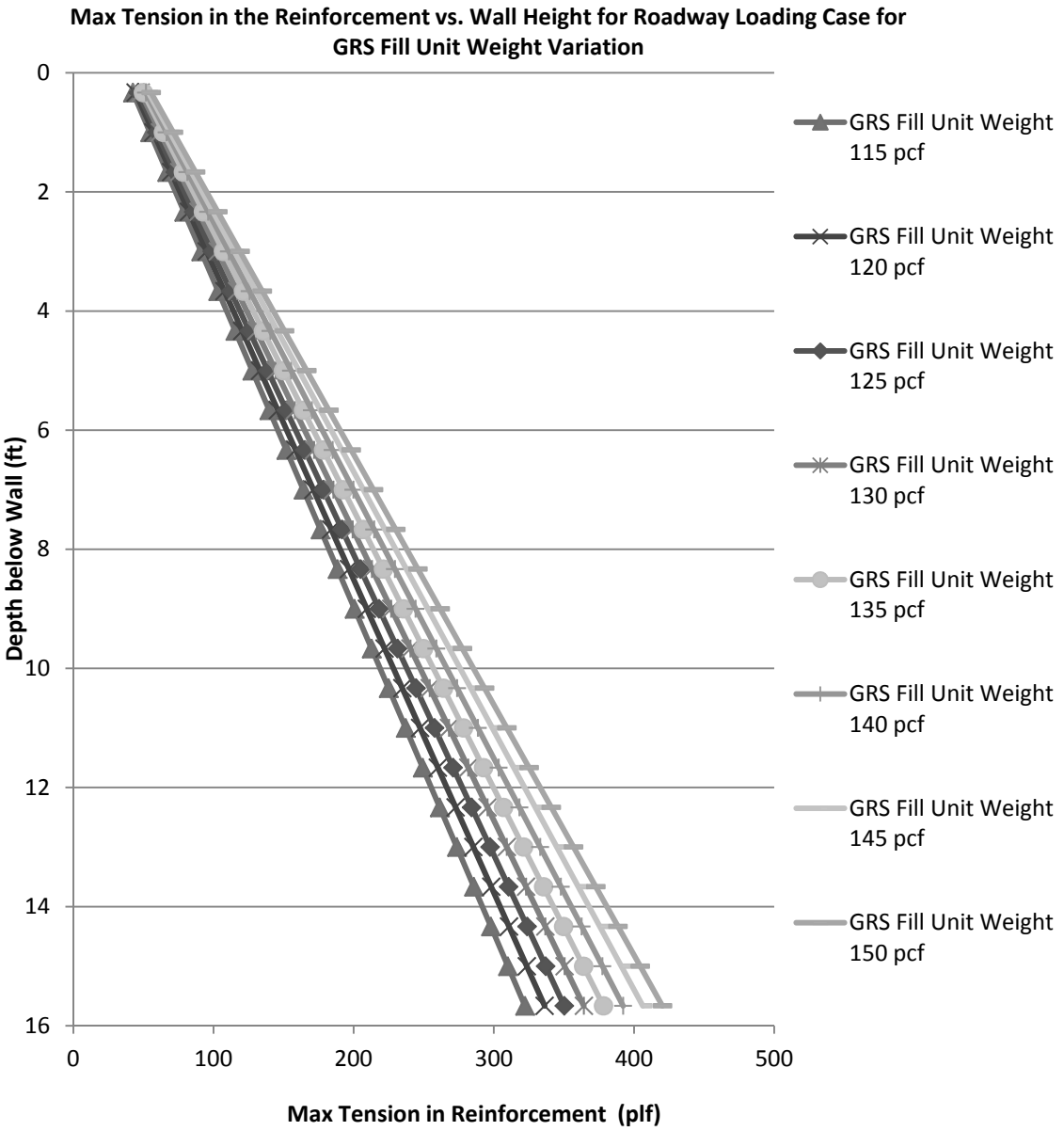

Figure 73: Influence of Unit Weight on Max Tensile Load in the Reinforcement for Roadway Loading for Method 4: NCHRP GRS Method

Figure 73 shows that for Method 4, increasing reinforced fill unit weight will increase the nominal maximum tensile load, T_{max}, at all depths below the top of the reinforced zone. The shape of each distribution remains linear through the entire soil profile.

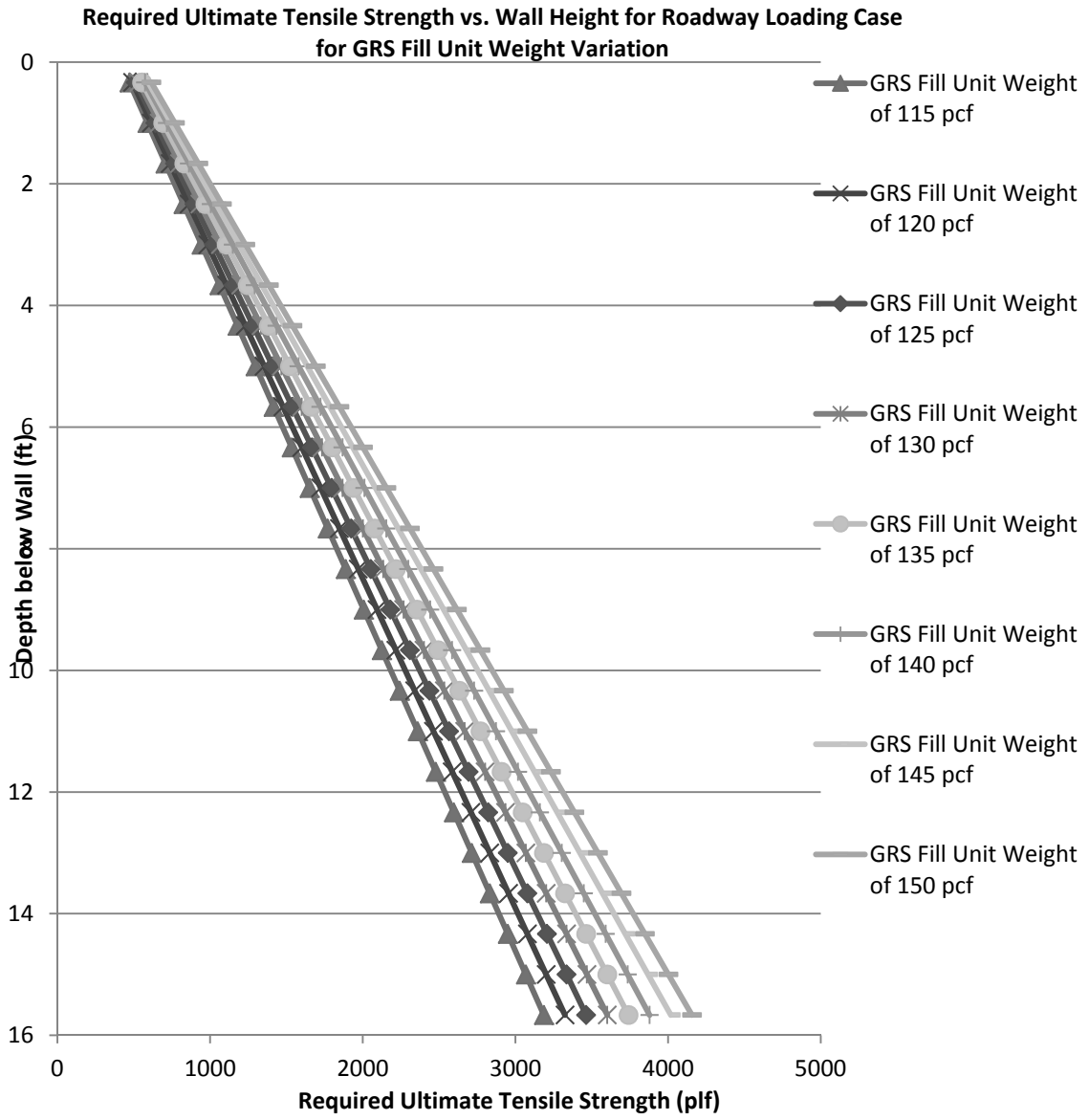

Figure 74: Influence of Unit Weight on Ultimate Required Tension for Roadway Loading for Method 5: FHWA GRS-IBS Method Analytic Solution

For Method 5's analytic solution, as unit weight of the reinforced fill increases the predicted required ultimate tensile strength, T_{req}, increases for the entire soil profile as shown in Figure 74. All distributions are linear at all depths. The increase in T_{req} is greater at the bottom than at the top of the wall.

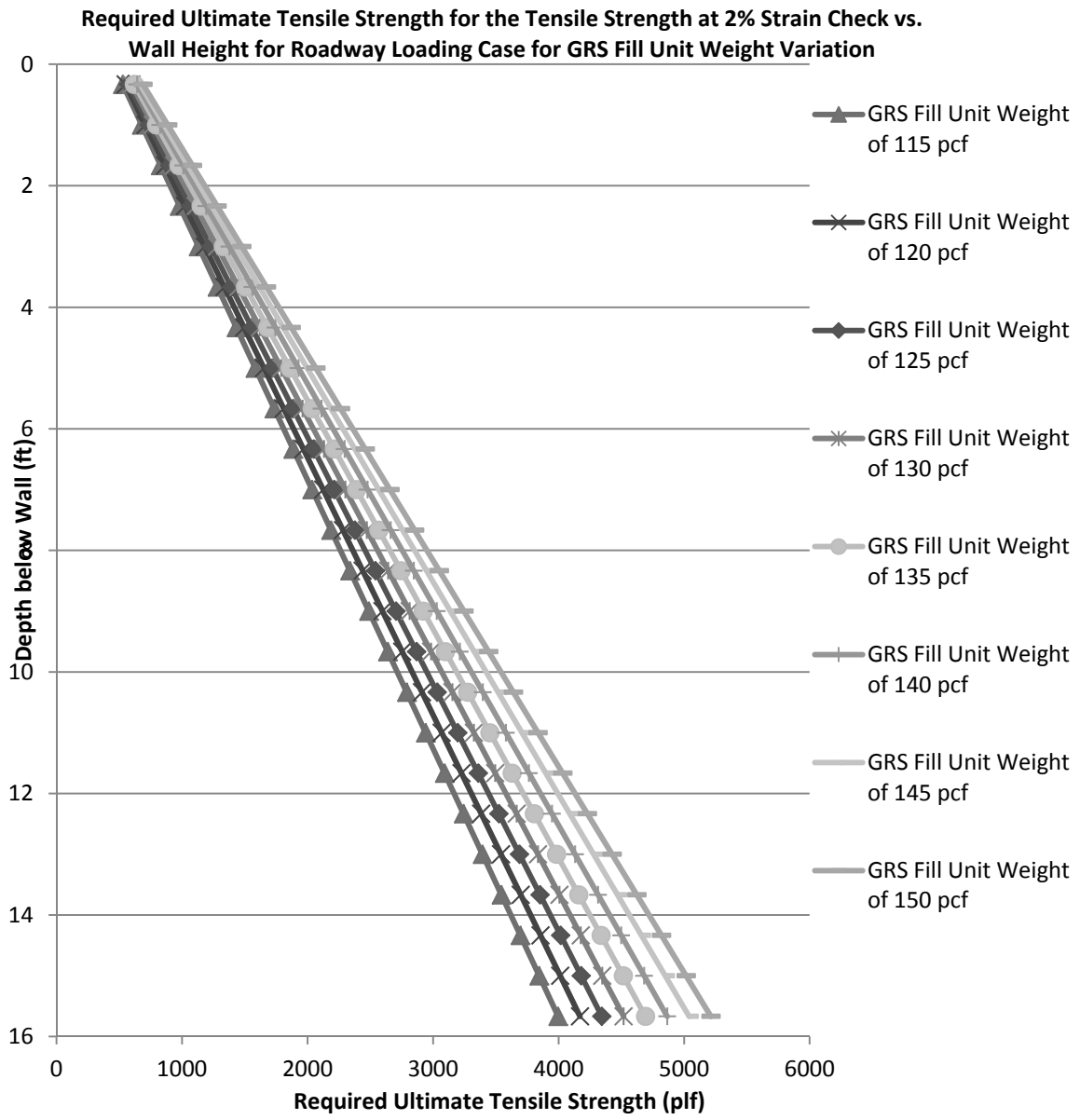

Figure 75: Influence of Unit Weight on Ultimate Required Tension for Roadway Loading for Method 5: FHWA GRS-IBS Method Tensile Strength at 2% Strain Check

Figure 75 shows that for Method 5's tensile strength at 2% strain equivalent T_{req} calculation, the increase in reinforced fill unit weight will increase the predicted required ultimate tensile strength, $T_{req.}$ The predicted values of T_{req} are higher than that predicted by the analytic solution. The distributions remain linear for the entire soil profile similarly to the analytic solution.

The third check required by Method 5 guidance requires the ultimate tensile strength to be greater than or equal to 4,800 lb/ft. This requirement is not plotted but would plot as a straight line at the value of 4,800 lb/ft. For this parameter variation, T_{req} is controlled by

either the 2% strain equivalent or 4,800 lb/ft, and the 2% strain equivalent only controls in the lower portions of walls with high unit weight fill.

For the roadway loading scenario, both T_{max} and T_{req} can be compared across all methods. The maximum values of T_{max} and T_{req} are shown in Figure 76 and Figure 77, respectively.

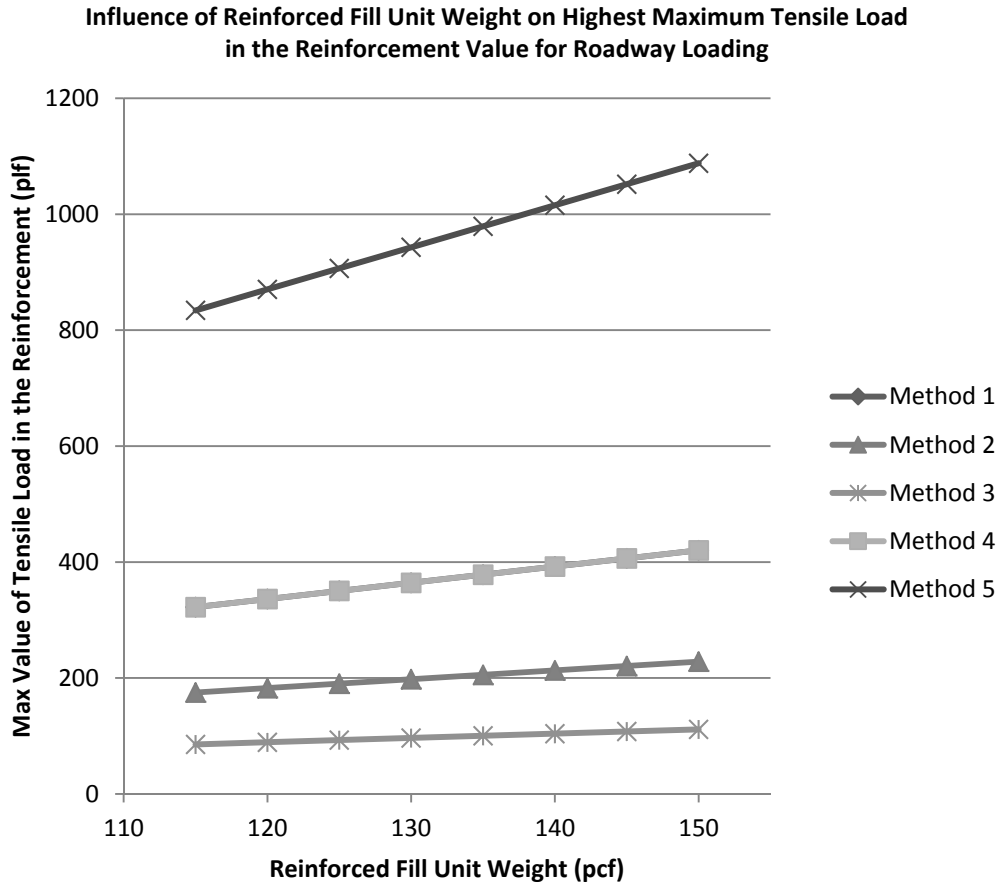

Figure 76: Influence of Unit Weight on Max Load in the Reinforcement for the Roadway Loading Condition

Figure 76 shows that the highest value of maximum load in the reinforcement, T_{max}, increases linearly with increasing reinforced fill unit weight. Values predicted by Method 4 are identical to Method 1 and thus appear as a single line. Values predicted by Method 2 and 3 have roughly the same slope and thus are most likely similarly influenced by reinforced fill unit weight. Method 5 appears to be the most influenced by unit weight as it has the highest slope. Additionally, Method 5 predicts the highest values of T_{max} in comparison to all other methods.

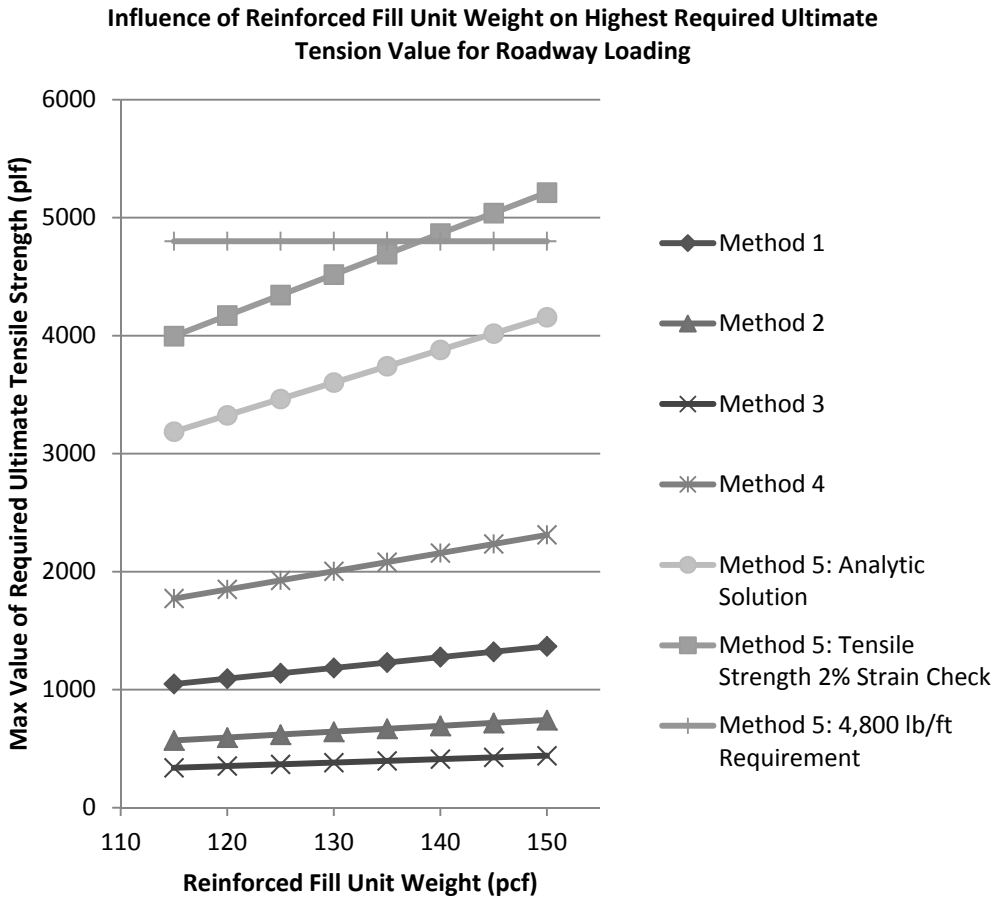

Figure 77: Influence of Unit Weight on the Highest Predicted Ultimate Required Tension for the Roadway Loading Condition

For all but one of the lines plotted in Figure 77, the highest predicted ultimate required tensile strength, T_{req}, also increases linearly with increasing reinforced fill unit weight. The degree of influence that unit weight has varies from method to method but can be correlated to the slope of the linear lines. Unit weight has a similar level of influence on Methods 2 and 3. Method 1 and Method 4 are influenced slightly more by unit weight.

Method 5 has three requirements to establish T_{req} values for design. The first is an analytic solution, the second is a check of tensile strength at 2% strain, and the last is a requirement that T_{req} be at least equal to or above 4,800 lb/ft. The value chosen for design is the highest of the three ultimate strength values. All three of these predicted values are plotted in Figure 77. The first and second requirements are similarly influenced by unit weight but the tensile strength at 2% strain check predicts a higher value. The last requirement plots as a straight horizontal line at 4,800 lb/ft.

Bridge Loading: Method 3, the K-Stiffness Method, was not adapted for the bridge loading case for the parametric study. Figure 78, Figure 79, Figure 80, Figure 81, Figure

82, and Figure 83 show the variation in tension for the entire soil profile with change in unit weight for each of the methods compared.

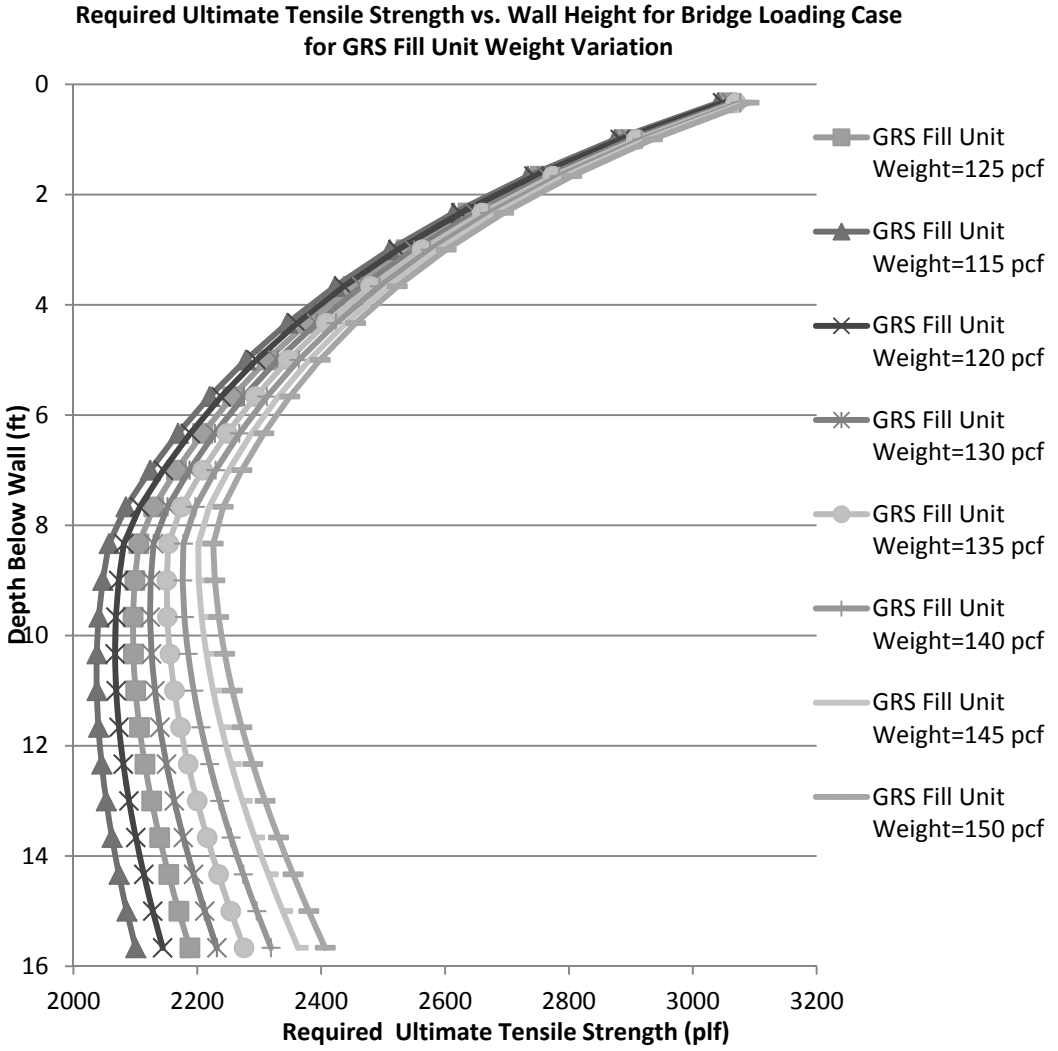

Figure 78: Influence of Unit Weight on Ultimate Required Tension for Bridge Loading for Method 1: The Simplified Procedure

For Method 1, as unit weight of the reinforced fill increases, the predicted required ultimate tensile strength, T_{req}, increases as shown in Figure 78. All distributions have a curved shape for the entire soil profile with the degree of curvature increasing with increasing reinforced fill unit weight. The T_{req} value both at the top and the bottom increase with unit weight of the reinforced fill, with the increase at the bottom being greater than at the top of the wall.

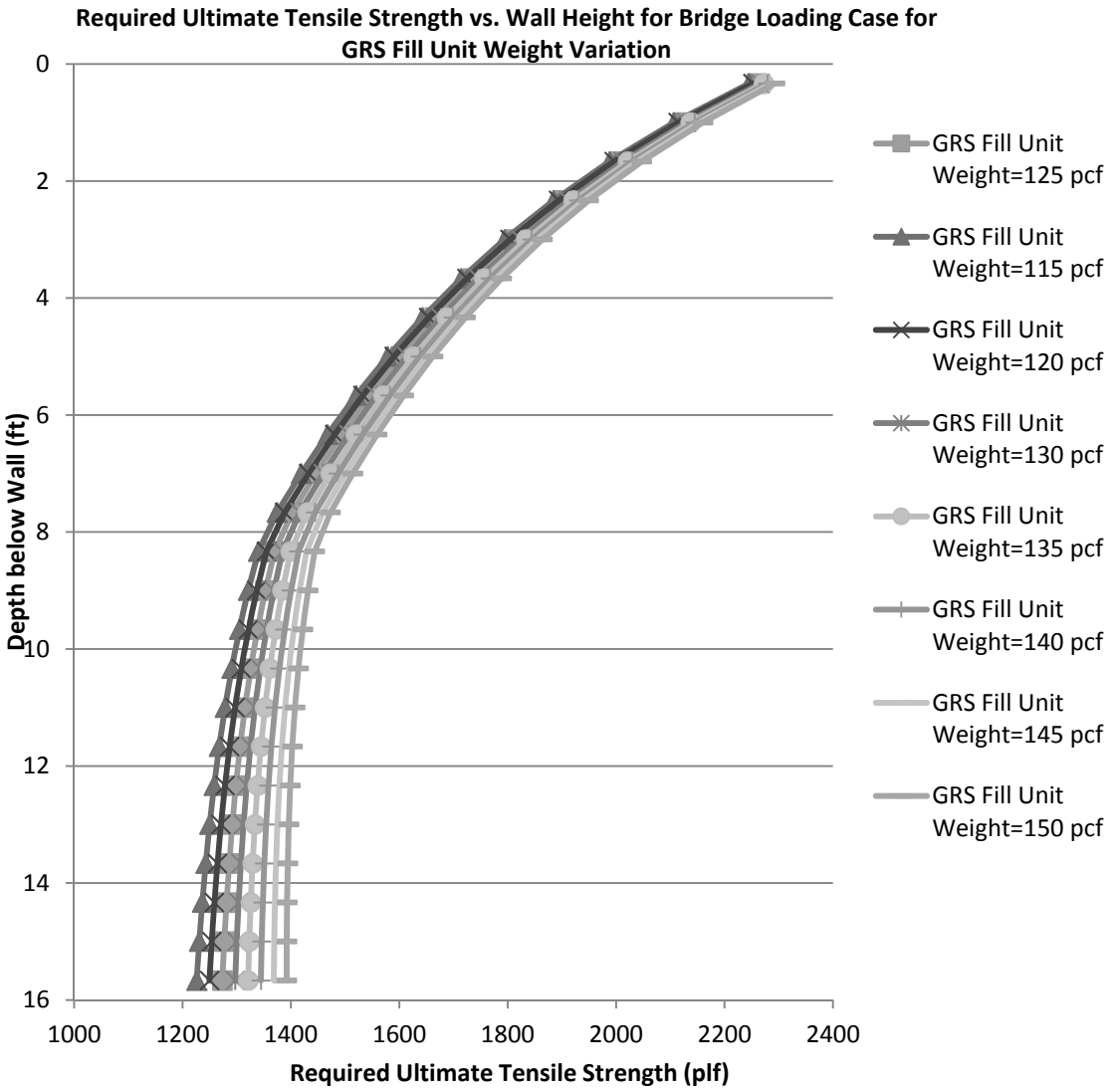

Figure 79: Influence of Unit Weight on Ultimate Required Tension for Bridge Loading for Method 2: The Simplified Procedure with K_r/K_a Adjusted

For Method 2, as unit weight of the reinforced fill increases the predicted required ultimate tensile strength, T_{req}, increases as shown in Figure 79. All distributions have a curved shape for the entire soil profile with the degree of curvature increasing with increasing reinforced fill unit weight. The T_{req} value both at the top and the bottom increase with unit weight of the reinforced fill with the increase at the bottom being greater than at the top of the wall.

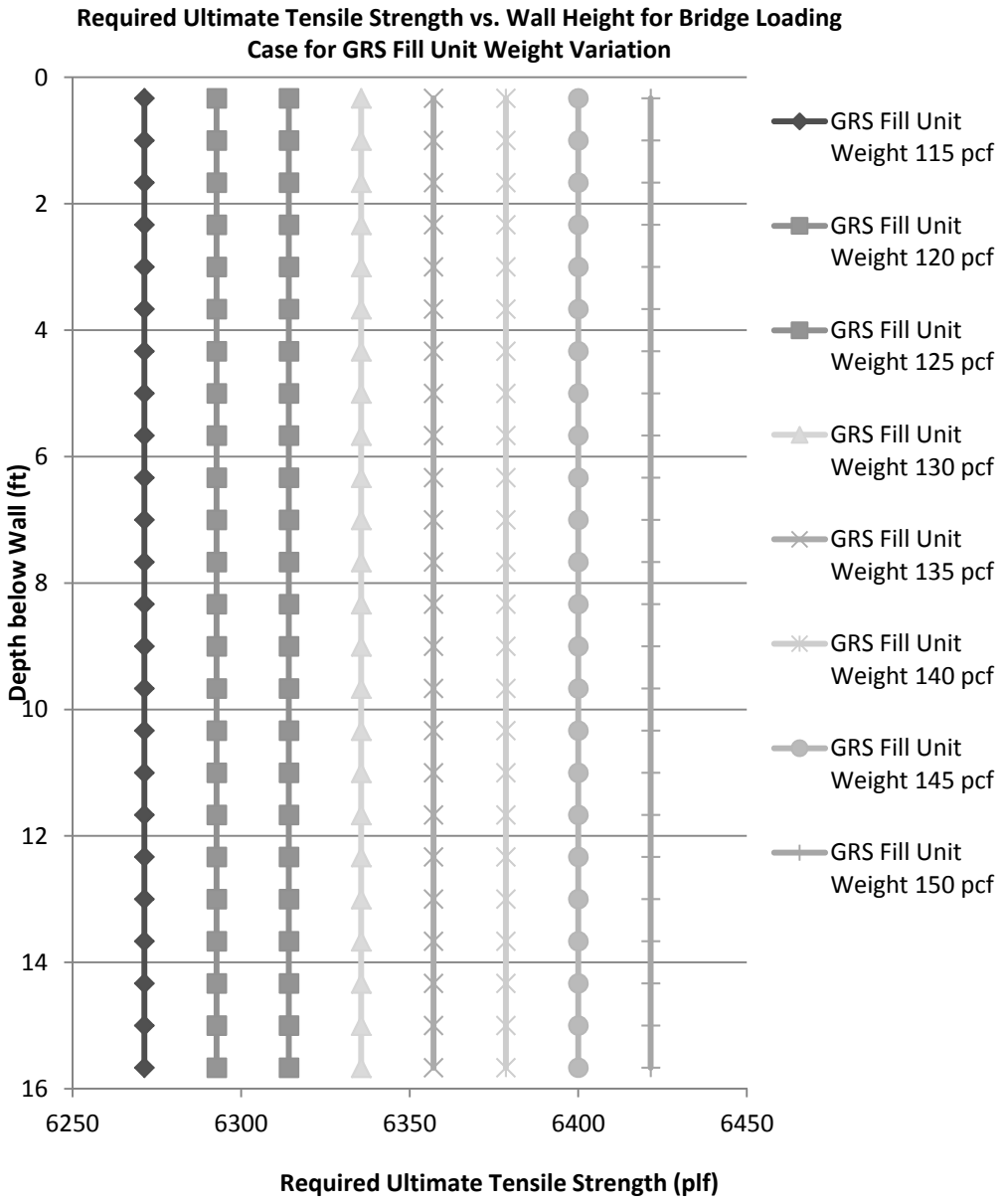

Figure 80: Influence of Unit Weight on Ultimate Required Tension for Bridge Loading for Method 4: NCHRP GRS Method

Figure 80 shows that for Method 4, the entire profile is assigned a required ultimate tensile strength, T_{req}, value equal to the highest value that occurs in the wall. Therefore, the distributions plot as vertical lines. With increasing reinforced fill unit weight, the maximum T_{req} value in the profile increases, but the magnitude of the increase is small. To look more closely at the variation of tension at each reinforcement layer, the variation in nominal maximum tensile load, T_{max}, with depth was plotted for each variation in unit weight. These relationships are plotted in Figure 81.

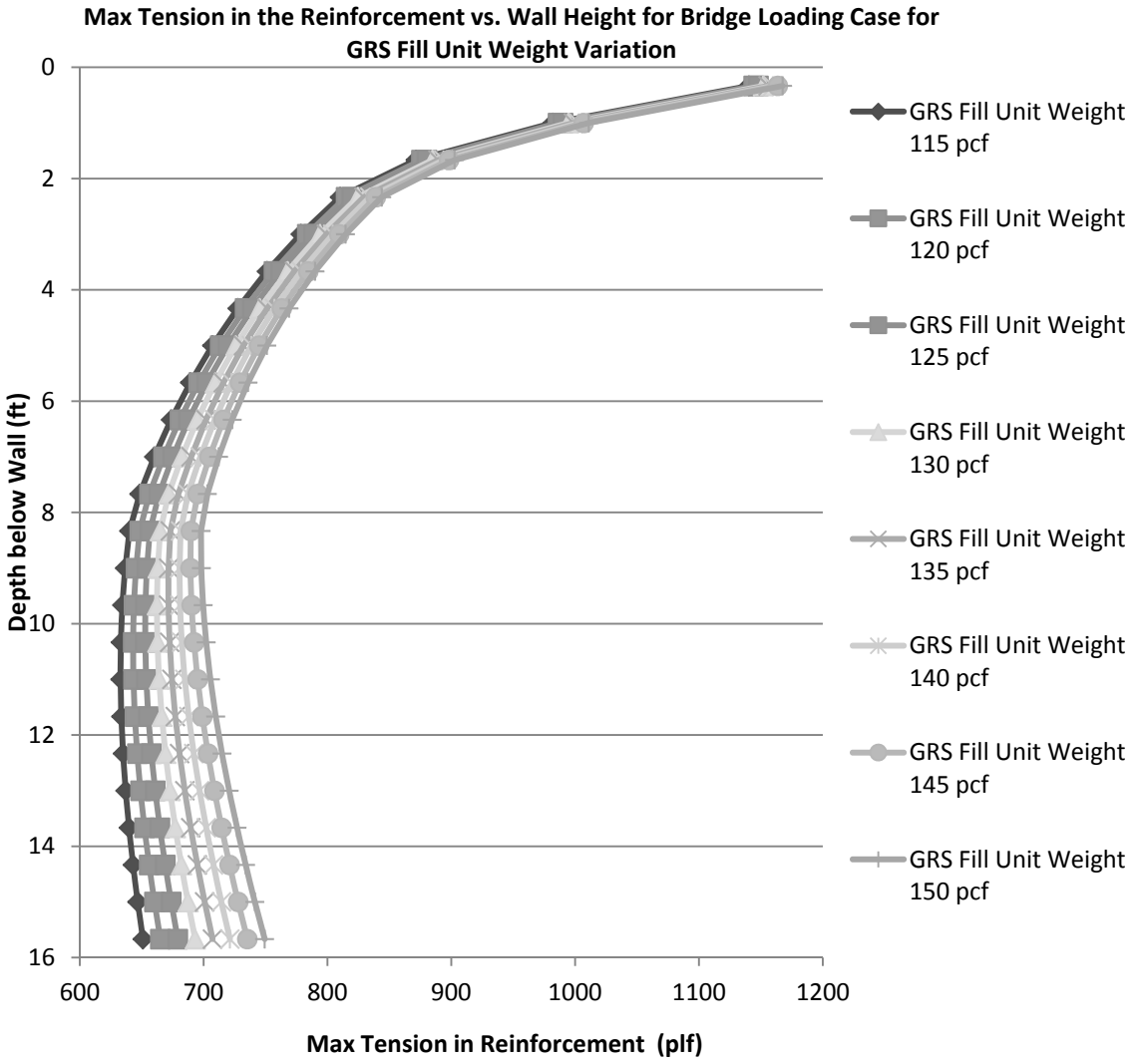

Figure 81: Influence of Unit Weight on Max Tensile Load in the Reinforcement for Bridge Loading for Method 4: NCHRP GRS Method

Figure 81 shows that for Method 4, increasing reinforced fill unit weight increases the nominal maximum tensile load, T_{max}, at all depths below the top of the reinforced zone. The shape of each distribution is curved with increasing degree of curvature as reinforced fill unit weight increases.

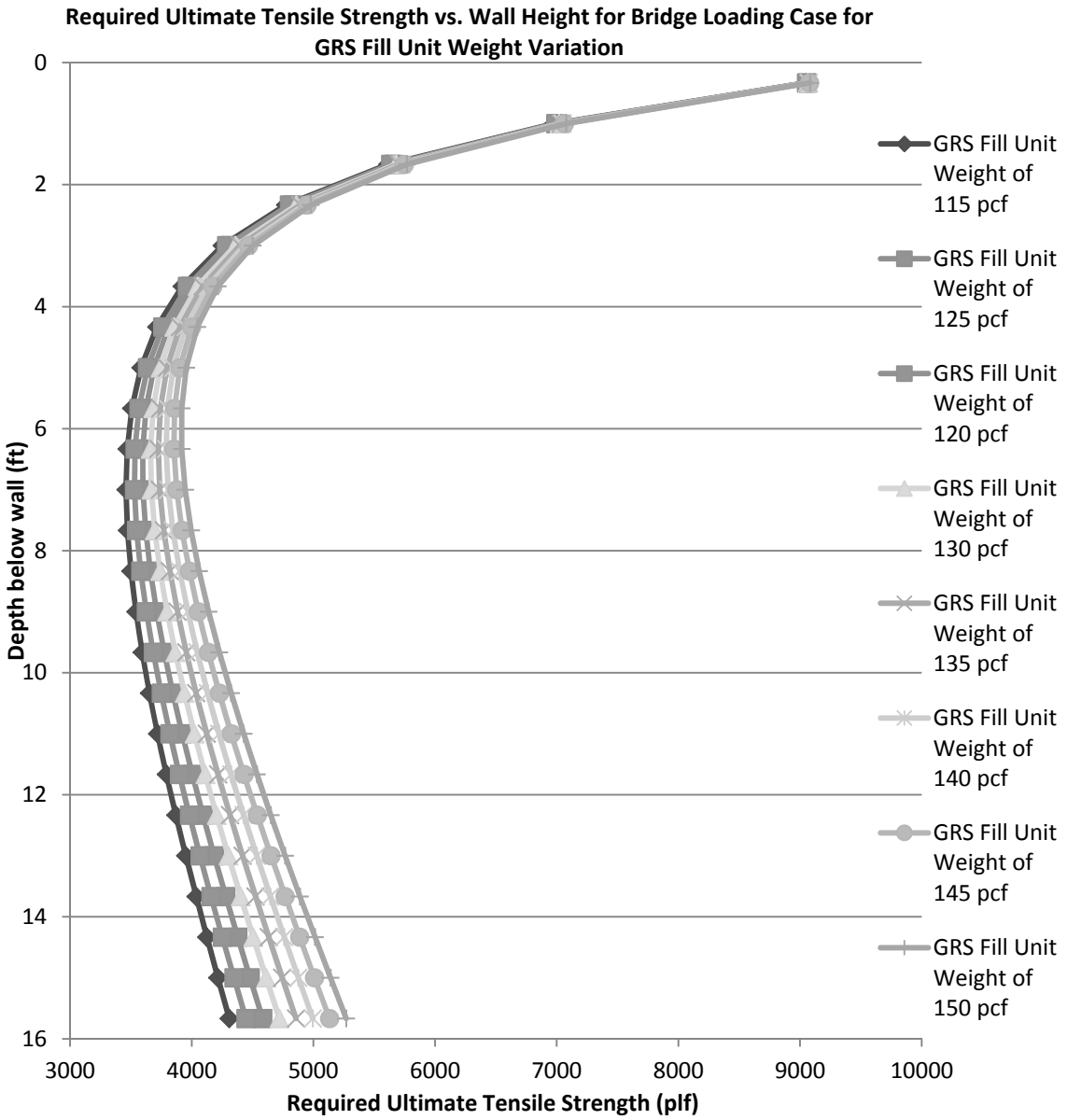

Figure 82: Influence of Unit Weight on Ultimate Required Tension for Bridge Loading for Method 5: FHWA GRS-IBS Method Analytic Solution

For Method 5's analytic solution, as unit weight of the reinforced fill increases the predicted required ultimate tensile strength, T_{req}, increases for the entire soil profile as shown in Figure 82. All distributions have a curved shape that increases in degree with increasing unit weight. The increase in T_{req} is greater at the bottom than at the top of the wall.

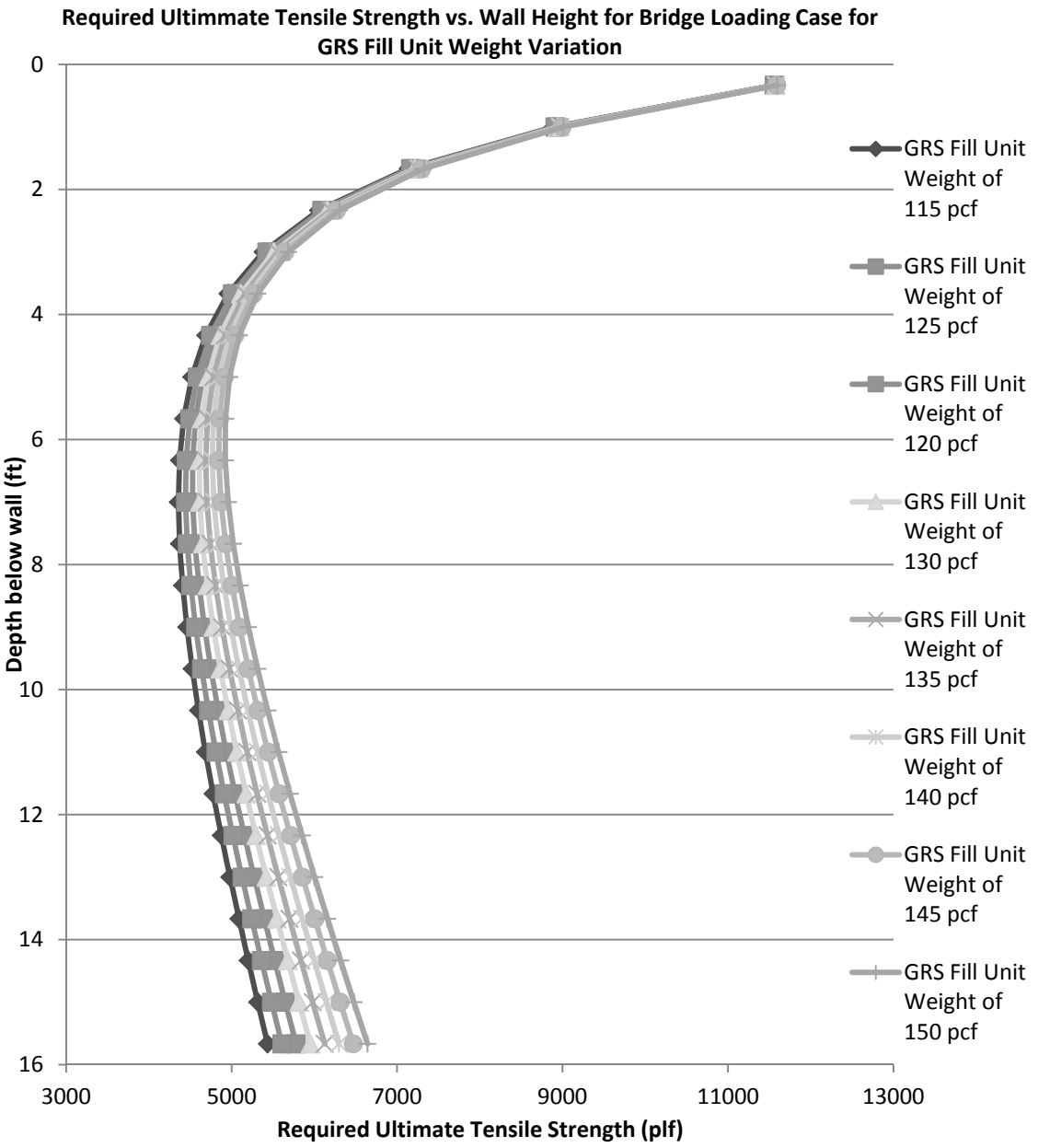

Figure 83: **Influence of Unit Weight on Ultimate Required Tension for Bridge Loading for Method 5: FHWA GRS-IBS Method Tensile Strength at 2% Strain Check**

Figure 83 shows that for Method 5's tensile strength at 2% strain equivalent T_{req} calculation, the increase in reinforced fill unit weight will increase the predicted required ultimate tensile strength, $T_{req.}$ The predicted values of T_{req} are higher than that predicted by the analytic solution but the distributions have very similar shapes.

There is a third check required by Method 5 guidance that requires the ultimate tensile strength to be greater than or equal to 4,800 lb/ft. This requirement is not plotted but would plot as a straight line at the value of 4,800 lb/ft. Which of the three requirements that controls can vary within the soil profile. In general, the tensile strength at 2% strain

controls for the upper and lower portions of the wall profile for all unit weights. The 4,800 lb/ft requirement controls for some of the unit weights less than 140 pcf for the center portion of the profile.

Method 3, the K-Stiffness Method, was not adapted for the bridge loading case for the parametric study. The maximum values of T_{max} and T_{req} are shown in Figure 84 and Figure 85, respectively.

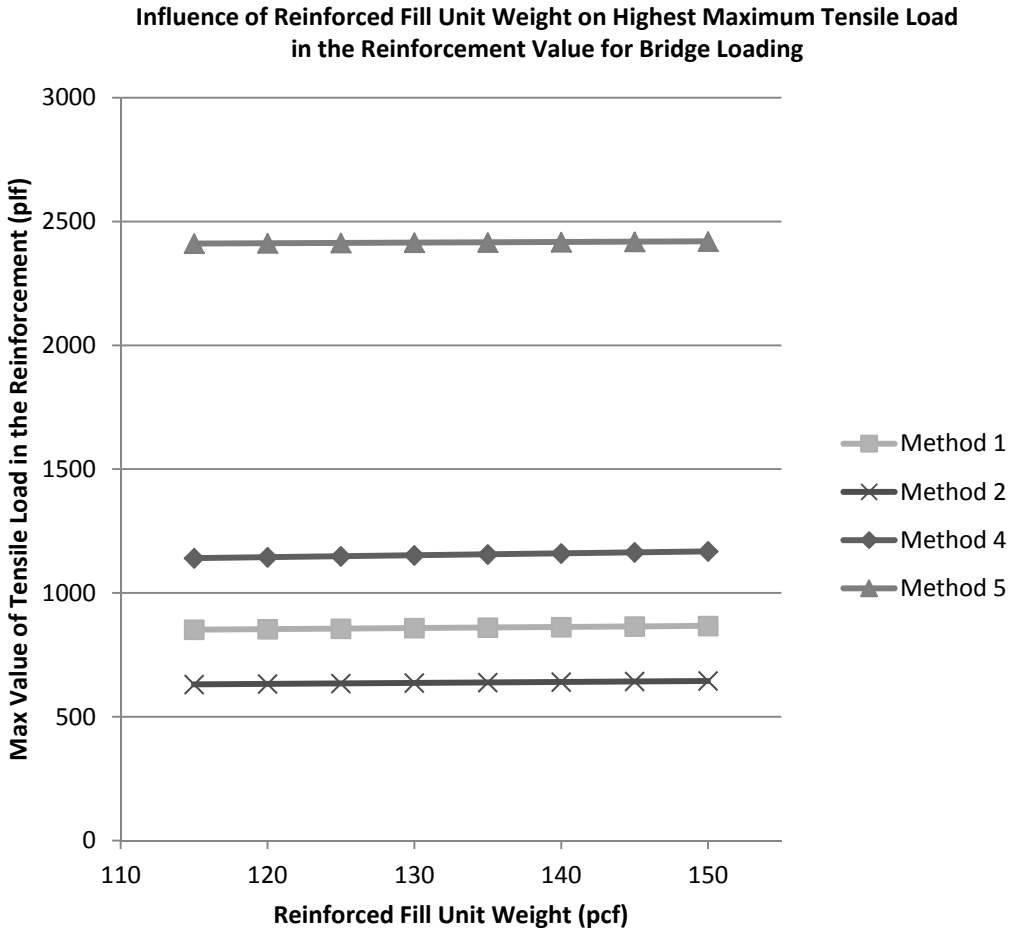

Figure 84: Influence of Unit Weight on Max Load in the Reinforcement for the Bridge Loading Condition

Figure 84 shows that the highest value of maximum load in the reinforcement, T_{max}, is at the top of the wall profile for the bridge loading condition. Therefore, Methods 1, 2, 4, and 5 have maximum T_{max} values that plot as a straight horizontal line in Figure 84. The Method 5 tensile strength at 2% check predicts the highest T_{req} values and Method 2 the lowest.

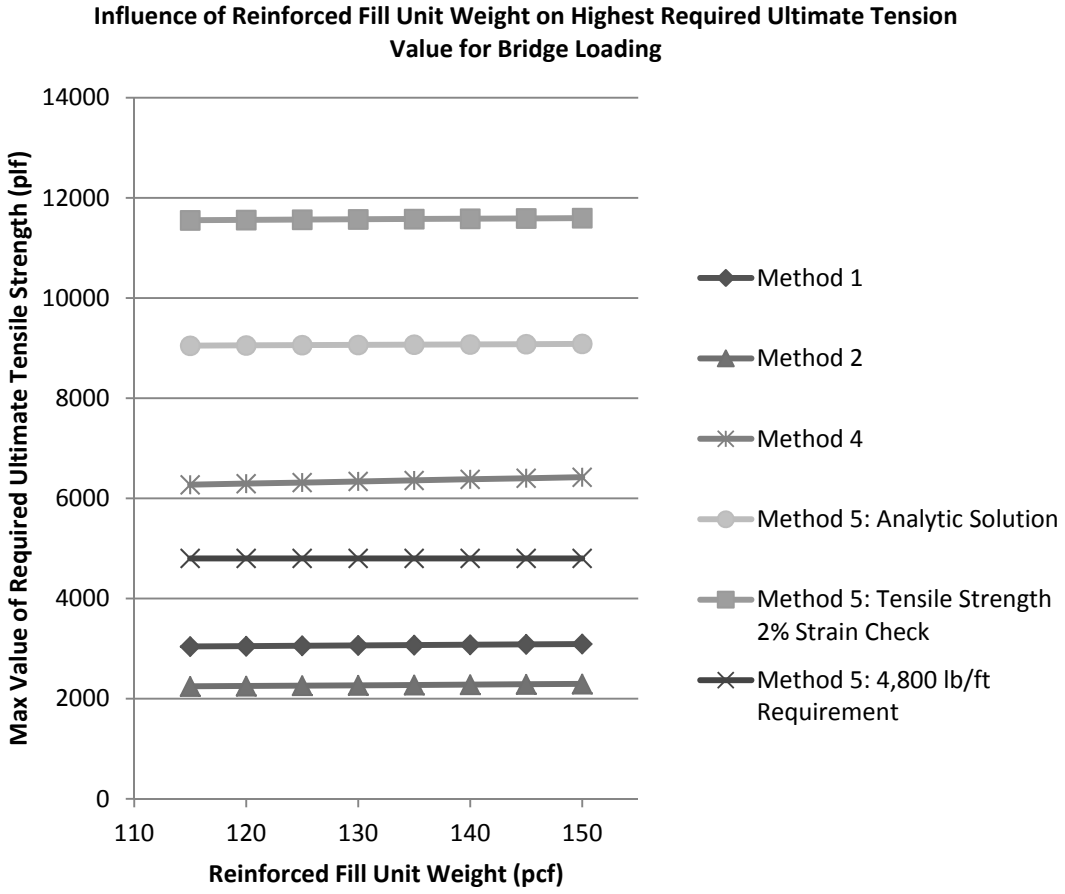

Figure 85: Influence of Unit Weight on the Highest Predicted Ultimate Required Tension for the Bridge Loading Condition

Figure 85 shows that the highest predicted ultimate required tensile strength, T_{req}, is at the top of the wall profile for the bridge loading condition. Therefore, Methods 1, 2, 4, and 5 have maximum T_{req} values that plot as a straight horizontal line in Figure 85. The Method 5 tensile strength at 2% check predicts the highest T_{req} values and Method 2 the lowest.

Impact of Friction Angle Variation: The following section explores the influence of varying the reinforced fill friction angle over the range detailed in Table 4 for the roadway loading condition and Table 5 for the bridge loading case.

Roadway Loading: For the roadway loading scenario, both T_{max} and T_{req} can be compared across all methods. The friction angle was varied from a minimum value of 34° to a maximum value of 55°. The base case value of the friction angle was 38°. Figure 86, Figure 87, Figure 88, Figure 89, Figure 90, Figure 91 and Figure 92 show the variation in tension for the entire soil profile with change in friction angle for each of the 5 methods.

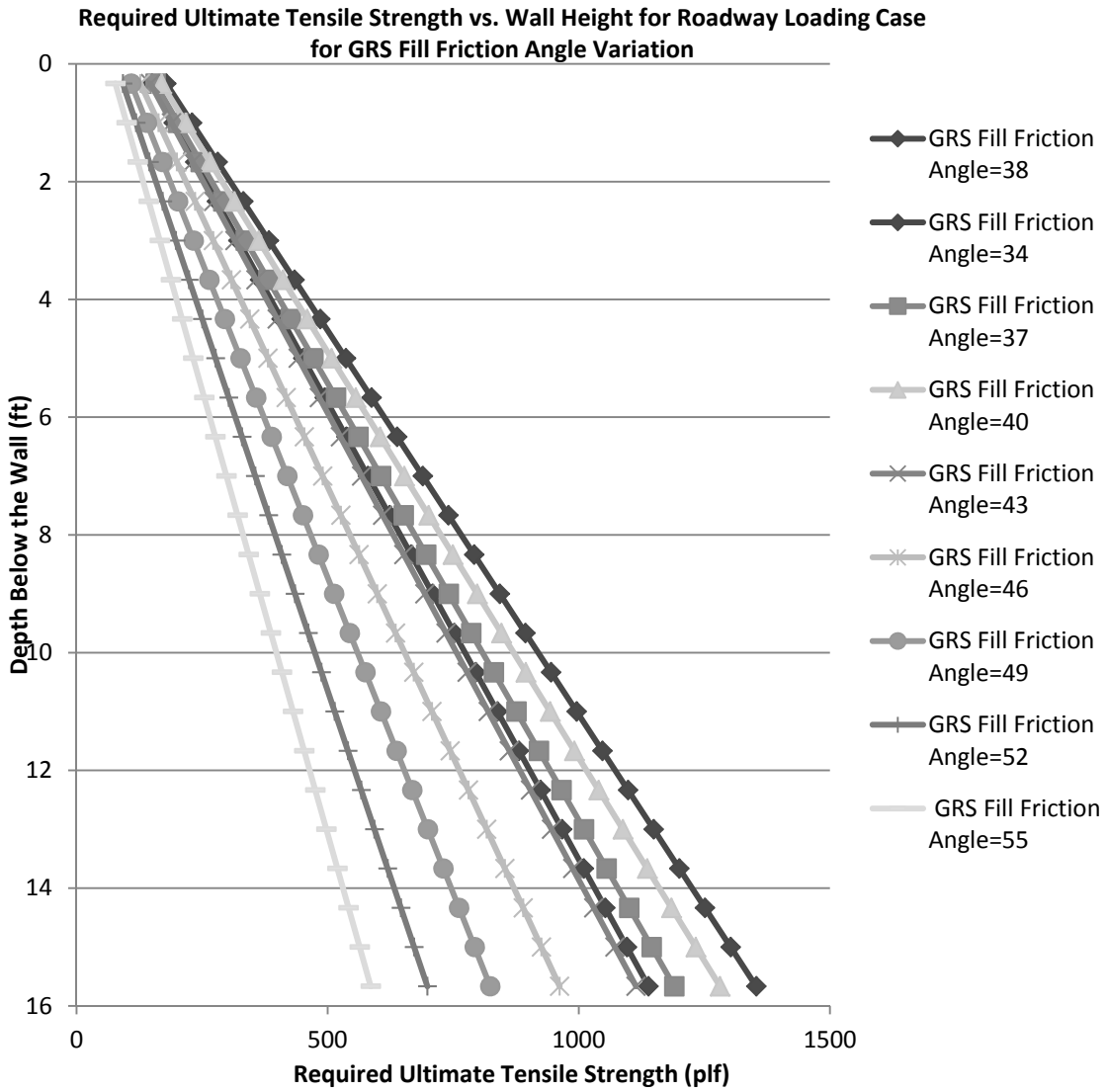

Figure 86: Influence of Friction Angle on Ultimate Required Tension for Roadway Loading for Method 1: The Simplified Procedure

For Method 1, in general as friction angle of the reinforced fill increases the predicted required ultimate tensile strength, T_{req}, decreases as shown in Figure 78. However, the reduction factor for installation damage is partly dependent on friction angle. Once friction angle of the reinforced fill is equal to or above 40° the reduction factor increases to 1.8 from 1.3 for the base case. This causes some parameter variations to not fall in a progressive sequence. All distributions have a linear shape for the entire soil profile. The T_{req} value both at the top and the bottom decrease with increasing friction angle of the reinforced fill with the decrease at the bottom being greater than at the top of the wall.

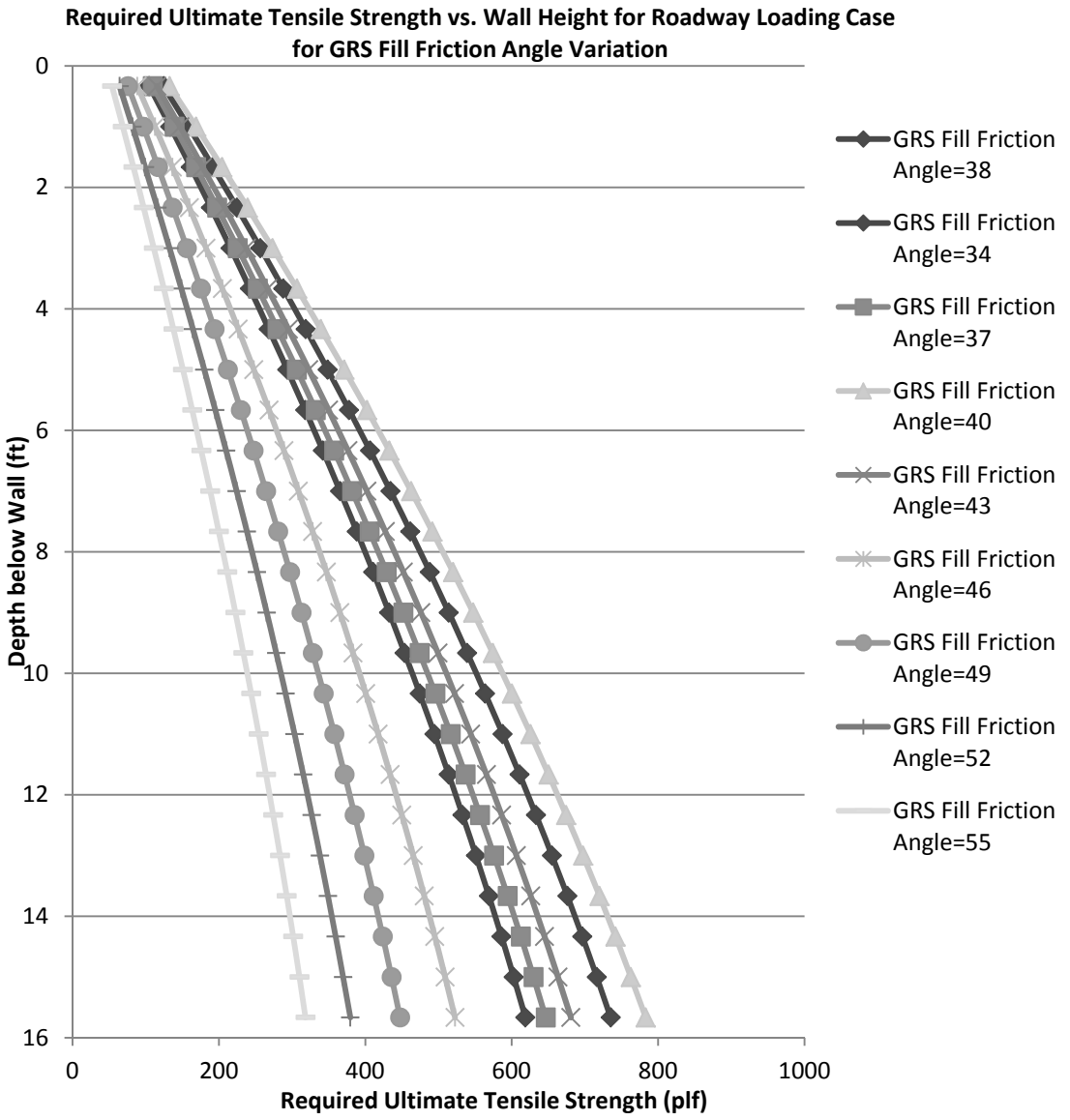

Figure 87: Influence of Friction Angle on Ultimate Required Tension for Roadway Loading for Method 2: The Simplified Procedure with K_r/K_a Adjusted

For Method 2, in general as friction angle of the reinforced fill increases the predicted required ultimate tensile strength, T_{req}, decreases as shown in Figure 87. However, the reduction factor for installation damage is partly dependent on friction angle. Once friction angle of the reinforced fill is equal to or above 40° the reduction factor increases to 1.8 from 1.3 for the base case. This causes some parameter variations to not fall in a progressive sequence. All distributions have a slightly curved shape that decreases with increasing friction angle. The T_{req} value both at the top and the bottom decrease with increasing friction angle of the reinforced fill with the decrease at the bottom being greater than at the top of the wall.

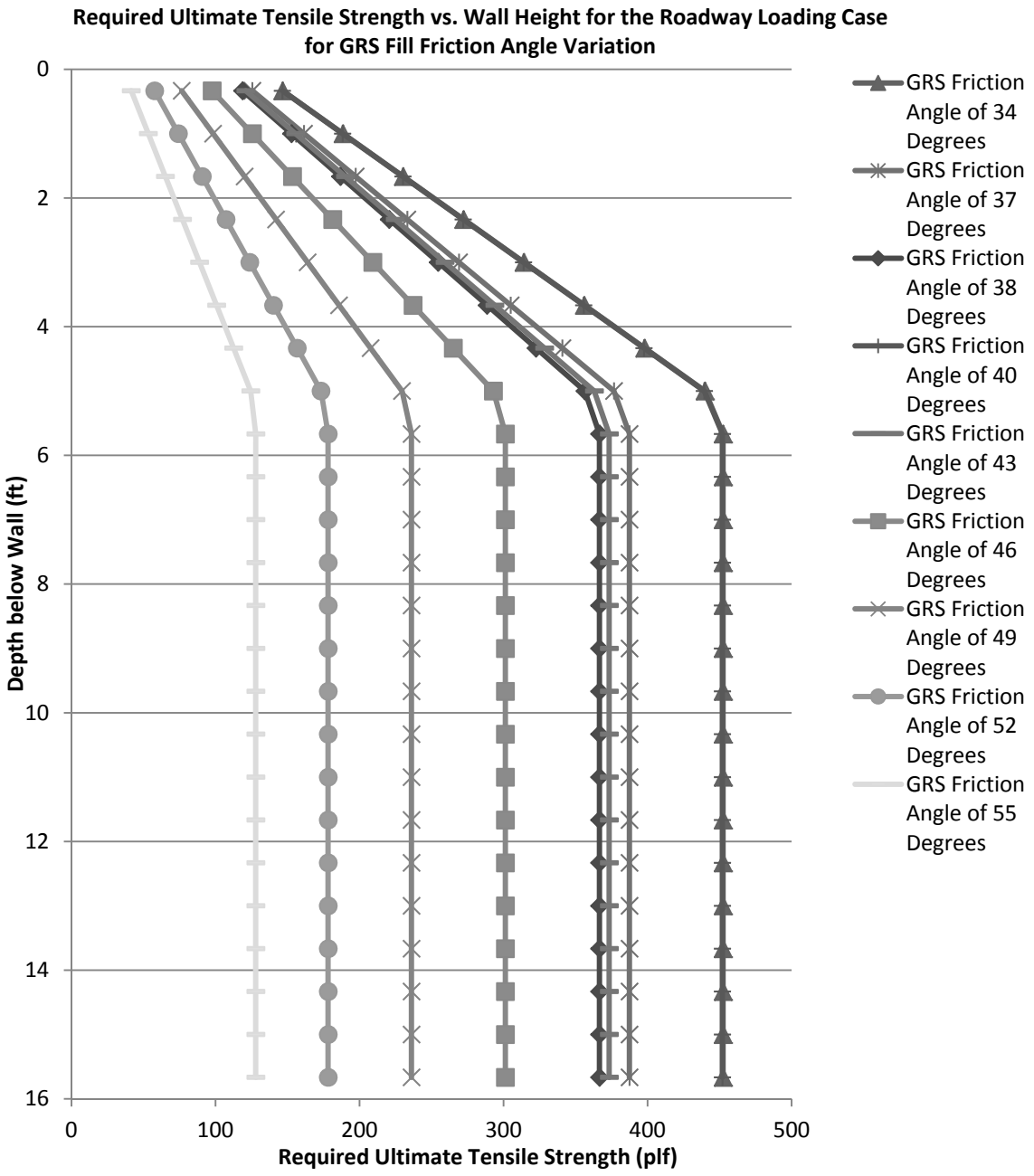

Figure 88: Influence of Friction Angle on Ultimate Required Tension for Roadway Loading for Method 3: K-Stiffness Method

For Method 3, as friction angle of the reinforced fill increases the predicted required ultimate tensile strength, T_{req}, decreases for the entire soil profile as shown in Figure 88. However, the reduction factor for installation damage is partly dependent on friction angle. Once friction angle of the reinforced fill is equal to or above 40° the reduction factor increases to 1.8 from 1.3 for the base case. This causes some parameter variations to not fall in a progressive sequence. The shape of the distribution is controlled by the

load distribution factor. Values predicted using Method 3, K-Stiffness, are lower in comparison to other methods.

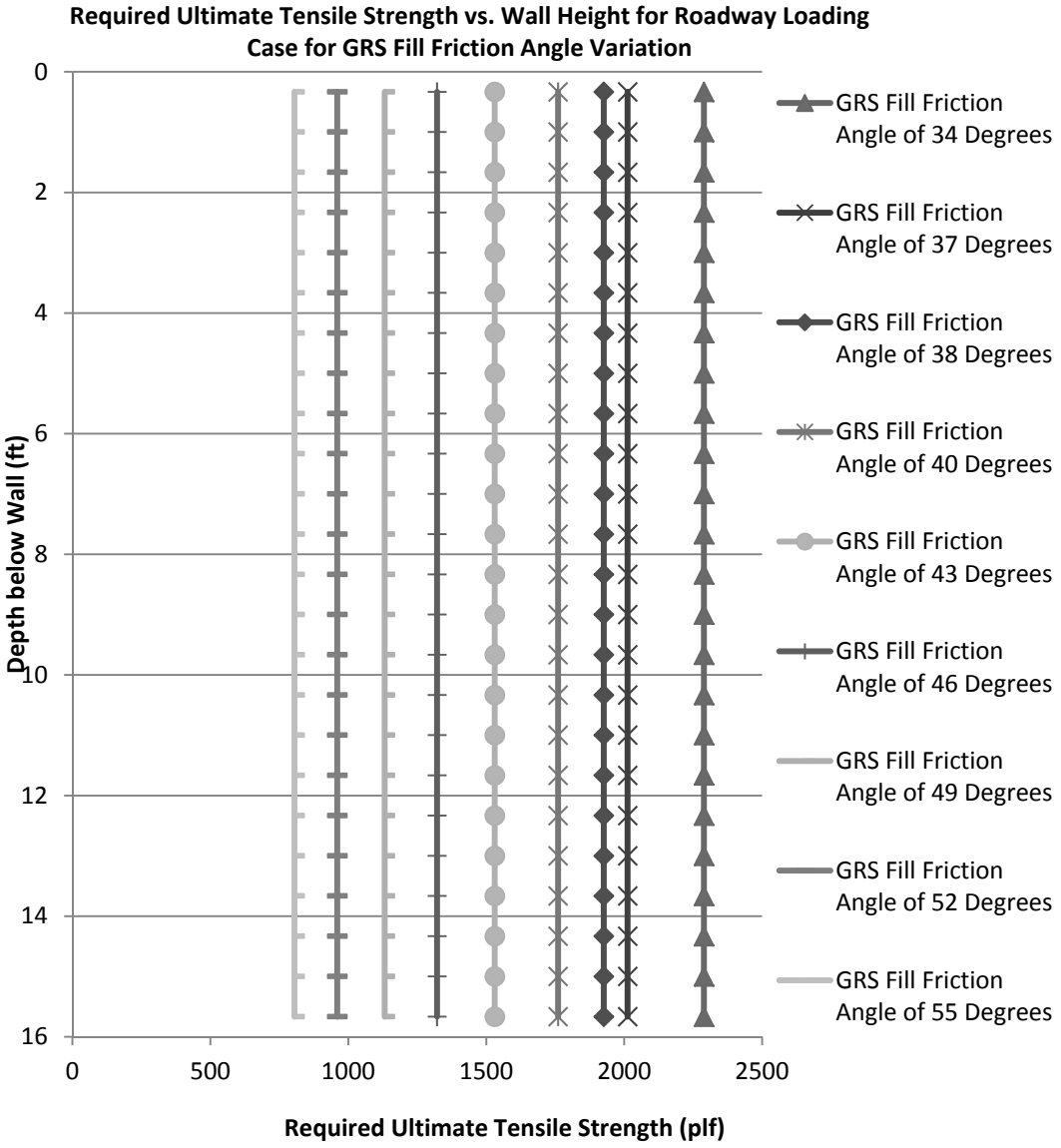

Figure 89: Influence of Friction Angle on Ultimate Required Tension for Roadway Loading for Method 4: NCHRP GRS Method

Figure 89 shows that for Method 4, the entire profile is assigned a required ultimate tensile strength, T_{req}, value equal to the highest value that occurs in the wall. Therefore, the distributions plot as vertical lines. With increasing friction angle of the reinforced fill, the maximum T_{req} value in the profile decreases. To look more closely at the variation of tension at each reinforcement layer, the variation in nominal maximum tensile load, T_{max}, with depth was plotted for each variation in friction angle. These relationships are plotted in Figure 90.

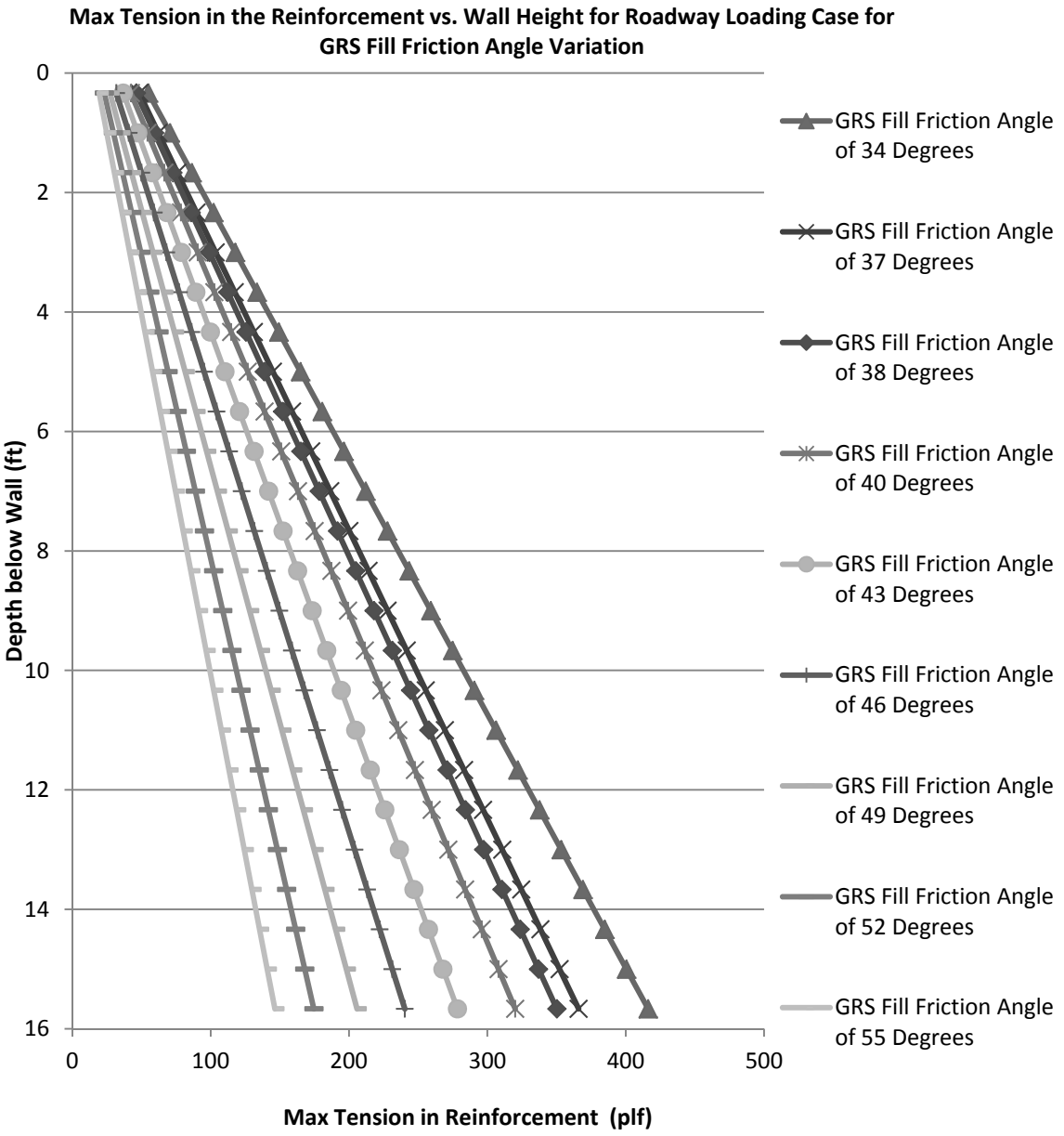

Figure 90: Influence of Friction Angle on Max Tensile Load in the Reinforcement for Roadway Loading for Method 4: NCHRP GRS Method

Figure 90 shows that for Method 4, increasing friction angle of the reinforced fill will decrease the nominal maximum tensile load, T_{max}, at all depths below the top of the reinforced zone. The shape of each distribution is linear.

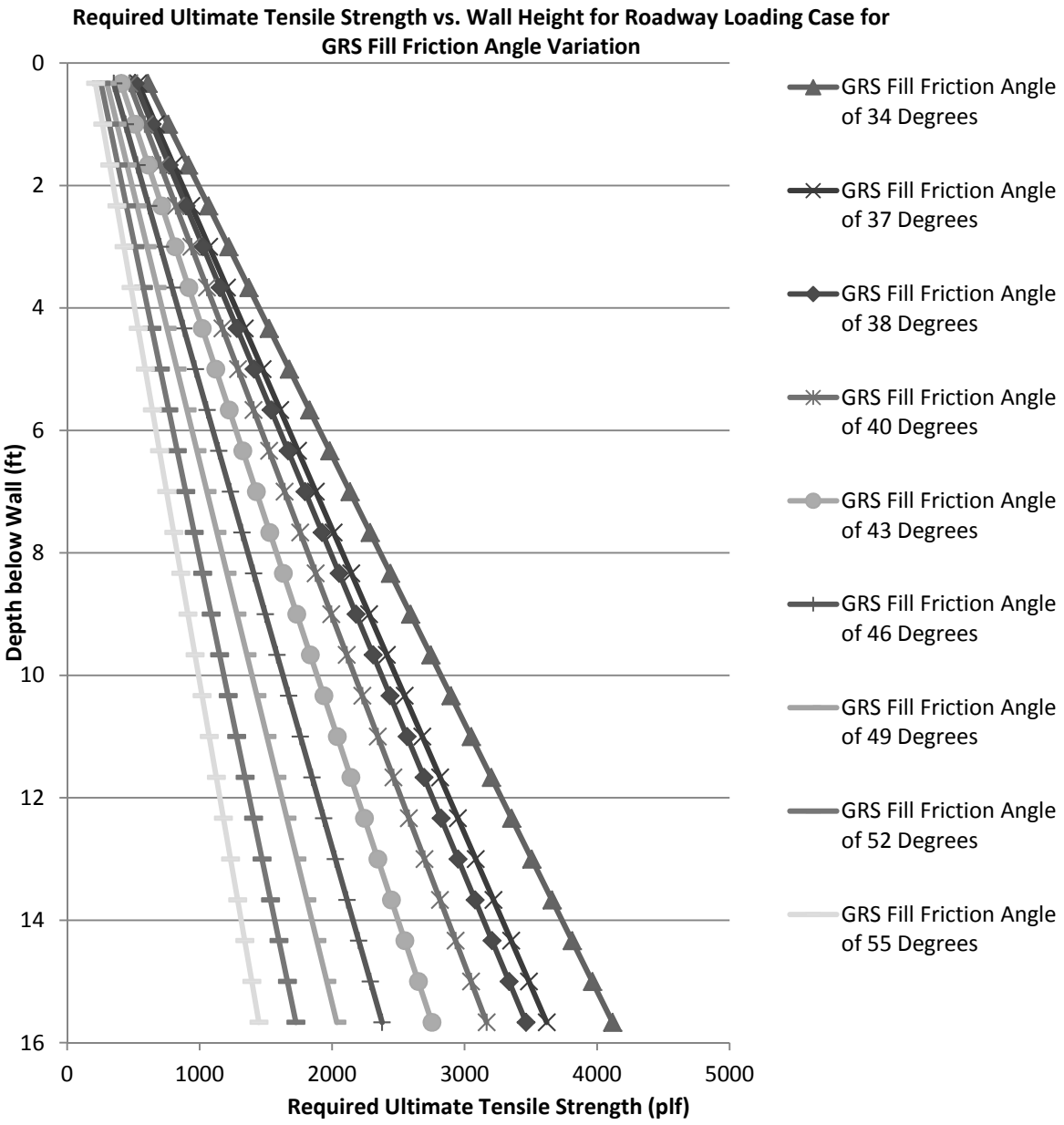

Figure 91: Influence of Friction Angle on Ultimate Required Tension for Roadway Loading for Method 5: FHWA GRS-IBS Method Analytic Solution

For Method 5's analytic solution, as friction angle of the reinforced fill increases the predicted required ultimate tensile strength, T_{req}, decreases for the entire soil profile as shown in Figure 91. All distributions are linear at all depths. The decrease in T_{req} is greater at the bottom than at the top of the wall.

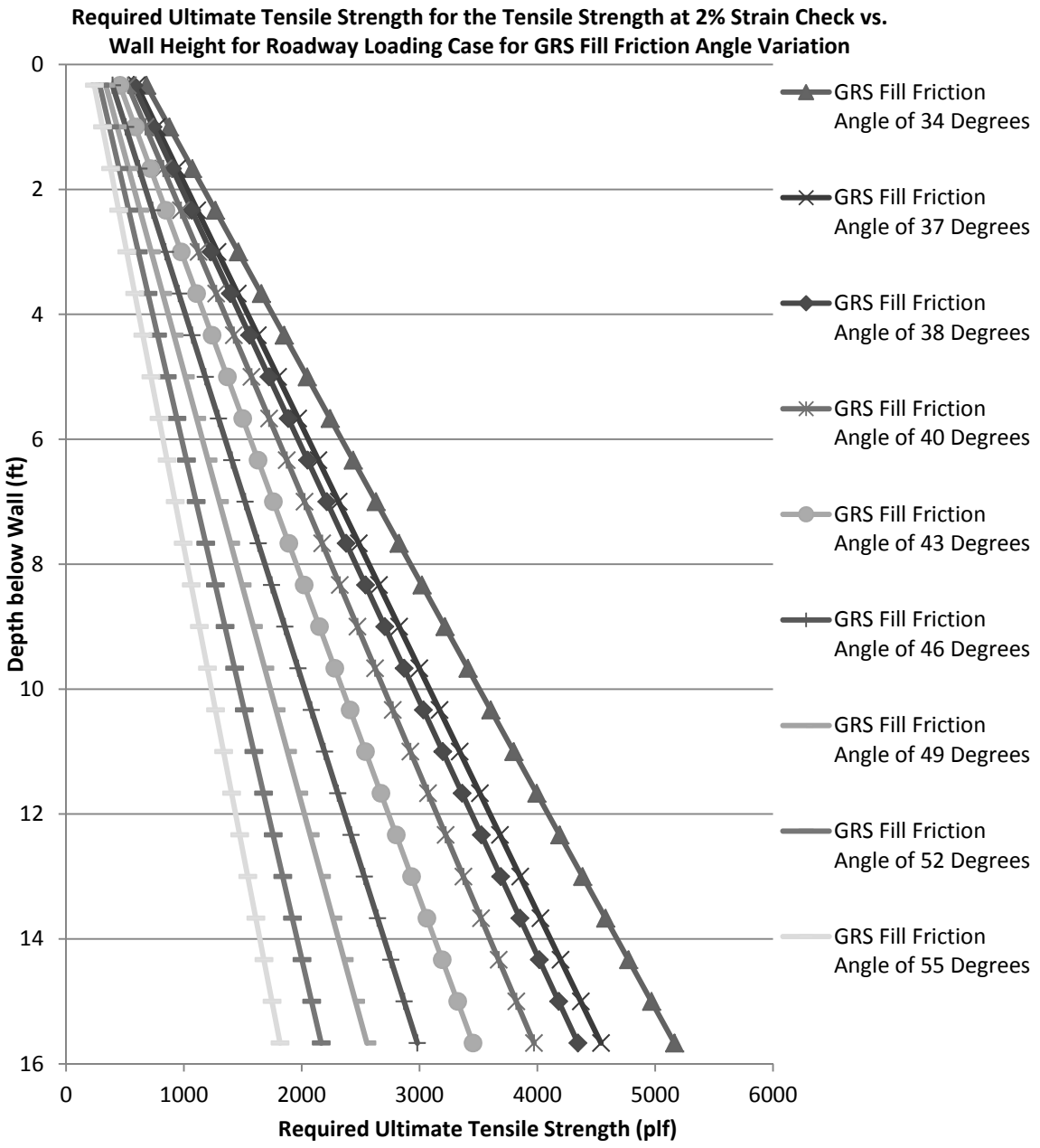

Figure 92: Influence of Friction Angle on Ultimate Required Tension for Roadway Loading for Method 5: FHWA GRS-IBS Method Tensile Strength at 2% Strain Check

Figure 92 shows that for Method 5's tensile strength at 2% strain equivalent T_{req} calculation, the increase in reinforced fill friction angle will decrease the predicted required ultimate tensile strength, $T_{req.}$ The predicted values of T_{req} are higher than that predicted by the analytic solution. The distributions remain linear for the entire soil profile similarly to the analytic solution.

There is a third check required by Method 5 guidance that requires the ultimate tensile strength to be greater than or equal to 4,800 lb/ft. This requirement is not plotted but

would plot as a straight line at the value of 4,800 lb/ft. Which of the three requirements that controls can vary within the soil profile. For the roadway loading condition the 4,800 lb/ft requirement would control for all but the lowest variation in friction angle, 34°, at the very bottom of the wall for the 2% tensile strength check. The analytic solution for Method 5 does not control at any point.

The maximum values of T_{max} and T_{req} are shown in Figure 93 and Figure 94, respectively.

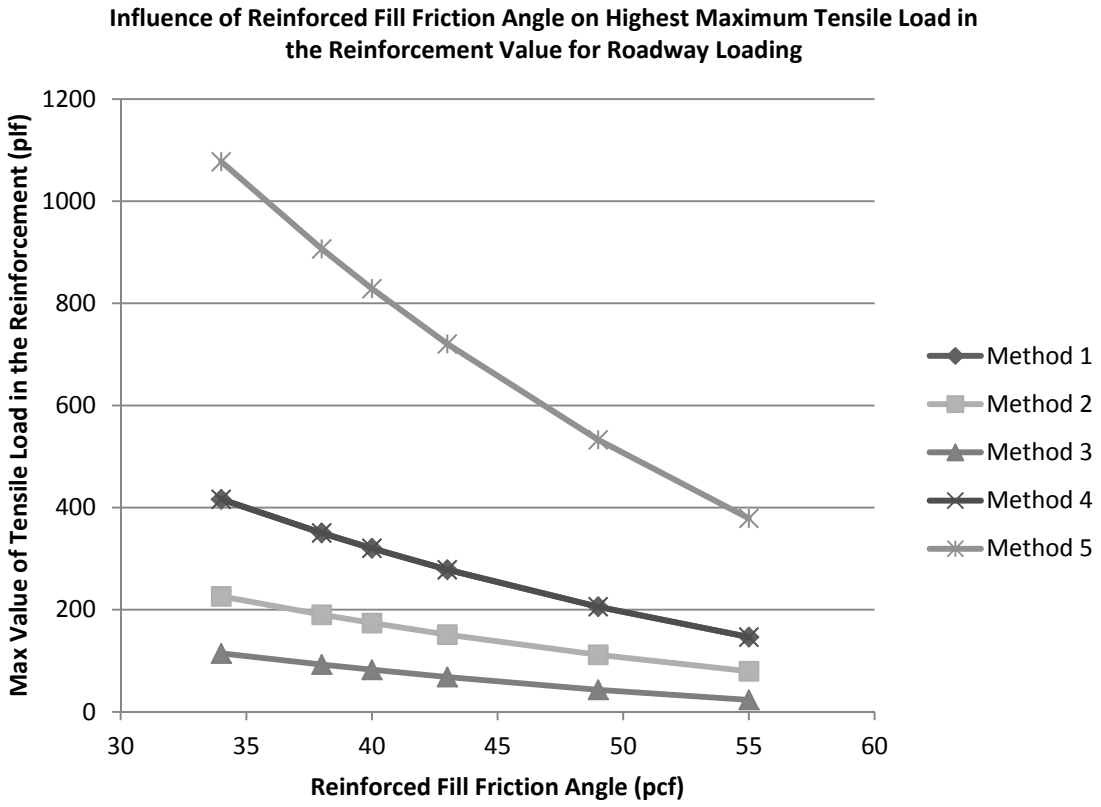

Figure 93: Influence of Friction Angle on Max Load in the Reinforcement for the Roadway Loading Condition

Figure 93 shows that the highest value of maximum load in the reinforcement, T_{max}, decreases close to linearly for all methods with increasing reinforced fill friction angle. Values predicted by Method 4 are identical to Method 1 and thus appear as a single line. Values predicted by Method 2 and 3 have roughly the same slope and thus are most likely similarly influenced by reinforced fill friction angle. Method 5 appears to be the most influenced by friction angle as it has the highest slope. Additionally, Method 5 predicts the highest values of T_{max} in comparison to all other methods.

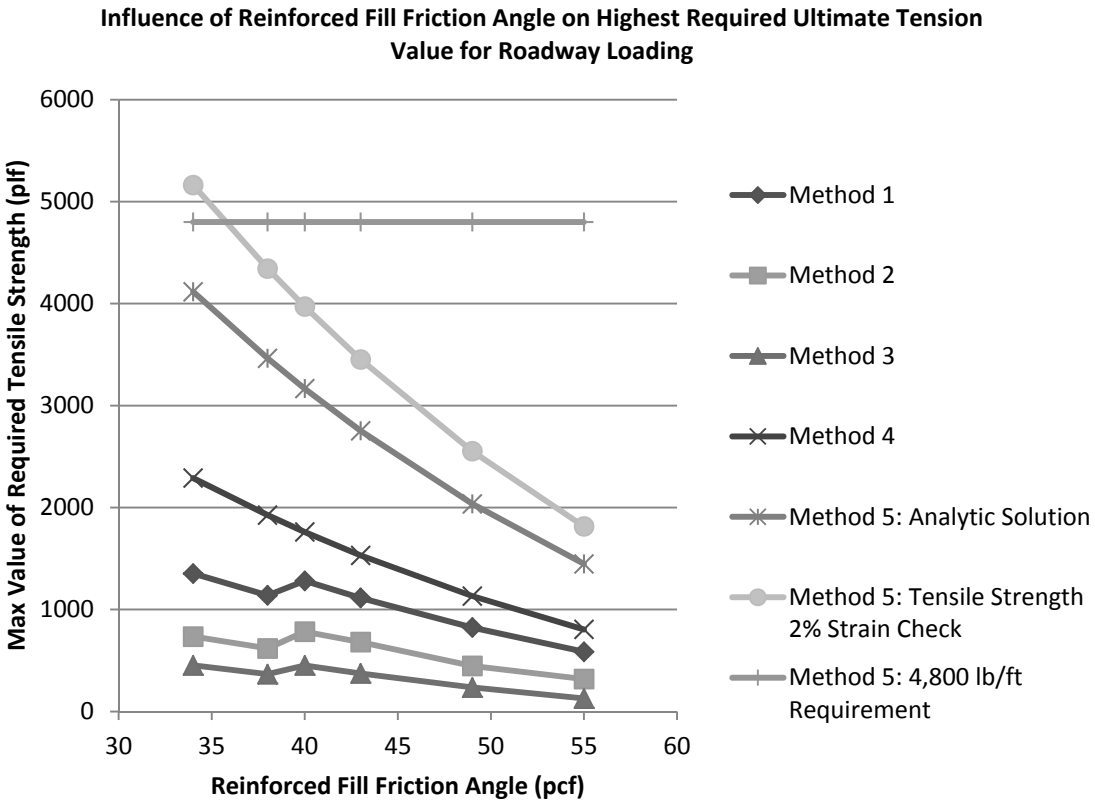

Figure 94: Influence of Friction Angle on the Highest Predicted Ultimate Required Tension for the Roadway Loading Condition

Figure 94 shows that the highest predicted ultimate required tensile strength, T_{req}, also decreases with increasing reinforced fill friction angle. Methods 1, 2, and 3 have a section of increase at a reinforced fill friction angle of 40°. This is the result of the reduction factor accounting for installation damage which increases from 1.3 to 1.8 for the base case at 40°. The *FHWA NHI-9-87* report by V. Elias, K. Fishman, B. Christopher, and R. Berg (2009), which was a reference for Methods 1, 2, and 3 governing equations, was utilized in selecting the value of this factor. Method 3 predicts the lowest value of T_{req}.

Method 5 has three requirements to establish T_{req} values for design. The first is an analytic solution, the second is a check of tensile strength at 2% strain, and the last is a requirement that T_{req} be at least equal to or above 4,800 lb/ft. The value chosen for design is the highest of the three ultimate strength values. All three of these predicted values are plotted in Figure 94. The first and second requirements are similarly influenced by friction angle but the tensile strength at 2% strain check predicts a higher value. The last requirement plots as a straight horizontal line at 4,800 lb/ft.

Bridge Loading: Method 3, the K-Stiffness Method, was not adapted for the bridge loading case for the parametric study. Figure 95, Figure 96, Figure 97, Figure 98, Figure

99, and Figure 100 show the variation in tension for the entire soil profile with change in friction angle for each of the other methods compared.

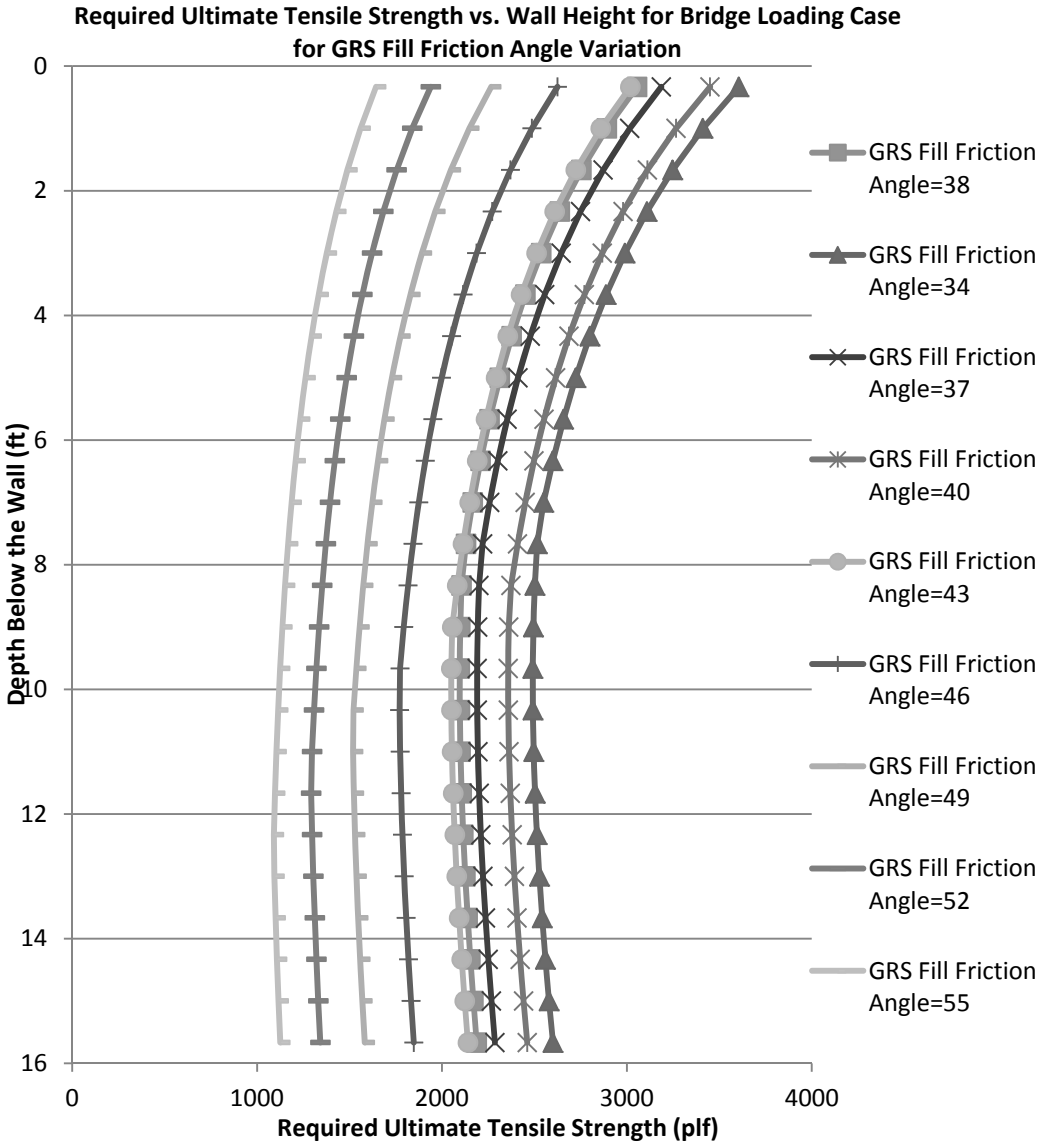

Figure 95: Influence of Friction Angle on Ultimate Required Tension for Bridge Loading for Method 1: The Simplified Procedure

For Method 1, in general as friction angle of the reinforced fill increases the predicted required ultimate tensile strength, T_{req}, decreases as shown in Figure 95. However, the reduction factor for installation damage is partly dependent on friction angle. Once friction angle of the reinforced fill is equal to or above 40° the reduction factor increases to 1.8 from 1.3 for the base case. This causes some parameter variations to not fall in progressive order. All distributions have a curved shape for the entire soil profile with the degree of curvature decreasing slightly with increasing reinforced fill friction angle. The T_{req} value both at the top and the bottom decrease with increasing friction angle of the

reinforced fill with the increase at the bottom being slightly less than at the top of the wall.

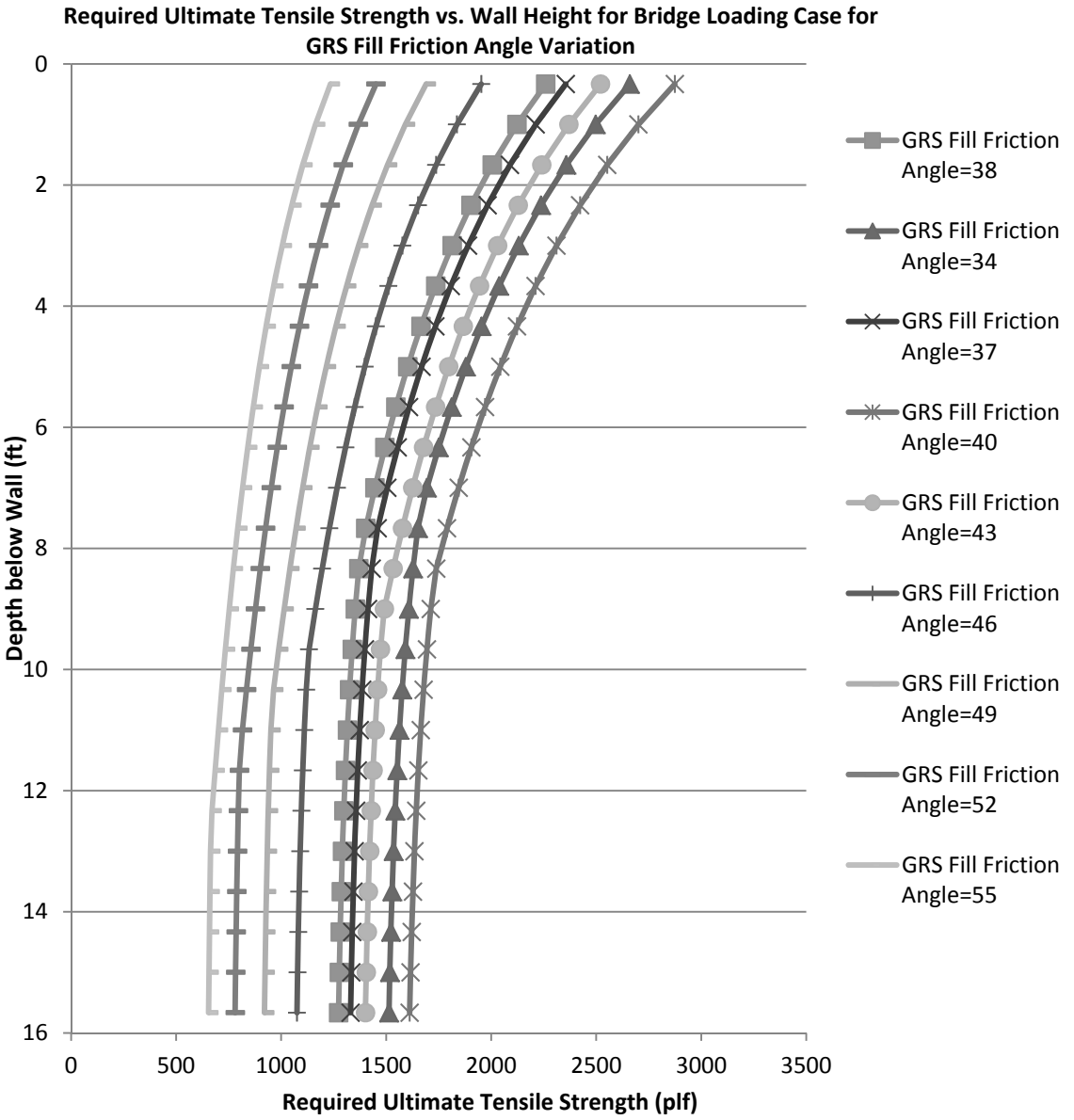

Figure 96: Influence of Friction Angle on Ultimate Required Tension for Bridge Loading for Method 2: The Simplified Procedure with K_r/K_a Adjusted

For Method 2, in general as friction angle of the reinforced fill increases the predicted required ultimate tensile strength, T_{req}, decreases as shown in Figure 96. However, the reduction factor for installation damage is partly dependent on friction angle. Once friction angle of the reinforced fill is equal to or above 40° the reduction factor increases to 1.8 from 1.3 for the base case. This causes some parameter variations to not fall in progressive order. All distributions have a curved shape for the entire soil profile with the degree of curvature decreasing slightly with increasing reinforced fill friction angle. The

T_{req} value both at the top and the bottom decrease with increasing friction angle of the reinforced fill with the increase at the bottom being slightly less than at the top of the wall.

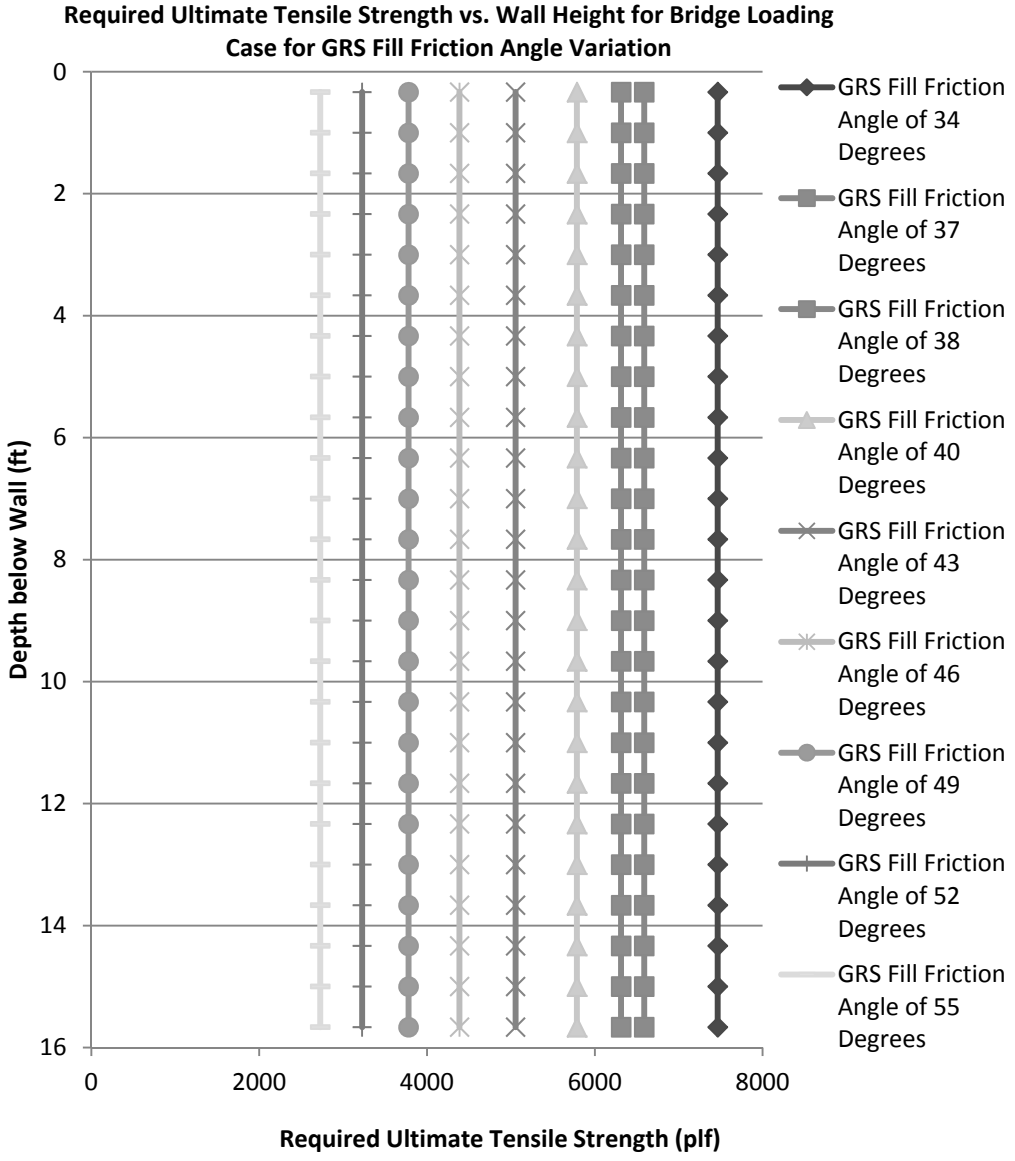

Figure 97: Influence of Friction Angle on Ultimate Required Tension for Bridge Loading for Method 4: NCHRP GRS Method

Figure 97 shows that for Method 4, the entire profile is assigned a required ultimate tensile strength, T_{req}, value equal to the highest value that occurs in the wall. Therefore, the distributions plot as vertical lines. With increasing friction angle of the reinforced fill, the maximum T_{req} value in the profile decreases. To look more closely at the variation of tension at each reinforcement layer, the variation in nominal maximum tensile load, T_{max}, with depth was plotted for each variation in friction angle. These relationships are plotted in Figure 98.

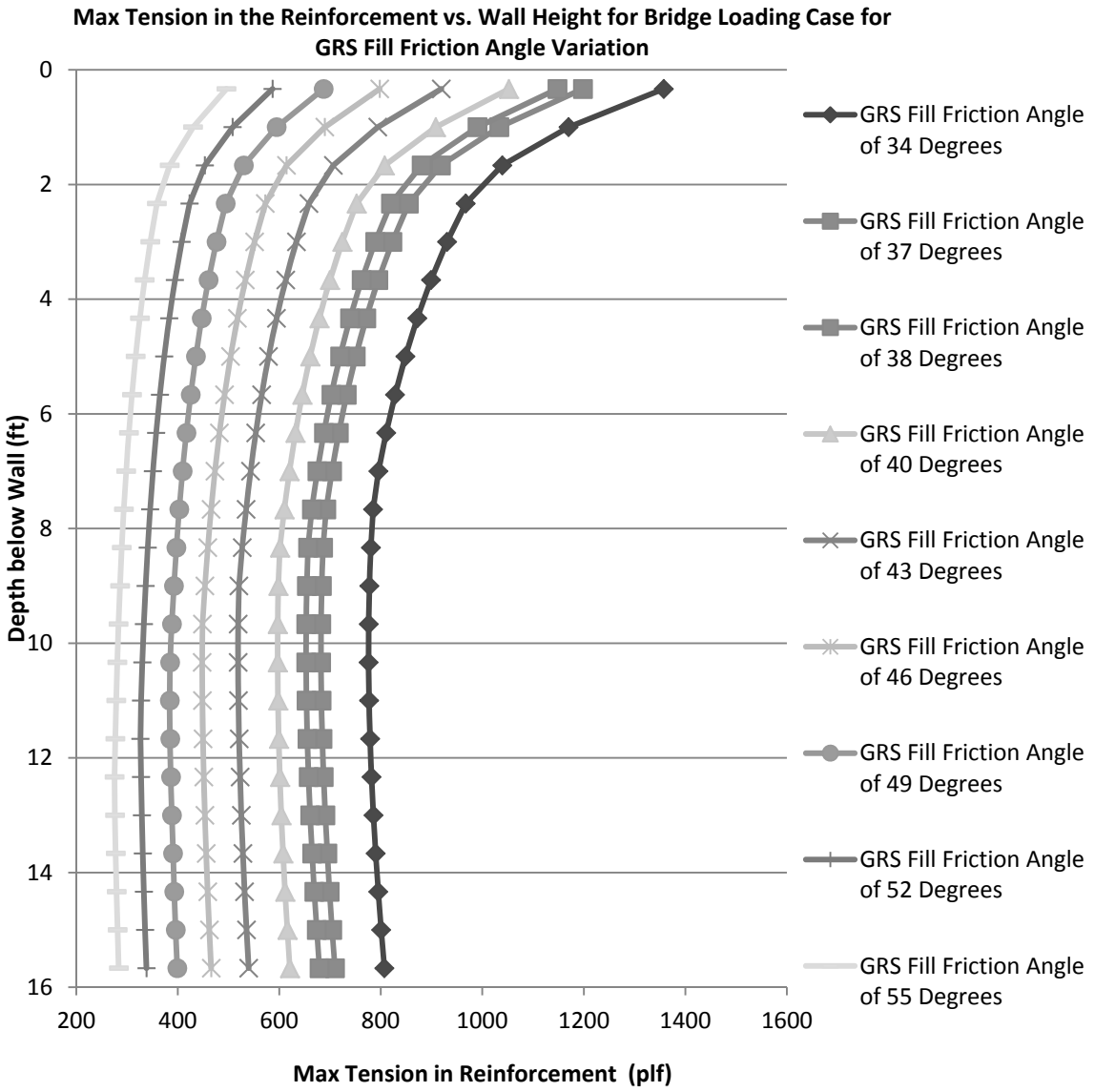

Figure 98: Influence of Friction Angle on Max Tensile Load in the Reinforcement for Bridge Loading for Method 4: NCHRP GRS Method

Figure 98 shows that for Method 4, increasing friction angle of the reinforced fill will decrease the nominal maximum tensile load, T_{max}, at all depths below the top of the reinforced zone. The shape of each distribution is curved.

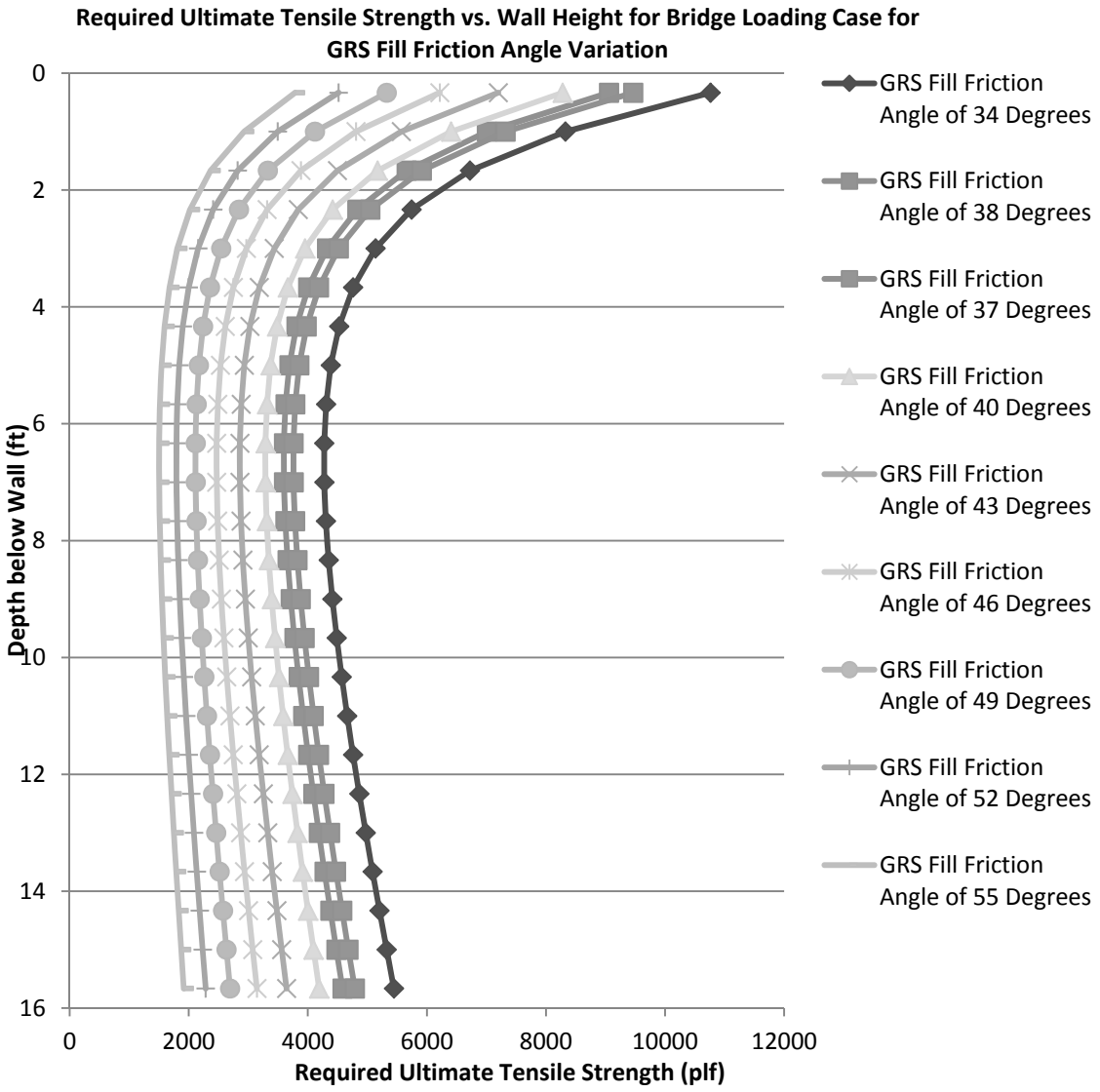

Figure 99: Influence of Friction Angle on Ultimate Required Tension for Bridge Loading for Method 5: FHWA GRS-IBS Method Analytic Solution

For Method 5's analytic solution, as friction angle of the reinforced fill increases the predicted required ultimate tensile strength, T_{req}, decreases for the entire soil profile as shown in Figure 99. All distributions have a curved shape. The decrease in T_{req} is greater at the top than at the bottom of the wall.

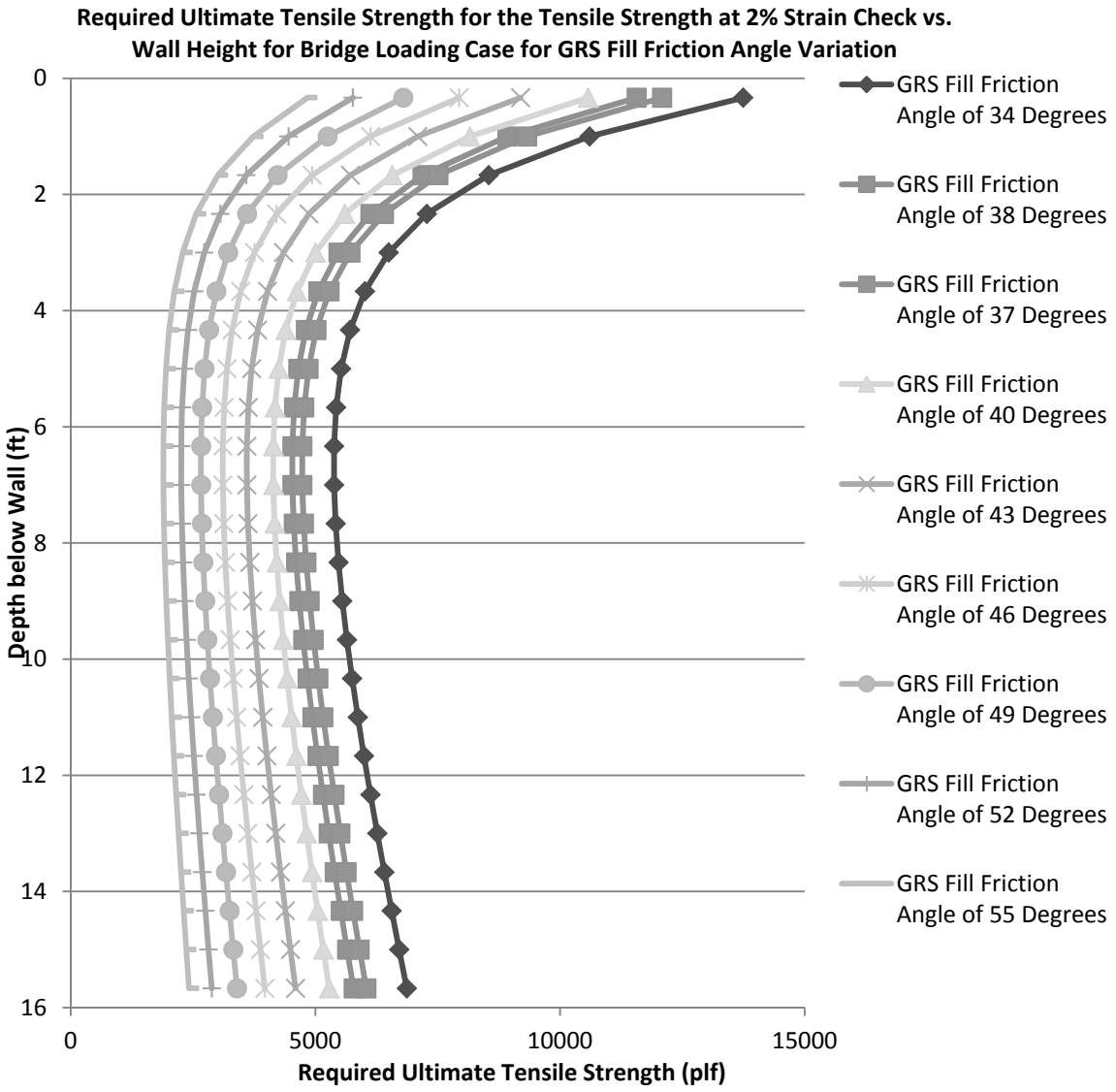

Figure 100: Influence of Friction Angle on Ultimate Required Tension for Bridge Loading for Method 5: FHWA GRS-IBS Method Tensile Strength at 2% Strain Check

Figure 100 shows that for Method 5's tensile strength at 2% strain equivalent T_{req} calculation, the increase in reinforced fill friction angle will decrease the predicted required ultimate tensile strength, $T_{req.}$ The predicted values of T_{req} are higher than that predicted by the analytic solution but the distributions have very similar shapes.

There is a third check required by Method 5 guidance that requires the ultimate tensile strength to be greater than or equal to 4,800 lb/ft. This requirement is not plotted but would plot as a straight line at the value of 4,800 lb/ft. Which of the three requirements that controls can vary within the soil profile.

Method 3, the K-Stiffness Method, was not adapted for the bridge loading case for the parametric study. The variation in maximum values of T_{max} and T_{req} are shown in Figure 101 and Figure 102, respectively.

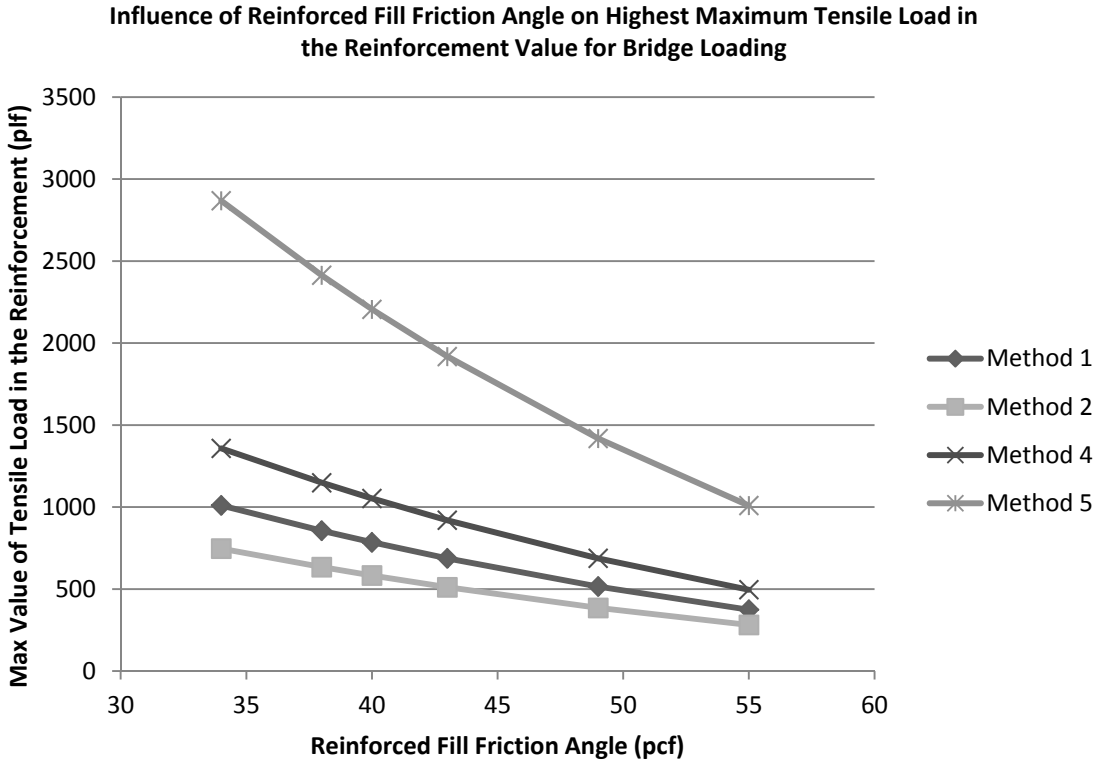

Figure 101: Influence of Friction Angle on Max Load in the Reinforcement for the Bridge Loading Condition

Figure 101 shows that the highest value of maximum load in the reinforcement, T_{max}, decreases nearly linearly for all methods with increasing reinforced fill friction angle. Values predicted by Method 1, 2 and 4 have roughly the same slope and thus are most likely similarly influenced by reinforced fill friction angle. Method 5 appears to be the most influenced by friction angle as it has the highest slope. Additionally, Method 5 predicts the highest values of T_{max} in comparison to all other methods.

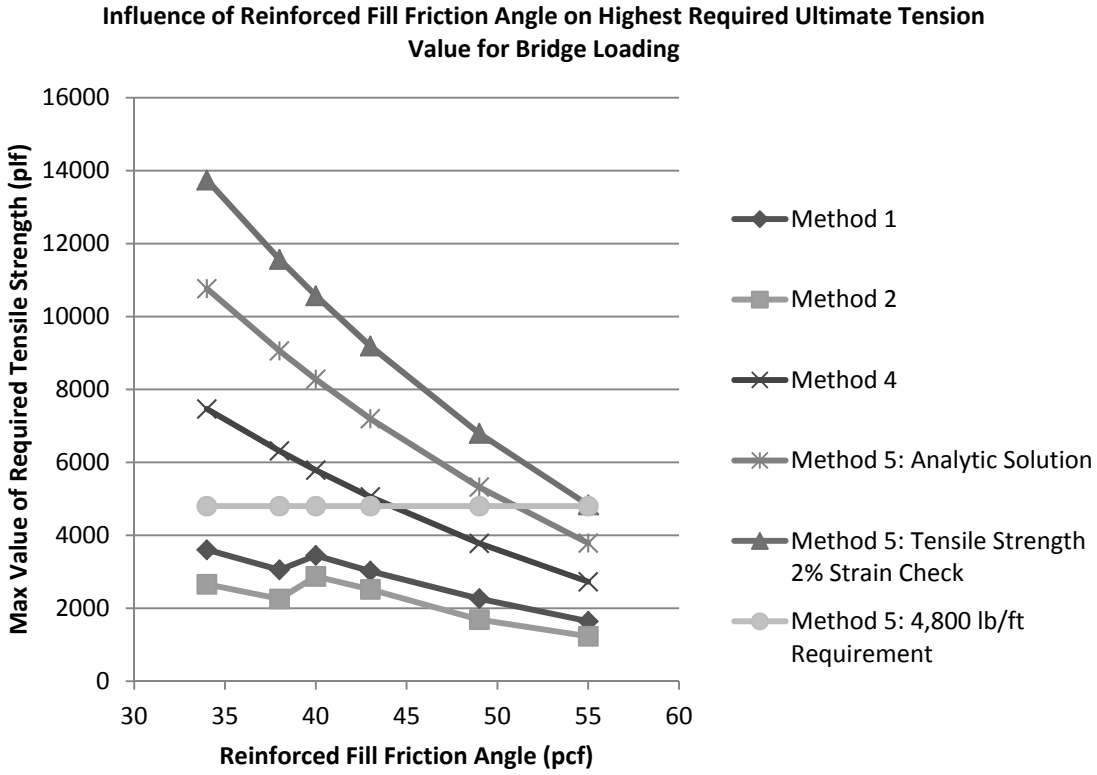

Figure 102: Influence of Friction Angle on the Highest Predicted Ultimate Required Tension for the Bridge Loading Condition

Figure 102 shows that the highest predicted ultimate required tensile strength, T_{req}, also decreases with increasing reinforced fill friction angle. Methods 1 and 2 have a section of increase at a reinforced fill friction angle of 40°. This is the result of the reduction factor accounting for installation damage which increases from 1.3 to 1.8 for the base case at 40°. The *FHWA NHI-9-87* report by V. Elias, K. Fishman, B. Christopher, and R. Berg (2009), which was a reference for Methods 1 and 2 governing equations, was utilized in selecting the value of this factor.

Method 5 has three requirements to establish T_{req} values for design. The first is an analytic solution, the second is a check of tensile strength at 2% strain, and the last is a requirement that T_{req} be at least equal to or above 4,800 lb/ft. The value chosen for design is the highest of the three ultimate strength values. The value chosen for design is the highest of the three ultimate strength values. All three of these predicted values are plotted in Figure 102. The first and second requirements are similarly influenced by friction angle but the tensile strength at 2% strain check predicts a higher value. The last requirement plots as a straight horizontal line at 4,800 lb/ft.

Impact of Reinforcement Type Variation: The following section explores the influence of varying reinforcement type over the range detailed in Table 4 for the roadway loading condition and Table 5 for the bridge loading case.

Roadway Loading: For the roadway loading scenario, both T_{max} and T_{req} can be compared across all methods except Method 4. Method 4, the NCHRP Method, assumes reinforcement type has only a secondary effect on performance. Method 4 does not incorporate reductions factors; it only includes a factor of safety that is not dependent on reinforcement type. The reinforcements compared for the other methods are illustrative of typical reinforcement types that could be applied in design of walls in practice. Figure 103, Figure 104, Figure 105, and Figure 106 show the variation in ultimate required tensile strength, T_{req}, and the influence of reinforcement type predicted by each method individually. The variation of T_{req} for the entire soil profile is presented.

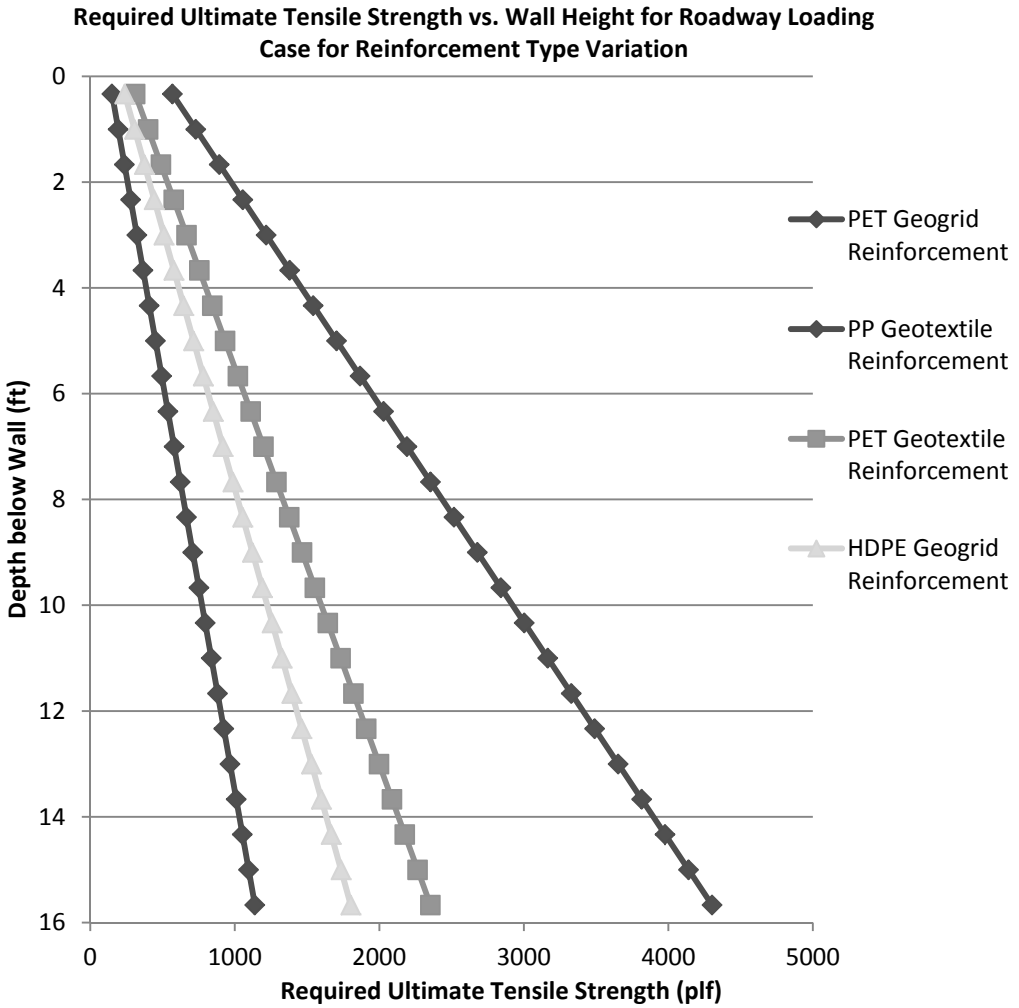

Figure 103: Influence of Reinforcement Type on Ultimate Required Tension for Roadway Loading for Method 1: The Simplified Procedure

Figure 103 shows that for Method 1, each reinforcement type predicted a variation in predicted required ultimate tensile strength, T_{req}, which was linear for the entire soil profile. The highest value of T_{req} for the entire distribution was for the polypropylene (PP) geotextile reinforcement type and the lowest for the polyester (PET) geogrid

reinforcement type. Reinforcement type influences T_{req} through the application of reduction factors. These reduction factors are calibrated by manufacturers to account for installation damage, creep, and degradation. Each polymer type had different reduction factors. Method 1 reference material was utilized in selecting these reduction factors.

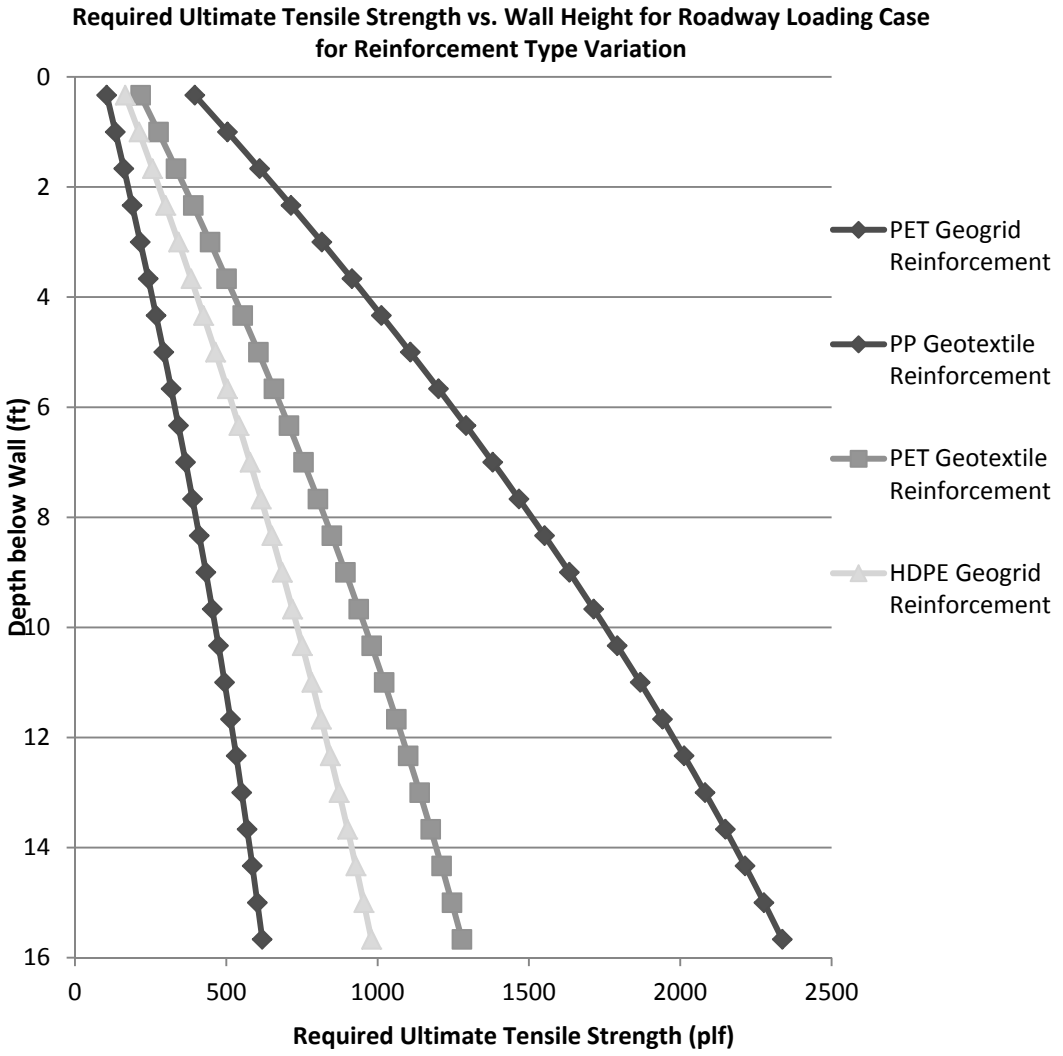

Figure 104: Influence of Reinforcement Type on Ultimate Required Tension for Roadway Loading for Method 2: The Simplified Procedure with K_r/K_a Adjusted

Figure 104 shows that for Method 2, each reinforcement type predicted a variation in predicted required ultimate tensile strength, T_{req}, which was slightly curved. The highest value of T_{req} for the entire distribution was for the polypropylene (PP) geotextile reinforcement type and the lowest for the polyester (PET) geogrid reinforcement type. Reinforcement type influences T_{req} through the application of reduction factors. These reduction factors are calibrated by manufacturers to account for installation damage, creep, and degradation. Each polymer type had different reduction factors. Method 2 reference material was utilized in selecting these reduction factors.

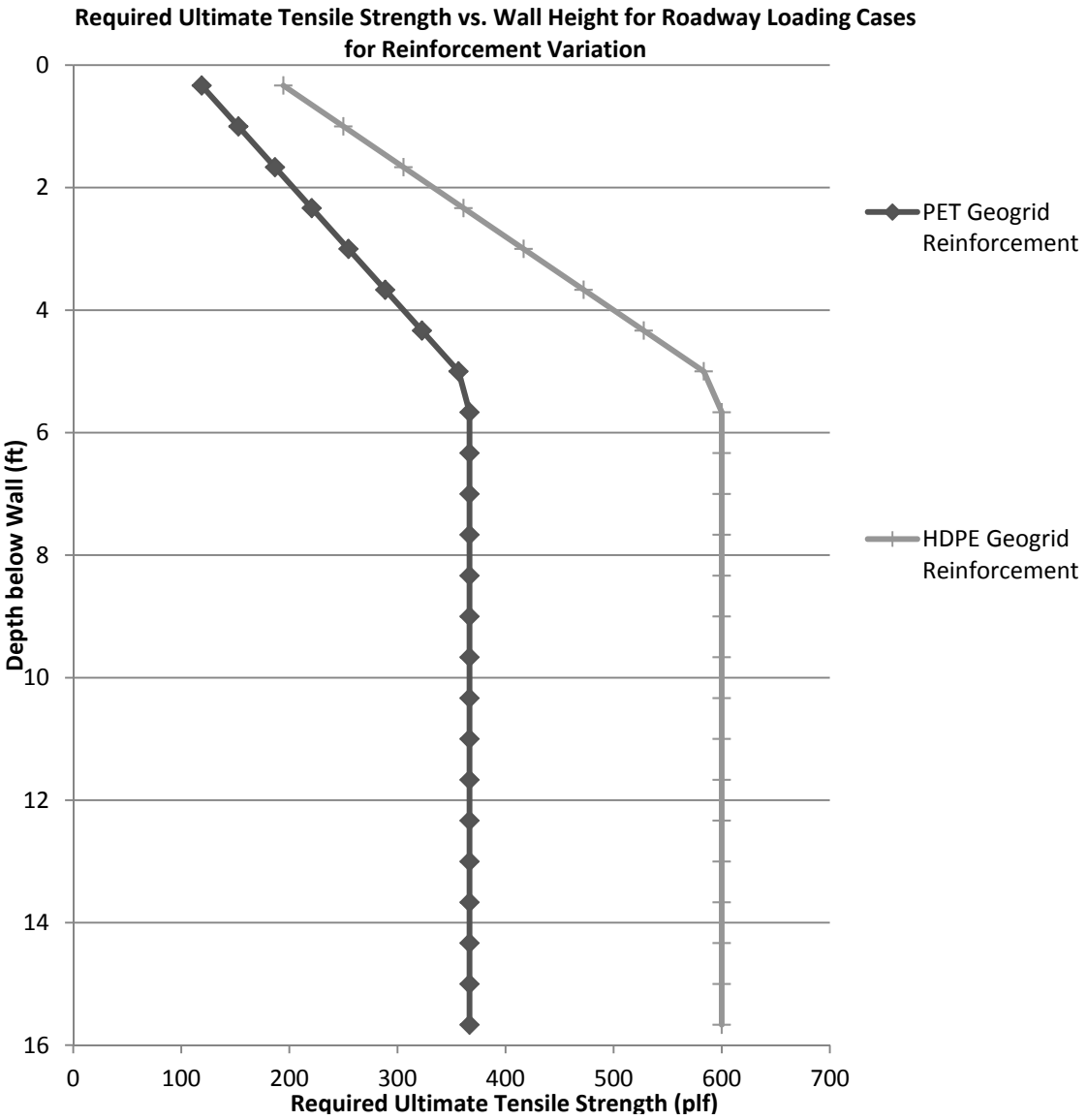

Figure 105: Influence of Reinforcement Type on Ultimate Required Tension for Roadway Loading for Method 3: The K-Stiffness Method

Due to limited creep information, only PET and HDPE geogrids could be assessed for Method 3. Figure 105 shows that the highest value of T_{req} for the entire distribution was for the HDPE geogrid reinforcement type and the lowest for the PET geogrid reinforcement type. The use of different reduction factors, RF values, for each reinforcement type influence the final predicted T_{req} values. Additionally, Method 3 utilizes a creep stiffness value at 2% for calculating T_{req}. This value is different between a PET and HDPE geogrid as shown in Equation 41 and Equation 42.

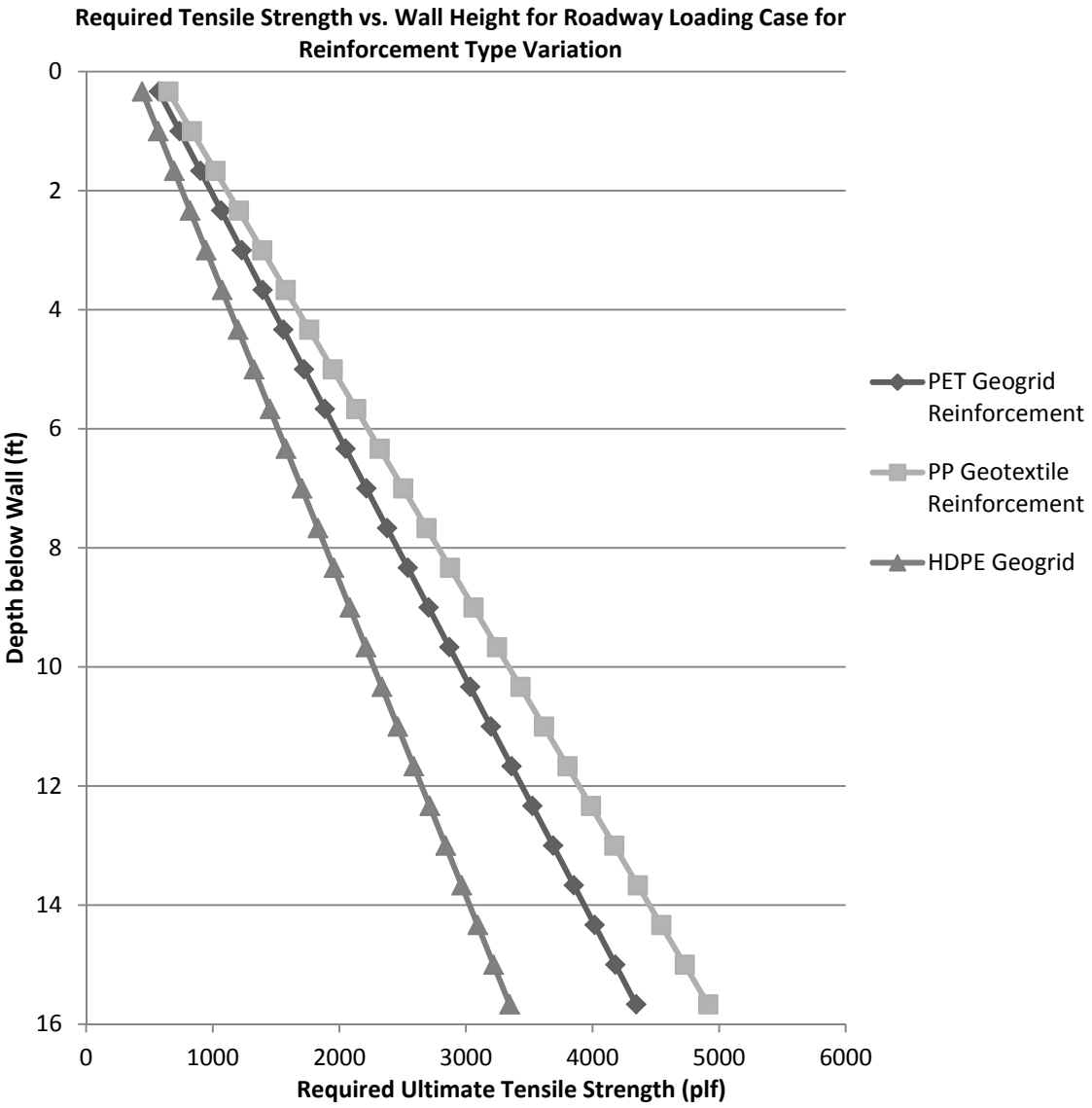

Figure 106: Influence of Reinforcement Type on Ultimate Required Tension for Roadway Loading for Method 5: FHWA GRS-IBS Method Tensile Strength at 2% Strain Check

Figure 106 shows the variation in Method 5's tensile strength at 2% strain check. Only the tensile strength at 2% strain check imposed by Method 5 varies due to the influence of reinforcement type because the ratio of ultimate strength to strength at 2% stain is material specific.. The analytic solution predicts the same T_{req} value for any reinforcement type and the 4,800 lb/ft requirement remains constant as well. HDPE predicts the lowest T_{req} value for Method 5, and PP geotextile the highest.

For the roadway loading scenario, both T_{max} and T_{req} can be compared across all methods except Method 4. Method 4, the NCHRP Method, assumes reinforcement type has only a secondary effect on performance. Method 4 does not incorporate reductions factors; it only includes a factor of safety that is not dependent on reinforcement type. The

reinforcements compared for the other methods are illustrative of typical reinforcement types that could be applied in design of walls in practice. Figure 107 and Figure 108 show the effects of reinforcement variation on highest predicted values of T_{max} and T_{req} respectively for all applicable methods for the roadway loading condition.

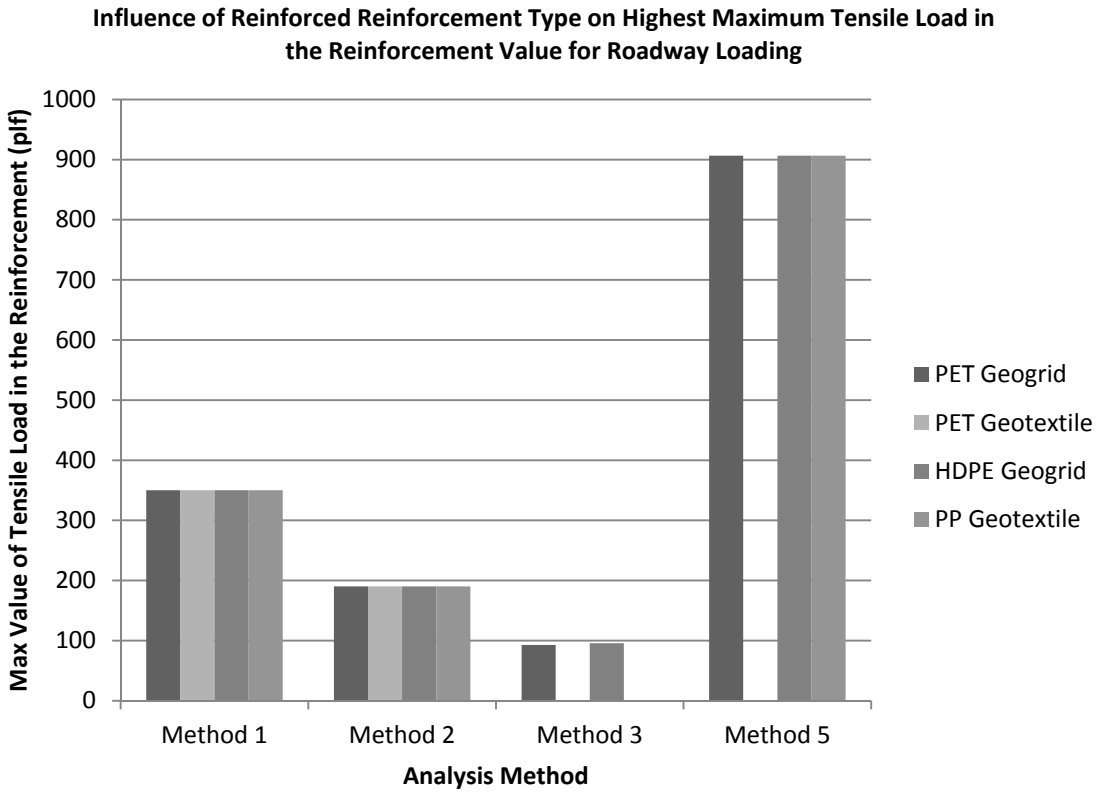

Figure 107: Influence of Reinforcement Type on Max Load in the Reinforcement for the Roadway Loading Condition

Figure 107 shows that the maximum tensile load carried by the reinforcement, $T_{max,}$ is not influenced by reinforcement type for Methods 1, 2, 3 and 5 for the roadway loading condition.

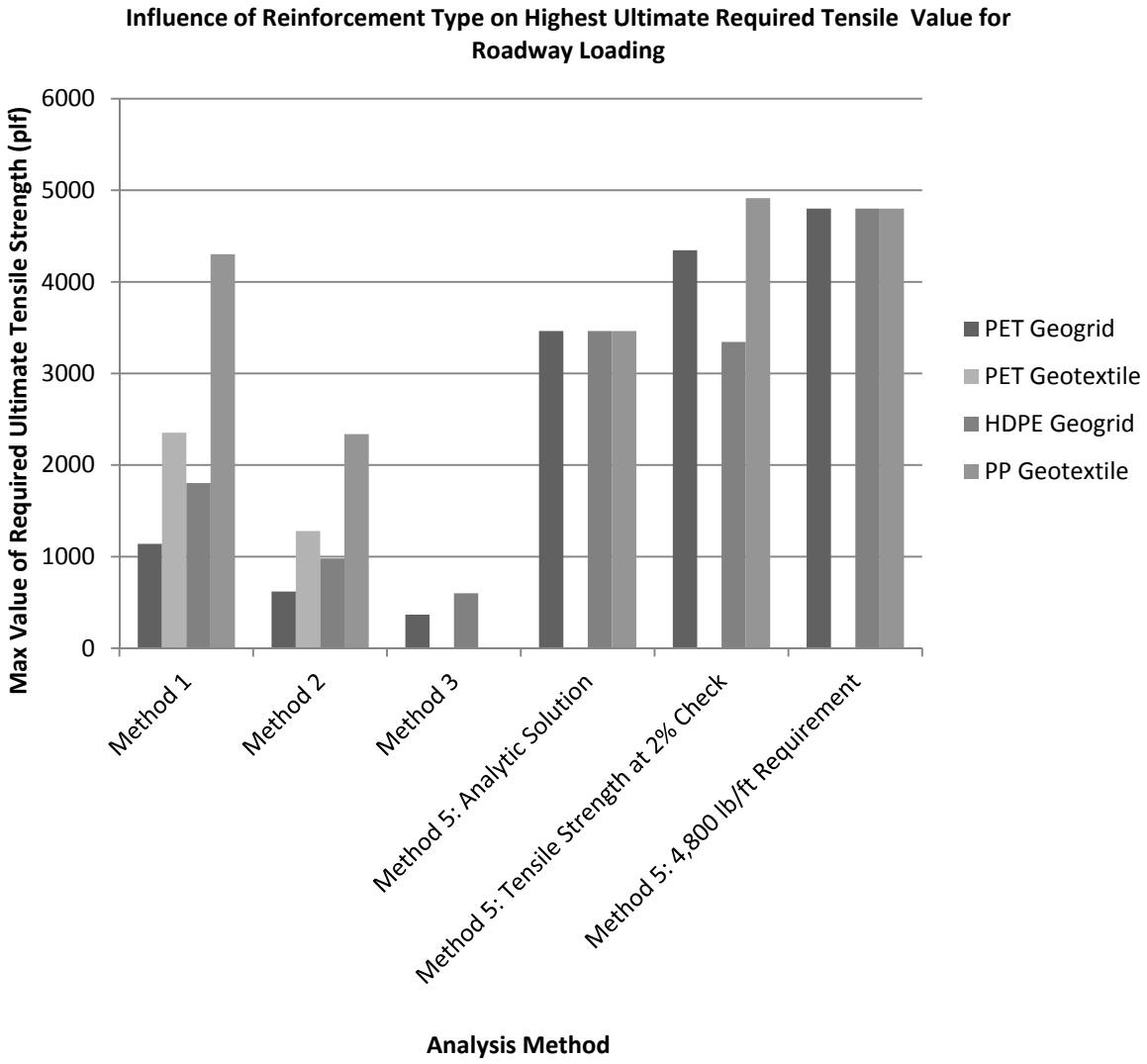

Figure 108: Influence of Reinforcement Type on the Highest Predicted Ultimate Required Tension for the Roadway Loading Condition

Figure 108 shows that for Method 1, a PP geotextile will yield the highest prediction for ultimate required reinforcement strength, T_{req}, followed by a PET geotextile, HDPE geotextile, and then a PET geogrid, the chosen base case reinforcement. The same trend is true for Method 2. For method 3 not all reinforcement type could be compared due to a limited amount of information from reinforcement product manufacturers about creep stiffness. HDPE geotextile reinforcement will predict a higher T_{req} value than a PET geogrid. Of Method 5's three requirements for evaluating T_{req}, only the Tensile strength at 2% strain check is influence by reinforcement type. For this Method 5 requirement, the predicted value of T_{req} is highest for a PP geotextile, followed by a PET geogrid, and then a HDPE geogrid.

Bridge Loading: Method 3, the K-Stiffness Method, was not adapted for the bridge loading case for the parametric study. Additionally, Method 4 could not be compared

because it is not influenced by the variation of reinforcement type. The reinforcements compared are illustrative of typical reinforcement types that could be applied in design of walls in practice. Figure 109, Figure 110, Figure 111, and Figure 121 show the variation in ultimate required tensile strength, T_{req}, and the influence of reinforcement type predicted by each method individually. The variation of T_{req} for the entire soil profile is presented.

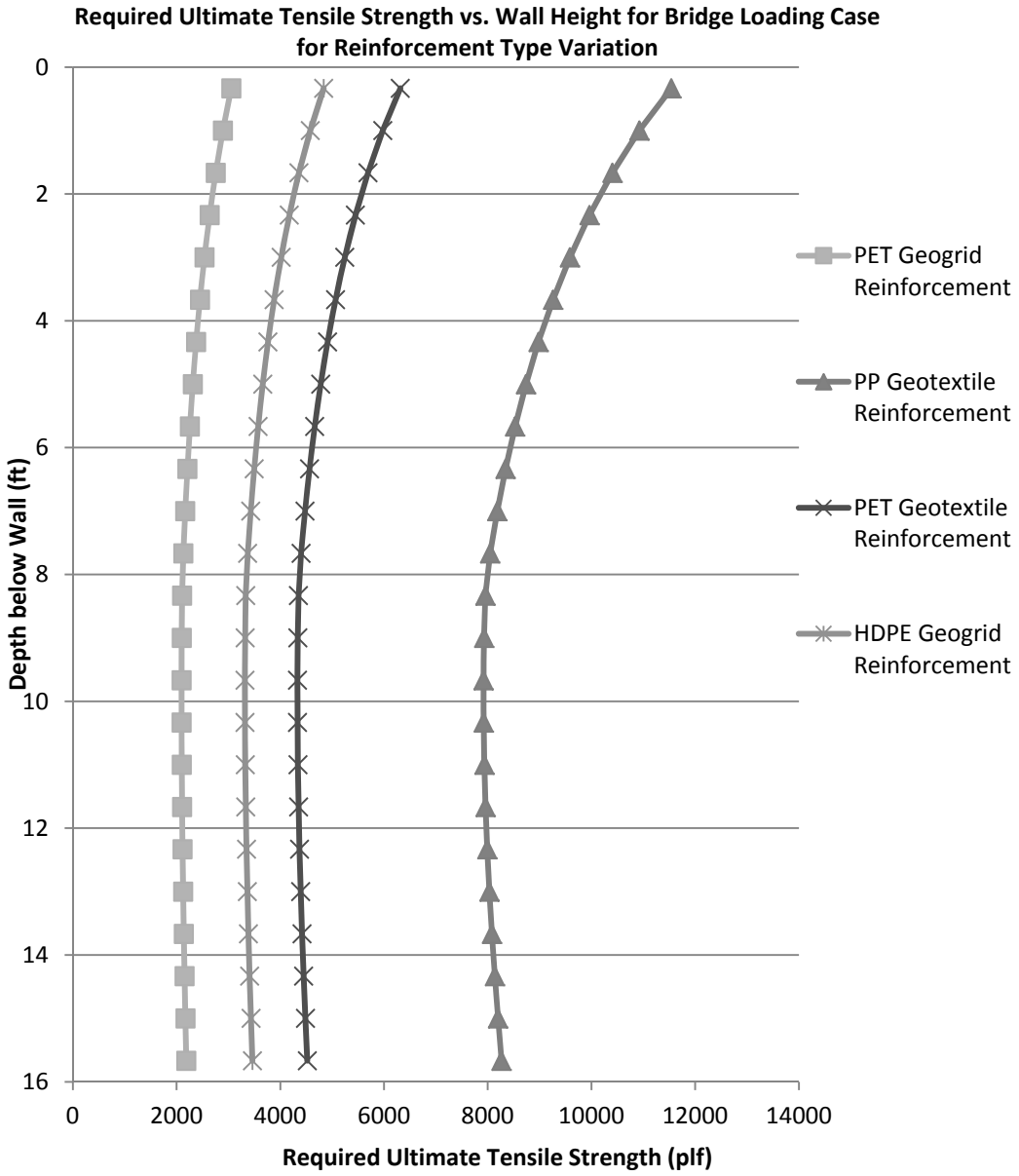

Figure 109: Influence of Reinforcement Type on Ultimate Required Tension for Bridge Loading for Method 1: The Simplified Procedure

Figure 109 shows that for Method 1, each reinforcement type predicted a variation in predicted required ultimate tensile strength, T_{req}, which was curved. The highest value of T_{req} for the entire distribution was for the polypropylene (PP) geotextile reinforcement

type and the lowest for the polyester (PET) geogrid reinforcement type. Reinforcement type influences T_{req} through the application of reduction factors. These reduction factors are calibrated by manufacturers to account for installation damage, creep, and degradation. Each polymer type had different reduction factors. Method 1 reference material was utilized in selecting these reduction factors.

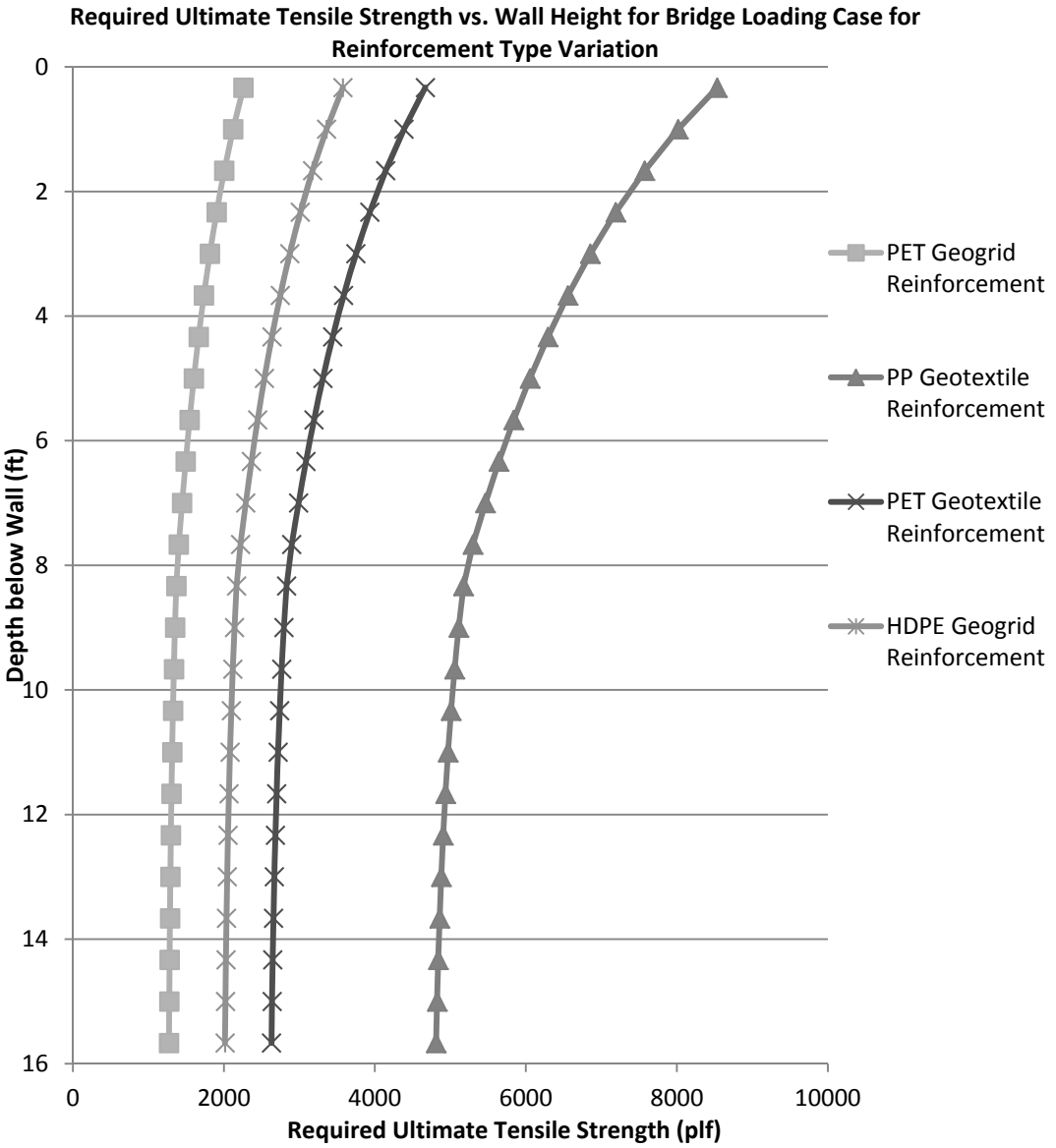

Figure 110: Influence of Reinforcement Type on Ultimate Required Tension for Bridge Loading for Method 2: The Simplified Procedure with K_r/K_a Adjusted

Figure 110 shows that for Method 2, each reinforcement type predicted a variation in predicted required ultimate tensile strength, T_{req}, which was curved. The highest value of T_{req} for the entire distribution was for the polypropylene (PP) geotextile reinforcement type and the lowest for the polyester (PET) geogrid reinforcement type. Reinforcement type influences T_{req} through the application of reduction factors. These reduction factors

are calibrated by manufacturers to account for installation damage, creep, and degradation. Each polymer type had different reduction factors. Method 2 reference material was utilized in selecting these reduction factors.

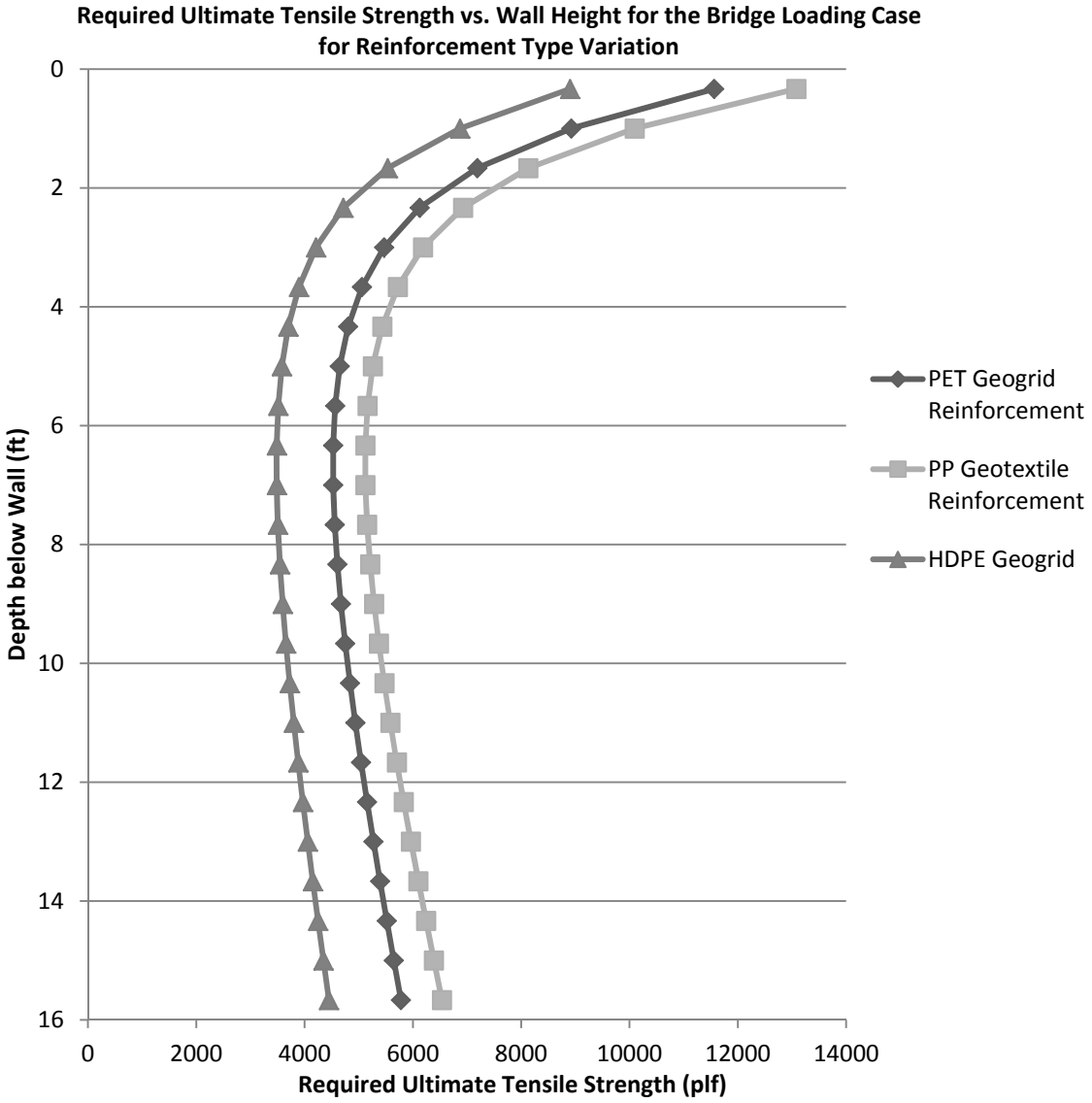

Figure 111: Influence of Reinforcement Type on Ultimate Required Tension for Bridge Loading for Method 5: FHWA GRS-IBS Method Tensile Strength at 2% Strain Check

Figure 111 shows the variation in Method 5's tensile strength at 2% strain check. Only the tensile strength at 2% strain check imposed by Method 5 varies due to the influence of reinforcement type because the ratio of ultimate strength to strength at 2% stain is material specific. The analytic solution predicts the same T_{req} value for any reinforcement type and the 4,800 lb/ft requirement remains constant as well. HDPE predicts the lowest T_{req} value for Method 5, and PP geotextile the highest.

Method 3, the K-Stiffness Method, was not adapted for the bridge loading case for the parametric study. Additionally, Method 4 could not be compared because it is not influenced by the variation of reinforcement type. The reinforcements compared are illustrative of typical reinforcement types that could be applied in design of walls in practice. Figure 112 and Figure 113 show the effects of reinforcement variation on highest predicted values of T_{max} and T_{req} respectively for all applicable methods for the bridge loading condition.

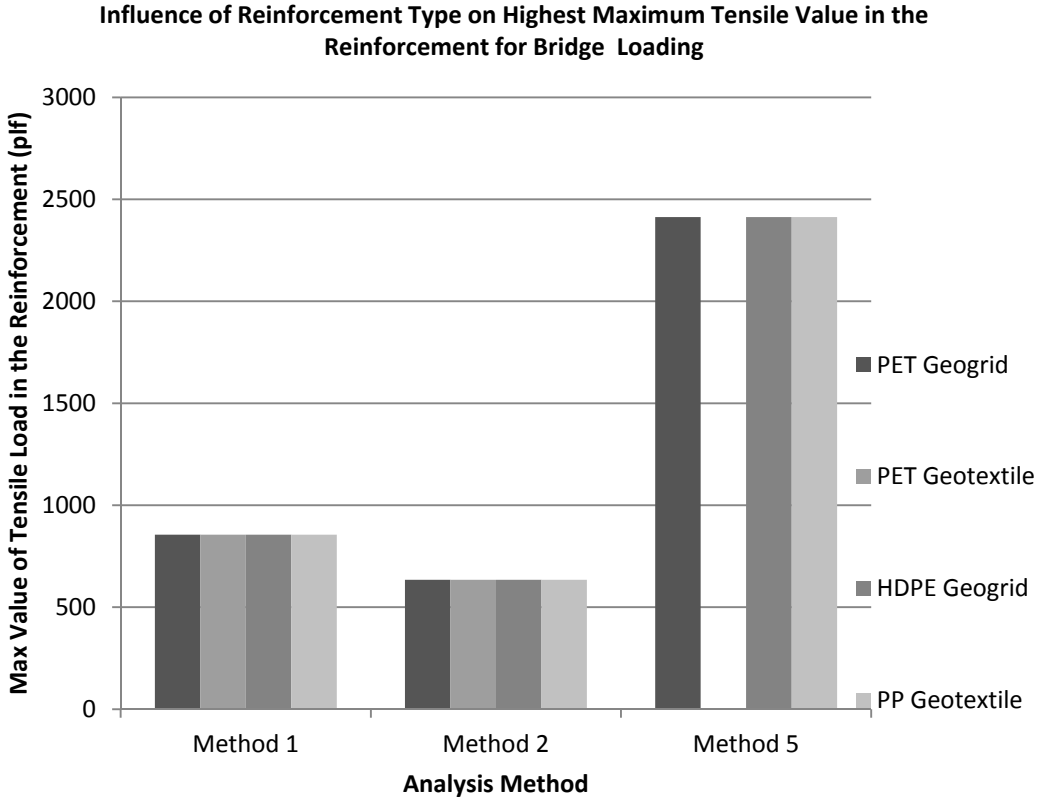

Figure 112: Influence of Reinforcement Type on Max Load in the Reinforcement for the Bridge Loading Condition

Figure 112 shows that reinforcement type does not influence the maximum load carried by the reinforcement, T_{max}, for Methods 1, 2, and 5 for the bridge loading condition.

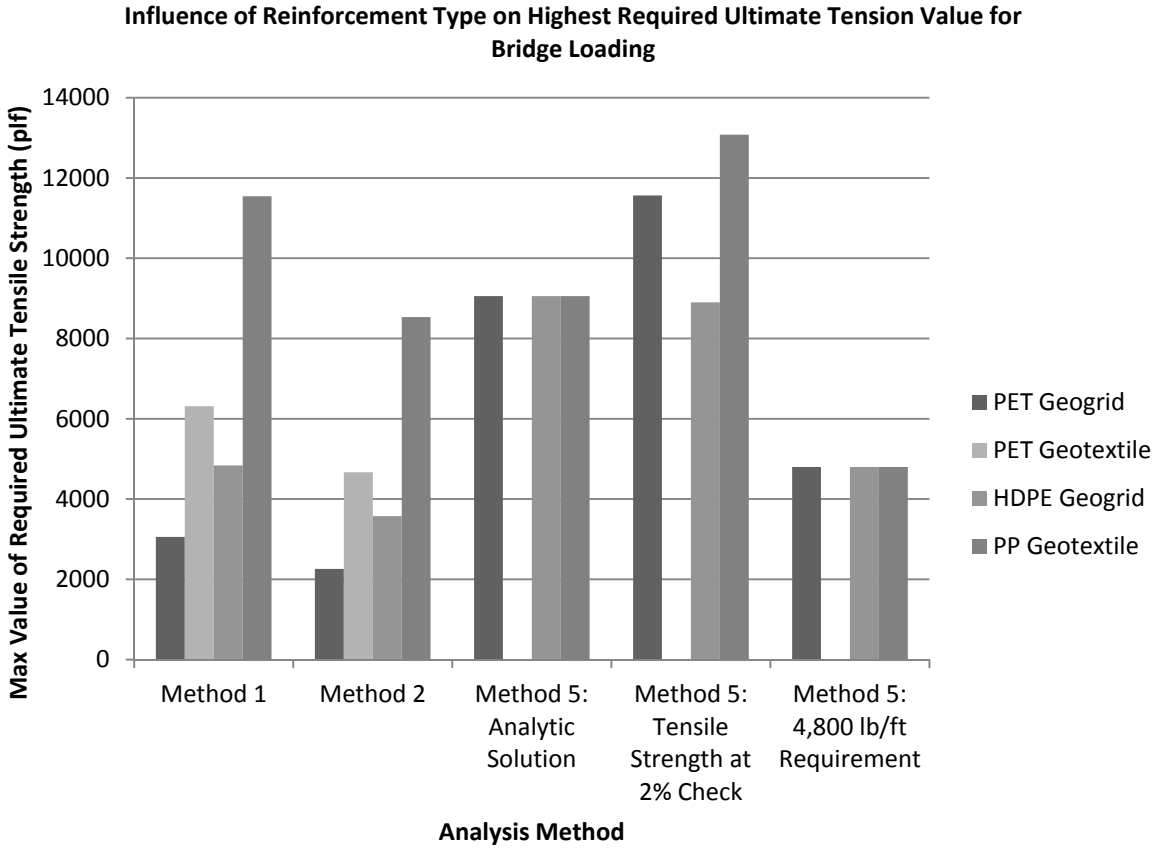

Figure 113: Influence of Reinforcement Type on the Highest Predicted Ultimate Required Tension for the Bridge Loading Condition

Figure 113 shows that for Method 1, a PP geotextile will yield the highest prediction for ultimate required reinforcement strength, T_{req}, followed by a PET geotextile, HDPE geotextile, and then a PET geogrid, the chosen base case reinforcement. The same trend is true for Method 2. Of Method 5's three requirements for evaluating T_{req}, only the Tensile strength at 2% strain check is influence by reinforcement type. For this Method 5 requirement, the predicted value of T_{req} is highest for a PP geotextile, followed by a PET geogrid, and then a HDPE geogrid.

Impact of Reinforcement Spacing Variation: The following section explores the influence of varying reinforcement spacing over the range detailed in Table 4 for the roadway loading condition and Table 5 for the bridge loading case.

Roadway Loading: For the roadway loading scenario, both T_{max} and T_{req} can be compared across all methods. The reinforcement spacing was varied from 8 inches to 24 inches. The base case value was 8 inches. To present the results clearly, only tributary areas equal to the spacing variation were plotted. In other words, if the tributary area at the very bottom of the wall did not fit evenly into the distribution of wall height, then the final reinforcement layer was not plotted. Lastly, Method 4 and Method 5 the two GRS

analysis methods set limits on reinforcement spacing of 16 inches and 12 inches respectively. Variations above these values are for comparison purposes with MSEW methods which allow for larger spacings. Figure 114, Figure 115, Figure 116, Figure 117, Figure 118, Figure 119, and Figure 120 show the variation in tension for the entire soil profile with change in reinforcement spacing for each of the 5 methods.

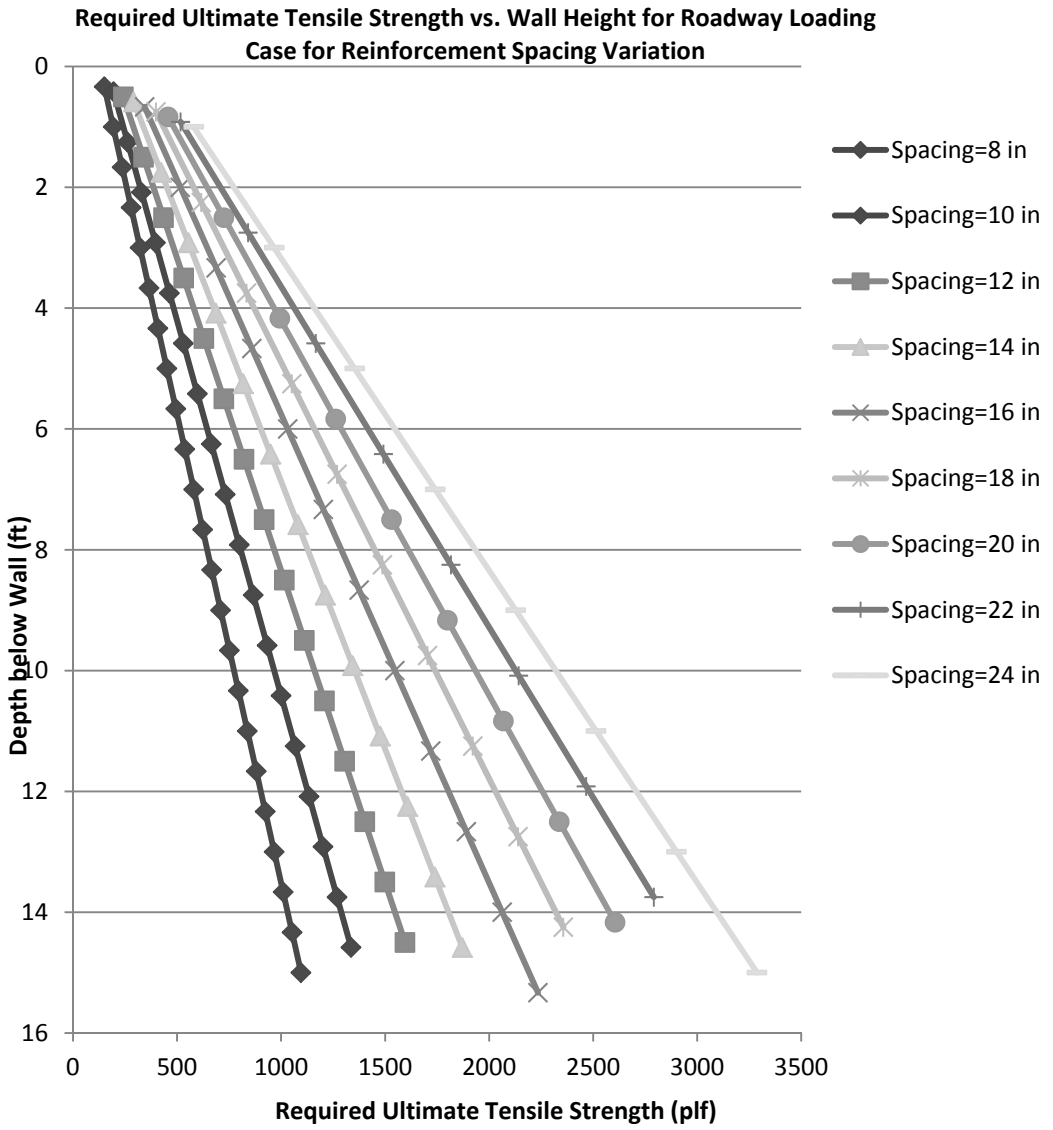

Figure 114: Influence of Reinforcement Spacing on Ultimate Required Tension for Roadway Loading for Method 1: The Simplified Procedure

For Method 1, the increase in spacing results in an increase in the predicted required ultimate tensile strength, T_{req}, for the entire soil profile as shown Figure 114. All distributions have a linear shape for the entire soil profile. The T_{req} value both at the top and the bottom increase with increasing reinforcement spacing. The increase at the bottom is greater than at the top of the wall.

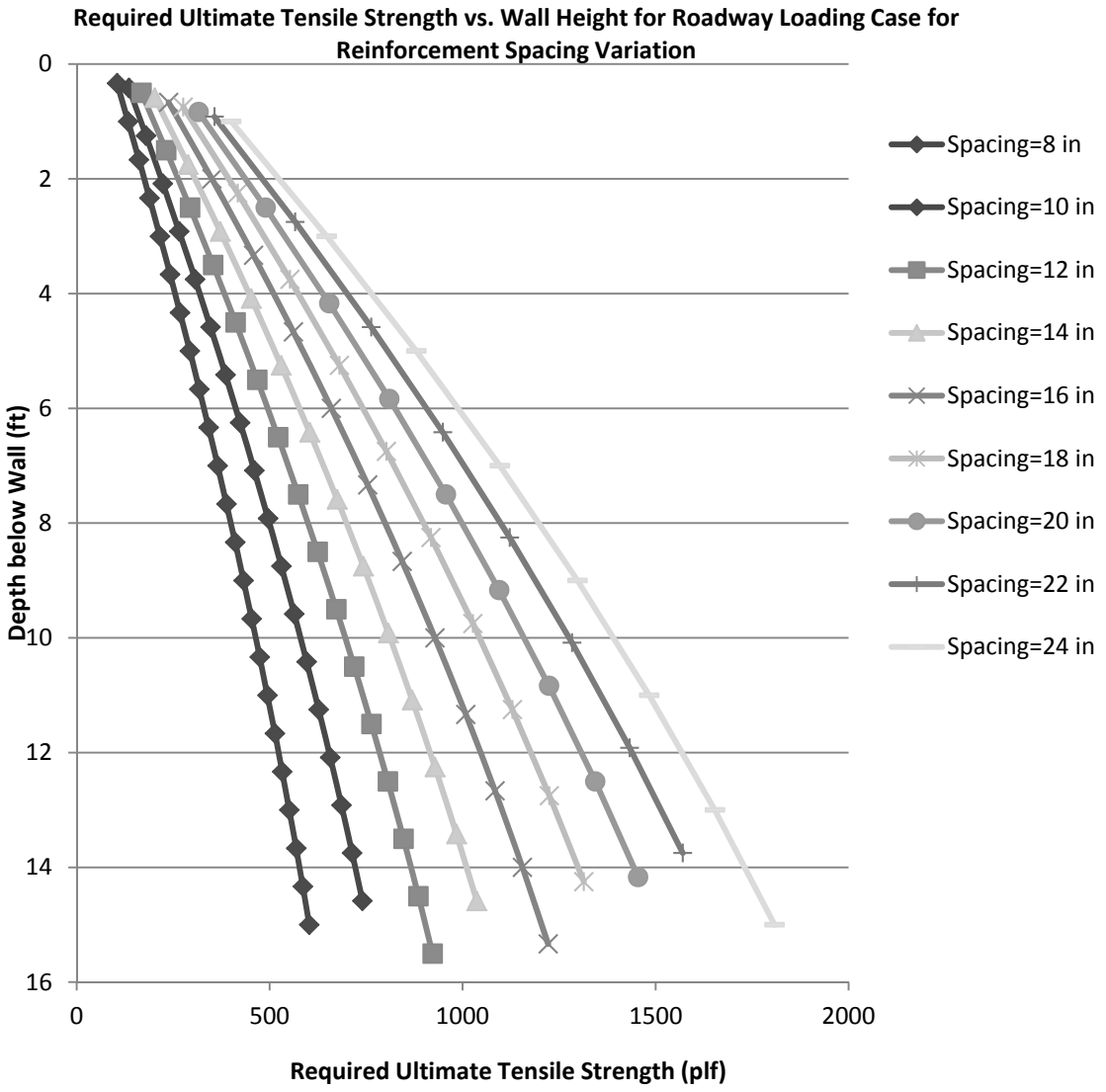

Figure 115: Influence of Reinforcement Spacing on Ultimate Required Tension for Roadway Loading for Method 2: The Simplified Procedure with K_r/K_a Adjusted

For Method 2, the increase in spacing results in an increase in the predicted required ultimate tensile strength, T_{req}, for the entire soil profile as shown Figure 115. All distributions have a slightly curved shape. The T_{req} value both at the top and the bottom increase with increasing reinforcement spacing. The increase at the bottom is greater than at the top of the wall.

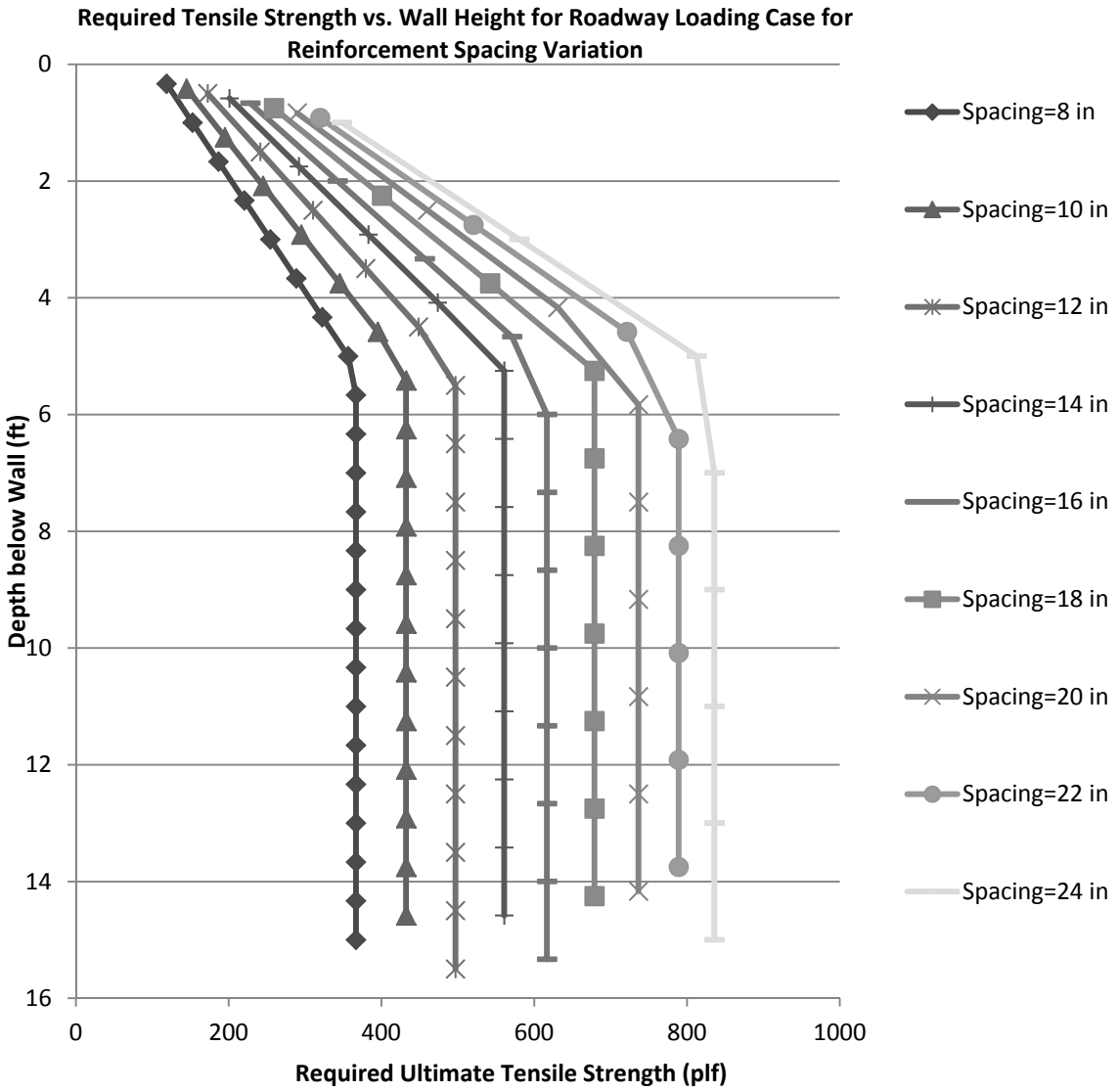

Figure 116: Influence of Reinforcement Spacing on Ultimate Required Tension for Roadway Loading for Method 3: K-Stiffness Method

For Method 3, as reinforcement spacing increases the predicted required ultimate tensile strength, T_{req}, increases for the entire soil profile as shown in Figure 116. The shape of the distribution is controlled by the load distribution factor. Values predicted using Method 3, K-Stiffness, are lower in comparison to other methods.

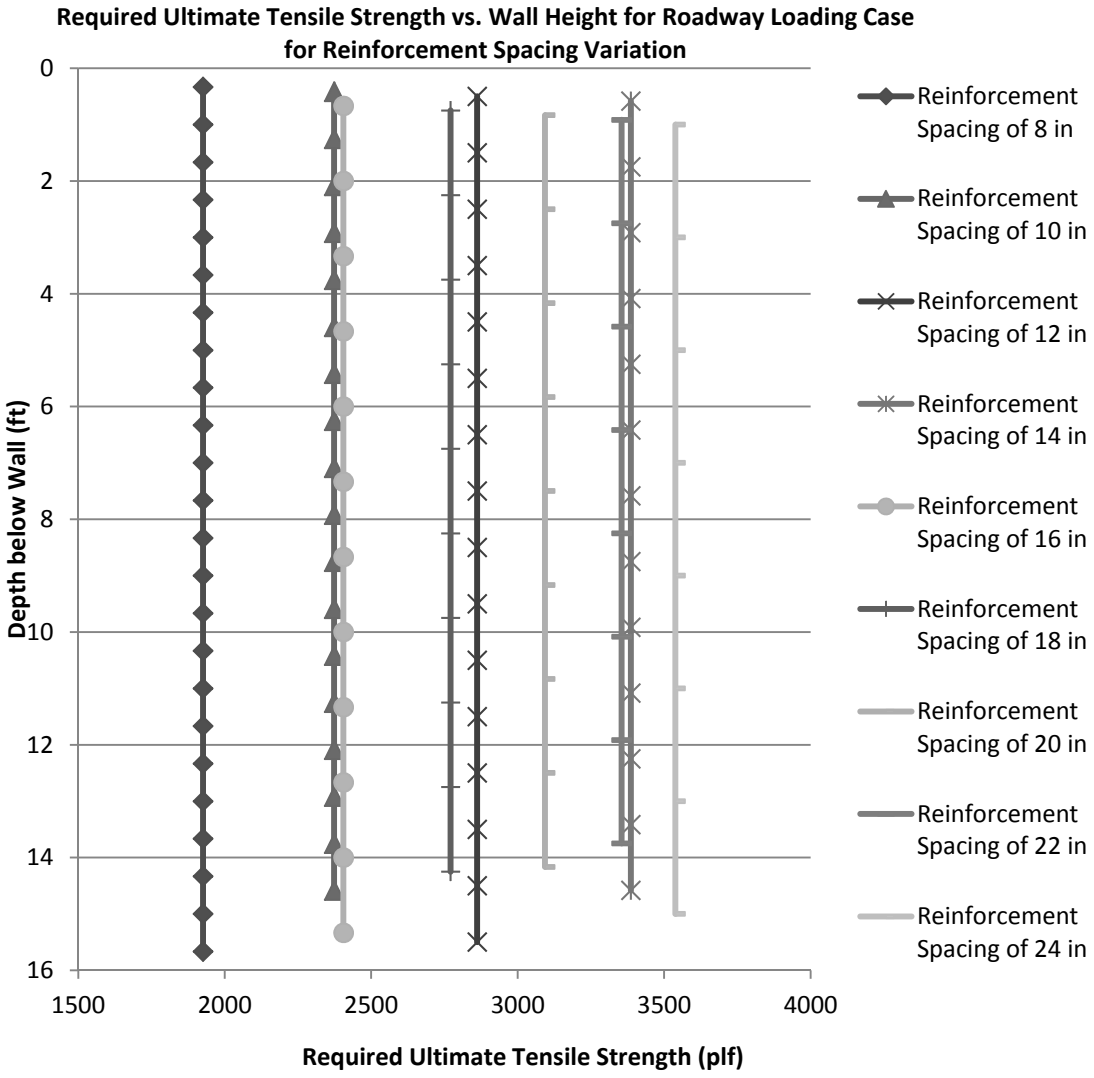

Figure 117: Influence of Reinforcement Spacing on Ultimate Required Tension for Roadway Loading for Method 4: NCHRP GRS Method

Figure 117 shows that for Method 4, the entire profile is assigned a required ultimate tensile strength, T_{req}, value equal to the highest value that occurs in the wall. Therefore, the distributions plot as vertical lines. In general, with increasing reinforcement spacing, the maximum T_{req} value in the profile increases. However, Method 4 predicts a T_{req} value that is dependent on a FS value, as shown in Equation 56. This FS value is influence by reinforcement spacing and changes at 16 inches. Therefore the vertical lines do not always progress in order. To look more closely at the variation of tension at each reinforcement layer, the variation in nominal maximum tensile load, T_{max}, with depth was plotted for each variation in reinforcement spacing. These relationships are plotted in Figure 118.

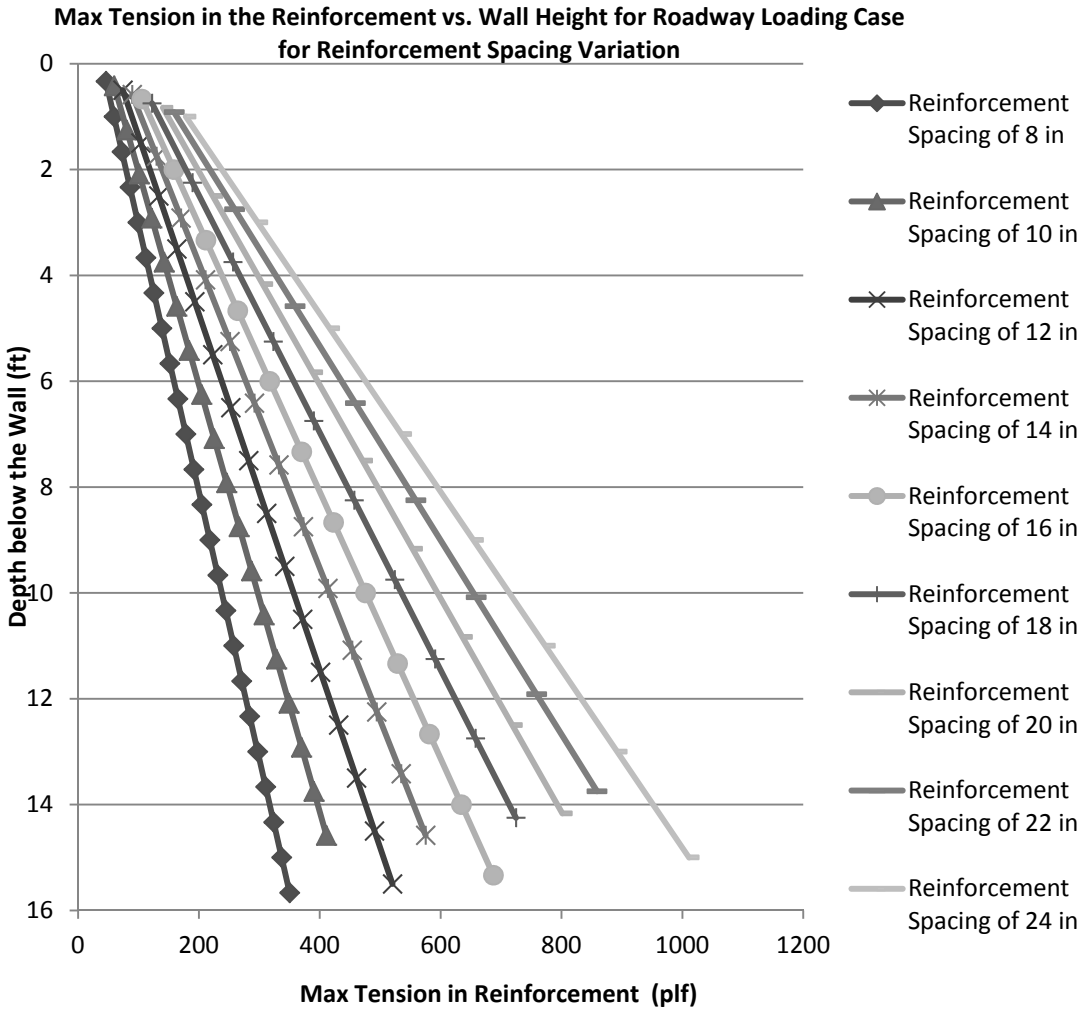

Figure 118: Influence of Reinforcement Spacing on Max Tensile Load in the Reinforcement for Roadway Loading for Method 4: NCHRP GRS Method

Figure 118 shows that for Method 4, increasing reinforcement spacing will increase the nominal maximum tensile load, T_{max}, at all depths below the top of the reinforced zone. The shape of each distribution remains linear for the entire soil profile.

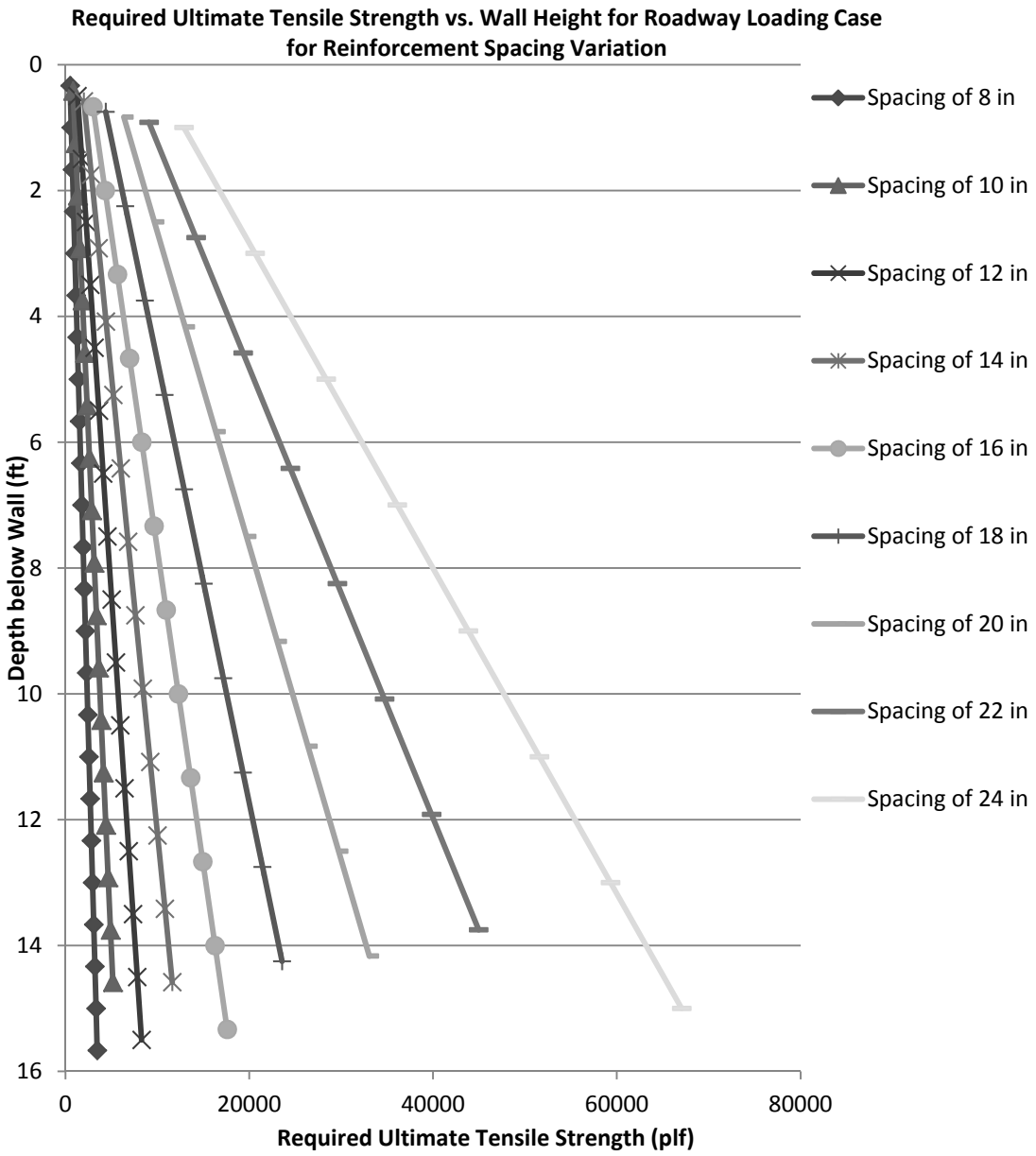

Figure 119: Influence of Reinforcement Spacing on Ultimate Required Tension for Roadway Loading for Method 5: FHWA GRS-IBS Method Analytic Solution

For the Analytic solution for Method 5, as reinforcement spacing increases, the predicted required ultimate tensile strength, T_{req}, increases for the entire soil profile, as shown in Figure 119. All distributions are linear at all depths. The increase in T_{req} is greater at the bottom than at the top of the wall.

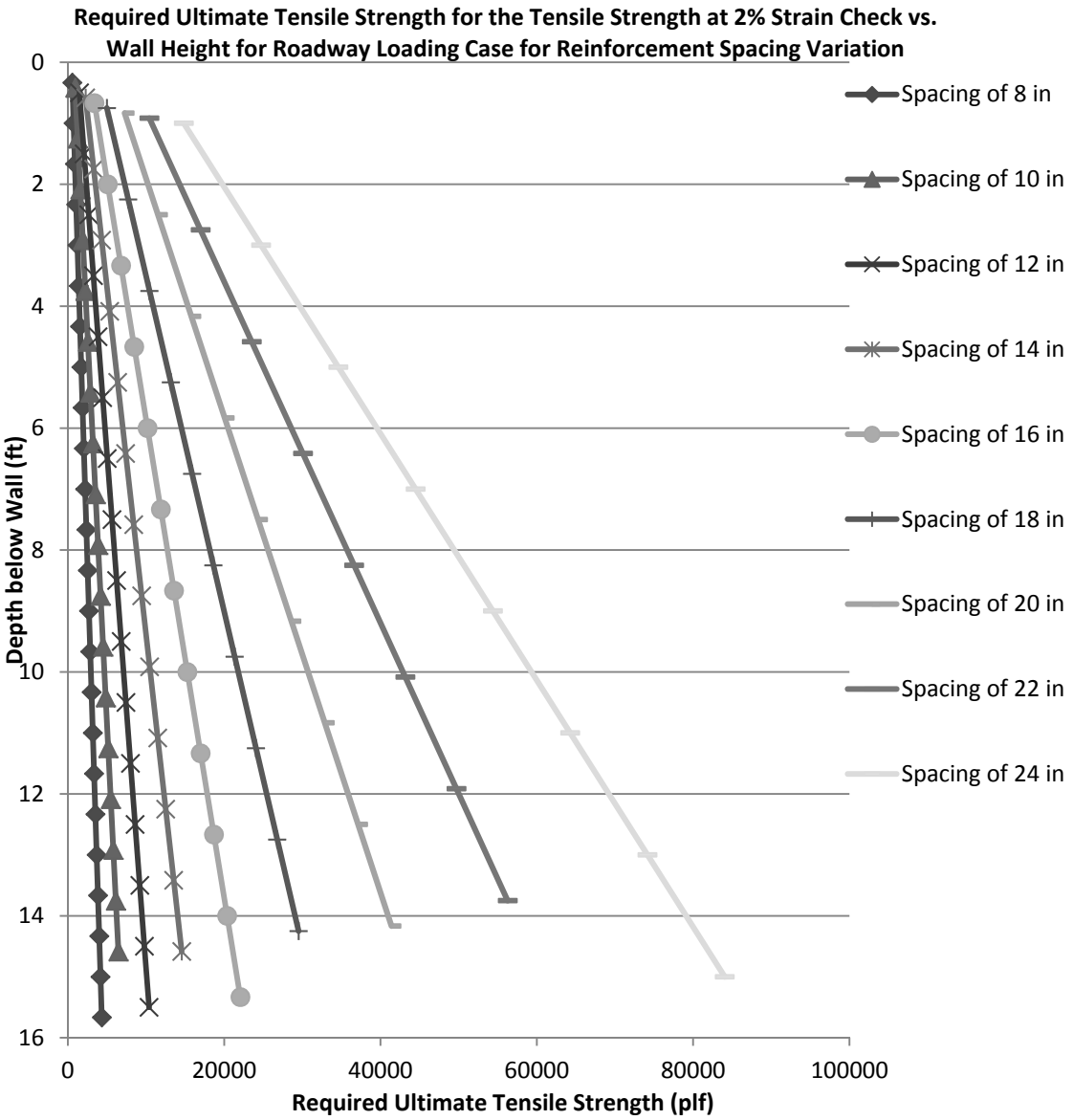

Figure 120: Influence of Reinforcement Spacing on Ultimate Required Tension for Roadway Loading for Method 5: FHWA GRS-IBS Method Tensile Strength at 2% Strain Check

Figure 120 shows that for Method 5's tensile strength at 2% strain equivalent T_{req} calculation, the increase in reinforcement spacing will increase the predicted required ultimate tensile strength, $T_{req.}$ The predicted values of T_{req} are higher than that predicted by the analytic solution. The distributions remain linear for the entire soil profile similarly to the analytic solution.

There is a third check required by Method 5 guidance that requires the ultimate tensile strength to be greater than or equal to 4,800 lb/ft. This requirement is not plotted but would plot as a straight line at the value of 4,800 lb/ft. Which of the three requirements that controls can vary within the soil profile.

In order to compare the methods against one another, the highest values of T_{max} and T_{req} are plotted versus reinforcement spacing in Figure 121 and Figure 122, respectively for all methods.

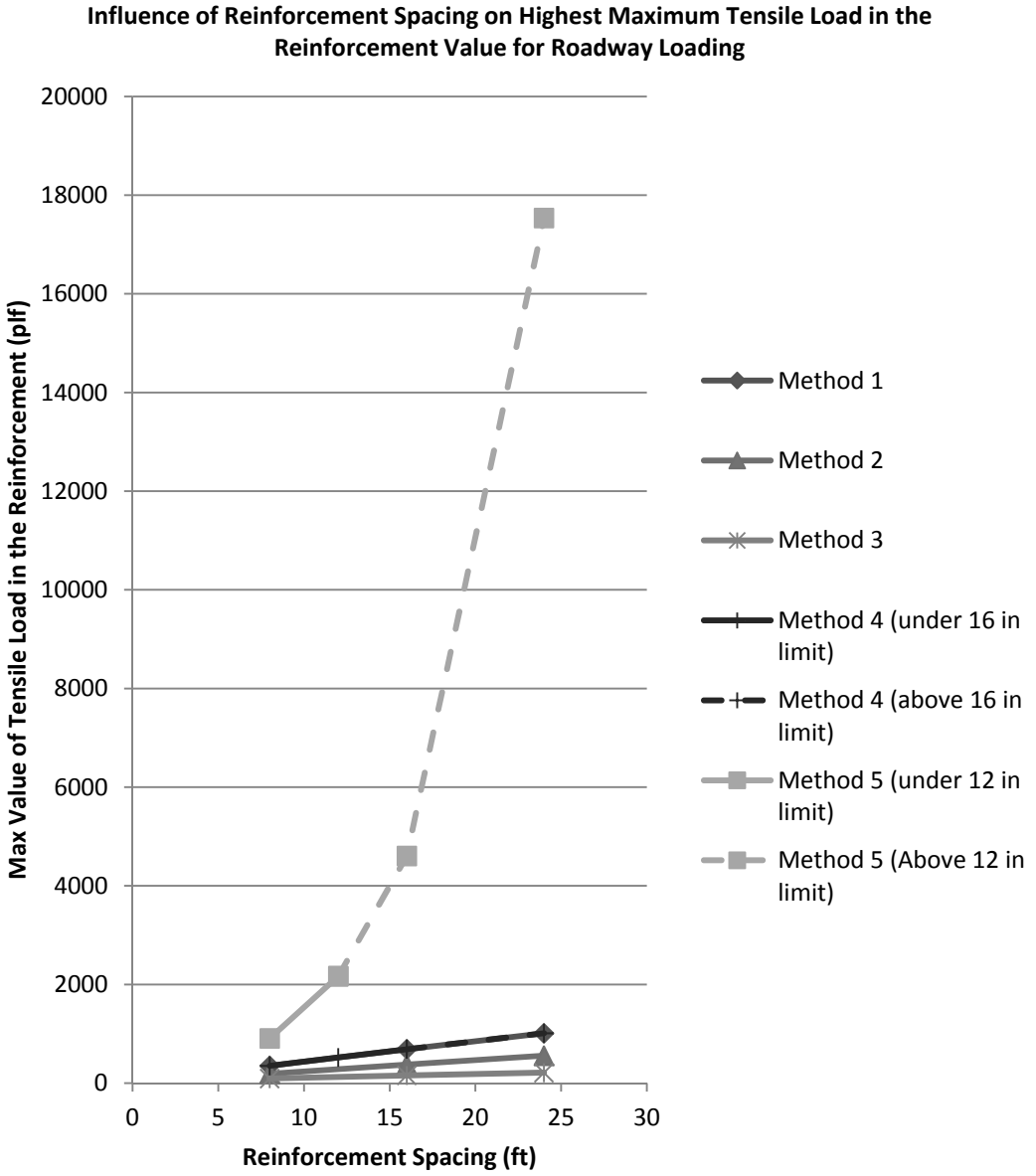

Figure 121: Influence of Reinforcement Spacing on Max Load in the Reinforcement for the Roadway Loading Condition

Figure 121 shows that the highest value of maximum load in the reinforcement, T_{max}, increases with increasing reinforcement spacing. Values predicted by Method 4 are identical to Method 1 and thus appear as a single line. However, Method 4 limits reinforcement spacing to 16 inches. Therefore, spacing values above this limit are indicated with a dashed line and are extrapolated for comparison with MSEW methods

that allow for higher spacings. Similar to Method 4, Method 5 sets a spacing limit of 12 inches. Therefore spacing values above this limit are indicated with a dashed line and are for comparison purposes. Method 5 appears to be the most influenced by reinforcement spacing. This is likely because Method 5 has a very different relationship for predicting T_{max}, where spacing appears in the denominator, shown in Equation 60. This is different than predictive relationships for other methods. Additionally, Method 5 predicts the highest values of T_{max} in comparison to all other methods.

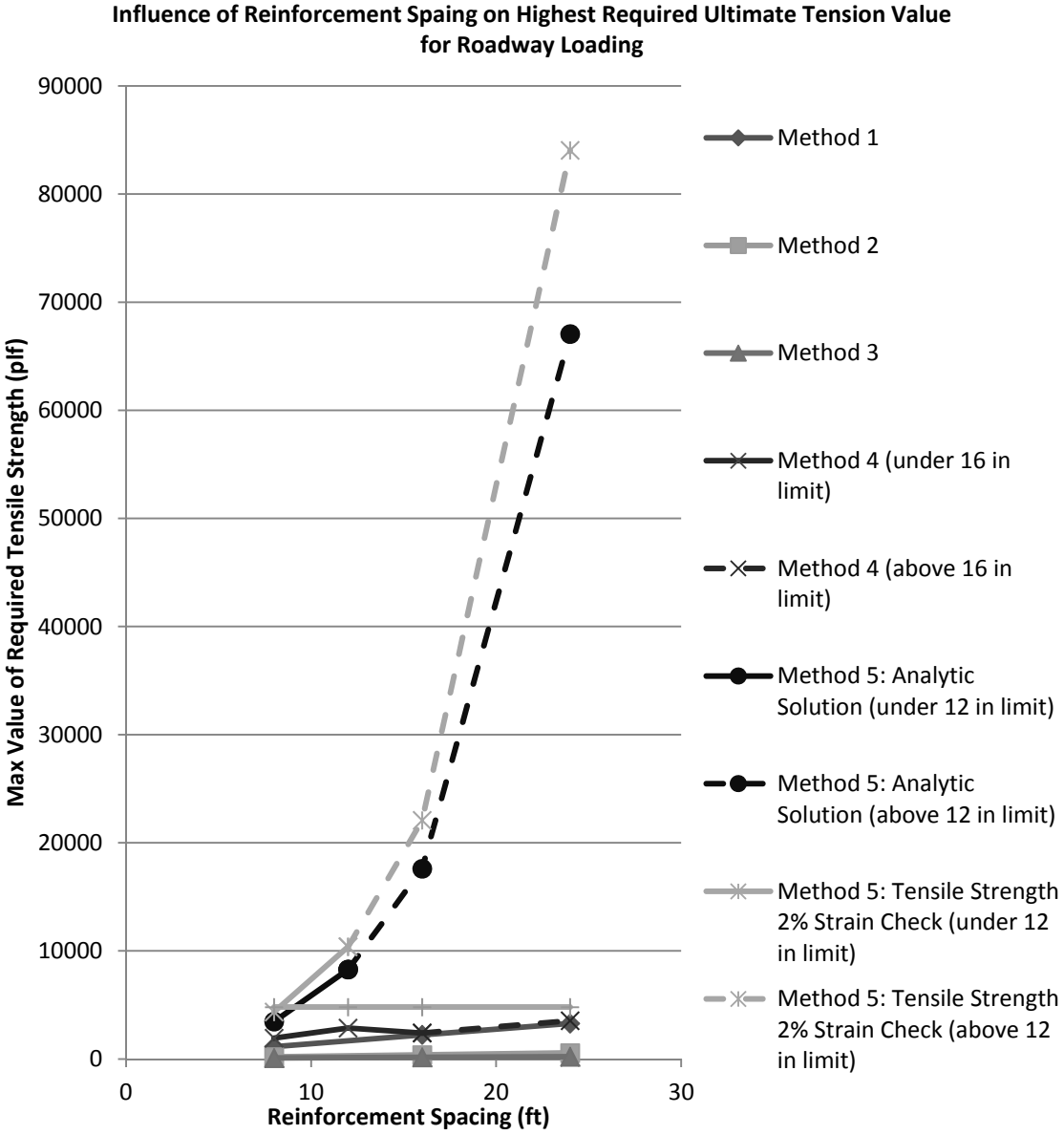

Figure 122: Influence of Reinforcement Spacing on the Highest Predicted Ultimate Required Tension for the Roadway Loading Condition

Figure 122 show that the highest predicted ultimate required tensile strength, T_{req}, also increases with increasing reinforcement spacing. Method 4 limits reinforcement spacing

to 16 inches. Therefore, spacing values above this limit are indicated with a dashed line and are extrapolated for comparison with MSEW methods that allow for higher spacings. Due to the fact that Method 4 utilizes a FS value in its calculation of T_{req}, shown in Equation 56, which varies with spacing, the predicted T_{req} variation is not constant. Similar to Method 4, Method 5 sets a spacing limit of 12 inches. Therefore spacing values above this limit are indicated with a dashed line and are for comparison purposes. Method 5 appears to be the most influenced by reinforcement spacing. This is likely because Method 5 has a very different relationship for predicting T_{max} which is an input into T_{req}. Additionally, Method 5 predicts the highest values of T_{req} in comparison to all other methods.

Method 5 has three requirements to establish T_{req} values for design. The first is an analytic solution, the second is a check of tensile strength at 2% strain, and the last is a requirement that T_{req} be at least equal to or above 4,800 lb/ft. The value chosen for design is the highest of the three ultimate strength values. All three of these predicted values are plotted in Figure 122. The first and second requirements are similarly influenced by reinforcement spacing but the tensile strength at 2% strain check predicts a higher value. The last requirement plots as a straight horizontal line at 4,800 lb/ft.

Bridge Loading: Method 3, the K-Stiffness Method, was not adapted for the bridge loading case for the parametric study and is therefore not included in this section. The reinforcement spacing was varied from 8 inches to 24 inches. The base case value was 8 inches. To present the results clearly, only tributary areas equal to the spacing variation were plotted. In other words, if the tributary area at the very bottom of the wall did not fit evenly into the distribution of wall height, then the final reinforcement layer was not plotted. Lastly, Method 4 and Method 5 the two GRS analysis methods set limits on reinforcement spacing of 16 inches and 12 inches respectively. Variations above these values are for comparison purposes with MSEW methods which allow for larger spacings. Figure 123, Figure 124, Figure 125, Figure 126, Figure 127, and Figure 128 show the variation in tension for the entire soil profile with change in reinforcement spacing for each of the 5 methods.

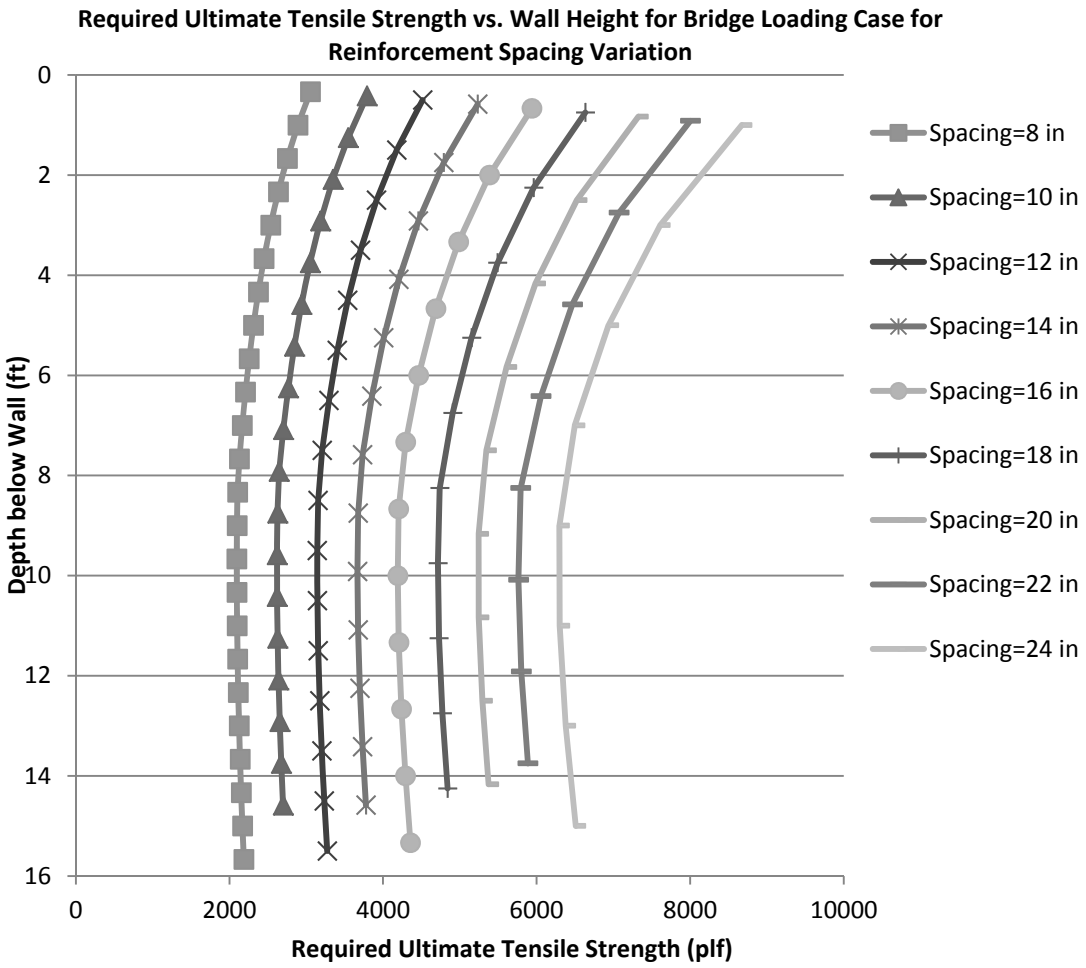

Figure 123: Influence of Reinforcement Spacing on Ultimate Required Tension for Bridge Loading for Method 1: The Simplified Procedure

For Method 1, the increase in spacing results in an increase in the predicted required ultimate tensile strength, T_{req}, for the entire soil profile as shown in Figure 123. All distributions have a curved shape that increases in degree with increase in reinforcement spacing. The T_{req} value both at the top and the bottom increase with increasing reinforcement spacing. The increase at the bottom is less than at the top of the wall.

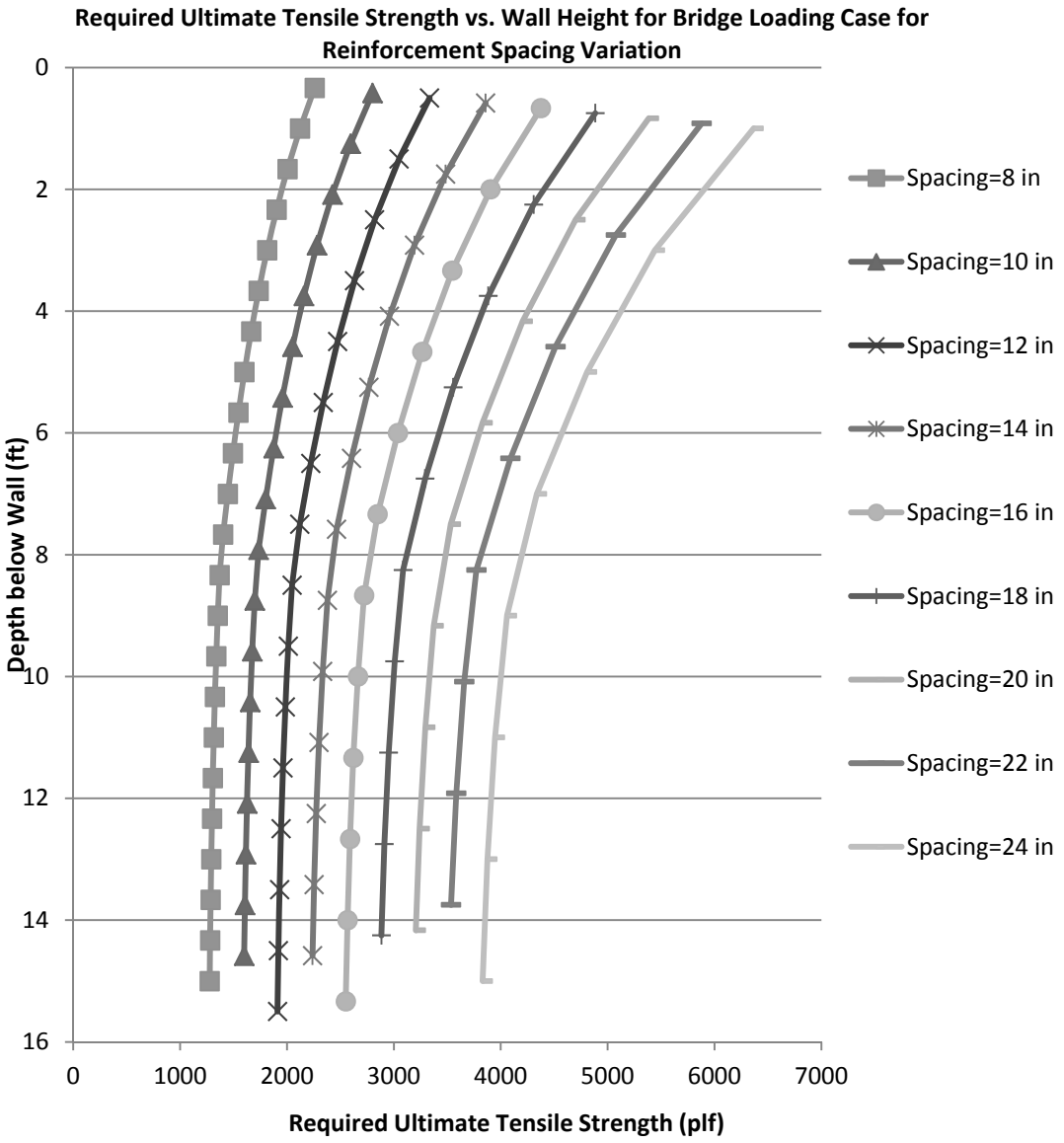

Figure 124: Influence of Reinforcement Spacing on Ultimate Required Tension for Bridge Loading for Method 2: The Simplified Procedure with K_r/K_a Adjusted

For Method 2, the increase in spacing results in an increase in the predicted required ultimate tensile strength, T_{req}, for the entire soil profile as shown in Figure 124. All distributions have a curved shape that increases in degree with increase in reinforcement spacing. The T_{req} value both at the top and the bottom increase with increasing reinforcement spacing. The increase at the bottom is less than at the top of the wall.

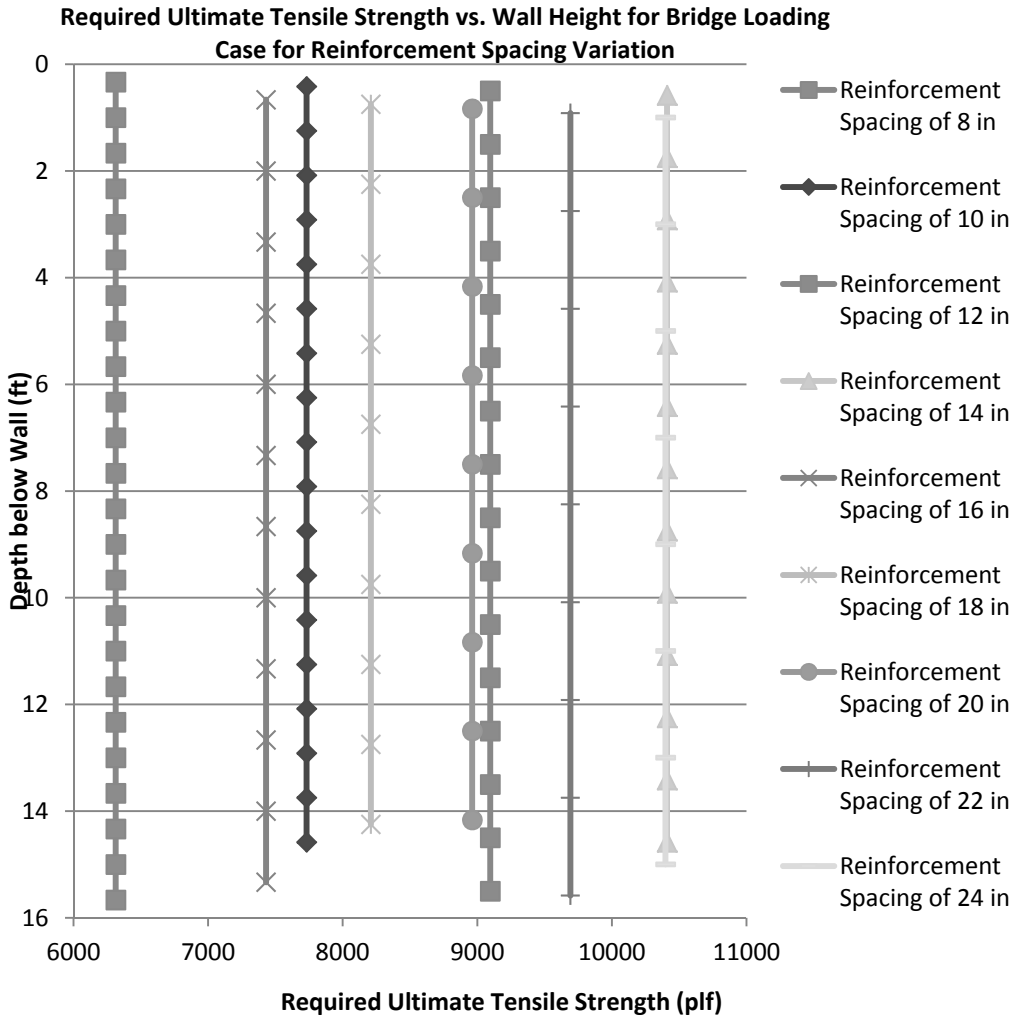

Figure 125: Influence of Reinforcement Spacing on Ultimate Required Tension for Bridge Loading for Method 4: NCHRP GRS Method

Figure 125 shows that for Method 4, the entire profile is assigned a required ultimate tensile strength, T_{req}, value equal to the highest value that occurs in the wall. Therefore, the distributions plot as vertical lines. In general, with increasing reinforcement spacing, the maximum T_{req} value in the profile increases. However, Method 4 predicts a T_{req} value that is dependent on a FS value, as shown in Equation 58. This FS value is influence by reinforcement spacing and changes at 16 inches. Therefore the vertical lines do not always progress in order. To look more closely at the variation of tension at each reinforcement layer, the variation in nominal maximum tensile load, T_{max}, with depth was plotted for each variation in reinforcement spacing. These relationships are plotted in Figure 126.

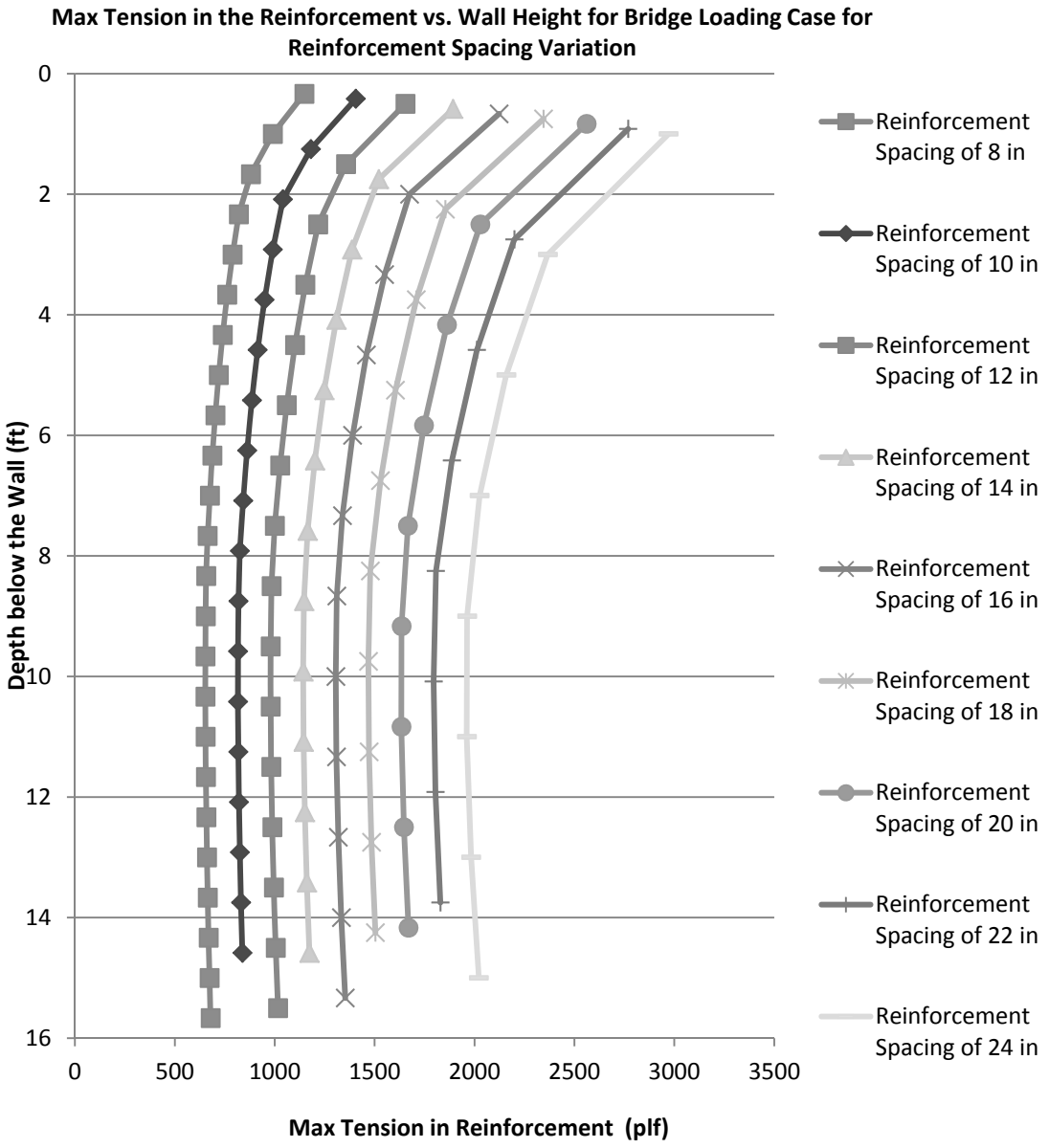

Figure 126: Influence of Reinforcement Spacing on Max Tensile Load in the Reinforcement for Bridge Loading for Method 4: NCHRP GRS Method

Figure 126 shows that for Method 4, increasing reinforcement spacing will increase the nominal maximum tensile load, T_{max}, at all depths below the top of the reinforced zone. The shape of each distribution is curved with increasing degree of curvature with increasing reinforcement spacing.

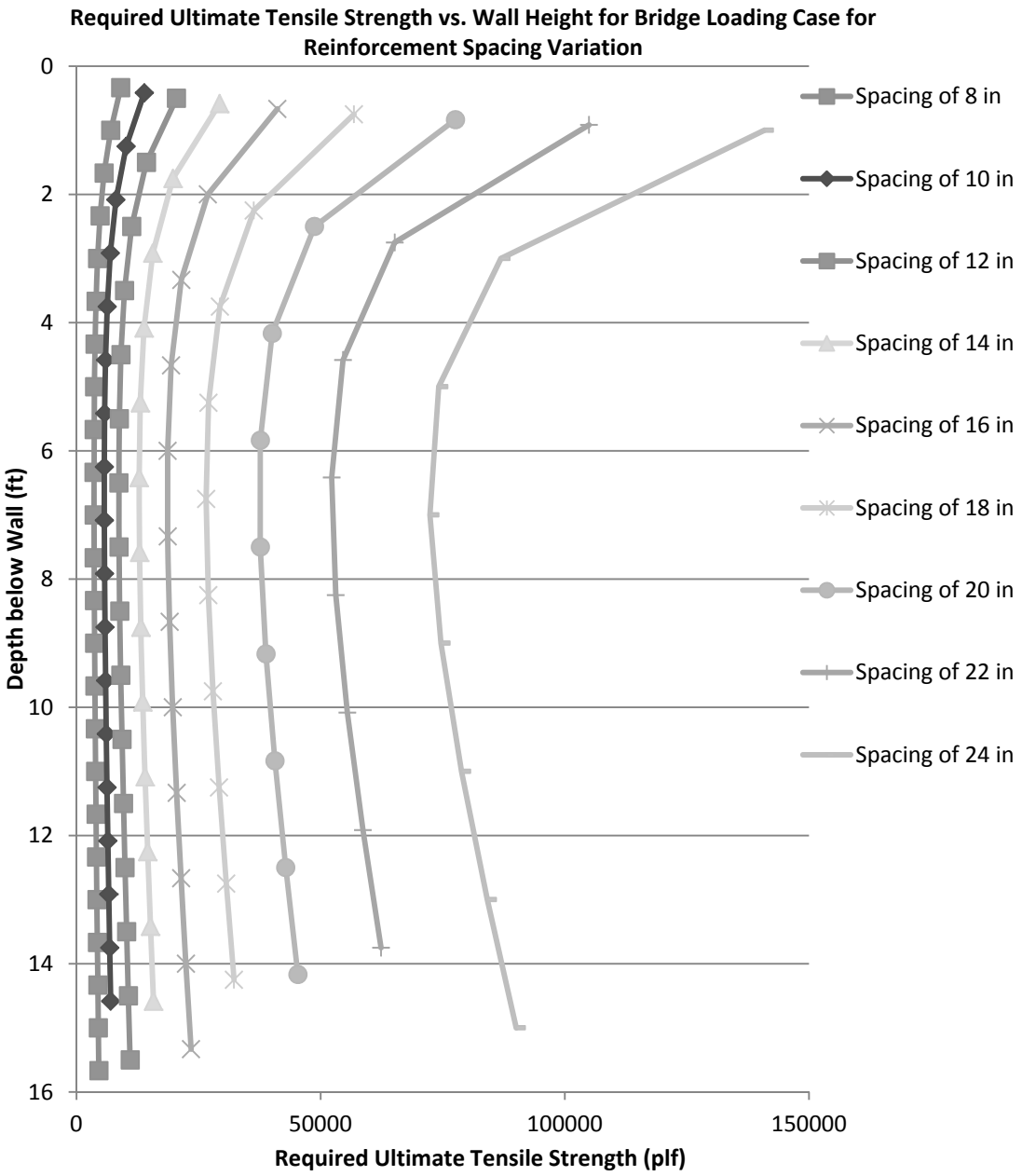

Figure 127: **Influence of Reinforcement Spacing on Ultimate Required Tension for Bridge Loading for Method 5: FHWA GRS-IBS Method Analytic Solution**

Fort the analytic solution for Method 5, as reinforcement spacing increases, the predicted required ultimate tensile strength, T_{req}, increases for the entire soil profile, as shown in Figure 127. All distributions have a curved shape. The increase in T_{req} is greater at the top than at the bottom of the wall.

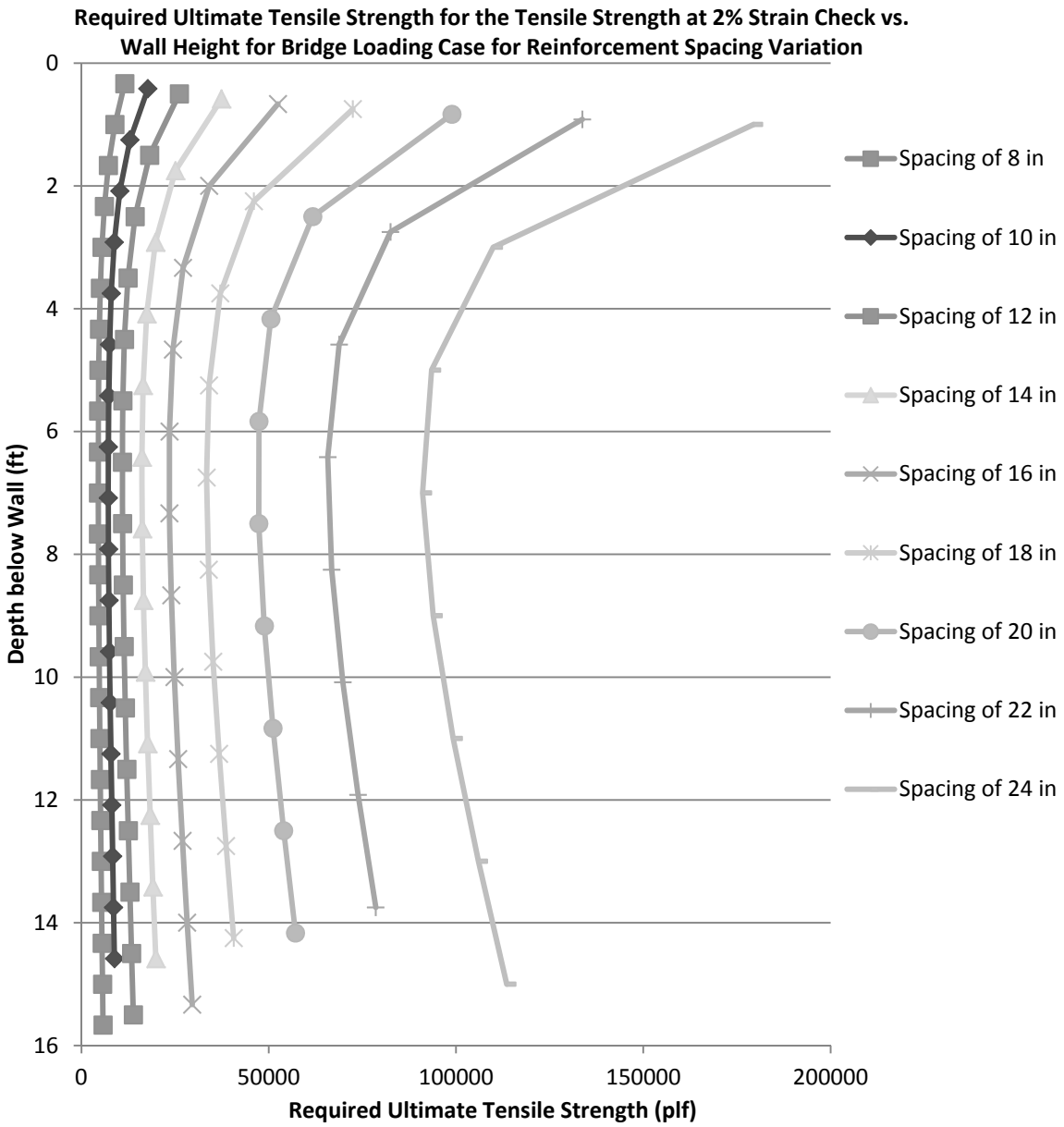

Figure 128: Influence of Reinforcement Spacing on Ultimate Required Tension for Bridge Loading for Method 5: FHWA GRS-IBS Method Tensile Strength at 2% Strain Check

Figure 128 shows that For Method 5's tensile strength at 2% strain equivalent T_{req} calculation, the increase in reinforcement spacing will increase the predicted required ultimate tensile strength, $T_{req.}$ The predicted values of T_{req} are higher than that predicted by the analytic solution but the distributions have very similar shapes. Higher spacing values for Method 5 are much greater than those predicted by other methods.

There is a third check required by Method 5 guidance that requires the ultimate tensile strength to be greater than or equal to 4,800 lb/ft. This requirement is not plotted but

would plot as a straight line at the value of 4,800 lb/ft. Which of the three requirements that controls can vary within the soil profile.

In order to compare the methods against one another, the highest values of T_{max} and T_{req} are plotted versus reinforcement spacing in Figure 129 and Figure 130, respectively for all applicable methods.

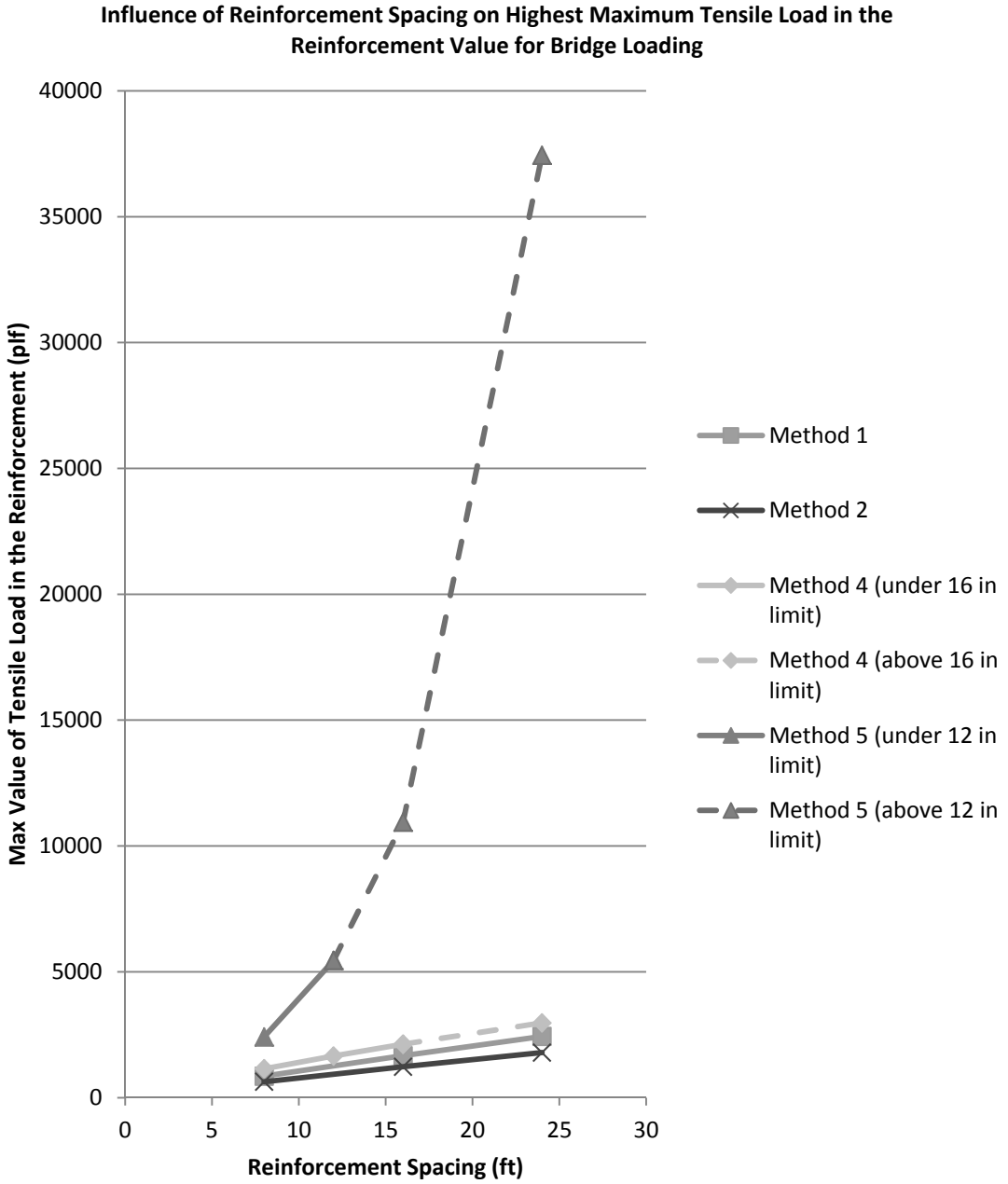

Figure 129: Influence of Reinforcement Spacing on Max Load in the Reinforcement for the Bridge Loading Condition

Figure 129 shows that the highest value of maximum load in the reinforcement, T_{max}, increases with increasing reinforcement spacing. Values predicted by Method 4 are identical to Method 1 and thus appear as a single line. However, Method 4 limits reinforcement spacing to 16 inches. Therefore, spacing values above this limit are indicated with a dashed line and are extrapolated for comparison with MSEW methods that allow for higher spacings. Similar to Method 4, Method 5 sets a spacing limit of 12 inches. Therefore spacing values above this limit are indicated with a dashed line and are for comparison purposes. Method 5 appears to be the most influenced by reinforcement spacing. This is likely because Method 5 has a very different relationship for predicting T_{max}, where spacing appears in the denominator, shown in Equation 63. This is different than predictive relationships for other methods. Additionally, Method 5 predicts the highest values of T_{max} in comparison to all other methods.

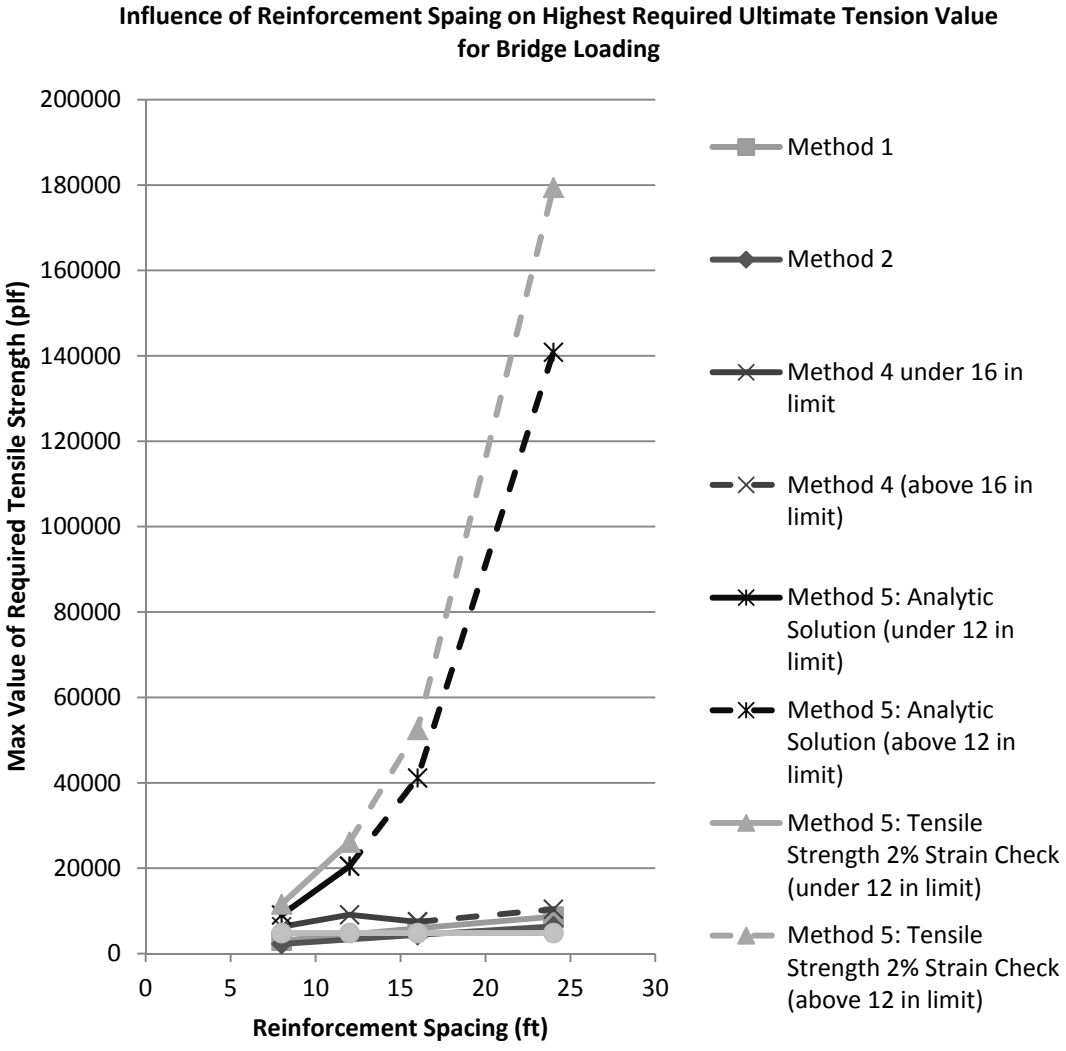

Figure 130: Influence of Reinforcement Spacing on the Highest Predicted Ultimate Required Tension for the Bridge Loading Condition

Figure 130 show that the highest predicted ultimate required tensile strength, T_{req}, also increases with increasing reinforcement spacing. Method 4 limits reinforcement spacing to 16 inches. Therefore, spacing values above this limit are indicated with a dashed line and are extrapolated for comparison with MSEW methods that allow for higher spacings. Due to the fact that Method 4 utilizes a FS value in its calculation of T_{req}, shown in Equation 58, which varies with spacing, the predicted T_{req} variation is not constant. Similar to Method 4, Method 5 sets a spacing limit of 12 inches. Therefore spacing values above this limit are indicated with a dashed line and are for comparison purposes. Method 5 appears to be the most influenced by reinforcement spacing. This is likely because Method 5 has a very different relationship for predicting T_{max} which is an input into T_{req}. Additionally, Method 5 predicts the highest values of T_{req} in comparison to all other methods.

Method 5 has three requirements to establish T_{req} values for design. The first is an analytic solution, the second is a check of tensile strength at 2% strain, and the last is a requirement that T_{req} be at least equal to or above 4,800 lb/ft. The value chosen for design is the highest of the three ultimate strength values. All three of these predicted values are plotted in Figure 130. The first and second requirements are similarly influenced by reinforcement spacing but the tensile strength at 2% strain check predicts a higher value. The last requirement plots as a straight horizontal line at 4,800 lb/ft.

Impact of Maximum Aggregate Size Variation: The following section explores the influence of varying maximum aggregate size over the range detailed in Table 4 for the roadway loading condition and Table 5 for the bridge loading case. This variation only influences Method 5. None of the other methods utilize this parameter for calculation of T_{max} and $T_{req.}$

Roadway Loading: For the roadway loading scenario, both T_{max} and T_{req} can be calculated for Method 5 the FHWA GRS-IBS Method. Figure 131 and Figure 132 show the variation in tension for the entire soil profile with change in maximum aggregate size for Method 5.

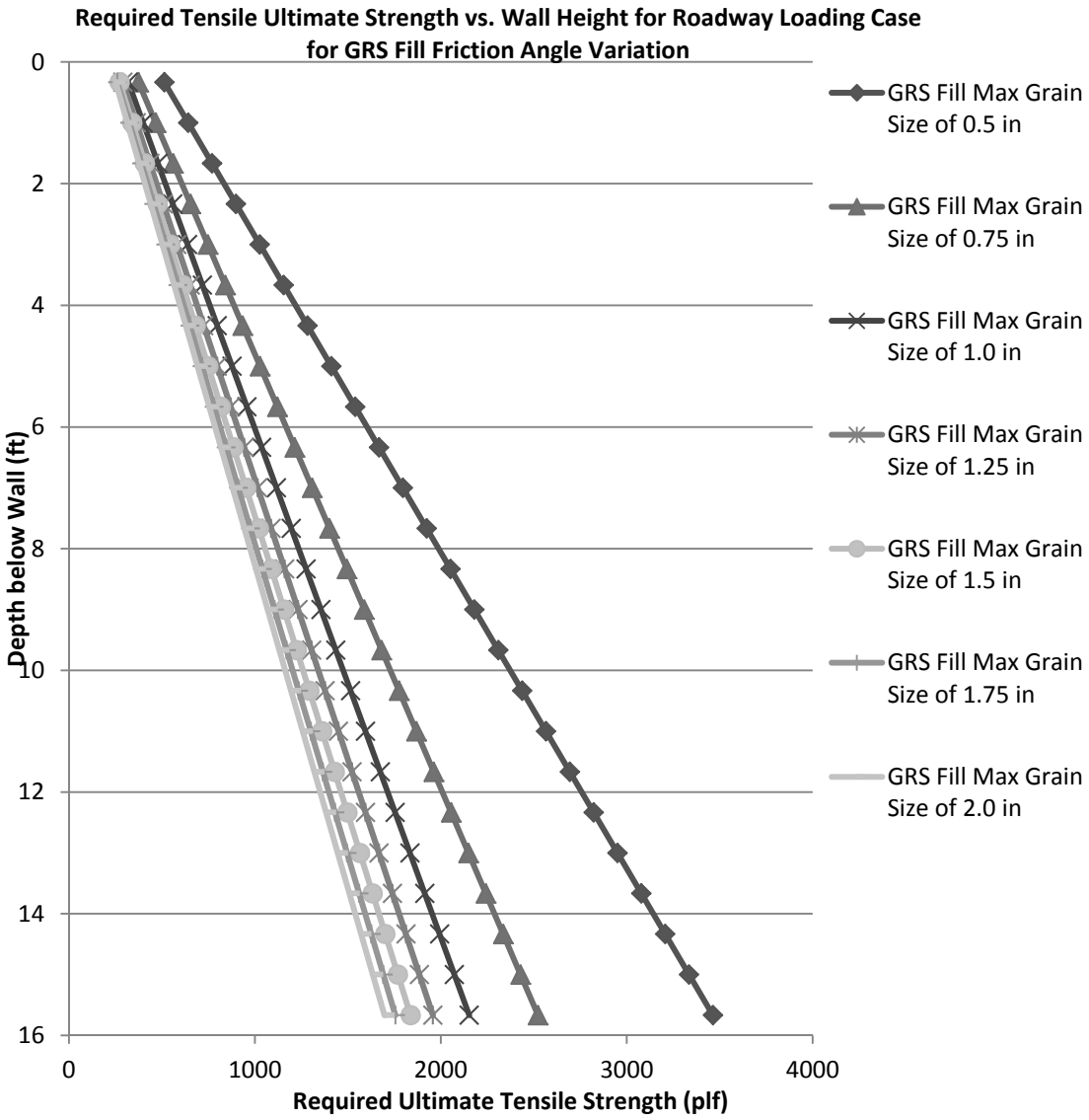

Figure 131: **Influence of Maximum Aggregate Size on Ultimate Required Tension for Bridge Loading for Method 5: FHWA GRS-IBS Method Analytic Solution**

For Method 5's analytic solution, as maximum aggregate size increases the predicted required ultimate tensile strength, T_{req}, decreases for the entire soil profile as shown in Figure 131. All distributions are linear at all depths. The decrease in T_{req} is greater at the bottom than at the top of the wall.

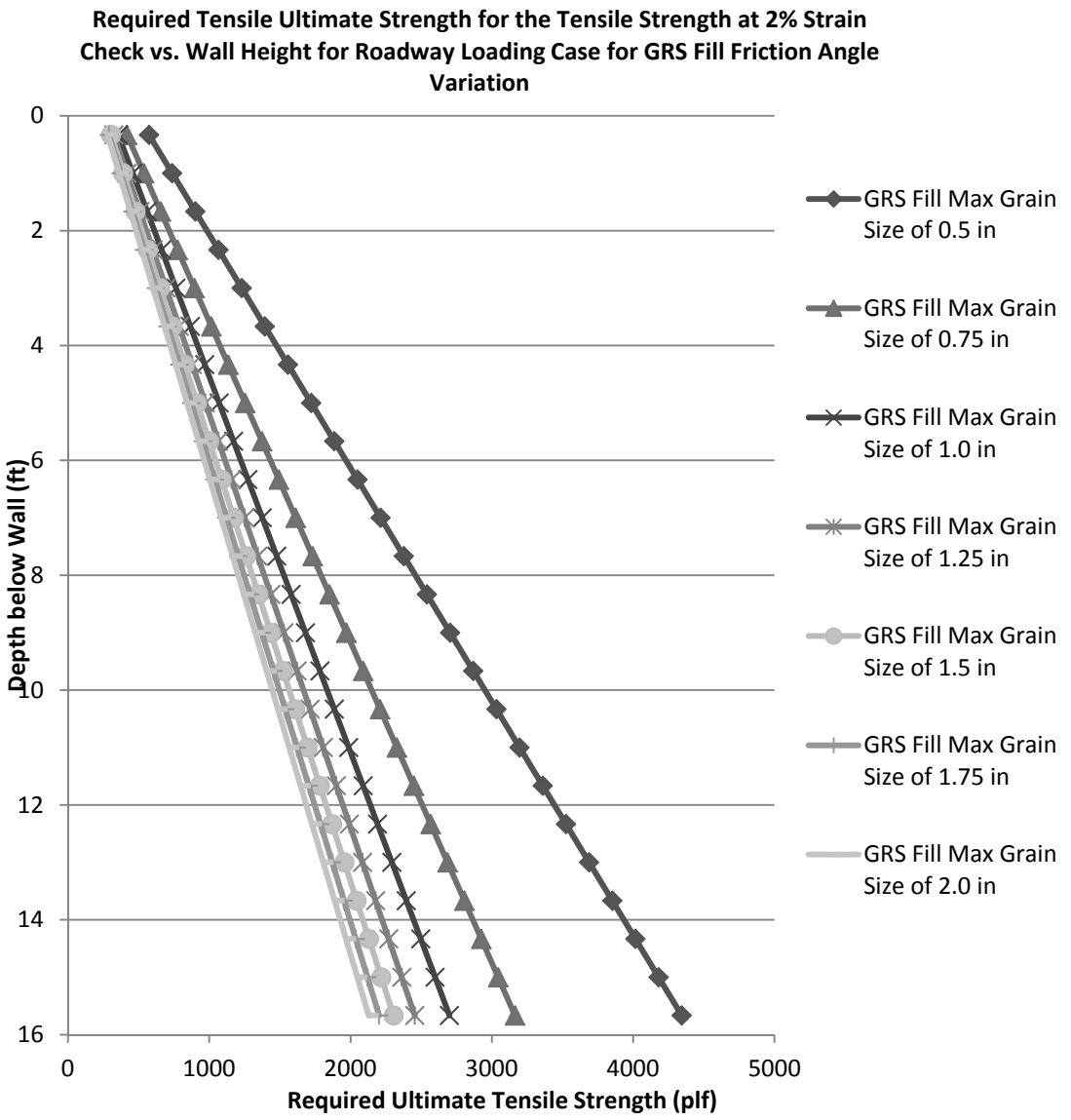

Figure 132: Influence of Maximum Aggregate Size on Ultimate Required Tension for Bridge Loading for Method 5: FHWA GRS-IBS Method Tensile Strength at 2% Strain Check

Figure 132 shows that for Method 5's tensile strength at 2% strain equivalent T_{req} calculation, the increase in maximum aggregate size will decrease the predicted required ultimate tensile strength, $T_{req.}$ The predicted values of T_{req} are higher than that predicted by the analytic solution. The distributions remain linear for the entire soil profile similarly to the analytic solution.

There is a third check required by Method 5 guidance that requires the ultimate tensile strength to be greater than or equal to 4,800 lb/ft. This requirement is not plotted but would plot as a straight line at the value of 4,800 lb/ft. For the roadway loading condition this check would control at all depths.

The relationships presented in Figure 133 and Figure 134 only show the variation of the highest values of T_{max} and T_{req}.

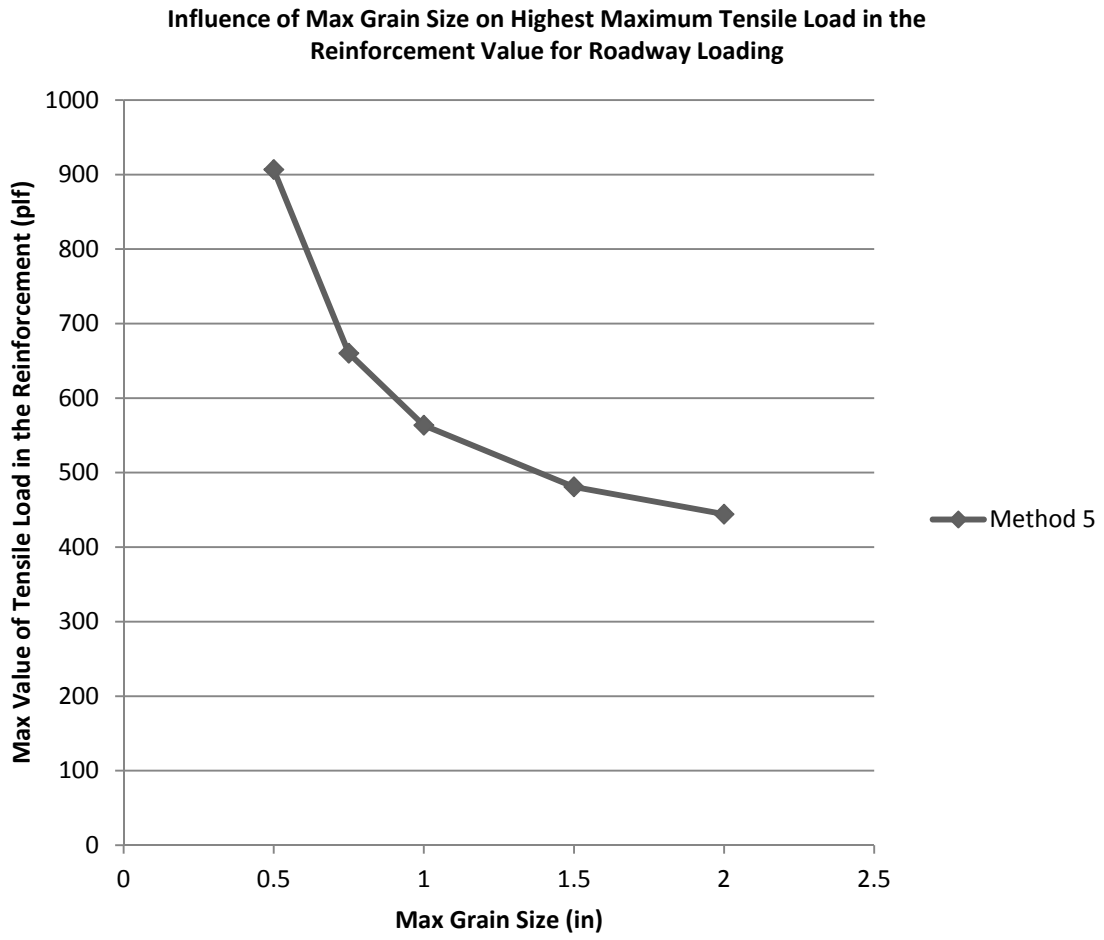

Figure 133: Influence of Maximum Aggregate Size on Max Load in the Reinforcement for the Bridge Loading Condition

Figure 133 shows that the highest value of maximum load in the reinforcement, T_{max}, decreases with increasing maximum aggregate size of the reinforced fill. The highest predicted ultimate required tensile strength, T_{req}, also decreases with increasing maximum aggregate size as shown in Figure 134.

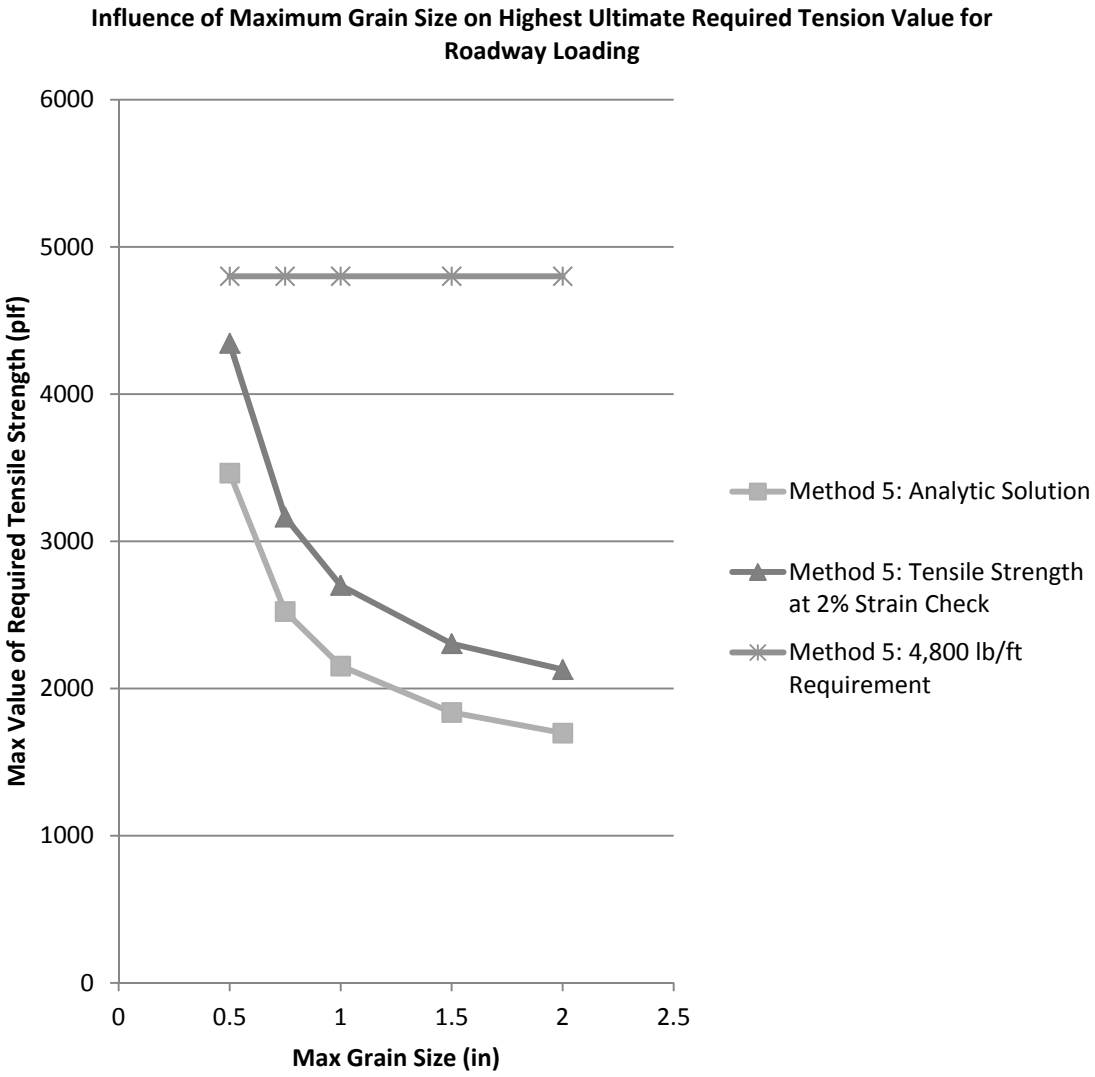

Figure 134: Influence of Maximum Aggregate Size on the Highest Predicted Ultimate Required Tension for the Roadway Loading Condition

Method 5 has three requirements to establish T_{req} values for design. The first is an analytic solution, the second is a check of tensile strength at 2% strain, and the last is a requirement that T_{req} be at least equal to or above 4,800 lb/ft. The value chosen for design is the highest of the three ultimate strength values. All three of these predicted values are plotted in Figure 134. The first and second requirements are similarly influenced by maximum aggregate size but the tensile strength at 2% strain check predicts a higher value. The last requirement plots as a straight horizontal line at 4,800 lb/ft.

Bridge Loading: For the bridge loading scenario, both T_{max} and T_{req} can be calculated for Method 5 the FHWA GRS-IBS Method. Figure 135 and Figure 136 show the variation in tension for the entire soil profile with change in maximum aggregate size for Method 5.

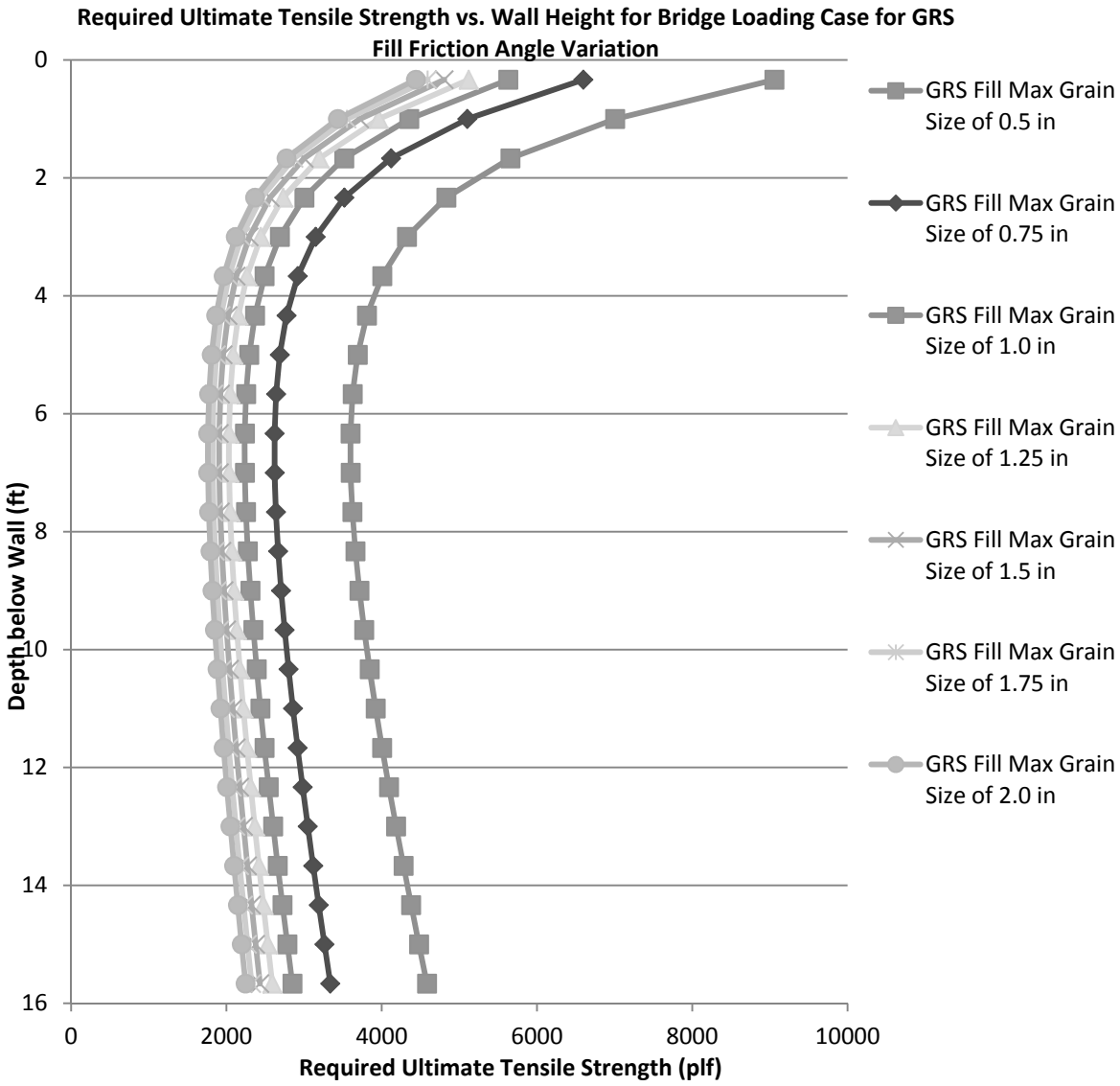

Figure 135: **Influence of Maximum Aggregate Size on Ultimate Required Tension for Bridge Loading for Method 5: FHWA GRS-IBS Method Analytic Solution**

For Method 5's analytic solution, as maximum aggregate size increases the predicted required ultimate tensile strength, T_{req}, decreases for the entire soil profile as shown in Figure 135. All distributions have a curved shape.

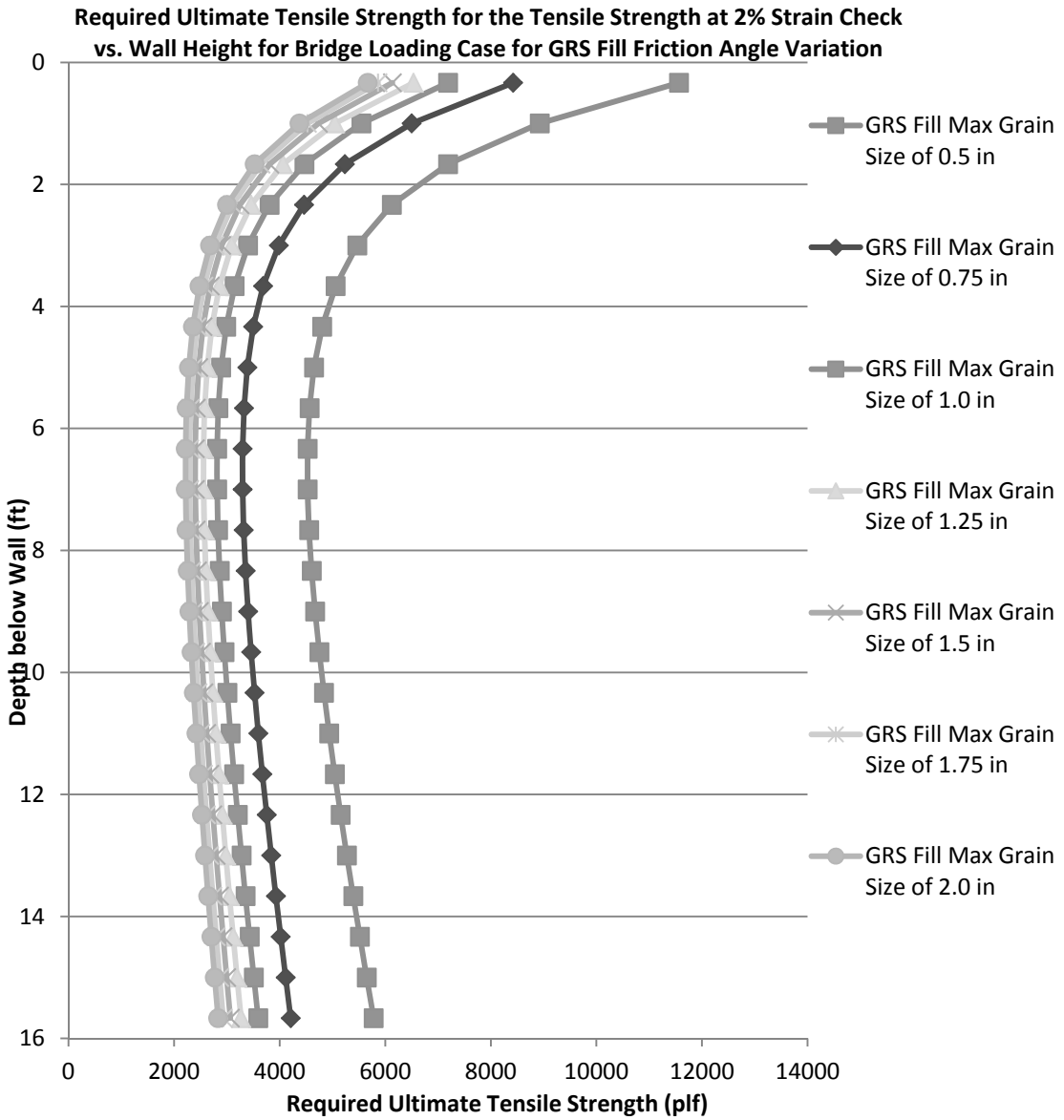

Figure 136: Influence of Max Aggregate Size on Ultimate Required Tension for Bridge Loading for Method 5: FHWA GRS-IBS Method Tensile Strength at 2% Strain Check

Figure 136 shows that for Method 5's tensile strength at 2% strain equivalent T_{req} calculation, the increase in maximum aggregate size will decrease the predicted required ultimate tensile strength, $T_{req.}$ The predicted values of T_{req} are higher than that predicted by the analytic solution but the distributions have very similar shapes.

There is a third check required by Method 5 guidance that requires the ultimate tensile strength to be greater than or equal to 4,800 lb/ft. This requirement is not plotted but would plot as a straight line at the value of 4,800 lb/ft. Which of the three requirements that controls can vary within the soil profile.

The relationships presented in Figure 137 and Figure 138 only show the variation of the highest values of T_{max} and T_{req}.

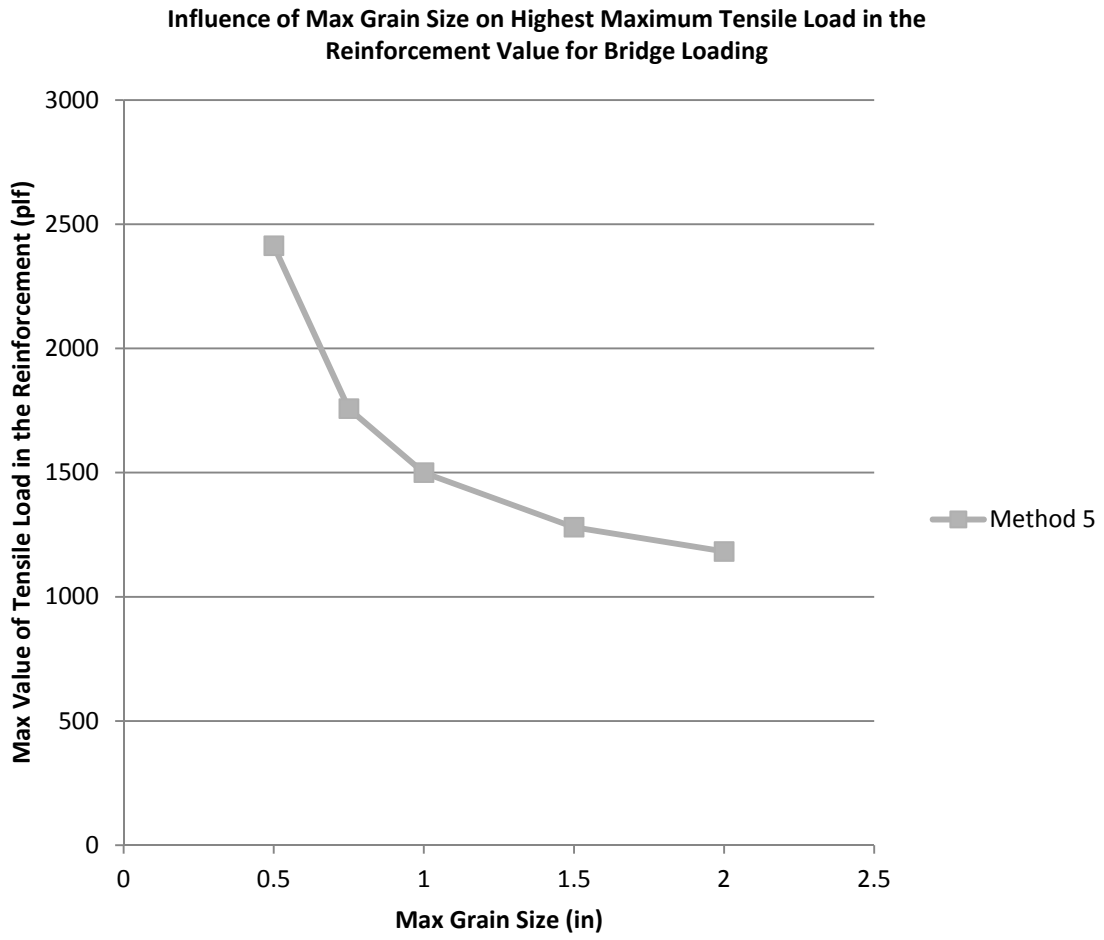

Figure 137: Influence of Maximum Aggregate Size on Max Load in the Reinforcement for the Bridge Loading Condition

Figure 137 shows that the highest value of maximum load in the reinforcement, T_{max}, decreases with increasing maximum aggregate size of the reinforced fill. The highest predicted ultimate required tensile strength, T_{req}, also decreases with increasing maximum aggregate size as shown in Figure 138.

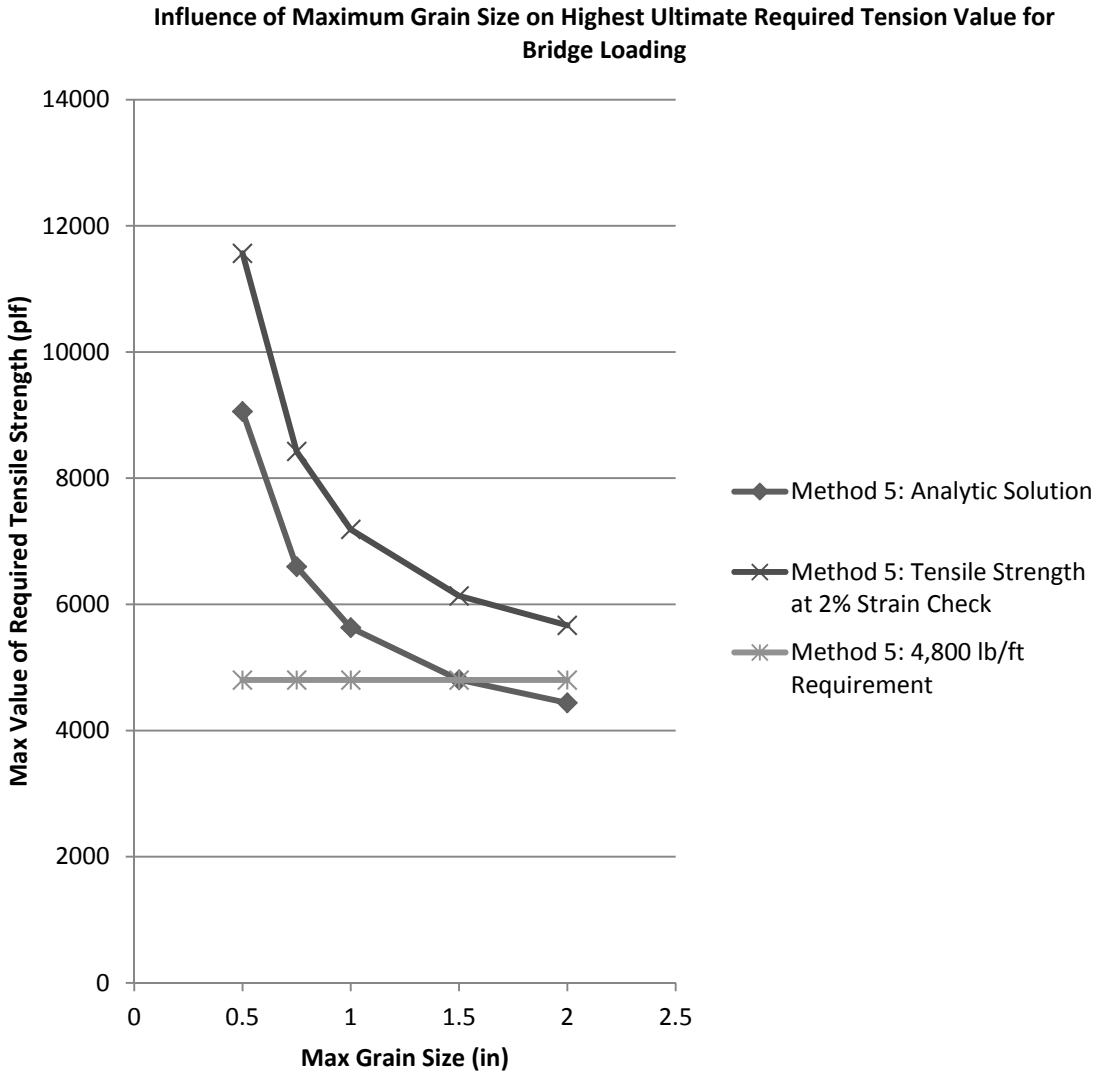

Figure 138: Influence of Maximum Aggregate Size on the Highest Predicted Ultimate Required Tension for the Bridge Loading Condition

Method 5 has three requirements to establish T_{req} values for design. The first is an analytic solution, the second is a check of tensile strength at 2% strain, and the last is a requirement that T_{req} be at least equal to or above 4,800 lb/ft. The value chosen for design is the highest of the three ultimate strength values. All three of these predicted values are plotted in Figure 138. The first and second requirements are similarly influenced by maximum aggregate size but the tensile strength at 2% strain check predicts a higher value. The last requirement plots as a straight horizontal line at 4,800 lb/ft.

Impact of Facing Block Dimension Variation: The following section explores the influence of varying the facing block dimensions over the range detailed in Table 4 for the roadway loading condition. This variation only influences Method 3. All other methods do not utilize this parameter for calculation of T_{max} and T_{req}.

Roadway Loading: For the roadway loading scenario, both T_{max} and T_{req} can be calculated for Method 3 the K-Stiffness Method. The influence of facing block dimensions on T_{req} for the entire soil profile is shown in Figure 139.

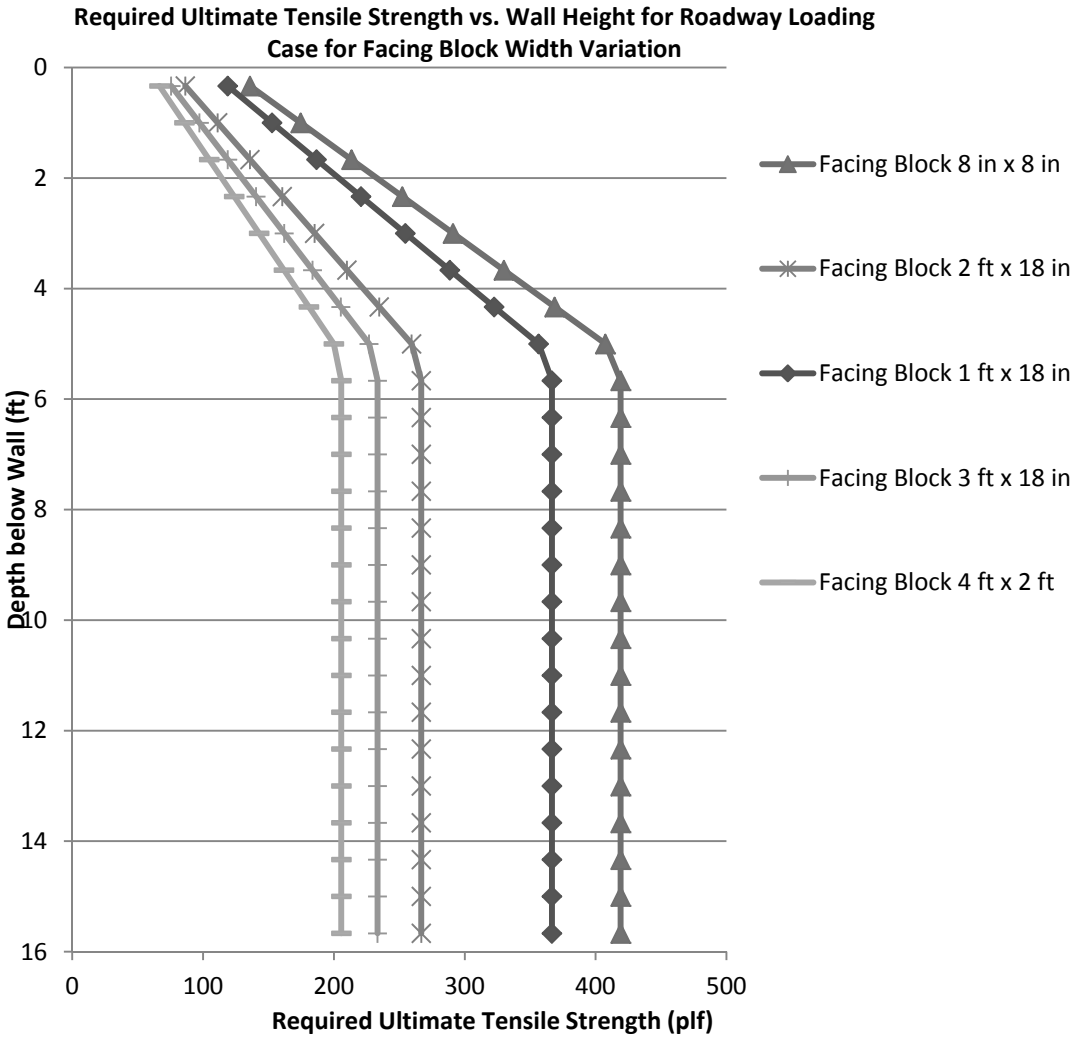

Figure 139: Influence of Facing Block Dimensions on Ultimate Required Tension for Roadway Loading for Method 3: K-Stiffness Method

As facing block dimensions increased in size, the predicted required ultimate tensile strength, T_{req}, for the entire soil profile decreased as shown in Figure 139. It should be noted, that block width had a greater influence on this decrease than block width. The distribution shape is still controlled by the load distribution factor. Method 3, even for smaller facing block elements, produces values lower than other methods by comparison.

A comparison of how block dimensions influence the highest predicted values of T_{max} and T_{req} is shown in Figure 140 and Figure 141.

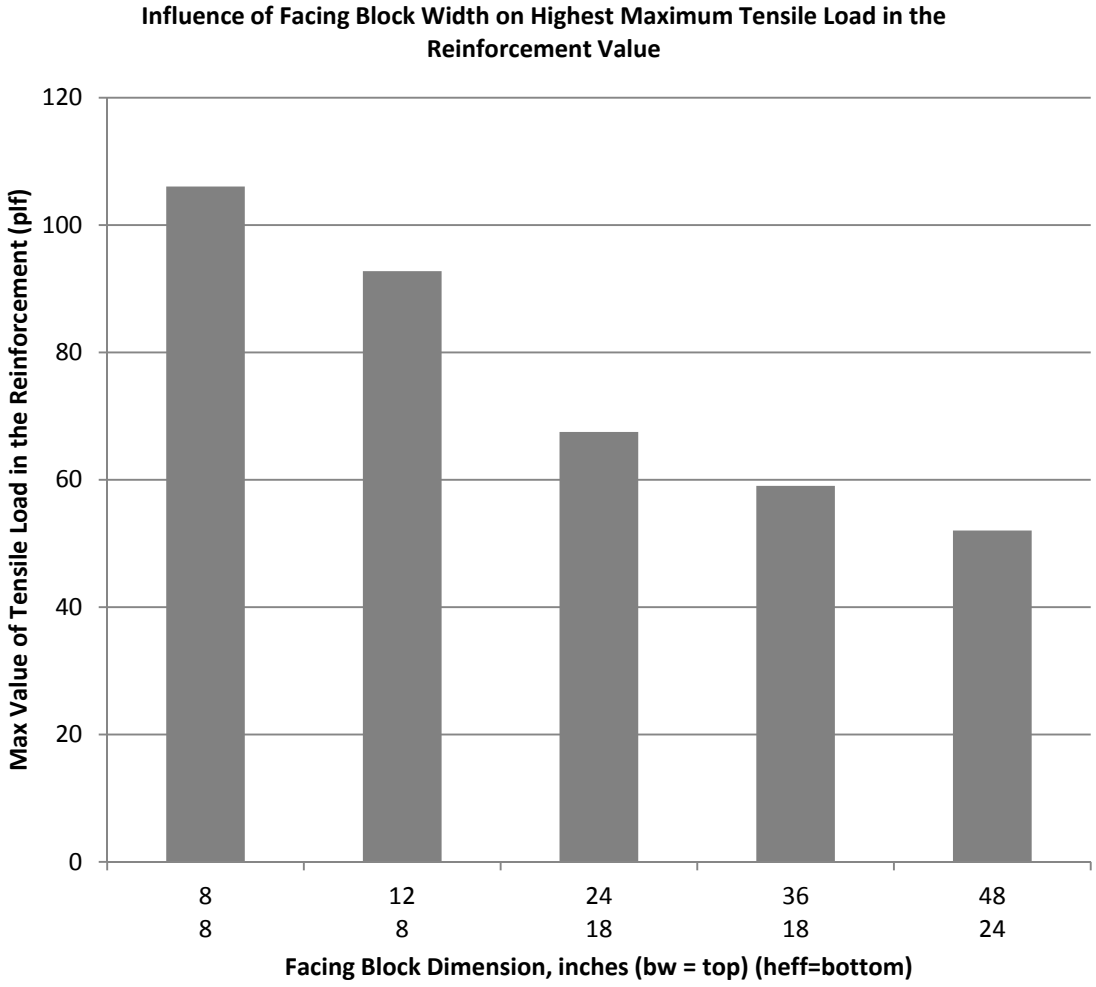

Figure 140: Influence of Facing Block Dimensions on Max Load in the Reinforcement for the Roadway Loading Condition

Figure 140 shows that for Method 3, the increase in block size causes a decrease in the predicted nominal maximum tensile load carried by the reinforcement, T_{max}, for the entire soil profile. It should be noted that block width has a greater influence on this decrease than block height.

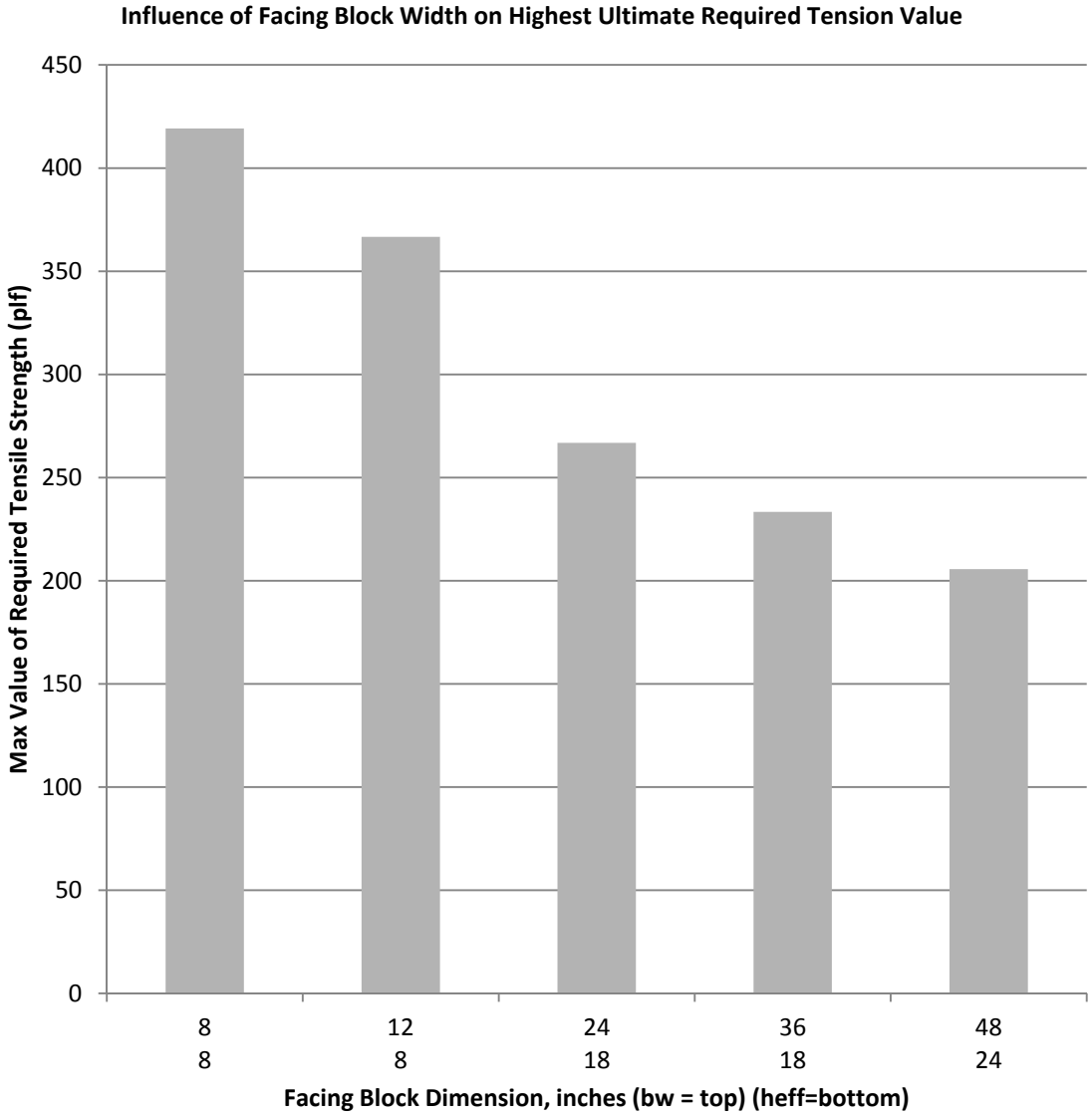

Figure 141: Influence of Facing Block Dimensions on the Highest Predicted Ultimate Required Tension for the Roadway Loading Condition

Figure 141 shows that for Method 3, the increase in block size causes a decrease in the predicted required ultimate tensile strength, T_{req}, for the entire soil profile. It should be noted that block width has a greater influence on this decrease than block height.

Impact of Upper Wall Height Variation: The following section explores the influence of varying the upper wall height over the range detailed in Table 5 for the bridge loading case. This parameter is unique to the bridge loading scenario and therefore is not applicable for the roadway loading condition. Only the influence on bridge loading conditions will be explored in this section.

Bridge Loading: Method 3, the K-Stiffness Method, was not adapted for the bridge loading case for the parametric study. The upper wall height was varied from 1 foot to 5

feet in 6 inch intervals. The base case was 3 feet. The relationships presented in Figure 148 and Figure 149 only show the variation of the highest values of T_{max} and T_{req}. Figure 142, Figure 143, Figure 145, Figure 146, and Figure 147 show the variation in tension for the entire soil profile with change in upper wall height for each of the methods compared.

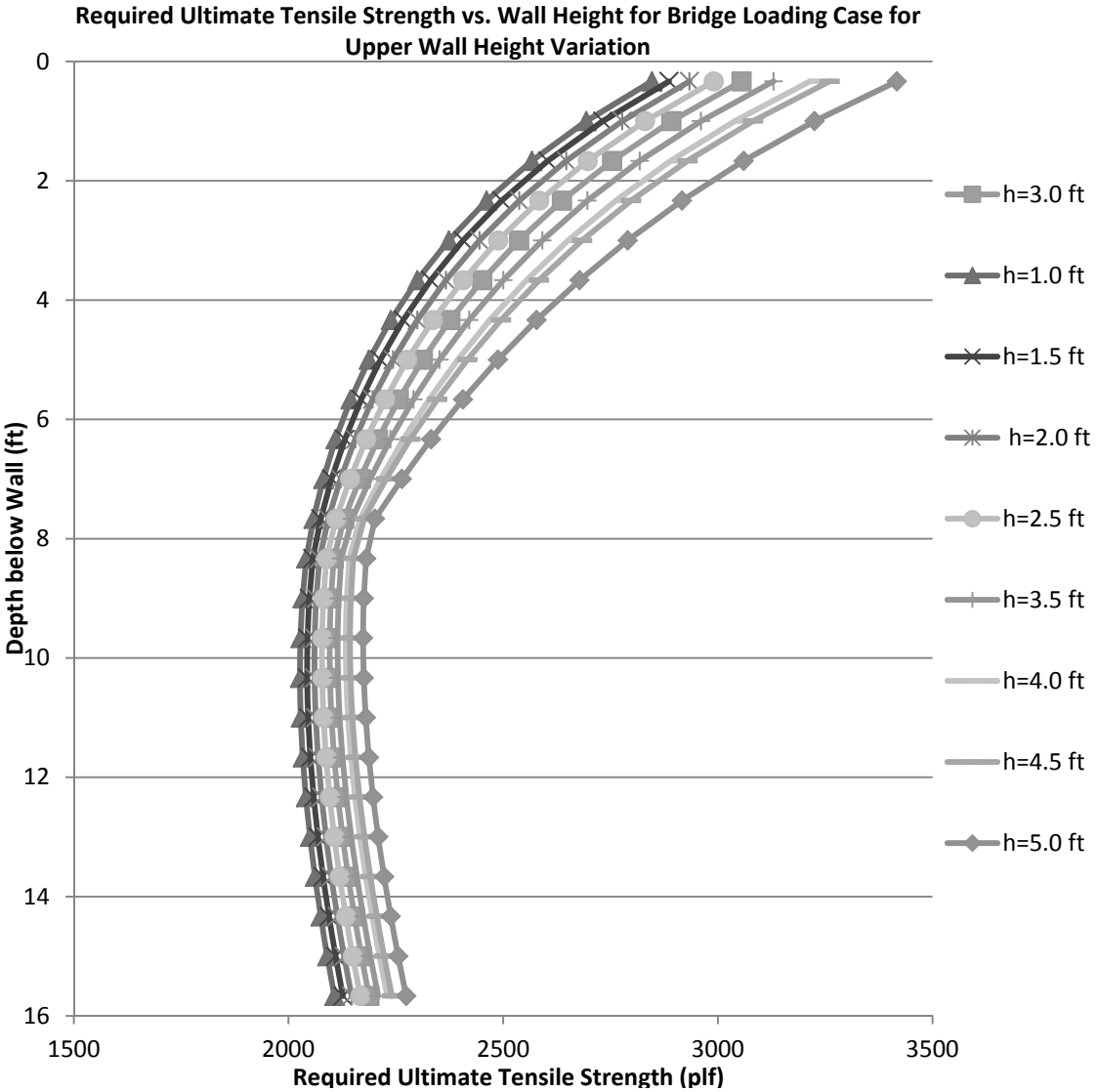

Figure 142: Influence of Upper Wall Height on Ultimate Required Tension for Bridge Loading for Method 1: The Simplified Procedure

For Method 1, the increase in upper wall height leads to an increase in predicted required ultimate tensile strength, T_{req}, for the entire soil profile as shown in Figure 142. All distributions have a curved shape that increases in degree with increase in upper wall height. The T_{req} value both at the top and the bottom increase with increasing upper wall height. The increase at the bottom is less than at the top of the wall.

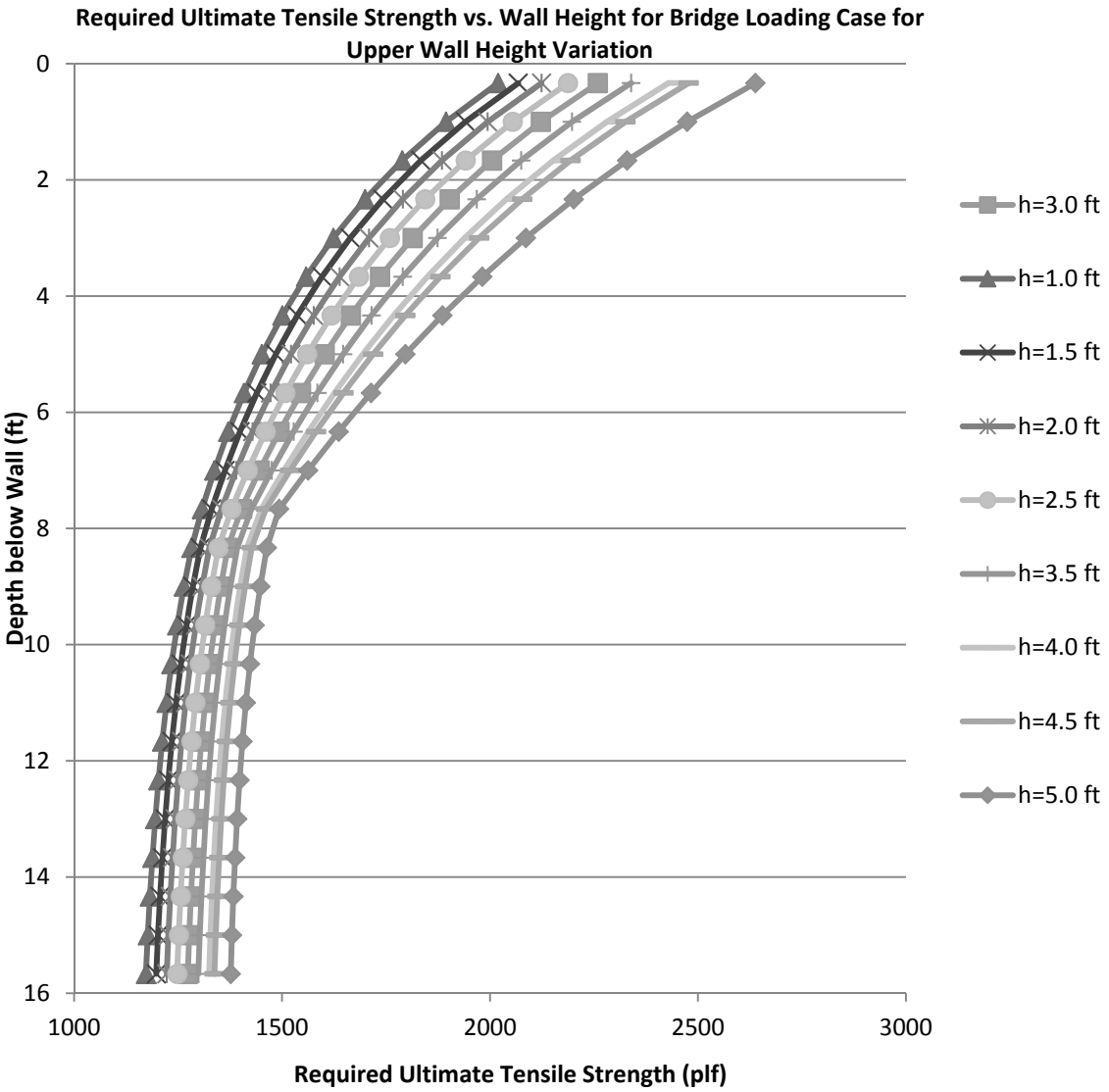

Figure 143: Influence of Upper Wall Height on Ultimate Required Tension for Bridge Loading for Method 2: The Simplified Procedure with K_r/K_a Adjusted

For Method 2, the increase in upper wall height leads to an increase in predicted required ultimate tensile strength, T_{req}, for the entire soil profile as shown in Figure 143. All distributions have a curved shape that increases in degree with increase in upper wall height. The T_{req} value both at the top and the bottom increase with increasing upper wall height. The increase at the bottom is less than at the top of the wall.

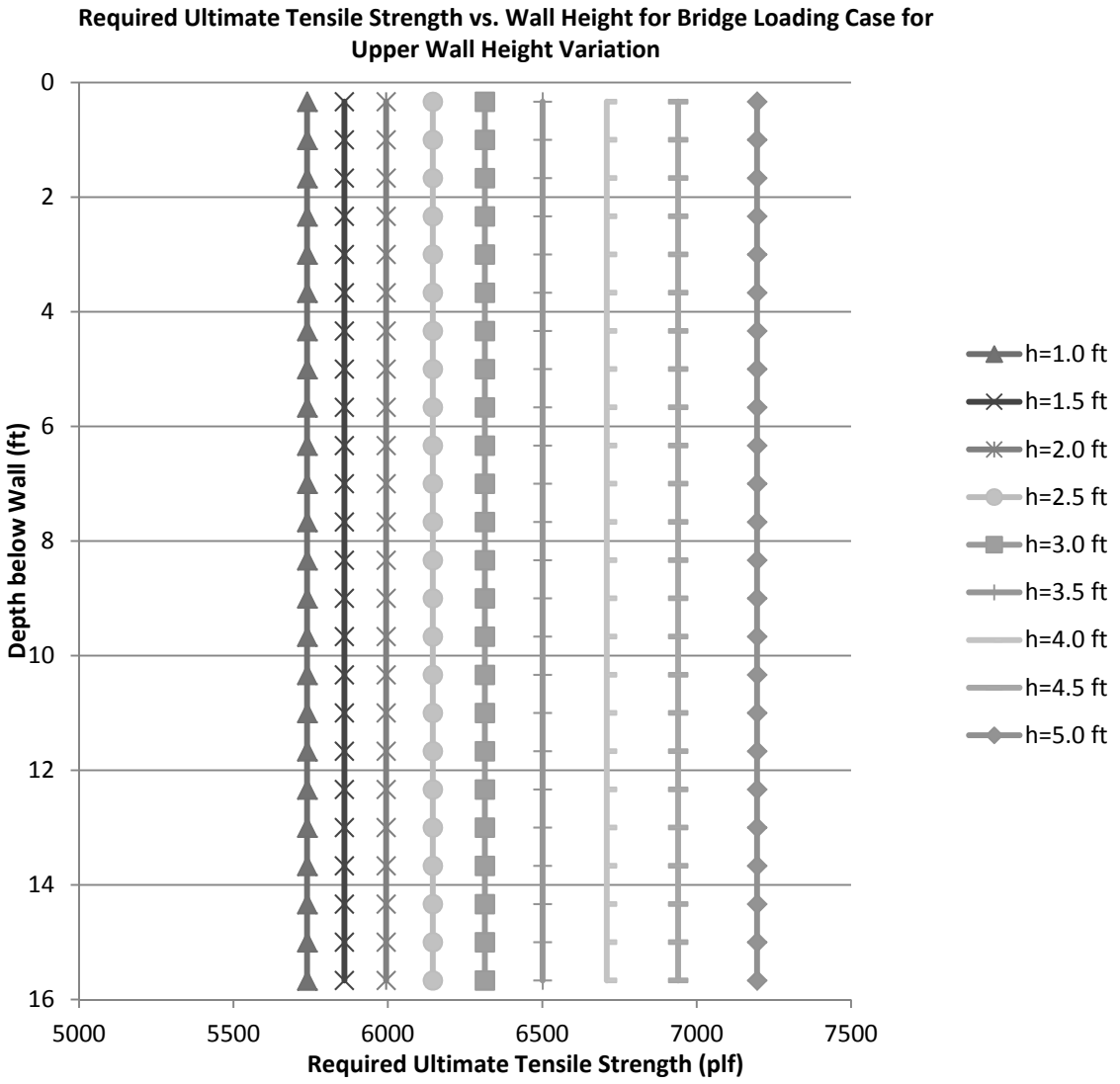

Figure 144: Influence of Upper Wall Height on Ultimate Required Tension for Bridge Loading for Method 4: NCHRP GRS Method

Figure 144 shows that for Method 4, the entire profile is assigned a required ultimate tensile strength, T_{req}, value equal to the highest value that occurs in the wall. Therefore, the distributions plot as vertical lines. With increasing upper wall height, the maximum T_{req} value in the profile increases. To look more closely at the variation of tension at each reinforcement layer, the variation in nominal maximum tensile load, T_{max}, with depth was plotted for each variation in upper wall height. These relationships are plotted in Figure 145.

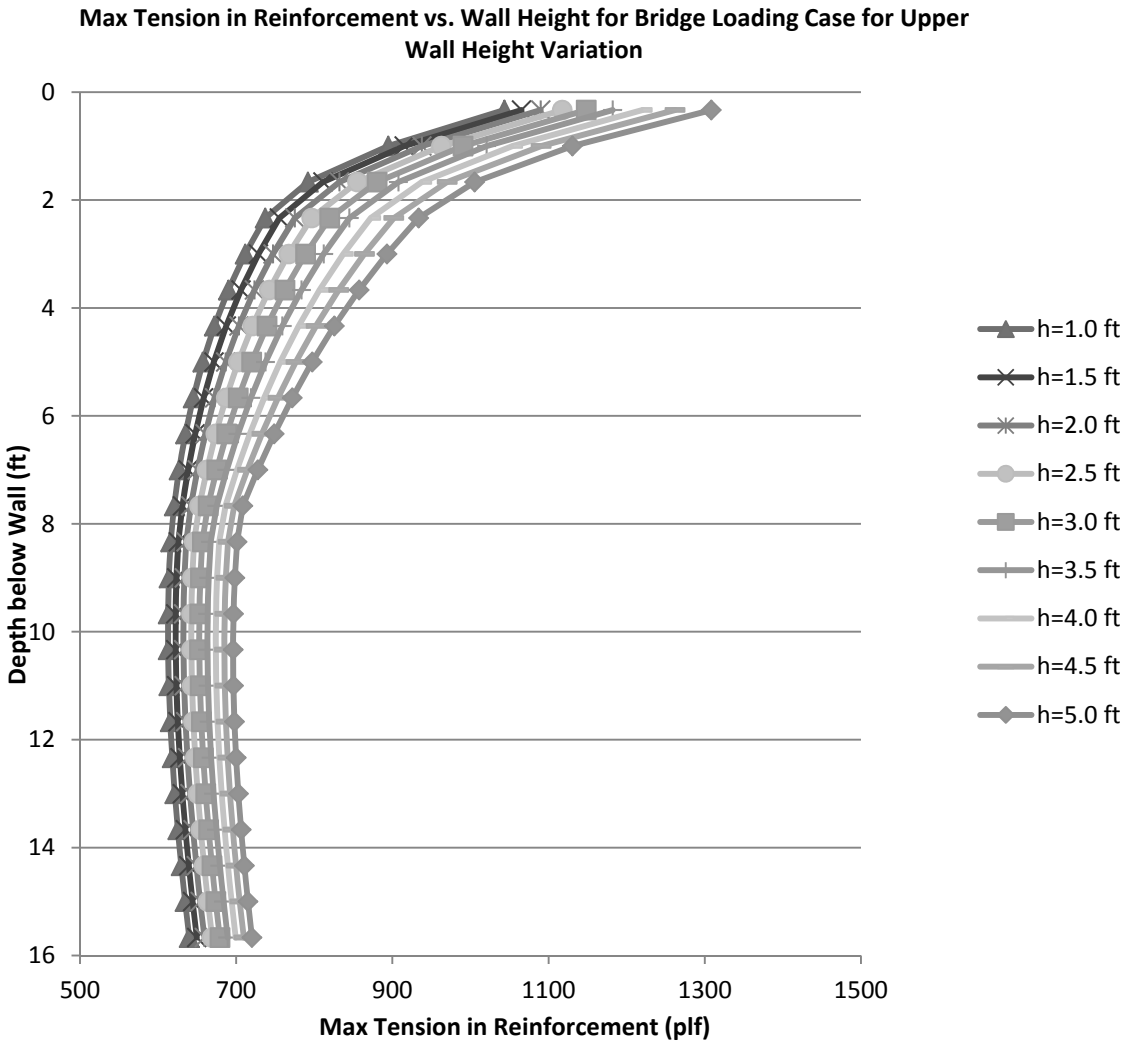

Figure 145: Influence of Upper Wall Height on Max Tensile Load in the Reinforcement for Bridge Loading for Method 4: NCHRP GRS Method

Figure 145 shows that for Method 4, increasing upper wall height will increase the nominal maximum tensile load, T_{max}, at all depths below the top of the reinforced zone. The shape of each distribution is curved.

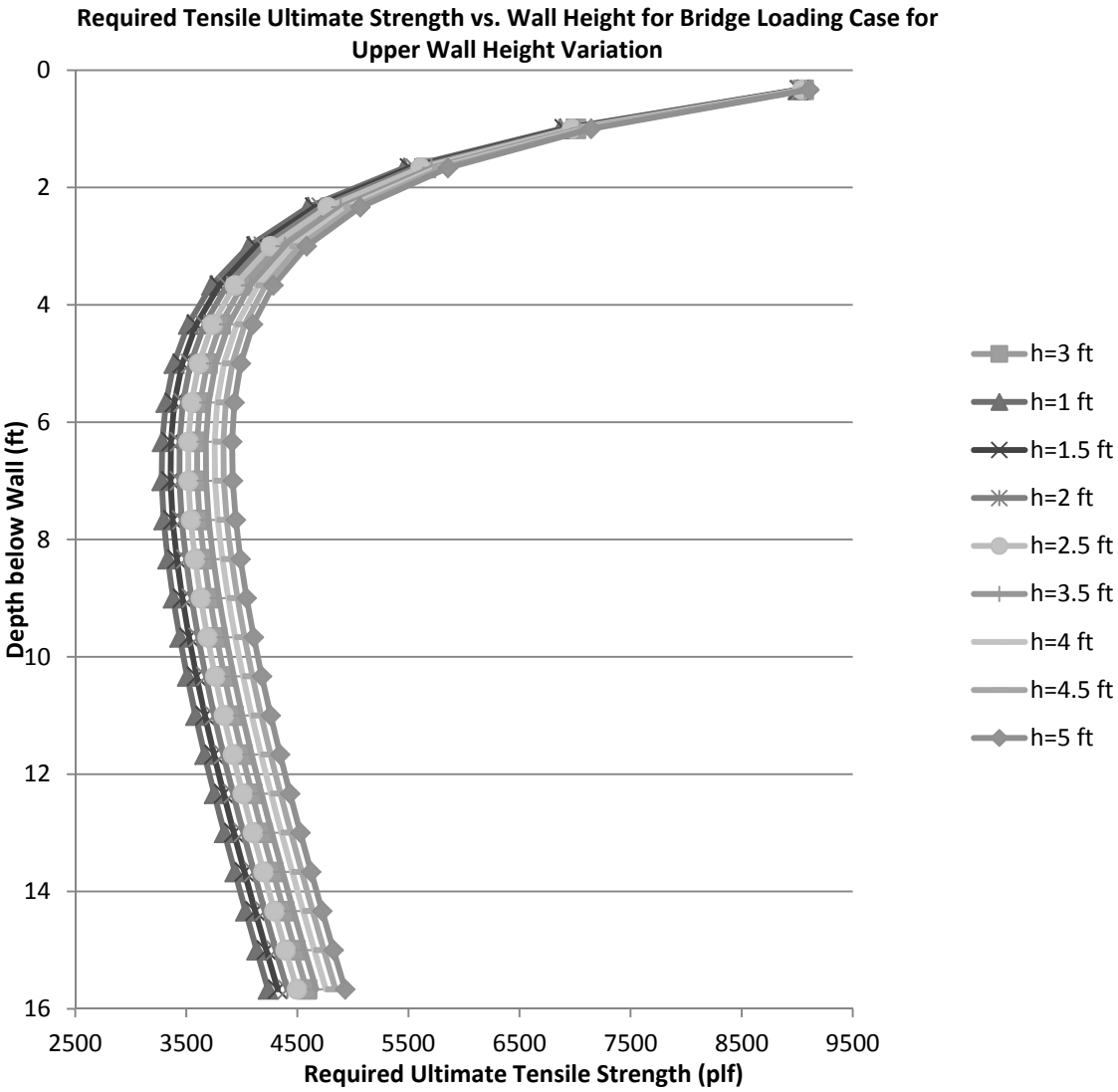

Figure 146: Influence of Upper Wall Height on Ultimate Required Tension for Bridge Loading for Method 5: FHWA GRS-IBS Method Analytic Solution

For Method 5's analytic solution, as upper wall height increases the predicted required ultimate tensile strength, T_{req}, increases for the entire soil profile as shown in Figure 146. All distributions have a curved shape. The increase in T_{req} at the top is lower than at the bottom of the wall.

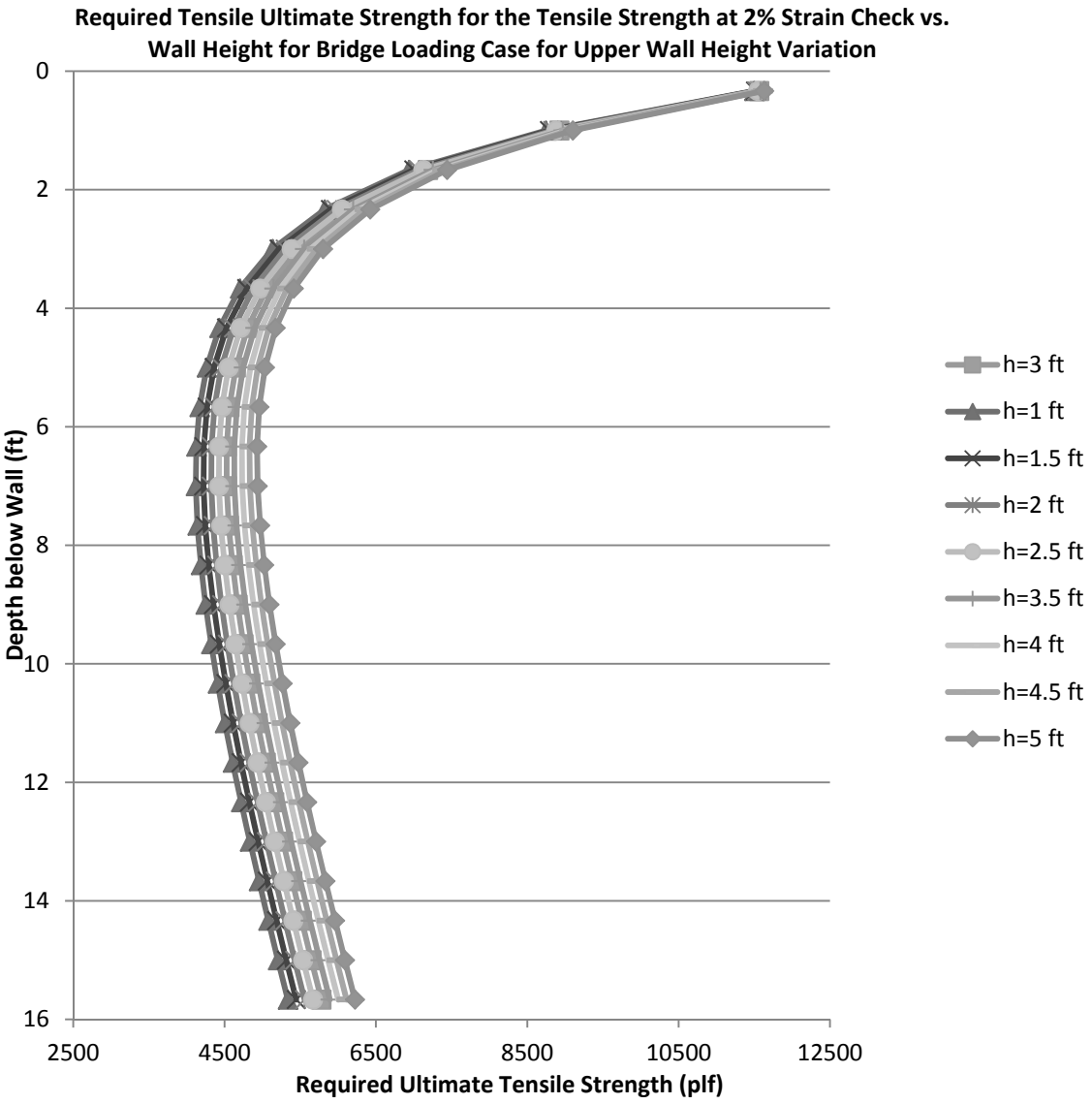

Figure 147: Influence of Upper Wall Height on Ultimate Required Tension for Bridge Loading for Method 5: FHWA GRS-IBS Method Tensile Strength at 2% Strain Check

Figure 147 shows that for Method 5's tensile strength at 2% strain equivalent T_{req} calculation, the increase in upper wall height will increase the predicted required ultimate tensile strength, $T_{req.}$ The predicted values of T_{req} are higher than that predicted by the analytic solution but the distributions have very similar shapes.

There is a third check required by Method 5 guidance that requires the ultimate tensile strength to be greater than or equal to 4,800 lb/ft. This requirement is not plotted but would plot as a straight line at the value of 4,800 lb/ft. Which of the three requirements that controls can vary within the soil profile.

The highest values of T_{max} and T_{req} are shown in Figure 148 and Figure 149, respectively for applicable methods.

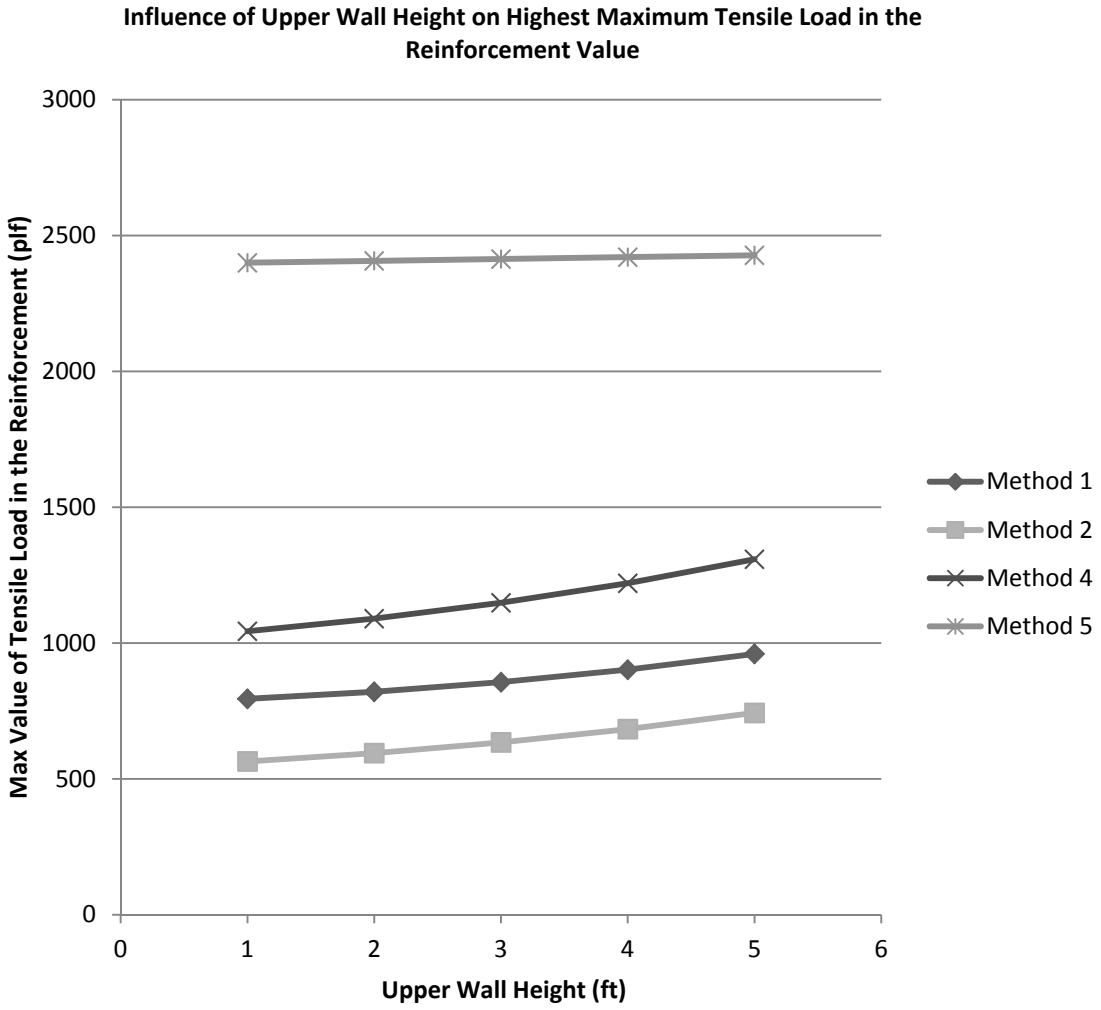

Figure 148: Influence of Upper Wall Height on Max Load in the Reinforcement for the Bridge Loading Condition

Figure 148 shows that the highest value of maximum load in the reinforcement, T_{max}, increases with increasing upper wall height. Values predicted by Method 1 and 1 have roughly the same shape and thus are most likely similarly influenced by upper wall height. Method 4 is influenced slightly more by upper wall height. Method 5 appears to be the least influenced by upper wall height as it has the lowest slope, nearly flat. Method 5 predicts the highest values of T_{max} in comparison to all other methods.

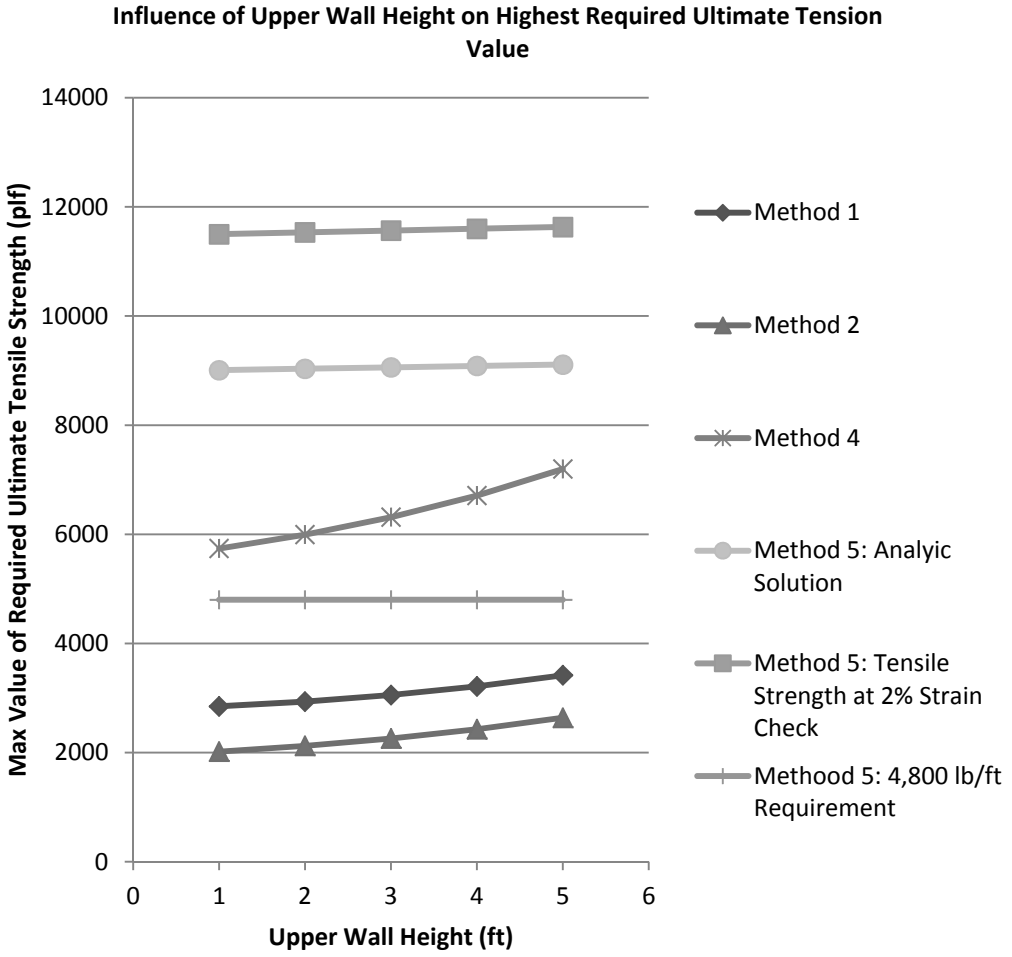

Figure 149: Influence of Upper Wall Height on the Highest Predicted Ultimate Required Tension for the Bridge Loading Condition

Figure 149 shows that the highest predicted ultimate required tensile strength, T_{req}, also increases with increasing upper wall height. The degree of influence upper wall height has varies from method to method but can be correlated to the slope of the lines. Upper wall height has a similar level of influence on Method 1 and 2. Method 4 is influenced more by upper wall height.

Method 5 has three requirements to establish T_{req} values for design. The first is an analytic solution, the second is a check of tensile strength at 2% strain, and the last is a requirement that T_{req} be at least equal to or above 4,800 lb/ft. The value chosen for design is the highest of the three ultimate strength values. All three of these predicted values are plotted in Figure 149. The first and second requirements are similarly influenced by upper wall height but the tensile strength at 2% strain check predicts a higher value. The last requirement plots as a straight horizontal line at 4,800 lb/ft.

Impact of Sill Width Variation: The following section explores the influence of varying the sill width over the range detailed in Table 5 for the bridge loading case. This

parameter is unique to the bridge loading scenario and therefore is not applicable for the roadway loading condition. Only the influence on bridge loading conditions will be explored in this section.

Bridge Loading: Not all methods predict T_{max} and T_{req} values for the bridge loading condition. Method 3, the K-Stiffness Method, was not adapted for the bridge loading case for the parametric study. Sill width was varied from 2 feet to 7 feet at 6 inch intervals. The base case sill width was 3 feet. The loading across the sill was held constant. Therefore, for wider sills, the unit load per foot was less. Figure 150, Figure 151, Figure 152, Figure 153, Figure 154, and Figure 155 show the variation in tension for the entire soil profile with change in sill width for each of the methods compared.

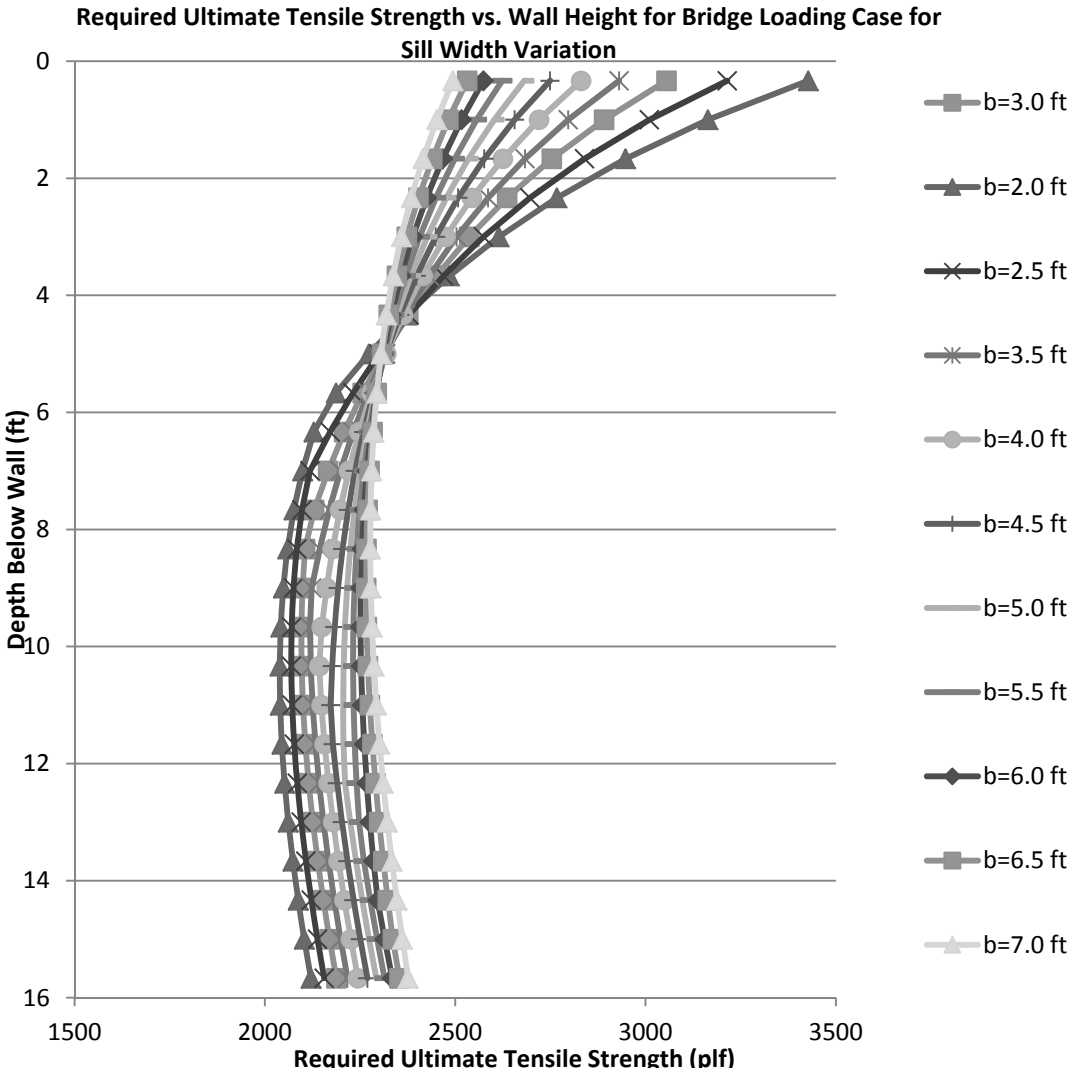

Figure 150: Influence of Sill Width on Ultimate Required Tension for Bridge Loading for Method 1: The Simplified Procedure

For Method 1, the influence of sill width on predicted required ultimate tensile strength is complicated, as shown in Figure 150. As sill width increases the T_{req} value decreases at

the top and increases at the bottom. The loading across the sill was held constant. Therefore, for wider sills, the unit load per foot was less. This led to a reduction in change in vertical stress and change in horizontal stress with increasing sill width. However this only influenced the upper portion of the wall. Due to the fact that the eccentricity of the system decreased with increasing sill width, the depth to which bridge loads penetrated increased. This resulted in increases of T_{req} at lower depths. This also resulted in a reduction in degree of curvature of the T_{req} distribution with increasing sill width.

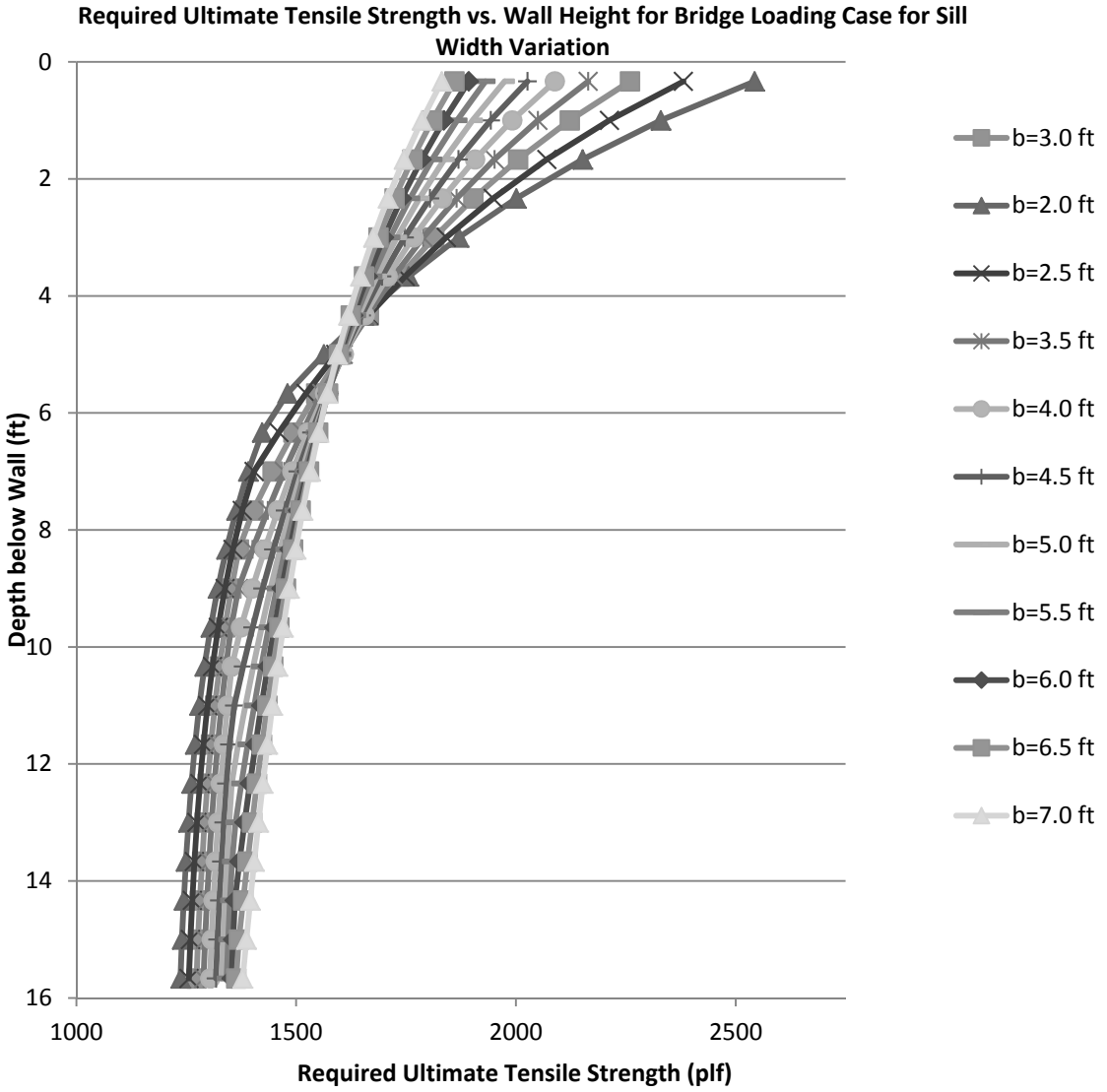

Figure 151: Influence of Sill Width on Ultimate Required Tension for Bridge Loading for Method 2: The Simplified Procedure with K_r/K_a Adjusted

For Method 2, the influence of sill width on predicted required ultimate tensile strength is complicated similar to Method 1, as shown in Figure 151. As sill width increases the T_{req} value decreases at the top and increases at the bottom. The loading across the sill was

held constant. Therefore, for wider sills, the unit load per foot was less. This led to a reduction in change in vertical stress and change in horizontal stress with increasing sill width. However this only influenced the upper portion of the wall. Due to the fact that the eccentricity of the system decreased with increasing sill width, the depth to which bridge loads penetrated increased. This resulted in increases of T_{req} at lower depths. This also resulted in a reduction in degree of curvature of the T_{req} distribution with increasing sill width. This behavior is nearly identical to that predicted by Method 1.

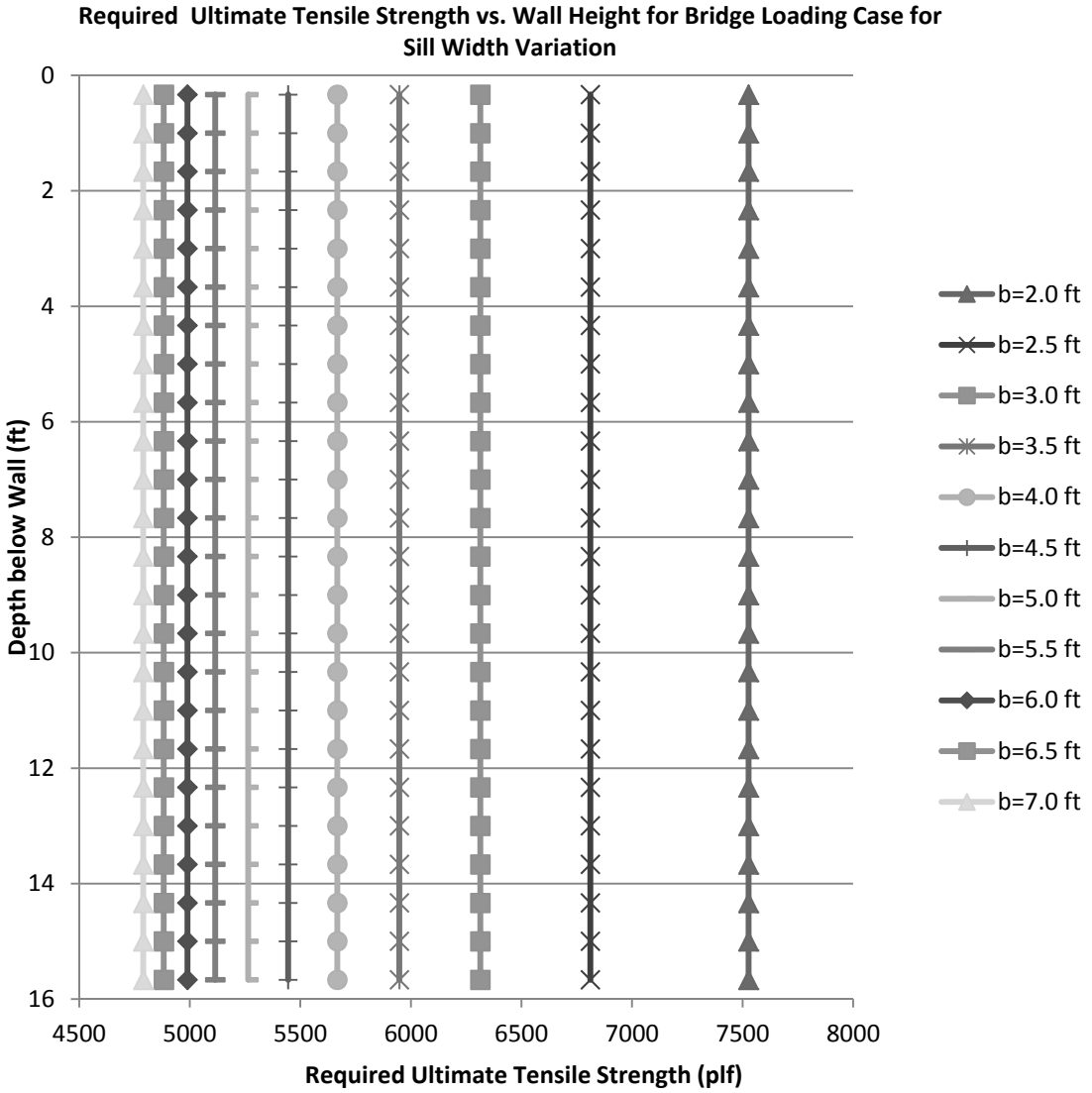

Figure 152: Influence of Sill Width on Ultimate Required Tension for Bridge Loading for Method 4: NCHRP GRS Method

Figure 152 shows that for Method 4, the entire profile is assigned a required ultimate tensile strength, T_{req}, value equal to the highest value that occurs in the wall. Therefore, the distributions plot as vertical lines. With increasing sill width, the maximum T_{req} value in the profile decreases. To look more closely at the variation of tension at each

reinforcement layer, the variation in nominal maximum tensile load, T_{max}, with depth was plotted for each variation in sill width. These relationships are plotted in Figure 153.

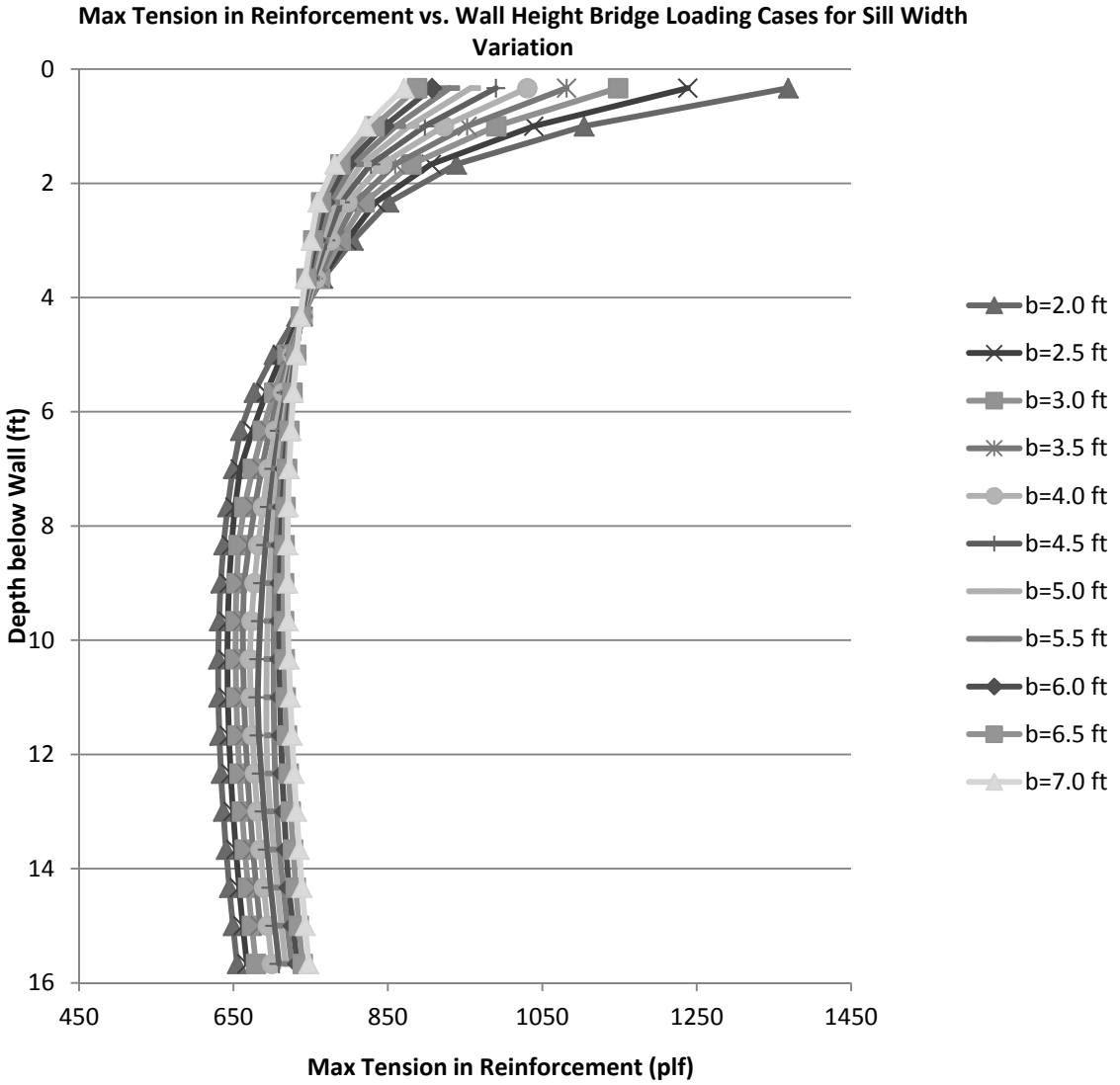

Figure 153: Influence of Sill Width on Max Tensile Load in the Reinforcement for Bridge Loading for Method 4: NCHRP GRS Method

Figure 153 shows that for Method 4 like other methods, the influence of sill width on the nominal maximum tensile load, T_{max}, is complicated. As sill width increases the T_{max} value decreases at the top and increases at the bottom. The loading across the sill was held constant. Therefore, for wider sills, the unit load per foot was less. This led to a reduction in change in vertical stress and change in horizontal stress with increasing sill width. However this only influenced the upper portion of the wall. Due to the fact that the eccentricity of the system decreased with increasing sill width, the depth to which bridge loads penetrated increased. This resulted in increases of T_{max} at lower depths. This also

resulted in a reduction in degree of curvature of the T_{max} distribution with increasing sill width.

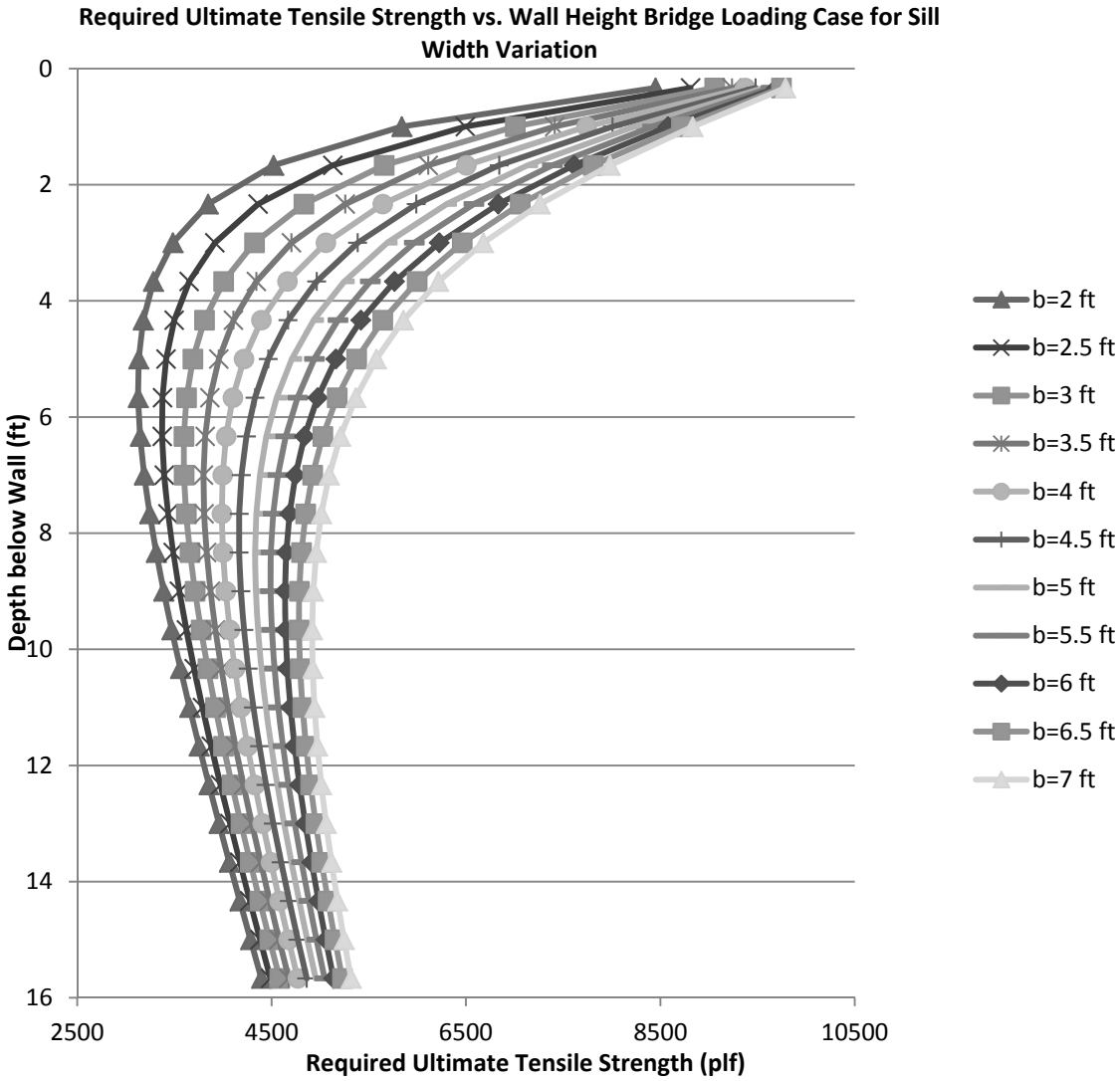

Figure 154: Influence of Sill Width on Ultimate Required Tension for Bridge Loading for Method 5: FHWA GRS-IBS Method Analytic Solution

For Method 5's analytic solution, as sill width increases the predicted required ultimate tensile strength, T_{req}, increases for the entire soil profile as shown in Figure 154. All distributions have a curved shape that is different from other methods.

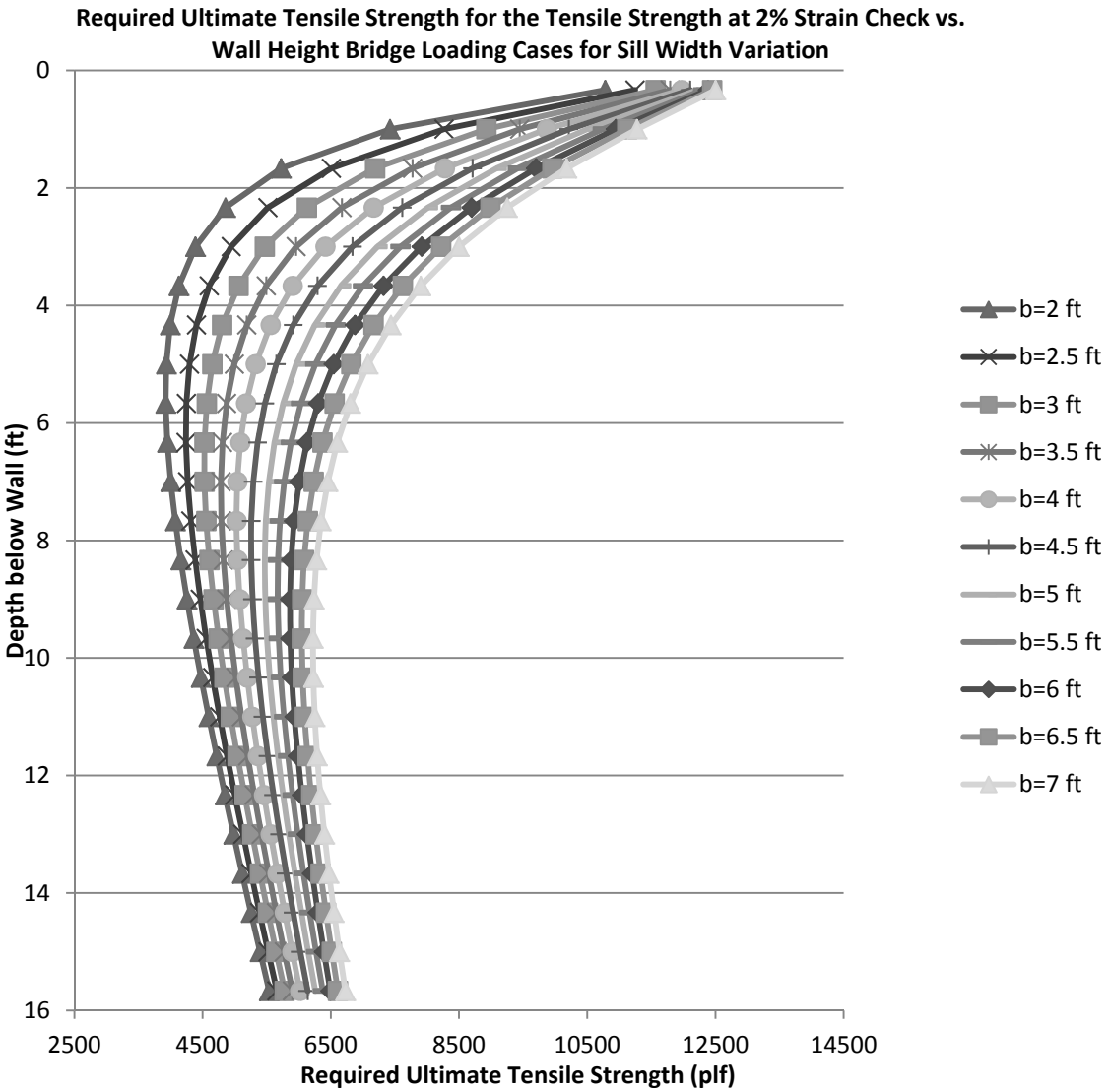

Figure 155: Influence of Sill Width on Ultimate Required Tension for Bridge Loading for Method 5: FHWA GRS-IBS Method Tensile Strength at 2% Strain Check

Figure 155 shows that for Method 5's tensile strength at 2% strain equivalent T_{req} calculation, the increase in sill width will increase the predicted required ultimate tensile strength, $T_{req.}$ The predicted values of T_{req} are higher than that predicted by the analytic solution but the distributions have very similar shapes. The distributions for Method 5 are different from those predicted by other methods. This is likely due to the fact that other parameters are influencing the distributions of Method 5 that are not utilized in other methods, such as the angles α and β used in the calculation of change in vertical pressure from bridge loading.

There is a third check required by Method 5 guidance that requires the ultimate tensile strength to be greater than or equal to 4,800 lb/ft. This requirement is not plotted but

would plot as a straight line at the value of 4,800 lb/ft. Which of the three requirements that controls can vary within the soil profile.

The variation in maximum values of T_{max} and T_{req} are shown in Figure 156 and Figure 157, respectively, for all applicable methods.

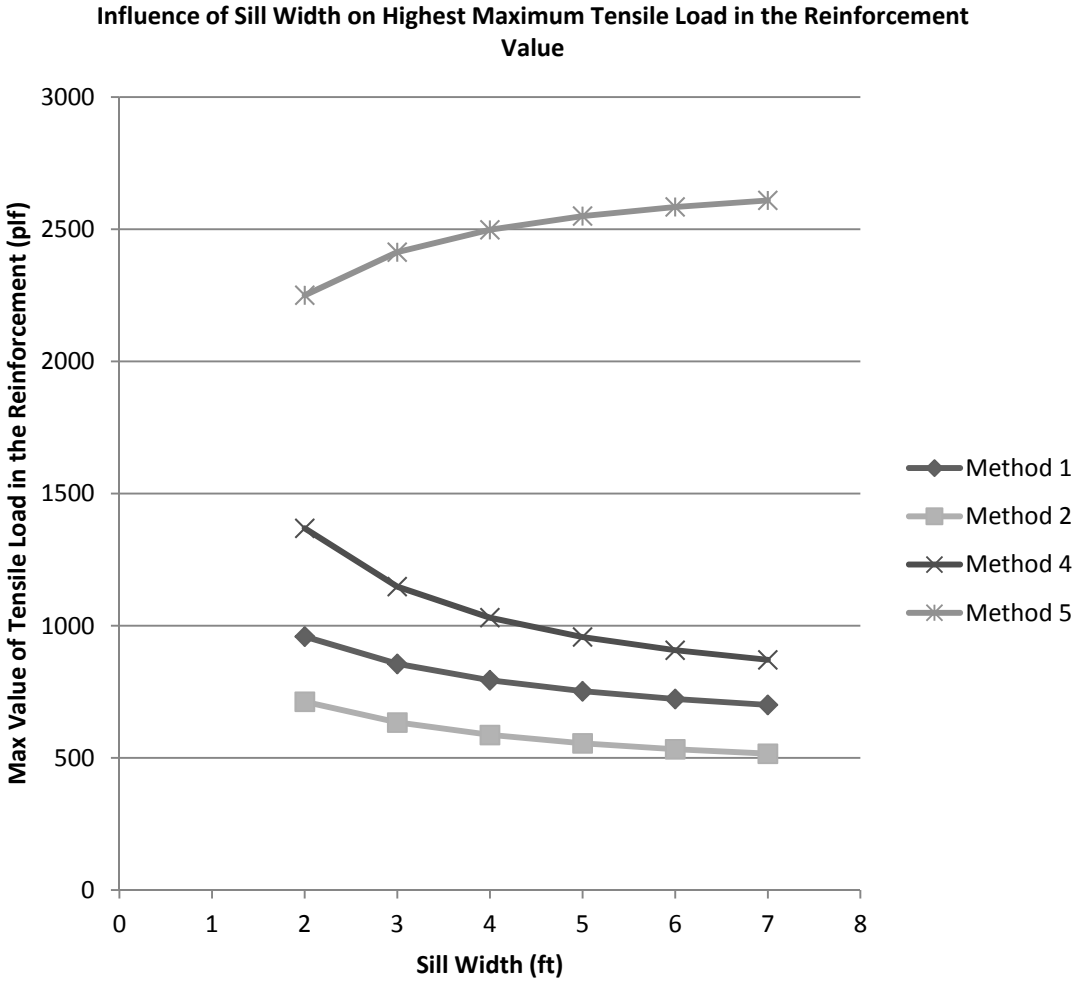

Figure 156: Influence of Sill Width on Max Load in the Reinforcement for the Bridge Loading Condition

Figure 156 shows that the highest value of maximum load in the reinforcement, T_{max}, decreases with increasing sill width for Methods 1, 2, and 4. Values predicted by these methods seem to be similarly influenced by sill width. Method 5 appears to be influence differently by sill width. It predicts a T_{max} value that increases with increasing sill width. This is likely due to the fact that other parameters are influencing the distributions of Method 5 that are not utilized in other methods, such as the angles of α and β used in calculating the change in vertical pressure distribution from bridge loading. Additionally, Method 5 predicts the highest values of T_{max} in comparison to all other methods.

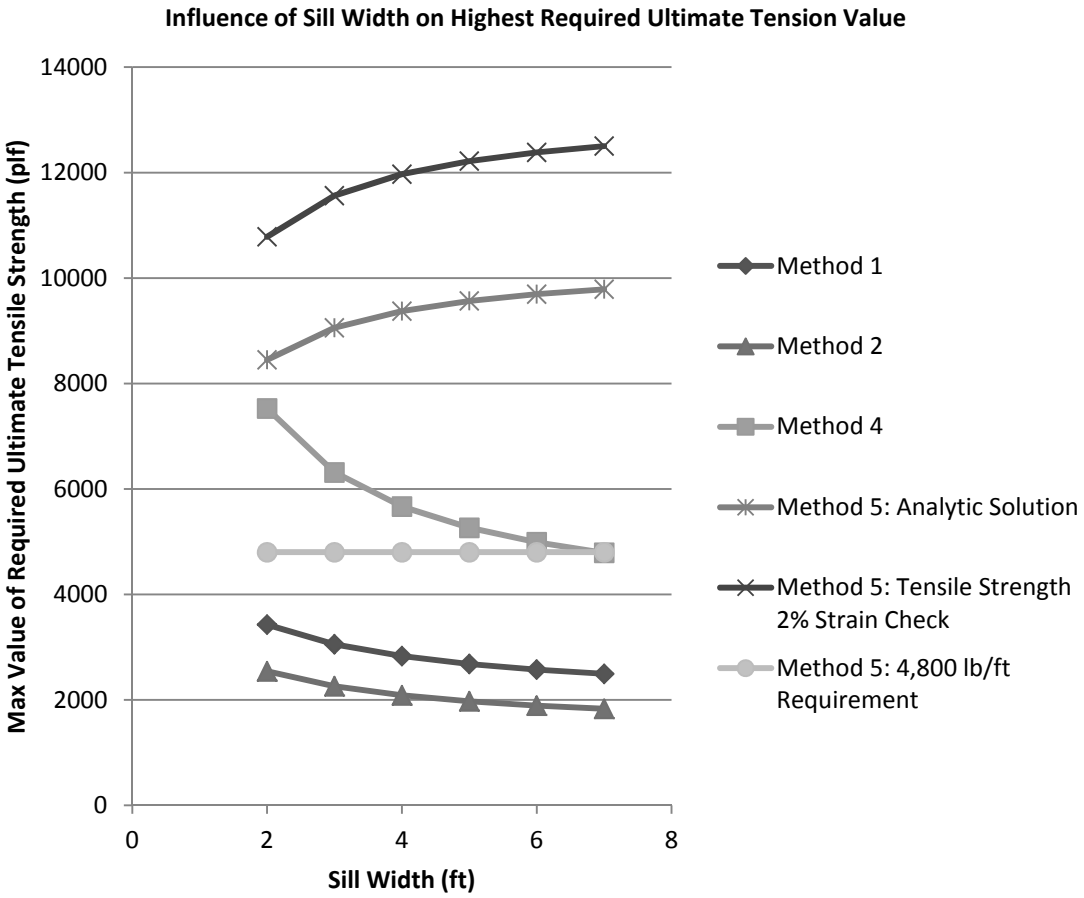

Figure 157: Influence of Sill Width on the Highest Predicted Ultimate Required Tension for the Bridge Loading Condition

Figure 157 shows that the highest predicted ultimate required tensile strength, T_{req}, also decreases for Methods 1, 2, and 4 with increasing sill width. Methods 1 and 2 are influenced similarly by sill width. Method 4 is more sensitive to sill width.

Method 5 has three requirements to establish T_{req} values for design. The first is an analytic solution, the second is a check of tensile strength at 2% strain, and the last is a requirement that T_{req} be at least equal to or above 4,800 lb/ft. The value chosen for design is the highest of the three ultimate strength values. All three of these predicted values are plotted in Figure 157. The first and second requirements are similarly influenced by sill width but the tensile strength at 2% strain check predicts a higher value. The last requirement plots as a straight horizontal line at 4,800 lb/ft. Method 5 also predicts values that increase with increasing sill width which is different than the other methods compared. This is likely due to the fact that other parameters are influencing the distributions of Method 5 that are not utilized in other methods, such as the angle that control the distribution of vertical stress with depth from bridge loads, α and β.

Impact of Setback Distance Variation: The following section explores the influence of varying the setback distance over the range detailed in Table 5 for the bridge loading case. This parameter is unique to the bridge loading scenario and therefore is not applicable for the roadway loading condition. Only the influence on bridge loading conditions will be explored in this section.

Bridge Loading: Not all methods predict T_{max} and T_{req} values for the bridge loading condition. Method 3, the K-Stiffness Method, was not adapted for the bridge loading case for the parametric study. Setback distance was varied from 1 foot, which was the base case value, up to 2.3 feet. For Method 5, the parameter setback distance is not an input. Therefore its variation will have no influence on T_{req} values and it is not included in this section. Figure 158, Figure 159, Figure 160, and Figure 161 show the variation in tension for the entire soil profile with setback distance for each of the methods compared.

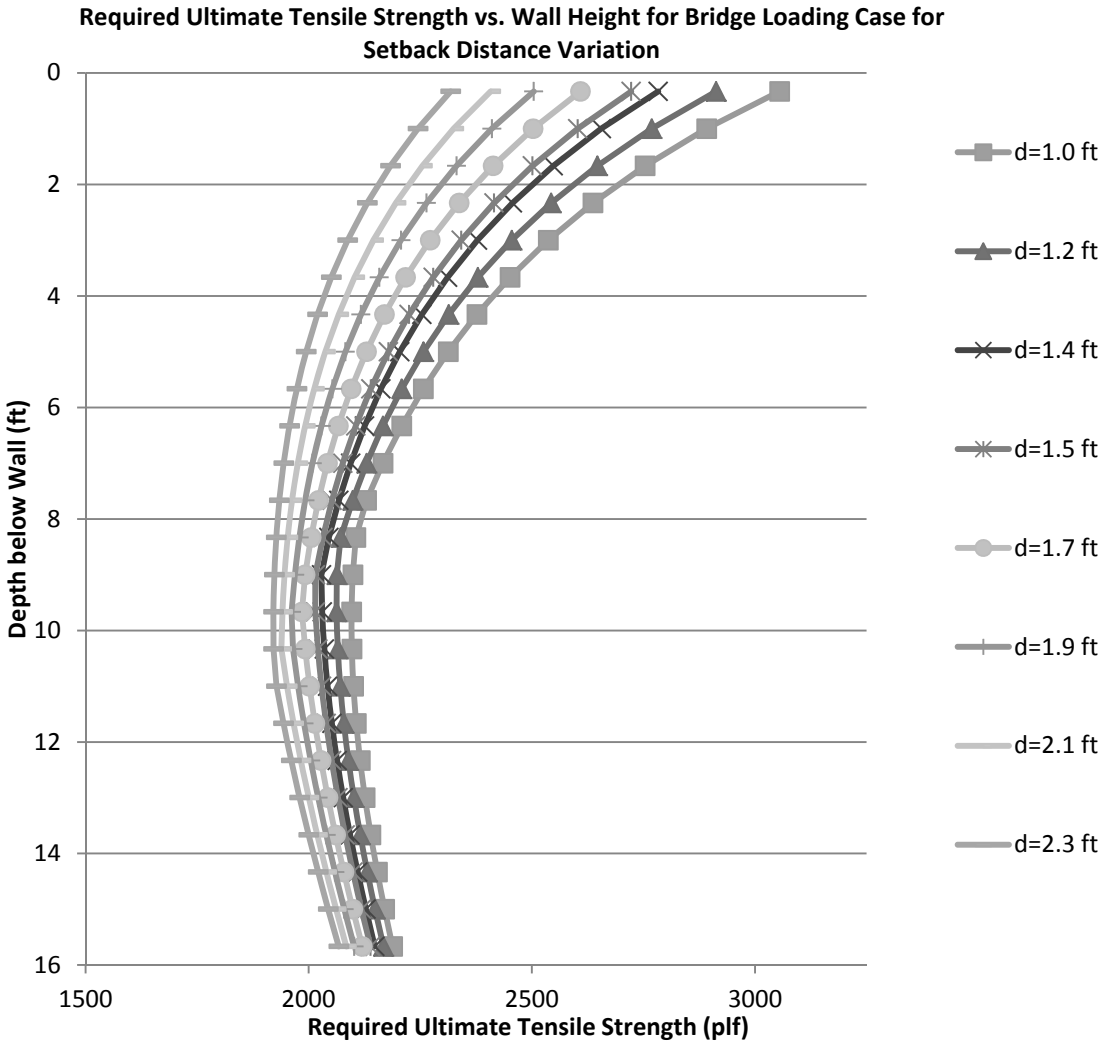

Figure 158: Influence of Setback Distance on Ultimate Required Tension for Bridge Loading for Method 1: The Simplified Procedure

For Method 1, the increase in setback distance lead to a decrease in predicted required ultimate tensile strength, T_{req}, for the entire soil profile as shown in Figure 158. All distributions have a curved shape that decrease in degree with increase in setback distance. This is likely due to the more uniform influence for bridge loads with increasing setback distance. The T_{req} value both at the top and the bottom decrease with increasing setback distance. The decrease at the bottom is less than at the top of the wall. This is likely due to the fact that the lateral and vertical earth pressures caused by bridge loading decrease with increasing setback distance for Method 1.

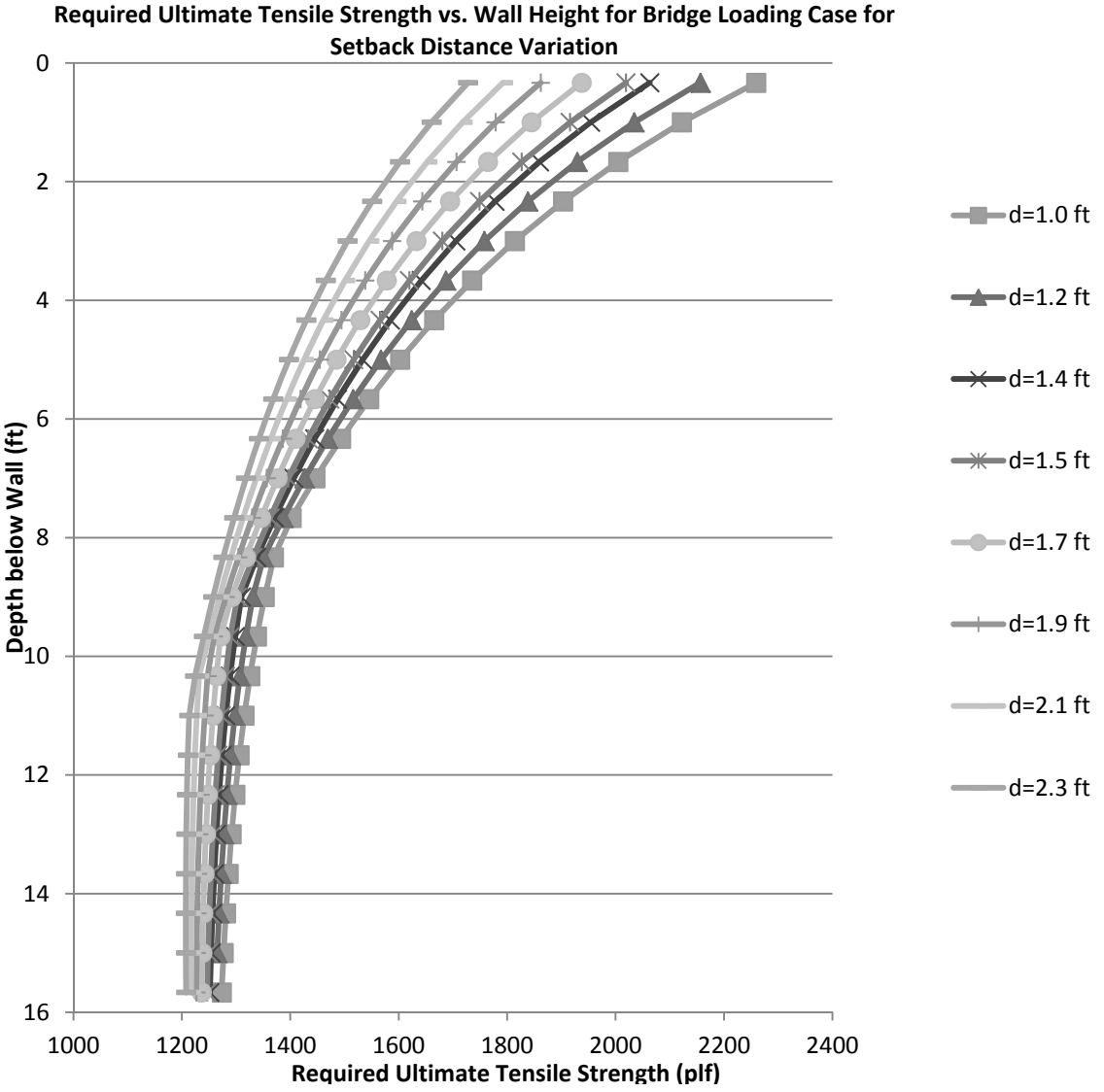

Figure 159: Influence of Setback Distance on Ultimate Required Tension for Bridge Loading for Method 2: The Simplified Procedure with K_r/K_a Adjusted

For Method 2 similar to Method 1, the increase in setback distance lead to a decrease in predicted required ultimate tensile strength, T_{req}, for the entire soil profile as shown in Figure 159. All distributions have a curved shape that decrease in degree with increase in

setback distance. This is likely due to the more uniform influence for bridge loads with increasing setback distance. The T_{req} value both at the top and the bottom decrease with increasing setback distance. The decrease at the bottom is less than at the top of the wall. This is likely due to the fact that the lateral and vertical earth pressures caused by bridge loading decrease with increasing setback distance for Method 2.

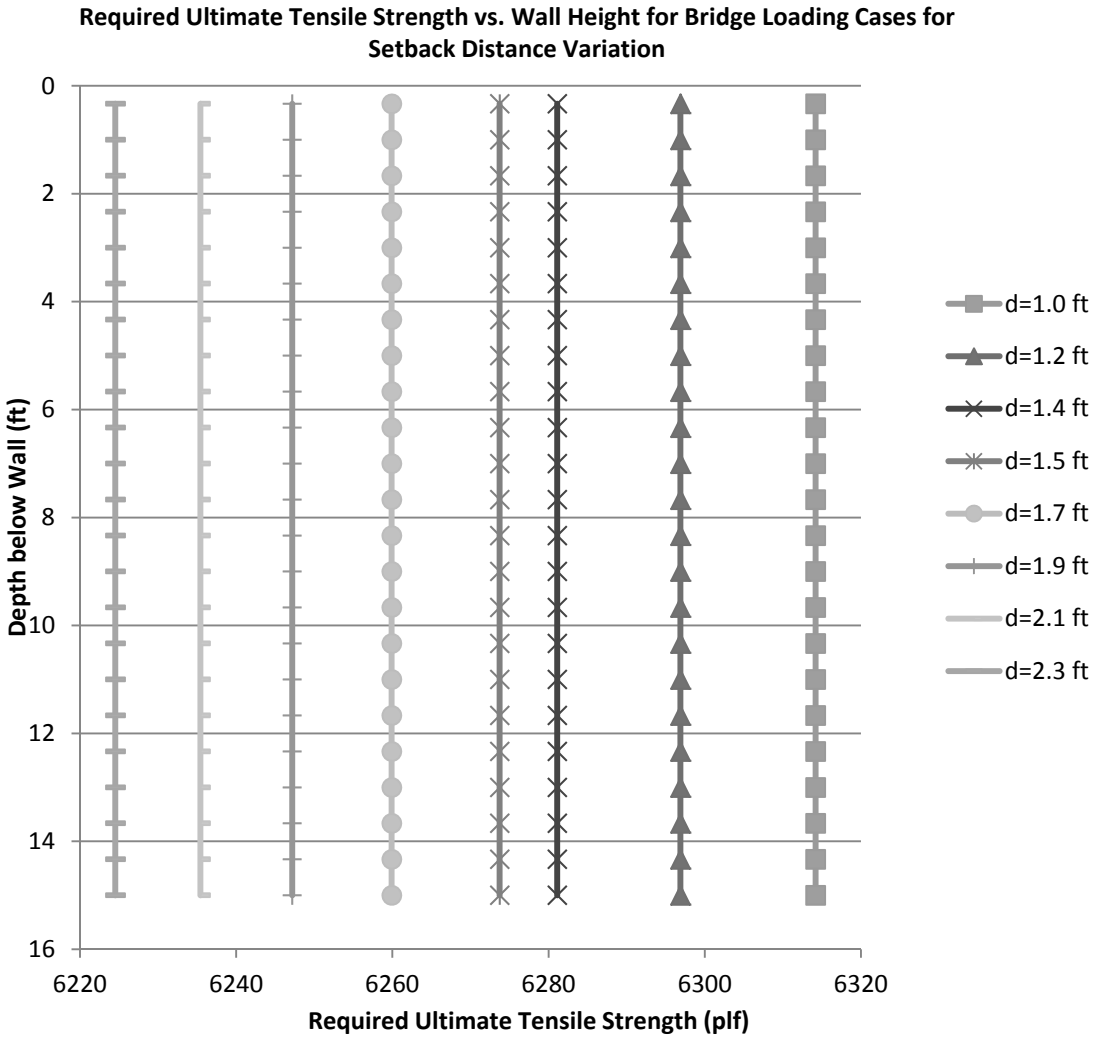

Figure 160: Influence of Setback Distance on Ultimate Required Tension for Bridge Loading for Method 4: NCHRP GRS Method

Figure 160 shows that for Method 4, the entire profile is assigned a required ultimate tensile strength, T_{req}, value equal to the highest value that occurs in the wall. Therefore, the distributions plot as vertical lines. With increasing setback distance, the maximum T_{req} value in the profile decreases. To look more closely at the variation of tension at each reinforcement layer, the variation in nominal maximum tensile load, T_{max}, with depth was plotted for each variation in setback distance. These relationships are plotted in Figure 161.

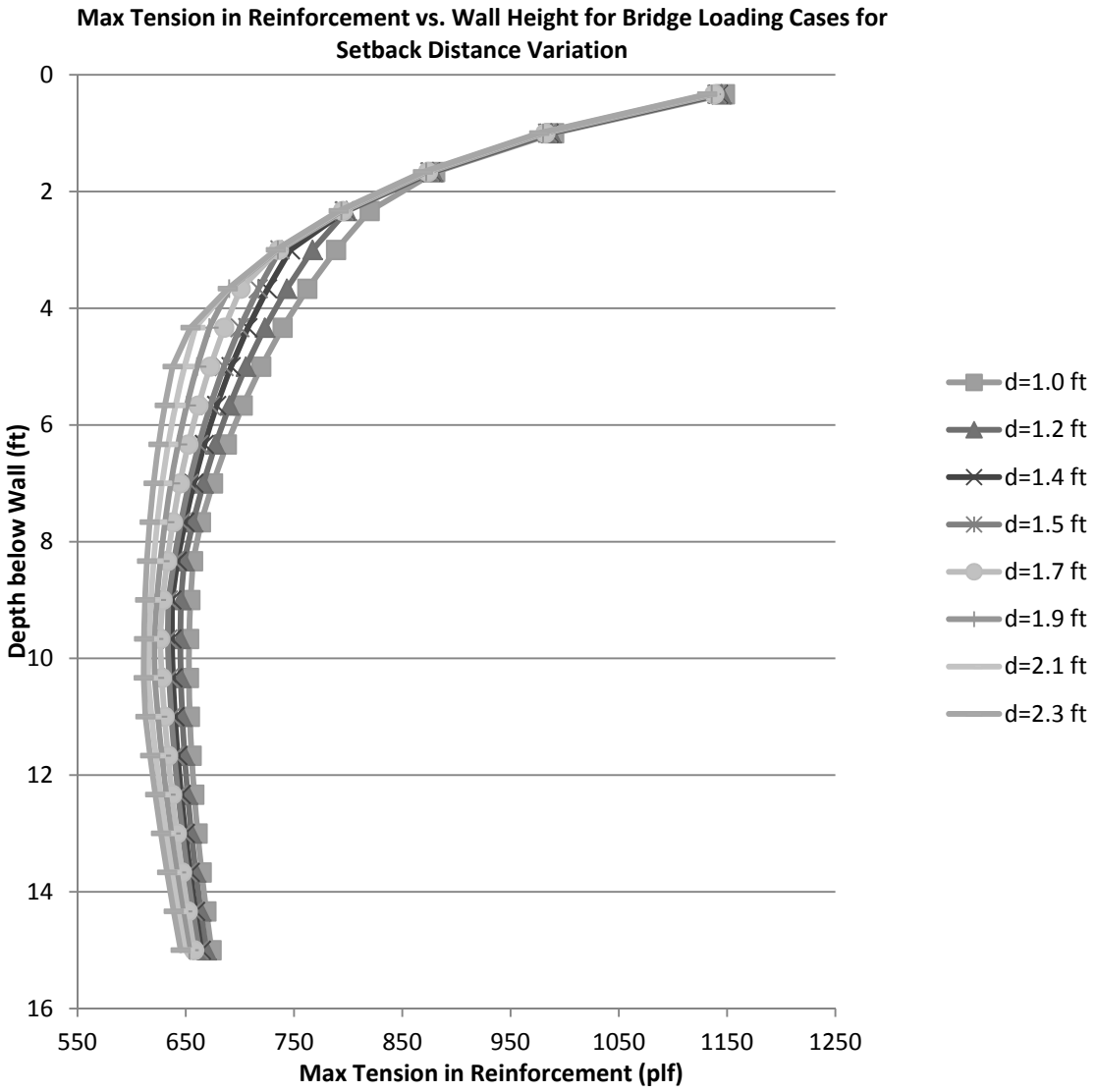

Figure 161: Influence of Setback Distance on Max Tensile Load in the Reinforcement for Bridge Loading for Method 4: NCHRP GRS Method

Figure 161 shows that for Method 4, increasing setback distance will decrease the nominal maximum tensile load, T_{max}, at all depths below the top of the reinforced zone. However, the decrease along the upper portion of the wall is much lower than the center and bottom of the wall. This is different than predicted by Methods 1 and 2. For Methods 1 and 2 the change in vertical stress decreases with increasing setback distance. Therefore, the distribution is most affected for these methods in the upper portion of the wall. For Method 4, the top portion is least affected by setback distance.

The variation in maximum T_{max} and T_{req} are shown in Figure 162 and Figure 163, respectively for all applicable methods.

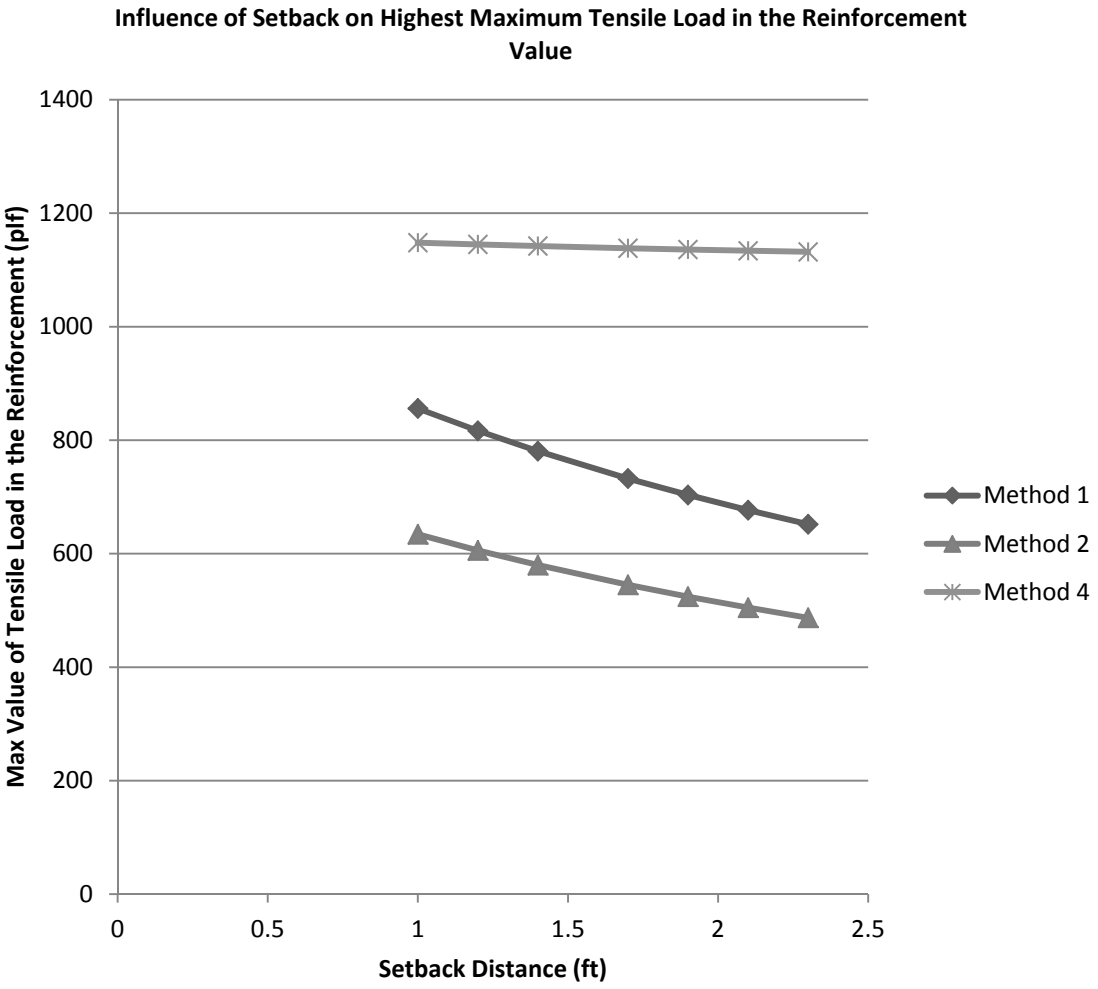

Figure 162: Influence of Setback Distance on Max Load in the Reinforcement for the Bridge Loading Condition

Figure 162 shows that the highest value of maximum load in the reinforcement, T_{max}, decreases linearly with increasing setback distance. Values predicted by Method 1 and 2 are similarly influenced by setback distance. Method 4 is less influenced by setback distance and predicts the highest value of the methods compared.

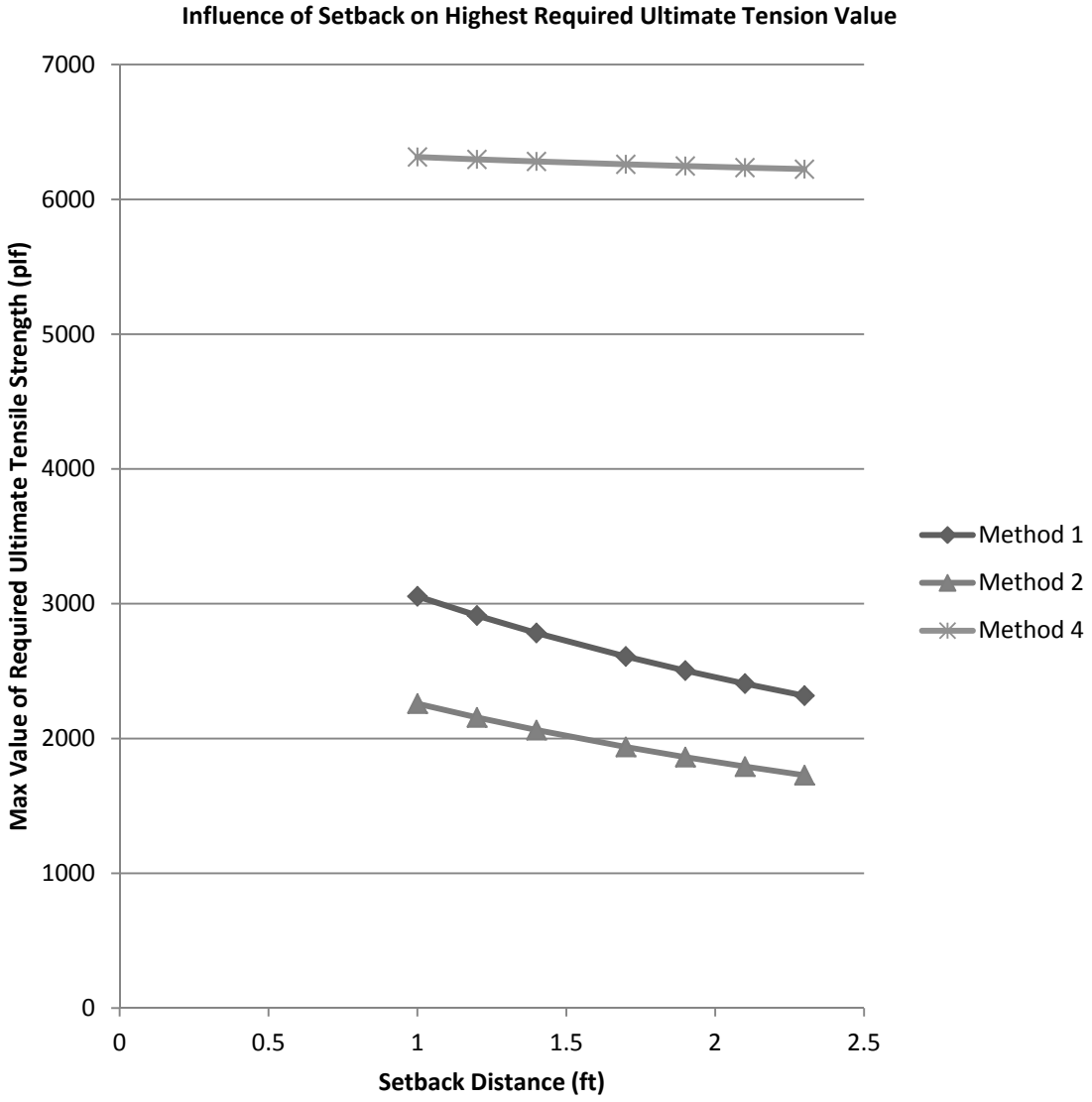

Figure 163: Influence of Setback Distance on the Highest Predicted Ultimate Required Tension for the Bridge Loading Condition

Figure 163 shows that the highest predicted ultimate required tensile strength, T_{req}, also decreases linearly with increasing setback distance. Values predicted by Method 1 and 2 are similarly influenced by sill width. Method 4 is less influenced by sill width and predicts the highest value of the methods compared.

Impact of Bridge Dead Load Variation: The following section explores the influence of varying the bridge dead load over the range detailed in Table 5 for the bridge loading case. This parameter is unique to the bridge loading scenario and therefore is not applicable for the roadway loading condition. Only the influence on bridge loading conditions will be explored in this section.

Bridge Loading: Method 3, the K-Stiffness Method, was not adapted for the bridge loading case for the parametric study. Bridge dead load was varied from 1.3 ksf to 6.5 ksf. The base case value was 3.34 ksf. The sill width was held constant at the base case value of 3.0 feet for this investigation. Figure 164, Figure 165, Figure 166, Figure 167, Figure 168, and Figure 169 show the variation in tension for the entire soil profile with change in bridge dead load for each of the methods compared.

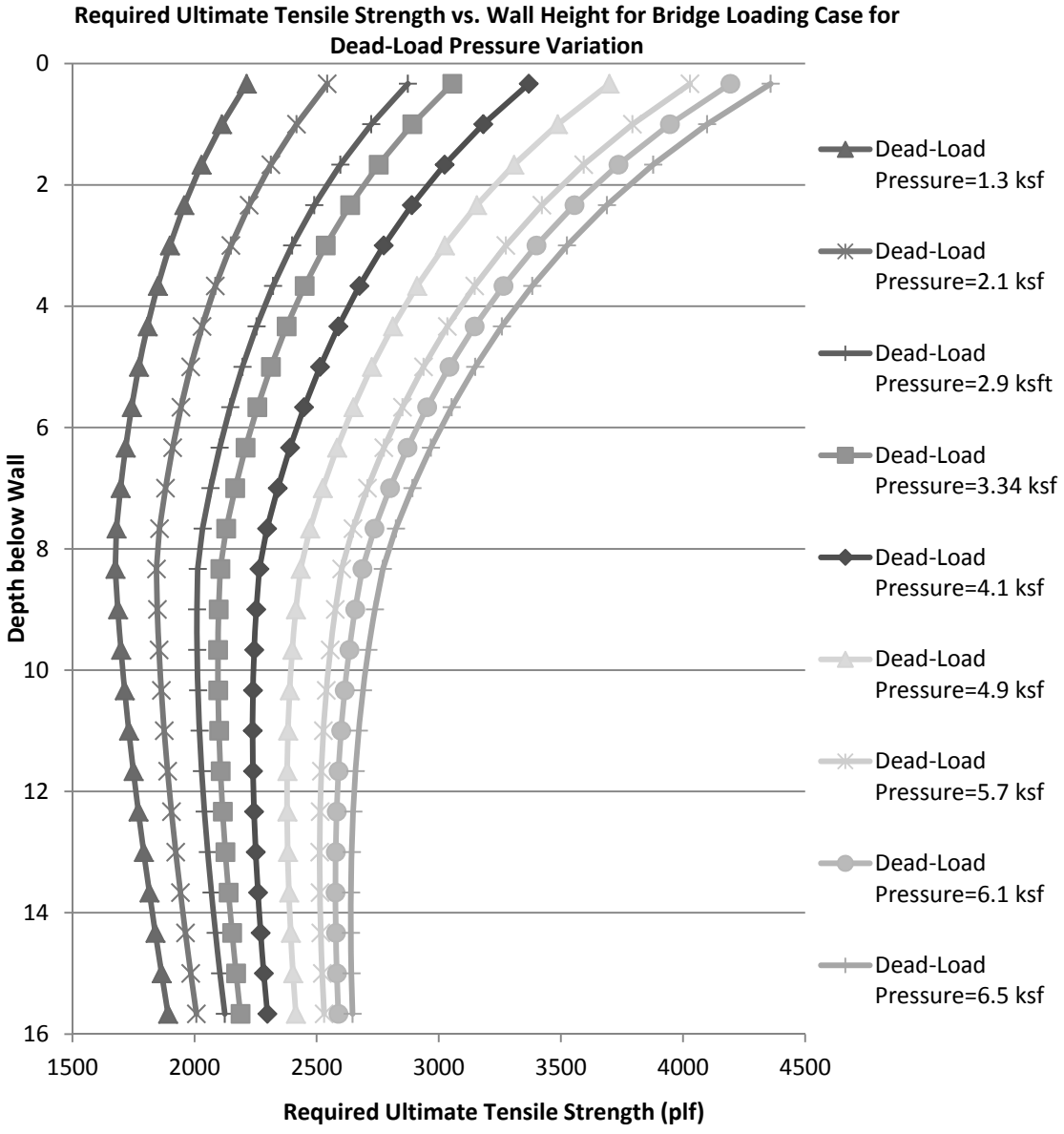

Figure 164: Influence of Dead Load on Ultimate Required Tension for Bridge Loading for Method 1: The Simplified Procedure

For Method 1, the increase in bridge dead load leads to an increase in predicted required ultimate tensile strength, T_{req}, for the entire soil profile as shown in Figure 164. All distributions have a curved shape that increases in degree with increase in bridge dead load. The T_{req} value both at the top and the bottom increase with increasing dead load.

The increase at the bottom is less than at the top of the wall. This is due to the fact that bridge load primarily influence the upper portion of the wall for this loading case.

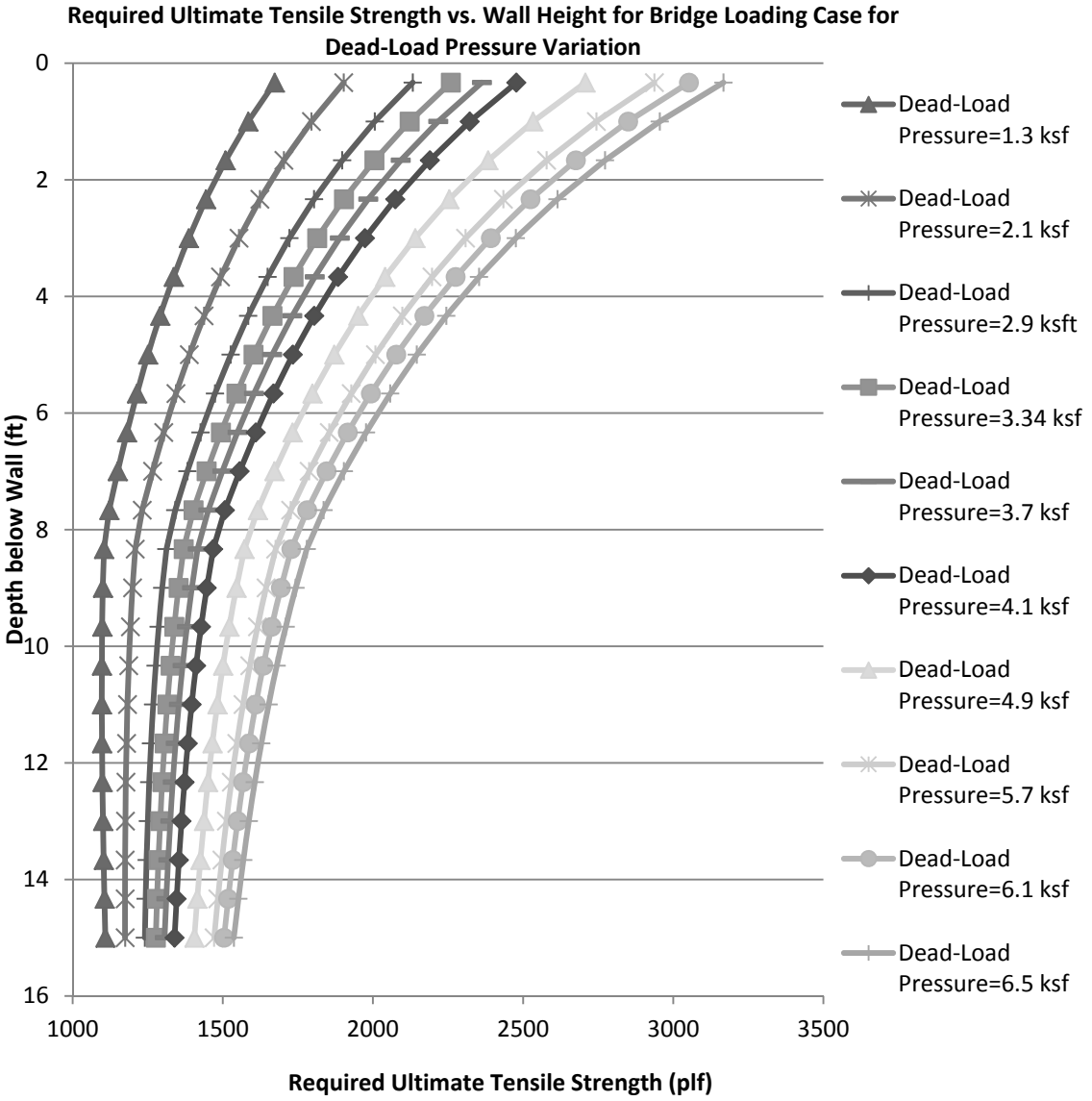

Figure 165: Influence of Dead Load on Ultimate Required Tension for Bridge Loading for Method 2: The Simplified Procedure with K_r/K_a Adjusted

For Method 2, the increase in bridge dead load leads to an increase in predicted required ultimate tensile strength, T_{req}, for the entire soil profile as shown in Figure 165. All distributions have a curved shape that increases in degree with increase in dead load. The T_{req} value both at the top and the bottom increase with increasing bridge dead load. The increase at the bottom is less than at the top of the wall. This is due to the fact that bridge load primarily influence the upper portion of the wall for this loading case similarly to Method 1.

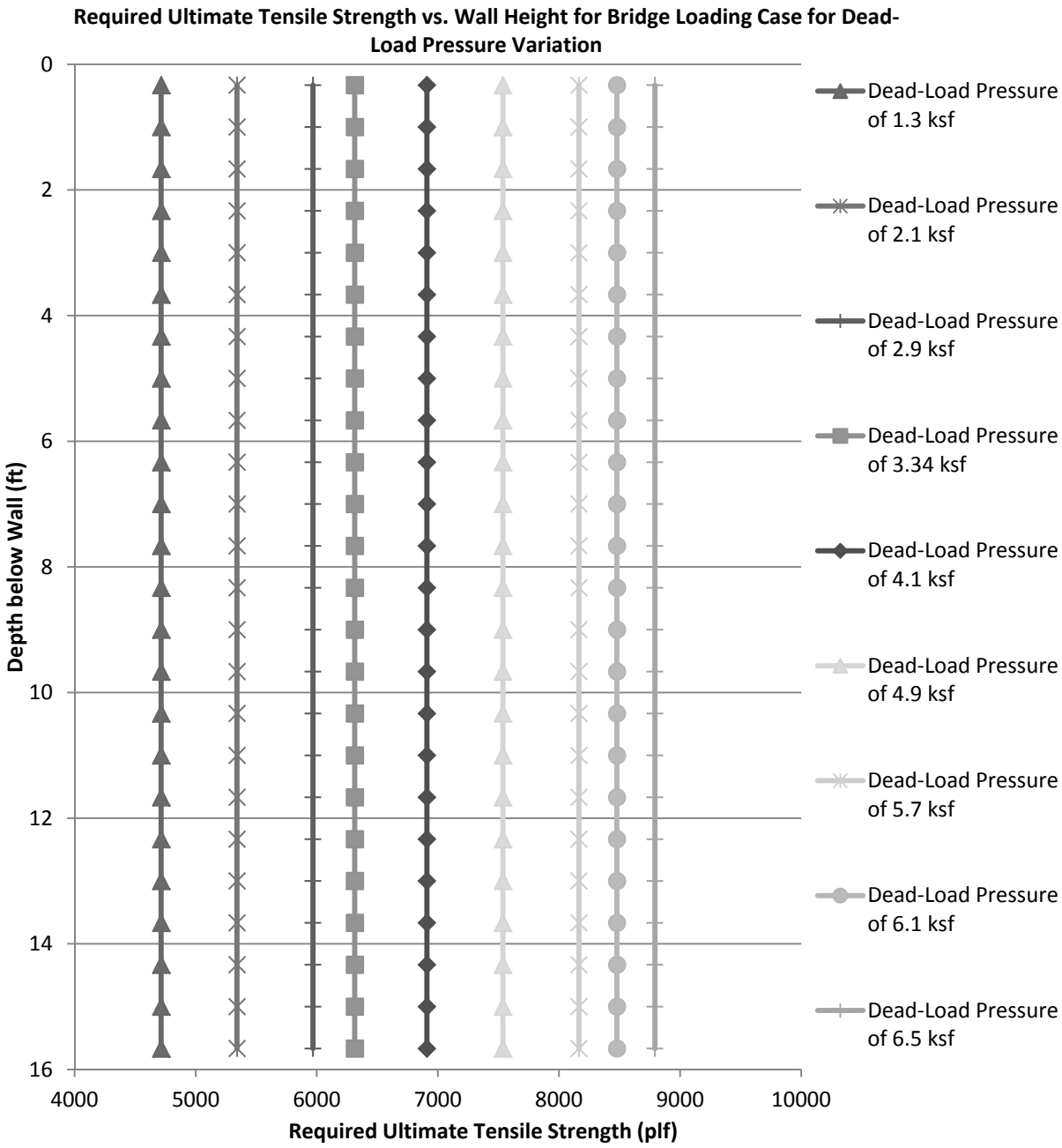

Figure 166: Influence of Dead Load on Ultimate Required Tension for Bridge Loading for Method 4: NCHRP GRS Method

Figure 166 shows that for Method 4, the entire profile is assigned a required ultimate tensile strength, T_{req}, value equal to the highest value that occurs in the wall. Therefore, the distributions plot as vertical lines. With increasing dead load, the maximum T_{req} value in the profile increases. To look more closely at the variation of tension at each reinforcement layer, the variation in nominal maximum tensile load, T_{max}, with depth was plotted for each variation in dead load. These relationships are plotted in Figure 167.

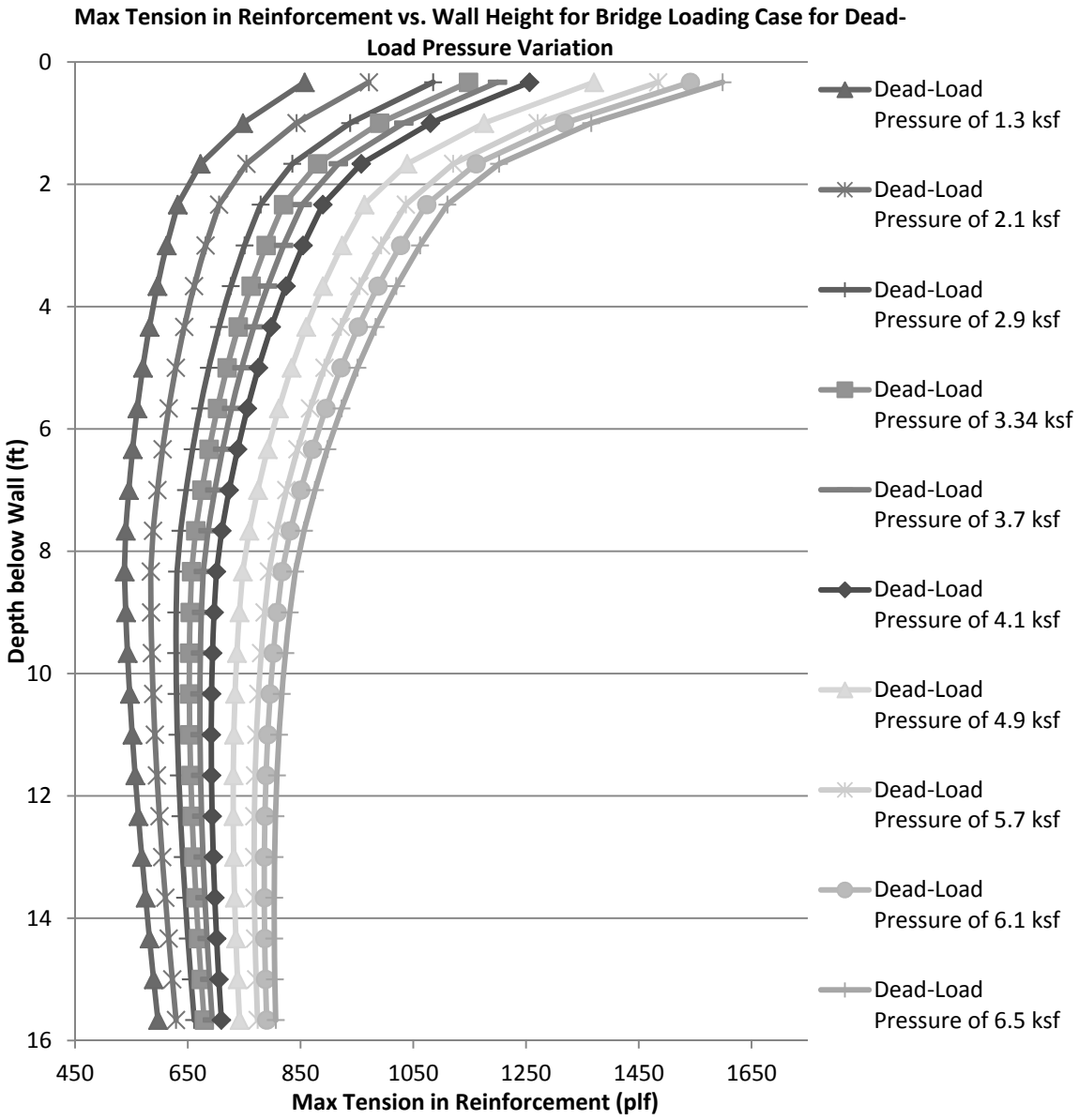

Figure 167: Influence of Dead Load on Max Tensile Load in the Reinforcement for Bridge Loading for Method 4: NCHRP GRS Method

Figure 167 shows that for Method 4, increasing dead load pressure will increase the nominal maximum tensile load, T_{max}, at all depths below the top of the reinforced zone. The shape of each distribution is curved. The increase in T_{max} is greater at the top than the bottom. This is due to the fact that bridge loads influence the upper portion of the wall more for this loading condition.

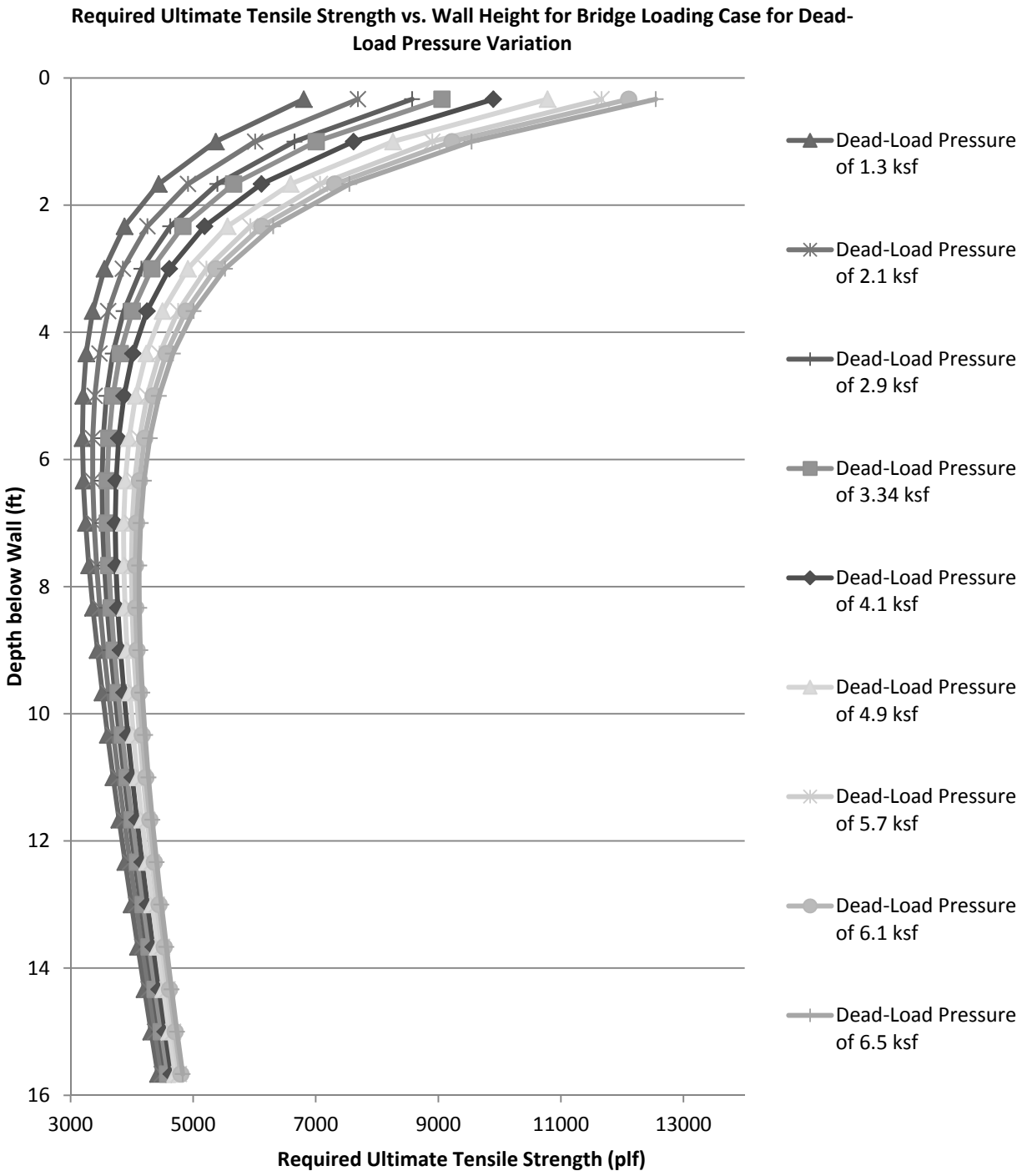

Figure 168: Influence of Dead Load on Ultimate Required Tension for Bridge Loading for Method 5: FHWA GRS-IBS Method Analytic Solution

For Method 5's analytic solution, as bridge dead load increases the predicted required ultimate tensile strength, T_{req}, increases for the entire soil profile as shown in Figure 168. All distributions have a curved shape. The increase in T_{req} values is much greater near the top of the wall than the bottom for this loading condition.

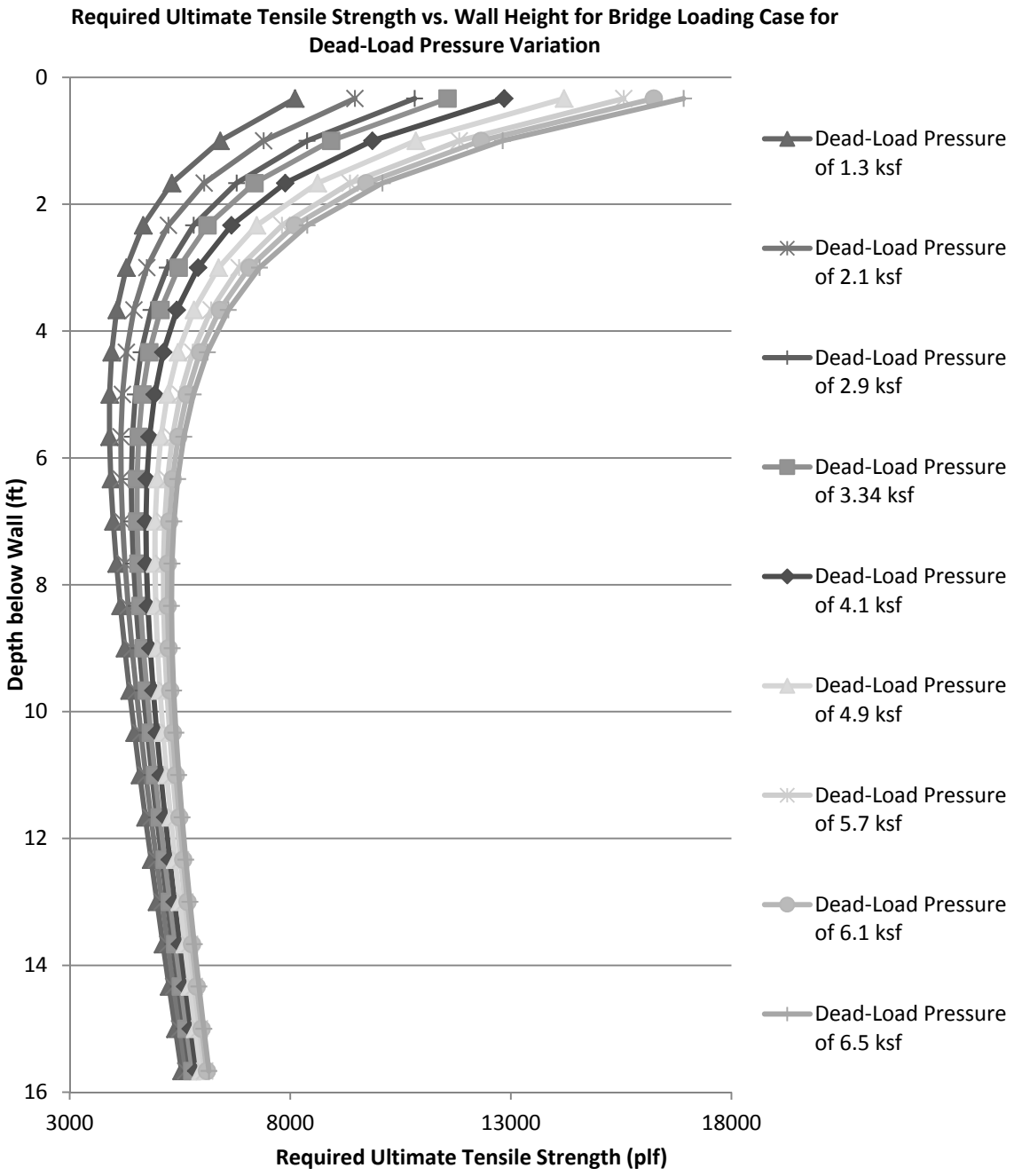

Figure 169: Influence of Dead Load on Ultimate Required Tension for Bridge Loading for Method 5: FHWA GRS-IBS Method Tensile Strength at 2% Strain Check

Figure 169 shows that for Method 5's tensile strength at 2% strain equivalent T_{req} calculation, the increase in bridge dead load will increase the predicted required ultimate tensile strength, $T_{req.}$ The predicted values of T_{req} are higher than that predicted by the analytic solution but the distributions have very similar shapes.

There is a third check required by Method 5 guidance that requires the ultimate tensile strength to be greater than or equal to 4,800 lb/ft. This requirement is not plotted but

would plot as a straight line at the value of 4,800 lb/ft. Which of the three requirements that controls can vary within the soil profile.

The variation in maximum value of T_{max} and T_{req} is shown in Figure 170 and Figure 171, respectively for all applicable methods.

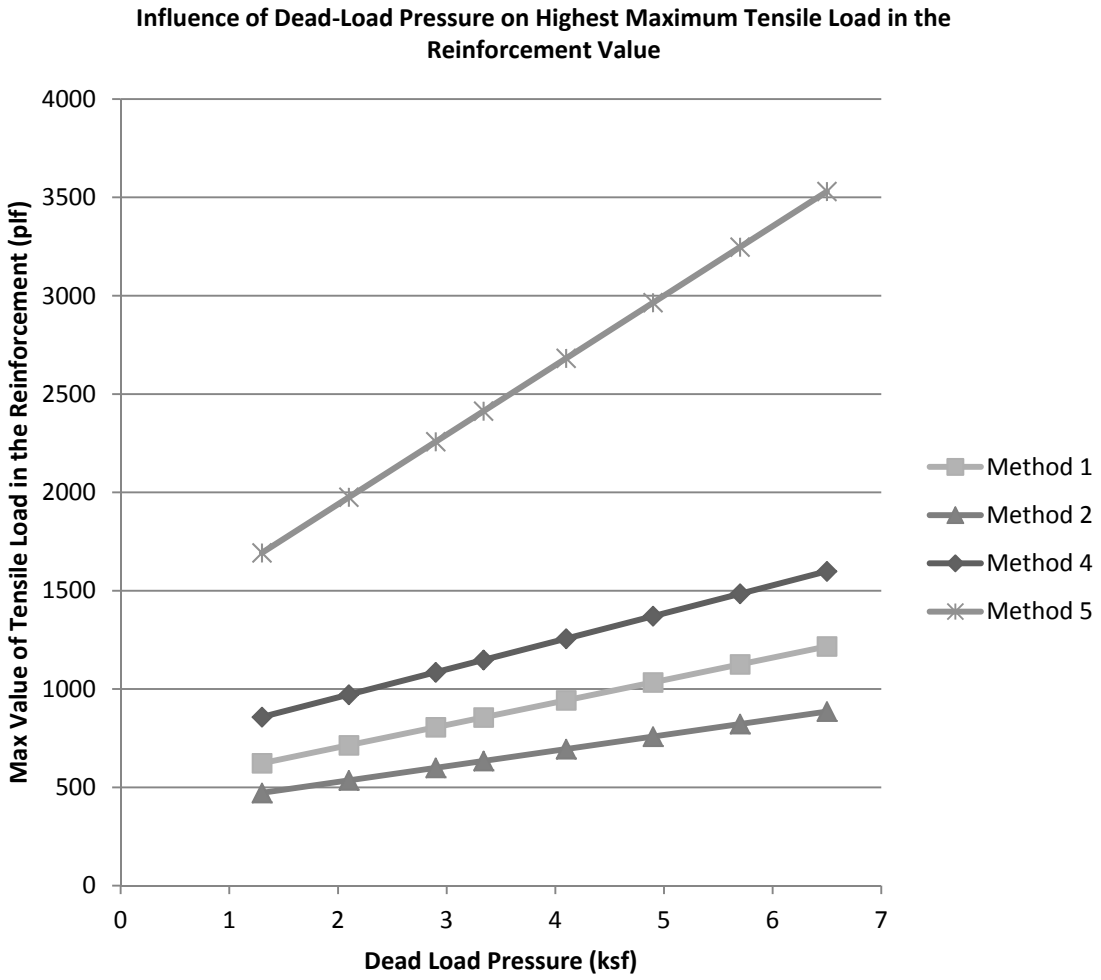

Figure 170: Influence of Dead Load on Max Load in the Reinforcement for the Bridge Loading Condition

Figure 170 shows that the highest value of maximum load in the reinforcement, T_{max}, increases linearly with increasing bridge dead load. Methods 1, 2, and 4 are more closely influenced by bridge dead load in comparison to each other than Method 5. Method 5 appears to be the most influenced by bridge dead load. Additionally, Method 5 predicts the highest values of T_{max} in comparison to all other methods.

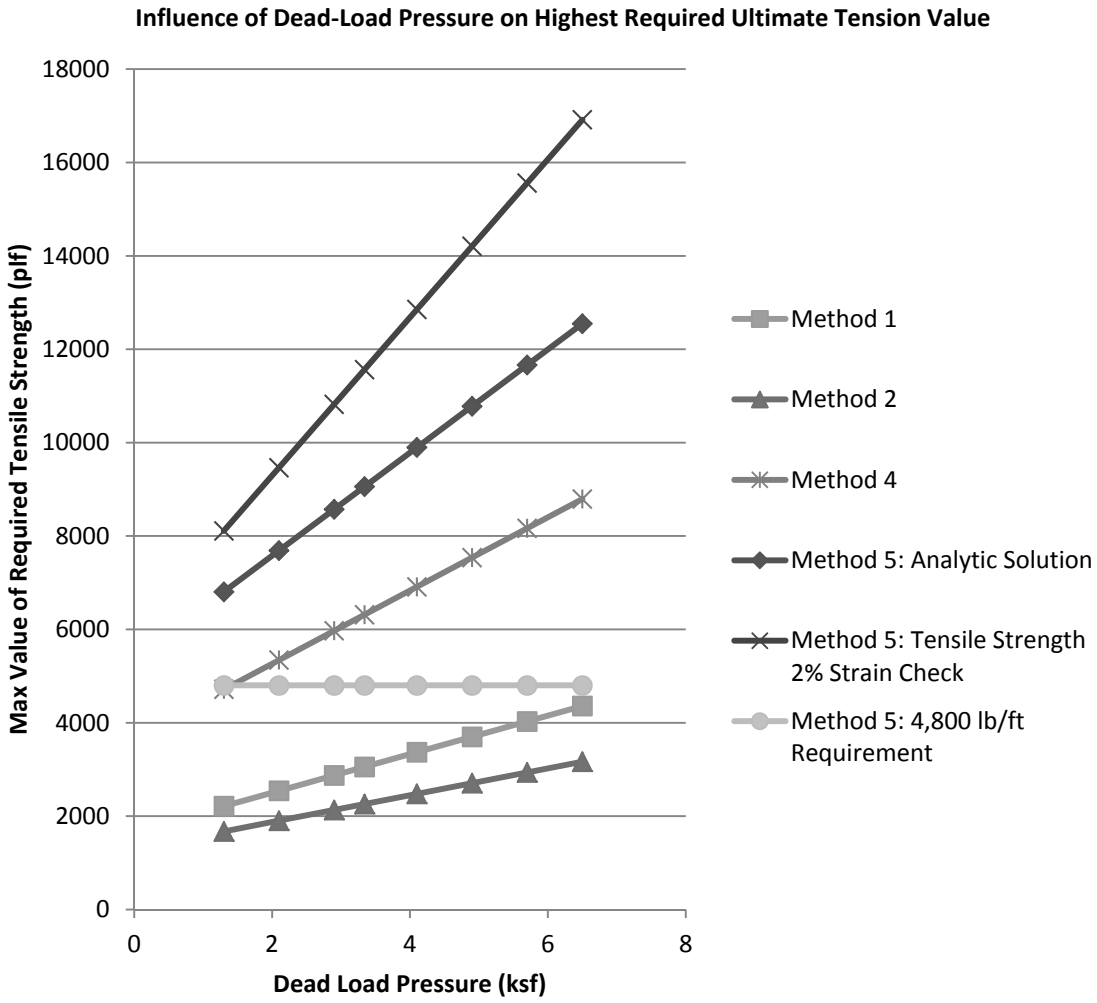

Figure 171: Influence of Dead Load on the Highest Predicted Ultimate Required Tension for the Bridge Loading Condition

Figure 171 shows that the highest predicted ultimate required tensile strength, T_{req}, also increases linearly with increasing bridge dead load. Methods 1 and 2 are similarly influenced by bridge dead load. Method 4 is more sensitive to bridge dead load than Methods 1 and 2.

Method 5 has three requirements to establish T_{req} values for design. The first is an analytic solution, the second is a check of tensile strength at 2% strain, and the last is a requirement that T_{req} be at least equal to or above 4,800 lb/ft. The value chosen for design is the highest of the three ultimate strength values. All three of these predicted values are plotted in Figure 171. The first and second requirements are similarly influenced by bridge dead load but the tensile strength at 2% strain check predicts a higher value. The last requirement plots as a straight horizontal line at 4,800 lb/ft.

Impact of Bridge Live Load Variation: The following section explores the influence of varying the bridge Live load over the range detailed in Table 5 for the bridge loading

case. This parameter is unique to the bridge loading scenario and therefore is not applicable for the roadway loading condition. Only the influence on bridge loading conditions will be explored in this section. The variation of live load was explored separately from the dead load to account for difference in load factors for methods utilizing a LRFD design platform.

Bridge Loading: Method 3, the K-Stiffness Method, was not adapted for the bridge loading case for the parametric study. Bridge live load was varied from 1.5 ksf to 4.3 ksf. The base case value was 3.34 ksf. The sill width was held constant at the base case value of 3.0 feet for this investigation. Figure 172, Figure 173, Figure 174, Figure 175, Figure 176, and Figure 177 show the variation in tension for the entire soil profile with change in live load for each of the methods compared.

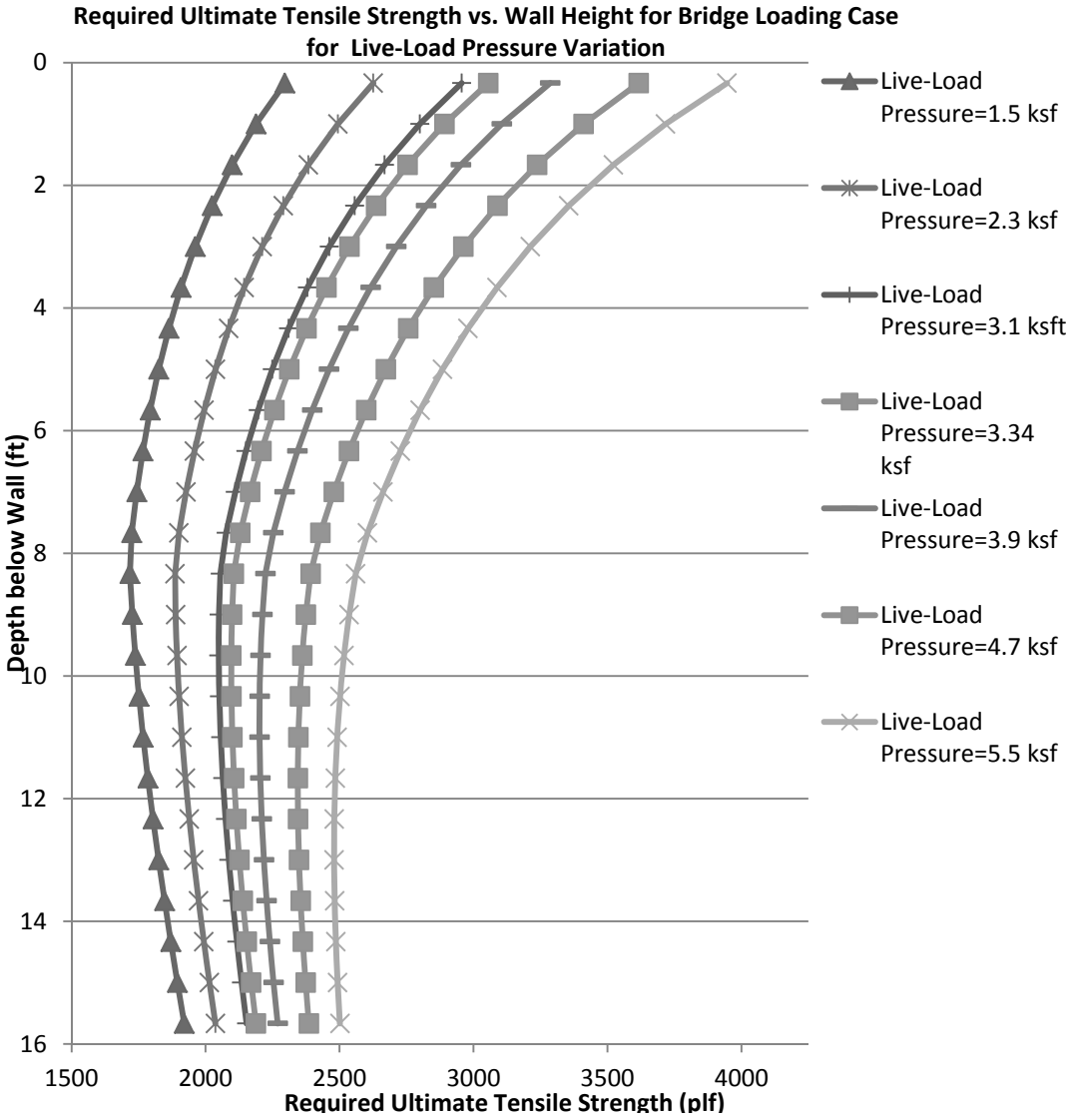

Figure 172: Influence of Live Load on Ultimate Required Tension for Bridge Loading for Method 1: The Simplified Procedure

For Method 1, the increase in bridge live load leads to an increase in predicted required ultimate tensile strength, T_{req}, for the entire soil profile as shown in Figure 172. All distributions have a curved shape that increases in degree with increase in live load. The T_{req} value both at the top and the bottom increase with increasing bridge live load. The increase at the bottom is less than at the top of the wall. This is due to the fact that bridge load primarily influence the upper portion of the wall for this loading case.

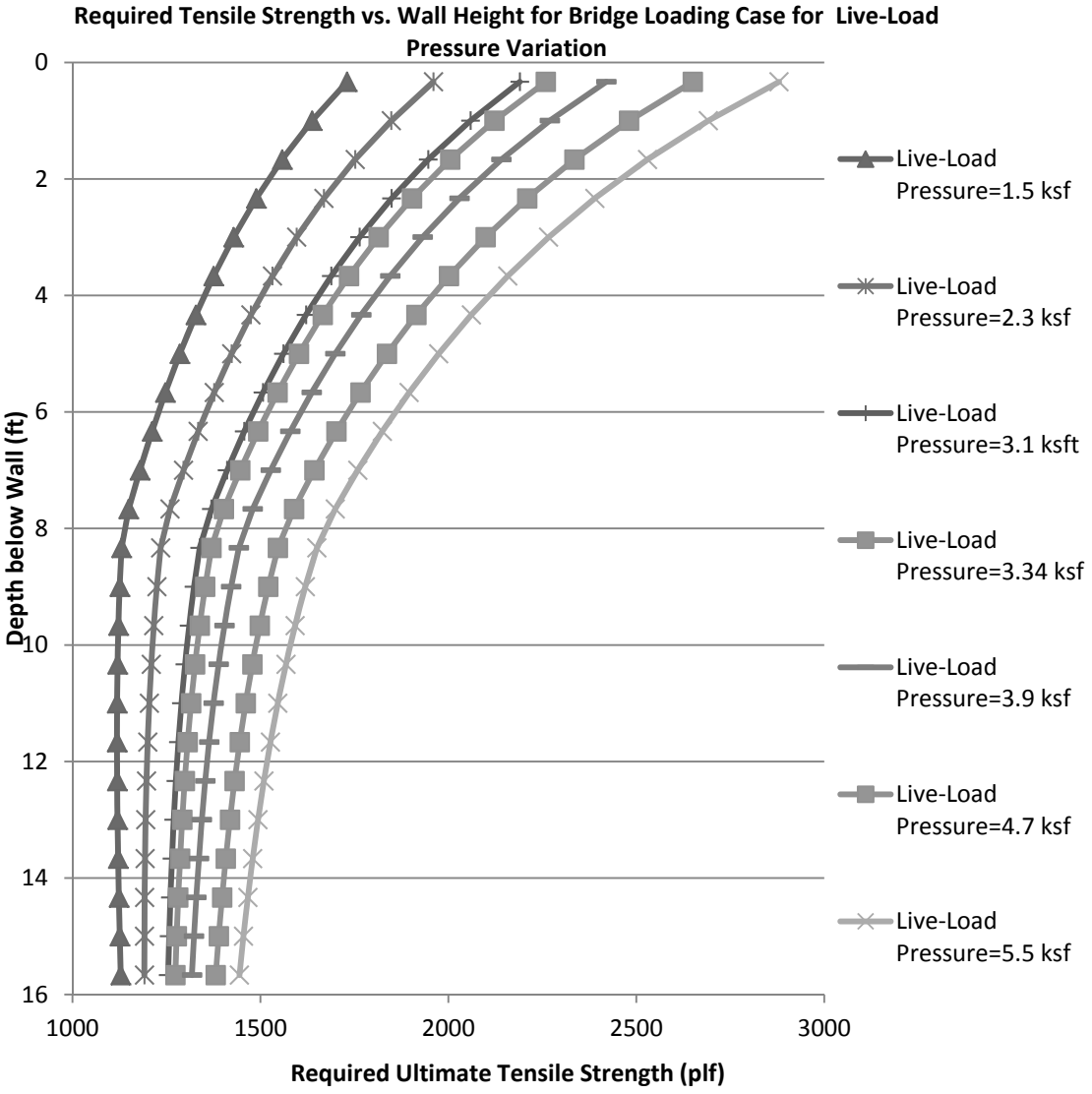

Figure 173: Influence of Live Load on Ultimate Required Tension for Bridge Loading for Method 2: The Simplified Procedure with K_r/K_a Adjusted

For Method 2, the increase in bridge live load leads to an increase in predicted required ultimate tensile strength, T_{req}, for the entire soil profile as shown in Figure 173. All distributions have a curved shape that increases in degree with increase in upper wall height. The T_{req} value both at the top and the bottom increase with increasing bridge live load. The increase at the bottom is less than at the top of the wall. This is due to the fact

that bridge load primarily influence the upper portion of the wall for this loading case similar to Method 1.

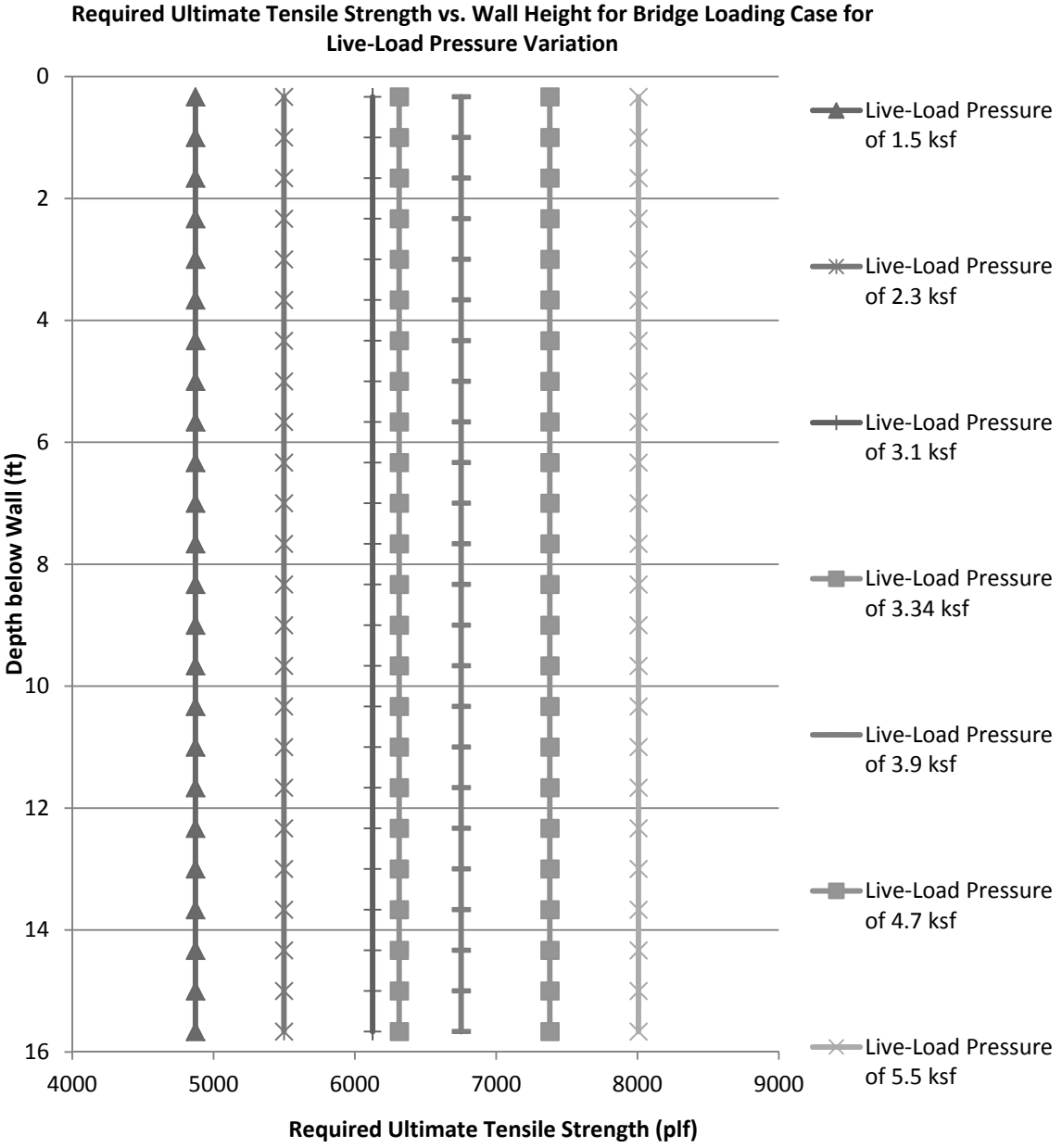

Figure 174: Influence of Live Load on Ultimate Required Tension for Bridge Loading for Method 4: NCHRP GRS Method

Figure 76 shows that for Method 4, the entire profile is assigned a required ultimate tensile strength, T_{req}, value equal to the highest value that occurs in the wall. Therefore, the distributions plot as vertical lines. With increasing live load, the maximum T_{req} value in the profile increases. To look more closely at the variation of tension at each reinforcement layer, the variation in nominal maximum tensile load, T_{max}, with depth was plotted for each variation in live load. These relationships are plotted in Figure 175.

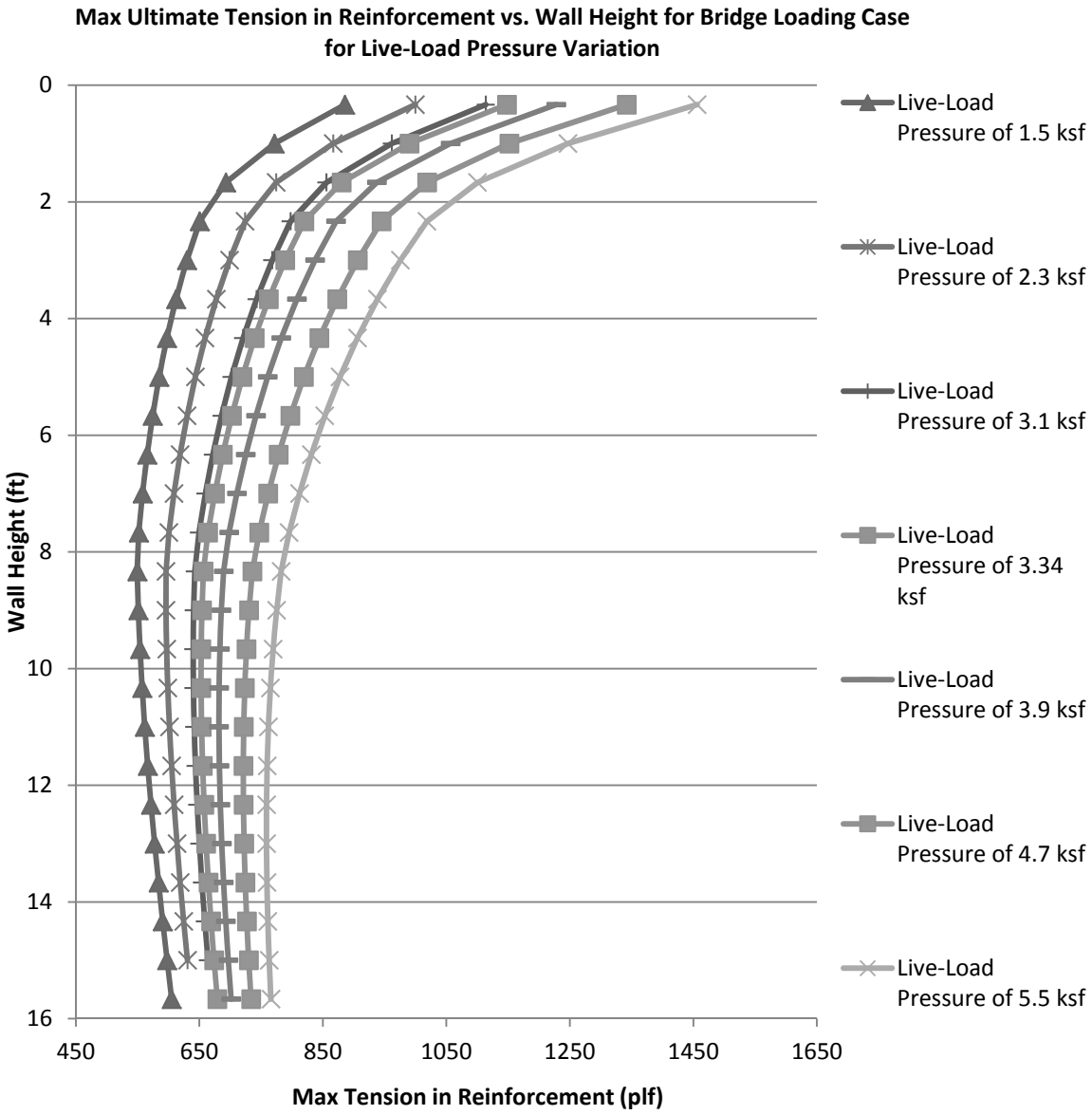

Figure 175: Influence of Live Load on Max Tensile Load in the Reinforcement for Bridge Loading for Method 4: NCHRP GRS Method

Figure 175 shows that for Method 4, increasing live load pressure will increase the nominal maximum tensile load, T_{max}, at all depths below the top of the reinforced zone. The shape of each distribution is curved. The increase in T_{max} is greater at the top than the bottom. This is due to the fact that bridge loads influence the upper portion of the wall more for this loading condition.

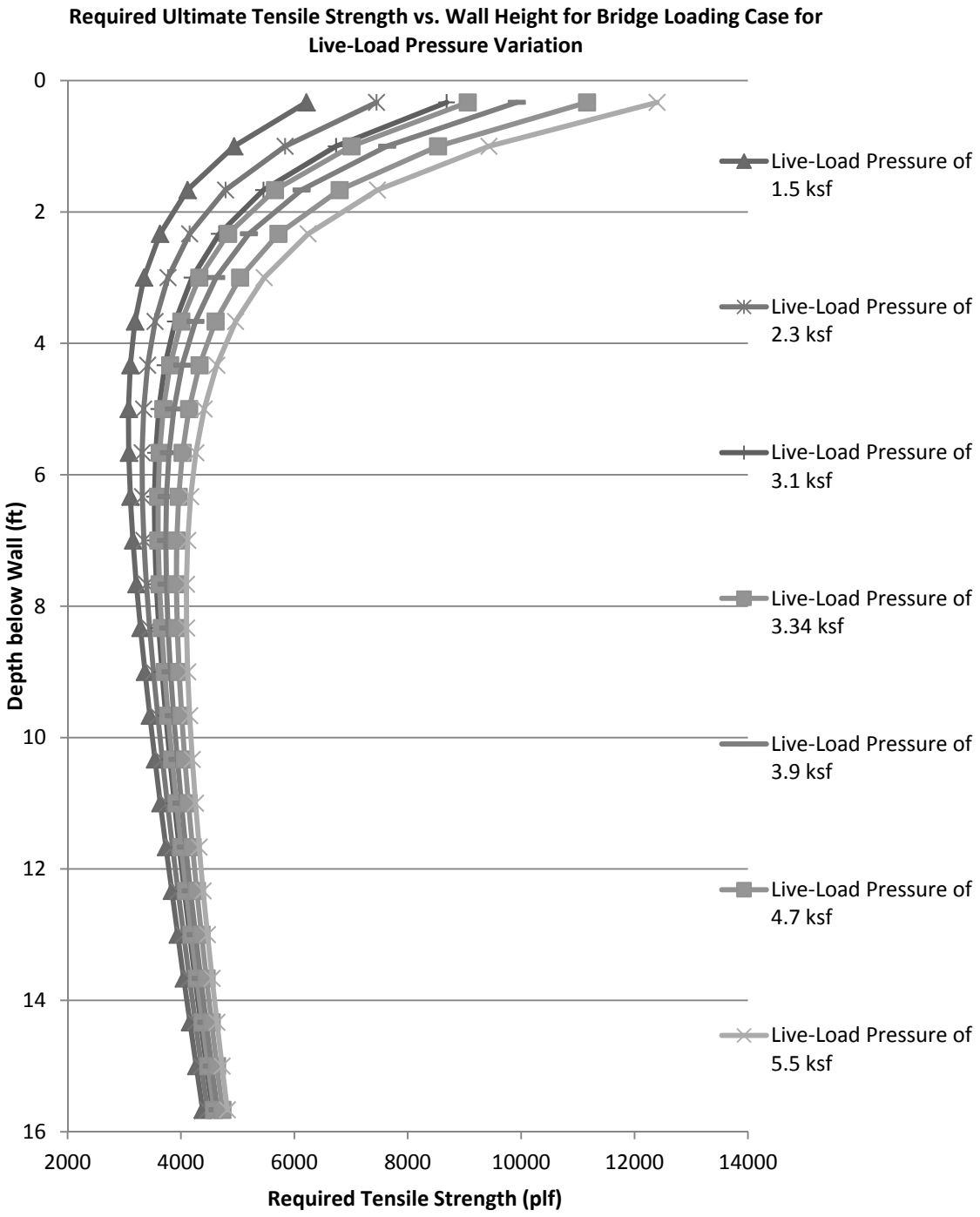

Figure 176: Influence of Live Load on Ultimate Required Tension for Bridge Loading for Method 5: FHWA GRS-IBS Method Analytic Solution

For Method 5's analytic solution, as bridge live load increases the predicted required ultimate tensile strength, T_{req}, increases for the entire soil profile as shown in Figure 176. All distributions have a curved shape. The increase in T_{req} values is much greater near the top of the wall than the bottom for this loading condition.

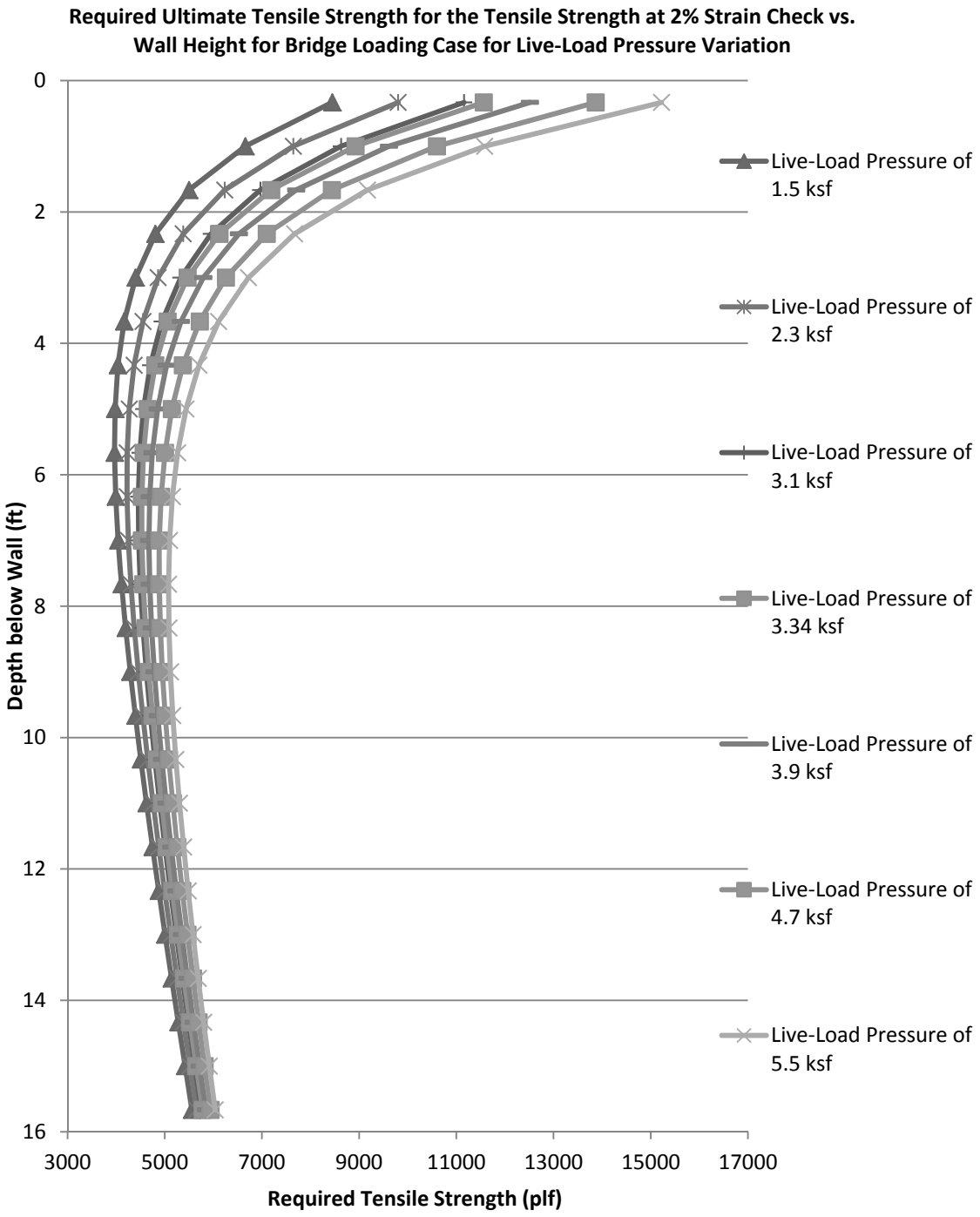

Figure 177: Influence of Live Load on Ultimate Required Tension for Bridge Loading for Method 5: FHWA GRS-IBS Method Tensile Strength at 2% Strain Check

Figure 177 shows that for Method 5's tensile strength at 2% strain equivalent T_{req} calculation, the increase in bridge live load will increase the predicted required ultimate tensile strength, $T_{req.}$ The predicted values of T_{req} are higher than that predicted by the analytic solution but the distributions have very similar shapes.

There is a third check required by Method 5 guidance that requires the ultimate tensile strength to be greater than or equal to 4,800 lb/ft. This requirement is not plotted but would plot as a straight line at the value of 4,800 lb/ft. Which of the three requirements that controls can vary within the soil profile.

The variation in maximum value of T_{max} and T_{req} is shown in Figure 178 and Figure 179, respectively for all applicable methods.

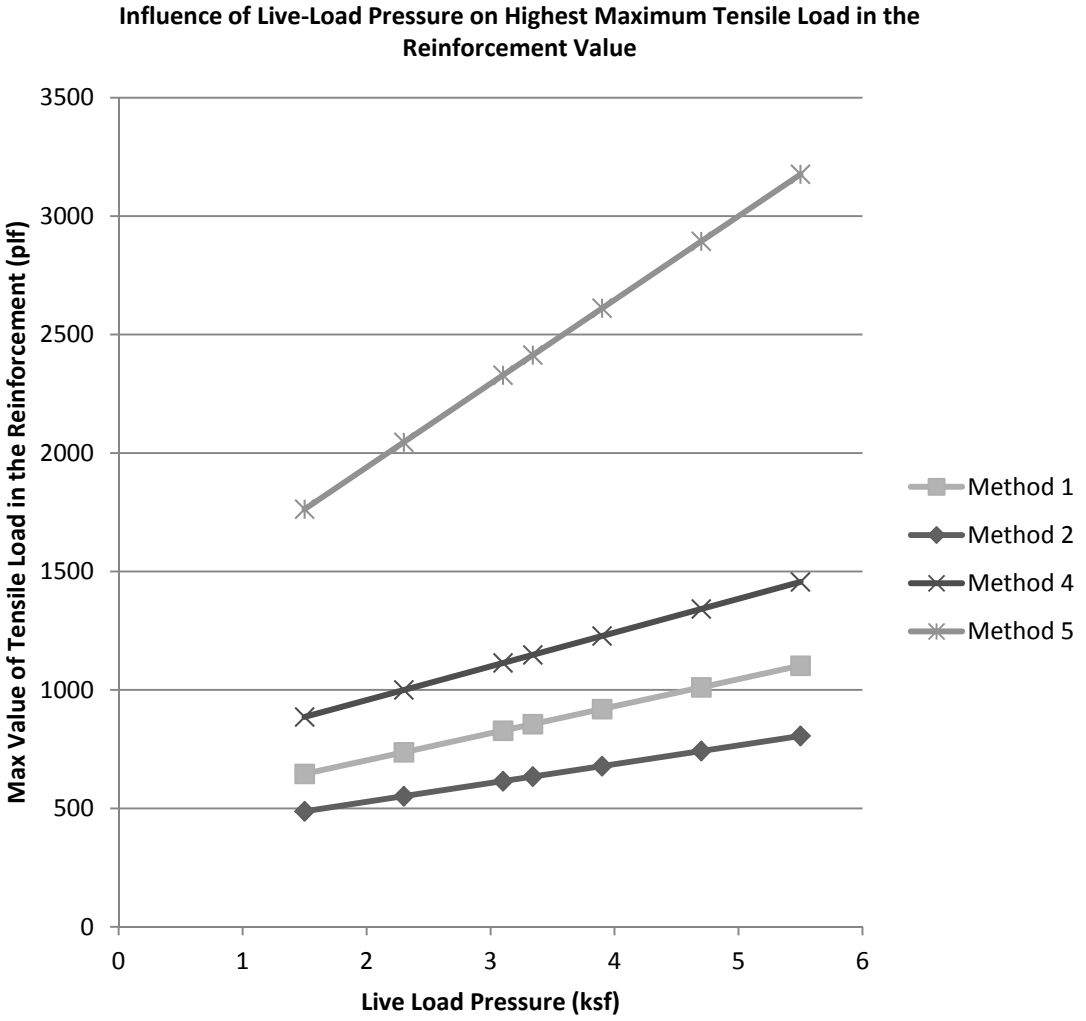

Figure 178: Influence of Live Load on Max Load in the Reinforcement for the Bridge Loading Condition

Figure 178 shows that the highest value of maximum load in the reinforcement, T_{max}, increases linearly with increasing bridge live load. Methods 1, 2, and 4 are similarly influenced by bridge live load. Method 5 is more sensitive to live load and predicts the highest values of T_{max} for all methods compared.

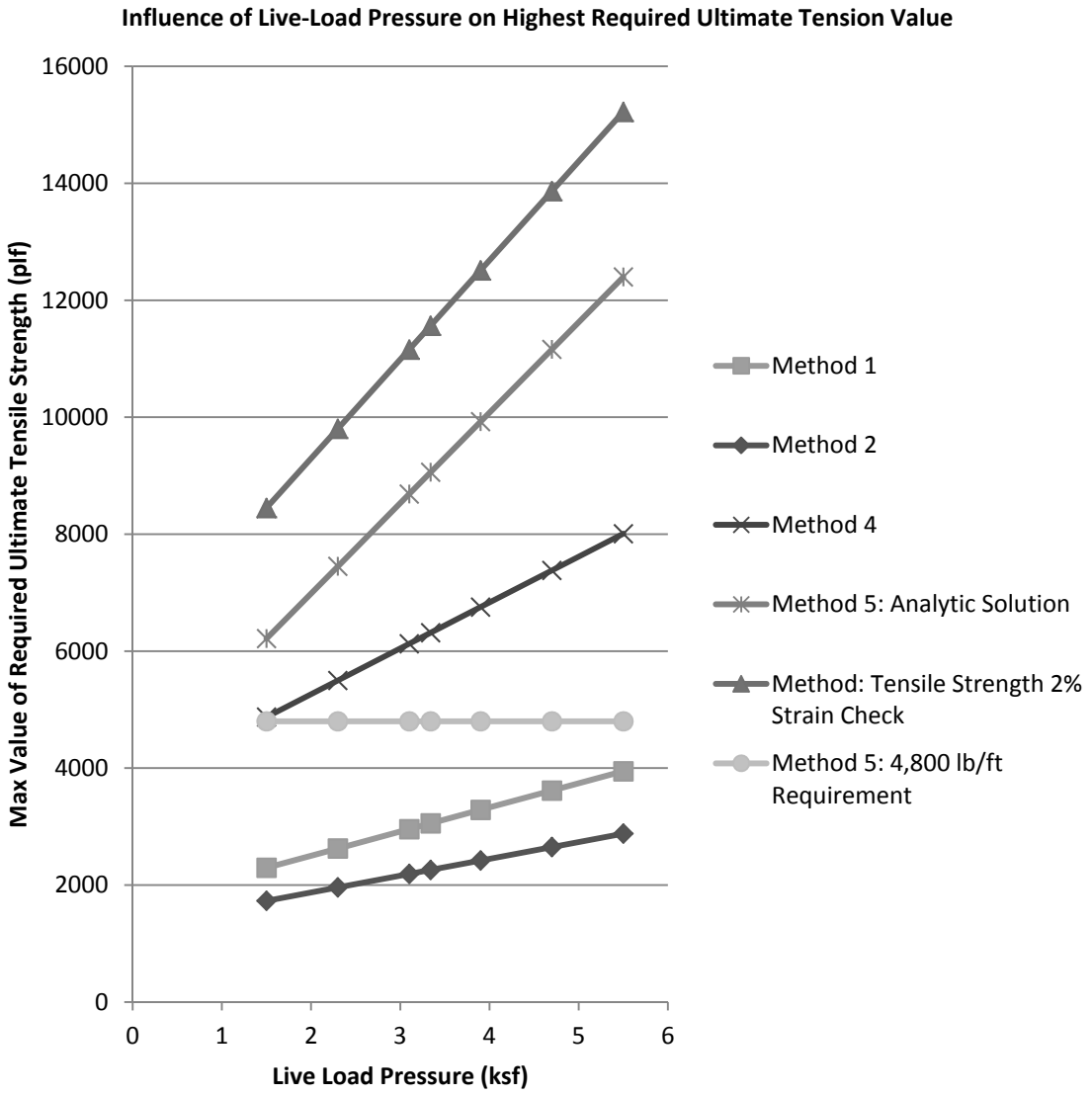

Figure 179: Influence of Live Load on the Highest Predicted Ultimate Required Tension for the Bridge Loading Condition

Figure 179 shows that the highest predicted ultimate required tensile strength, T_{req}, also increases linearly with increasing bridge live load pressure. Methods 1 and 2 are similarly influence by live load while Method 4 is more sensitive to live load.

Method 5 has three requirements to establish T_{req} values for design. The first is an analytic solution, the second is a check of tensile strength at 2% strain, and the last is a requirement that T_{req} be at least equal to or above 4,800 lb/ft. The value chosen for design is the highest of the three ultimate strength values. All three of these predicted values are plotted in Figure 179. The first and second requirements are similarly influenced by live load but the tensile strength at 2% strain check predicts a higher value. The last requirement plots as a straight horizontal line at 4,800 lb/ft.

CHAPTER 4 - DISCUSSION AND CONCLUSIONS

Of the five methods assessed, many differences in the calculation procedures and results exist. These differences are the result of each method employing slightly or significantly different assumptions. This section outlines the fundamental principles behind each of the five methods, and it describes how differences in these principles produce different outcomes. Overall conclusions are also presented.

4.1 DISCUSSION OF UNDERLYING ASSUMPTIONS

The assumptions underlying the calculations for each method are often the results of multiple assumptions and basic theories, and they sometimes include newer empirical observations. The goal of this section is to discuss the most basic theoretical assumptions each method employs. At the end of the section, a discussion of the major differences between each method's basic principles is included. Additionally, the ways that these differences influence predicted required tension T_{req} and maximum nominal tensile load in the reinforcement T_{max} is discussed.

Method 1-FHWA Simplified Procedure Assumptions: Method 1 is the most current and widely used design method for MSEW technology. It classifies the major design components as the reinforcement, the facing elements, and the reinforced fill. The soil and reinforcement together create a composite soil mass with improved tensile performance. The reinforcement provides a degree of confinement that produces a stiffer soil mass. Method 1 is considered a limit-equilibrium design methodology that is empirically derived (Berg et al. 2009).

Stress Transfer Mechanisms: Stress is transferred from the soil to the reinforcement via friction and/or passive resistance. The stress transfer mechanism of friction develops from the normal force of soil particles against reinforcement and a pulling force from wall loading that mobilized frictional forces. This mechanism is depicted in Figure 180. The passive resistance is the result of the shape of the reinforcement. For geosynthetics, a grid shape will yield passive resistance built up from bearing stresses along transverse surfaces as shown in Figure 181 (Berg et al. 2009).

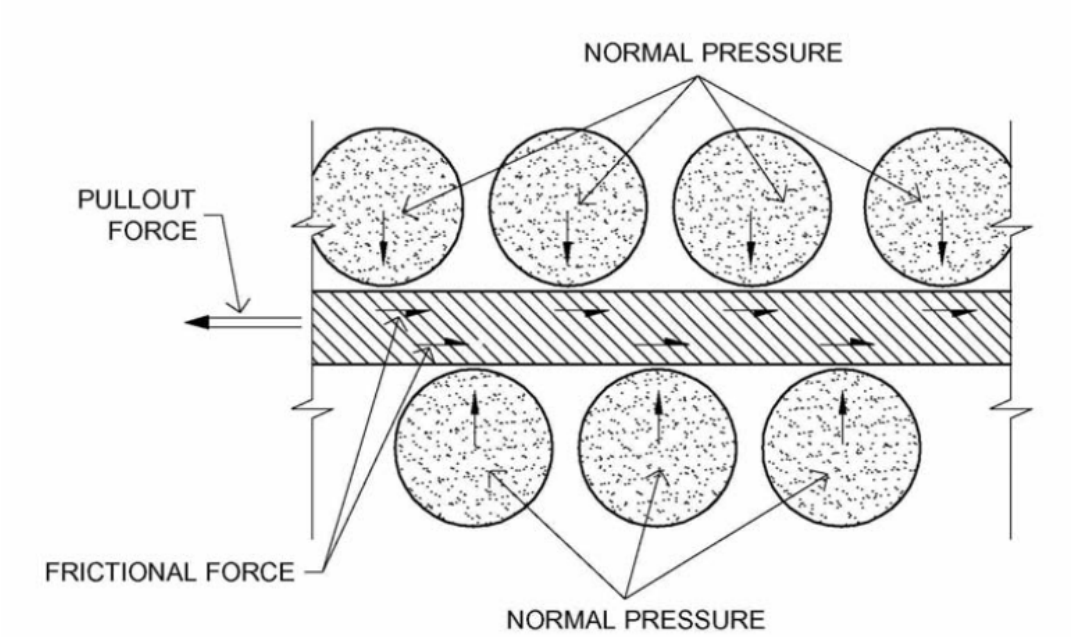

Figure 180: Frictional Stress Transfer between Soil and Reinforcement Berg, R. R., Christopher, B. R., and Samtani, N. (2009). "Mechanically Stabilized Earth Walls and Reinforced Slopes, Design and Construction Guidelines." *Vol. I - FHWA-NHI-10-024, Vol. II – FHWA-NHI-10-025*, Federal Highway Administration, Washington, D.C. Used under fair use, 2014.

Geosynthetic reinforcement is classified as "extensible." This means that the reinforcement can elongate more than the soil before failure. Additionally, the load in the reinforced zone is first transferred to the soil, which mobilizes stress that are then picked up by the reinforcement. It should be noted that confining pressure and soil type also play a role in this interaction. There is a level of allowable displacement of the reinforced fill soil relative to the reinforcement to allow for full mobilization of the tensile force in the reinforcement (Berg et al. 2009).

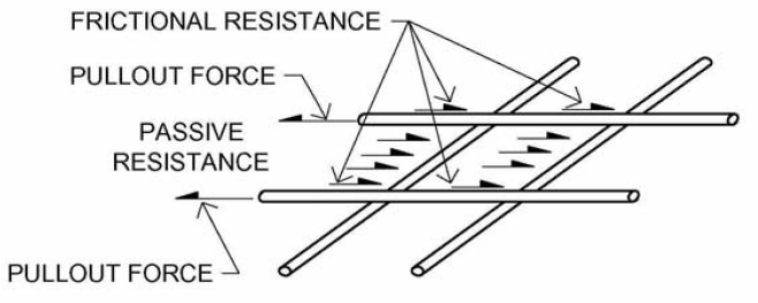

Figure 181: Passive Resistance on Transverse Reinforcement Surfaces Berg, R. R., Christopher, B. R., and Samtani, N. (2009). "Mechanically Stabilized Earth Walls and Reinforced Slopes, Design and Construction Guidelines." *Vol. I - FHWA-NHI-10-024, Vol. II – FHWA-NHI-10-025*, Federal Highway Administration, Washington, D.C. Used under fair use, 2014.

Long Term Strength Loss: Long term strength losses of the reinforcement are captured using reduction factors. These factors account for installation damage, creep from long-term sustained loading, and durability issues associated with degradation. Figure 182 captures this reduction in strength of the reinforcement over the life of the structures. Equation 30 and Equation 31 developed from Method 1 design guidance reflect the long-term strength concepts associated with geosynthetic reinforcement (Berg et al. 2009).

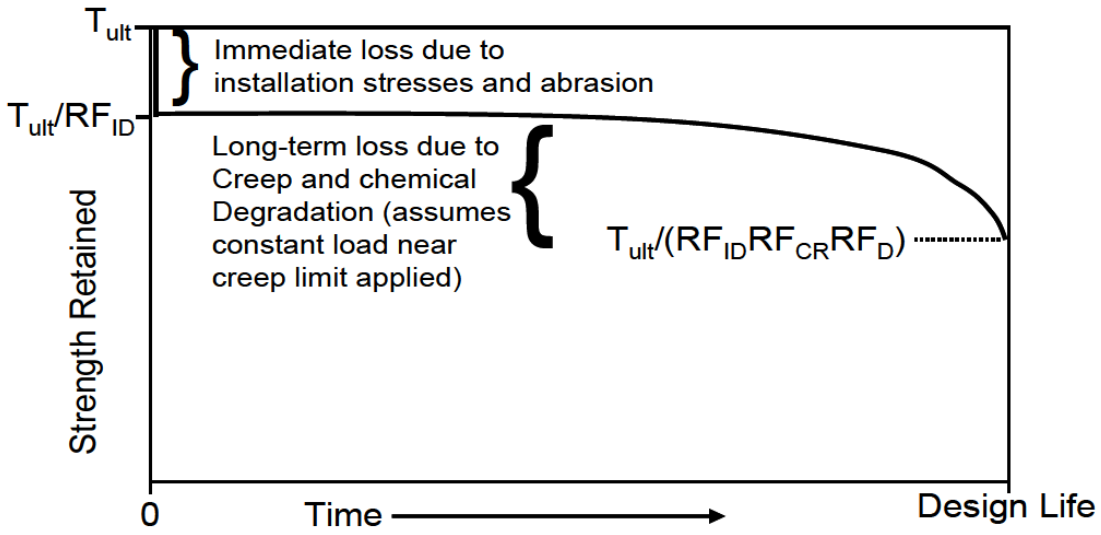

Figure 182: Long Term Strength of Geosynthetic Reinforcement Berg, R. R., Christopher, B. R., and Samtani, N. (2009). "Mechanically Stabilized Earth Walls and Reinforced Slopes, Design and Construction Guidelines." *Vol. I - FHWA-NHI-10-024, Vol. II – FHWA-NHI-10-025*, Federal Highway Administration, Washington, D.C. Used under fair use, 2014.

The long term displacements of the wall are influenced by the creep properties of the soil and reinforcement. Since coarse grained fill is utilized most often for reinforced fill, the soil itself should not be susceptible to creep to the extent that a cohesive soil would be. Creep of the reinforcement is often dependent on polymer type for geosynthetics. Additionally, confining stress often improves the long term durability and creep performance of geosynthetic reinforcements. However, this phenomenon is not accounted for in the calculation of nominal long term reinforcement strength (Berg et al. 2009).

Reinforced Fill Properties: Method 1 guidance assumes an internal friction angle of the reinforced fill utilized in design of 34° if gradation requirements were met. A value greater than 34° can only be used if additional testing can substantiate a higher value. Such testing includes triaxial testing per AASHTO T-296 and direct shearing testing per AASTO T-236. Method 1 guidance also limits the friction angle used in design to 40° even if testing indicates the value is higher. The cohesion of the reinforced fill is always assumed to be zero (Berg et al. 2009).

Lateral Earth Pressure Coefficient of the Reinforced Fill: Method 1 design guidance utilizes the "Simplified Method" in determining the ratio of lateral earth pressure

coefficient of the reinforced fill, K_r, to the Rankine lateral earth pressure coefficient, K_a. This relationship is dependent on reinforcement type (Berg et al. 2009). The goal of the "Simplified Method" was to take into account differences in reinforcement type and global stiffness without creating complex iterative calculations. Therefore, curves were developed based simply on reinforcement type that provided a variation in K_r/K_a (Allen et al. 2001). The curve for geosynthetics is illustrated in Figure 42 and the ratio of K_r/K_a is equal to 1.0.

It should be noted that for vertical walls, such as was assumed for the parametric analysis, the Rankine earth pressure coefficient equals that determined from the Coulomb earth pressure relationship. Rankine theory assumes that the interface friction between the wall and reinforced fill soil is equal to the slope of the backfill. Additionally, the assumption is made that the soil is homogenous and isotropic. For the Coulomb lateral earth pressure equation to equal that of Rankine's for the active earth pressure condition, the assumption is made that there is no wall friction and that the backfill is level (Berg et al. 2009). The resulting equation to determine K_a is shown in Equation 3.

Failure Surface Assumptions for Internal Stability: A classic Coulomb failure surface is assumed in Method 1 design guidance. Geosynthetic reinforcement is considered to not have an influence on failure surface shape due to the fact that its propensity for elongation will produce strains that are higher than that of the soil in the reinforced zone prior to failure (Berg et al. 2009).

The failure surface is considered to pass through the toe of the wall and to be planar in the case of geosynthetic reinforcements. Per AASHTO, Coulomb earth pressure theory illustrated in Figure 183 is utilized in defining the shape of the critical slip surface (Berg et al. 2009).

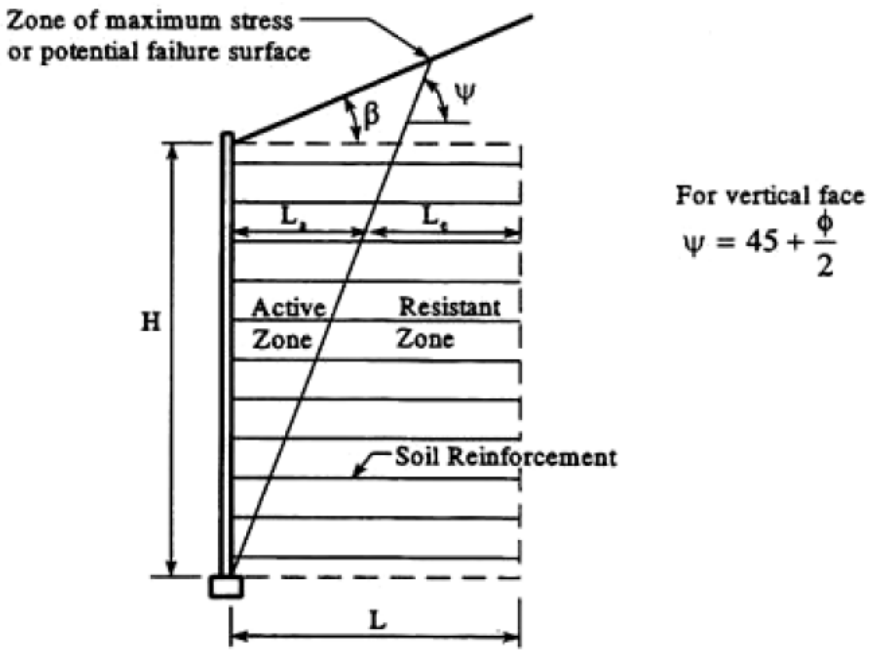

Figure 183: Coulomb Definition of Failure Surface Berg, R. R., Christopher, B. R., and Samtani, N. (2009). "Mechanically Stabilized Earth Walls and Reinforced Slopes, Design and Construction Guidelines." *Vol. I - FHWA-NHI-10-024, Vol. II – FHWA-NHI-10-025,* Federal Highway Administration, Washington, D.C. Used under fair use, 2014.

It is recommended that reinforcement extend past the active failure wedge into the resisting or anchorage zone. As the failure wedge moves forward and pushes against the facing material, resisting forces are engaged in the anchorage zone. The reinforcing elements act as tiebacks into the soil mass behind the active zone that restrain the wall facing system. Therefore the facing elements are structural in nature and support the soil mass (Kost et al. 2013).

Estimation of Horizontal Stresses: Calculation of all horizontal stress within the reinforced zone follows principles of classic soil mechanics. Since no water is present in the fill material, all stresses are expressed as total stresses. Equation 2 and Equation 7 which are used to find the horizontal stress per Method 1 guidance utilize no empirical corrections or manipulations (Berg et al. 2009). For example, horizontal stresses from the soil column itself are estimated to have a linear distribution as shown in Figure 184. The horizontal stress profile for the soil column plus an equivalent soil surcharge would have a distribution similar to that shown in Figure 185.

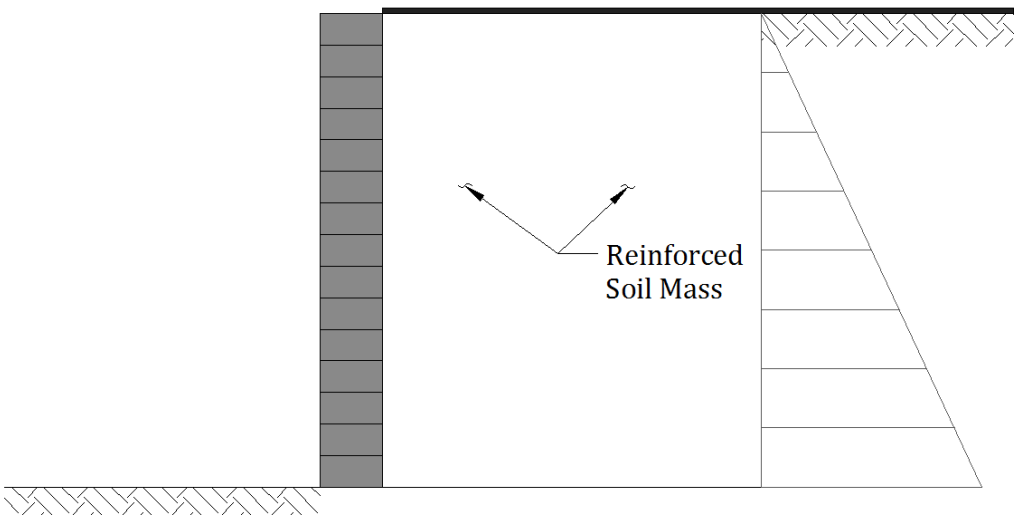

Figure 184: Assumed Horizontal Stress Distribution for a Simple Wall Scenario

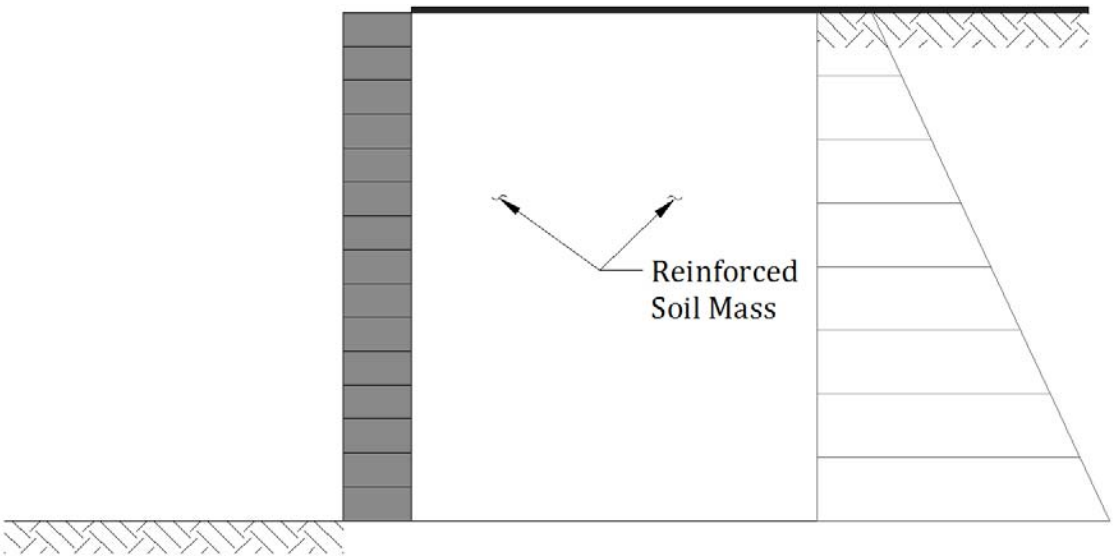

Figure 185: Assumed Horizontal Stress Distribution for a Simple Wall with Surcharge

Estimation of Maximum Tension: Equation 1 defines the maximum tension in a reinforcement layer per unit width determined using Method 1 guidance. The horizontal earth pressure at each reinforcement layer is calculated at the center of the contributory height, S_v. Figure 186 illustrates the concept of contributory height or tributary area. The only inputs into determining maximum tension load to be carried by a reinforcement layer are the horizontal earth pressure at that layer depth and the contributory height of the layer (Berg et al. 2009).

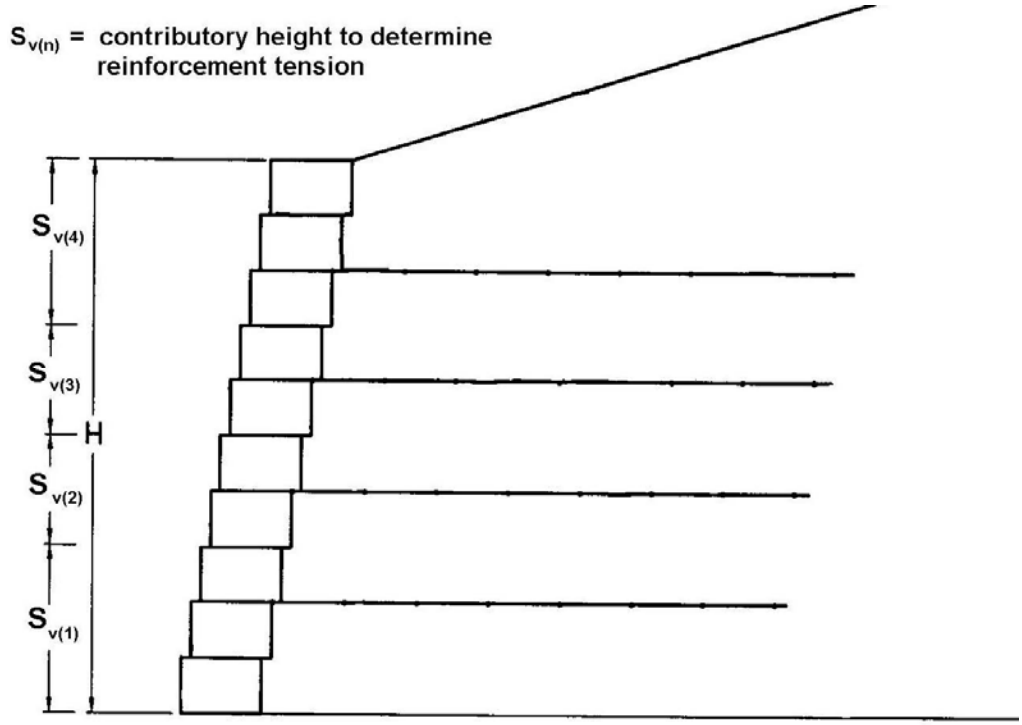

Figure 186: Contributory Height or Tributary Area of a Reinforcing Element Berg, R. R., Christopher, B. R., and Samtani, N. (2009). "Mechanically Stabilized Earth Walls and Reinforced Slopes, Design and Construction Guidelines." *Vol. I - FHWA-NHI-10-024, Vol. II – FHWA-NHI-10-025,* Federal Highway Administration, Washington, D.C. Used under fair use, 2014.

Limit States and Load/Resistance Factor Design: The FHWA Simplified Procedure, Method 1, designs for particular strength and extreme event limit states but does not evaluate directly service limit states. Based on success of in-service walls designed using Method 1, the conclusion can be made that meeting certain strength limit states will ensure the serviceability requirements are met (WSDOT 2012).

Method 1 is a limit equilibrium analysis and, as such, assesses the reinforced soil system in static equilibrium at failure, or just prior to collapse. The soil and reinforcement within the reinforced zone are assumed to reach their peak strength at the same time. It should be noted that this is not likely the case for geosynthetic reinforcement which will strain well past the failure strain of the surrounding soil (Allen and Bathurst 2013). However, limit equilibrium allows for a simplified platform for design that allows classic soil mechanism principals to be employed.

Since geosynthetic reinforced systems can be considered ductile at failure, the resistance factor applied for geosynthetic reinforcement for the Strength I limit state is 0.9 which is higher than steel, which is characterized by a brittle failure. The resistance factor accounts for uncertainties in long term reinforcement strength and any nonuniform loading which could cause local overstress of the reinforcement (Berg et al. 2009).

In geosynthetic reinforced systems, the reinforced fill soil will control how much the composite soil and reinforcement mass strains. Since coarse grained reinforced fills are often used, the strain of the composite mass is much lower than the rupture strain of the reinforcement. Any local overstress of the reinforcement would not result in sudden collapse, and effects of this overstress would likely be visible. Additionally, stress measurements taken within in-service walls indicate that design stresses are much higher than in-service stresses. This also contributes to selection of the resistance factor of 0.9 for geosynthetics (Berg et al. 2009).

Load factors are broken into two categories: permanent and transient loads. Within these categories, suggested minimum and maximum factors are given for a particular loading type, such as a dead-load earth fill. A minimum or maximum value should be selected depending on whether it impacts stability. A minimum value should be used if the load is applied to increases stability and a maximum value should be used if the load reduces stability (Berg et al. 2009).

Method 2 – Simplified Procedure with K_r/K_a Adjusted Assumptions: All aspects of the supporting soil theory for this proposed revision to Method 1, the Simplified Procedure, are identical to Method 1 with the exception of determining the lateral earth pressure coefficient of the reinforced fill.

Lateral Earth Pressure Coefficient of the Reinforced Fill: The proposed revision in determining the ratio of K_r/K_a came from observations of in-service walls. The lateral earth pressure coefficient of the reinforced fill can be estimated using Equation 32 and Figure 44. As a result of the revised ratio, the lateral earth pressure of the reinforced fill is predicted to be lower than the Rankine active lateral earth pressure coefficient up to a depth of 20 feet. Therefore, predicted horizontal earth pressures and maximum tensile loads are lower for Method 2 in comparison to Method 1, which assumes $K_r = (1.0)\ K_a$.

Method 3 - K-Stiffness Method Assumptions: The K-Stiffness Method uses calibration factors developed from instrumented case histories of in-service walls to predict the ultimate required tensile strength needed for design. The method is considered to predict more accurate loads within reinforced soil walls in comparison to Method 1. The components of the wall design are the same as Method 1. However, the K-Stiffness method is a working stress method with input parameters fitted to measured reinforcement strains from field data. The K-Stiffness Method should not be applied to designs where a reinforced soil mass is supporting other structures (WSDOT 2012). There is no difference between Method 1 and Method 3 in terms of assumed stress transfer mechanisms and the developed failure surface. Developers of Method 3 did not explicitly explore these concepts; instead, they adopted the specifications detailed by Method 1 for all aspects of design outside the scope of the K-Stiffness approach.

Long Term Strength Loss: The major design principal of the K-Stiffness Method for walls utilizing geosynthetics is in relation to the soil strain relative to the reinforcement

stiffness. For geosynthetic reinforced zones, the soil will reach its peak strength much sooner than the reinforcement will. Therefore, the soil can move past its peak strength and into the range of its residual strength. Limiting the soils strain to prevent the strength moving to a residual state improves wall performance by preventing excessive deformation (Berg et al. 2009).

Additional long term strength loss is captured using the same principal of reduction factors utilized in Method 1. These reduction factors, RF values, account for installation damage, creep, and degradation effects on long term reinforcement strength (WSDOT 2012). These factors are material specific and vary depending on which polymer type of reinforcement is used. The same RF values were used in Method 3 as in Method 1.

Reinforced Fill Properties: The initial development of the K-Stiffness Method was only applicable for coarse grained reinforced fill. The initial calibration of the method utilized 11 case history walls that had no cohesion. In later revisions to the method, the effects of cohesion were included. Newer walls added to the method for calibration had fines contents that could be assessed (Bathurst et al. 2008). However, for the parametric analysis, only coarse grained fill was considered. Backfill should meet specifications outlined in Chapter 5 of the WSDOT GDM and GSDOT Standard Specifications for gravel borrow material used in construction (WSDOT 2012).

Lateral Earth Pressure Coefficient of the Reinforced Fill: The lateral earth pressure coefficient for Method 3, the K-Stiffness Method, is determined using Equation 35 and Equation 36. Unlike Method 1, the Simplified Procedure, an at-rest lateral earth pressure coefficient is used instead of an active lateral earth pressure coefficient. Additionally, the friction angle utilized in the analysis is the secant peak plane strain friction angle of the soil, not the friction angle obtained from testing the soil in a triaxial or direct shear test like in Method 1. These differences are the result of calibrating the predicted loads in the wall with case history data. The K-Stiffness Method uses the at-rest condition as an index and does not assume at rest conditions are occurring in the wall fill from a classic soil mechanics stand point.

Estimation of Horizontal Stresses: Horizotal loads developed behind the wall are calcualted at a depth approximately halfway down the wall instread of the full height as in Method 1 and traditional soil mechanics. The principles for estimating the load at this location are consistent with Method 1. However, the load distribution is adjusted to fit observed field stress distributions using a factor called, D_{tmax} (WSDOT 2012). It was noted that in-service walls had a horizontal stress distribution shape that was more trapezoidal than linear as predicted by Method 1 (Bathurst et al. 2008). For geosynthetic reinforced walls, Figure 187 should be used for calculating the variation in D_{tmax} with depth. The parameters on the y-axis are the depth, z, the equivalent surcharge height, S, and the wall height, H. It should be noted that h_{eq} was the variable utilized in the

calculation summary of the parametric study for equivalent surcharge height, not S. The variation of D_{tmax} shown in Figure 187 assumes a wall constructed on a firm foundation. A wall on soft soil or rock may have a different distribution (WSDOT 2012).

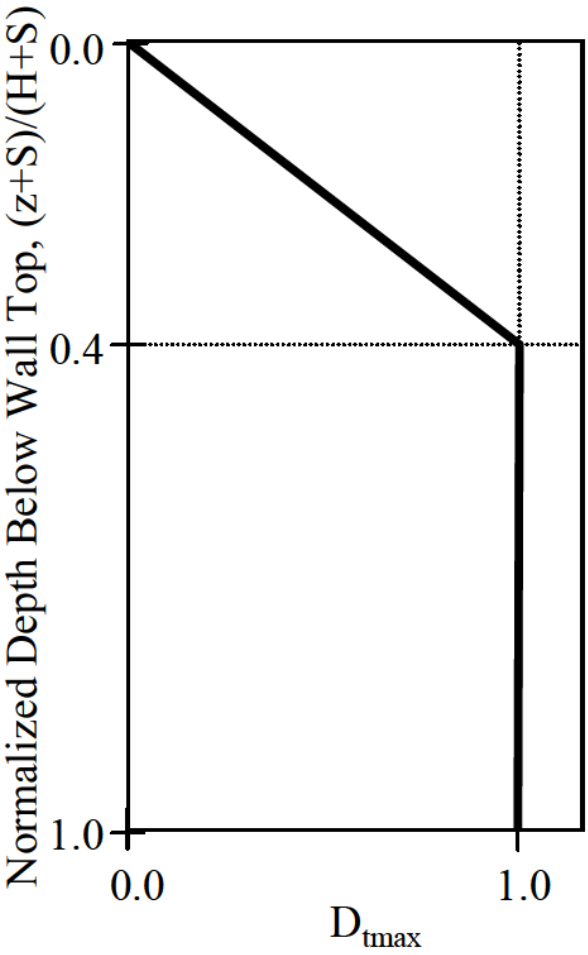

Figure 187: Variation in Load Distribution Factor for Geosynthetic Reinforced Walls WSDOT (2012). "Geotechnical Design Manual." *M6-03.07,* Environmental and Engineering Programs, Geotechnical Services. Used under fair use, 2014.

For a simple wall with soil surcharge, the variation of horizontal distriution predicted by Methods 1 and 3 is shown in Figure 188. The distribution in red shows the stresses predicted by Method 1, and the distribution in blue shows the stresses predicted by Method 3. Method 3, the K-Stiffness Method, has an empirically adjusted distribution that is quite different from that predicted by the most widely utilized MSEW method, the Simplified Procedure.

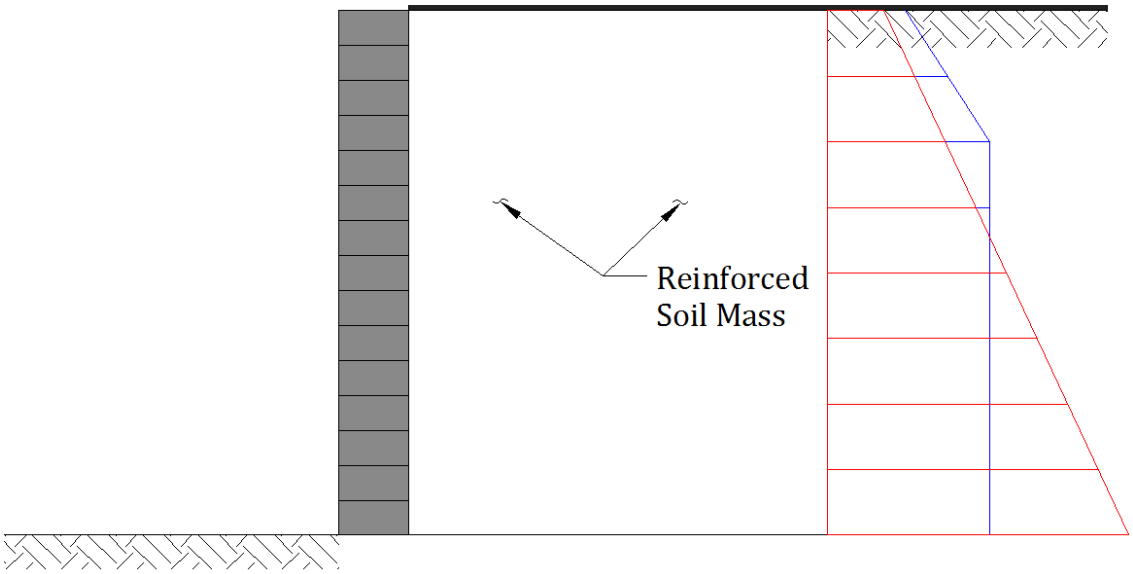

Figure 188: Horizontal Stress Distribution Predictions for Methods 1 (red) and 3 (blue) for the Roadway Loading Condition

The varition of wall height and any surcharge loading present will influence the horizontal stress distribution predicted by the K-Stiffness method. Raising the wall height will raise the break point in Figure 187. Additionally, increasing the wall height will increase the horizontal stress value at that point. This is shown in Figure 189 where the distribution in blue has a wall height lower than the distribution in green. Increasing the surcharge load's equivalent soil height will raise the break point in Figure 187. Additionally, increasing the equivalent heigth will increase the horizontal stress value at this location. This is shown in Figure 190 where the original distribution is shown in blue and the distribution in magenta represents the anticipated stress from increasing the equivalent soil surcharge height.

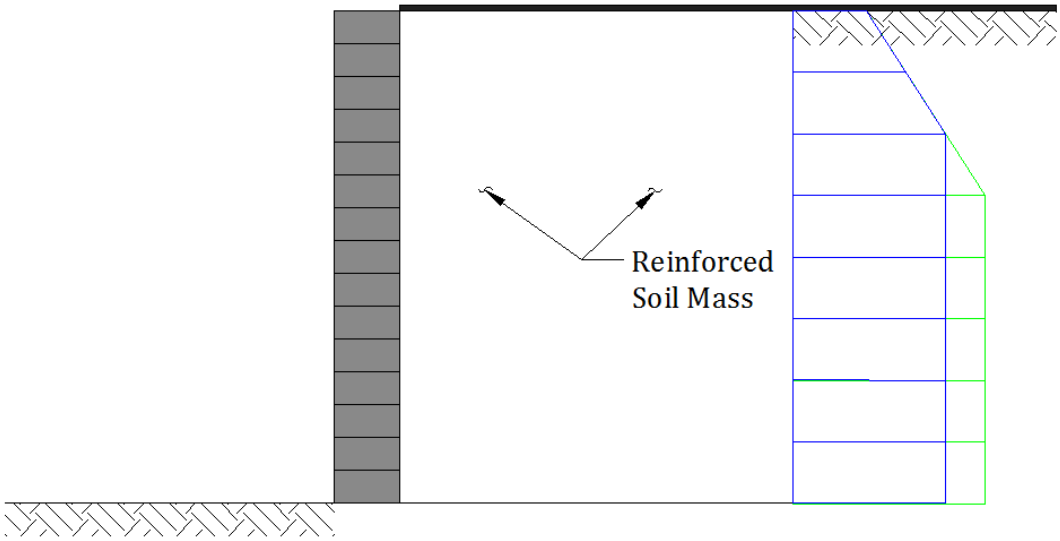

Figure 189: Horizontal Stress Variation with Increase in Wall Height

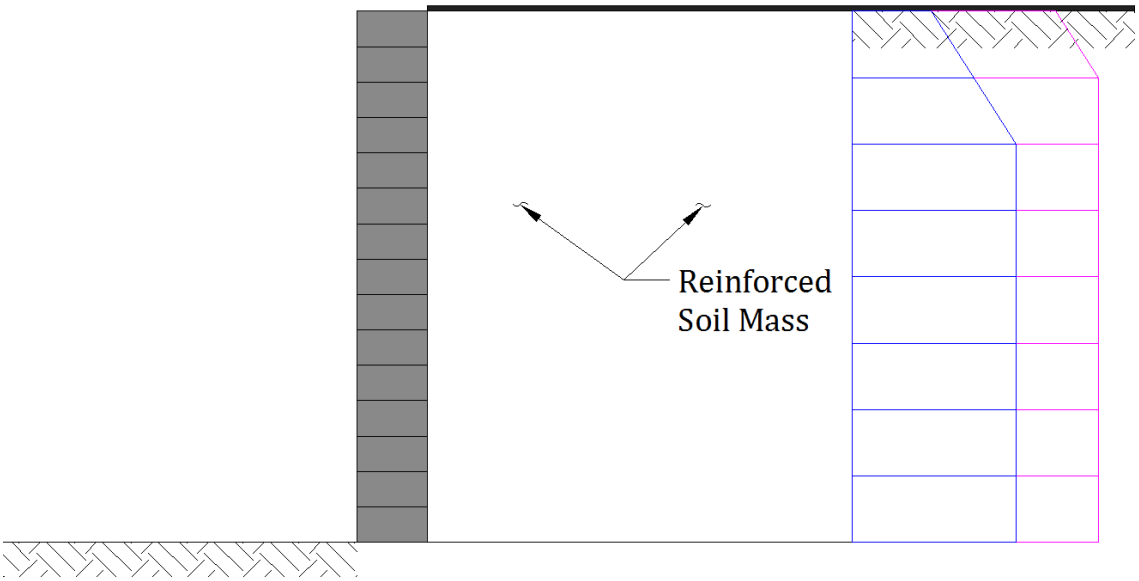

Figure 190: Horizontal Stress Distribution with Increase in Equivalent Surcharge Height

Estimation of Maximum Tension: Equation 33 defines the maximum tension carried in a reinforcement layer, T_{max}, predicted by the K-Stiffness Method. Unlike Method 1 guidance, Method 3 utilizes a series of factors to adjust the predicted tensile load to account for stiffness of various wall components. Additionally, these factors have been calibrated against field data, and predicted T_{max} values are more likely to represent values seen in the field. Other components of the T_{max} equation such as contributory height are the same as Method 1. The contributory area, which correlates to the reinforcement spacing for most layers, is recommended to be less than 2.7 feet, approximately 32 inches, for Method 3 (WSDOT 2012). The spacing or contributory area is illustrated in Figure 186.

Three of the factors incorporated in the K-Stiffness Method were given a value of 1.0 for the parametric analysis. The first was the factor to account for the effects of facing batter ϕ_{fb}; the second was the factor accounting for cohesion effects ϕ_c, and lastly the local stiffness factor ϕ_{local}. The wall utilized in the parametric analysis was vertical therefore a correction for facing batter was unnecessary. Secondly, since the backfill for the parametric analysis had no cohesion, no correction was required.

The third factor utilized in the analysis that had a value of 1.0, shown in Equation 46, was the local stiffness factor ϕ_{local}. The local stiffness factor attempts to capture the influence of reinforcement density and resulting stiffness. Therefore, it incorporates the ratio of S_{local} over S_{global}. For geosynthetics, an exponent of 1.0 is applied to this ratio. S_{local} captures the stiffness of a particular reinforcement layer and S_{global} captures the average reinforcement stiffness of the entire wall. If the same stiffness of reinforcement was utilized for the entire wall then ϕ_{local} would equal 1.0 at every reinforcement level

(Bathurst et al. 2008). If there were no stiffness in a given reinforcement layer than theoretically ϕ_{local} would equal zero. For the parametric analysis a single stiffness of reinforcement was assumed for the entire wall profile for the purpose of calculating the local stiffness factor. Therefore, ϕ_{local} equaled 1.0.

The first factor utilized in the analysis, shown in Equation 38, was the global stiffness factor ϕ_g. This factor attempts to capture the influence of the global wall stiffness and reinforcement spacing over the entire wall height. The S_{global} term is normalized by atmospheric pressure. Then, from empirically fitting data, the exponent β and coefficient α are applied, each having a value of 0.25. As the reinforcement stiffness increases, the global average reinforcement stiffness increases, which causes the predicted maximum load in the reinforcement, T_{max}, to increase due to the application of a higher ϕ_g. Additionally, as the reinforcement spacing increases, the load in the reinforcement will also increase. This is another relationship captured by ϕ_g (Bathurst et al. 2008). If there were no reinforcement in the wall then theoretically the stiffness would be zero and thus the value of ϕ_g would be zero. Additionally, the value of ϕ_g is not capped at a value of 1.0. The power function utilized in the calculation of ϕ_g was meant to be applicable for both geosynthetic reinforcement and steel strip reinforcements. Theoretically, with increasing global stiffness, ϕ_g would approach infinity; however, the values of α and β equal to 0.25 tend to keep ϕ_g at a low level. The highest value of ϕ_g from the parametric analyses was 0.496.

The second factor utilized in the analysis, shown in Equation 43 is the facing stiffness factor ϕ_{fs}. The parameter F_f defines a normalized stiffness for the facing column. As the wall face increases in height, the value of F_f decreases. This causes a reduction in rigidity, resulting in the face carrying fewer loads, and the reinforcement picks up the loads within the reinforced soil mass. Overall, as wall height increases, reinforcement load would be expected to increase (Bathurst et al. 2008). If a defect were to occur in the facing system causing deflection of the face, the reinforcement is anticipated to carry more of the load (WSDOT 2012). This behavior is captured in ϕ_{fs} (Bathurst et al. 2008). Additionally, from field observations it was noted that walls using segmental concrete blocks as facing elements had reduced reinforcement loads. For modular block systems, the parameter h_{eff} can be approximated as the height of the facing column between reinforcement layers. If multiple blocks are present between layers, they are assumed to behave as if continuous. Due to the difficulty in predicting facing stiffness for flexible facing systems, it is recommended to use a ϕ_{fs} value equal to 1.0. Additionally, wall height has a large influence on the facing stiffness factor. Due to the limited number of tall case history walls calibrated, any wall design over 35 feet tall should be approved by those with familiarity with the method, for example the Washington State Geotechnical Engineer or the K-Stiffness Method developers (WSDOT 2012).

Limit States and Load/Resistance Factor Design: The K-Stiffness method defines a particular limit state that is different than other methods; it is a soil failure limit state (Berg et al. 2009). This occurs when the soil moves from its peak strength to its residual strength. To prevent the wall from reaching this failure limit state, the strain that the reinforcement can develop over the service life of the structure must be limited. For geosynthetic reinforced soil walls, the reinforcement strain is kept below 3%. Preventing this limit state will ensure large deformations do not occur and serviceability requirements are met. In addition to the failure limits state, the K-Stiffness Method assesses the same strength limit states and extreme event cases, such as a seismic event, as Method 1 (WSDOT 2012).

The K-Stiffness Method can be applied to wall design using an LRFD platform. Application of load factors using the K-Stiffness Method is the same as Method 1 with the exception of the values applied. Permanent loads are given unique load factor ranges for the K-Stiffness Method and are detailed in the WSDOT Geotechnical Design Manual. Transient loads factors should be obtained from Method 1 guidance which utlizes the AASHTO LRFD specifications. A reisistance factor of 0.85 was utilized for the parametric analysis. This was selected after evaluating the section on safety against structural failure for external stability, specifically Table 15-8 (WSDOT 2012).

Its should be noted that Method 3 was intially developed to better correlate observed wall performance with design methods. Method 3 developers demonstrated that there is inherent conservatism built into the Simplified Procedure, Method 1, before the application of load and resistance factors. It was estimated that ignoring the effects of apparent cohesion resulted in a "hidden" conservatism in Method 1 that resulted in predictions of reinforcement loading 1.2 to 3.5 times greater than in the field. Additionally, not matching the reinforcement strength to the demand for a particular layer results in an additional "hidden" conservatism which predicts reinforcement loads 1.4 to 1.5 times that observed in field conditions. These two causes of inherent conservatism likely results in "hidden" factors of safety between 1.5 to 4. The K-Stiffness method reduces this "hidden" conservatism, and therefore its predicted reinforcement loads more closely resembling loads anticipated in field conditions (Bathurst et al. 2008).

Method 4 - NCHRP GRS Method Assumptions: The NCHPR GRS Method was the first major design methodology for GRS abutments. Its design methodology built upon an earlier publication of Method 1, the Simplified Procedure, before the inclusion of LRFD. The NCHRP Method, or Method 4, was based on an extensive literature review, full scale experiments, and a numerical study. The goal of the method was to provide revisions to the earlier publication of Method 1 in order to capture the behavior observed for GRS (Wu et al. 2006a).

Stress Transfer Mechanisms: In addition to the frictional and passive resistance developed from the interaction of reinforcement and soil particles, Method 4 briefly explores the concept of "locked-in" lateral stresses. Method 4 recommends the use of closer reinforcement spacing. It sets a limit of 16 inches and many of the test walls explored reinforcement spacing of 8 inches. The close reinforcement spacing creates a more "coherent" reinforced mass. This improvs the interaction between ths soil and the reinforcement detailed for Method 1, such as the development of frictional and passive resistance. Secondly, the benefits of quality compaction would be even greater with closer reinforcement spacing as the soil adjacent to the reinforcement could "lock-in" the lateral stresses (Wu et al. 2006a).

Long Term Strength Loss: Long term creep is considered negligible under service loads if quality fill material is used and the reinforced fill is properly compacted. For field measured conditions of GRS abutments examined for the NCHPR report, the range of reinforcement strains were 0.1 to 1.6%. It should be noted that the reinforcement strain correlated to the quality and strength of the reinforced fill material. Additionally, the reinforcement type, and thus its strength loss characteristics, was found to only have a secondary effect on wall performance in comparison to reinforced fill quality. No specific reduction factors, such as those detailed for degradation, installation damage, and creep in Method 1 guidance, are included in the design methodology for Method 4. However, a comprehensive factor of safety is applied to the required ultimate tensile strength, T_{req}, to capture long term performance issues (Wu et al. 2006a).

Reinforced Fill Properties: Method 4 stressed the importance of quality fill material. With well-graded coarse grained fill that has been compacted properly, the movements of the wall face are anticipated to be small, in comparison to a poor quality fill material. Method 4 correlated performance heavily with fill quality and specifically placement density. Method 4 also selects a range of friction angle utilized in design of 34 to 40 degrees (Wu et al. 2006a).

Lateral Earth Pressure Coefficient of the Reinforced Fill: Method 4 defines the lateral earth pressure coefficient by setting it equal to the Rankine lateral earth pressure coefficient for the active conditions (Wu et al. 2006a). This is defined in Equation 53. This is different from Method 1, which uses the Simplified Method to predict a ratio of K_r/K_a. Figure 42 was not referenced for Method 4. Even though the resulting coefficient has the same value as Method 1, the methodology used to arrive at this value is not the same.

Failure Surface Assumptions for Internal Stability: The distance the reinforcement extends into the reinforced fill material was found to have only a secondary effect on wall performance in comparison to fill quality. This would therefore diminish the benefits outlined in the Method 1 theory section of having reinforcing elements that act as "tie-

backs" into the soil mass. Nonetheless, a Rankine active earth pressure failure surface is assumed for the condition of a vertical surcharge in Method 4 guidance. The angle of inclination of the failure plane is $45 + \phi'_r/2$, and the slip surface is the same as the Coulomb surface presented in Figure 183 (Wu et al. 2006a).

Estimation of Horizontal Stresses: For the basic roadway loading scenario, Method 4 is identical to Method 1. However, for the bridge loading scenario, a different relationship was utilized in defining the change in vertical stress due to bridge loading, $\Delta\sigma_v$, than Method 1. The horizontal stress for Method 4 for the bridge loading condition is defined using Equation 52 through Equation 55. Unlike Method 1, Method 4 assumes that the relationship that defines $\Delta\sigma_v$ is not constant with depth. The width over which the vertical forces acting on the bridge sill act, defined by the variable D, varies with depth. This causes a slightly different distribution of horizontal pressures between Method 1 and 4. The predicted load at the top of the wall is higher than that predicted by Method 1. The assumptions made by Method 1 are based on principles of the load spread methodology for assessing changes in vertical pressure with depth. Method 4 is based on a modified load spread approach where the load is more concentrated at the top and spread out further towards the bottom of the wall.

Figure 191 shows an anticipated horizontal stress distribution for Method 1, shown in red, and Method 4, shown in blue. Depending on the height of the wall, the shape of the distribution at the bottom could change. A taller wall could have the distribution curving out as the stress starts to increase at the bottom. This phenomenon would be capture by both Method 1 and Method 4. Method 4 predicts a typical stress distribution expected for a bridge loading condition.

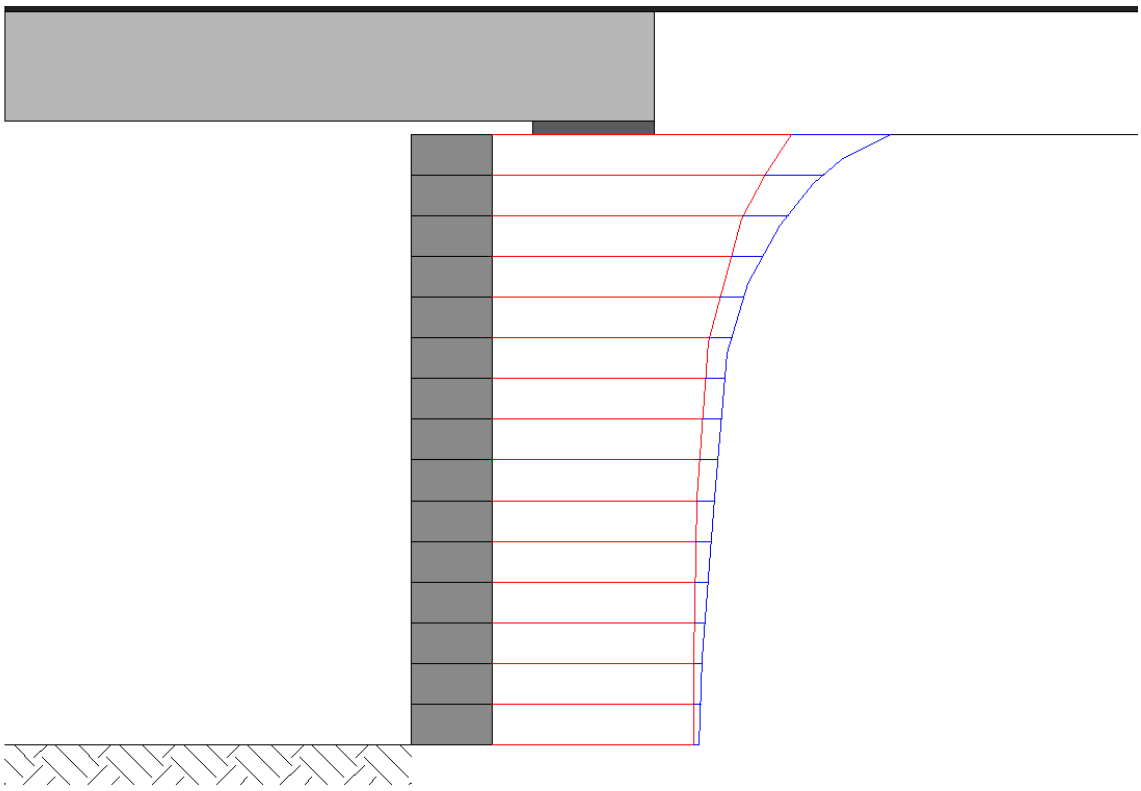

Figure 191: Horizontal Stress Distributions Predicted by Methods 1 (red) and 4 (blue) for the Bridge Loading Condition

Estimation of Maximum Tension: The relationship that defines the maximum tensile strength for a reinforcement layer for Method 4 is Equation 51. This definition is the same as Method 1 with the exception that the horizontal stress for the bridge loading case is calculated differently for the two methods. Method 4 also utilizes the contributory spacing illustrated in Figure 186.

Factors of Safety: Unlike Methods 1, 2, and 3, Method 4 does not apply a LRFD platform to its design methodology. Additionally, Method 4 applied a single recommended ultimate required tensile strength, T_{req}, to the entire soil profile instead of varying it like other methods. This calculation process is defined in Equation 56 through Equation 59.

Method 4 recommends a combined factor of safety instead of applying resistance and load factors. The factor of safety value is dependent on reinforcement spacing, as defined in the variable definitions of Equation 56 and Equation 58. This factor of safety captures uncertainties expected from construction to long term service (Wu et al. 2006a).

Method 5 - FHWA GRS-IBS Method Assumptions: GRS-IBS is a unique technology with design and construction details outlined by Method 5 references. The technology has been made an "Every Day Counts" initiative and is considered an ideal design alternative for single span bridges. Method 5 is based on a synthesis of 40 years of

research at the state and federal levels on GRS technology. GRS technology can be applied to both wall and bridge abutment loading scenarios. Method 5 guidance primarily focuses on the use of GRS for bridge abutments. Method 5 also presents two design approaches for GRS-IBS, an analytical and empirical method. The analytic approach is outlined in the governing equation section of this report. The empirical method allows for a performance test to be conducted using the proposed materials for the site. If the proposed materials are the same as the performance test with results reported in Method 5 guidance, then no test is needed. These materials can be employed directly on site as long as all material requirements are satisfied (Adams et al. 2011a).

The components of design for Method 5 are the same as Method 1; facing elements, reinforcement, and reinforced fill material. However, unlike Method 1, Method 5 assumes that the facing elements are nonstructural. Additionally, Method 5 limits the height of a reinforced soil wall to 30 feet. Bearing stress from bridge loads is also limited to 4.0 ksf. Finally, Method 5 assumes the implementation of a reinforced soil foundation (RSF). The parametric study assumed that the foundation material was competent. Other methods do not require the construction of a RSF (Adams et al. 2011a).

Stress Transfer Mechanisms: In addition to the passive and frictional resistance detailed in the Method 1 soil theory section, Method 5 explores the effects of compaction induced stresses (CIS). These stresses are developed prior to loading, when the wall is under construction. The idea is that the process of compacting the reinforced fill, especially at such close spacing, results in the transfer of stress from the soil into the reinforcement. Therefore, prior to loading and the development of passive and frictional resistance, the reinforcement is already under tension. Consequently, higher loads are required to generate movement of the GRS mass than predicted by other methodologies (Adams et al. 2011b).

Long Term Strength Loss: The anticipated creep deformation of a select coarse grained fill material is considered to be low. The creep rate of the geosynthetic reinforcement is dependent on the interaction it has with the reinforced fill soil. If the creep of the soil is low, the geosynthetic creep will likely be small. Method 5 guidance estimates that the creep of the soil and geosynthetic will not exceed the value at the end of construction. Additionally, due to the close reinforcement spacing exhibited in a GRS mass, the confinement plays a role in the long term performance of the wall. The reinforcement and the soil strain together, and the resulting movements are considered to be very low (Adams et al. 2011b).

To account for difference in load deformation behavior of varying reinforcement polymer types, an additional tensile strength check is required for Method 5. The additional check requires that the nominal tensile load carried by the reinforcement, T_{max}, be less than the reinforcement's tensile strength at 2% strain. If T_{max} is greater than the tensile strength at 2% strain, then an alternative reinforcement should be selected (Adams et al. 2011a).

The procedure utilized for evaluating this requirement for the parametric analysis is detailed in Equation 72, Equation 73, Equation 77, and Equation 78 (Adams et al. 2011a).

Additionally, it should be noted that the resistance factor applied for the LRFD analysis in Appendix C of the FHWA-HRT-11-02 Report accounts for creep, durability, and installation damage. No additional reduction factors were applied for these mechanisms of strength loss (Adams et al. 2011b).

Reinforced Fill Properties: The reinforced fill is considered structural in nature. Only coarse grained fill is recommended for use by Method 5 guidance. The friction angle of the reinforced fill must be at least 38°. If submergence is ever a concern, an open graded gravel that allows for drainage should be employed. The parametric analysis assumed no water would be present in the fill. Maximum aggregate size is limited to 2 inches to ensure proper compaction. Fines content should not exceed 12 percent. Method 5 guidance provides information regarding gradation. In nearly all cases the cohesion is assumed to be zero for the reinforced fill; though if cohesion will be present during the service life of the structure, a relationship is provided to capture its effects (Adams et al. 2011b). Cohesion was not incorporated into the parametric analysis.

Lateral Earth Pressure Coefficient of the Reinforced Fill: Method 5 defines the lateral earth pressure coefficient by setting it equal to the Rankine lateral earth pressure coefficient for the active condition (Adams et al. 2011a). This is defined in Equation 53. This is different from Method 1, which uses the Simplified Method to predict a ratio of K_r/K_a. Figure 42 was not referenced for Method 5. Even though the resulting coefficient has the same value as Method 1, the methodology used to arrive at this value is not the same.

Failure Surface Assumptions for Internal Stability: Method 5 assumes that a GRS mass is internally stable and freestanding without the requirement of facing elements being in place (Adams et al. 2011b). No active Rankine failure wedge is considered to develop behind the wall face as detailed in Methods 1 and 4. Therefore reinforcement length is not dependent on identifying the boundary between an active zone and an anchorage zone. Instead, the minimum reinforcement length is recommended to have a base to height ratio of 0.3 at the lowest level. The reinforcement length is then recommended to follow the cut slope of the backfill. This continues up to a point where a base to height ratio of 0.7 is achieved if applicable (Adams et al. 2011a).

Estimation of Horizontal Stresses: For the basic roadway loading scenario, Method 5 is identical to Method 1 in predicting nominal lateral earth pressure. The factored form of the equation is different and is shown in Equation 62 for Method 5. The distribution of lateral earth pressure will have a triangular shape typically assumed for wall loading.

For the bridge loading scenario, a different relationship was utilized in defining the horizontal earth pressure in comparison to the other methods. The horizontal stress for Method 5 for the bridge loading condition is defined using Equation 64 and Equation 69.

The anticipated difference in nominal horizontal stress between Methods 1 and 5 is shown in Figure 192. Method 1 is in red and Method 5 in blue. Depending on the wall height and bridge load, the distribution of Method 5 could intersect that of Method 1 at different locations. Method 5 has a more pronounced curved shape in comparison to Method 1.

The more pronounced shape is likely due to the fact that horizontal stress for Method 5 is dependent on shape factor angles α and β while other methods do not include these parameters. α and β are derived from applying Boussinesq load distribution theory to the reinforced zone soil mass under bridge loads which act on the bearing pad. (Adams et al. 2011a). This approach of estimating the change in stress with depth is different than Methods 1 and 4, which utilize the load spread methodology principals and separate relationships for $\Delta\sigma_v$ and $\Delta\sigma_h$.

Additionally, Method 5 assumes there is no thrust force acting on the wall face from lateral pressures induced from bridge loading. Any thrust that is generated within the reinforced zone will be taken up by the reinforcement and none will transmit to the wall face. This phenomena is explained by Bin Pressure Theory (Adams et al. 2011b).

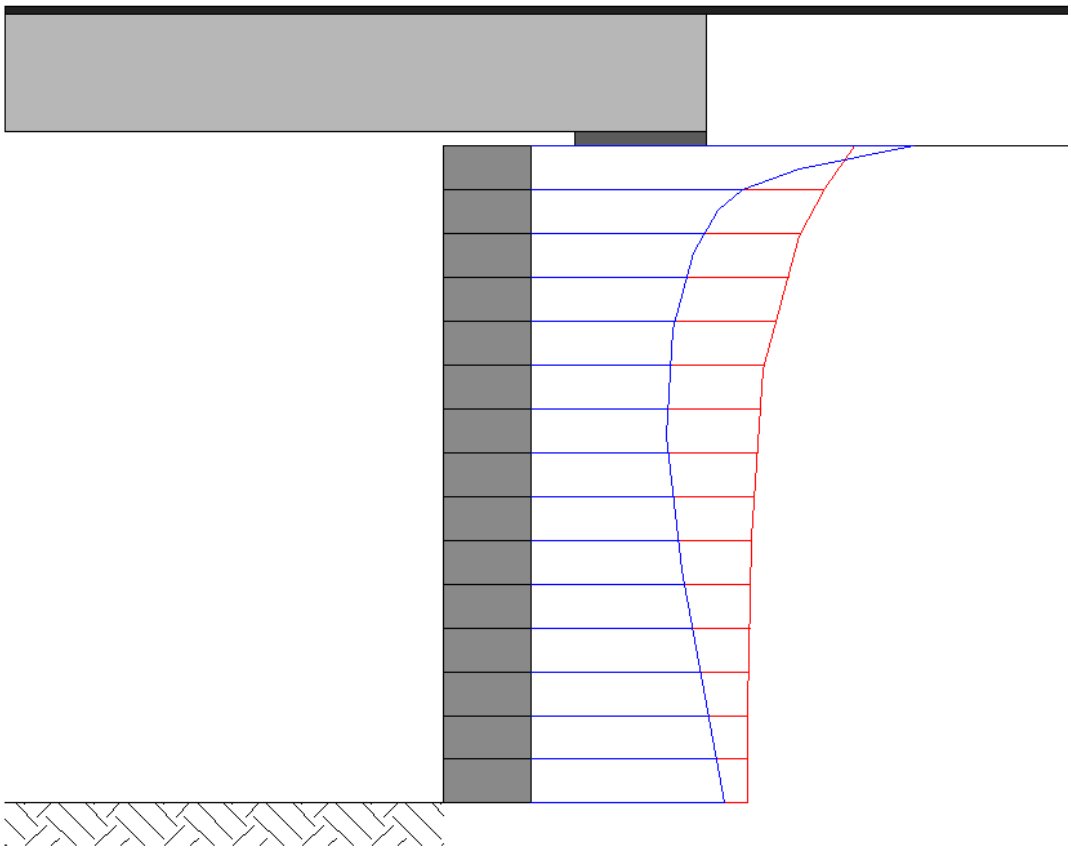

Figure 192: Horizontal Stress Distribution Predicted by Methods 1 (red) and 5 (blue) for the Bridge Loading Condition

Estimation of Maximum Tension: The relationship utilized by Method 5 guidance for determination of tensile load in the reinforcement, shown in Equation 63 and Equation 68, is quite different from other methods. The relationship depends on an additional variable not used in other methods, d_{max}, which is the maximum diameter of the aggregate. The form of the equation is designed to capture an additional aspect of the behavior of a composite reinforced soil mass called compaction induced stresses (CIS). These stresses are "locked in" stresses as similarly described in Method 4 guidance. Due to the influence of CIS, a higher lateral load than previously thought would be needed to generate movement of the reinforced soil mass (Adams et al. 2011b).

The ultimate tensile capacity of a GRS mass is a function of the quality of the soil, specifically the friction angle and maximum aggregate size, the reinforcement strength, and reinforcement spacing. The reinforcement spacing is thought to have a much higher influence on ultimate tensile capacity than the reinforcement strength (Adams et al. 2011b). The reinforcement spacing is equivalent to the contributory height illustrated in Figure 186.

Limit States and Load/Resistance Factor Design: The FHWA GRS-IBS Method, Method 5, designs for particular strength and extreme event limit states and provides an LRFD design approach in the Appendices of the FHWA-HRT-11-02 Report. The LRFD procedure outlined by Method 5 predicts the same values as the ASD procedure presented in the main body of the guidance document. Load factors for Method 5 are detailed in Table 16 of Appendix C of the FHWA-HRT-11-02 Report. Unlike Method 1 and 3, which use resistance factors of 0.9 and 0.85 respectively, Method 5 recommends a much lower value of 0.4. This resistance factor is meant to account for the uncertainties of reinforcement strength, such as creep, durability, and installation damage. The final T_{req} predictions using the recommended resistance factor and load factors will produce an equivalent solution to that predicted using the ASD approach with a FS=3.5 presented in the main body of the report. It should be noted that LRFD methodology for internal stability is still evolving. There is not a lot of statistical data on GRS, and as more information is gathered factors may be adjusted in the future (Adams et al. 2011a).

4.2 DEGREE OF PARAMETER INFLUENCE

This section explores which parameters influenced the predicted require reinforcement strength the most for each of the methods. Particular parameters drove predicted behavior for multiple methods, while others only influenced a single method.

Parametric study results showed that all methods were sensitive to wall height for the roadway loading condition. The increase in wall height from the base case value of 16 feet to the highest variation of 28 feet resulted in large percent increases in the highest reported ultimate tensile strength required, T_{req}. Methods 1, 4, and 5 predicted the same level of increase, 68%. Increases predicted by other methods included 55% for Method 2 and 113% for Method 3. For the bridge loading condition, the wall height has no

influence on highest predicted T_{req} value because the largest value occurs at the top of the wall profile for the bridge load used in the base case. However, it can still be concluded that all methods have a high degree of sensitivity to wall height.

All methods were sensitive to friction angle of the reinforced fill. The increase in friction angle from the base case value of 38° to 55° resulted in a 49% decrease in predicted T_{req} values for the roadway loading condition for Methods 1 and 2. The decrease was even greater for the other methods. Methods 4 and 5 had decreases of 58% for the roadway loading case. And for Method 3, a decrease of 75% was predicted. For the bridge loading scenario, Methods 1 and 2 predict decreases of 46% and 45%, respectively. Method 3 is not applicable for the bridge loading condition. Method 4 and 5 predict decreases of 57% and 58% respectively.

The variation of maximum grain size of the reinforced fill only influences Method 5. However, the highest predicted T_{req} value for Method 5 is quite sensitive to this parameter. Method 5 defines all tensile values in terms of this parameter. Increasing the maximum aggregate size from 0.5 inches, the base case, to 2 inches results in a 51% decrease in highest predicted T_{req} value for both the roadway and bridge loading condition.

Unit weight of the reinforced fill was not as influential as other soil properties. Unit weight was increased from 125 pcf, the base case value, to 150 pcf as part of the parametric study. This increase resulted in a 20% increase in the highest predicted T_{req} values for all methods for the roadway loading condition. All methods were less sensitive to unit weight for the bridge loading scenario because the highest predicted T_{req} value occurs at the top of the wall profile. Thus, only the influence unit weight has on the equivalent soil surcharge plays a role in increasing T_{req} for the bridge loading case.

The variation in reinforcement spacing, which can also be thought of as the tributary area or contributory height, results in major changes to the highest predicted T_{req} value, especially for Method 5. Method 5 is not meant to have spacing values exceeding 12 inches. The parametric study pushed the variation past this boundary solely for the purpose of investigating the nature of the relationship. The spacing was varied from 8 inches, the base case up to 24 inches, a typical MSEW spacing. This increase for the roadway loading condition produced increases of 186% for Method 1, 192% for Method 2, 128% for Method 3, 83% for Method 4, and 1,834% for Method 5. For the bridge loading condition, increases were 183% for Method 1, 182% for Method 2, 65% for Method 4, and 1,451% for Method 5. Method 3 is not applicable for bridge loading.

The variation in facing block size, h_{eff} by *b*, only influences Method 3 for the roadway loading condition. Increasing in block size from an 8 inch by 12 inch block to a 24 inch by 48 inch block results in a 44% decrease in the highest predicted T_{req} value. Therefore, it can be concluded that Method 3 is sensitive to facing block size.

All methods that assess bridge loading conditions are influenced by bridge loads, both live loads and dead loads. Dead load was increased from the base case of 3.34 ksf to 6.5 ksf. This increases resulted in an increase in predicted T_{req} value of 43% for Method 1, 40% in Method 2, 39% for Method 4, and 46% for Method 5. Live load increase from 3.34 ksf to 5.5 ksf resulted in T_{req} increases of 29% for Method 1, 27% for Method 2 and 4, and 37% for Method 5. For all methods except Method 5, the increases in T_{req} for dead loads and live loads are similar if the difference in load increase is accounted for. For Method 5, the increase in T_{req} for live loads is larger than would be expected based on the increase for dead loads, this is due to the application of different load factors for each quantity.

The variation for the bridge loading condition of certain geometries, such as sill width, setback distance, and upper wall height, produced lower percentages changes in highest predicted T_{req} value than other parameters. All percentage changes were less than 25% for all applicable methods and in some cases quite low. Methods 1, 2, 4 are considered to be sensitive to setback distance, but the influence is smaller for Method 4. Method 5 does not incorporate setback distance. Methods 1, 2, 4, and 5 are all sensitive to sill width and upper wall height, with Method 5 being the least sensitive for both parameters.

In summary, the parameters that are the most influential across all methods are wall height, reinforcement spacing, and friction angle. For individual methods, Method 5 is significantly influenced by maximum grain size and Method 3 by facing block size. For the bridge loading condition, the bridge load magnitude is important. Of these most influential parameters, if one parameter was selected as the most influential for the required ultimate tensile strength, T_{req}, in a wall, it would be reinforcement spacing.

4.3 CONCLUSIONS

For the base case wall, the geometry, reinforcement spacing, and fill material selected were representative of a typical GRS wall. Utilizing the characteristics of GRS while following other design analysis methods yielded valuable comparisons.

For the roadway loading condition, the nominal lateral earth pressures, σ_h, predicted by Methods 1, 4, and 5 were identical. Method 2, the FHWA Simplified Procedure with K_r/K_a Adjusted, predicted the lowest lateral earth pressure values for the entire reinforced zone profile. Method 3, the K-Stiffness Method, predicted higher lateral earth pressures at the top of the profile and lower pressures at the bottom in comparison to Methods 1, 4, and 5. For the roadway loading condition, the nominal predicted tensile loads, T_{max} values, were highest for Method 5, the FHWA GRS-IBS Method, and lowest for Method 3, the K-Stiffness Method. Due to the fact that the K-Stiffness Method was calibrated against case history field data, it may reasonably be assumed that the tensile loads predicted by the method would most closely resemble anticipated field measurements from instrumentation. However, the database of case histories for Method 3 does not include many walls with close reinforcement spacing characteristic of GRS.

Even though Method 5 has the same predicted σ_h as some of the other Methods, the differences in the relationship for determining T_{max} result in large differences in anticipated tensile load carried by the reinforcement for the roadway loading condition. The application of Method 5 to roadway loading scenarios may prove conservative compared to the other methods.

When factors of safety, reduction factors, load and resistance factors and other limiting conditions are added to the relationship to produce a required ultimate tensile value, T_{req}, needed for design, an extra degree of complexity is added to the comparison for the roadway loading condition. This comparison is presented in Figure 46. It can be concluded that for a design engineer, selecting which method should be employed over another is not always straight forward and the variation in T_{req} final results can be great.

For the bridge loading condition, the nominal lateral earth pressure, σ_h, predicted by Methods 1, 2, 4, and 5 was compared. Method 3 is not applicable for the bridge loading condition. Method 2 predicted the lowest lateral earth pressure values at the top and bottom of the reinforced zone profile. Method 5 predicted the lowest values for the center portion. Method 4, the NCHRP GRS Method, predicted the highest values for the entire profile. All methods predict a distinct curved shaped distribution anticipated for the bridge loading scenario, with Method 5's distribution being the most pronounced. For the bridge loading condition, the nominal predicted tensile loads, T_{max} values, were highest for Method 5 and lowest for Method 2. There is no ideal comparison to anticipated field values at this time for the bridge loading condition. Therefore, it is difficult to assess whether one method is more accurate than another.

Once factors of safety, reduction factors, load and resistance factors and other limiting conditions are added to the relationship to produce a required ultimate tensile value, T_{req}, needed for design, an extra degree of complexity is added to the comparison for the bridge loading condition. This comparison is presented in Figure 50. Similar to the roadway loading case, for the bridge loading condition, selection of appropriate methods to employ is challenging. Additionally, the relationships utilized by the various methods compared to predict T_{req} produce a wide variety of final values.

Finally, it should be noted that if a limit exists where behavior of the wall systems transitions from GRS to MSEW, this change is not reflected in predictive relationships presented for each design analysis method for the roadway loading condition. Only one of the analysis methods, Method 5, captures the effects of compaction induced stresses for determining tensile load, but the limit of when this interaction no longer applies seems arbitrarily set at 12 inches, the maximum spacing allowed by the design method. MSEW design methods do not consider this issue. If Method 5 is utilized for a wall with spacing as high as 24 inches, the predictive relationship results in an enormous tensile load in comparison to other methods, which is likely not accurate.

At this time, the results of this study can be used to evaluate influential parameters and to evaluate difference in predictive relationships for tensile load and ultimate required tensile strength for a variety of methods. However, the most critical conclusion of this study is that not all methods predict similar results. Furthermore, this variation in predicted results could be inaccurate and costly. Further investigation and clarity regarding selection of design guidance for reinforced soil systems is needed.

4.4 RECOMMENDATIONS FOR FUTURE WORK

In order to ascertain a degree of accuracy in the predictions for each method compared in the parametric study, a comparison against field instrumented data is needed. A closer look at how the reinforcement tensions at each reinforcement layer, throughout the reinforced zone, would provide valuable insight. There have been instrumented bridge supports but often only at one or two reinforcement layer elevations. A full exploration of how each reinforcement layer tensions and strains overtime is needed. For the roadway loading condition, the predictions made by Method 3, the K-Stiffness Method, have been calibrated to reflect in-service tensile loads. The methodology was based on instrumented data gathered from a variety of walls with varying surcharge load and geometries. A similar comprehensive investigation has not been performed to date for reinforced walls supporting bridge abutments. Additionally, case histories that would classify as GRS could be added to the K-Stiffness Method calibration. An exploration of parameter influence based on field data is needed. A field investigation which examines the effects of close reinforcement spacing on tension at each reinforcement layer for both a roadway and bridge loading condition would prove valuable. Understanding how close design analysis methods predict tensile values in comparison to field conditions is a critical step in understanding how and when to use the many available reinforced soil analysis methods.

Another useful approach would be to validate a comprehensive numerical analysis against the instrumented GRS data that is available, even though that data is not as comprehensive as would be ideal. Then, the validated numerical model could be used in a parameter study to conduct numerical investigations to determine which existing analysis methods best agree with the numerical analyses over a realistic range of parameter values. Such a study could be used to help establish which existing analysis method is most accurate and reliable, and whether modifications are necessary.

Test results, case history data, and validated numerical analyses could also be used to evaluate potential differences and boundaries/transitions between MSEW and GRS response. If different analysis and design procedures are needed for each, then such studies could be used to help define the boundaries and transitions, which would benefit engineers greatly and reduce confusion surrounding the selection of design methodology and philosophy.

Lastly, a full cost comparison against typical MSEW walls without deep foundation elements for a bridge loading condition should be compared against GRS-IBS. A comparison of anticipated labor costs and material cost would prove valuable. GRS-IB is known to be more cost effective than bridge abutments using deep foundations, but the extent of its cost savings when compared to MSEW abutments with small spread footings supporting bridge loads is unclear. Additionally, a comparison of both GRS and MSEW walls that do not support additional structures, using the typical range of design properties unique to each design philosophy, would be insightful.

REFERENCES

Abu-Hejleh, N., Outcalt, W., Wang, T., and Zornberg, J. G. (2000a). "Performance of Geosynthetic Reinforced Walls Supporting the Founders/Meadows Bridge and Approaching Roadway Structures - Report 1: Design, Materials, Construction, Instrumentation, and Preliminary Results." *CDOT-DTD-R-2000-5*, Colorado Department of Transportation, Denver, CO.

Abu-Hejleh, N., Wang, T., and Zornberg, J. G. (2000b). "Performance of Geosynthetic-Reinforced Walls Supporting Bridge and Approaching Roadway Structures." *Advances in Transportation and Geoenvironmental Systems Using Geosynthetics*, ASCE, Reston, VA, 218-243.

Abu-Hejleh, N., Zornberg, J. G., Wang, T., McMullen, M., and Outcalt, W. (2001). "Performance of Geosynthetic-Reinforced Walls Supporting the Founders/Meadows Bridge and Approaching Roadway Structures-Report 2: Assessment of the Performance and Design of the Front GRS Walls and Recommendations for Future GRS Abutments." *CDOT-DTD-R-2001-12*, Colorado Department of Transportation, Denver, CO.

Abu-Hejleh, N., Zornberg, J. G., Wang, T., and Watcharamonthein, J. (2002). "Monitored Displacements of Unique Geosynthetic-Reinforced Soil Bridge Abutments." *Geosynthetics International*, 9(1), 71-95.

Adams, M. (1997). "Performance of a Prestrained Geosynthetic Reinforced Soil Bridge Pier." *Proc., International Symposium on Mechanically Stabilized Backfill*, J.T.H. Wu (Ed) A.A. Balkema, Rotterdam, 35-53.

Adams, M., Ketchart, K., Ruckman, A., DiMillio, A. F., Wu, J. T. H., and Satyanarayana, R. (1999). "Reinforced Soil for Bridge Support Applications on Low-Volume Roads." Transportation Research Board, Washington, D.C.

Adams, M., Ketchart, K., and Wu, J. T. H. (2007a). "Mini Pier Experiments: Geosynthetic Reinforcement Spacing and Strength as Related to Performance." *Geosynthetics in Reinforcement and Hydraulic Applications (GSP 165)*, Gabr, and Bowders (Eds.), Reston, VA, 98-106.

Adams, M., Lillis, C. P., Wu, J. T. H., and Ketchart, K. V. (2002). "Vegas GRS Mini Pier Experiment and the Postulate of Zero Volume Change." *Proc., 7th International Conference on Geosynthetics*, P. Delmas, J. P. Gourc, and H. Girard (Eds.). Swets & Zeitlinger, Lisse, France, 389-394.

Adams, M., Nicks, J., Stabile, T., Wu, J. T. H., Schlatter, W., and Hartmann, J. (2011a). "Geosynthetic Reinforced Soil Integrated Bridge System—Interim Implementation Guide." *FHWA-HRT-11-026*, Federal Highway Administration, McLean, VA.

Adams, M., Nicks, J., Stabile, T., Wu, J. T. H., Schlatter, W., and Hartmann, J. (2011b). "Geosynthetic Reinforced Soil Integrated Bridge System—Synthesis Report." *FHWA-HRT-11-027*, Federal Highway Administration, McLean, VA.

Adams, M., Schlatter, W., and Stabile, T. (2007b). "Geosynthetic-Reinforced Soil Integrated Abutments at the Bowman Road Bridge in Defiance County, Ohio." *Geosynthetics in Reinforcement and Hydraulic Applications (GSP 165)*, Gabr, and Bowders (Eds.). ASCE, Reston, VA, 119-129.

Allen, T., Christopher, B., Elias, V., and DiMaggio, J. (2001). "Development of the Simplified Method for Internal Stability Design of Mechanically Stabilized Earth Walls." *WA-RD 513.1*, Washington State Department of Transportation, U.S. Department of Transportation, Federal Highway Administration.

Allen, T. M., and Bathurst, R. J. (2003). "Prediction of Reinforcement Loads in Reinforced Soil Walls." *WA-RD 522.2*, Washington State Department of Transportation, Seattle, WA.

Allen, T. M., and Bathurst, R. J. (2013). "Comparison of Working Stress and Limit Equilibrium Behavior of Reinforced Soil Walls." *ASCE Geotechnical Special Publication*, 230, 499-513.

Barrett, R., and Ruckman, A. (2007). "GRS – A New Era in Reinforced Soil Technology." *Geosynthetics in Reinforcement and Hydraulic Applications (GSP 165)*, Gabr, and Bowders (Eds.). ASCE, Reston, VA, 153-164.

Bathurst, R. J., Miyata, Y., Nernheim, A., and Allen, A. M. (2008). "Refinement of K-stiffness Method for Geosynthetic Reinforced Soil Walls." *Geosynthetics International*, 15(4), 269-295.

Berg, R. R. (2013). "Simplified Procedure with Kr/Ka Adjusted." E. K. Phillips, ed.

Berg, R. R., Allen, T. M., and Bell, J. R. (1998). "Design Procedures for Reinforced Soil Walls- A Historic Perspective." *Sixth International Conference on Geosynthetics*.

Berg, R. R., Christopher, B. R., and Samtani, N. (2009). "Mechanically Stabilized Earth Walls and Reinforced Slopes, Design and Construction Guidelines." *Vol. I* -

FHWA-NHI-10-024, Vol. II – FHWA-NHI-10-025, Federal Highway Administration, Washington, D.C.

Berg, R. R., Collin, J. G., and Bell, J. R. (1998). "Design Procedures for Reinforced Soil Walls- A Historic Perspective." *Sixth International Conference on Geosynthetics*.

Carter, J. P., and Balaam, N. P. (1990). "Program AFENA, A General Finite Element Algorithm." Center for Geotechnical Research, Univerity of Sydney, NSW Australia.

Christopher, B. R., Holtz, R. D., Berg, R. R., and Stulgis, R. P. (2013). "Reinforced Soil Walls and Slopes: In Retrospect (i.e. The Good, the Bad, and the Ugly)."

Elton, D. J., and Patawaran, M. A. B. (2004). "Mechanically Stabilized Earth Reinforcement Tensile Strength from Tests of Geotextile-Reinforced Soil." Transportation Research Board, Washington, D.C.

FHWA (2011). "Geosynthetic Reinforced Soil Integrated Bridge System (GRS-IBS)." *Every Day Counts Presentation*, U.S. Department of Transportation.

FHWA (2011). "GRS-IBS Case Study: The Bowman Bridge." <http://www.fhwa.dot.gov/bridge/abc/grscasestudy.cfm>. (February 5, 2014).

Gotteland, P., Gourc, J. P., and Villard, P. (1997). "Geosynthetics Reinforced Structures as Bridge Abutments: Full Scale Experimentation and Comparison with Modelisations." *Proc., International Symposium on Mechanically Stabilized Backfill*, J. T. H. Wu (Ed.) A.A. Balkema, Rotterdam, 25-34.

Hallquist, J. O., and Whiley, R. G. (1989). "Dyna3d User's Manual: Nonlinear Dynamics Analysis of Structures in Three Dimensions." *Rep. UCID-19592*, University of California, Lawrence Livermore National Laboratory, Rev. 5.

Helwany, S. M. B., Wu, J. T. H., and Froessl, B. (2003). "GRS Bridge Abutments - An Effective Means to Alleviate Bridge Approach Settlement." *Geotextiles and Geomembranes*, 21(3), 177-196.

Helwany, S. M. B., Wu, J. T. H., and Kitsabunnarat, A. (2007). "Simulating the Behavior of GRS Bridge Abutments." *Journal of Geotechnical and Geoenvironmental Engineering*, 133(10), 1229-1240.

Keller, G. R., and Devin, S. C. (2003). "Geosynthetic-Reinforced Soil Bridge Abutments." Transportation Research Board, Washington, D.C.

Ketchart, K., and Wu, J. T. H. (1997). "Performance of Geosynthetic-Reinforced Soil Bridge Pier and Abutment." *Proc., International Symposium on Mechanically Stabilized Backfill*, J. T. H. Wu (Ed.) A.A.Balkema, 101-116.

Ketchart, K., and Wu, J. T. H. (2002). "A Modified Soil-Geosynthetic Interactive Performance Test for Evaluating Deformation Behavior of GRS Structures." *Geotechnical Testing Journal*, 25(4), 405-413.

Kost, A., Filz, G., and Cousins, T. (2014). "Differential Settlement of a GRS Abutment: Full-Scale Investigation." *Virginia Center for Transportation Innovation and Research* Charlottesville, VA.

Kost, A., Santacruz, K., and Filz, G. (2013). "Technology Summary: Geosynthetic-Reinforced Soil Interated Bridge System (GRS-IBS)." The Charles E. Via, Jr. Department of Civil and Environmental Engineering, Virginia Tech.

Lee, K. Z. Z., and Wu, J. T. H. (2004). "A Synthesis of Case Histories on GRS Bridge-Supporting Structures with Flexible Facing." *Geotextiles and Geomembranes*, 22(4), 181-204.

Mohamed, K., Abouzakhm, M., and Elias, M. (2011). "Applications and performance of geosynthetic-reinforced soil abutments on soft subsurface soil conditions.", Transportation Research Board.

Nguyen, Q. (2012). "GRS Abutments for Bridge Replacement National Wildlife Refuge." A New Era of Partnerships - Investing in America's Treasures, U.S. Department of Transportation, FHWA, EFLHD.

Ohta, H., and Iizuka, A. (1986). "DACSAR, Deformation Analysis Considering Stress Anisotropy and Reorientation." *Soil Mechanics and Foundation Engineering Lab Report*, Department of Civil Engineering, Kanazawa Univeristy, Japan.

Pham, T. (2009). "Investigating Composite Behavior of Geosynthetic-Reinforced Soil (GRS) Mass." University of Colorado at Denver, Denver, CO.

Skinner, G. D., and Rowe, R. K. (2005). "Design and Behaviour of a Geosynthetic Reinforced Retaining Wall and Bridge Abutment on a Yielding Foundation." *Geotextiles and Geomembranes*, 23(3), 234-260.

Wang, T. (2002). "Case History of GRS Abutment." Workshop on Geotechnical Composite Systems, Sponsored by National Science Foundation and Virginia Tech, Roanoke, VA.

Warren, K. A., Schlatter, W., Adams, M., Stabile, T., and LeGrand, D. (2010). "Preliminary Results for a GRS Integrated Bridge System Supporting a Large Single Span Bridge." *Proc., Earth Retention Conference 3*, ASCE, Reston, VA, 612-619.

Warren, K. A., Whelan, M., Adams, M., and Nicks, J. (2013). "Preliminary Evaluation of Thermally Induced Strains and Pressured Developed in GRS Integrated Bridge System." *Geosynthetics Conference* Long Beach, CA.

WSDOT (2012). "Geotechnical Design Manual." *M6-03.07*, Environmental and Engineering Programs, Geotechnical Services.

Wu, J. T. H. (2007). "Lateral Earth Pressure against the Facing of Segmental GRS Walls." *Geosynthetics in Reinforcement and Hydraulic Applications (GSP 165)*, Gabr, and Bowders (Eds.). ASCE, Reston, VA, 165-175.

Wu, J. T. H., and Adams, M. (2007). "Myth and Fact on Long-Term Creep of GRS Structures." *Geosynthetics in Reinforcement and Hydraulic Applications (GSP 165)*, Gabr, and Bowders (Eds.). ASCE, Reston, VA, 107-118.

Wu, J. T. H., and Helwany, S. M. B. (1996). "A Performance Test for Assessment of Long-Term Creep Bhavior of Soil-Geosynthetic Composites." *Geosynthetics International*, 3(1), 107-124.

Wu, J. T. H., Ketchart, K., and Adams, M. (2001). "GRS Bridge Piers and Abutments." *FHWA-RD-00-38*, Federal Highway Administration, McLean, VA.

Wu, J. T. H., Ketchart, K., and Crouse, P. E. (1997). "How to Assess Long-Term Deformation of a GRS Structure?" *Proc., International Symposium on Mechanically Stabilized Backfill*, J. T. H. Wu (Ed.) A.A.Balkema, Rotterdam, 345-350.

Wu, J. T. H., Lee, K. Z. Z., Helwany, S. M. B., and Ketchart, K. (2006a). "Design and Construction Guidelines for GRS Bridge Abutment with a Flexible Facing." *Report No. 556*, National Cooperative Highway Research Program, Washington, D.C.

Wu, J. T. H., Lee, K. Z. Z., and Pham, T. (2006b). "Allowable Bearing Pressures of Bridge Sills on GRS Abutments with Flexible Facing." *Journal of Geotechnical and Geoenvironmental Engineering*, 132(7), 830-841.

Wu, J. T. H., Pham, T. Q., and Adams, M. T. (2013). "Composite Behavior of Geosynthetic Reinforced Soil Mass." *Publication No. FHWA-HRT-10-077*., Federal Highway Administration, McLean, VA.

APPENDIX

Table A1: Variable Definitions

NA	Not Applicable
	Not defined in the method but information from other sources was utilized to define parameter
	Not specifically defined in the method but parameter can be established from other parameters in the same method
	Not defined or utilized in the method

		Variable Definition					
Parameter Definition	*Units*	*Method*					*Parametric Analysis*
		1	2	3	4	5	
Maximum factored load in the reinforcement	plf	T_{max}	T_{max}			$T_{req,f}$	$T_{max,f}$
Factored horizontal stress	psf	σ_H	σ_H			$\sigma_{h,f}$	$\sigma_{h,f}$
Reinforcement spacing	ft	S_v	S_v	S_v	s	S_v	S_v
Facing Block Height	ft			h_{eff}			
Lateral earth pressure coefficient of the reinforced fill	NA	K_r	K_r	K	$K_{a(rf)}$	K_{ar}	K_r
Unit weight of the reinforced fill	pcf	γ_r	γ_r	γ_r	γ_{rf}	γ_r	γ_r
Depth below top of reinforced zone	ft	Z	Z	z	z	z	z
Equivalent uniform soil surcharge height	ft	h_{eq}	h_{eq}	s	h_{eq}	h_{eq}	h_{eq}
Load factor corresponding to a vertical pressure from a dead load earth fill	NA	$\gamma_{EV\text{-}MAX}$	$\gamma_{EV\text{-}MAX}$	γ_{EV}			$\gamma_{EV\text{-}MAX}$
Rankine lateral earth pressure coefficient for the	NA	K_a	K_a	K_a	K_a	K_a	K_a

active condition							
Peak secant plane strain reinforced fill friction angle	Deg.			ϕ_{ps}			ϕ_{ps}
Friction angle of the reinforced fill	Deg.	ϕ'_r	ϕ'_r		ϕ'_{rf}	ϕ_r	ϕ'_r
Maximum nominal load in the reinforcement	plf			T_{max}	T_{max}	T_{req}	T_{max}
Nominal horizontal stress	psf				σ_h	σ_h	σ_h
Height of the upper wall also known as the back wall	ft	h	h		H_2	h	h
Unit weight of the upper wall soil	pcf	γ_2	γ_2		γ_2		γ_u
Nominal vertical pressure at the base of the bearing pad	psf	$\Delta\sigma_{v\text{-footing}}$	$\Delta\sigma_{v\text{-footing}}$		$\Delta\sigma_v$		$\Delta\sigma_v$
Load factor corresponding to earth surcharge loading	NA	$\gamma_{P\text{-}ES}$	$\gamma_{P\text{-}ES}$			$\gamma_{ES\text{-}MAX}$	$\gamma_{ES\text{-}MAX}$
Nominal horizontal pressure from upper wall	psf	$\Delta\sigma_H$	$\Delta\sigma_H$		$\Delta\sigma_h$		$\Delta\sigma_h$
Nominal load on the base of the bearing pad	plf	P_{wL}	P_{wL}				P_{wL}
Sill width or width of the bearing pad	ft	b_f	b_f		B	b	b
eccentricity from the center of bearing pad	ft	e_f	e_f		e'		e
Clear or setback distance	ft	c_f	c_f		d		d
Sum of the nominal vertical forces from the bearing pad	plf	V_{Ab}	V_{Ab}		ΣV_A		V_{Ab}

Nominal vertical load from the weight of the bearing pad	plf	V_1	V_1		V1		V_1
Nominal dead load from the bridge	plf	DL	DL		DL		DL
Nominal live load on the bridge	plf	LL	LL		LL		LL
Unit weight of concrete	pcf	γ_c	γ_c		$\gamma_{concrete}$		γ_c
Height of the bearing pad	ft	h_1	h_1		t		h_1
Nominal dead load pressure from the bridge	psf					q_b	q_b
Nominal live load pressure on the bridge	psf					q_{LL}	q_{LL}
Sum of horizontal nominal pressures from upper wall	plf	F_A	F_A		ΣF_a		F_A
Depth of influence for the lateral load acting on the base of the bearing pad	ft	L_1	L_1		l_1		L_1
Location of the resultant from point A, which corresponds to the location of the front edge of the footing closest to the wall face	ft	a_{wl}	a_{wl}				a_{wl}
Nominal moment at point A, which corresponds to the location of the front edge of the footing closest to the wall face	lb-ft/ft	M_A	M_A		ΣM_{RA}		M_A
Moment due to the nominal vertical force from the	lb-ft/ft	MV_1	MV_1				MV_1

weight of the footing							
Moment due to the nominal dead load from the bridge	lb-ft/ft	MDL	MDL				MDL
Moment due to the nominal live load on the bridge	lb-ft/ft	MLL	MLL				MLL
Moment due to the horizontal nominal earth pressure force from upper wall soil	lb-ft/ft	MF_1	MF_1				MF_1
Moment due to the horizontal nominal earth pressure force from traffic surcharge	lb-ft/ft	MF_{S1}	MF_{S1}				MF_{S1}
Horizontal nominal earth pressure force from the upper wall soil	Plf	F_1	F_1		F1		F_1
Horizontal nominal earth pressure force from traffic surcharge	plf	F_{S1}	F_{S1}		F_q		F_{S1}
Lateral earth pressure coefficient of the upper wall	NA	K_{a2}	K_{a2}				$K_{a,u}$
Friction angle of the upper wall soil	Deg.	ϕ'_u	ϕ'_u				ϕ'_u
Required tensile strength	plf						T_{req}
Reduction factor accounting for installation damage	NA	RF_{ID}	RF_{ID}	RF_{ID}			RF_{ID}
Reduction factor accounting for creep	NA	RF_{CR}	RF_{CR}	RF_{CR}			RF_{CR}

Reduction factor accounting for degradation	NA	RF_D	RF_D	RF_D			RF_D
Resistance factor accounting for geosynthetic reinforcement	NA	ϕ	ϕ	ϕ_{rr}		ϕ_{reinf}	ϕ
Correction factor for wall face batter	NA			Φ_{fb}			Φ_{fb}
Correction factor for soil cohesion	NA			Φ_c			Φ_c
Correction factor for global stiffness	NA			Φ_g			Φ_g
Correction factor for facing stiffness	NA			Φ_{fs}			Φ_{fs}
Correction factor for local reinforcement stiffness	NA			Φ_{local}			Φ_{local}
Nominal vertical stress at depth within the reinforced fill	psf						σ_v
Load distribution factor based on layer location that modifies reinforcement load	NA			D_{tmax}			D_{tmax}
Height of the wall	ft			H			H
Influence exponent resulting from empirically fitting case history data for local stiffness	NA			a			a
Influence factor coefficient resulting from empirically fitting case history data for global stiffness	NA			α			α
Global reinforcement	psf			S_{global}			S_{global}

stiffness							
Local reinforcement stiffness	psf			S_{local}			S_{local}
Atmospheric pressure	psf			P_a			P_a
Influence factor exponent resulting from empirically fitting case history data for global stiffness	NA			β			β
Sum of reinforcement stiffness at 2% strain in each reinforcement layer	plf			ΣJ			ΣJ
Reinforcement stiffness at 2%	plf			$J_{2\%}$			$J_{2\%}$
Influence factor coefficient resulting from empirically fitting case history data for facing stiffness	NA			η			η
Facing stiffness parameter	NA			F_f			F_f
Influence factor exponent resulting from empirically fitting case history data for facing stiffness	NA			k			k
Modulus of the facing material	psf			E			E
Width of the facing block	ft			*b*			*b*
Target reinforcement strain for the soil failure limit, strain check	NA			ε_{targ}			ε_{targ}

Resistance factor for the soil failure limit state	NA			ϕ_{sf}			ϕ_{sf}
Effective width of applied bridge load at depth	ft				D		D
Minimum reinforcement stiffness	plf				$T_{@\varepsilon=1\%}$		$T_{@\varepsilon=1\%}$
Factor of safety accounting for reinforcement	NA				FS		FS
Nominal maximum horizontal stress	psf				$\sigma_{h,max}$		$\sigma_{h,max}$
Maximum particle diameter	ft					d_{max}	d_{max}
Load factor accounting for horizontal earth pressure in the active condition	NA					γ_{EH-MAX}	γ_{EH-MAX}
Load factor corresponding to live load surcharge	NA					γ_{LS}	γ_{LS}
Factored lateral earth pressure from equivalent bridge load	psf					$\sigma_{h,bridge,eq,f}$	$\sigma_{h,bridge,eq,f}$
Load factor accounting for components and attachments	NA					γ_{DC-MAX}	γ_{DC-MAX}
Load factor accounting for live load	NA					γ_{LL}	γ_{LL}
Adjustment parameter for location of bridge pressure acting on the sill	NA					α_b	α_b
Adjustment	NA					β_b	β_b

parameter for location of bridge pressure acting on the sill							
Nominal lateral earth pressure from equivalent bridge load	psf					$\sigma_{h,bridge,eq}$	$\sigma_{h,bridge,eq}$